TRANSPORTATION RESEARCH

RECORD

No. 1449

Pavement Design, Management, and Performance

Design and Rehabilitation of Pavements

A peer-reviewed publication of the Transportation Research Board

TRANSPORTATION RESEARCH BOARD
NATIONAL RESEARCH COUNCIL

NATIONAL ACADEMY PRESS
WASHINGTON, D.C. 1994

Transportation Research Record 1449
ISSN 0361-1981
ISBN 0-309-06056-7
Price: $49.00

Subscriber Category
IIB pavement design, management, and performance

Printed in the United States of America

Sponsorship of Transportation Research Record 1449

GROUP 2—DESIGN AND CONSTRUCTION OF TRANSPORTATION FACILITIES
Chairman: Charles T. Edson, Greenman Pederson Inc.

Pavement Management Section
Chairman: Joe P. Mahoney, University of Washington

Committee on Rigid Pavement Design
Chairman: Gary Wayne Sharpe, Kentucky Transportation Cabinet
Don R. Alexander, Mark W. Bintzer, Brian T. Bock, Larry J. Buttler, Judith B. Corley-Lay, Kathleen T. Hall, John E. Hunt, Anastasios M. Ioannides, Walter P. Kilareski, Starr D. Kohn, Roger M. Larson, Jo A. Lary, Brian R. McWaters, Theodore L. Neff, William Albert Nokes, Mauricio R. Poblete, Robert J. Risser, Jr., Mark B. Snyder, Shiraz D. Tayabji, Mang Tia, John P. Zaniewski, Dan G. Zollinger

Committee on Flexible Pavement Design
Chairman: Newton C. Jackson
Secretary: Stephen B. Seeds, Nichols Consulting Engineers
Douglas I. Anderson, Uno Arebratt, Chris A. Bell, Jacques Bonnot, Elton R. Brown, James L. Brown, Stephen F. Brown, Albert J. Bush III, George R. Cochran, N. F. Coetzee, Judith B. Corley-Lay, Raymond A. Forsyth, C. R. Freeme, W. Charles Greer, Jr., Jerry J. Hajek, John P. Hallin, W. N. Lofroos, Kenneth H. McGhee, Carl L. Monismith, William Albert Nokes, Cesar A. V. Queiroz, Lutfi Raad, John L. Rice, Cheryl A. Richter, Peter Sebaaly, Gary Wayne Sharpe, Marshall R. Thompson

Committee on Pavement Rehabilitation
Chairman: David E. Newcomb, University of Minnesota
Secretary: Roger C. Olson, Minnesota Department of Transportation
Janice L. Arellano, Fouad M. Bayomy, Thomas L. Boswell, James L. Brown, Alfred B. Crawley, Denis E. Donnelly, Kathleen T. Hall, Joseph B. Hannon, Don M. Harriott, Thomas M. Hearne, Jr., Mustaque Hossain, Ira J. Huddleston, Tom J. Kazmierowski, Walter P. Kilareski, Aramis Lopez, Jr., Joe P. Mahoney, Emmanuel B. Owusu-Antwi, Elias H. Rmeili, Gary Wayne Sharpe, Eugene L. Skok, Jr., Shiraz D. Tayabji, Gerald F. Voigt

GROUP 3—OPERATION, SAFETY, AND MAINTENANCE OF TRANSPORTATION FACILITIES
Chairman: Jerome W. Hall, University of New Mexico

Task Force on Statistical Methods in Transportation
Chairman: Olga Pendleton, Texas A&M University System
Secretary: Patricia S. Hu, Oak Ridge National Laboratory
Charles E. Antle, Kenneth L. Campbell, Lynda T. Carlson, Michael I. Darter, Gary A. Davis, Michael S. Griffith, Irit Hocherman, David T. Hunt, Robert L. Mason, Edward V. Milton, Frank C. Sonsini, Gary S. Spring, Delbert E. Stewart, Peter R. Stopher, Russell G. Thompson, Richard M. Weed, Robert E. White

Transportation Research Board Staff
Robert E. Spicher, Director, Technical Activities
D. W. Dearasaugh, Jr., Engineer of Design
Richard F. Pain, Transportation Safety Coordinator
Nancy A. Ackerman, Director, Reports and Editorial Services
Luanne Crayton, Editor

The organizational units, officers, and members are as of December 31, 1993.

Transportation Research Record 1449

Contents

Foreword

The TRB Committees on Rigid Pavement Design, Flexible Pavement Design, and Pavement Rehabilitation and the Task Force on Statistical Methods in Transportation sponsored various sessions on pavement design and rehabilitation during the 1994 Annual Meeting, and most of the papers in this volume were presented at those sessions. However, the first five papers were presented in sessions on pavement performance and reliability in pavement design during the 1993 Annual Meeting. Gopinath et al. present a two-component performance model representing both functional performance and structural integrity of the pavement. Pendleton encourages appropriate use of reliability in pavement design by summarizing its historical evolution, addressing issues relating to its use, and presenting applications and misuses of reliability. Kulkarni describes a rigorous, yet practical methodology for evaluating pavement design reliability. Zollinger and McCullough present concepts for determination of rational, mechanically based reliability and design calibration factors. Brown reviews the background, definition, and details of reliability in pavement design and describes the weaknesses and strengths of using reliability in pavement design.

The next six papers are on flexible pavement design. Hall and Thompson investigate the use of soil index properties to estimate the subgrade resilient modulus for structural pavement design. Attoh-Okine and Roddis discover the pronounced effect that thickness variability has on the structural characteristics and in-service performance of a pavement. Noureldin et al. describe a procedure that uses values of the mean and coefficient of variation of flexible pavement layer thicknesses and strength parameters to estimate the standard deviation of predicted pavement performance. Aglan et al. discuss the concept of the specific energy of damage as a fracture criterion for flexible pavements and present four case studies to demonstrate its validity. Riley et al. use the World Bank HDM-III model to analyze new pavement design standards for highways in Thailand derived by using a life cycle costing approach. Baladi and Thomas present and discuss a full factorial experiment design that can be used to conduct a mechanistic evaluation of the AASHTO flexible pavement design equations.

The next eight papers in the Record are focused on rigid pavement design. Chatti et al. present a new dynamic finite-element computer program, DYNA-SLAB, for analyzing jointed concrete pavements subjected to moving transient loads. Zollinger et al. suggest an approach based on fracture mechanics analysis for estimating appropriate sawcut depths for concrete pavement joints. Lee and Darter present prediction models to determine edge stresses in concrete slabs caused by the combined effects of wheel loading and thermal curling. Senadheera and Zollinger propose a framework based on survival analysis that can be used to incorporate crack spalling in the design of concrete pavements. Zaghloul et al. use a three-dimensional dynamic finite-element method (3D-DFEM) to analyze the effects of heavy loads on concrete pavements in Indiana. Suh and McCullough evaluated various factors, including construction season, coarse aggregate type, amount of steel, and time of occurrence, that affect crack width in continuously reinforced concrete pavement. Bendanã et al. describe the development of a mechanistic-empirical procedure to verify the designs that were presented in a new manual for thickness design of concrete pavements in New York State. Byrum and Hansen present a technique for analyzing the interactions between typical highway loads and jointed rigid pavements using influence functions and compare the results with field surveys of a test pavement in Michigan.

The next nine papers deal with pavement rehabilitation; four cover the design and performance of concrete overlays. Tayabji et al. present the details of the field investigations, data analysis, and the rehabilitation design process used to arrive at the final design for the unbonded plain-jointed concrete overlay of I-495 in Delaware. Kazmierowski and Sturm describe the design and construction of an unbonded concrete overlay in Canada and detail the results of a comprehensive performance monitoring program. Khazanovich and Ioannides present a new method of analyzing the effects of combined traffic loading and temperature differentials on the stresses and deflections of an unbonded concrete overlay using a formulation proposed by Totsky that is implemented into ILLI-SLAB, a finite-element program. Bodocsi et al. show how the type of base, season of the year,

joint spacing and pattern, presence of dowels, type of dowels, and time of day affect deflections at the joints of an experimental pavement built in Ohio in 1972. Pierce provides an overview of the performance of concrete pavements in Washington State and discusses the construction, analysis, and initial performance of a specific concrete pavement rehabilitation project involving retrofitted dowel bars, a tied concrete shoulder, and pavement grinding. Complementing their previous paper in this record, Zaghloul et al. use the 3D-DFEM to analyze composite pavements with verification both for static, linear elastic analysis and for dynamic, nonlinear analysis. Moody presents the preliminary results of a research project to design, construct, and evaluate the effectiveness of seven pavement rehabilitation strategies for reducing the extent and severity of reflective cracking of asphalt concrete overlays constructed over jointed concrete pavements. Reddy and Pandey correlated data collected on pavement sections in India to the mechanistic response of the pavement to develop criteria to predict the performance of bituminous overlays on flexible pavements. Taha et al. report the results of a survey of current practices for undersealing concrete pavements in the United States.

In the last paper, Lee and Darter present statistical algorithms for predictive modeling techniques for pavements.

Modeling Performance of Highway Pavements

DINESH GOPINATH, MOSHE BEN-AKIVA, AND ROHIT RAMASWAMY

A highway performance prediction model predicts the performance of highway pavements as a function of explanatory variables such as pavement characteristics, ambient climate, usage of the system, and so on. However, there is no unambiguous approach that can be used to directly measure the performance of the highway pavement. Performance is considered to be unobservable (latent). The problems with developing performance deterioration models include the definition of the aforementioned unobservable performance in terms of the observed or measurable distress measures of the system and simultaneously relating the performance to the explanatory variables. Previous research is extended by exploring the existence of a two-component performance measure for highway pavements: a latent variable to represent functional performance and another variable to represent the structural integrity or structural performance of the pavement. A case study is conducted on a data set from Brazil compiled by the World Bank.

Why are performance deterioration models necessary? The determination of cost-effective maintenance actions requires information on:

- Current condition (obtained from an inspection of the facility), and
- Anticipated conditions for different maintenance and rehabilitation actions (obtained from performance deterioration models).

The emergence of a large variety of automated technologies (such as video, laser, radar, and infrared technologies) that can be used to collect information on pavement conditions has made available large quantities of data for the analysis of pavement performance. These new technologies require new methods for processing their nascent outputs to a manageable size meaningful for decision making. On the other hand existing approaches to pavement performance analysis are based on subjective indexes that use a predetermined set of distress measures selected at a time when less developed data collection technologies were used [e.g., measures like present serviceability index (PSI) (*1*) and pavement condition index (*2*)]. There is a need for an improved performance analysis methodology to exploit these enhanced data collection capabilities. By using new methods for performance analysis, it should be possible to plan more cost-effective maintenance actions for highway pavements.

PAVEMENT MANAGEMENT PROCESS

This section outlines the different facets of the pavement management process. The reader is directed to Ben-Akiva et al. (*3,4*) for a more comprehensive treatment of the pavement management process. The pavement maintenance management problem consists of the allocation of limited resources for the maintenance and rehabilitation of different pavements over both spatial and temporal dimensions. The pavement management process can be divided into the following three task areas:

- Data collection and analysis (including inspection);
- Performance analysis and modeling; and
- Maintenance and rehabilitation (M&R) and inspection strategy selection.

These tasks are related in the manner shown in Figure 1. The facility condition data collected by using different technologies are used in two ways. First, they are one of the items used in the estimation of pavement performance models. Second, they provide the initial values in the prediction of future performance. In addition to M&R strategies, the third block includes models for the selection of future inspection strategies. This effect is represented by the feedback loop of Figure 1.

Data Collection and Analysis

Data on the extent of pavement damage (such as area or length and severity of damage), on the causal variables that affect deterioration such as usage, age, environmental conditions, and pavement type are collected. The data may be collected by visual inspection, through manual measurements, or through automated techniques. The data collected, after suitable processing, can be used as inputs to performance analysis. The data collected can also be used for monitoring purposes to validate model predictions and update a model system after it has been implemented.

Performance Analysis and Modeling

A deterioration model links a measure of the condition of the facility to a vector of explanatory variables. The condition measure in its simplest form is just the extent of damage; more complex indexes that combine the extent of different types of damage may also be used.

This paper addresses the issue of estimating pavement performance deterioration models. The framework presented by Ben-Akiva et al. (*5,6*) is used to estimate two-component performance deterioration models. Hence, this paper concentrates on this block of the pavement management process.

D. Gopinath and M. Ben-Akiva, Department of Civil and Environmental Engineering, Massachusetts Institute of Technology, Cambridge, Mass. 02139. R. Ramaswamy, AT&T Bell Laboratories, Cranfords Corner Road, Room 3K-308, Holmdel, N.J. 07733.

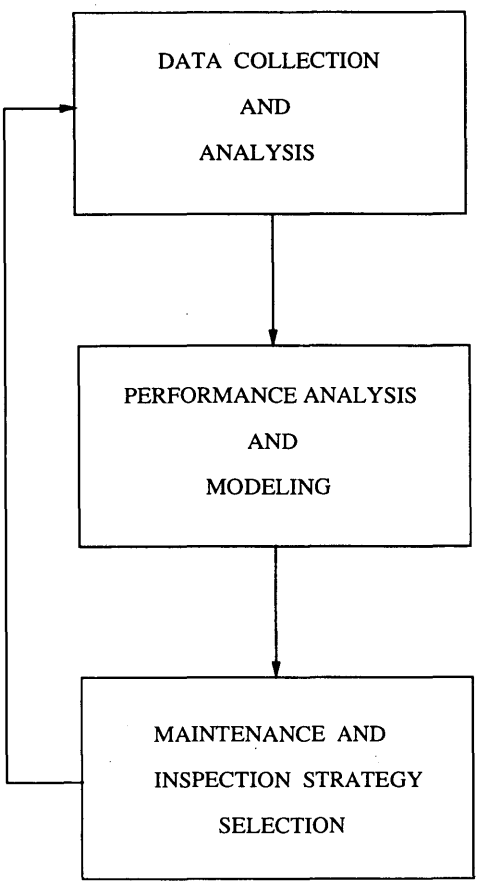

FIGURE 1 Highway pavement management process.

M&R and Inspection Strategy Selection

This block involves the choice of an optimal maintenance activity and inspection strategy that minimizes the total costs over the planning horizon subject to various resource and technical constraints. A methodology that recognizes the trade-offs between inspection costs (which increase with the accuracy of the measurement technology used) and the added costs of M&R (which decrease with the increased accuracy of the information provided by this technology) to address the inspection decisions in a systematic manner is presented by Madanat and Ben-Akiva (*7*).

FRAMEWORK OF MODELING PAVEMENT PERFORMANCE

The framework of modeling pavement performance is presented in Figure 2. The independent variables affecting the performance of the facility form X: $(K \times 1)$. These factors can be classified broadly into the following categories:

1. Inherent factors (factors associated with the facility itself, such as facility type and construction quality), and
2. Extraneous factors (which include facility usage, maintenance actions performed, and environmental factors.

Since the facility performance is not directly observable, it is characterized by a latent variable vector, $S : (M \times 1)$. The latent

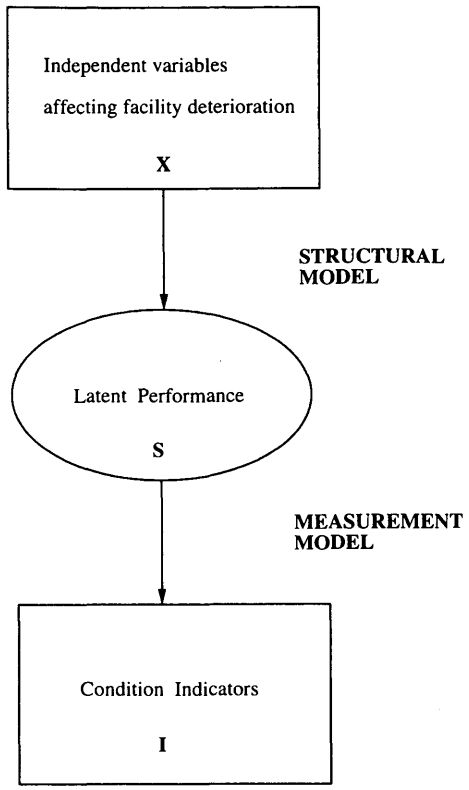

FIGURE 2 Pavement performance modeling framework.

performance of the facility manifests itself in the form of measurable indicators $I : (P \times 1)$. The indicators of the latent pavement performance are roughness, cracking, rutting, surface patching, raveling, and so on. The relationships among the independent variables X and the performance vector S form the structural model (Equation 1). The mapping from the latent performance S to the indicators I form the measurement model (Equation 2). Using linear functional forms the model system is written as

$$S = \gamma X + \zeta \quad (1)$$

$$I = \Lambda S + \epsilon \quad (2)$$

where

$\gamma : (M \times K)$ and $\Lambda : (P \times M)$ = parameter matrices to be estimated,
$\zeta : (M \times 1)$ = error component in structural model, and
$\epsilon : (P \times 1)$ = error component in measurement model.

Without any loss of generality, all observed variables are written as deviations from their respective means, or else the intercepts must be included in both the structural and measurement models. A comprehensive treatment of the theory and estimation of latent variable models is found in work by Everitt (*8*) and Bollen (*9*).

CASE STUDY

Description of Data

The data used in the study described here were collected during World Bank road deterioration studies undertaken in Brazil from

TABLE 1 Descriptive Statistics of Selected Variables

Variable	Units	Mean	Std. dev	Minimum	Maximum
Age since rehabilitation	years	8.19	4.53	0.007	23.05
Equivalent Standard axles	80 kip load $\times 10^6$	2.226	3.2	0.00011	30.28
Cumulative precipitation	meter	2.58	1.92	0.00	7.22
Roughness	QI in counts/km	40.53	15.36	12.92	99.69
Cracking	% surface area	15.16	25.70	0.00	100.00
Rut depth	mm	3.71	2.19	0.00	15.75
Surface patching	% surface area	2.47	8.65	0.00	86.29
Ravelling	% surface area	7.61	19.70	0.00	100.00
Benkelman deflection	mm	0.65	0.36	0.12	2.03
Structural number	units	4.12	1.03	1.62	7.73

1975 to 1982 under the *Research on Interrelationships Between the Costs of Highway Construction and Utilization* (*10*).

Surfacing Type

There were 3,149 observations [an average of 8.3 observations per highway section (one lane of 280 to 560 m in length) at approximately half-yearly intervals] of the pavement condition, cumulative traffic, environmental factors, maintenance status, and pavement strength at given dates as they evolved during the study period. There were four main types of pavement surfaces at the first observation dates:

1. Asphalt concrete, original (AC);
2. Double surface treatment, original (DST);
3. Asphalt concrete overlay on original asphalt concrete surfacing (ACOVL); and
4. Asphalt concrete overlay on original double surface treatment (DSTOV).

Explanatory Variables

The important explanatory variables, which affect performance deterioration, available in the data set are

1. Age since the most recent rehabilitation (AGER), measured in years.
2. Cumulative number of equivalent standard axles (ESAXL) since the most recent rehabilitation at the date of observation.
3. Cumulative precipitation since the most rehabilitation (CP), in meters.
4. Structural number (SNC), a measure of pavement strength, obtained from the thicknesses and stiffnesses of different pavement layers.

Condition Indicators

The indicators of pavement performance are roughness, cracking, rutting, surface patching, and raveling. Roughness (RQI), a measure of the longitudinal irregularity of the road surface, is measured in quarter-car index with units in counts per kilometer. As a measure of cracking, the area of indexed cracking (CRX) as a percentage of the surface area is also available. Rutting (RDMN) is measured as the mean rut depth under a 1.2-m straightedge across two wheelpaths and four test points per wheelpath. Surface patching (SPAT) is measured as the sum of the areas of surface patching expressed as a percentage of the surface area. Raveling (RAV) is measured as the sum of the areas raveled expressed as a percentage of the section area. The indicators of highway pavement strength are Benkelman deflection (DEFS) and rut depth. The descriptive statistics of selected variables are given in Table 1.

Model 0: Present Serviceability Index Type Deterioration Model

In the PSI type deterioration model, which uses the formula for PSI described previously (*11*), the PSI for each highway segment is fitted as the function of condition indicators. The fitted PSI variable is regressed on a set of variables, which include pavement age, cumulative axle loading, precipitation, and structural number, to obtain the deterioration model as shown here:

$$\widehat{PSI} = \alpha_0 + \alpha_1 \text{AGER/SNC} + \alpha_2 \text{ESAXL/SNC} + \alpha_3 \text{CP/SNC} + \epsilon \quad (3)$$

The estimated model is presented in Table 2. All of the estimated coefficients are significant and have the right signs. The fit of the

TABLE 2 Model 0: PSI-Type Deterioration Model

Independent variable	Estimate	t-statistic
Intercept	5.023	76.08
AGER/SNC	-0.388	-15.05
ESAXL/SNC	-0.117	-2.51
CP/SNC	-0.201	-3.18

model is poor, with an R^2 of 0.19 (number of observations = 1,571). Model 0 serves as the base model against which the estimated latent performance models are compared.

Estimated Latent Performance Models

In the next two sections latent performance deterioration models estimated on the basis of the data set are presented. The models are broadly classified into

- Models in which performance is characterized by a single latent variable.
- Models in which performance is characterized by two-component latent vector.

Comparisons of different models are primarily based on squared multiple correlation, a measure of goodness-of-fit similar to R^2 in a regression model, of each equation in the model, the "correctness" of the estimated parameters, and their significance. All of the models are estimated by using the unmaintained highway segments. Thus, the number of observations used in the analysis is less than the total number of observations in the data set. Furthermore, all observations are pooled under the assumption of no temporal dependence of the deterioration process for each highway segment.

The covariance matrix of the error term in the structural model is unconstrained (all the elements are free parameters that are estimated), whereas the covariance matrix of the error term in the measurement model is constrained to a diagonal matrix. This is a realistic assumption because the measurement processes for the different indicators are independent.

Single Latent Performance Models

In this section models are estimated on the basis of the hypothesis that the performance of the highway facility can be characterized by a single latent variable. The measured damage components are directly used as indicators of the underlying latent variable.

Model 1 In Model 1 the performance of the pavement is hypothesized to be affected by AGER, CP, and ESAXL, which represents traffic loading or usage of the highway. Thus the effects of facility usage, environmental conditions, and age of the pavement on performance are captured in the deterioration model.

In the measurement model, the observed damage measurements—RQI, CRX, RDMN, SPAT, and RAV—are used directly as indicators of the latent performance of the pavement segment because of the absence of a priori information regarding the manifestation process of the underlying performance variable. Since the latent variable is unobserved it does not have a definite scale. Hence it is necessary to fix one parameter in each column of the Λ matrix in the measurement model to unity. This defines the unit of measurement of the latent variable to be the same as that of the corresponding observed variable. In this model the scale of the performance variable is set equal to that of roughness. The structural and the measurement models are given in the following: for the structural model,

$$S = \gamma_1 \text{AGER} + \gamma_2 \text{ESAXL} + \gamma_3 \text{CP} + \zeta$$

TABLE 3 Structural Model, Model 1

Independent variable	Estimate	t-statistic
Age since rehabilitation	1.097	15.01
Equivalent standard axles	0.295	3.52
Cumulative precipitation	0.141	1.09

Coefficient of determination= 0.36

For the measurement model,

$$\text{RQI} = S + \epsilon_1$$

$$\text{CRX} = \lambda_2 S + \epsilon_2$$

$$\text{RDMN} = \lambda_3 S + \epsilon_3$$

$$\text{SPAT} = \lambda_4 S + \epsilon_4$$

$$\text{RAV} = \lambda_5 S + \epsilon_5$$

The estimated model system is presented in Tables 3 through 5. The coefficients of AGER and ESAXL are significant, whereas the coefficient of cumulative precipitation is insignificant, implying inconsequential effects of precipitation on pavement performance deterioration. In the measurement model the squared multiple correlation (SMC) is a measure of the variance of the indicator explained by the latent variable; a higher value of SMC for a particular measurement equation implies that the associated indicator is a better measure of the latent variable than an indicator with a lower value of SMC. In Model 1 roughness, cracking, and rut depth have relatively high SMCs (approximately 0.4), implying that these damage components are good indicators of performance. On the other hand patching and raveling appear to be poor measures of the latent performance of the pavement. The overall fit of the measurement model is 0.63, which is higher than the overall fit of the structural model (0.36). It must be noted that the fit of the structural model (0.36) is higher than the R^2 of 0.19 in Model 0.

In the equation for the estimated value of latent performance as a linear function of the indicators, the coefficients of the different indicators are calculated by using the full information extraction method described by Gopinath (*12*). The adjusted R^2 (a measure of the goodness-of-fit of the model) for this extracted latent performance model is 0.68, with all of the estimated coefficients being statistically significant. It can be seen that the *t*-statistics of roughness, cracking, and rut depth are more than those of patching and raveling, reiterating the relative importance of the former measures. This model can be used to estimate the performance given the distress measurements from an inspection of the facility.

TABLE 4 Measurement Model, Model 1

Indicator	Estimate	t-statistic	squared multiple correlation
Roughness	1.000	–[a]	0.35
Cracking	1.778	16.50	0.40
Rut depth	0.150	16.45	0.39
Surface patching	0.348	11.28	0.13
Ravelling	0.431	6.53	0.04

[a]Fixed parameter.
Coefficient of determination= 0.63

TABLE 5 Extracted Latent Performance Model, Model 1

Indicator	Estimate	t-statistic
Roughness	0.145	14.33
Cracking	0.134	23.17
Rut depth	1.556	23.21
Surface patching	0.099	5.91
Ravelling	0.063	9.41

Adjusted R^2= 0.68
Total number of observations= 1571

TABLE 7 Measurement Model, Model 2

Indicator	Estimate	t-statistic	squared multiple correlation
Roughness	1.000	–[a]	0.356
Cracking	1.458	17.27	0.306
Rut depth	0.178	21.35	0.498
Surface patching	0.235	8.98	0.071
Ravelling	0.555	8.67	0.061

[a]Fixed parameter.
Coefficient of determination= 0.62

Model 2 Model 2 SNC, which is a measure of the strength of pavement on the basis of the thickness and stiffness of the different pavement layers, is used as an additional explanatory variable in the structural model corresponding to Model 1. This variable is expected to capture the effects of pavement strength on the deterioration process, and thus differentiate among different pavement types. One would expect a stronger pavement to have a slower rate of deterioration than a weaker pavement. Therefore, the explanatory variables AGER, ESAXL, and CP are divided by SNC to model these interaction effects in the structural model.

The estimated model system is presented in Tables 6 through 8. The fit of the structural model incrased from 0.36 (in Model 1) to 0.61, implying that structural strength is an important explanatory variable affecting the deterioration process. In the measurement model the fit of the rut depth equation increased to 0.5 from 0.39 in Model 1. This observation is also reflected in the increase in the value of the rut depth coefficient in the extracted latent performance model. The surface patching coefficient is statistically insignificant in the extracted latent performance model. Thus, the addition of a strength-related explanatory variable suggests the presence of a performance variable related to the structural integrity of the pavement. Of the two single latent performance models presented so far, this model has good fits for the structural and the extracted latent performance models. Thus, it can be used to predict the future condition of the pavement as well as to calculate present performance if the facility is inspected (i.e., the indicators are measured) for the present period.

The observations made in Model 2 suggest the presence of another dimension to pavement performance—a pavement strength-related dimension as seen in the relative importance of the rut depth indicator (a strength-related variable)—in addition to a surface quality-related dimension. In the next section a two-component latent performance vector—a latent variable, S_{func}, to represent ride quality or functional performance and a latent variable, S_{struc}, to represent pavement strength or structural performance—is used to characterize the performance of the pavement.

Two-Component Latent Performance Model (Model 3)

In Model 3 it is hypothesized that the functional performance of the pavement is characterized by a latent variable, S_{func}, and the structural integrity of the pavement is characterized by another latent variable, S_{struc}. The functional aspect of pavement performance is related to the surface characteristics such as roughness, cracking, and raveling that affect user costs. The structural aspect of performance is of no perceptible concern to the user, whereas it is extremely important to the highway agency because the future functional performance may depend on the present structural condition. Furthermore, the maintenance actions could be chosen with the objective of improving the functional performance (crack filling, resurfacing, thin overlay) or improving the structural performance (preventive maintenance, reconstruction). The indicators of latent functional performance are those distress measurements that affect the user costs directly (usually surface distresses). The indicators of latent structural performance are those related to the strength of the pavement. The functional performance is hypothesized to be affected by the age of the pavement, traffic loading, precipitation, and pavement strength. Similarly, the structural performance is written as a function of the age of the pavement, traffic loading, and pavement strength.

In this specification the functional and structural performances are hypothesized to be affected by the age of the pavement, precipitation, traffic loading, and structural number. The explanatory variables are specified as in Model 2 to model the effects of pavement strength on the functional and structural performance deterioration processes. In the measurement model the scale of S_{func} performance is set equal to that of roughness, whereas the scale of S_{struc} performance is set equal to Benkelman deflection. The loadings of the indicators of functional and structural performance are chosen after extensive experiments. For the structural model,

$$S_{func} = \gamma_1 \text{AGER/SNC} + \gamma_2 \text{ESAXL/SNC} + \gamma_3 \text{CP/SNC} + \zeta_1$$

$$S_{struc} = \beta_1 \text{AGER/SNC} + \beta_2 \text{ESAXL/SNC} + \beta_3 \text{CP/SNC} + \zeta_2$$

TABLE 6 Structural Model, Model 2

Independent variable	Estimate	t-statistic
AGER/SNC	3.482	16.30
ESAXL/SNC	4.078	12.15
CP/SNC	1.503	3.75

Coefficient of determination= 0.61

TABLE 8 Extracted Latent Performance Model, Model 2

Indicator	Estimate	t-statistic
Roughness	0.171	16.89
Cracking	0.092	17.87
Rut depth	2.016	31.35
Surface patching	0.021	1.21
Ravelling	0.082	10.76

Adjusted R^2= 0.69
Total number of observations= 1571

TABLE 9 Structural Model for Latent Functional Performance, Model 3

Independent variable	Estimate	t-statistic
AGER/SNC	4.322	16.25
ESAXL/SNC	0.401	0.88
CP/SNC	3.207	5.05

Squared multiple correlation= 0.47

For the measurement model,

$$RQI = S_{func} + \epsilon_1$$

$$CRX = \lambda_2 S_{func} + \epsilon_2$$

$$RDMN = \lambda_5 S_{struc} + \epsilon_3$$

$$SPAT = \lambda_3 S_{func} + \epsilon_4$$

$$RAV = \lambda_4 S_{func} + \epsilon_5$$

$$DEFS = S_{struc} + \epsilon_6$$

The estimated structural and measurement models are presented in Tables 9 through 11, and the extracted latent performance model is presented in Table 12. Both the functional and structural performance equations in the structural model have decent fits (0.47 and 0.43, respectively). The overall fit of the structural model is 0.68. The significant explanatory variables affecting functional performance are AGER/SNC and CP/SNC. This observation suggests that the age of the pavement and precipitation are important factors in the functional performance deterioration process, whereas traffic loading has inconsequential effects. On the other hand, as seen in the significance of the explanatory variables in the structural performance equation, the important variables affecting structural performance are traffic loading and the age of the pavement, whereas precipitation is found to be insignificant.

In the measurement model the SMC of rut depth equation is 0.86, indicating that rut depth is a good measure of structural performance. Furthermore, the SMC of the Benkelman deflection equation is 0.31, indicating that deflection is also a reasonable measure of structural performance. The SMC of the roughness measurement equation is 0.55, from which one can infer that roughness is a good measure for representing the functional performance of the pavement. The overall fit of the measurement model is 0.93. The fits of the structural and functional performance equations in the extracted latent performance model have good fits (0.87 and 0.95, respectively). All of the estimated parameters are significant.

TABLE 10 Structural Model for Latent Structural Performance, Model 3

Independent variable	Estimate	t-statistic
AGER/SNC	0.055	12.04
ESAXL/SNC	0.126	13.81
CP/SNC	0.000	0.17

Squared multiple correlation= 0.43
Total coefficient of determination of structural model= 0.68

TABLE 11 Measurement Model, Model 3

Indicator	Functional perf.		Structural perf.		sq. multiple
	estimate	t-stat	estimate	t-stat	correlation
Roughness	1.000	–[a]	–	–	0.55
Cracking	1.253	16.70	–	–	0.30
Rut depth	–	–	9.994	18.17	0.86
Surface patching	0.331	13.72	–	–	0.19
Ravelling	0.361	6.90	–	–	0.04
Benkelman defs.	–	–	1.000	–	0.31

[a]Parameter fixed or not estimated.
Total coefficient of determination of measurement model= 0.93

CONCLUSIONS

In this paper various highway pavement performance deterioration models were presented. Structural number, a pavement strength–related variable, is found to be an important explanatory variable affecting the performance deterioration process of the pavement. By including structural number, a measure of the thickness and stiffness of the different pavement layers, in the structural deterioration model the effects of pavement strength on the deterioration process are captured.

The hypothesis of the performance of the pavement characterized by a two-component latent performance vector—one latent variable that represents functional performance and another one that represents structural performance—was tested. The good fits for the structural and functional performance deterioration equations and the extracted latent performance model demonstrate the identification and effectiveness of two-component latent performance models. Roughness and cracking are found to be good indicators of functional performance, whereas Benkelman deflection and rut depth are the indicators of structural performance. Further work is needed to study the specific effects of different maintenance actions on the progression of structural and functional performance.

The primary motivation for modeling the functional and structural performance deterioration processes separately stems from the use of these deterioration models in the context of a pavement management system. M&R activities are undertaken to preserve the surface quality and structural integrity of the pavement. These activities consist of surface maintenance (routine maintenance, resurfacing, etc.) and structural maintenance (reconstruction). Also, in the case of preventive maintenance actions, one needs to model

TABLE 12 Extracted Latent Performance Model, Model 3

Indicator	Functional performance		Structural performance	
	estimate	t-stat	estimate	t-stat
Roughness	0.426	69.19	–[a]	–
Cracking	0.136	37.42	–	–
Rut depth	–	–	0.077	143.42
Surface patching	0.096	8.94	–	–
Ravelling	0.051	11.89	–	–
Benkelman defs.	–	–	0.068	21.14
Squared multiple correlation	0.87		0.95	

[a]Parameter not estimated.
Total coefficient of determination= 0.98
Total number of observations= 1543

the structural performance deterioration because the structural aspect is of no immediate concern to the users, whereas it is critical to the highway agency so that it can avoid more expensive corrective measures in the future.

ACKNOWLEDGMENTS

The authors are indebted to W. D. O. Paterson from the World Bank for providing the data set used in the case study, without which this work would have been impossible. Support was provided in part from a grant from the Army Research Office to the Center for Construction Research and Education at the Massachusetts Institute of Technology.

REFERENCES

1. Carey, W. N., and P. E. Irick. The Pavement Serviceability Performance Concept. *Bulletin 250*, HRB, National Research Council, Washington, D.C., 1960.
2. Shahin, M., and S. Kohn. *Pavement Management System for Roads and Parking Lots*. Technical Report M-294. Construction Engineering Research Lab, U.S. Army Corps of Engineers, 1981.
3. Ben-Akiva, M., F. Humplick, S. Madanat, and R. Ramaswamy. Infrastructure Management Under Uncertainty: Latent Performance Approach. *Journal of Transportation Engineering*, ASCE, Vol. 119, No. 1, January/February 1993.
4. Ben-Akiva, M., F. Humplick, S. Madanat, and R. Ramaswamy. Latent Performance Approach to Infrastructure Management. In *Transportation Research Record 1311*, TRB, National Research Council, Washington, D.C., 1992.
5. Ben-Akiva, M., and R. Ramaswamy. Estimation of Latent Pavement Performance from Damage Measurements. *Proc., 3rd International Conference on Bearing Capacity of Roads and Airfields*, Trondeim, Norway, 1989.
6. Ben-Akiva, M., and R. Ramaswamy. An Approach for Predicting Latent Infrastructure Performance Deterioration. *Transportation Science*, Vol. 27, No. 2, May 1993.
7. Madanat, S., and M. Ben-Akiva. Optimizing Sequential Decisions Under Measurement and Forecasting Uncertainty: Application to Infrastructure Inspection, Maintenance and Rehabilitation. *Transportation Science* forthcoming.
8. Everitt, B. S. An Introduction to Latent Variable Models. In *Monographs on Statistics and Applied Probability*, Chapman & Hall, 1984.
9. Bollen, K. *Structural Equations with Latent Variables*. Wiley Series in Probability and Mathematical Statistics. John Wiley & Sons, Inc., New York, 1989.
10. GEIPOT. *Research on Interrelationships Between the Costs of Highway Construction and Utilization*, 12 vols. Ministerio dos Transportes, Brasilia, Brazil, 1982.
11. *Special Report 61E: The AASHO Road Test, Report 5: Pavement Research*. HRB, National Research Council, Washington, D.C., 1961.
12. Gopinath, D. *Modeling Infrastructure Performance and User Costs*. M.S. thesis. Department of Civil Engineering, Massachusetts Institute of Technology, Cambridge, Jan. 1992.

Publication of this paper sponsored by Committee on Flexible Pavement Design.

Reliability in Pavement Design: Issues, Concepts, and Significance

OLGA J. PENDLETON

Reliability as both a concept and a methodology has been an integral part of scientific research for centuries. As a methodology, however, it has not been widely embraced by the pavement design research community. A historical summary of the evolution of reliability methods in other disciplines, specifically medicine, is provided. Several issues relating reliability to pavement design and evaluation are addressed. Applications and misuses of reliability methods as related to pavement performance modeling are then presented. The object is to encourage the appropriate use of reliability methods in building, evaluating, and validating pavement performance models, thus dissipating the clouds of skepticism and distrust that have surrounded this well-founded and powerful methodology.

Reliability. The word itself conjures thoughts of dependability, trustworthiness, and credibility. But when preceded by the adjective *statistical*, reactions may vary from skepticism to fear. Yet statistical reliability is nothing more than a measurement device, a yardstick, by which one can scientifically access a process in an objective, unbiased manner. So why the mixed reviews? In this paper several issues relating reliability to pavement design and evaluation are addressed in the hopes of clarifying misconceptions and dissipating the clouds of skepticism and distrust that have surrounded this well-founded and powerful methodology.

When searching for a definition of statistical or mathematical reliability the most common definitions are

- A methodology concerned with random occurrences of undesirable events (*1*).
- The probability that a system, when operating under stated environmental conditions, will perform its intended function (*1*).
- The study of the proper functioning of equipment and systems (*2*).
- The study of a random variable that represents the lifetime or time to failure of a unit (*3*).
- The probability that a unit survives until a fixed time (*4*).

So which is it: a study or a probability? Mathematically, it is a probability, namely

$$1 - P \text{ [failure]}$$

or, simply put, the probability that something will *not* fail. Specifically, in the area of pavement performance, AASHTO defines it as

> the probability that the pavement system will perform its intended function over its design life and under the conditions (or environment) encountered during operation. . . . the probability that any particular type of distress will remain below or within a permissible level . . . during the design life. (*5*)

Yet in reading textbooks on the subject, one finds reliability methods covering everything from survival analysis to least-squares regression modeling, from hypothesis testing to the formulation of prediction intervals, from normal probability distributions to Weibulls. In other words the term *reliability*, depending on the setting, may refer to something far more general than a single probability. The origin of this more global interpretation of the term probably stems from the grammatical definition of reliability.

Webster's defines "reliability" as "the state or quality of being dependable, sound, irrefutable, unquestionable, conclusive, incontestable, and infallible." The thesaurus provides antonyms such as "undependable" and even "dangerous". Probability theory, statistical inference, and the scientific method are all synonymous with methodologies that attempt to arrive at conclusions that are reliable. So it is quite logical that the term "reliability" would take on a broader meaning than merely a probability of not failing. Regardless of personal preferences as to the meaning of the term, it is important that the more general context of the word be recognized to understand the vast array of methodologies available to achieve reliability in scientific experimentation.

Historically, reliability has always been met with some skepticism. Early in the developmental history of the scientific method the recognition of variability within populations being studied brought out natural questions about the mechanisms causing the variability. These mechanisms were, unavoidably, the chance mechanisms that are the subject of probability theory. One of the oldest disciplines to first embrace the union of probability concepts with scientific experimentation was medicine. However, when Francis Galton and Karl Pearson, founders of the science of biometry, first proposed the concept at the turn of the century, the Royal Society of London (the British Academy of Science) strongly opposed it. How incredulous to recommend the mixing of mathematics and biology!

Although biometry is now a well-ingrained part of the medical field, it would appear that other sciences are still at the turn of the century with regard to acknowledging the importance of probability concepts in drawing scientific conclusions. The field of pavement design and evaluation would appear to be among these sciences. There appears to exist some reluctance toward accepting and implementing reliability theory into the modeling process. This is most unfortunate because not only has much of the difficult theory been developed but computer software is also readily available for straightforward implementation and interpretation. Many of the biomedical computer packages could be applied to the pavement area, avoiding the reinvention of the wheel, so to speak.

Texas Transportation Institute, TTI/CE Building, Suite 508, College Station, Tex. 77843.

In 1973 several scientists recognized this link between reliability and biometry and held a symposium from which proceedings were published (*6*). In reply to the question "What do reliability and biometry have in common?", the proceedings' preface states:

> Both disciplines apply statistical methods to predict, estimate, and hopefully extend lifelength. In reliability, the lifelength under study is generally that of an engineering system; in biometry, the lifelength is that of a living creature. However, aside from the presence or absence of animation . . ., the two disciplines are remarkably alike in their main goals and the tools that can be used for reaching these goals. And yet, in looking back over the history of the two subjects, one is struck by the fact that the development of the two fields has proceeded largely independently by separate groups (*6*).

Although this was acknowledged nearly 20 years ago, it would appear that the two disciplines have not made much progress toward recognizing these similarities and taking advantage of the "tools" developed by the other.

Many of the difficult problems that have resulted in complex theoretical developments are held in common by both groups. One such example is the problem of censoring. In the pavement area one is faced with the dilemma of what to do about pavements that had not yet failed up to some point in time but then were changed in some way that affected their failure time. In medical clinical trials, some patients are lost to follow-up either because they did not properly follow their treatment regimen, dropped out of the study, or died as a result of something unrelated to the disease, like a car accident. Yet there is still some valuable information about these patients in that their condition is known up to the time that they were dropped from the trial. Similarly, there is valid information in knowing that the changed pavements had not failed up to the time that the change was made. These data are generally termed "censored data," and methods exist for incorporating the valid information about these data without classifying them as "failed."

Similarly, in medicine and pavement evaluation there is the situation of "complex repairable systems." In pavements the "repair" may consist of maintenance procedures performed over the life of the pavement. In medicine the "repair" may be biological, as in the case of infant mortality as a result of some disease. As the infant matures the body internally "repairs" itself through the immune system. This is a factor that cannot be controlled for, but it can be modeled as a nonhomogeneous Poisson process. This same model would appear to be relevant to modeling pavement failure rates, including the maintenance process.

Many of the problems addressed in biometry are difficult because they cannot be controlled through experimental design. This is also true of pavement evaluation. The point is that many of these problems have been resolved in biometry and could easily be applied to pavements. The time has come for the pavement design discipline to take advantage of these developments and emerge from the cloud of skepticism and fear. It is hoped that this paper will result in a significant first step toward this end.

RELIABILITY MODELS

Reliability models are built on the assumption that there are three inherent sources of variability in the model:

- Variability in the output variables,
- Variability in the explanatory or input variables, and
- Sampling variability or experimental error.

Figure 1 represents a schematic depicting this modeling process. The input portion of the model may consist of known equations and relationships such as physical or mechanistic laws of nature. Or the input model may be a known or hypothesized probability model. It may even, in fact, be a black box in which nothing is known about either the mathematical form of the functions or even the input variables that belong in the box. But regardless of what is or is not known about the input box, a reliability model acknowledges that there is always an error associated with any experimental modeling process. Of course, the objective is to determine what form of the input box will minimize the amount of error in the model and thus produce reliable, predictable outputs.

As a simplistic example consider the relationship between the amount of stress required to deflect a beam to some degree and the physical and material properties of the beam. The exact relationship is known by using the physical and mechanistic laws of nature. Yet for a sample of beams there may be some variation from this known relationship because of differences in environmental conditions at the time of experimentation (humidity, temperature), physical properties (manufacturing differences in production of the beams' dimensions), or material properties. In this example many of the factors contributing to this variability could be controlled, especially in a laboratory setting. However, now suppose that these samples of beams have been buried underground for different periods of time and at different locations. Now the environmental factors cannot be controlled. It may be that data can be collected and these factors recorded retrospectively, in which case they go into the input box and are taken out of the error box. Suppose also that because of their submersion in the earth their physical and material properties have changed from what they were initially. A sample might have to be drawn and the extent of change in properties might need to be measured and put into the input box, again reducing the magnitude of the error box, or the uncertainty. Now, suppose this example is not about a beam at all but a section of pavement.

This, in a nutshell, is the objective of reliability modeling: to reduce the magnitude of the error box and, in so doing, to explain the dynamics of the input box. Reliability theory and methodology help to get a handle on the uncertainty or error in the models in a scientific, objective, and unbiased way. And an essential part of doing this involves understanding variability and its sources.

The importance of variability and covariability in describing pavement performance is essential and critical in designing pavements. Reliability methods provide a means of incorporating variability and covariability in developing pavement designs. More important, these methods provide an unbiased and scientifically accepted procedure for developing deformation models at acceptable confidence levels.

Some reliability models differ from other types of statistical models (i.e., regression models) in that they incorporate variability inherent in the input as well as the output variables. This is done

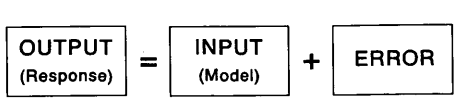

FIGURE 1 Schematic depicting reliability modeling.

through the assumption that these input variables are themselves random rather than fixed quantities and as such follow some probability distribution defined by some shape and scale parameters. The most common such distributions are the normal, lognormal, Gumbel, and Weibull distributions. The methodology exists for handling any of these four models, and tests exist for determining which model best describes the system on the basis of a sample of representative data.

Reliability theory plays a critical role in any scientific experiment from beginning to end or modification. In the beginning reliability in the design of the experiment is critical if the end product is to be optimal. The use of the concepts of probability and variability helped to establish minimum sample size requirements. Controlling the levels of certain key factors can contribute to reduced experimental variability. In addition experimental design conditions can sometimes reduce the number of samples needed by optimally sampling at the extremes or where the variability is greatest. This is design reliability.

During the course of the experiment or study reliability in management and testing (estimation) and model building are important. And, finally, reliability concepts provide a means of assessing the goodness and reproducibility of the model (reliability demonstration), which in turn allow modification of the model. Once modified, it may be desirable to redesign the experiment and begin the process again until the optimal model is obtained. So reliability plays a dynamic, not stochastic, role in any experimental process. Like the testing of a product, such as a motor vehicle, which consists of many component processing steps, the entire system, not just the end product, must be tested. So, too, must reliability methodology be used at every juncture of a scientific experiment.

COMMON ERRORS IN RELIABILITY MODELING

In this section some common errors and misapplications of the concepts of reliability and probability in engineering are illustrated. One such misconception is that a level of reliability can be generated from plotted data. The appropriate probability distribution can be found and statistically tested for goodness of fit by using the data, but ultimately it is this distribution that theoretically determines the level of any degree of reliability.

Another misconception is that model inputs are known and without error. These inputs or model components are random variables that follow some probability distribution and that have some variability, and, subsequently, coefficients of variations, that must be accounted for in the development of reliable designs and models for pavement performance. These are not fictitious or unrealistic concepts and can easily be applied to pavement performance modeling.

Specifically, the following example is presented. It shows that the variance of the log of traffic (N) is reduced by the inclusion of the (positive) correlation between material fatigue parameters. Since N is a function of these parameters, if they are treated as random variables with some bivariate probability distribution, then N, and hence the variability of N, must depend on their mean values as well as their variability and correlation. Likewise, a negative correlation among the input variables will result in a larger estimate of variability, and exclusion of this correlation produces an underestimate of the true variability. Another example of this can be seen in modeling the relationship of stress and strain to estimate expected pavement life.

Another error that is often committed is the use of the variance of means in place of the variance of individual observations. The central limit theorem states that, regardless of the distribution of a random variable, a sample of means of the variable will be normally distributed and the variability of these means is less than the variability of the random variable by a factor of $1/n$ because n, the sample size, tends to infinity. Thus, the use of means in place of individual observations is wrong and assumes a much smaller variance than what is really in effect.

Still another area of concern is in the description of the relationship between cracking and load applications. Here it is essential that the variability inherent in both of these random variables be considered. In the assumed relationship of Figure 2, for example, had a least-squares solution been used to develop this relationship using this "cloud of points," the resulting model would have assumed that the explanatory variable N was a fixed variable with no error. This would only be true if somehow in measuring cracking (C) one could specify various load applications, that is, go out and find roads that had N_1, N_2, etc., traffic loads and measure the cracking on those roads. In practice, one cannot do this. A sample of roads is selected and then whatever values of N and C result are taken. In this way, N must be treated just like C, that is, as a random variable that had some probability of occurrence in the sample and that is variable; that is, if another experiment was performed (drew another sample), there is a good likelihood that, for the same cracking level, one would observe a different load application from the previous one. Similarly, on repeated sampling for the same value of load application one would in all likelihood observe a different degree of cracking. This is what the "normal" distributions mean in Figure 2.

Another disconcerting fact is that if one were to reverse the roles of cracking and load application—that is, put load application on the y-axis and cracking on the x-axis and fit a least-squares regression model—the model and reliability levels would be different for the reversed case. The reaon for this is that cracking has now been assumed to be fixed without error and only the variability in load application is accounted for. The only way that the same model would result regardless of the roles of these variables in the least-squares modeling procedure is the very restricted case in which both random variables have exactly the same variabilities.

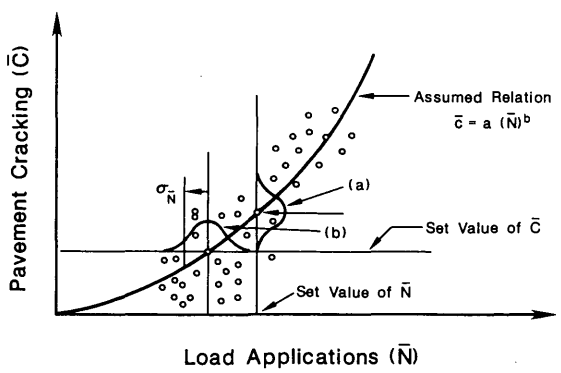

FIGURE 2 Pavement cracking versus load application.

Another common yet erroneous practice is the use of *means* rather than the observed individual cracking values as datum points. The means, as discussed earlier, have a much smaller variability, and hence the relationship appears to be better (more reliable) than it really is. The greater the number of pavements sampled, the worse this error becomes and the model appears to be better than it is. In fact a designer could arbitrarily make a model look good using this trick of modeling means.

Some researchers have recommended that rather than fit a model to the "cloud" of datum points a separate curve be established for each pavement using a model form that satisfies the necessary limits of the variables (*7*). By selecting an arbitrary but small lower value and then finding the curve parameters that will fit the observed point and the assumed lower point, a separate curve can be established for each pavement. This modeling method offers the advantage of controlling for other outside factors that make the pavements behave differently from each other. That is, suppose the cloud of points shows no relationship, yet the sample consists of pavements of one type that are known to have very steep curves and pavements of another type that are known to have relationships witha very low slope. Combining these pavements together as a cloud and trying to find one model that represents them all will result in a very poor model that does not represent any of them. The sketch in Figure 3 is an attempt to describe this situation. If separate models were established for each of the two types of pavements, this problem could be circumvented. In reality, however, one does not have knowledge of the factor type or any of a number of other factors that could result in similar obscurities. By letting each pavement stand alone, models that control for these unknown confounding effects are built.

Reliability can be established either on the basis of the number of load applications, that is, the probability that the traffic will not exceed a maximum level, or on the basis of cracking, that is, the probability that the cracking areas will not exceed a maximum acceptable level. For either case even if the probability distributions are not known, any of the four most common ones can readily be applied and tested to see which one is the best.

Another common misconception is that the material properties used in construction specifications to control quality can be considered to control reliability. Controlling the construction quality by monitoring test values of a single variable does not guarantee a specified design reliability. Design specifications are generally set arbitrarily. Yet implicit in these specifications are factors that affect design reliability, namely, the means and variances or coefficients of variation. To control the reliability knowledge of and experience with these coefficients of variation are essential. To set specifications without this knowledge is a dangerous practice.

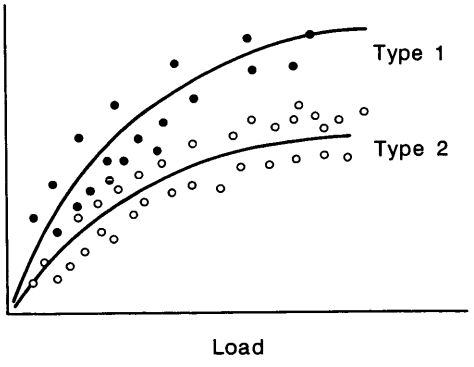

FIGURE 3 Example of mixing pavements of different types.

Returning to the schematic of Figure 1, another popular practice is the adoption of the "black box" approach when, in fact, there is knowledge of some of the interrelationships and interactions that take place in the input box. This "blind" approach in the face of knowledge makes absolutely no scientific sense. In fact examples can be constructed to show how futile it is in some cases to ever arrive at the known, true relationship if this "naive" approach is used.

CONCLUSIONS

Both empirical and nonempirical approaches should be merged in any modeling effort to produce a reliable design. Empirical relationships based on data should serve as guidelines in pavement design and performance modeling but cannot stand alone as conclusive and absolute indicators of the reliability of the models. The reason for this is the error box, the inherent error owing to variability of the random variables being observed. Each datum point represents only one realization in many, and it is the variability of the many that dictates the reliability of the models developed. Knowledge of the distribution of the random variables, which is available through the nonempirical mechanistic design relationships, can be used to incorporate this variability and hence establish reliability levels for the resulting pavement performance models.

In many areas of science little if any knowledge exists regarding the true relationships of observed phenomena. Investigators in these scientific disciplines have no choice but to blindly follow the observed data dictates and make decisions in the absence of known relationships. The result is often disappointing, and many replications and redesigns of experiments are required before progress, if any, can be achieved. The discipline of pavement performance modeling appears to have the advantage of a vast field of knowledge in the form of known physical laws and properties to serve as foundations on which to build models using empirical evidence along the way. It is truly a step backward in the scientific pursuit of truth to blindly pursue the naive, empirical approach and forsake all known engineering concepts.

The purely empirical approach has the additional, most dangerous potential of introducing bias and unfair practices in the inferential process. The statement "you can prove anything with statistics" emerged as a result of this all too inevitable bias. The fact is, it is not the "figures (statistics) that lie but the liars that figure," and this is causing the problem. It is the subtle and perhaps even unintentional use of noncomparable models or hidden, invalid assumptions that allows bias to creep into the scientific method.

In short what is currently being proposed by this and other papers in this Record is the application of a standard, well-accepted mathematical methodology, along with the use of the principles of mechanistic design, to develop, in a scientific and unbiased way, pavement performance models that will be comparable and free of bias. It is appalling to think that an area as critical and costly as the designing of highway pavements has received such little attention from the standpoint of sound mathematical and scientific treatment, especially in light of the fact that both the mathematics and engi-

neering principles have been in existence for nearly a century or more and are used routinely in so many other scientific arenas. It is not too late to begin implementing these procedures. The tools for accomplishing this have been refined over the years and are available and within practicable reach. One needs only to step forward, outside the cloud of skepticism and fear, to see them.

REFERENCES

1. Shooman, M. L. *Probabilistic Reliability: An Engineering Approach.* McGraw-Hill Book Co., New York, 1968.
2. Kotz, S., and N. L. Johnson. *Encyclopedia of Statistical Science*, Vol. 8. John Wiley & Sons, Inc., New York, 1988.
3. Kapur, K. C., and L. R. Lamberson. *Reliability in Engineering Design.* John Wiley & Sons, Inc., New York, 1977.
4. Bain, L. J. *Statistical Analysis of Reliability and Life-Testing Models.* Marcel Dekker, Inc., New York, 1978.
5. *AASHTO Guide for Design of Pavement Structures.* AASHTO, Washington, D.C., 1986.
6. Proschan, F., and R. J. Serfling. *Reliability and Biometry.* Society for Industrial and Applied Mathematics, Philadelphia, Pa., 1974.
7. Lytton, R. L., and D. G. Zollinger. Modeling Reliability in Pavements. Presented at 72nd Annual Meeting of the Transportation Research Board, Washington, D.C., 1993.

Publication of this paper sponsored by Committee on Flexible Pavement Design.

Rational Approach in Applying Reliability Theory to Pavement Structural Design

RAM B. KULKARNI

A rigorous yet practical methodology for evaluating pavement design reliability is described. Pavement design reliability is expressed in terms of the probability that a pavement will withstand the actual number of load applications—that is, the traffic—on it during a selected design life while maintaining its structural integrity. Traffic is selected as the design element to which the reliability analysis should be applied because it is the only factor common to all pavement types. The methodology therefore provides a uniform basis for evaluating the reliability of alternative pavement designs with different pavement types. Alternative expressions of reliability (such as the probability of not exceeding a specified level of pavement distress) do not provide a proper comparison of alternative pavement types. A mathematical model that can be used to evaluate the reliability of alternative pavement designs and to calculate the design traffic for the selected design is presented. A systematic process for updating and improving initial estimates of the statistical parameters needed for the evaluation of reliability is also described.

The reliability theory provides a rational framework for addressing uncertainties in evaluating the projected performance of a facility during its intended life. In the context of pavements, pavement design reliability is defined as the probability that a pavement as designed will withstand the actual number of load applications on it during a selected design life while maintaining its structural integrity. Neither the actual traffic loading that will pass on a pavement during its design life nor the pavement's capacity to withstand traffic loading can be determined with certainty. Methods of reliability analysis formally address these uncertainties in the selection of a pavement design. The objective of reliability analysis is to provide a specified degree of (probabilistic) assurance that the pavement will perform satisfactorily while being subjected to the traffic and environmental conditions encountered during its design life.

A uniform method of evaluating pavement design reliability is essential in selecting the most appropriate pavement type for a given project location and in evaluating alternative pavement designs for a given pavement type. The choice of a pavement type may be made on the basis of estimated life-cycle costs. However, life-cycle costs of the selected designs for alternative pavement types cannot be directly compared unless the designs achieve the same level of reliability evaluated by a uniform method. Without a common definition of reliability and a uniform method of evaluating reliability, the comparison of life-cycle costs of alternative pavement types would be misleading and could result in the selection of a less cost-effective pavement type.

To provide uniformity pavement design reliability is defined as the probability that the pavement's traffic load capacity exceeds the cumulative traffic loading on the pavement during a selected design life. An alternative definition of reliability such as the probability of not exceeding a specified level of pavement distress is not useful for a direct comparison of the design reliabilities of different pavement types. This is because flexible and rigid pavements display different types of distresses. Traffic, however, provides a common basis because projected traffic at a given projected location can be assumed to be independent of the pavement type.

This paper describes a mathematical model for evaluating pavement design reliability and discusses the estimation of model parameters by using the types of data that are generally available to highway agencies. The final section contains recommendations regarding the proper use of reliability theory in the design and selection of pavement type at a given project location. Although the focus of the paper is on initial pavement design, the same approach can also be used in evaluating rehabilitation alternatives for in-service pavements.

MATHEMATICAL MODEL FOR EVALUATING PAVEMENT DESIGN RELIABILITY

The reliability R of a pavement design is defined as

$$R = \text{probability } [N > n] \tag{1}$$

where N is the number of traffic load applications that the pavement can withstand before losing its structural integrity, and n is the actual number of load applications on the pavement during a specified design life. If N exceeds n the pavement would maintain its structural integrity during its entire design life. Reliability is the probability that this condition would be met.

The evaluation of the probability in Equation 1 requires an assumption about the probability distributions of the two variables N and n. Field data suggest that the distributions of both variables are positively skewed (i.e., with longer tails to the right) and, consequently, assuming a lognormal probability distribution, is appropriate. Previous studies have commonly made this assumption (*1*).

With the assumption of lognormal probability distribution for N and n, Equation 1 can be rewritten as:

$$R = \text{probability } [\ln N > \ln n] = \text{probability } [\ln N - \ln n > 0] \tag{2}$$

where ln represents the natural logarithm of a variable. Since N and n are lognormally distributed, it follows that ln N and ln n would be normally distributed. Figure 1 is a schematic representation of the two distributions in which the overlap between the

Woodward-Clyde Consultants, 500 12th Street, Suite 100, Oakland, Calif. 94607-4014.

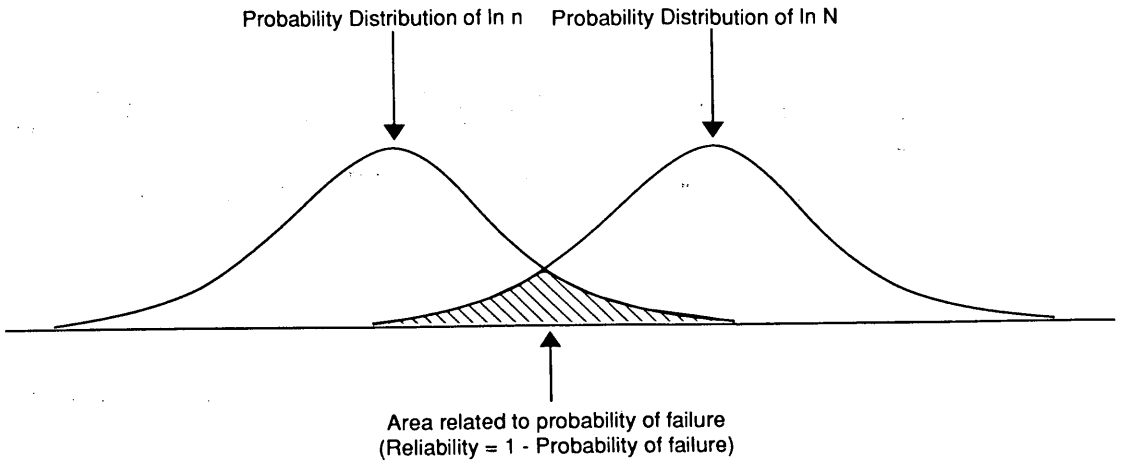

FIGURE 1 Probability distributions of ln n and ln N.

two distributions is related to the failure probability (i.e., the probability that ln N is less than ln n) and reliability is 1 minus the failure probability.

The greater the separation between ln N and ln n, the higher the design reliability would be. Thus, one may define the safety margin (SM) of a design as

$$\text{SM} = \ln N - \ln n \tag{3}$$

A convenient measure of design reliability is the reliability index (β), defined as the ratio of the expected value of SM, denoted by $E[\text{SM}]$, and the standard deviation of SM, denoted by $SD[\text{SM}]$. Thus,

$$\beta = \frac{E[\text{SM}]}{SD[\text{SM}]} \tag{4}$$

$$= \frac{E[\ln N] - E[\ln n]}{\sqrt{\text{var}[\ln N] + \text{var}[\ln n]}} \tag{5}$$

in which $E[\cdot]$, $SD[\cdot]$, and var[•] represent the expected value, standard deviation, and variance, respectively, of a random variable.

The design reliability R can now be related to β as follows:

$$\begin{aligned} R &= \text{probability } [\ln N - \ln n > 0] \\ &= \text{probability } [\text{SM} > 0] \\ &= 1 - F_U\left(\frac{0 - E[\text{SM}]}{SD[\text{SM}]}\right) \\ &= 1 - F_U(-\beta) \\ &= 1 - [1 - F_U(\beta)] \\ &= F_U(\beta) \end{aligned} \tag{6}$$

where F_U is the cumulative distribution function of a unit normal variate. Figure 2 illustrates the relationship between R and β.

The reliability index β thus expresses the mean safety margin (i.e., the mean separation between ln N and ln n) in terms of

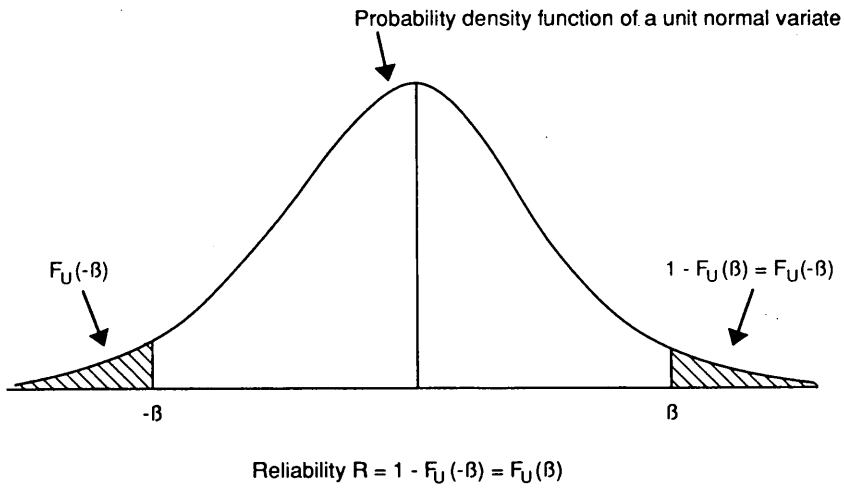

FIGURE 2 Reliability in terms of reliability index.

multiples of the standard deviation of the safety margin. Higher values of β are associated with greater levels of reliability. For given variances of ln N and ln n, β increases as the difference between the mean values of ln N and ln n increases. Similarly, for given mean values of ln N and ln n, β increases as the variances of ln N and ln n decrease. Thus, the reliability of a pavement design can be increased by increasing the average structural capacity (to withstand a greater number of load applications) or reducing the uncertainties in estimating the structural capacity and traffic loading.

The concept of the reliability index has been used for the design of structures (*2*), offshore platforms (*3*), and geotechnical facilities (*4*). The index provides a consistent and convenient basis for comparing the reliabilities of alternative designs of a given facility. With regard to pavement designs, life-cycle costs of alternative pavement types could be directly compared only if each type is designed to achieve the same reliability index.

ESTIMATION OF MODEL PARAMETERS

The input parameters needed to calculate the reliability index are

- The definition of "failure" criterion,
- Mean value and variance of ln N, and
- Mean value and variance of ln n.

The estimation of these parameters and the calculation of design traffic are discussed in this section.

Definition of Failure Criterion

In estimating a pavement's capacity to withstand traffic, one needs to define a "failure" criterion in a functional or structural mode. For mechanistic pavement designs the failure criterion may be stated in terms of a threshold level of pavement distress at which the pavement would be assumed to have lost it structural integrity. It should be noted that pavement structures do not fail catastrophically. A pavement failure is characterized by the development of a specific type of distress (such as fatigue cracking on a flexible pavement) of sufficient severity and extent at different points within a pavement section. This type of failure, sometimes referred to as a "stochastic failure," implies that a pavement section is not homogeneous in strength along its entire length. A pavement section designed and constructed the same way exhibits random variations in material properties and as-built characteristics. Locations at which several deficiencies coincide may fail, although the remaining section maintains its structural integrity.

Hence, the structural failure of a pavement may not necessarily imply that the pavement has fallen below an acceptable level of serviceability. Conversely, a pavement may fall below an acceptable level of serviceability prior to a structural failure. Thus, a time lag may exist between the structural failure and serviceability failure, as illustrated schematically in Figure 3.

In evaluating the reliabilities of alternative pavement types, the structural failure criteria should be selected such that this time lag to reach a given level of serviceability is similar for the alternative pavement types. That is, the degree of conservatism in the selected structural failure criteria as established from the analysis of actual performance data (e.g., nature and extent of failure manifestations, surface rideability, and maintenance records) and from judgment and experience should be the same for the alternative pavement types. Figure 3 illustrates the contrast between structural and serviceability failure.

Mean Value and Variance of ln N

It is assumed that a specific design procedure (equation) is used to estimate N, the number of load applications that a given design would withstand before reaching the threshold distress level. For mechanistic design the design equation is developed by using the pavement's structural response parameters (stresses, strains, deformations) and is validated by using data on past pavement failures.

Let the actual traffic load capacity of the pavement N be related to the estimated capacity $\hat{N}$, as follows:

$$N = \hat{N}\alpha_1$$

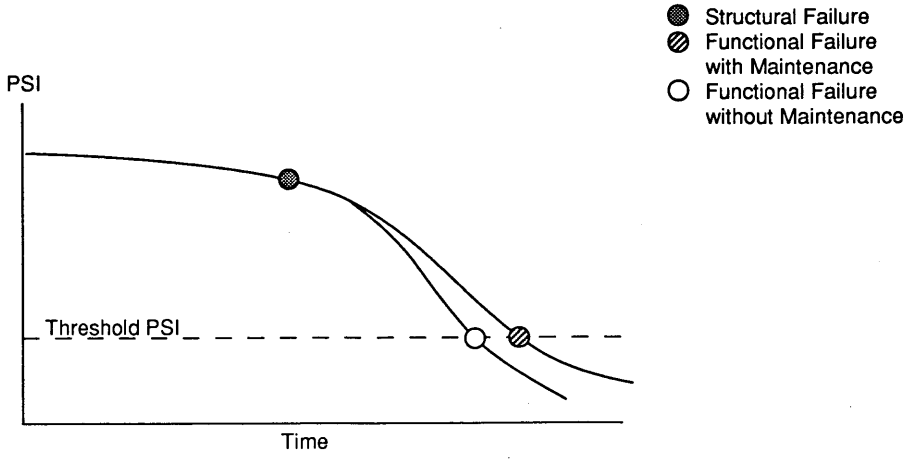

FIGURE 3 Present serviceability index (PSI) versus time showing functional and structural failures.

or

$$\ln N = \ln \hat{N} + \ln \alpha_1 \quad (7)$$

where $\ln \alpha_1$ is the deviation between the logs of actual and estimated traffic load capacity.

It is assumed that $\ln \alpha_1$ is a random error term that does not introduce any bias in the estimation procedure.

The mean and variance of $\ln N$ can be expressed as

$$E[\ln N] = \ln \hat{N} \quad (8)$$

$$\text{Var}[\ln N] = \text{var}[\ln \alpha_1] \quad (9)$$

Uncertainties in estimating traffic load capacity are captured in the variance of $\ln N$ (Equation 9). Thus, $\hat{N}$ should be the "best" (median) estimate of traffic load capacity that is obtained by using the median (rather than conservative) values of the design parameters such as material properties and structural response.

A number of sources of deviation could contribute to the overall deviation $\ln \alpha_1$, including

- Lack of fit of the design equation,
- Differences between design and as-built parameters,
- Construction variability, and
- Variability in the material properties.

The estimation of the variance of $\ln \alpha_1$ is an evolving process that begins with an initial estimate of $\ln \alpha_1$ on the basis of the available information from previous studies. This initial estimate is periodically updated as additional data specific to a given highway agency become available. The recommended steps in this process are described in the following:

1. Use the variance of $\ln \alpha_1$ derived in the AASHTO design guide (*1*) as an initial estimate. The AASHTO design guide estimates the variances of $\ln \alpha_1$ to be 0.194 and 0.114 for flexible and rigid pavements, respectively.
2. Compile pavement performance data over the past 10 years on sections of flexible and rigid pavements that have reached the applicable threshold distress levels. Although these sections may not have been designed by the current design methods, the percent variability of the deviation between the actual and estimated traffic load capacities can be expected to be similar for the recent and current design methods. This is because many components of the overall variability (such as construction practices, environmental conditions, and sources of raw materials) are likely to be similar.
3. Use the data compiled in Step 2 to estimate the traffic load capacity of each section. The cumulative traffic that has passed on the section is also estimated by using the available traffic data. The deviations between the log values of the actual cumulative traffic and the estimated traffic load capacity are then calculated and are used to estimate the variance of $\ln \alpha_1$. When data on a minimum of 10 pavement sections become available, the variance of $\ln \alpha_1$ calculated from these data should be used in place of the initial estimates in Step 1.
4. As pavement performance data from sections designed with the current design method become available, these sections should replace the older sections identified in Step 2. The analysis in Step 3 should then be updated with performance data compiled from the group of pavement sections designed by the current method.
5. The Long-Term Pavement Performance (LTPP) program initiated as a part of the Strategic Highway Research Program includes the collection of data on a large number of pavement sections nationwide. These sections have been selected by using a statistically based experimental design. This program is expected to accumulate sufficient information over the next few years for conducting a detailed analysis of the variability in pavement performance owing to variabilities in such factors as material properties, construction practice, design method, traffic projections, and environmental conditions. Formal statistical analysis of the data from LTPP should provide even more accurate estimates of the individual components of variance and the total variance of $\ln \alpha_1$. These estimates, when available, should then replace the prior estimates obtained in the preceding steps.

The steps outlined here will provide a reasonable initial estimate of the variance of $\ln \alpha_1$ and an evolving process to improve the accuracy of the initial estimate. The importance of this process is that it permits the application of reliability theory to pavement design even when data from statistically based road test programs are not available to estimate individual components of variability. The process yields reasonable estimates of the overall variability in traffic load capacity, N (and also in traffic loading, n). The estimates can be systematically updated and improved as additional data become available.

Mean Value and Variance of ln *n*

It is assumed that a specified traffic forecasting model is used to estimate the amount of cumulative traffic [in terms of number of equivalent single-axle loads (ESALs)] expected on a pavement. As with the traffic load capacity, the actual cumulative traffic n is related to the estimated cumulative traffic $\hat{n}$ as follows:

$$n = \hat{n}\, \alpha_2$$

or

$$\ln n = \ln \hat{n} + \ln \alpha_2 \quad (10)$$

It is again assumed that $\ln \alpha_2$ is a random error (without any bias). The mean and variance of $\ln n$ are then obtained from

$$E[\ln n] = \ln \hat{n} \quad (11)$$

$$\text{Var}[\ln n] = \text{var}[\ln \alpha_2] \quad (12)$$

As with the estimation of traffic load capacity, an evolving process can be used to estimate the variance of $\ln \alpha_2$. A reasonable initial estimate of this variance is 0.04, as derived in the AASHTO design guide (*1*). This estimate can be updated with traffic count data collected by the highway agency for a sample of pavement sections. The sample should include pavement sections constructed in the past 10 years for which actual traffic count data are available.

For example, using the current traffic forecasting model and the data that would have been available 10 years ago (but not using the traffic count data collected in the past 10 years), the total cumulative traffic (in terms of ESALs) during the past 10 years is estimated for each of the selected pavement sections. The de-

viations between the log values of both actual and estimated cumulative traffic are then used to estimate the variance of ln α_2 to replace the initial value of 0.04. This estimate can be further refined as additional data become available.

Calculation of Design Traffic To Achieve Desired Level of Reliability

For a specified level of design reliability, R^*, the corresponding reliability index can be calculated from Equation 6. Let this reliability index be denoted by β^*. Then the cumulative traffic for which the pavement should be designed is given by

$$\ln \hat{N} = \ln \hat{n} + \beta^* \sqrt{\text{var}[\ln \alpha_1] + \text{var}[\ln \alpha_2]} \quad (13)$$

Equation 13 can also be expressed as

$$\hat{N} = \hat{n}F \quad (14)$$

where F is defined as a traffic multiplier with the relationship to the reliability index β^* of

$$F = \exp\left(\beta^* \sqrt{\text{var}[\ln \alpha_1] + \text{var}[\ln \alpha_2]}\right) \quad (15)$$

Thus, if the pavement is designed for the cumulative traffic of $\hat{N}$ obtained from Equation 14, there is an R^* percent probability that the pavement would not fail (according to the defined failure criterion) before reaching the cumulative design traffic level.

SUMMARY AND RECOMMENDATIONS

A rigorous yet practical methodology for evaluating pavement design reliability was described in this paper. Pavement design reliability was expressed in terms of the probability that a pavement will withstand the actual number of load applications, that is, the traffic, on it during a selected design life while maintaining its structural integrity. Traffic was selected as the design element to which the reliability analysis should be applied because it is the only factor common to all pavement types. The methodology therefore provides a uniform basis for evaluating the reliability of alternative pavement designs with different pavement types. Alternative expressions of reliability (such as the probability of not exceeding a specified level of pavement distress) do not provide a proper comparison of alternative pavement types.

The methodology quantifies uncertainties in estimating a pavement's traffic load capacity and the actual cumulative traffic loading on the pavement during a specified design period. A reliability index was calculated for each alternative design, taking into account

1. The difference between the estimated traffic load capacity and the projected traffic loading,
2. The variance of the deviations between actual and projected traffic load capacities (caused by the variability in material properties and construction practices), and
3. The variances of the deviations between actual and estimated traffic loadings.

Procedures for systematically updating and improving initial estimates of the statistical parameters needed for the evaluation of reliability were described.

Finally, the reliability of a given design was calculated as a function of the reliability index, and appropriate probability distributions of the two variables (ln N and ln n) were used to define this index. These probability distributions were selected on the basis of the statistical evaluation and interpretation of the available data. The design that achieves a desired level of reliability with the minimum life-cycle cost may be selected. The reliability index of the selected design is then used to calculate a traffic multiplier (see Equation 14). When this traffic multiplier is applied to the projected traffic loading (expressed, for example, in terms of 18,000-lb ESALS for any mix of traffic) it establishes the level of traffic for which the pavement should be designed to achieve the specified reliability.

This is a proven methodology that has been used to evaluate the design reliabilities of highways as well as such engineered systems as landfills, dams, buildings, bridges, and offshore platforms. Its use is recommended in evaluating the reliabilities of alternative pavement designs with different pavement types for a given project. The selection of the most cost-effective pavement type can be made only after ensuring that the selected designs of the alternative pavement types achieve the same level of reliability and that a consistent procedure is used to evaluate design reliability so that the reliability levels calculated for the different pavement types are directly comparable to one another.

REFERENCES

1. *Guide for Design of Pavement Structures.* AASHTO, Washington, D.C., 1986.
2. Ang, A. H.-S., and C. A. Cornell. Reliability Basis of Structural Design and Safety. *Journal of the Structural Division,* ASCE, Vol. 100, No. ST9, 1974.
3. Bea, R. G. Reliability Considerations in Offshore Platform Criteria. *Journal of the Structural Division,* ASCE, Vol. 106, No. ST9, 1980.
4. Li, K. S., and P. Lumb. Probabilistic Design of Slopes. *Canadian Geotechnical Journal,* Vol. 24, 1987.

Publication of this paper sponsored by Committee on Flexible Pavement Design.

Development of Weibull Reliability Factors and Analysis for Calibration of Pavement Design Models Using Field Data

DAN G. ZOLLINGER AND B. FRANK MCCULLOUGH

With the growing popularity of mechanistic-empirical design concepts, a need exists to address design in an unbiased manner that incorporates the natural capability of these concepts to provide designs for any region, soil type, or environmental condition on a comparative basis. With these possibilities within reach, the calibration of these designs consequently stands out as a key ingredient to the successful application of their results to actual performance standards. Design calibration can be determined such that reliability coefficients are not unduly biased. On the basis of this premise, design calibration applies to both design and reliability parameters and as a consequence is influenced by the intrinsic material and structural characteristics germane to different pavement types and climates. With this perspective of mechanistic design concepts, the age of subjective factors of safety in pavement design has long since passed. The full benefit of using rational, mechanistically based reliability and calibration factors may be realized only when these factors consider the "underlying" mechanisms relative to the development of pavement distress. The analysis of pavement performance data conducted on this basis provides insight and understanding that reflect the type of mechanisms noted earlier and leads to the greatest utility of design model calibration efforts.

The object of any pavement design procedure [and particularly mechanistic-empirical (M-E) designs], plainly stated, is to provide the lowest life cycle cost pavement to carry the expected traffic at or above a specific level of safety, riding quality, and durability at a specified level of reliability, regardless of surface material type. These expectations must be achieved by simultaneously considering the paving materials to be used and their behaviors under different load and environmental conditions with respect to the design factors and pavement type. These design factors normally will include design life, traffic loads, subgrade conditions, construction quality and timing, aggregate sources and characteristics, material strengths and properties, and construction weather, among others. To achieve the greatest amount of predictability, all pavement designs should be calibrated to the extent possible.

It is important that design calibration not be confused with design reliability. However, design reliability and design calibration must be given equal consideration. Calibration methodology should be mechanistically oriented based on using the same models and assumptions as those used in the design process, and focused on the adjustment of the predicted level of pavement performance and the parameters (reliability coefficients) that describe the distribution of pavement performance relative to the qualification of the various levels of design reliability. This approach to the characterization of pavement material behavior and pavement performance factors, from a practical point of view, is much more efficient than the empirically based alternative, which requires data collection on many costly, time-consuming, and inherently labor-intensive field test sections that will take years to produce any type of usable results. Calibrated reliability coefficients that are developed in an effective, cost-efficient manner on the basis of engineering mechanics and statistics, the knowledge about highway materials that experienced highway engineers already have, and currently available performance data for existing pavements will provide the most sound and theoretically correct approach to design.

Reliability is defined simply as the probability that something will not fail. To put it another way, reliability is 1.0 minus the risk of failure (*1–3*). The application of reliability to pavements makes it possible to erect objective standards of performance and to provide for the selection of pavements that will best serve their intended functions of carrying the traveling public in comfort and safety while providing this service with durable materials placed and maintained with the least life cycle costs. This pavement function, as expressed in public law, is desired by the ultimate owner and user, the taxpaying public. Reliability must be applied correctly to pavements to achieve this objective, hence its ultimate importance.

Highway pavements fail when different modes of distress reach a prescribed level. If stress relations can be used to represent some of these modes of distress as design models, then it may be possible to relate the level of stress to the number of load repetitions to the level of associated distress (cracking, rutting, etc.). Since several factors can influence the development of the distress, such as factors related to climate, probabilistic concepts allow the variabilities associated with these factors to be quantified in the calculation of reliability.

The purpose of the calibration process is then to adjust or fine-tune the reliability factors or coefficients associated with the distributions that characterize the variabilities (in cracking, rutting, etc.) referred to earlier. Taking this approach, the examination of the variability that is particular to each uniform pavement section should provide as many different "sets" of reliability coefficients as sections considered. Once these sets have been established, the engineering process should determine the "particularities" that are key to the correlation of the generated sets of reliability co-

D. G. Zollinger, Department of Civil Engineering, Texas A&M University, College Station, Tex. 77843-3136. B. F. McCullough, Civil Engineering Department, University of Texas, Austin, Tex. 78712.

efficients. In this manner the calibration process can be achieved such that all sections are used to broaden the range of the calibrated coefficients, distributions, and design parameters. The emphasis of this paper is on the application and illustration of the Weibull distribution in a design model and reliability coefficient calibration process. Statistical calculations are included in an example to further elaborate and support the concepts and rationale presented in this paper.

APPLICATION OF RELIABILITY FACTORS IN DESIGN CALIBRATION

The methods discussed in the following pertain to any pavement distress for which deterministic engineering models are available to provide system responses. The examination presented will focus on pavement cracking (c) for purposes of illustrating the application of reliability concepts in design calibration.

Calibration Factors Based on Number of Load Applications To Reach Failure, N_f

The application of what pavement engineers know about pavements also applies to the form of the equation that defines the relation between cracking and the number of load applications. It is known that cracking does not occur at the same time over the entire length of the pavement. It is also known that it does not occur uniformly at all locations along a pavement section of uniform construction. Thus, it is known and has been represented in mechanics as the result of a stochastic process. Analysis of the cracking behavior of a pavement as a function of estimated traffic, if it is to respect what is known of its behavior, must make use of the forms of equations that are used in probability.

The question of which form of equation to use may be posed by asking which of the relations (a), (b), or (c) in Figure 1 should

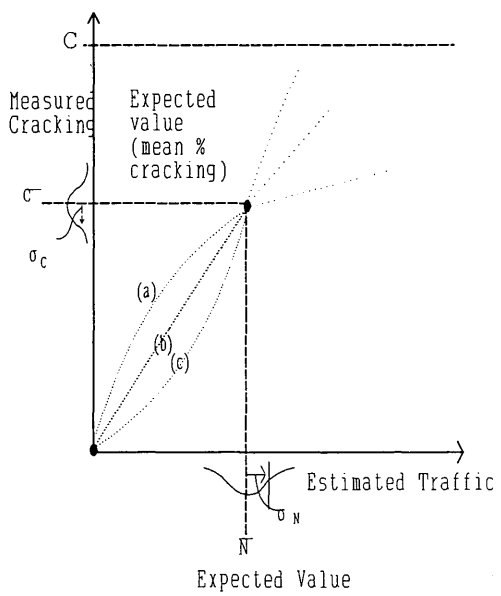

FIGURE 1 Possible relations between mean c and N for single pavement section.

be used to relate the expected value of cracking (c) to the expected value of the traffic load application ($\overline{N}$).

With cracking data, one must analyze the relationship between two probabilistic quantities: traffic and cracking. The recorded traffic is an estimate of the actual traffic and has, as have all traffic estimates, an expected value ($\overline{N}$) as its most likely value and a likely range within which the actual value will fall. Thus, the estimate of N, the number of traffic load applications, has a probability density function (PDF) that can be characterized by its mean (μ), its standard deviation (σ), and its mathematical form. Commonly used mathematical forms used with traffic data are normal, lognormal, and Poisson.

The recorded cracking is also a mean value (c) measured over an entire pavement section that is of constant cross section and thickness and subjected to equal traffic along the section, although the occurrence of cracking in the section is by no stretch of the imagination uniformly distributed. Instead, c is arrived at by measuring all of the cracking along the pavement section and dividing by a theoretical maximum cracking level (e.g., the total area of pavement that could be cracked). Thus, the recorded value of cracking (c) is also an estimate of the expected value and represents a range of values that are likely to occur on the pavement from point to point. This indicates that cracking also has a PDF that is represented by a mean, a standard deviation, and its mathematical form. Commonly used forms of equations used to describe cracking frequency are normal, lognormal, and Weibull.

This leads to the question of how c and N are related. In the first place, it is recognized that this relation, whatever it is, is unique to the particular pavement on which it is measured. Second, it is recognized that the value of c has absolute limits of 0 and 1. Any mathematical form of the relation between c and N that allows c to go below 0 or above 1 is automatically invalid. Thus, the relations

$$\overline{c} = a\,\overline{N}^b$$

and

$$\overline{c} = a + b\,\overline{N} \tag{1}$$

which are illustrated in Figure 1 as Curves (c) and (b), respectively, are inappropriate mathematical forms to use in describing the relationship between c and N.

On the other hand, an appropriate mathematical relation is illustrated in Figure 1, Curve (a). The form of this equation is

$$\overline{c} = \text{prob [damage} > 1.0]$$

where

$$\text{damage} = \sum_{i=1}^{k} \frac{n_i}{N_{fi}},$$

n_i = number of load applications of load level i,
N_{fi} = number of load applications of load level i to cause failure, and
k = number of periods.

If a form of load equivalency is used to characterize the number of load applications for the traffic estimate, then the damage equation simplifies to

$$D = \text{damage} = \frac{N}{N_{fi}}$$

It is assumed for design proposes that when the damage ratio equals 1.0 at a given spot on the road surface, the crack, which has been working its way through the pavement, appears on the surface. The amount of mean cracking can be interpreted in probabilistic terms as the area under the damage distribution curve bounded by the damage values greater than or equal to 1.0. The relationship between the mean values of cracking and traffic load applications is governed by the probabilistic relationship that the mean value of cracking (c) is related to the mean value of traffic ($\bar{N}$) by the probability that the damage ratio (N/N_f) is equal to 1.0. That is

$$\bar{c} = \int_1^{\infty} p(x)\, dD$$

where x is defined in this paper for a Weibull distribution in terms of fatigue damage D. For a Weibull distribution,

$$p(x) = \gamma\lambda(\lambda x)^{\gamma-1} \exp\left[-(\lambda x)^{\gamma}\right]$$

where λ is the Weibull scale parameter and γ is the Weibull shape parameter. The cumulative PDF $P(x)$, which corresponds to the Weibull PDF, is the following exponential function:

$$\bar{c} = P(x) = \exp\left[-(\lambda x)^{\gamma}\right]$$

and

$$x = D_c \cong \frac{\bar{N}_c}{\bar{N}_f|_{\bar{N}_c=\bar{N}_f}} = 1$$

where D_c is the critical level damage beyond which pavement cracking occurs. The form of this expression can be used to correlate the $\bar{c}-\bar{N}$ pairs of datum points.

Any of the aforementioned cumulative distribution functions (normal, lognormal, and Weibull) can be used to fit the $c-N$ pairs of data recorded for each pavement section one section at a time. Under most circumstances only two datum points are known for each pavement section:

1. The origin where $\bar{N}$ is equal to 1 and the cracking is an assumed small value, say, 0.001.
2. The actual measured point, c and N (x represents N in the equations $\bar{c} = \exp\left[-(\lambda x)^{\gamma}\right]$. A mathematical form (i.e., Equation 1) can be used to formulate either $c-N$ or $c-D$ relationships (discussed later).

Therefore, it is possible to find distribution parameters for each pavement section by using these two points on the curve by using the Weibull exponential functions (other forms such as normal or lognormal may also be considered).

To elaborate further, it is also possible, then, taking one pavement section at a time, to determine a relationship that can be used to find a value of $\bar{N}$ corresponding to some preset value of c and a corresponding value of $\bar{c}_{max}$ that the design engineer determines to be a maximum acceptable level of cracking. Also, the value of $\bar{c}_{max}$ leads to a value of $\bar{N}_f$ that is particular to the pavement in question and that can be used in the definition of damage. Consequently, the value of $\bar{N}_f$ is a design calibration parameter.

With a Weibull cumulative distribution, the scale and shape factors, λ and γ, respectively, can be determined by linear regression, one pavement section at a time, by the equation

$$y_i = a + b\, x_i \tag{2}$$

where

$y_i = \ln(-\ln \bar{c}_i)$,

$x_i = \ln \bar{N}_i$,

$b = -\gamma$,

$a = \gamma \ln \lambda$, and

$\lambda = \exp(-a/b)$.

Once these factors are known, the value of N_f can be found by using the following formula:

$$\bar{N}_f = \frac{1}{\lambda}\left[-\ln(\bar{c}_{max})\right]^{\frac{1}{\gamma}} \tag{3}$$

Values of N_f can be determined for each pavement section by this means. The value of N_f that is determined is a unique property of each individual pavement section and is a value by which each pavement section may be compared because it represents the number of load applications at which a standard condition of distress of each pavement section is reached. In a similar manner, the scale and shape parameters also represent design calibration terms. The value of N_f determined in this way can be used as the dependent variable in an expression that represents the number of load cycles required to reach failure.

Design Calibration Based on Reliability Factors Derived from Field Data

In light of the preceding discussion, the following is provided as an illustration of design calibration using field data obtained from 22 project sites in Minnesota listed in the Concrete Pavement Evaluation System (COPES) data base (*4*) to develop calibration constants that involve reliability factors derived from the COPES data. This illustration constitutes an approach to the consideration of the pavement distress of slab cracking that is unique in that it directly considers the performance data of each project individually rather than as a combination of the whole. In this manner this approach to calibration is constructed by using consistent statistical concepts as they would apply to a design philosophy that considers one pavement section at a time (as most of them do) in the quantification of pavement structure design parameters.

The data for the concrete pavement sections in the COPES data base for Minnesota were listed with respect to pavement design and construction data and pavement performance and environmental data. These data were also associated with the survey project identification number and the county where the project was located. Although the date of construction was listed in September of the year of construction for all of the listed projects, it was assumed that the actual paving occurred between May and August of the construction year. The percentage cracking for each project was calculated from the listed cracking data and was found by considering all reported transverse cracking, regardless of the level of severity, to account for all cracks that had occurred since con-

struction (discounting controlled cracks). If all possible cracks, whether controlled or not, can be considered to include those cracks that may occur at intervals of 4.44ℓ (where ℓ is the radius of relative stiffness) and those that may occur midway between the cracks at intervals of 4.44ℓ, then the total possible number of cracks is 2 times the survey length (LEN) (in inches) divided by 4.44ℓ rounded to the nearest whole number. Subtracting from this the number of sawcut or controlled cracks results in the maximum number of cracks (nc_{max}) that may occur:

$$nc_{max} = \text{LEN}\left(\frac{24}{4.44\ell} - \frac{1}{\text{joint spacing}}\right)$$

Dividing the observed cracking (in terms of the number of 12-ft transverse cracks) by nc_{max} results in the percentage of cracking for each project in the data base. Heating degree-days (D-day) that are listed for the assumed paving period are based on a reference temperature of 65°F. It is noted that a D-day is 1°F difference between the reference temperature and the mean temperature over a 1-day period. D-day data were not available in the COPES data base.

An illustration of the project site performance data for all 22 projects is shown in Figure 2. Figure 2 tends to suggest that a broad scatter exists between pavement cracking in the field and applied wheel load applications [equivalent single-axle loads (ESALs)]. Because of this observed variability and the obvious difficulties in correlating these datum points, it is much more advantageous from a calibration standpoint to consider each of these sections on an individual basis. This can be achieved by considering the $c-N$ relationship for each individual project shown in Figure 2 to follow one of the previously described distributions. A Weibull distribution is selected here for illustration purposes, but other previously mentioned distributions may be considered.

As pointed out previously, two known pairs of pavement performance data are assumed to be available for each project site if the data plotted in Figure 2 constitute one set of data and if the data representing the pavement performance at the time of pavement opening can represent the second set of data. The opening mean traffic level (N) is assumed to be 1 (however, some truck traffic during construction operations may have occurred before the opening of the pavement section). The initial cracking level may be considered to be close to 0 (0.0001 is suggested because

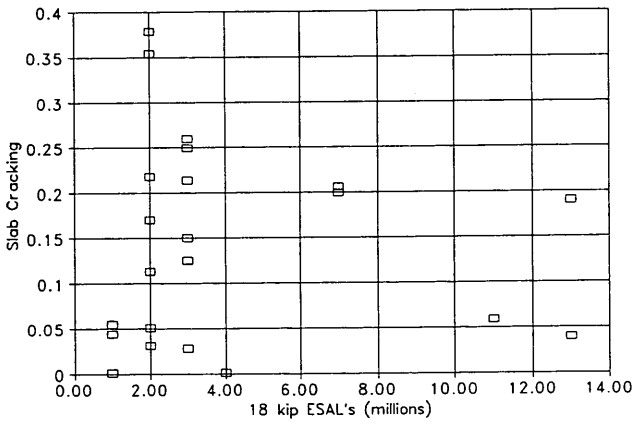

FIGURE 2 Field performance data for 22 sites in Minnesota.

of the mathematical nature of a Weibull distribution), but it has been noted that paving during warm temperatures can cause a certain amount of slab cracking before opening the pavement to traffic. Data obtained from test sites in Illinois (*5*) emphasize the effects that temperature conditions at the time of construction can have on the cracking performance of the pavement system. Experience has suggested that the initial cracking may range between 3 and 8 percent and is significantly affected by the pavement joint spacing. For reasons discussed subsequently, initial levels of cracking were assigned to each project, depending on the surveyed cracking level. These levels were subtracted from the observed cracking levels listed in the COPES data base to provide a more accurate accounting of wheel load–induced cracking. The initial cracking distribution is given in Table 1 with respect to four categories or groupings of cracking.

Using linear regression techniques for the expressions shown in Equation 2, the terms a, $b(\gamma)$, and λ can be found for each project for the assigned values of x_i and y_i. The correlation between log (λ) and the mean slab cracking (c) for the 22 project sites is shown in Figure 3. Significant trends for λ are noted within each cracking category. Similar correlations are noted for the coefficient γ but are not shown. On the basis of this observation it is of interest to correlate the λ and γ coefficients to pavement design parameters such that a comprehensive calibration process will result for all 22 project sites.

A characteristic parameter of jointed concrete pavements noted to be related to environmental factors (*6,7*) is L/ℓ, where L is the joint spacing. The radius of relative stiffness (ℓ) is

$$\ell = \left[\frac{Eh^3}{12(1 - \nu^2)k}\right]^{1/4}$$

where

E = concrete modulus of elasticity (FL^{-2}),
h = slab thickness (L),
ν = Poisson's ratio, and
k = foundation modulus (FL^{-2}/L)

The correlation trends between L/ℓ and the slab cracking data are shown in Figure 4. Other correlations to slab cracking shown in Figure 5 were found from the annual rainfall (for the year of construction) and D-day data for the assumed period. Since L/ℓ indicated signs of correlation to slab cracking and it is known that weather conditions at the time of construction can have a significant effect on slab cracking, it is not surprising that paving D-days correlate well to slab cracking. On the basis of these findings relationships between L/ℓ, rainfall $(r)/\ell$, D-day, λ, and γ were investigated. The usefulness of such relations is a key to the calibration process.

Preliminary correlations (measured in terms of the goodness of fit, r^2) of γ to the parameter D-day suggested that the D-day data should be partitioned according to the level of surveyed cracking. Even though the dates of construction were listed in September of the year of opening for each project, it was assumed that the actual construction took place sometime between May and August. Since the actual paving dates were unknown for each project, the D-day data were used to partition each project with respect to either an early or a late summer construction period. The early summer construction was assumed to be from May to June, and the late summer construction was assumed to be from June to August. Each project was partitioned with respect to the cracking

TABLE 1 Project Partitioning and Data Correlation Parameters

Survey Cracking Level (%)	Partitioning	Initial Crack Level (%)	Correlation Parameters	
			γ	λ
0 - 10	Early Summer	0	r/ℓ	r/ℓ
10 - 20	Late Summer	3	L/ℓ, D-Days	L/ℓ, D-Days
20 - 30	Late Summer	8	L/ℓ, D-Days	L/ℓ, D-Days
30 - 40	Late Summer	15	L/ℓ, D-Days	L/ℓ, D-Days

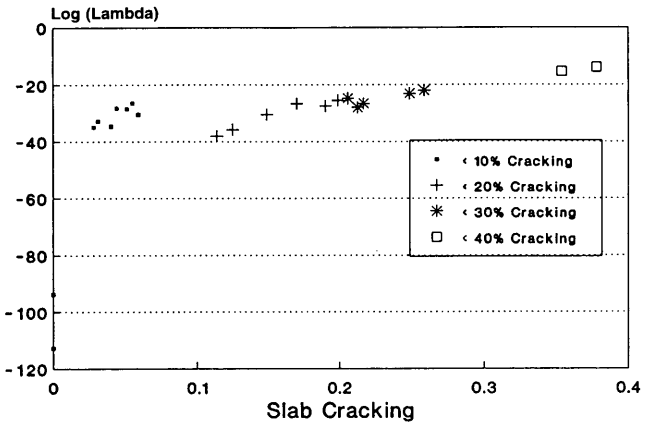

FIGURE 3 Correlation between mean slab cracking (c) and λ.

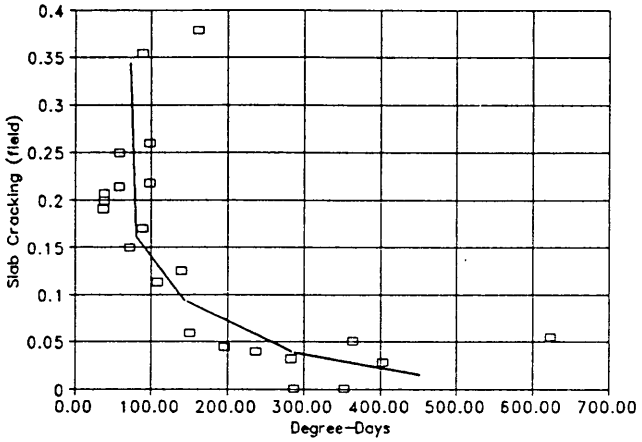

FIGURE 5 Correlation between slab cracking and heating degree-days.

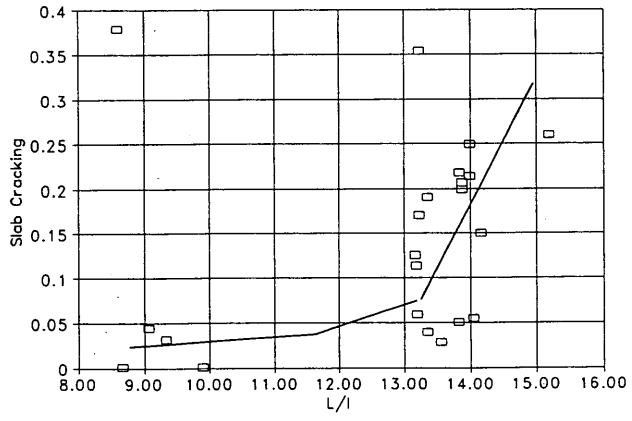

FIGURE 4 Correlation between slab cracking and L/ℓ.

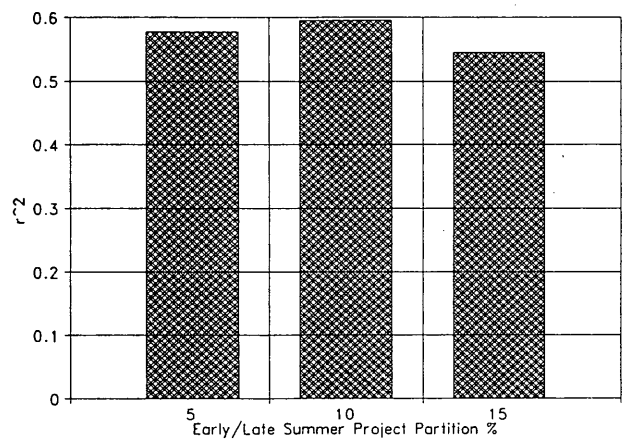

FIGURE 6 Partitioning of project sites by cracking level.

levels shown in Figure 6. Figure 6 also indicates the resulting r^2 for the correlation between γ and D-day on the basis of whether the surveyed cracking level was above or below the given level of cracking. As shown, the 10 percent cracking level resulted in the greatest correlation for γ; therefore, pavement sections showing 10 percent cracking or less were assigned to the early summer period. All remaining sections were assigned to the later summer period and, consequently, different levels of initial cracking, as shown in Table 1.

It should be noted that the adjustments and partitioning just described would not be necessary if sufficient construction data were available to properly assess the environmental conditions during paving. Since these modifications represent certain as-

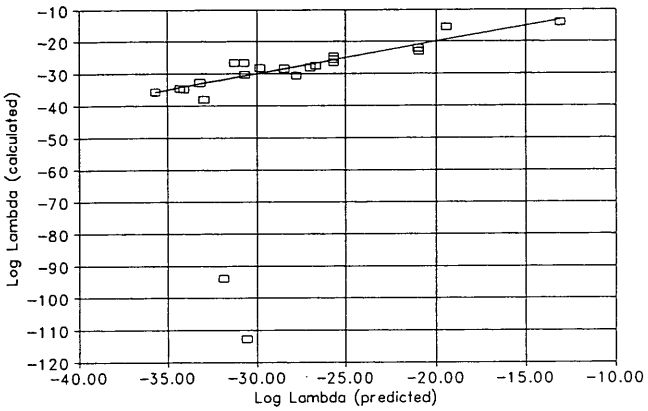

FIGURE 7 Comparison of predicted λ to calculated λ.

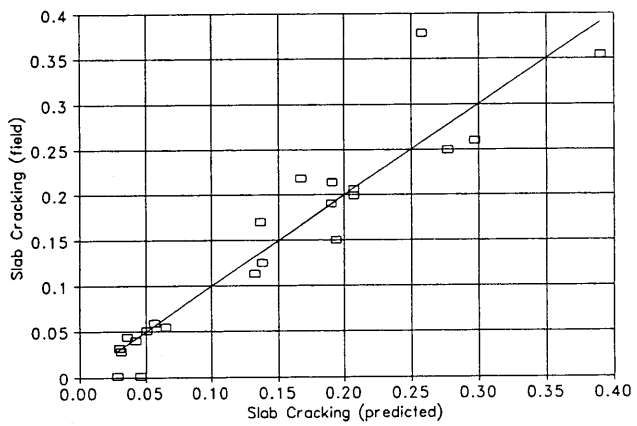

FIGURE 8 Comparison of predicted cracking to field cracking.

sumptions that can be used to improve the assessment of the performance data, some discontinuities in the data may have resulted (shown later in Figures 7 and 8). However, these discontinuities were not entirely apparent in the prediction equations for λ, even though these equations were delineated with respect to cracking category as a function of annual rainfall in the year of construction or D-day and the L/ℓ value. The correlation parameters for these expressions are presented in Table 1, and the regression statistics are given in Table 2. Note that rainfall was defined as a dimensionless parameter of rainfall/ℓ for the first category of slab cracking.

Figure 7 compares the predicted λ values with the calculated λ values in which two outliers represent datum points (of nearly zero cracking levels) that were not well accounted for by either of the correlation parameters shown in Table 1. Otherwise, the predicted value of λ is considered to be very good, as is the case with the predicted slab cracking (Figure 8). On the basis of Figures 7 and 8 it is apparent that the scatter in the data shown in Figure 2 can largely be accounted for through correlations of the Weibull distribution scale and shape functions (λ and γ, respectively) to factors that strongly influence early pavement behavior within the first week of construction.

With these correlations and the design engineer's maximum allowable cracking (c_{max}) level, the maximum allowable loads to failure (N_f) may be found for each project by using Equation 3. Therefore, N_f may be considered to be calibrated on the basis of the slab L/ℓ and the D-days to which a pavement may be subjected during construction.

It should be noted that N_f (which may be referred to as a calibrated value, N_{f_c}) will vary with the chosen level of maximum slab cracking. The term N_{f_c} is used to develop a universally applicable cracking damage curve as explained later and can be defined in terms of design for pavements meeting similar conditions according to the D-days, rainfall/ℓ, and L/ℓ ratios. It is apparent, however, that N_{f_c} is independent of r (the stress ratio) and that different strength (MR) and stress (σ_{WLS}) requirements different from those for the calibrated pavement may be desired design requirements, and therefore it is of interest with respect to these requirements to use a value of N_f that is also a function of the stress ratio (r).

The following discussion explains how this can be achieved. An expression for N_f based on laboratory fatigue data is often used in the determination of accumulated fatigue damage (D) (*8*).

$$\log N_{f_{LAB}} = k_1 + k_2 r$$

where

k_i = fatigue coefficients (k_1 = 17.61; k_2 = −17.61),
r = stress ratio (σ/MR for an existing pavement with known $c-N$ data),

TABLE 2 Regression Statistics ($y = a + bw + cx$)

Survey Cracking Level (%)	Parameter	a	b	c	r^2	SEE
0 - 10%	γ	3.58×10^{-2}	-1.4×10^{-1}	0	0.96	1.72×10^{-3}
	Ln (λ)	-76.38	59.53	0	0.94	0.89
10 - 20%	γ	-1.38×10^{-1}	1.72×10^{-4}	6.15×10^{-3}	0.52	5.79×10^{-3}
	Ln (λ)	-52.28	-0.084	2.16	0.58	3.52
20 - 40%	γ	-3.82×10^{-2}	-5.3×10^{-5}	9.34×10^{-5}	0.99	2.247×10^{-4}
	Ln (λ)	-9.38	2.68×10^{-2}	-0.94	0.65	4.71

* w = rainfall/ℓ or D-days (See Table 1)
x = L/ℓ

σ_{WLS} = wheel load stress,
MR = concrete modulus of rupture, and
$N_{f_{LAB}}$ = laboratory-based value of N_f.

The value of N_{f_c} may be adjusted in terms of the design r value (r_d), which can account for design configurations being different from calibrated design conditions. For design purposes this adjustment may be formulated in terms of a calibrated multiplying factor (MF_c) for stress ratios (r) other than the stress ratio for the calibrated projects, as shown here:

$$MF_c = \frac{N_{f_{LAB}}(r)}{N_{f_c}(L/\ell, \text{ D-days})}$$

$$r_c = r - \frac{\ell n \ MF_c}{k_2 \ell n 10}$$

Note the consistency in the above expression with respect to the stress ratio (r). The term r_c accounts for environmental affects not considered in r. A design multiplying factor (MF_d) using r_d is computed as

$$MF_d = \exp [k_2(r_d - r_c) \ \ell n 10]$$

leading to a design N_{f_c} as

$$N_{f_d} = \frac{N_{f_{LAB}}(r_d)}{MF_d}$$

Therefore, the design loads to failure (NF_d) are a function of both design parameters and calibration parameters. By this process design features and material properties other than the ones used in the calibration for the design may be incorporated in the design calculations of new projects.

In addition to N_{f_d}, the damage scale and shape parameters (η, ζ), using the form of a Weibull distribution shown in Equation 2, should be determined to complete the calibration process. These parameters are calibrated as a function of N_{f_d} and the known values of $\bar{c}$ and $\bar{N}$ as:

$$y_i = a + b \ x$$

where

$$y_i = \ln (-\ln \bar{c}_i)$$

$$x_i = \ln \bar{D}_i$$

$$b = \zeta = \frac{y_2 - y_1}{x_2 - x_1}$$

$$a = -\zeta \ln \eta = y_1 - bx_1$$

$$\eta = \exp \left[- \frac{a}{b} \right]$$

The $\bar{c}$–$\bar{D}$ pairs are defined at the c_{max} level when $\bar{D}$ is 1 and at the known $\bar{c}$ where $\bar{D}$ is N/N_{f_d}. The following outlines the steps taken in the calibration process illustrated in this example:

1. Find the λ and γ scale and shape parameters by fitting $\bar{c}$–$\bar{N}$ pairs of data.
2. Set the value of c_{max}.
3. Determine N_{f_c} and N_{f_d}.
4. Find the η and ζ scale and shape parameters by fitting c–D pairs of data.

Use the following expression to predict cracking:

$$\bar{c} = \exp [-(\bar{D}/\eta)^{\zeta}]$$

where $D = n/N_{f_d}$.

5. If there are multiple points of c–N data, then follow the same procedure as outlined in Steps 1 through 4. Check that the assumed distribution, in this case the Weibull distribution, fits the actual data. If so,

$$\prod_{i=1}^{n} b = \left[\frac{y_2 - y_1}{x_2 - x_1} \right]^n$$

and

$$\prod_{i=1}^{n} a = [y_1 - b_1 x_1]^n$$

and then determine η and ζ. If not, return to Step 1 and try another distribution such as a lognormal or a normal distribution.

CONCLUSIONS

Several implications can be drawn from the correlations and analysis shown and discussed in this paper. It is apparent that the calibration portion of a pavement design procedure not only affects the overall utility of the procedure but encompasses the very core of how reliability can be or is considered in the design process. It should also be apparent that calibration not only applies to the design parameters (mean estimates of distress) but also to the reliability coefficients used to characterize the distress distribution. This also means that the distributions and assumptions used in the calibration process must be applied consistently to the design model to ensure accurate calibrated designs. Therefore, design calibration entails more than an aimless effort of overlaying scattered clouds of datum points with statistical distributions that result in unacceptable r^2 factors. On the basis of the evidence presented in this paper, dramatic improvements in representing field data in the design model calibration process are warranted.

The correlations presented in this paper suggest that paving conditions at the time of construction significantly affect the long-term performance of concrete pavements. It is also apparent that any correlation in fatigue performance that involves the ratio of L over ℓ will also involve other parameters that are directly related to the climatic conditions under which the pavement was constructed. These observations are evident because the correlations indicated here were developed for real field data under real conditions using real distributions.

It is evident from the results of the example presented that the use of reliability concepts combined with what engineers know about pavement behavior can serve as extremely powerful tools in the calibration of pavement performance with field data. By using a process of considering each pavement section, one at a time, the interpretation of what appeared to be very confusing

patterns of performance data (Figure 4) was transformed into a form of order and understanding suitable for the application in design.

REFERENCES

1. Kher, R. K., and M. L. Darter. *Probabilistic Concepts and Their Application to AASHO Interim Guide for Design of Rigid Pavements.* Center for Highway Research, University of Texas at Austin (n.d.).
2. Lemer, H. C., and F. Moavenzadeh. Reliability of Highway Pavements. In *Highway Research Record 362*, HRB, National Research Council, Washington, D.C., 1971.
3. Harr, M. E. *Reliability Based Design in Civil Engineering.* McGraw-Hill Book Company, New York, 1987.
4. Becker, J. M., M. I. Darter, M. B. Snyder, and R. E. Smith. *Concrete Pavement Evaluation System (COPES), User's Manual*, Vol. 2. Department of Civil Engineering, University of Illinois at Urbana-Champaign, Dec. 1984.
5. Zollinger, D. G., and E. J. Barenberg. *Pavement Mechanistic Based Design Procedure for Jointed Concrete Pavements.* Research Report for Project IHR-518. Civil Engineering Studies, Transportation Engineering Series 57, Illinois Cooperative Highway Research Program Series 225, May 1989.
6. Westergaard, H. M. Stresses in Concrete Pavements Computed by Theoretical Analysis. *Public Roads*, Vol. 7, No. 2, April 1926.
7. Bradbury, R. D. *Reinforced Concrete Pavements.* Wire Reinforcement Institute, Washington, D.C., 1938.
8. Darter, M. I., and E. J. Barenberg. *Zero-Maintenance Pavement: Results of Field Studies on the Performance Requirements and Capabilities of Conventional Pavement Systems.* Report FHWA-RD-76-105. University of Illinois; FHWA, U.S. Department of Transportation, April 1976.

Publication of this paper sponsored by Committee on Flexible Pavement Design.

Reliability in Pavement Design? Who's Kidding Whom?

JAMES L. BROWN

There is a considerable divergence of opinion among members of the pavement community about the various aspects of reliability in the pavement design process. Additional considerations have plagued the author while using the original work in Texas for 18 years. Confidence level, life cycle reliability, the consequences of failure, the 1986 AASHTO design guide, and reliability and the pavement type selection process are discussed, followed by a summary.

The background on the introduction of reliability into the pavement design process, based on an oral presentation at the 1992 Meeting of TRB's Committee on Flexible Pavement Design, is presented. Newt Jackson, who requested that the presentation be written so that it could be considered for publication, believes that there is a considerable divergence of opinion among members of the pavement community about the various aspects of reliability in the pavement design process. Additionally, the researchers Marshall Thompson and Ernest Barenberg have struggled with how to handle reliability in their NCHRP Project 1-26, "Calibrated Mechanistic Design Procedures." Thompson and Barenberg have done a superb job of reviewing previous work published on this subject. However, additional considerations that are not published have plagued the author during the last 18 years of using the original work in Texas. Finally, industry reviewers of NCHRP Project 1-26 have differing opinions on this subject. This paper is an attempt to clarify the background, definition, details, weaknesses, and strengths of reliability in pavement design. Additionally, a correct interpretation of the subject is offered, and ideas on proper usage follow from that interpretation.

CONFIDENCE LEVEL

During the 1960s Frank Scrivner was charged with translating the AASHO Road Test findings to Texas' conditions and with developing a flexible pavement design procedure from the results (*1*). The author was the technical coordinator for the Texas Highway Department for much of the project. Scrivner's product was named the Texas Flexible Pavement Design (FPS) system (*2*). It was a life cycle cost pavement design system that attempted to minimize the costs of a variety of design strategies, each of which met certain design criteria. Trial implementation with engineers from five pilot districts revealed that all engineers believed that the pavement structures were too thin and unsafe (*3*). This was not unanticipated; no safety factor had been incorporated within the design system.

Scrivner's satellite study terminated and a large joint effort between the Center for Transportation Research, the Texas Transportation Institute, and the Texas Highway Department continued the effort (*4*). While a sensible sensitivity study was being attempted, it was discovered that the overall uncertainty in the mathematical system could be determined if the uncertainty in each portion could be estimated (*5*). This effort was influenced by Leland Barclay's error analysis methods from University of Texas surveying classes. The uncertainties (variance components) owing to the lack of fit, pure error, and the uncertainty owing to translating the AASHO Road Test to Texas in a time period different from the Road Test (exceeding the inference space) were all needed as well as materials, subgrade, traffic prediction, and environmental uncertainties. An enthusiastic doctoral candidate, Michael Darter, and colleagues undertook the challenge of trying to estimate these variance components (*6,7*).

The reader should note that the Texas Highway Department considered this approach to be valuable for two reasons, neither of which was the calculation of reliability. First, the procedure provided an excellent method of comparing the sensitivity of the output to each input variable while considering the other uncertainties in the process. Such a comparison was as valid because the relative uncertainties of the various components of variance were known.

Second, the method provided a convenient manner for applying a safety factor. All that remained was for someone to say how many standard deviations away from the mean we should design. No one had the slightest notion of what this should be. However, it was reasoned that if the experienced designers could determine that the originally proposed answers were unsafe, they could possibly tell us the safe or correct solution.

For various classes of highways ranging from rural secondary through urban freeways, pavement designs were prepared by using the mean design traffic and the mean design traffic plus one, two, three, four, and five standard deviations (overall standard deviation). The method described above was used to obtain the overall variance. (The log of traffic was used because the AASHO Road Test showed performance to be related to this transformed version of traffic.) From these six solutions the experienced designers were asked to select the right answer. A reasonably consistent pattern developed. For rural secondary roads the design that used the log of the mean design traffic plus two standard deviations was selected as the correct solution. For urban freeways the design based on adding four standard deviations was selected (*8*). The results as implemented are taken from the FPS user's manual as shown below. They were still in use in 1993.

Rev. June 4, 1974

3.5 Design Confidence Level

This variable controls the reliability with which the specified quality of pavement service will be satisfied. Its choice should depend largely upon the consequences of failing to provide the specified quality throughout the indicated analysis period. As an example, sup-

404 West Ninth Street, Suite 203C, Georgetown, Tex. 78726.

pose one highway carrying 28,000 vehicles per lane per day must be overlaid or reconstructed prematurely. The consequences will be much more severe if it does not have continuous frontage roads or some other convenient detour with sufficient capacity available. (The designer is cautioned to remember that the FPS program takes into account user costs for *planned* overlays).

The problems arising because of failure to provide the specified quality throughout the analysis period depend upon the type of repair required to restore serviceability, the relative amount of traffic using the facility during this repair, and the availability of a detour for this traffic.

The designer must specify confidence levels by coding a letter A, B, C, D, E, F, or G. The reliability (probability of success) increases with each succeeding letter—A being the lowest reliability and G the highest.

It is recommended that the guidelines shown in Table 3.1 be used in selecting the Design confidence level.

	The highway will be operating at greater than 50 percent of capacity sometime during the analysis period.	The highway will be operating at less than 50 percent of capacity throughout the analysis period.
The highway is or will become urban before the end of the analysis period.	E	C or D
The highway will remain rural.	C or D	C

LIFE CYCLE RELIABILITY

One modeling problem that still exists today surfaced. As discussed above, the FPS design system models and uses the performance of an initial pavement construction and the performance after maintenance and rehabilitation interventions. The computed performance of the total strategy (the life cycle) will vary greatly depending on whether the various performance periods are connected in series or parallel or something in between. The following scenarios illustrate this problem and the solution chosen to handle it.

- *Scenario 1:* A series of pavements is designed to last at least 10 years with a probability of success of 0.95. The structural model being used says an overlay of t thickness will be required to make the pavement last at least 10 more years with a probability of success of 0.95. A similar overlay of d thickness is required for the third period. The pavements are always treated just as planned: that is, those that last until the end of the 10-year periods are overlaid with the preplanned overlays. Those that fail prematurely are completely reconstructed.
- *Scenario 2:* A series of pavements is designed to last at least 30 years with a probability of success of 0.48. However, a monitoring system that determines threshold conditions of needed rehabilitation is in place. These conditions are analyzed frequently, and whenever a threshold condition is reached, the pavement is redesigned and rehabilitated to last until the end of the 30-year period, again with a probability of success of 0.48. Note that rehabilitation funding is always available, there is always a structurally feasible solution available, and traffic can be handled in a safe and economically feasible manner.
- *Scenario 3:* A series of pavements is designed to last at least 10 years with an 85 percent probability of success. They are monitored, and when funds are available, the pavements that reach a needed overlay condition level are overlaid. For some of those in good condition at the end of 10 years, the planned overlay was postponed so that a better job could be done on the pavements that wore out early. The process is repeated throughout the 30-year period with enough average funding so that 85 percent of the pavements last the 30 years without requiring either more than two overlays or reconstruction.

What is the reliability of these designs? What are the key issues in deciding the answer to that question? Scenario 1 is analogous to the bad employee who does exactly what you tell him or her every time without thinking. Scenario 2 is most likely unachievable because some distresses cannot be corrected. Midcourse corrections may not be possible for either structural, traffic handling, or financial reasons. The composite, Scenario 3, is the most probable case.

The author's estimate of the interventions and failures that occur in each scenario is given in Table 1. The resulting reliability is also presented. A reader who computes different results for this table should not be alarmed. The author admits that he does not know how to compute an accurate answer for these scenarios, and he doubts whether anyone else knows either.

It should be readily apparent from these examples that the true reliability for a life cycle depends not only on design factors for the pavement and subsequent rehabilitation interventions but also on how these interventions are applied. Operational restraints such as unavailable funding or traffic-handling limitations can severely limit the advantages of midcourse corrections. Technical restraints

TABLE 1 Required Actions for Three Scenarios

Activity	Scenario One	Scenario Two	Scenario Three
No Overlay Required	0	53	0
Single Overlays	95	25	86
Double Overlays	95	12	86
Reconstruction*	15	15	15
Reliability	85	85	85

*Assuming that any pavement that failed to last 30 years with two overlays had to be reconstructed.

such as the inability to know when a correction is needed or not having a rehabilitation technique that can correct a specific distress can also limit the ability to make effective midcourse corrections. Conversely, in most cases it is incorrect, in the author's opinion, to adopt the approach taken in Scenario 1. Incidentally, this is the approach used in the 1986 AASHTO *Guide for Design of Pavement Structures* (*9*). Most state highway agencies have some ability to detect and treat potentially failing pavements. Probably all of them have the capacity to delay rehabilitation interventions when the pavement is showing no sign of distress.

As a middle ground, the Texas Highway Department adopted for the FPS system a predicted reliability (confidence level) for the entire performance period that is exactly equal to that used for nonstaged construction (*8*).

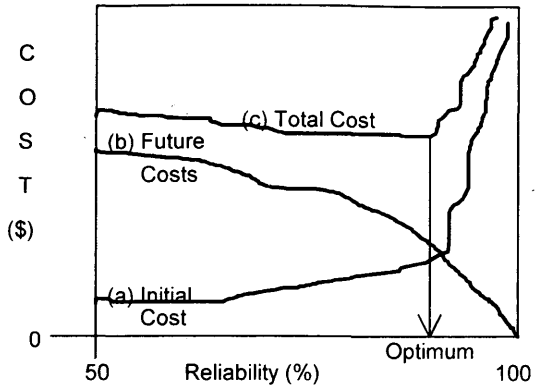

FIGURE 1 Approach to identifying optimum reliability level for a given facility (*9*,p.I-63).

CONSEQUENCES OF FAILURE

One would be remiss in discussing the background to reliability if the very important contribution of J. W. Hewett was not noted. During the period under discussion, Hewett was Assistant Branch Chief of FHWA's Pavement Design Branch. In a conversation about the subject, he noted, "the correct confidence or reliability to select must depend upon *the consequences of failure.*" To a pavement designer and one teaching pavement design, this statement has been invaluable. Such important but unquantifiable factors as availability of detours, amount of traffic, speed of traffic, difficulty of required repair, availability of resources (money, workers, and equipment to make the required repairs), and the public image cost vary a great deal from project to project and from agency to agency. Despite their nebulous natures these factors must be considered in assigning a factor of safety or confidence level or design reliability level. Hewett's simple explanation, that one must look at the consequences of failure to select an appropriate certainty level for design, has been useful to those who have been applying these concepts.

1986 AASHTO GUIDE

The 1986 AASHTO *Guide for Design of Pavement Structures* (*9*) introduced the reliability concepts of the Texas FPS system to a broad audience for the first time. In Appendix EE, Volume 2 and Chapter 4, Part 1, Paul Irick has treated the calculations with mathematical rigor. In Appendix EE, R. L. Lytton has collected, from the available data and from his experience, a set of estimates of the variances for all of the inputs to the design equations, much as Darter had done a decade before for the Texas equations. The author supplied the conceptual Figure 4.5, reproduced herein in Figure 1. The concepts illustrated in the figure grew out of the preceding discussion on the selection of a proper design reliability.

The AASHTO Joint Task Force on Pavement Design, which is responsible for producing the guide, tried an exercise to select the appropriate reliability design in the same manner that Texas had used in the 1970s. They had questionable success. The effort was undertaken by having the task force members get the pavement designers from their home states to submit a correct design solution for a series of design problems. The staff then tried to match these answers to a reliability level required to achieve the same design solutions using the guide. The results were wildly scattered. The author contributes this scatter almost exclusively to one factor: the inference space over which the guide was being applied was much too large. As examples, neither thin-surfaced asphalt roads, such as those used in Texas with much success, nor continuously reinforced concrete pavements were even used at the Road Test. An even larger expansion of inference space is today's modern urban freeway loaded with traffic compared to anything being considered by the personnel developing the present serviceability concept at the Road Test (Table 2.2 of the guide). Suggested levels of reliability for various functional classifications (p. II-10 of the guide) is the result of that exercise. It is not so bad as a guideline. Any agency that uses the guide must recognize that it has total responsibility for adjusting the guide so that it matches the agency's experience. The agency must adjust the guide to the conditions under which it is to be applied.

RELIABILITY AND PAVEMENT TYPE SELECTION PROCESS

A troublesome bit of rhetoric evolved in the presentations that were used to introduce the new guide to the pavement community. It has created false expectations for the reliability concept. The statement usually takes a form like the following: "Reliability is the probability that a pavement will achieve its design function. Therefore, for comparing pavement designs for the purpose of pavement type selection, each competing design should have the same reliability."

Although this statement is correct, it has no practical application at this time. Let us examine it part by part. First, the term "its design function" implies that a single number, like the present serviceability index, represents the performance of the pavements. Only if the competing pavements are being designed for some global and equal functional design criteria does the statement work. It should be readily apparent that the reliability against faulting in a concrete pavement is not of the same importance as the reliability against rutting in an asphalt pavement. Another problem exists if we further consider the consequences of failure; it may be much easier to rehabilitate a thin-surfaced alligator-cracked asphalt pavement than a very thick alligator-cracked asphalt pavement.

The problem of staged construction or future interventions also makes the earlier statement almost useless in selecting pavement

type. Life cycle costs must be considered in pavement type selection, yet we have not resolved how to couple future interventions for a specific design reliability.

SUMMARY

To summarize, the advantages and disadvantages of the reliability methodology were reviewed. First, however, it is stated again that by the reliability methodology the author means estimating and correctly combining all of the uncertainties associated with a particular design model into an overall variance. Such an exercise lets us examine the contribution of each uncertainty to the total. Knowing the importance of each design input lets us know how important it is for us to spend efforts to get better data for design. If subgrade stiffness is very important we can run more tests; if the present percentage of trucks is important we can count the trucks. If our prediction models are so poor that better design data will not improve our answers, we can spend more on research to improve the equations.

The reliability methodology provides a very convenient method for applying a safety factor to our design equations. We *must* calibrate any of our equations to our experience. This can be done by using the reliability methodology.

The disadvantages are all of the nature of misapplication, misunderstanding, or incomplete knowledge preventing us from reaching the full potential of this technology. First, we have the "innocents," who use percent reliability as if they were precise with their calculations. In fact, they are very inexact and probably biased to the low side. It is not too hard to envision a representative in a congressional hearing saying, "you designed it for 99.99 percent reliability and it failed anyway!"

Next comes the very difficult problem of how to handle the coupling of various stages in life cycle problems. All of us are going to have to give our operating processes a closer look before we select the model that should be used to couple these various stages.

Reliability as being applied today is the probability that the pavement will not exceed some distress criteria being treated by the design model. This probability is valid only for the inference space that was encompassed by the data set from which the model was derived. Our experience with the Strategic Highway Research Program's Long-Term Pavement Performance Program experiment designs teaches us that all of our present data bases are very limited.

Despite confusing rhetoric otherwise, reliability technology offers little help in the pavement type selection process. We can and should attempt to design different pavement types to have the same overall life cycle reliability. However, we must continue to let the responsible engineer weigh these results and make his or her final selection on the basis of all of the data and judgment that he or she can deploy. We cannot limit ourselves to using a very imperfect model instead of applying the wisdom of the ages.

REFERENCES

1. Scrivner, F. H., and W. M. Moore. *Application of AASHO Road Test Results to Texas Conditions.* Texas Highway Department Research Study Number 32. Texas Transportation Institute. July 1962–Aug. 1969.
2. Scrivner, F. H., and W. M. Moore. *A Systems Approach to the Flexible Pavement Design Problem.* Texas Highway Department Research Report 32-11. Texas Highway Department, Oct. 1968.
3. Buttler, L. J., and H. E. Orellana. *Implementation of a Complex Design System.* Texas Highway Department Research Report 123-20. Texas Highway Department, June 1973.
4. Brown, J. L., F. H. Scrivner, W. R. Hudson, et al. Texas Highway Department Research Study 123. *A System Analysis of Pavement Design and Research Implementation,* Nov. 1968–Aug. 1975. Texas Highway Department, Texas Transportation Institute, and Center for Highway Research.
5. Kher, R. K., and M. I. Darter. Probabilistic Concepts and Their Applications to the AASHO Interim Guide for the Design of Rigid Pavements. In *Highway Research Record 466,* HRB, National Research Council, Washington, D.C., 1973.
6. Darter, M. I., and W. R. Hudson, *Probabilistic Design Concepts Applied to a Flexible Pavement Design System.* Texas Highway Department Research Report 123-18. Texas Highway Department, 1973.
7. Darter, M. I., W. R. Hudson, and J. L. Brown. Statistical Variations of Flexible Pavement Properties and Their Consideration in Design. *Proc., Annual Meeting of the Association of Asphalt Paving Technologists,* 1973.
8. Brown, J. L., L. J. Buttler, et al. *A Recommended Texas Highway Department Pavement Design System User's Manual.* Texas Highway Department Research Report 123-2. Texas Highway Department, 1970.
9. *Guide for Design of Pavement Structures.* AASHTO, Washington, D.C., 1986.

Publication of this paper sponsored by Committee on Flexible Pavement Design.

Soil-Property-Based Subgrade Resilient Modulus Estimation for Flexible Pavement Design

KEVIN D. HALL AND MARSHALL R. THOMPSON

Subgrade soils play an integral part in pavement performance. The nature and properties of subgrade soils must be considered in structural pavement design. Many highway agencies, particularly those that administer local or low-volume pavements, do not have the resources to conduct comprehensive subgrade evaluation programs. The use of soil index properties obtained from county soil surveys published by the Soil Conservation Service to estimate the subgrade resilient modulus for structural pavement design is investigated. Soils data and nondestructive pavement testing data from five counties in Illinois were used in the analyses. Subgrade resilient modulus is estimated from soil index properties by using relationships developed for Illinois subgrade soils. Resilient modulus is also estimated from pavement surface deflections by using equations developed from the ILLI-PAVE finite-element pavement model. Soil-property-based modulus estimates are compared with deflection-based modulus estimates. Two methodologies are described that were used to adjust soil-property-based modulus estimates to design values for pavements based on comparisons with deflection-based modulus estimates. One method is based on the natural drainage class of the soil. The second method uses the moisture adjustment ratio, which is the ratio of the design in situ moisture condition of the soil to the soil's optimum moisture content. For many of the soils investigated, design soil-property-based subgrade modulus estimates relate well to the corresponding deflection-based modulus estimates. However, local soils are best represented by soil-property-based modulus estimates when the methodologies described are applied specifically to local conditions rather than when generic or blanket relationships developed for a wide range of soils are relied upon.

Subgrade soil characterization is one of the critical factors in structural pavement design. Most methods of determining pavement thickness requirements for projected traffic loading include a subgrade input, whether as an explicit variable or implicitly in design curves. Ideally a subgrade investigation program would be conducted for each pavement project to determine classification and strength data for each soil encountered on the project. Unfortunately, time and monetary considerations generally preclude such investigations or severely limit their scope. This is true particularly for agencies involved in the design and construction of low-volume roads.

The primary subgrade property of interest in the structural pavement design of flexible pavements is the resilient modulus, E_R. In the absence of subsurface exploration or nondestructive pavement testing programs, highway agencies (particularly local agencies) need methods of obtaining or developing reasonable estimates of the subgrade resilient modulus. Techniques for estimating E_R from soil index properties such as plasticity index (PI) and percent clay have been developed. A large body of index property data for soils exists and is readily available to the pavement designer. In this paper methodologies are described for estimating the subgrade resilient modulus for pavement design purposes by using established techniques and readily available soil property information. Soil-property-based estimates of the subgrade resilient modulus are compared with modulus values estimated from the results of nondestructive pavement testing. On the basis of the comparisons, soil-property-based estimates are adjusted to design values for use in pavement design activities.

The following items should be noted concerning the analyses that follow:

1. The methodologies presented are based on soils and conditions in Illinois. Because of the relatively uniform soil conditions present in Illinois, typically only three or four soil series are encountered per mile on a project. Extrapolation to areas in which soil and climatic conditions are substantially different from those in Illinois must be performed with caution.
2. The primary application of the methodologies presented is to low-volume roads, in which the pavement is typically constructed directly on the natural subgrade soil.
3. The analyses described in this paper demonstrate an approach to modulus estimation; they are not intended to be a cookbook procedure for providing the resilient modulus of the subgrade soil.
4. The methodologies described are not intended to replace field investigation of subgrade soils; however, they may provide a workable alternative to the do-nothing option when fieldwork is not feasible.

ESTIMATING RESILIENT MODULUS

Using Soil Index Properties

A number of studies have been conducted to develop subgrade modulus predictive equations based on soil properties such as Atterberg limits and percent clay. An excellent summary of the major efforts is contained in the Final Report of NCHRP Project 1-26 (*1*), on which the following discussion is based.

Drumm et al. (*2*) developed subgrade modulus predictive equations based on standard soil tests using 11 typical Tennessee soils. Resilient modulus was related to the soil's plasticity, percent fines, density, saturation, and unconfined compressive strength. The authors concluded that the modulus predictive equation provides "a good characterization of response for the soils investigated."

K. D. Hall, Department of Civil Engineering, 4159 Bell Engineering Center, Fayetteville, Ark. 72701. M. R. Thompson, Department of Civil Engineering, University of Illinois at Urbana-Champaign, 1208 NCEL, 205 North Mathews, Urbana, Ill. 61801.

Elliott et al. (*3*) tested 15 typical Arkansas soils for resilient modulus. Subgrade modulus predictive equations were developed for repeated deviator stress levels of 27.5 and 55 kPa (4 and 8 psi). The subgrade modulus was related to the percent clay, PI, and optimum moisture content. The resilient modulus data used in developing the predictive equations represented soils at approximately 120 percent AASHTO T-99 moisture content and 95 percent compacted dry density.

Farrar and Turner (*4*) published the results of a laboratory resilient modulus testing program for 13 typical Wyoming subgrade soils. The subgrade modulus was related to the degree of saturation, repeated deviator stress, confining pressure, PI, and percent passing the No. 200 sieve.

Thompson and Robnett (*5*), in the first comprehensive study of its type, investigated the repeated load behavior of 50 typical Illinois fine-grained soils. The subgrade modulus was significantly correlated with liquid limit, PI, group index (from the AASHTO soil classification system), silt content, clay content, specific gravity, and organic carbon content. A stepwise regression analysis was performed on the data to develop modulus predictive equations from soil properties. Thompson and LaGrow (*6*) proposed using the following regression equation for conventional flexible pavement design:

$$E_{Ri}(\text{OPT}) = 4.46 + 0.098C + 0.119\text{PI}$$

$$(R^2 = 0.63, \text{SEE} = 2.7 \text{ ksi}) \qquad (1)$$

The regression algorithm is improved if soil organic carbon content is included:

$$E_{Ri}(\text{OPT}) = 6.90 + 0.0064C + 0.216\text{PI} - 1.97\text{OC}$$

$$(R^2 = 0.76, \text{SEE} = 2.3 \text{ ksi}) \qquad (2)$$

where

E_{Ri}(OPT) = subgrade resilient modulus (ksi) at AASHTO T-99 optimum moisture content and 95 percent compaction,
C = percent clay (<2 μm),
PI = plasticity index (percent),
OC = percent organic carbon,
R^2 = coefficient of determination, and
SEE = standard error of the estimate.

Thompson and Robnett (*5*) modeled the stress softening behavior of fine-grained soils as a bilinear curve (Figure 1). Their modulus equations (Equations 1 and 2) predict the breakpoint resilient modulus (E_{Ri}), which commonly occurs at approximately 41.3 kPa (6 psi) deviator stress for Illinois soils (*5*). E_{Ri} is a good indicator of soil resilient behavior. The slope values in Figure 1, k_1 and k_2, display less variability and influence pavement structure response to a smaller degree than does E_{Ri} (*7*).

The E_{Ri} estimate obtained from the predictive equations for Illinois soil represents a soil at optimum moisture content and 95 percent compaction (AASHTO T-99). Subgrade soils, particularly fine-grained ones, are moisture sensitive. In other words, the resilient modulus of the soil depends on the moisture content of the soil. Relationships between E_{Ri} and the degree of saturation of the soil (*5*) demonstrate that subgrade modulus decreases with increasing moisture content.

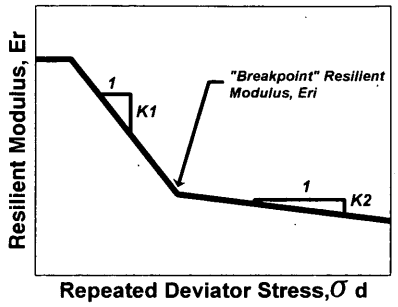

FIGURE 1 Bilinear model of resilient behavior of fine-grained soils (*5*).

Thompson and LaGrow (*6*) analyzed the Illinois data (*5*) to develop moisture adjustment factors based on the U.S. Department of Agriculture (USDA) textural classification of the soil. The moisture adjustment factor represents the decrease in E_{Ri} (in kips per square inch) for each 1 percent increase in moisture content above the optimum moisture content. In general, soils with higher values of clay content and PI (textural classification groups clay, silty clay, and silty clay loam) showed less sensitivity to changes in the degree of saturation. The moisture adjustment factors proposed by Thompson and LaGrow are shown in Table 1.

It is apparent from the preceding discussion that subgrade resilient modulus can be estimated from soil properties (percent passing a No. 200 sieve, percent <2-μm clay, PI, percent OC), moisture density conditions (consolidated in percent saturation), and stress state conditions. There is a difficulty in applying many of the predictive equations to everyday design situations, however. Many of the equations contain one or more quantities that are not routinely measured, such as values from unconfined compression or repeated load triaxial testing, and therefore represent information that is not readily available. Ideally, reasonable estimates of E_{Ri} could be made by using soil index properties (e.g., grain size and plasticity), which are used in the equations for Illinois soils (Equations 1 and 2).

TABLE 1 Moisture Adjustment Factors (*6*)

USDA Textural Class	Moisture Sensitivity (ksi / %)
clay silty clay silty clay loam	0.7
silt loam	1.5
loam	2.1

Notes: Moisture Adjustment Factor represents the decrease in Eri (ksi) for each 1% moisture increase above optimum

1 ksi = 6890 kPa

Sources of Soil Property Information

Equations 1 and 2 relate subgrade resilient modulus to laboratory test values of soil index properties. It is certainly ideal to conducting laboratory tests of the actual soils encountered on a paving project; however, in the absence of field sampling and laboratory testing, soil property information may yet be readily available. Perhaps the single largest source of soil property information is the USDA Soil Conservation Service (SCS). The SCS maintains records on more than 17,000 soils mapped in the United States. The primary source of SCS soils data most accessible to the pavement designer is the SCS county soil survey (the county soils report).

The SCS county soils report contains a significant amount of information concerning local soils. Tables in the county soils report list items such as USDA textural class, Unified and AASHTO classifications, grain size distribution, Atterberg limits, percent clay, and percent organic matter. Most soil property data items are listed as a range of values, which reflect the variability of the property for that soil in the county. Soils are listed in the county soils report on the basis of their pedologic classifications. *Pedology* is a field of study involving the processes of soil genesis, classification, morphology, survey, and interpretation (*8*). Studies have indicated that pedology-based subgrade classification can be advantageous to pavement design activities (*5,6,9*). In addition, many state highway agencies (SHAs) are using pedologic concepts in subgrade evaluation. A summary of current SHA efforts is given elsewhere (*7*).

Using Nondestructive Testing Data

The subgrade resilient modulus can be back-calculated by using pavement surface deflections generated from a falling-weight deflectometer (FWD). There are many methods of back-calculating subgrade modulus from pavement surface deflections, including direct-solution procedures, elastic layer program (ELP)-based procedures, and stress-dependent finite-element model (FEM)-based procedures. The question of the best method for back-calculating subgrade modulus from deflection data has received much attention in the pavement engineering community. The focus of this research is to relate back-calculated values of modulus to soil-property-based modulus values, not to assess back-calculation procedures. A brief discussion of the procedures used in this research follows.

Studies at the University of Illinois (*10,11*) have resulted in algorithms for estimating the subgrade resilient modulus from pavement surface deflections. The algorithms, which relate E_{Ri} to D_3 [the surface deflection (in mils) at 914 mm (36 in.) from the point of loading], are regression equations developed from a data base of pavement responses to load. The data base was generated by the ILLI-PAVE finite-element structural pavement model. Equations 3 through 6 show the E_{Ri} back-calculation algorithms:

For surface treatment/granular base pavements:

$$E_{Ri} = 24.2 - 5.71D_3 + 0.35D_3^2$$

$$(R^2 = 0.98, \text{SEE} = 0.57 \text{ ksi}) \quad (3)$$

For conventional flexible pavement (3-in.-minimum asphalt concrete/granular base):

$$E_{Ri} = 25.0 - 5.25D_3 + 0.29D_3^2$$

$$(R^2 = 0.97, \text{SEE} = 0.76 \text{ ksi}) \quad (4)$$

For full-depth asphalt concrete pavements:

$$E_{Ri} = 24.7 - 5.41D_3 + 0.31D_3^2$$

$$(R^2 = 0.98, \text{SEE} = 0.64 \text{ ksi}) \quad (5)$$

For all flexible pavements:

$$E_{Ri} = 24.1 - 5.08D_3 + 0.28D_3^2$$

$$(R^2 = 0.97, \text{SEE} = 0.76 \text{ ksi}) \quad (6)$$

The ILLI-PAVE-based algorithms shown have been used in many studies conducted at the University of Illinois and give reasonable estimates of subgrade modulus (*9*).

DATA ANALYSIS

Results from FWD testing (pavement surface deflections) are used to estimate the subgrade resilient modulus by using the ILLI-PAVE algorithms given above. The subgrade modulus is also estimated by using soil index properties obtained from county soil surveys for pedologic soil series encountered by FWD testing. The two estimates of subgrade modulus, deflection-based and soil-property-based, are compared to determine whether a relationship exists.

Soil property and FWD data from Champaign County, Illinois are used to develop relationships between soil-property-based and deflection-based estimates of E_{Ri}. The relationships developed with the Champaign County data are verified with soil property and FWD data from four additional counties in Illinois: Sangamon, Livingston, Mercer, and Marion.

Development of Relationships: Deflection-Based Versus Soil-Property-Based E_{Ri}

FWD Results: Deflection-Based Estimates of Subgrade Modulus

In March 1992 a nondestructive (FWD) pavement testing program was performed on approximately 68.4 lane-km (42.5 lane-mi) of flexible pavement located in Champaign County. Testing sites were identified by using soil maps contained in the Champaign County soil survey (*12*). A total of 15 sites located in five county soil associations were identified and tested. The testing program was designed to obtain test results for the major pedologic soil series of the county. A complete description of the testing program is given elsewhere (*9*). The soil series encountered during testing represents the soils on approximately 89 percent of the total county area. For major soil series, relatively long continuous segments are typically encountered. On a typical pavement project only a small number of soil series needs to be considered.

The ILLI-PAVE-based algorithm appropriate for the pavement structure present at each FWD testing site is used to estimate E_{Ri}. If the specific pavement structure is not known, Equation 6 is used. Within each testing site (or project) the E_{Ri} values representing a particular soil series are grouped into a mean value (the project mean). Analyses performed for this research and by others have indicated that the project mean is an appropriate level at which to consider E_{Ri} data (*9,13*). Table 2 shows the results of FWD data analysis for Champaign County.

Soil-Property-Based Estimates of Subgrade Modulus

The subgrade modulus is estimated from soil index properties by using Equations 1 and 2. Mid-range soil index properties are obtained from the Champaign County soil survey (*12*). An E_{Ri} estimate is generated for each of the soil's genetic horizons. Equation 1 is used to estimate E_{Ri} for B and C horizons, whereas Equation 2 is used to estimate E_{Ri} for A horizons [the surficial horizon that typically has a significant amount of organic matter (OM)]. For use in Equation 2, OM is expressed as OC through the following relationship (*9*):

$$\text{Percent OC} = \frac{\text{percent OM}}{1.7} \tag{7}$$

For routine purposes agronomists typically assume that the OC content is 58 percent of the total OM content.

Table 3 shows midrange values of soil properties and E_{Ri}(OPT) estimates for the major soil series in Champaign County. The designation E_{Ri}(OPT) is used to denote the fact that Equations 1 and 2 yield the subgrade modulus at optimum moisture content.

The moisture adjustment factors shown in Table 1 are used to adjust E_{Ri}(OPT) estimates to moisture contents in excess of the optimum. The adjustment factor is a function of the USDA textural class of the soil, which is given in the county soil survey. Table 3 shows the major soil series of Champaign County, with estimates of E_{Ri}(OPT) and for moisture contents up to (OPT+6 percent). Because of differences in the textural class of horizons within the same soil series, the E_{Ri}(OPT) estimate of each horizon

TABLE 2 Results of FWD Data Analysis for Champaign County

FWD Site	Soil Series	No. Obs	Mean Eri (ksi)	Std Dev	COV (%)	FWD Site	Soil Series	No. Obs	Mean Eri (ksi)	Std Dev	COV (%)
1-1	152 Drummer	6	0.93	0.04	5	2-4	146 Elliott	7	10.08	1.40	14
	153 Pella	13	0.92	0.03	3		152 Drummer	5	9.17	1.04	11
	154 Flanagan	19	1.29	0.85	66						
	171 Catlin	2	1.70	0.44	26	3-1	56 Dana	18	5.19	4.11	79
							152 Drummer	9	1.21	0.59	49
1-2	152 Drummer	13	4.47	1.66	37		221 Parr	12	5.81	3.45	59
	153 Pella	5	4.64	1.38	30		481 Raub	13	3.02	2.34	77
	154 Flanagan	36	5.22	1.85	35						
1-3	152 Drummer	38	3.19	2.61	82	5-1	152 Drummer	42	0.93	0.06	6
	154 Flanagan	11	4.68	1.64	35		198 Elburn	11	1.81	1.28	70
	198 Elburn	5	1.82	0.70	39						
						5-2	148 Proctor	2	5.94	0.87	15
1-4	152 Drummer	32	1.63	0.72	44		149 Brenton	2	1.84	0.81	44
	153 Pella	5	2.92	0.59	20		152 Drummer	23	1.02	0.27	27
	154 Flanagan	16	2.66	1.39	52						
						5-3	152 Drummer	16	1.94	1.43	74
1-5	67 Harpster	2	1.65	0.38	23		154 Flanagan	17	3.99	2.81	70
	150 Onarga	2	5.48	0.66	12		198 Elburn	12	2.49	1.09	44
	152 Drummer	31	2.57	1.09	43		199 Plano	5	3.28	0.46	14
	153 Pella	10	1.81	0.61	34		221 Parr	1	7.80	0.00	0
	154 Flanagan	6	3.06	0.91	30						
	171 Catlin	2	2.19	0.11	5	7-1	146 Elliott	22	6.73	1.25	19
							152 Drummer	2	4.92	0.06	1
2-1	148 Proctor	4	2.58	1.26	49		223 Varna	6	6.96	2.52	36
	152 Drummer	20	2.48	2.18	88		232 Ashkum	10	6.31	1.37	22
	481 Raub	5	3.48	1.69	49		330 Peotone	3	8.19	1.14	14
							402 Colo	2	7.78	1.07	14
2-2	148 Proctor	1	8.67	0.00	0		481 Raub	4	6.61	3.15	48
	152 Drummer	10	7.01	2.12	30		490 Odell	4	7.77	2.45	32
	221 Parr	8	6.89	2.73	40						
	481 Raub	1	10.21	0.00	0	7-2	56 Dana	4	5.41	0.98	18
							146 Elliott	23	5.82	2.20	38
2-3	148 Proctor	6	5.76	0.48	8		232 Ashkum	27	4.97	2.54	51
	149 Brenton	4	6.93	1.24	18						
	152 Drummer	10	5.27	0.77	15						
	481 Raub	2	5.28	1.03	20						

NOTE: 1 ksi = 6890 kPa

TABLE 3 Average Soil Properties and E_{Ri} Estimates for Champaign County Soils

Soil Series	Horizons Thick (in)	Sym	USDA Textural Class	Average Values PI (%)	%CL	%OC	Eri (OPT) (ksi)	Eri (ksi) @ OPT+: 1	2	3	4	5	6
56 Dana	12	A	SiL	10	17	1.50	6.2	4.7	3.2	1.7	1.0	1.0	1.0
	22	B	SiCL	26	31		10.6	9.9	9.2	8.5	7.8	7.1	6.4
	5	IIB	CL	24	31		10.3	9.3	8.3	7.3	6.3	5.3	4.3
	21	IIB/IIC	L	8	21		7.5	5.4	3.3	1.0	1.0	1.0	1.0
	COMPOSITE:						**8.6**	**7.2**	**5.9**	**4.4**	**3.9**	**3.6**	**3.3**
146 Elliott	12	A	SiL	13	26	2.65	4.7	3.2	1.7	1.0	1.0	1.0	1.0
	29	IIB	SiC,SiCL	19	40		10.6	9.9	9.2	8.5	7.8	7.1	6.4
	19	IIC	SiCL,CL	18	31		9.6	8.9	8.2	7.5	6.8	6.1	5.4
	COMPOSITE:						**9.1**	**8.2**	**7.4**	**6.7**	**6.1**	**5.6**	**6.0**
152 Drummer	14	A	SiCL	23	31	3.50	5.1	4.4	3.7	3.0	2.3	1.6	1.0
	27	B	SiCL	23	31		10.2	9.5	8.8	8.1	7.4	6.7	6.0
	6	IIB	L,SiL,CL	23	28		9.8	8.3	6.8	5.3	3.8	1.0	1.0
	13	IIC	SaL/SiCL	14	24		8.4	7.7	7.0	6.3	5.6	4.9	4.2
	COMPOSITE:						**8.6**	**7.8**	**7.0**	**6.2**	**5.5**	**4.6**	**3.9**
154 Flanagan	18	A	SiL	23	25	2.65	6.7	5.2	3.7	2.2	1.0	1.0	1.0
	27	B	SiCL	23	39		10.9	10.2	9.5	8.8	8.1	7.4	6.7
	15	IIB/IIC	L,CL,SiL	18	25		9.0	7.5	6.0	4.5	1.0	1.0	1.0
	COMPOSITE:						**9.2**	**8.0**	**6.9**	**5.7**	**4.2**	**3.9**	**3.6**
232 Ashkum	17	A	SiCL	28	40	3.50	6.2	5.5	4.8	4.1	3.4	2.7	2.0
	22	B	SiCL,SiC	28	40		11.7	11.0	10.3	9.6	8.9	8.2	7.5
	21	IIB/IIC	SiCL	23	35		10.6	9.9	9.2	8.5	7.8	7.1	6.4
	COMPOSITE:						**9.8**	**9.1**	**8.4**	**7.7**	**7.0**	**6.3**	**5.6**
481 Raub	18	A	SiL	10	24	1.80	5.7	4.2	2.7	1.2	1.0	1.0	1.0
	14	B	SiCL	28	31		10.8	10.1	9.4	8.7	8.0	7.3	6.6
	8	IIB	CL,SiCL	20	31		9.9	9.2	8.5	7.8	7.1	6.4	5.7
	20	IIB/IIC	L,CL	8	26		7.9	6.4	4.9	3.4	1.0	1.0	1.0
	COMPOSITE:						**8.2**	**7.0**	**5.8**	**4.6**	**3.4**	**3.2**	**2.9**

NOTE: 1 ksi = 6890 kPa

is adjusted before a composite estimate of the subgrade modulus is calculated. The composite E_{Ri} estimate is calculated as a weighted average of the horizons by using horizon thickness as the weighting factor (*9*).

Comparison of Deflection-Based and Soil-Property-Based Subgrade Modulus Estimates

Table 3 shows subgrade modulus estimates for soils at moisture conditions ranging from optimum to 6 percent wet of optimum. The natural, in situ moisture condition of subgrade soils is not likely to be constant but a function of soil properties such as plasticity and grain size. Arbitrarily assigning a moisture condition to all subgrade soils (i.e., OPT + 3) may lead to errors in the soil-property-based modulus estimate. The question becomes, At what moisture condition should the pavement designer consider subgrade soils for design purposes? A comparison of soil-property-based subgrade modulus estimates and deflection-based estimates sheds some light on this question.

Figure 2 shows soil-property-based E_{Ri} estimates for a number of OPT + n moisture conditions and deflection-based E_{Ri} estimates for Champaign County soils. An estimate of the OPT + n condition or conditions required for soil-property-based modulus estimates to accurately reflect deflection-based estimates can be obtained from Figure 2. Soil series 56 Dana requires approximately OPT + 2 conditions. Soil series 146 Elliott is well represented by OPT + 4 moisture conditions, whereas soil series 152 Drummer requires approximately OPT + 7 conditions. A moisture condition of approximately OPT + 4 is required for soil series 154 Flanagan. Soil series 232 Ashkum is best represented by about OPT + 7 conditions, and soil series 481 Raub requires about OPT + 3 conditions.

The moisture condition required for deflection-based and soil-property-based subgrade modulus estimates to agree can be expressed in terms of a degree of saturation for the soil series. To do this, the optimum moisture content (w_{opt}) and maximum dry density (γ_d) of the soil are required. The Illinois Department of Transportation has developed equations for estimating w_{opt} and γ_d from soil index properties (*14*). The Illinois Department of Transportation equations, shown in Equation 8 (w_{opt}) and Equation 9 (γ_d), are based on data obtained for Illinois subgrade soils.

$$w_{opt} = 0.499\,LL - 0.354\text{PI} + 0.044P200 + 1.86 \qquad (R^2 = 0.928) \qquad (8)$$

$$\gamma_d = -1.10LL + 0.769\text{PI} - 0.062P200 + 138.96 \qquad (R^2 = 0.921) \qquad (9)$$

where

w_{opt} = optimum moisture content, (percent),
γ_d = maximum dry density [pcf (1 pcf = 159 N/m^3)],
LL = liquid limit (percent),
PI = plasticity index (percent),
$P200$ = percent passing a No. 200 sieve, and
R^2 = coefficient of determination.

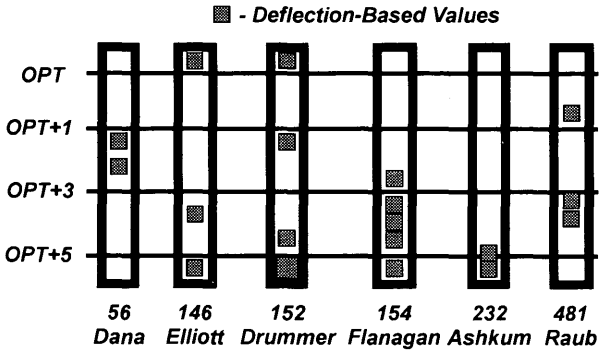

FIGURE 2 Soil-property-based and deflection-based subgrade modulus estimates for Champaign County soil series.

By using estimates of the optimum moisture content and maximum dry density obtained with Equations 8 and 9, the degree of saturation required for soil-property-based E_{Ri} estimates to reflect deflection-based estimates is determined. The required degree of saturation is related to the USDA natural drainage class of the soil. Table 4 shows the Champaign County soil series and the requirements for soil-property-based and deflection-based modulus estimates to relate, expressed in terms of moisture condition (OPT + n) and degree of saturation, and the soil's natural drainage class. By using Table 4, it is possible to identify the following relationships: poorly drained soils (152 Drummer and 232 Ashkum) are nearly 100 percent saturated, somewhat poorly drained soils (146 Elliott, 154 Flanagan, and 481 Raub) are nearly 90 percent saturated, and moderately well drained soils (56 Dana) are nearly 80 percent saturated. Note that the degree of saturation required to relate E_{Ri} estimates increases as the natural drainage of the soil gets poorer. This trend is not surprising; for a given position of the water table, amount of precipitation, and so on, soils with poorer natural drainage characteristics will show higher degrees of saturation.

Another method of developing design soil-property-based modulus values uses the difference between the predicted E_{Ri}(OPT) value and the deflection-based value for a particular soil series. This difference, when divided by the moisture adjustment factor (Table 1) appropriate for the soil, is expressed as the required moisture adjustment for the soil (literally, the n in the OPT + n required for E_{Ri} estimates to relate). The required moisture adjustment for a particular soil series is related to the soil's optimum moisture content. The moisture adjustment ratio (MAR) is the ratio of the required moisture adjustment to the optimum moisture content of the soil.

Table 5 shows the required moisture adjustment and MAR for each Champaign County soil series used in this study. An average MAR of 0.29 is calculated for Champaign County soils. The average MAR is used to determine design soil-property-based E_{Ri} values for the soil series shown. The MAR is multiplied by the optimum moisture content to determine design moisture conditions (the n in OPT + n). The design value of E_{Ri} either can be determined from a table such as Table 3 or can be calculated directly by using the appropriate moisture adjustment factor (Table 1). Table 5 shows design E_{Ri} values determined by both methods.

MAR values calculated for Champaign County soil series exhibit relatively large variabilities (coefficient of variation equal to about 45 percent), most likely because of the relative lack of uniformity of soil parent material across the county. Soil series mapped in regions with more uniform parent materials may show less variable MAR values.

Validation of Relationships

Validation Methodology

Four sets of soils data and corresponding FWD test data are used to validate relationships between soil-property-based and deflection-based estimates of subgrade modulus developed with Champaign County data. The validation data represent soils located in Sangamon, Livingston, Mercer, and Marion counties in Illinois. The analyses conducted for each set of data involve five basic steps, as follows.

1. E_{Ri} is back-calculated from FWD deflection data by using the appropriate ILLI-PAVE-based algorithm (Equations 3 through 6).
2. E_{Ri}(OPT) is estimated for each soil horizon by using soil index properties obtained from the appropriate county soil survey and Equations 1 and 2.
3. The E_{Ri}(OPT) estimate is adjusted for moisture contents above optimum (OPT + n) by using the appropriate moisture adjustment factor from Table 1.
4. A composite E_{Ri} estimate is developed for each moisture condition to account for soil horizonation by using the relative horizon thickness for all horizons.

TABLE 4 Relationship Between USDA Drainage Class and Degree of Saturation for Champaign County Soils

Soil Series	USDA Natural Drainage Class	Design Moisture Condition (OPT+n)	Req'd Deg. of Saturation (%)	Design Deg. of Saturation (%)	Design Eri (ksi)
56 Dana	Mod. Well	1.9	79	80	4.2
146 Elliott	SW Poor	3.7	93	90	6.9
152 Drummer	Poor	5.8	107	100	4.4
154 Flanagan	SW Poor	3.9	88	90	3.6
232 Ashkum	Poor	6.5	102	100	5.9
481 Raub	SW Poor	4.0	86	90	2.4

NOTE: 1 ksi = 6890 kPa

TABLE 5 Moisture Adjustment Ratios for Champaign County Soils

Soil Series	Moisture Adjustment Factor (Table 1)	Required Moisture Adjustment	Optimum Moisture Content (%)	Moisture Adjustment Ratio MAR	Design Moisture Condition* OPT+ :	Design Eri** (ksi)	Design Eri*** (ksi)
56 Dana	1.9	1.68	13.6	0.12	3.94	1.6	0.2
146 Elliott	0.7	4.29	17.6	0.24	5.10	6.0	5.9
152 Drummer	0.7	7.14	13.6	0.53	3.94	5.6	5.6
154 Flanagan	1.4	3.57	14.6	0.24	4.23	1.7	3.1
232 Ashkum	0.7	7.00	18.9	0.37	5.48	6.9	6.6
481 Raub	1.4	3.21	12.8	0.25	3.71	1.5	2.8

NOTES: * *Determined using Champaign County average MAR = 0.29*
** *Determined from Table 5*
*** *Calculated Value*

1 ksi = 6890 kPa

5. Design soil property-based E_{Ri} values are estimated by using the relationship between soil drainage class and degree of saturation and MAR concepts developed for Champaign County soils.

Evaluation of Validation Results

Comparisons of soil-property-based E_{Ri} values and deflection-based modulus estimates produce mixed results. In many cases soil-property-based estimates compare favorably with deflection-based estimates. However, for some soil series the E_{Ri} values estimated by using soil properties overestimate or underestimate the subgrade modulus compared with those obtained by using deflection-based estimates.

MAR-Based Design E_{Ri} Figure 3 shows a comparison of deflection-based E_{Ri} values and soil-property-based E_{Ri} values calculated by using the Champaign County average MAR (0.29). Ideally, points would group around the 1:1 line, indicating good agreement between different estimates of the subgrade modulus. Most of the points shown in Figure 3 fall below the 1:1 line, indicating that values of E_{Ri} calculated with the Champaign County average MAR underestimate the subgrade modulus compared with those calculated with deflection-based estimates. A best-fit line developed by linear regression is shown on Figure 3. This line reflects a rather poor fit (r^2 = 0.06; correlation coefficient, 0.25) to the data. Although some soils are adequately represented in Figure 3, it is apparent that use of the MAR relationship developed for one area (e.g., Champaign County) to estimate the E_{Ri} for soils in other areas may not give accurate, consistent results.

The overall average and standard deviation MAR determined with information from all soils investigated are 0.24 and 0.12, respectively (coefficient of variation = 50 percent). The large variability in MAR values, as indicated by the relatively high coefficient of variation, suggests that a single value of MAR cannot adequately represent all subgrade soils. Linear regression performed on soil-property-based E_{Ri} values calculated by using the overall MAR average and corresponding deflection-based values shows a better fit to the data (r^2 = 0.11; correlation coefficient, 0.33), but many soils continue to be poorly represented.

Soil-property-based E_{Ri} values calculated with a single MAR value may adequately estimate the subgrade modulus for some soil series, whereas they may significantly overestimate or underestimate the modulus for other soil series. It is apparent from the analyses that the most promising method of using MAR concepts is to establish individual MAR relationships for regions (e.g., counties) containing relatively uniform soils. Figure 4 is a plot similar to that shown in Figure 3, with soil property-based E_{Ri}

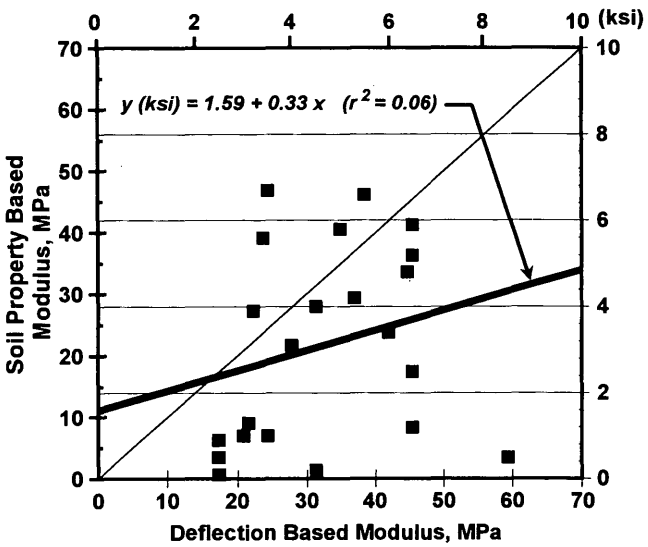

FIGURE 3 Comparison of design soil-property-based and deflection-based subgrade modulus using Champaign County average MAR.

values calculated by using the specific "county MAR average" for the county (or testing site) in which the soil is encountered. The plot shown in Figure 4 is the best relationship between MAR-based E_{Ri} values and deflection-based values. The linear regression fit is characterized by an r^2 value of 0.31 and a correlation coefficient of 0.56.

Natural Drainage Class–Degree of Saturation Based E_{Ri}

There is a relationship between the natural drainage class of the soil and the in situ moisture conditions required for soil-property-based E_{Ri} estimates to match FWD deflection-based estimates. In general, less-well-drained soils relate to higher moisture conditions. The natural drainage–moisture condition relationships developed by using information on Champaign County soils may or may not apply to many of the soils from other Illinois counties. Figure 5 shows soil-property-based E_{Ri} values determined by using the Champaign County drainage class–degree of saturation relationship plotted against corresponding FWD deflection-based E_{Ri} estimates. Many of the points group closely to the 1:1 line, but there are a number of outlying points. A line fit to the data by linear regression (r^2 = 0.008; correlation coefficient, 0.091) suggests that adjusting soil-property-based modulus estimates by using degree of saturation relationships yields results similar to those obtained by using the overall average MAR adjustment.

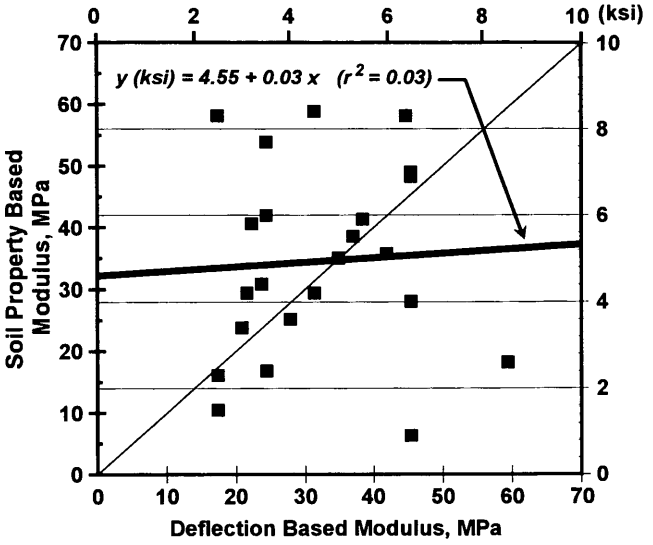

FIGURE 5 Comparison of design soil-property-based and deflection-based subgrade modulus using relationship between natural drainage class and degree of saturation.

SUMMARY

Two methods were developed to relate soil-property-based E_{Ri} estimates and FWD deflection-based E_{Ri} estimates. The methods include the use of an MAR, which is a function of the optimum moisture content of the soil, and a relationship between the soil's natural drainage class and the required degree of saturation.

Figures 3 through 5 illustrate the relationship between soil-property-based and target FWD deflection-based values of E_{Ri}. The points shown in the figures represent the 23 major pedologic soil series encountered during FWD testing in Champaign, Sangamon, Livingston, Mercer, and Marion counties in Illinois. Analyses of the data indicate that the best method of using the MAR is to determine the average MAR for the specific county in which FWD testing is performed.

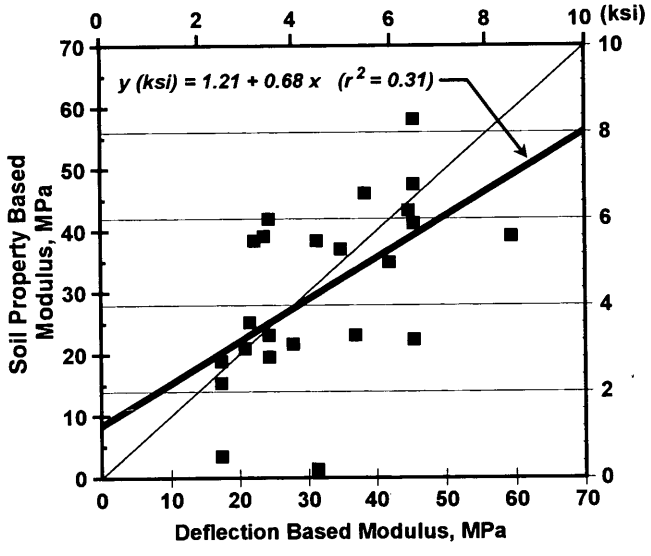

FIGURE 4 Comparison of design soil-property-based and deflection-based subgrade modulus using individual county average MAR.

The average difference between soil-property-based and deflection-based E_{Ri} estimates for the points shown in Figures 3 through 5 are as follows: Figure 3, 15.2 MPa (2.2 ksi); Figure 4, 9.7 MPa (1.4 ksi); and Figure 5, 13.1 MPa (1.9 ksi). A difference in E_{Ri} of 10.3 to 13.8 MPa (1.5 to 2.0 ksi) may represent only 1 percent moisture in subgrade soils on the basis of the moisture adjustment factors shown in Table 1. In addition sensitivity analyses performed on current flexible pavement design procedures indicate for most cases that a variation in E_{Ri} of 6.9 to 13.8 MPa (1 to 2 ksi) is not significant in pavement design (*9*). The coefficients of variation for average differences in soil-property- and deflection-based E_{Ri} values for Figures 3 to 5 range from about 80 percent to about 100 percent, indicating a wide range of differences. However, it should be noted that in situ subgrade modulus values within a given project will vary; in the present study the coefficient of variation of deflection-based modulus estimates for a particular soil series ranged from about 10 percent to as high as about 80 percent, with a typical range of values being 30 to 50 percent (*9*). In many cases the principles developed in the research for determining design E_{Ri} values on the basis of soil index properties give reasonable estimates of the subgrade modulus.

There are difficulties in comparing values of subgrade modulus that are estimated by dissimilar procedures. In the present study the differences between soil-property-based and deflection-based modulus estimates are analyzed solely on the basis of moisture content and the moisture adjustment factors shown in Table 1. It is apparent that factors other than moisture content should be considered to totally explain the observed differences in the modulus estimate. One example of other considerations concerns the fact that soil properties are listed in the county soil survey as ranges

of values. The present analysis used midrange values for soil properties. The variation in soil properties within a particular soil series explains some of the differences in modulus estimates.

Another consideration in analyses such as those described in this paper concerns the time of year in which deflection testing is performed to estimate in situ subgrade modulus. The FWD testing for the present study was performed in March, which could be considered the worst time of year with respect to subgrade moisture in central Illinois. Whether an agency decides to use extreme subgrade conditions to develop a conservative design or average conditions with an applied reliability factor, care must be taken to ensure that the actual subgrade conditions are representative of the target conditions. The time of year of FWD testing will have an impact on the relationship between deflection-based modulus estimates and soil-property-based estimates.

The analyses described in this paper suggest that the relationship between soil-property-based E_{Ri} and deflection-based E_{Ri} depends somewhat on the predominant soil series of an area. The most reliable and consistent method of characterizing the resilient properties of soil series in a particular area requires deflection testing in the area to correlate with soil-property-based subgrade modulus estimates. The use of generic or blanket relationships between soil-property-based and deflection-based E_{Ri} estimates may lead to less accurate modulus estimates for local soils. The methodologies presented here are easily adapted by pavement agencies to local conditions, potentially providing a valuable alternative to doing nothing with regard to subgrade evaluation for pavement design.

ACKNOWLEDGMENTS

This research is based primarily on Project IHR-527, Mechanistic Design for Local Roads, conducted by the University of Illinois at Urbana-Champaign. The project was sponsored by the Illinois Department of Transportation.

REFERENCES

1. *Final Report, NCHRP Project 1-26: Calibrated Mechanistic Structural Analysis Procedures for Pavements,* Vol. 2. TRB, National Research Council, Washington, D.C., 1990.
2. Drumm, E. C., Y. Boateng-Poku, and T. J. Pierce. Estimation of Subgrade Resilient Modulus from Standard Tests. *Journal of the Geotechnical Division,* ASCE, Vol. 116, No. 5, May 1990.
3. Elliott, R. P., et al. *Resilient Properties of Arkansas Subgrades.* Final Report, TRC 94. Arkansas Highway and Transportation Research Center, University of Arkansas, Fayetteville, 1988.
4. Farrar, M. J., and J. P. Turner. *Resilient Modulus of Wyoming Subgrade Soils.* MPC Report 91-1. Mountain Plains Consortium, 1991.
5. Thompson, M. R., and Q. L. Robnett. Resilient Properties of Subgrade Soils. *Transportation Engineering Journal,* ASCE, Vol. 105, No. TE1, January 1979.
6. Thompson, M. R., and T. LaGrow. A Proposed Conventional Flexible Pavement Thickness Design Procedure. In *Civil Engineering Studies.* Transportation Engineering Series No. 55. University of Illinois, 1988.
7. *Final Report, NCHRP Project 1-26: Calibrated Mechanistic Structural Analysis Procedures for Pavements,* Vol. 1. TRB, National Research Council, Washington, D.C., 1990.
8. Buol, S. W., F. D. Hole, and R. J. McCracken. *Soil Genesis and Classification,* 3rd ed. Iowa State University Press, Ames, 1989.
9. Hall, K. D. *Pedologic Based Subgrade Characterization for Low-Volume Pavement Design.* Ph.D. thesis. University of Illinois, Urbana, 1993.
10. Elliott, R. P., and M. R. Thompson. Mechanistic Design Concepts for Conventional Flexible Pavements. In *Civil Engineering Studies.* Transportation Engineering Series No. 42. University of Illinois, 1985.
11. Gomez-Achecar, M., and M. R. Thompson. ILLI-PAVE Based Response Algorithms for Full-Depth Asphalt Concrete Flexible Pavements. In *Transportation Research Record 1095,* TRB, National Research Council, Washington, D.C., 1986.
12. *Soil Survey of Champaign County, Illinois.* Soil Conservation Service, U.S. Department of Agriculture, 1990.
13. Wilson, T., and M. R. Thompson. Pedologic Soil Series-Resilient Moduli Relations. Document 89-51-03. Advanced Construction Technology Center (sponsored by the Army Research Office), University of Illinois, 1989.
14. *Soils Manual.* Bureau of Design, Illinois Department of Transportation, Springfield.

Publication of this paper sponsored by Committee on Flexible Pavement Design.

Pavement Thickness Variability and Its Effect on Determination of Moduli and Remaining Life

NII OTOKUNOR ATTOH-OKINE AND W. M. KIM RODDIS

Variation in layer thickness can result in variations in the structural characteristics and in-service performance of a pavement. Pavements can vary substantially in thickness within one pavement management section. Discrete thickness measurement approaches, such as coring, may miss significant changes in the continuous thickness profile. The effects of variable asphalt pavement layer thickness on the composite back-calculated moduli and remaining life before overlay are investigated. In-service pavements selected to cover a range of thickness, structural, and functional conditions were investigated. Ground-penetrating radar was used to measure continuous thickness profiles of pavement sections so that the actual thickness variability of in-place pavements was used as the basis for the study. Discrete pavement thickness was obtained by destructive coring. Dynaflect testing was performed to measure pavement deflection. By using the continuous thickness profile obtained from the radar survey, the effect of variability of asphalt cement-bound layer thickness on the remaining life before overlay and back-calculated moduli of the asphalt cement-bound layers was investigated. The effect of variability of thickness on remaining life prior to overlay is very pronounced.

Knowledge of asphalt layer thickness is important in many areas of pavement management. The layer thicknesses, which represent an element of the Pavement Management System (PMS) data base, are required for load rating, overlay design, and setting of maintenance and rehabilitation priorities. A rational Project Optimization System requires correct pavement thickness data for performance prediction modeling. Negative economic effects and reductions in remaining life are consequences of both underestimates and overestimates of actual pavement thickness. For direct overlay projects an underestimate of existing pavement thickness will result in a conservative overlay design with excessive cost, whereas an overestimate will result in a design that will not achieve the desired service life. For milling and recycling projects, an underestimate of existing thickness may falsely indicate that a direct overlay would be more cost-effective, whereas an overestimate may result in an inadequate amount of material for reuse. Possible equipment breakthrough on the reduced structure of the milled pavement may also occur.

Layer thickness can be determined from historical data base records or coring. Thicknesses from historic data base records are frequently inaccurate or nonexistent, whereas coring is destructive, time-consuming, expensive, and intrusive to traffic. Ground-penetrating radar (GPR) is a noncontact technique that has the potential for use in surveying pavement thickness while operating at near highway speed, and the GPR-generated continuous pavement thickness profiles provide important data for pavement management systems.

Asphalt layer thickness is an important variable in the back-calculated moduli of pavements. Minor changes in asphalt layer thickness can produce significant changes in the analytical results of elastic properties of the pavements (*1*). Normally, one or more cores are used to directly measure in situ layer thickness. Variation in construction and natural terrain make some variability in layer thickness inevitable. The impact of variation of asphalt layer thickness on the back-calculated modulus has been investigated by Irwin (*2*) and Rodriguez-Gomez et al. (*3*). In those studies all of the thickness data were based on simulation.

The purpose of this paper is to investigate the effect of variable asphalt layer thickness on the composite back-calculated moduli and remaining life before overlay. The study described here, unlike the previous studies, investigates in-service pavements selected to cover a wide range of pavement thickness, structural, and functional conditions. Furthermore, continuous thickness profiles of pavement sections were obtained from the GPR survey so that the actual thickness variabilities of in-place pavements were used as the basis for the study.

FIELD STUDY

The objective of the site selection was to ensure that the selected pavement segments would be a representative cross-section of a highway population unit managed at the network and project levels, in particular, the highways of the Kansas Department of Transportation (KDOT) road system.

The KDOT PMS classifies paved highways into 23 categories by pavement type, function, traffic level, and width as illustrated in Figure 1. The pavement types are (*a*) portland cement concrete (PCC); (*b*) composite pavement (Comp), PCC pavement, or brick that has been overlaid with asphalt concrete; (*c*) full design bituminous pavement (FDBit), designed and constructed to carry expected traffic; and (*d*) partial design bituminous pavement (PDBit), not designed or constructed to carry expected traffic. The two functional classifications of the road categories are "Interstate" and "other." The traffic levels are based on annual average daily traffic (AADT) counts expressed in terms of daily equivalent 18-kip axle loads (ESALs) in one direction and are categorized as low (less than 87 ESALs), medium (between 87 and 162 ESALs), or high (greater than 162 ESALs) use. Widths are categorized as less than 32 feet or 32 feet and greater.

N. O. Attoh-Okine, Department of Civil Engineering, Florida International University, Miami, Fla. 33199. W. M. K. Roddis, Department of Civil Engineering, 2008 Learned Hall, University of Kansas, Lawrence, Kans. 66045.

Pavement Type		PPC			Comp			FDBit			PDBit		
Traffic		L	M	H	L	M	H	L	M	H	L	M	H
Function	Width												
Interstate	< 32 ft	1		2	3		4	5					
	32 ft												
Other	< 32 ft	6	7	8	9	10	11	12	13	14	18	19	20
	32 ft							15	16	17	21	22	23

FIGURE 1 Kansas highway network road categories.

For the purpose of the present study pavement type is the most important road characteristic because the objective depends on the effect of variable asphalt layer thicknesses. Therefore only the asphalt pavement types (Comp, FDBit, PDBit) are of interest. The 23 road categories used for the entire Kansas road network were reduced to 10 road categories for inclusion in the study, as indicated by the shaded cells in Figure 1.

The primary criterion in selecting the specific road segments to represent each category was that the in-service segments chosen have documented construction history, maintenance history, and current pavement surface condition. This allowed a choice of road segments with a range of physical characteristics. Additional criteria were to have multiple asphalt overlays in place on several sites. The sites selected covered a range of subbase materials (bituminous-treated, lime-treated, crushed limestone, natural gravel, and cement-treated bases).

Table 1 lists the pavement structures of the sites included in the thickness survey. The individual layers of the structure in Table 1 were obtained from data in the KDOT pavement management data base. Discrepancies were found between KDOT pavement management data base records and the in-place pavements with regard to pavement type. Site 15 was classified in the records as a fully designed bituminous category. From the cores it was clear that the site is a partially designed pavement. Site 23 was classified in the records as a partially designed bituminous category. The cores showed that the site is a fully designed pavement. Maintenance histories earlier than 1970 were not available. Before 1970 the KDOT standard operating procedure was to apply a seal coat every 3 years. For this reason when using data base values to determine asphalt thicknesses, KDOT's rule of thumb was to add 0.1 in. for each year of pavement service prior to 1970. This accounts for pavement thickness build-up because of repeated applications of seal coating. This adjustment is included in Table 1.

DATA COLLECTION

GPR was used to obtain continuous thickness data at the selected sites. Each site was 1,000 ft long, and GPR data were acquired at longitudinal intervals of 5 ft. Each site was tested with one pass of the radar van, in the inner wheelpath of the outside lane. At Site 3 radar surveys were conducted in both the inner wheelpath and between the wheelpaths of the passing lane. By subtracting the two computed thicknesses, rut depth throughout the section can be computed. All radar data were digitized and stored on hard disk by using an IBM-compatible 386 computer housed in the van. The radar thickness data were subsequently analyzed by Infrasense, Inc., Cambridge, Massachusetts, by using its PAVLAYER customized software for the radar pavement application. Continuous thickness profiles were generated for each site. Figure 2 shows the thickness profile for Site 21.

Locations for coring were determined after preliminary analysis of the continuous thickness profiles generated from the radar data. This analysis revealed locations where significant variations in thickness occurred. The first 10 field sites listed in Table 1 were cored to determine total asphalt-bound thickness and individual mixture layer thickness.

TABLE 1 Pavement Layers from KDOT Data Base

	Asphalt											
	Layer 1			Layer 2			Layer 3			Base Layer		
Road Category	(in.) Thick	Material	Year	(in.) Thick	Material	Year	(in.) Thick	Material	Year	(in.) Thick	Material	Year
3	3.0	BM2	1979	1.0	BM1	1979			1950-70	9.0	PCCPAV	1950
4	1.0	BM1	1980	3.0	BM2	1980				9.0	PCCPAV	1956
5	0.75	BM2	1981	1.0	HM31	1973	1.0	HM3	1973	16.0	ACB3	1973
11	1.0	BM1	1984	2.0	BM7	1984				9.0	PCCPAV	1968
12	1.5	BM1	1979							2.0	BITCOV	1979
15	1.5	BM2A	1990	1.5	BM2	1983	2.3	Maint	1947-70	2.0	BITCOV	1947
17	4.0	BM3	1975							9.0	BM4	1975
18	2.0	BM2	1988	0.75	BM2	1988	2.3	Maint	1947-70	6.0	BM2A	1947
21	2.0	BM1B	1990	1.5	BM1	1981	1.8	Maint	1952-70	2.0	BITCOV	1952
23	1.5	BM2	1982	1.0	BITCOV	1950	2.0	Maint	1950-70	6.0	AB	1950
SHRP*	4.0	HM3	1972							7.5	ACB3	1972

Legend

AB	Aggregate binder	HM3	Hot mixture 3
ACB3	Asphalt concrete base mix	HM31	Hot mixutre 31
BITCOV	Bituminous cover	HM6	Hot mix
BM1	Bituminous mixture 1	PCCPAV	Portland cement concrete
BM1B	Bituminous mixture 1B	Maint	Maintenance seal
BM2	Bituminous mixture2		
BM2A	Bituminous mixture2A		
BM3	Bituminous mixture3		

*SHRP LTPP GPS 201005 Site, Road Category 17

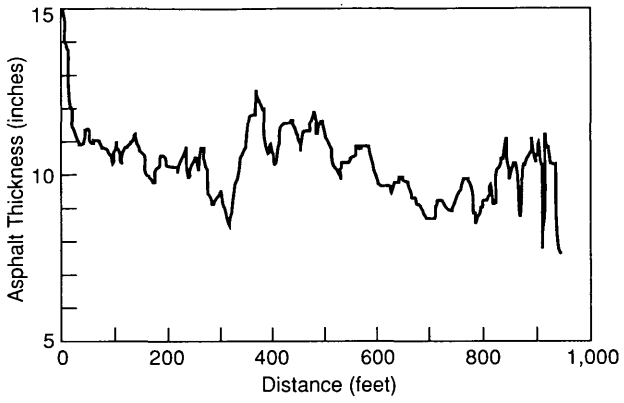

FIGURE 2 Continuous asphalt thickness profile for Site 21.

DEFLECTION TESTING

KDOT evaluates pavement structural condition by using the Dynaflect system. Dynaflect deflection measurements were made at 50-ft intervals located within each 1,000-ft test site in the inner wheelpath. This is far in excess of the number of tests required for routine pavement evaluation. The large quantity of data was obtained to allow assessment of variable thickness on deflection and hence on modulus. The Dynaflect system consists of a dynamic force generated mounted on a small two-wheel trailer with a control unit. It applies a cyclic dynamic load that generates a force with an amplitude of 1,000 lb on each wheel at a fixed frequency of 8 Hz. The load is applied at two points, and surface deflections are measured by geophones.

DATA ANALYSIS

After the continuous radar survey was completed, cores were obtained from the pavement and total and mixture layer thicknesses were recorded. Deflection measurements, coupled with asphalt concrete thickness layers, were used to estimate the composite back-calculated moduli. The moduli were subsequently used to determine the 1986 AASHTO design guide (*4*) layer coefficients of the composite asphalt concrete layers. The above layer coefficients were subsequently used to calculate the effective structural number, allowing the determination of the AASHTO remaining life before overlay of flexible pavements.

Variability of Asphalt-Bound Layer Thickness

A measure of variability of asphalt concrete layer thickness can be expressed in terms of the mean squared deviation from the mean thickness, that is, the variance, as defined in Equation 1, where x_i is the thickness of core i, $\bar{x}$ is the mean of all core thicknesses, and n is the sample size. However, the variability of the layer thickness can be more easily interpreted in terms of two statistical measures related to the variance. These are the standard deviation (Equation 2) and the coefficient of variation, defined as the standard deviation of the mean (Equation 3).

$$\text{Variance} = \sigma^2 = \sum_{i=1}^{n} \frac{|(x_i - \bar{x})|}{n - 1} \quad (1)$$

$$\text{Standard deviation} = \sigma = \sqrt{\sigma^2} \quad (2)$$

$$\text{Coefficient of variation} = V = \frac{\sigma}{\bar{x}} \quad (3)$$

The standard error (i.e., standard deviation) of the mean thickness, $\sigma_{\bar{x}}$, for a particular sample size can be estimated by (*5*)

$$\sigma_{\bar{x}} = \frac{\sigma}{\sqrt{n}} \quad (4)$$

where n is the number of cores, and σ is the population standard deviation of individual sampling units. Because it is not possible to know beforehand what the population standard deviation will be, σ is replaced with S_R, the standard deviation of thickness from the radar survey for the 1,000-ft test section (about 200 points).

In a random sampling of n cores, if the sampling process were repeated a large number of times, the distribution of the resulting sample means would approximate a normal distribution, as predicted by the central limit theorem. The average value of these sample means would be expected to equal the true thickness of the pavement section. Because of the normality assumptions, 68 percent of the sample mean thickness values would be expected to fall within ± 1.0 standard deviation of the actual thickness, and 95 percent of the thickness values will fall within ± 1.96 standard deviations of the actual thickness. In a more precise way, it can be expected that at the 68 percent confidence level that thickness from a particular location estimate is within ± 1.0 standard deviation of the actual thickness and at the 95 percent confidence level that the estimated thickness is within ± 1.96 standard deviations of the actual thickness.

To state the desired accuracy of a particular estimate, it is first necessary to specify an acceptable degree of error between the estimated and actual thicknesses, and then a degree of confidence that represents an acceptable difference or error between the estimated thicknesses and actual thicknesses is selected:

$$\epsilon = Z\sigma_{\bar{x}} \quad (5)$$

where ϵ is the acceptable error, and Z, the standard normal value, is a parameter based on the desired degree of confidence. Taking S_c as the standard deviation of thickness from the cores, the number of cores required is then equal to

$$n = \left(\frac{S_c Z}{\epsilon}\right)^2 \quad (6)$$

For a particular pavement type it is useful to know how many cores are required to achieve a specified acceptable error. Table 2 shows the pavement thickness data statistics comparing continuous GPR profiles, discrete destructive cores, and KDOT data base records. By using the radar standard deviation measured over the entire test section as a measure of variability, for composite pavement (Sites 3, 4, and 11) the highest variability is 0.40 (Site 3) and the lowest variability is 0.21 (Site 11). For FDBit (Sites 5, 12, 17, 23, 17SHRP) the lowest variability is 0.61 (Site 17) and the highest variability is 1.3 (Site 17SHRP). For PDBit (Sites 15, 18, and 21) the lowest variability is 0.38 (Site 15) and the highest variability is 1.07 (Site 21). This variability is based on the radar-generated continuous thickness profiles, sampling approximately

TABLE 2 Pavement Layers from KDOT Data Base

Road Category	AVERAGES at Core Sites Radar (in.)	Cores (in.)	DIFFERENCES Between Radar and Cores Inches	%	STANDARD DEVIATION Radar at core sites	Radar complete section	Cores	KDOT DATA BASE KDOT Data (inches)	Differences KDOT Core
3	4.64	4.41	0.23	5.30	0.23	0.40	0.22	4.0	–0.41
4	3.30	2.79	0.51	18.28	0.27	0.24	0.26	4.0	1.2
5	21.66	19.17	2.49	13.00	0.54	0.63	0.76	18.75	–0.42
5[d]	19.19	19.17	0.02	0.10					
11	2.82	2.63	0.19	7.31	0.22	0.21	0.22	3.0	0.37
12	7.37	7.41	–0.04	–0.57	0.92	0.80	0.87	3.5	–3.91
15	9.60	8.36[a]	1.23	14.76	0.54	0.38	1.03	7.3[e]	–1.03
17	14.32	14.03	0.30	2.11	0.86	0.61	0.24	13.0	–1.03
18	11.92	10.12[b]	1.79	17.70	0.30	0.44	0.11	11.05[e]	0.93
21	10.91	10.71	0.20	1.87	1.99	1.07	1.04	7.3[e]	–3.41
23	12.46	12.55	–0.09	–0.70	1.35	0.62	0.89	10.5[e]	–2.05
17(SHRP)	14.20	13.35	0.85	6.39	0.16	1.3	[c]	11.5	–1.85

Notes: [a] questionable data due to poorly defined asphalt/soil base
[b] questionable data due to core damage during drilling
[c] insufficient data (less than 5 cores)
[d] calibrated by 1 core
[e] for the period 1950-1970, these figures assume one chip seal every 3 years, with an average thickness of 0.33 inches/chip seal

TABLE 3 Number of Required Cores per 1,000 ft for 0.25-in. Acceptable Error

Pavement Type	Number of Cores	
	95 Percent Confidence Intervals	68 Percent Confidence Intervals
COMP	3	1
FDBit	29	8
PDBit	32	8

200 points on each 1,000-ft roadway section. Using average standard deviations and setting an acceptable error of 0.25 in. for illustration, the numbers of cores required within a 1,000-ft section were computed by using Equation 6 and Z values of 1.96 for 95 percent confidence intervals and 1.0 for 68 percent confidence intervals. The results are presented in Table 3.

The high number of cores obtained at the 95 percent confidence limit indicates that with the exception of composite pavements, a considerable amount of destructive coring is needed to achieve the 95 percent confidence limit. In contrast the radar can be used to obtain the same confidence limit without destructive coring.

Deflection Testing and Interpretation

Deflection testing and interpretation refer to the direct use of representative pavement surface deflections and deflection basin parameters as a means of quantifying the structural adequacy (or lack thereof) of a pavement structure without relating that adequacy to the fundamental properties of the pavement and the materials with which it was constructed (*6*). Deflection basin parameters are widely used for three major applications: (*a*) to check the structural integrity of in-service pavements, (*b*) to define critical pavement response, and (*c*) to calculate the in situ layer moduli.

For the present study the deflection basin parameters were used to calculate the in situ combined layer (all asphalt-bound layers) moduli. Hall and Mohsenni (*7*) outlined the limitations of existing back-calculation methods for estimating the modulus of an asphalt concrete overlay of a PCC pavement. For this reason, modulus back-calculation in the present study was limited to FDBit and PDBit pavements. Deflection testing was conducted at five sites; two were FDBit (Sites 5 and 17) and three were PDBit (Sites 15, 18, and 21). The mean, standard deviation, and coefficient of variation of the five Dynaflect sensors at each site were determined, and the variability across the sites was studied (Table 4). Since the coefficient of variation has a normalizing effect, Houston and

TABLE 4 Sensor Values

Site	Std.* Dev.	Coefficients of Variation (%) S1	S2	S3S4		S5	Average for site
5	0.63	8.3	8.0	7.4	8.1	7.3	7.8
15	0.38	14.0	12.9	14.6	16.1	21.3	15.7
17	0.61	35.9	21.4	23.1	25.4	22.2	25.6
18	0.44	14.6	15.3	16.6	17.6	19.4	16.7
21	1.07	19.7	15.3	16.6	17.6	19.4	20.8
Average Across Sites		18.5	14.6	15.7	17.0	17.9	16.7

* Complete Radar Data

Perera (*8*) commented that an average coefficient of variation of greater than 13 percent is the result of a material or site change.

The average coefficient of variation for the five Dynaflect sensors across the sites is 18 percent and is the result of site differences. The sites showing the greatest variability for the Dynaflect test were Sites 17 and 21, having average coefficients of variation of 25.6 and 20.8 percent, respectively. Table 4 shows that the variability in pavement thickness, as measured by the standard deviation for the complete section radar profile, generally correlates (r = 0.46) with the variation in deflection sensor values. The exception is Site 5, which was found to be thick and stiff. Thus, the deflection variation is small, as would be expected for a stiff pavement. The 0.63-in. standard deviation in thickness is also a small variation in the total pavement thickness of 20 in.

Four parameters were computed from the Dynaflect measurements, in which S_1, S_2, S_3, S_4, and S_5 are deflections at sensors 1, 2, 3, 4, and 5, respectively.

1. Dynaflect maximum deflection (DMD) = S_1,
2. Surface curvature index (SCI) = $S_1 - S_2$,
3. Base curvature index (BCI) = $S_4 - S_5$, and
4. Spreadability (SPD) = 100 $(S_1 + S_2 + S_3 + S_4 + S_5)/5S_5$.

Dynaflect maximum deflection is a measure of the pavement structural capacity and support conditions. The surface curvature index is predominantly an indicator of the structural condition of the surface layer. The base curvature index measures base support conditions. Spreadability measures the load-carrying capacity and the stiffness ratio of the pavement structure. Furthermore, Dynaflect maximum deflection has been shown to indirectly measure the subgrade modulus.

For each site the average values of DMD, SCI, BCI, and SPD were determined. Table 5 presents the results. Comparing the DMD and SCI values in Table 5 with the layer thicknesses in Table 2, the DMD and SCI values generally increase with decreasing thickness. This is typical for flexible pavement layers in good condition. Thus, Dynaflect measurements indicated that all test sections were typical of in-service flexible pavements without obvious defects in structural condition.

Back-Calculation of Layer Moduli

Back-calculation is a computational procedure that uses elastic-layer theory to define a plausible set of layer moduli that would theoretically result in a deflection basin that matches the measured deflection basin to within a specified tolerance. However, more than one set of moduli may satisfactorily produce a layered structure response that duplicates the measured deflection basin. If the tolerance is sufficiently tight and the deflection basin data are reliable, a reasonable set of comparable moduli can be found. Although it cannot be said that the moduli of the pavement materials are absolutely correct (*8*), they can be used to adequately model the behavior of the pavement under actual traffic loading.

Layer thickness is an important independent variable in the back-calculation of moduli. As the layer becomes thinner, the layer thickness input must be more precise. Although it is almost certain that some of the layers in a pavement system are nonlinear in their response to loading, pavements are modeled as linearly elastic systems in back-calculation algorithms.

The deflections calculated from the Dynaflect tests were used as inputs to MODULUS (*9*), a program that back-calculates the elastic composite modulus of the total asphalt layer. The numbers of pavement layers were determined from coring and radar waveforms. Two-layer or three-layer back-calculation analysis was performed as appropriate for the pavement structure determined by radar and corings. Two analyses were made:

1. Back-calculation using the thickness and structure obtained from the radar survey, and
2. Back-calculation using the thickness and structure obtained from destructive coring.

The following assumptions were made:

1. All asphalt layers were considered to be a single composite layer, giving one modulus for all asphalt-bound materials. Poisson's ratio was assumed to be equal to 0.35 for asphaltic concrete.
2. The material in each layer was linear, homogeneous, and isotopic.
3. The layers overlaying the elastic half space were weightless, finite in thickness, but infinite in the horizontal plane.
4. Inertia effects were neglected.
5. The boundary conditions were as follows:
   a. Layers were in continuous contact. There were no normal stresses outside the loaded area at the top of asphalt concrete layer; the surface was free from shearing stress.
   b. Horizontal strains across the interface were equal.
   c. Temperature effects were neglected.

A paired t-test was used to determine whether there was a significant difference between pavement moduli back-calculated from core thickness and radar thickness. With the exception of Site 5, the results of the paired t-test show that composite moduli of pavement are not significantly influenced by the procedure used to measure thickness. That is, radar and core data result in similar moduli. The anomalous behavior for radar on Site 5 is explained by the profile-generating software PAVLAYER. As used in the present study, the software model assumes constant dielectric properties for the pavement with respect to depth. For very thick pavements, such as at Site 5, which is 20 in. thick, this assumption does not match the actual trend of higher moisture content with depth. The radar method thus overestimated the thickness, resulting in a significant difference on the t-test. This difficulty occurs only on very thick pavements and can be corrected by use of a single calibration core when generating the profile as shown for Site 5 in Table 2 (footnote *d*).

Remaining Life Before Overlay

The remaining life of the existing pavement structure before the construction of an overlay is a difficult parameter to determine

TABLE 5 Dynaflect Parameters

Site	Mean			
	DMD	SCI	BCI	SPD
5	2.9	0.1	0.3	158
15	8.8	1.9	0.9	217
17	4.9	1.1	0.4	156
18	11.0	2.5	1.1	145
21	7.6	1.0	0.9	220

accurately. Remaining life is the estimated number of years or axle loads from a given date (usually from the last survey date) needed by a pavement section to accumulate distress equal to the threshold value.

In the present analysis the 1986 AASHTO design guide and a nondestructive testing approach were used. The remaining life before overlay was estimated by using a pavement condition factor, which is the percentage of remaining life before overlay found by comparing the effective structural number of the existing pavement (SN_{xeff} determined from radar survey and destructive coring) to the original structural number SN_0. The pavement condition factor C_x is calculated as

$$C_x = SN_{xeff}/SN_0 \quad (7)$$

given that SN_{xeff} equals $a_1D_1 + a_2D_2m_2 + a_3D_3m_3$, where

a_i = layer coefficients of pavement layers,
D_i = thicknesses of individual layers, and
m_i = drainage coefficients of individual layers.

Given C_x, the remaining life, RL_x, is determined from the 1986 AASHTO design manual, Figure 5.13, Remaining Life Estimate Predicted from Pavement Correction Factor (*4*). The SN_0 of the original pavement was assumed to be 4.50 on the basis of the standard assumption by KDOT for new pavement construction.

Only the asphalt concrete layers were considered in the computation of SN_{xeff}. This is because the thicknesses of other layers such as untreated base were not available from either the radar survey or destructive coring. At some sites the base consisted of stabilized asphalt, so the total thickness was used as the asphalt concrete layer.

By using the composite moduli obtained by using radar and core thicknesses, the layer coefficients of the asphalt material were determined by using AASHTO design manual Figure 2.5, Chart for Estimating Structural Layer Coefficient of Dense-Graded Asphalt Concrete Based on the Elastic (Resilient) Modulus (*4*). The value was then multiplied by the layer thickness obtained from the radar survey and destructive coring to obtain the effective structural number SN_{xeff}. The condition factor of the pavement C_x is then determined by Equation 7.

Figures 3 and 4 show the remaining life before overlay of selected sites. When C_x was greater than 1, the remaining life before overlay was assumed to be 100 percent. Figure 3 illustrates the

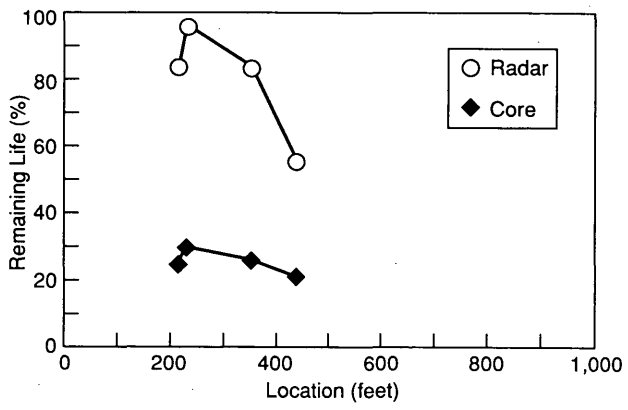

FIGURE 3 Remaining life before overlay for Site 18.

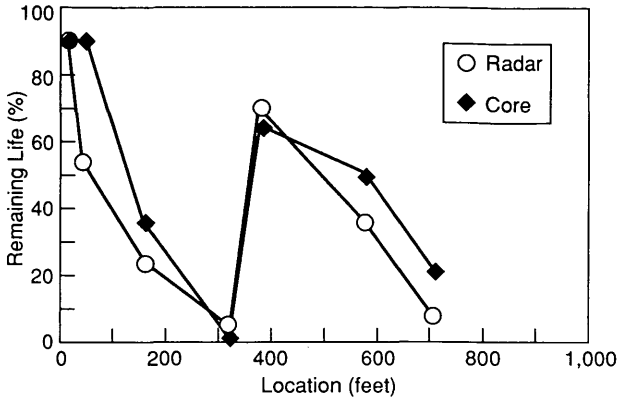

FIGURE 4 Remaining life before overlay for Site 21.

remaining life prediction for Site 18. The estimates of remaining life before overlay obtained by the radar approach were far greater than those obtained by the coring approach. The maximal difference in the remaining life estimates was about 70 percent. On this site there was a difference of 10 percent between the radar-based thickness and the core-based thickness, with radar giving the higher values. This shows how a small thickness difference may result in a larger difference in predicted remaining life.

Figure 4, in contrast, shows consistent behavior by using core and radar thickness data. When radar indicated a greater thickness, the radar-based remaining life was higher. When cores indicated a greater thickness, the core-based remaining life was higher. The thickness measurements at this site alternated; there were locations where the radar values were greater and there were locations where the core values were greater. Therefore, the remaining life pattern tracks the thickness pattern, as can be seen by comparing Figures 2 and 4.

The remaining life estimates obtained by this approach are relative. Depending on the design life, the life before overlay are obtained by multiplying the design life by the remaining life estimates.

CONCLUSION

1. A comparison of the composite layer moduli of asphalt concrete layers computed at discrete points shows that the thickness predictions from radar can be used as input for the back-calculation of the layer moduli. The paired *t*-test showed that radar-based moduli and the core-based moduli are statistically equivalently matched to the same discrete locations.
2. The predictions can also be used to investigate the effects of variable thickness of asphalt concrete layers on the back-calculation of layer moduli.
3. The combined use of GPR (continuous thickness) predictions and deflection studies can provide a standard by which the practical accuracy of composite back-calculation layer modulus results can be interpreted and used for further analysis and characterization of asphalt concrete pavement layers.
4. Most important, the continuous thickness profile, combined with deflection data, improves the interpretation and characterization of the structural integrity of an entire length of pavement. The use of discrete core thickness, which in some cases does not

correspond to the location of the measured deflections, will result in an inaccurate interpretation of the structural conditions of the site. This can lead to incorrect rehabilitation or maintenance decisions. The use of historical thickness information from a pavement management data base likewise may lead to incorrect decisions by forcing the choice of one, frequently inaccurate, thickness for an entire section.

ACKNOWLEDGMENTS

This research was funded by the KDOT Cooperative Research Program (K-TRAN), an ongoing, cooperative, and comprehensive research program addressing the transportation needs of the state of Kansas. The authors are also grateful to the University of Kansas for providing General Research Funds for this project. The authors gratefully acknowledge Infrasense, Inc., for providing additional data for analysis. Finally, the authors thank Ray Moore for many helpful discussions.

REFERENCES

1. Eckrose, R. A. Ground Penetrating Radar Supplements Deflection Testing To Improve Airport Pavement Evaluation. In *Symposium on Nondestructive Testing of Pavements and Backcalculation of Moduli,* STP 1026 (A. J. Bush and G. Y. Baladi, eds.). ASTM, Philadelphia, 1989, pp. 563–573.
2. Irwin, L. H., W. S. Yang, and R. N. Stubstad. Deflection Reading Accuracy and Layer Thickness Accuracy in Backcalculation of Pavement Layer Moduli. In *Symposium on Nondestructive Testing of Pavements and Backcalculation of Moduli,* STP 1026 (A. J. Bush and Baladi, G. Y., eds.). ASTM, Philadelphia, 1989, pp. 229–244.
3. Rodriguez-Gomez, J., C. Ferrugut, and S. Nazarian. Impact of Variability in Pavement Parameters on Backcalculated Moduli. *Proc., Conference on Road and Airport Pavement Response Monitoring Systems.* West Lebanon, N.H., 1991, pp. 261–275.
4. *Guide for Design of Pavement Structures.* AASHTO, Washington, D.C., 1986.
5. Mace, A. E. *Sample-Size Determination.* Reinhold Publishing Corp., New York, 1964.
6. Richter, C. A., and L. H. Irwin. *Application of Nondestructive Testing to Pavement Evaluation and Overlay Design.* Cornell Local Roads Program, Ithaca, N.Y., 1987.
7. Hall, K. T., and A. Mohsenni. Backcalculation of Asphalt Concrete-Overlaid Portland Cement Concrete Pavement Layer Moduli. In *Transportation Research Record 1293,* TRB, National Research Council, Washington, D.C., 1991, pp. 112–123.
8. Houston, S. L., and R. Perera. Impact of Natural Site Variability on Nondestructive Test Deflection Basins. *Journal of Transportation Engineering,* ASCE, Vol. 117, No. 5, 1991, pp. 550–565.
9. Uzan, J., R. L. Lytton, and P. F. Germann. General Procedure for Backcalculation of Moduli. In *Symposium on Nondestructive Testing of Pavement and Backcalculation of Moduli,* STP 1026 (A. J. Bush and Baladi, G. Y., eds.). ASTM, Philadelphia, 1989, pp. 217–228.

Publication of this paper sponsored by Committee on Flexible Pavement Design.

Estimation of Standard Deviation of Predicted Performance of Flexible Pavements Using AASHTO Model

A. SAMY NOURELDIN, ESSAM SHARAF, ABDULRAHIM ARAFAH, AND FAISAL AL-SUGAIR

Explicit inclusion of the reliability factor in pavement design was one of the major changes included in the 1986 version of the AASHTO *Guide for Design of Pavement Structures*. The design procedures for flexible (and rigid) pavements provide a common method for incorporating reliability into the design process on the basis of a shift in the design traffic. The guide recommended various levels of reliability (1 − risk of failure) for each roadway functional classification and suggested a range of values for the standard deviation of the combined traffic prediction and performance prediction (S_o). The S_o range suggested for flexible pavements is 0.4 to 0.5, with a typical value of 0.49. The guide also suggested that the variance of the performance prediction (S_N^2) represents about 82 percent of S_o^2 and the variance of the traffic prediction S_w^2 represents about 18 percent of S_o^2, where $S_o^2 = S_N^2 + S_w^2$. This means that the standard deviation of performance can be estimated to be in the range 0.36 to 0.45, with a typical value of 0.44. The manner in which the values of the mean and the coefficient of variation (which is equal to the standard deviation/mean) of flexible pavement layer thicknesses and strength parameters can be used as inputs to estimate the standard deviation of predicted pavement performance (S_N) is described. These values can be estimated easily by experienced pavement engineers, sometimes as well as they can be measured. The analysis resulted in an estimated S_N (typical S_N of 0.47) almost identical to what is recommended by the AASHTO guide (typical S_N of 0.44). However, the sequence leading to that estimation is believed to be of interest to users of the guide. In addition, the process of identifying the variability in pavement performance because of the variability of the factors that control that performance is demonstrated. This process is applicable to any pavement or overlay design model.

Any pavement thickness (or overlay) design method is usually based on six specific design parameters. These design parameters are the traffic characteristics, the subgrade soil characteristics, the pavement layer characteristics, the climatic conditions, the failure criteria, and the variabilities of all of those parameters.

In the 1986 AASHTO *Guide for Design of Pavement Structures* (*1*) all of the above design parameters are represented. In the design equation for asphalt pavements (flexible pavements),

1. The traffic characteristics are represented by the sum of equivalent single axle loads of 8.154 metric tons (18,000 lb) during the design period (ESAL or W_{t18}),
2. The subgrade soil characteristics are represented by the resilient modulus *MR*,
3. The pavement layer characteristics (thickness and material properties) are represented by the structural number *SN*,
4. The climatic conditions are represented implicitly within the design parameters *MR* and *SN*,
5. The failure criteria are represented by the drop in serviceability during the design period (ΔPSI), and
6. The variabilities of all of the above design parameters are represented by the standard normal deviate (Z_R) and the combined standard deviation of the traffic prediction and performance prediction (S_o). The inclusion of these variability parameters comes from the fact that each design parameter is actually a random variable with a specific distribution during the design period.

The traffic prediction equation can be expressed as follows:

$$\log W_{t18} = \log (\text{ADT} \cdot P \cdot D_d \cdot L_d \cdot \text{TF} \cdot 365 \cdot n \cdot \text{GF})$$

where

W_{t18} = predicted traffic in terms of accumulated number of ESALs (lb) during the design period,
ADT = average daily traffic,
P = percent trucks,
D_d = directional distribution,
L_d = lane distribution,
TF = truck factor, which is equal to the number of ESALs per truck,
n = design period (in years), and
GF = growth factor.

The standard deviation of the parameter log w_{t18} is termed S_w and is defined as the standard deviation of traffic prediction.

On the other hand the performance prediction equation is expressed as follows:

$$\log W_{t18} = 9.36 \log (SN + 1) - 0.2 + \frac{\log\left(\frac{\Delta PSI}{4.2 - 1.5}\right)}{0.4 + \left(\frac{1{,}094}{(SN + 1)^{5.19}}\right)} + 2.32 \log MR - 8.07$$

where

W_{t18} = predicted performance in terms of accumulated ESALs, (lb).
SN = structural number,

A. S. Noureldin, U.N. Development Program Experts Team, Ministry of Communications, Riyadh 11178, Saudi Arabia. E. Sharaf, A. Arafah, and F. Al-Sugair, Civil Engineering Department, King Saud University, Riyadh 11421, Saudi Arabia.

ΔPSI = drop in serviceability index, and
MR = resilient modulus.

The standard deviation of the parameter log W_{t18} is termed S_N and is defined as the standard deviation of performance prediction.

The AASHTO guide defines the combined standard deviation of traffic prediction and performance prediction (S_o) through the equation

$$S_o^2 = S_N^2 + S_w^2$$

where S_N is the standard deviation of the predicted performance of paving materials, and S_w is the standard deviation of the predicted amount of traffic that will use the facility.

This paper describes a simplified methodology for the estimation of S_N and the range of values of the associated design parameters.

RELIABILITY AND SOURCES OF MATERIAL VARIABILITY

Pavement thickness design for newly constructed roads (or overlay design for deteriorated roads) involves the selection of a specific value for each of the design factors. However, the design values used as inputs are seldom, if ever, unique or constant values. Every design value has some randomness in its measurement. The recognition of this stochastic or random nature of material properties has brought more attention to the explicit use of reliability concepts within the field of pavement thickness or overlay design.

Reliability is defined as the probability that the pavement system will perform its intended function over its design life and under the conditions (or environment) encountered during operation (*1*).

Material variability can be grouped into six main categories (*2,3*):

1. The inherent variability in the basic properties of materials known as *randomness*.
2. The variability in the properties of materials because of the lack of accuracy of the test method.
3. The variability that results from different laboratories and operators.
4. The variability in materials that results from circumstantial conditions during pavement service life (construction, climate, aging, traffic, etc.).
5. The modeling variability that results from inaccuracy in the design models, known as uncertainty.
6. The unexplained replication variability that still remains after considering all other categories of variability.

METHODS OF RELIABILITY ANALYSIS

Prediction of S_N can be done by several methods of reliability analysis. These methods have distinctive characteristics and assumptions and can be categorized into three distinct approaches (*3*):

1. Exact,
2. Approximation by using first-order second-moment (FOSM), and
3. Point estimate.

Exact Approach

Use of the exact approach requires the knowledge of the exact distribution (probability density function) for each of the independent variables associated with a random variable model (or function) (*3,4*). Suppose, for example, that the performance of a flexible pavement can be represented by the model

$$\log W_{t18} = 11.75 - 4.6 \log d_o$$

where W_{t18} represents the accumulated number of ESALs during the design period, and d_o represents the center deflection of a falling-weight deflectometer because of a 9,000-lb load at a pavement temperature of 20°C. The exact approach for the prediction of the standard deviation (S_N) of the random variable (log W_{t18}) requires the knowledge of the exact distribution of the random variable (d_o). In some instances the independent variable (d_o) can be assumed to be normally distributed, lognormally distributed, or uniform. After knowing (or assuming) the exact distributions of the independent variables, the exact distribution of the dependent variable can be obtained, and hence its standard deviation can be determined.

Approximation Approach

The approximation approach requires the knowledge of only the coefficients of variation (COVs) of the independent variables to predict the standard deviation of a dependent random variable (COV is the standard deviation divided by the mean). Cornell approximation (*4*) makes use of the first-order Taylor series expansion such that if F, for example, is a function of independent variables SN and MR given by the model

$$F = \phi\ (SN, MR)$$

then

$$\text{Mean of } F = \phi\ (\text{mean of } SN, \text{ mean of } MR)$$

$$\text{Variance of } F = \text{variance of } SN \cdot P_2 + \text{variance of } MR \cdot P_1$$

where

$$P_2 = \left(\frac{\partial F}{\partial SN} \text{ at mean of } SN\right)^2$$

= square of the partial derivative at mean SN

$$P_1 = \left(\frac{\partial F}{\partial MR} \text{ at mean of } MR\right)^2$$

= square of the partial derivative at mean MR

This approach is also called the FOSM approximation (*4*). Taking, for example, the model where

$$\log W_{t18} = 11.75 - 4.6 \log d_o$$

then

$$\text{Var}(\log W_{t18}) \cong \text{Var}(d_o) \cdot \left(\frac{4.6 \log e}{\bar{d}_o}\right)^2$$

and

$$S_N = \text{standard deviation of } \log W_{t18}$$

$$\cong \frac{\text{standard deviation of } d_o}{\bar{d}_o} \cdot 2$$

or

$$S_N = \text{standard deviation of } \log W_{t18}$$

$$\cong \text{COV}(d_o) \cdot 2$$

It can be noted that the standard deviation of W_{t18} (standard deviation for pavement performance) can be estimated to be a constant value multiplied by the value of the COV for center deflection for that model. An experienced pavement engineer can provide an estimate for the COV of center deflection (as good as the one measured), and hence can provide a good estimate of the standard deviation of log W_{t18}.

Point Estimate Approach

The point estimate approach does not use the Taylor series but instead uses measured values of the independent variables at different points to estimate the random dependent variable. This method is known as the point estimate approach (*5*).

Referring back to the example in which the model representing pavement performance is

$$\log W_{t18} = 11.75 - 4.6 \log d_o$$

d_o can be measured at different points, and hence, log W_{t18} can be calculated at these points by using the model. The mean, variance, standard deviation, or COV of the random variable (log W_{t18}) can then be obtained by using these calculated values.

ESTIMATION OF AASHTO S_N

The AASHTO design model for the design of flexible pavements is (*1*)

$$\log_{10}(W_{18}) = Z_R \times S_o + 9.36 \log_{10}(SN + 1) - 0.2 + \frac{\log_{10}\left(\frac{\Delta PSI}{4.2 - 1.5}\right)}{0.4 + \left[\frac{1{,}094}{(SN + 1)^{5.19}}\right]} + 2.32 \log_{10} MR - 8.07$$

where

W_{18} = predicted number of 8,154-kg (18-kip) ESALs,
Z_R = standard normal deviate,
S_o = combined standard error of the traffic prediction (S_w) and performance prediction (S_N) where $S_o^2 = S_N^2 + S_w^2$,
MR = resilient modulus (psi), and
ΔPSI = drop in serviceability during the design period.

SN is equal to the structural number indicative of the total pavement thickness required:

$$SN = a_1D_1 + a_2D_2m_2 + a_3D_3m_3$$

where

a_i = ith layer coefficient,
D_i = ith layer thickness (in.), and
m_i = ith layer drainage coefficient.

Tables 1 and 2 presents the suggested levels of reliability for various functional classifications and the corresponding Z_R values, respectively (*1*).

The estimation of S_N by the approximation approach for reliability analysis (see above) requires

1. An estimate of the coefficient of variation of the structural number SN,
2. An estimate of the coefficient of variation of the resilient modulus MR, and
3. An estimate of the COV of the drop in serviceability ΔPSI.

The following sections present how these estimates can be obtained for a fixed drop in ΔPSI of 1.7 ($\Delta PSI = 4.2 - 2.5 = 1.7$).

TABLE 1 Suggested Levels of Reliability for Various Functional Classifications (*1*)

Functional Classification	Recommended Level of Reliability	
	Urban	Rural
Interstate and other freeways	85 - 99.9	80 - 99.9
Principal Arterials	80 - 99	75 - 95
Collectors	80 - 95	75 - 95
Local	50 - 80	50 - 80

Note: Results based on a survey of the AASHTO Pavement Design Task Force

TABLE 2 Standard Normal Deviate (Z_R) Values Corresponding to Selected Levels of Reliability (*1*)

Reliability, R (percent)	Standard Normal Deviate, Z_R
50	-0.000
60	-0.253
70	-0.524
75	-0.674
80	-0.841
85	-1.037
90	-1.282
91	-1.340
92	-1.405
93	-1.476
94	-1.555
95	-1.645
96	-1.751
97	-1.881
98	-2.054
99	-2.327
99.9	-3.090

Estimation of COV for AASHTO Layer Coefficients

Figure 1 provides the relation between the layer coefficient of asphalt concrete layer (a_1) and its modulus (E_{AC}) suggested by the AASHTO guide (*1*) as a result of the research work reported in *NCHRP Report 128* (*6*). The average AASHO Road Test conditions suggest an average value of Marshall stability of 906 kg (2,000 lbs) and an average dynamic modulus, E_{AC} (axial loading), of 3103 MPa (450,000 psi) at 68°F (20°C), corresponding to a layer coefficient of 0.44 (*7*). It is imperative to indicate that the asphalt concrete layer coefficient (a_1) not only is dependent on the asphalt concrete modulus (or Marshall stability) but also is dependent on the thickness and material properties of the underlying paving layers. However, for the purposes of simplifying variability estimation, the relationship provided in Figure 1 can be utilized, since it is already usable for estimating the average value of a_1. The exact model for the relationship shown in Figure 1 does not need to be known to estimate the COV for the layer coefficient, which can be estimated as follows: Since a_1 is a function of E_{AC}

$$a_1 = \phi\ (E_{AC})$$

then

$$\text{Var}\ (a_1) \cong \text{Var}\ (E_{AC}) \cdot \left[\frac{\partial \phi(E_{AC})}{\partial E_{AC}}\right]^2$$

$$\frac{\text{Var}\ (a_1)}{\bar{a}_1^2\ \bar{E}_{AC}^2} \cong \frac{\text{Var}\ (E_{AC})}{\bar{a}_1^2\ \bar{E}_{AC}^2} \cdot (\text{slope of the relation at } \bar{E}_{AC})^2$$

where E_{AC} and a_1 are mean values

$$\overline{\text{COV}\ (a_1)}^2 \cong \frac{\bar{E}_{AC}^2}{\bar{a}_1^2} \cdot \overline{\text{COV}\ (E_{AC})}^2 \cdot \overline{\text{slope}}^2$$

$$\text{COV}\ (a_1) \cong \text{COV}\ (E_{AC}) \cdot \frac{450{,}000}{0.44} \cdot \frac{0.22}{450{,}000}$$

$$\text{COV}\ (a_1) \cong 0.5\ \text{COV}\ (E_{AC})$$

$$\text{where the slope} \cong \frac{0.22}{450{,}000}\ \text{(Figure 1)}$$

When the model for thickness equivalency of Odmark (*8*) is considered, then

$$a_1 = 3\sqrt{\frac{E_{AC}}{E_{\text{reference}}}}$$

or

$$a_1 = \frac{(E_{AC})^{1/3}}{\text{constant}}$$

then

$$\log a_1 = 1/3 \log E_{AC} - \log \text{constant}$$

and hence

$$\text{Var}\ (\log a_1) = 1/9\ \text{var}\ (\log E_{AC})$$

can be derived by using the approximation approach that

$$\text{Var}\ (\log a_1) \cong \frac{\overline{\text{COV}\ (a_1)}^2}{5.3}$$

and hence

$$\therefore \overline{\text{COV}\ (a_1)}^2 \cong \frac{1}{9}\ \overline{\text{COV}\ (E_{AC})}^2$$

$$\therefore \text{COV}\ (a_1) \cong \frac{\text{COV}\ (E_{AC})}{3}$$

Rada and Witczak (*9*) developed a relationship for granular base materials such that

$$a_2 = 0.249 \log MR - 0.977$$

where MR is the resilient modulus of the base materials, and a_2 is its layer coefficient. This relationship is also used to estimate the layer coefficient of the base material in the AASHTO guide (*1*). It is also essential to indicate that a_2 is also dependent on other pavement layer moduli as well as thicknesses. However, for

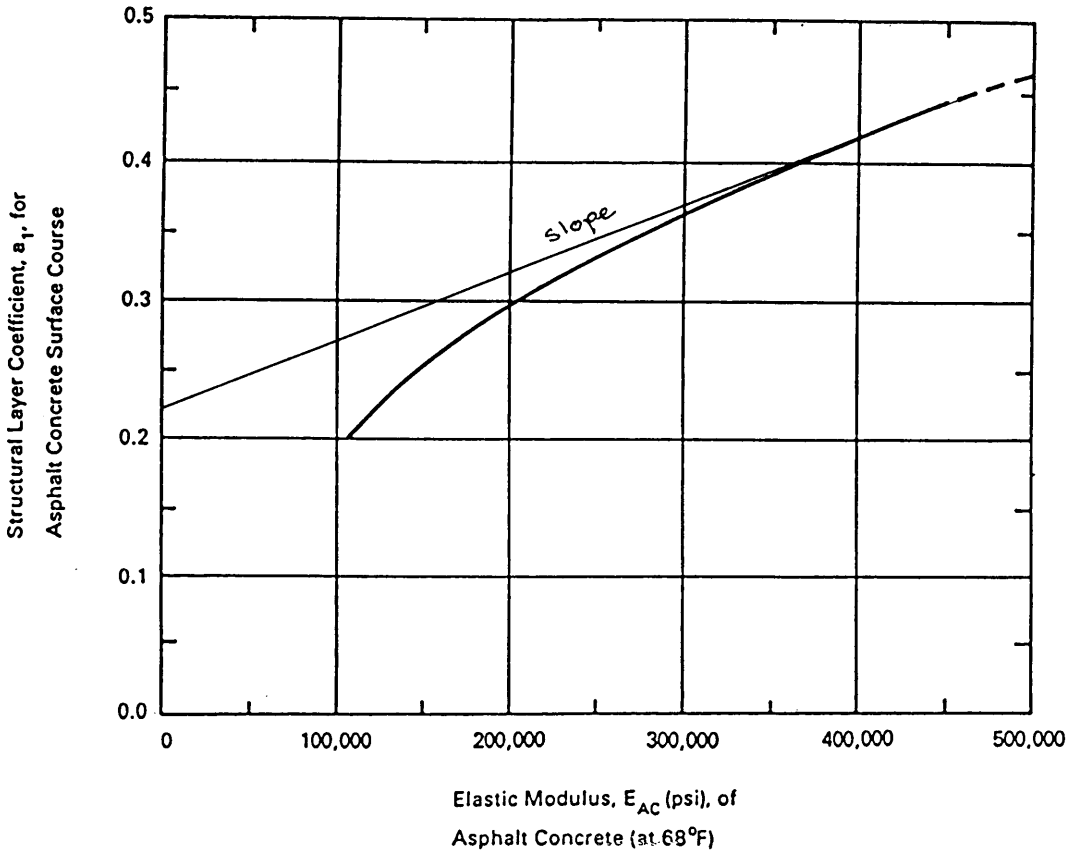

FIGURE 1 Chart for estimating structural layer coefficient of dense-graded asphalt concrete on the basis of elastic modulus (*1*).

purposes of simplifying the estimation of the COV for a_2, the above equation can be utilized as follows:

$$a_2 = \phi\ (MR)$$

$$\text{Var}\ (a_2) \cong \text{Var}\ (MR) \left[\frac{\partial \phi(MR)}{\partial MR}\right]^2$$

$$\text{Var}\ (a_2) \cong \text{Var}\ (MR) \left(\frac{0.249 \cdot 0.434}{\overline{MR}}\right)^2$$

$$\text{Var}\ (a_2) \cong \text{Var}\ (MR) \left(\frac{0.108139}{\overline{MR}}\right)^2$$

$$\frac{\text{Var}\ (a_2)}{\overline{a}_2^2} \cong \frac{\overline{MR}^2 \cdot \text{Var}\ (MR)}{\overline{a}_2^2 \cdot \overline{MR}^2} \left(\frac{0.108139}{\overline{MR}}\right)^2$$

$$\overline{\text{COV}\ (a_2)}^2 \cong \frac{\overline{MR}^2}{\overline{a}_2^2}\ \overline{\text{COV}\ (MR)}^2 \left(\frac{0.108139}{\overline{MR}}\right)^2$$

$$\text{COV}\ (a_2) \cong \frac{30{,}000}{0.14}\ \text{COV}\ (MR) \left(\frac{0.108139}{30{,}000}\right)$$

where the average modulus and layer coefficient of the base course during the AASHO road test were 207 MPa (30,000 psi) and 0.14, respectively.

Hence

$$\text{COV}\ (a_2) \cong 0.77\ \text{COV}\ (MR)$$

when using the model

$$a_2 = 3\sqrt{\frac{MR}{MR_{\text{reference}}}}$$

the COV for a_2 can be estimated as follows:

$$\text{COV}\ (a_2) \cong \frac{\text{COV}\ (MR)}{3}$$

Rada and Wiczak (*9*) established the following relationship between subbase modulus MR and layer coefficient a_3:

$$a_3 = 0.227 \log MR - 0.839$$

This equation is also being used in the AASHTO guide for estimating the layer coefficient a_3.

By using the same approach described previously, it can be shown that

$$\text{COV}\ (a_3) \cong 0.9\ \text{COV}\ (MR)$$

or

$$\text{COV}(a_3) \cong \frac{\text{COV}(MR)}{3}$$

for the model

$$a_3 = 3\sqrt{\frac{MR}{MR_{\text{reference}}}}$$

It can be concluded that the COVs for AASHTO layer coefficients can be estimated as follows:

$$\text{COV}(a_1) \cong (0.33 - 0.5)\ \text{COV}(E_{AC})$$

$$\text{COV}(a_2) \cong (0.33 - 0.77)\ \text{COV}(MR)$$

$$\text{COV}(a_3) \cong (0.33 - 0.9)\ \text{COV}(MR)$$

Since many highway agencies in the United States and all over the world have not yet equipped their laboratories with the equipment necessary to characterize paving layers in terms of *MR*, COVs for the AASHTO layer coefficients can be estimated in a more simple manner as follows:

$$\text{COV}(a_1) \cong (0.33 - 0.5)\ \text{COV of Marshall stability}$$

$$\text{COV}(a_2) \cong (0.33 - 0.77)\ \text{COV of CBR}$$

$$\text{COV}(a_3) \cong (0.33 - 0.9)\ \text{COV of CBR}$$

This is because *MR* can be modeled to be $MR \cong K \cdot \text{CBR}$, where *K* is a constant and hence

$$\text{Var}(MR) \cong K^2\ \text{Var}(\text{CBR})$$

$$\frac{\text{Var } MR}{\overline{MR}^2} \cong K^2 \frac{\text{Var}(\text{CBR})}{\overline{\text{CBR}}^2} \cdot \frac{\overline{\text{CBR}}^2}{\overline{MR}^2}$$

$$\overline{\text{COV}(MR)}^2 \cong K^2\ \overline{\text{COV}(\text{CBR})}^2 \cdot \frac{\overline{\text{CBR}}^2}{K^2\ \overline{\text{CBR}}^2}$$

$$\text{COV}(MR) \cong \text{COV}(\text{CBR})$$

Table 3 provides the COVs for some basic characteristics of pavement materials. The values in Table 3 are combined from previous reports (*2–4*) and from construction records in Saudi Arabia.

Table 4 summarizes the estimated COVs for the AASHTO layer coefficients on the basis of the values presented in Table 3.

Estimation of COVs for AASHTO Drainage Coefficients

Table 5 presents the drainage coefficients (m_i) recommended by AASHTO and as provided in the 1986 AASHTO guide (*1*). The ranges provided in Table 5 can be used to estimate the COVs employing the approach described by MS-17 of the Asphalt Institute (*10*) and reported by Yoder and Witczak (*2*), where

$$\text{COV} \cong \frac{\text{range} \cdot 0.3249}{\text{range midpoint}} \cdot 100$$

Using this equation it can be noted that the smallest estimated COV is for the condition of excellent drainage quality and less than 1 percent exposure to a moisture level approaching satura-

TABLE 3 Pavement Material COVs

Property	Coefficient of Variation, %	
	Range	Typical
Layer Thickness		
Bituminous Surface	3 - 12	7
Bituminous Base	5 - 15	10
Granular Base	10 - 15	12
Granular Subbase	10 - 20	15
Elastic Modulus		
Bituminous Layers	10 - 20	15
Granular Base	10 - 30	20
Granular Subbase	10 - 30	20
Subgrade	10 - 30	20
Marshall Stability	10 - 20	15
CBR		
Base	10 - 30	20
Subbase	10 - 30	20
Subgrade	10 - 30	20
Percent Compaction		
Surface	1 - 2	1.5
Base	2 - 3	2.5
Subbase	2 - 3	2.5
Subgrade	2 - 3	2.5
Maximum Deflection	10 - 30	20

TABLE 4 Estimated COVs of AASHTO Layer and Drainage Coefficients and AASHTO Structural Number

Parameter	Coefficient of Variation, %	
	Range	Typical
a_1	3 - 10	6
a_2	3 - 23	13
a_3	3 - 27	15
m_i	1.2 - 20	10
SN	5 - 18	11

tion. The COV at this condition can be estimated to be

$$\text{COV} \cong \frac{(1.4 - 1.35) \cdot 0.3249}{1.375} \cdot 100 \cong 1.2 \text{ percent}$$

On the other hand the largest estimated COV is for the condition of very poor drainage quality and 5 to 25 percent exposure to a moisture level approaching saturation. The COV at this condition can be estimated to be

$$\text{COV} \cong \frac{(0.75 - 0.4)\ 0.3249}{0.575} \cdot 100 \cong 20 \text{ percent}$$

In general the COVs for AASHTO drainage coefficients can be estimated to be in the range of 1.2 to 20 percent (Table 4).

Estimation of COV for AASHTO *SN*

The AASHTO structural number is defined by the equation (*1*)

$$SN = a_1D_1 + a_2m_2D_2 + a_3m_3D_3$$

where a_1, a_2, a_3, m_2, m_3, D_1, D_2, and D_3 are as defined above. By using the same approach described above, it can be concluded that

$$\begin{aligned}\text{Var}\,(SN) \cong\ & \bar{a}_1^2\ \text{Var}\,(D_1) + \bar{D}_1^2\ \text{Var}\,(a_1) \\ & + \bar{a}^2\,\bar{m}_2^2\ \text{Var}\,(D_2) + \bar{a}_2^2\ \text{Var}\,(m_2)\,\bar{D}_2^2 \\ & + \text{Var}\,(a_2)\,\bar{m}_2^2\,\bar{D}_2^2 + \bar{a}_3^2\,\bar{m}_3^2\ \text{Var}\,(D_3) \\ & + \bar{a}_3^2\ \text{Var}\,(m_3)\,\bar{D}_3^2 + \text{Var}\,(a_3)\,\bar{m}_3^2\,\bar{D}_3^2\end{aligned}$$

where a_1, a_2, a_3, m_2, m_3, D_1, D_2, and D_3 are the mean values, or

$$\begin{aligned}\overline{SN}^2\ \overline{\text{COV}\,(SN)}^2 \cong\ & \bar{a}_1^2\,\bar{d}_1^2\left[\overline{\text{COV}\,(a_1)}^2 + \overline{\text{COV}\,(d_1)}^2\right] \\ & + \bar{a}_2^2\,\bar{m}_2^2\,\bar{d}_2^2\left[\overline{\text{COV}\,(a_2)}^2 + \overline{\text{COV}\,(m_2)}^2\right. \\ & \left. + \overline{\text{COV}\,(d_2)}^2\right] + \bar{a}_3^2\,\bar{m}_3^2\,\bar{d}_3^2\left[\overline{\text{COV}\,(a_3)}^2\right. \\ & \left. + \overline{\text{COV}\,(m_3)}^2 + \overline{\text{COV}\,(d_3)}^2\right]\end{aligned}$$

TABLE 5 Recommended m_i Value for Modifying Structural Layer Coefficients of Untreated Base and Subbase Materials in Flexible Pavements (*1*)

Quality of Drainage	Percent of Time Pavement Structure is Exposed to Moisture Levels Approaching Saturation			
	Less Than 1%	1.5%	5.25%	Greater Than 25%
Excellent	1.40 - 1.35	1.35 - 1.30	1.30 - 1.20	1.20
Good	1.35 - 1.25	1.25 - 1.15	1.15 - 1.00	1.00
Fair	1.25 - 1.15	1.15 - 1.05	1.00 - 0.80	0.80
Poor	1.15 - 1.05	1.05 - 0.80	0.80 - 0.60	0.60
Very Poor	1.05 - 0.95	0.95 - 0.75	0.75 - 0.40	0.40

To illustrate the computation process consider a pavement section having

$\overline{D}_1$ = 6 cm (2.4 in.), $\overline{a}_1$ = 0.44

$\overline{D}_2$ = 18 cm (7.1 in.), $\overline{a}_2$ = 0.14

$\overline{D}_3$ = 23 cm (9.2 in.), $\overline{a}_3$ = 0.11

$\overline{m}_2$ = 1.0, $\overline{m}_3$ = 1.0, and $\overline{SN}$ = 3.06,

by employing the lower and upper values of the estimated COVs to estimate the COV for the structural number, it can be noted that the COV for *SN* can be estimated to be in the range of 5 to 18 percent for this pavement section. It can also be noted that the changes in thickness combination do not significantly affect this range.

Estimation of S_N

The AASHTO performance prediction equation for a fixed drop in ΔPSI of 1.7 (ΔPSI = 4.2 − 2.5 = 1.7) can be written as follows:

$$\log W_{t18} = \phi\ (MR, SN)$$

where *MR* is the resilient modulus and *SN* is the structural number. Then

$$S_N^2 = \text{Var}\ (\log W_{t18}) = \text{variance of performance prediction}$$

$$\cong \text{Var}\ (MR) \cdot P_1 + \text{Var}\ (SN) \cdot P_2$$

where P_1 is the variance component of *MR*

$$\cong \left(\frac{\partial \phi}{\partial\ MR}\ \text{at mean}\ MR\right)^2$$

$$\cong \left(\frac{2.32\ \log\ e}{\overline{MR}}\right)^2 \cong \frac{1}{\overline{MR}^2}$$

where *MR* is the mean of *MR*.

P_2 = variance component of *SN*

$$\cong \left(\frac{\partial \phi}{\partial SN}\ \text{at mean}\ SN\right)^2$$

$$\cong \left[\frac{4.065}{\overline{SN}\ +\ 1} - \frac{1135.57}{\left(0.4 + \frac{1{,}094}{(\overline{SN}\ +\ 1)^{5.19}}\right)^2 (\overline{SN}\ +\ 1)^{6.19}}\right]^2$$

where *SN* is the mean for *SN*.

$$S_N^2 = \overline{\text{COV}\ (MR)}^2 + P_2\ \overline{SN}^2 \cdot \overline{\text{COV}\ (SN)}^2$$

$$S_N = \sqrt{S_N^2}$$

Table 6 presents the P_2 values corresponding to the mean values of the structural number (*SN*), and Figure 2 illustrates the relationship between P_2 and *SN*.

TABLE 6 Variance Component P_2 Corresponding to Mean Value of Structural Number *SN*

Mean Structural Number $\overline{SN}$	Variance Component P_2
1	4.065
2	1.634
3	0.763
4	0.475
5	0.370
6	0.299
7	0.242
8	0.197
9	0.162
10	0.135

$$P_2 = \left[\frac{4.065}{\overline{SN}\ +\ 1} - \frac{1135.57}{\left(0.4 + \frac{1094}{(\overline{SN}\ +\ 1)^{5.19}}\right)^2 (\overline{SN}+1)^{6.19}}\right]^2$$

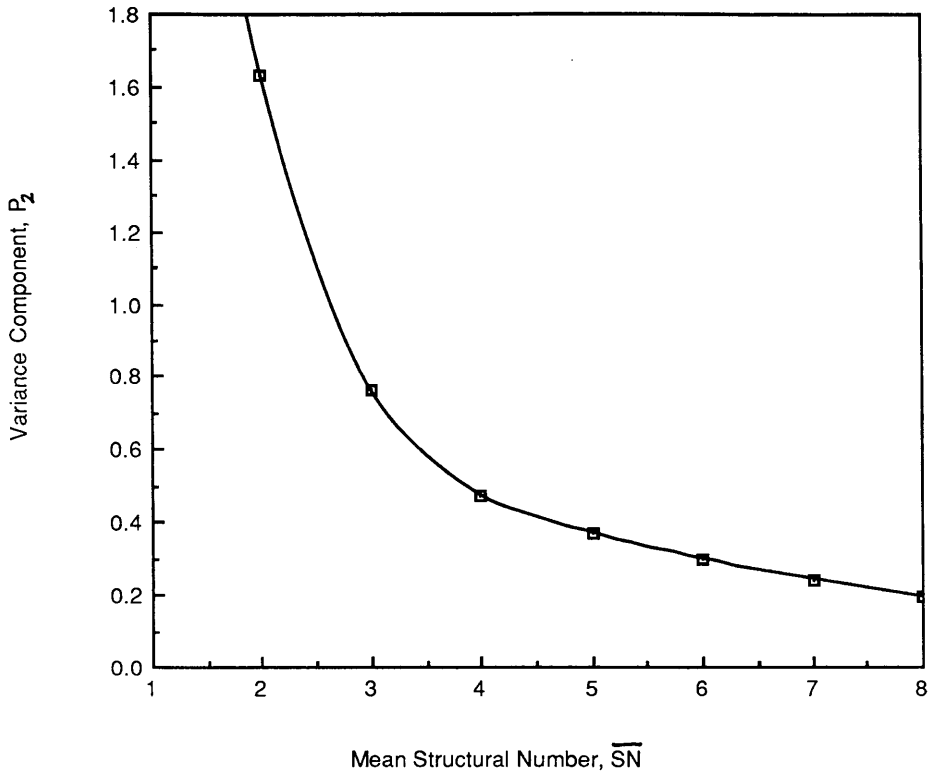

FIGURE 2 Relationship between mean structural number and variance component P_2.

By using the lower, upper, and typical values of the COV for the subgrade *MR* (10, 30, and 20 percent, respectively; Table 4) together with the lower, upper, and typical values of the COV for *SN* (5, 18, and 11 percent, respectively; Table 4); it can be shown that S_N is in the range of 0.17 to 0.58, with a typical value of 0.36 for a pavement with an *SN* of 4.0, for example.

When the lack-of-fit variance and unexplained replication variance of the AASHTO model itself [0.0763 + 0.0113 = 0.0876; Volume 2 of the guide (*11*)] are added to adjust the estimate for S_N, it can be computed that S_N is in the range of 0.34 to 0.66, with a typical value of 0.47, compared with the values recommended by AASHTO of 0.36 to 0.45, with a typical value of 0.44.

APPROXIMATION APPROACH VERSUS POINT ESTIMATE APPROACH

It is important to indicate that the presence of a correlation between independent variables of the performance prediction equation may result in an over- or underestimation of S_N when the approximation approach is used. If a negative correlation exists, for example, between *SN* and *MR*, the standard deviation estimated by the approximation approach will be overestimated. This case occurs for nonlinear "stress hardening" subgrades, in which the decrease in *SN* results in an increase in the stresses imposed on the subgrade, and hence an increase in *MR*. On the other hand if a positive correlation exists between *SN* and *MR*, the standard deviation estimated by the approximation approach will be underestimated. This case occurs for nonlinear "stress softening" subgrades, in which the decrease in SN results in an increase in the stresses imposed on the subgrade, and hence a decrease in *MR*.

In addition, the models used to estimate the coefficients of variation for the AASHTO layer coefficients (presented above) have their own uncertainties, and their added lack of fit variance may be significant so that it must be accounted for.

In those circumstances explained above the point estimate approach for reliability analysis may be preferred over the approximation approach, unless the covariances of the independent parameters can be quantified practically and the uncertainty in the models used is taken into consideration.

On the other hand usage of the point estimate approach, which requires measured values of the independent variables at different points to estimate the performance variable, may be not practical in comparison with the approximation approach.

However, in situ material characterization through back-calculation of paving layer moduli from deflection basins obtained during nondestructive testing of pavements can make the point estimate approach for reliability analysis as practical as the approximation approach.

The following example illustrates the fact that the two approaches may lead to almost identical estimations of S_N, regardless of the concerns expressed above.

Table 7 presents the back-calculated subgrade modulus and effective structural number for a 1,300-ft pavement segment [data are from Noureldin (*12*)]. The performance variable (log W_{t18}) was point estimated for each point by using the AASHTO model. When using the approximate approach S_N (without the inclusions

TABLE 7 Back-Calculated Subgrade Modulus (*MR*) Back-Calculated Effective Structural Number (*SN*), and Calculated Performance Variable (log W_{t18}) Along a 1,300-ft Pavement Segment

Distance Feet	Backcalculated Subgrade Modulus MR, PSI	Backcalculated Effective Structural Number SN_{eff}	Log W_{t18}
0	28,000	3.17	7.663
100	24,500	3.04	7.419
200	23,600	3.00	7.347
300	29,800	3.24	7.784
400	28,400	3.19	7.694
500	35,100	3.42	8.091
600	28,400	3.19	7.799
700	32,000	3.32	7.688
800	24,500	3.04	7.729
900	35,100	3.42	7.824
1000	26,000	3.09	7.843
1100	37,300	3.49	7.825
1200	24,200	3.02	7.517
1300	28,000	3.17	7.688
Mean	28,900	3.20	7.708
Std. Dev.	4,400	0.16	0.188
Coeff. of Var.	15.20%	5.00%	2.44%

of the unexplained and lack-of-fit variance of the AASHTO model) is estimated to be

$$S_N \cong \sqrt{\overline{\mathrm{COV}\ (MR)}^2 + P_2 \cdot \overline{SN}^2 \cdot \overline{\mathrm{COV}\ (SN)}^2}$$

$$\cong \sqrt{\overline{0.152}^2 + 0.675 \cdot \overline{3.2}^2 \cdot \overline{0.05}^2}$$

$$= 0.201$$

On the other hand, when using the point estimate approach, the standard deviation of performance parameter (log W_{t18}) is 0.188, as shown in Table 7. It can be noted that the two estimations are almost identical.

SUMMARY

The empirical or mechanistic pavement performance models usually used to predict the average performance of the pavement can also be used to predict the possible variations in that performance in terms of the statistical means, variances, standard deviations, or COVs.

The predicted average pavement performance requires knowledge of the predicted average of every independent variable affecting that performance and appearing in the design model. Likewise, the predicted variability in pavement performance requires the knowledge of the predicted variability of every independent variable affecting that performance. Rational quantification of these variabilities is essential for incorporating reliability into the design process.

Explicit quantification of these variabilities was presented in this paper in terms of the mean values and COVs of the independent variables that appear in the AASHTO pavement performance model. However, the concept presented is applicable for any other pavement performance model.

COVs of paving layer thicknesses and material properties for which ample data are available can be used by experienced pavement engineers to make realistic estimations that are almost as good as the values that can be measured; these were shown to be transferable into COVs for the independent variables of the AASHTO model.

The COVs for the independent variables of the AASHTO model were then shown to be a practical tool for quantifying the variability in flexible pavement performance and estimate the standard deviation of that performance.

ACKNOWLEDGMENTS

This paper was prepared through the study Adaptation of a Reliability Based Code for the Design of Flexible Pavement in the

Kingdom of Saudi Arabia, sponsored by King Abdel Aziz City for Science and Technology (KACST) under Grant AR-11-57. The authors appreciate the KACST sponsorship of the project and the Ministry of Communications, from which typical raw data were obtained.

REFERENCES

1. *Guide for Design of Pavement Structures*, Vol. I. AASHTO, Washington, D.C., 1986.
2. Yoder, E., and M. Witczak. *Principles of Pavement Design*, 2nd ed. John Wiley & Sons, Inc., New York, 1975.
3. Lytton, R. L., and D. Zollinger. Modeling Reliability in Pavement. Presented at 72nd Annual Meeting of the Transportation Research Board, Washington, D.C., January 1993.
4. Harr, M. E. *Reliability Based Design in Civil Engineering*. McGraw-Hill, New York, 1987.
5. Rosenblueth, E. Point Estimate for Probability Moments. *Proc., Mathematics*. National Academy of Sciences, Washington, D.C., 1975.
6. Van Til, C. J., F. McCullough, B. Vallerga, and G. Hicks. *NCHRP Report 128: Evaluation of AASHO Interim Guides for Design of Pavement Structures*. HRB, National Research Council, Washington, D.C., 1972.
7. *Special Report 61: The AASHO Road Test*. HRB, National Research Council, Washington, D.C., 1962.
8. Odmark, N. *Investigations as to the Elastic Properties of Soils and Design of Pavements According to the Theory of Elasticity*. Meddelande 77. Statens Vagenstitute, Stockholm, Sweden, 1949.
9. Rada, G., and M. Witczak. A Comprehensive Evaluation of Laboratory Resilient Moduli Results for Granular Material. In *Transportation Research Record 810*, TRB, National Research Council, Washington, D.C., 1981.
10. *Asphalt Overlays and Pavement Rehabilitation*. MS-17. Asphalt Institute, 1969.
11. *Guide for Design of Pavement Structures*, Vol. 2. AASHTO, Washington, D.C., 1986.
12. Noureldin, A. S. New Scenario for the Process of Backcalculation of Layer Moduli for Flexible Pavement. Presented at 72nd Annual Meeting of the Transportation Research Board, Washington, D.C., January 1993.

Publication of this paper sponsored by Committee on Flexible Pavement Design.

Specific Energy of Damage as Fracture Criterion for Asphaltic Pavements

H. AGLAN, A. OTHMAN, AND L. FIGUEROA

The concept of the specific energy of damage as a fracture criterion for asphaltic pavements is discussed. The theoretical and experimental aspects on which the specific energy of damage can be evaluated are outlined. These are the modified crack layer methodology and a simple fatigue crack propagation testing program. To demonstrate the validity of the proposed concept, four case studies are presented. These include the effects of additive loading, processing conditions, stress levels, and testing temperature on the fracture resistance of various asphaltic pavements. It was found that the specific energy of damage (γ') is capable of discriminating the subtle effects introduced by polymer additives as well as their loading percentages. It was also found that γ' reflects the increase in the fracture resistance of an asphalt mixture because it was enhanced by the dynamic/static compaction method. The value of γ' was found to be independent of stress level and testing temperature. The current findings attest to the fact that γ' can be viewed as a material parameter reflecting the fracture toughness of a material. On this basis a logical connection can be constructed among the chemical structure, processing conditions, as well as in-service conditions (stress level and temperature), and a long-term performance-related parameter, namely, the γ' of the mixture.

Traditionally, two main approaches have been used in the study of fatigue crack propagation, namely, a phenomenological approach and a fracture mechanics-based approach. The phenomenological or S-N approach to the fatigue lifetime of a pavement is based on the endurance concept that uses Wohler's technique (*1*), in which the number of cycles to failure is correlated with the applied stress or strain through empirical constants. Because of its simplicity this approach has been widely adopted (*2–5*); however, it carries severe limitations. It does not discriminate between crack initiation and propagation, and its constants are simply regression constants without physical meaning. In addition, even homogeneous materials exhibit an order of magnitude scatter in their fatigue lifetimes (*6,7*), so it is not reasonable to model a heterogeneous material such as pavement in such a manner. A good review of this approach has recently been given (*8*).

Fracture parameters such as the stress intensity factor K, based on linear elastic fracture mechanics theories, and the energy release rate J, based on elastic-plastic theory, have also been used as correlative tools in empirical formulas based on Paris and Erdogan's (*9*) power law equation to describe fatigue crack propagation (FCP) in various materials. This fracture mechanics-based approach carries its own difficulties, as outlined previously (*8*). Schapery (*10–12*) proposed a theory in an attempt to relate the constants obtained from the Paris and Erdogan (*9*) equation to some physical and mechanical properties of materials displaying viscoelastic responses. This theory has been examined by various researchers, for example, Majidzadeh et al. (*13*), Germann and Lytton (*14*), and Little et al. (*15*), on asphalt concrete mixtures. It appears from the literature that there are conflicting reports on the general applicability of Schapery's theory to characterizing various asphalt concrete mixtures to FCP.

The concept of a crack as an ideal cut with associated surface energy has led to the development of linear elastic fracture mechanics theories to evaluate the fracture resistance of brittle materials. Modern viscoelastic and viscoplastic materials challenge the adequacies of these theories for characterizing their fracture behaviors. Guided by the deformation theory of plasticity, which is essentially nonlinear elastic theory, Rice (*16*) extended Eshelby's (*17*) contour integrals, which are path independent by virtue of the energy conservation theorem, and formulated the energy release rate for materials displaying elastic-plastic responses. The path-independent J-integral proposed by Rice (*16*) was viewed by Begley and Landes (*18*) as a measure of the crack tip elastic-plastic field and can be evaluated from the load displacement curve associated with crack extension during monotonic loading. Little et al. (*15*) have modified the J-integral analysis to include unloading effects. They suggested that their modified analysis, namely J^*, is suitable for comparative analysis of the energy release rate among various asphalt binders.

Exploration of the combo-viscoplastic fundamental properties of asphaltic pavements demands a focused and innovative study of their micro- and macromechanical phenomena relevant to their long-term performances. These phenomena encompass deformation processes induced by the applied mechanical forces accelerated by environmental challenges. In this regard relevant micro- and macromechanical phenomena in pavement would involve localized irreversible deformation processes, for example, microcracking of the binder and binder-aggregate interface. Interfacial microcracking in the meantime relates to yet another fundamental phenomenon, that is, adhesion of the binder to the aggregate surfaces. It is also essential to recognize that micromechanical processes in the mixture are controlled to a great extent by the viscoelastic character of the asphalt, which in turn is influenced by the state of stress or strain, the processing conditions, and aging. Hence, it is fundamentally important to study the dependency of the viscoelastic character of the systems considered, particularly on design parameters such as stress level and aging (exposed to increased temperature).

This paper outlines an innovative approach for characterizing the micromechanical phenomena resulting from fatigue cracking in terms of the specific energy of damage concept. In this approach crack propagation and its associated damage are considered irreversible processes, and hence, the general framework of the thermodynamics of irreversible processes is employed for modeling the FCP phenomenon. The specific energy of damage,

H. Aglan, Mechanical Engineering Department, Tuskegee University, Tuskegee, Ala. 36088. A. Othman and L. Figueroa, Civil Engineering Department, Case Western Reserve University, Cleveland, Ohio 44106.

which is proposed as a candidate material parameter characteristic of asphaltic pavements' resistance to crack propagation (fracture toughness), is the energy required to transfer a unit volume of a material from the undamaged to the damaged state. The experimental and analytical procedures required to extract the specific energy of damage for various asphaltic pavements are discussed. Case studies demonstrating the consistency of the specific energy of damage concept for characterizing the resistance of asphaltic pavements to fatigue crack propagation are presented. The effect of chemical structure, processing conditions, stress levels, and environmental temperatures on the FCP resistances of different asphaltic pavements are studied in terms of the specific energy of damage concept.

SPECIFIC ENERGY OF DAMAGE CONCEPT

The development of fatigue crack-resistant asphaltic pavements necessitates the thorough understanding of the combo-viscoplastic behavior of the binders (asphalt) and the additives (modifiers), which have been shown to be the major constituents influencing asphaltic pavements' crack resistance. Recently, the modified crack layer (MCL) approach has been proposed (*19*). The capability of this approach for discriminating the subtle effects introduced by different chemical structures and processing conditions in asphaltic mixtures has been demonstrated (*20–22*). The MCL model essentially addresses the difficulties encountered in the general applicability of the crack layer model (*23,24*). These difficulties are the identification and quantification of damaged species associated with FCP in materials.

The MCL model has been expressed as

$$T\dot{S} = (J^* - \gamma' a)\dot{a} + \dot{D} \tag{1}$$

where

T = "ambient" temperature,
$\dot{S}$ = rate of change of the entropy of the system of the crack and the surrounding damage,
γ' = specific energy of damage,
a = crack length,
$\dot{a}$ = crack speed (see Equation 2),
$\dot{D}$ = rate of energy dissipation on material transformation associated with active zone evolution.

At minimum entropy the term $T\dot{S} = 0$ and Equation 1 can be written as

$$\dot{a} = \frac{\dot{D}}{(\gamma' a - J^*)} \tag{2}$$

where $\dot{a}$ is the crack speed, which can be expressed as da/dN for cyclic fatigue, with N being the number of cycles.

The energy release rate J^* can be evaluated experimentally. For stress control fatigue

$$J^* = \frac{1}{B}\left(\frac{\partial P}{\partial a}\right) \tag{3}$$

where P is the potential energy (area above the unloading curve) at each crack length a, and B is the specimen thickness. Under strain control fatigue, J can be used instead of J^*, and it is expressed as

$$J = -\frac{1}{B}\left(\frac{\partial U}{\partial a}\right) \tag{4}$$

where U is the strain energy (area under the loading curve at the corresponding crack length a).

It has been shown (*19,20*) that the cyclic rate of energy dissipation $\dot{D}$ associated with stress control loading can be expressed as

$$\dot{D} = \beta' \frac{dW_i}{dN} = \beta' \dot{W}_i \tag{5}$$

where β' is the coefficient of energy dissipation, and the quantity $\dot{W}_i$ is the change in work expended on damage formation and history-dependent viscous dissipative processes within the active zone of the propagating crack. It was also shown (*22*) that

$$\dot{W}_i = \frac{1}{B}(H_i - H_o) \tag{6}$$

where H_i is the area of hysteresis loop at any crack length, and H_o is the area of the hysteresis loop before crack initiation.

Substituting Equation 5 into Equation 2 and rearranging gives

$$\left(\frac{J^*}{a}\right) = \gamma' - \beta'\left[\frac{\dot{W}_i}{\left(\frac{da}{dN}\right)a}\right] \tag{7}$$

The quantities J^*, da/dN, $\dot{W}_i$, and a can be measured during fatigue crack propagation experiments as reported previously (*20–22*). It was shown that if the quantities between brackets in Equation 7 are plotted in the x-y domain a straight line is obtained, which attests to the fact that the theory is in accord with the experimental results. This will directly give the value of γ', which is the intercept of the straight line.

It should be emphasized that establishing the γ' criteria is based on measuring more fundamental parameters related to the fracture behavior of materials than any other FCP laws. These are the change in work $\dot{W}_i$ expended on damage formation and history-dependent viscous dissipation processes, the volumetric amount of damage, which is taken as a linear function of the crack length, the conventional crack speed, and the energy release rate J^*. This makes the specific energy concept a sound alternative for characterizing various asphaltic mixtures to FCP.

CASE STUDIES

Relationships Between Structure and γ'

In this section the γ' concept is used to discriminate the subtle effect introduced by varying the polymeric additive loading in two asphaltic mixtures. The γ', characteristic of the fracture toughness of the mixtures, and their dissipative character, β', have been extracted on the basis of FCP experiments by making use of Equation 7. Relationships between γ' and the additive loading (per-

centage of polymer in the asphalt) have been constructed. Two asphalt cement modifiers that belong to the general group of thermoplastic polymers have been studied. These modifiers are SBS Kraton® D4463 (thermoplastic rubber and styrenic block copolymer) and Elvax (ethylene vinyl acetate).

Gradation requirements corresponding to Ohio Department of Transportation (ODOT) specification item 403 (*25*) were adopted in the preparation of all specimens with the two additives. An optimum AC-5 asphalt cement content of 8 percent was used, as evaluated from maximum stability and unit weight. Additive loadings of 6, 10, and 15 percent were used for each polymer. The bulk polymer was first heated to the compaction temperature of 160°C (320°F) and was then blended with the asphalt cement with a high-speed electric mixer until a uniform blend was achieved. Beams measuring 381 mm long × 50.8 mm thick × 88.9 mm deep (15 × 2 × 3.5 in.) were prepared from the modified asphalt mixtures containing 8 percent asphalt by weight with a unit weight of 149 pcf by the following procedure. The aggregate, modified asphalt cement and the mold were preheated to 160°C (320°F) before blending and compaction. Beams were compacted by sustaining a 13.79-MPa (2,000-lb/in^2) pressure through a steel plate for 1 min in agreement with ASTM 3202-83. Beams were allowed to cool off in the compaction mold and were usually tested 7 days after preparation and conditioning. Conditioning consisted of subjecting each beam to a constant temperature of 60°C (140°F) for 1 day.

Fatigue tests were conducted at a constant frequency of 0.5 Hz under load control from zero to a constant maximum load of 289 N (65 lb). Each cycle consisted of a 0.2-sec load duration with a 2-sec rest period. Tests were conducted at room temperature [21.1°C (70°F)]. An initial notch of 6.35 mm (0.25 in.) was placed in each specimen with a saw before testing. Three specimens were tested at each set of conditions, and the average value of γ' was obtained.

The relationships between the values of γ' obtained from Equation 7 and the percentage of additive (chemical structure) are given in Figure 1 for both the Kraton and Elvax modified asphalt mixtures. It is seen from Figure 1 that γ' has an optimum value at about 10 percent Elvax loading, whereas there is no optimum value for the Kraton-based mixtures. The value of γ' increases with the increase in the Kraton loading within the range of percent Kraton tested.

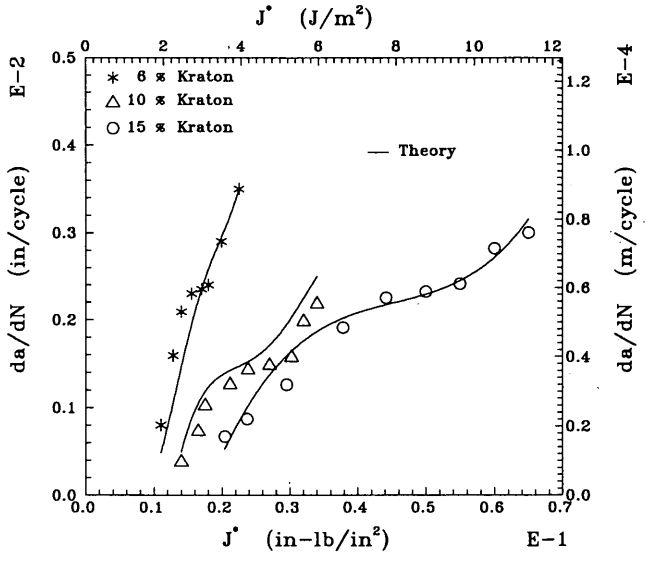

FIGURE 2 Theoretically predicted FCP speed on the basis of MCL model (together with experimental data) for modified AC-5 asphalt concrete mixtures with different Kraton loadings.

To demonstrate the relationship between γ' and the fracture toughness of the material, final results of FCP experiments for the Kraton-modified AC-5 with different loadings are discussed here. In Figure 2 the theoretically predicted FCP speed on the basis of the values of γ' and β', obtained from the modified crack layer model together with the experimental data, are shown. It is evident that the mixture with 15 percent additive, which has the highest γ', is the most resistant to FCP. This is easily established by comparing the value of J^* for the different mixtures at any constant crack speed. The higher the value of J^* the more resistant the material is to FCP.

The dissipative character, β', of each polymer-modified mixture was also extracted by using Equation 7. The relationships between the values of β' and the additive loadings for both Kraton- and Elvax-modified AC-5 asphalt mixtures are shown in Figure 3. It is evident from Figure 3 that the β'–percent additive relationship takes an opposing trend to the γ'–percent additive relationship for both the Kraton and Elvax asphalt mixtures. Such findings

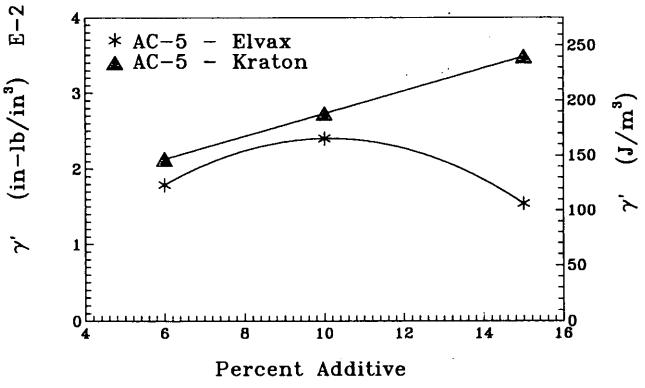

FIGURE 1 Relationship between γ' and percent additive loading.

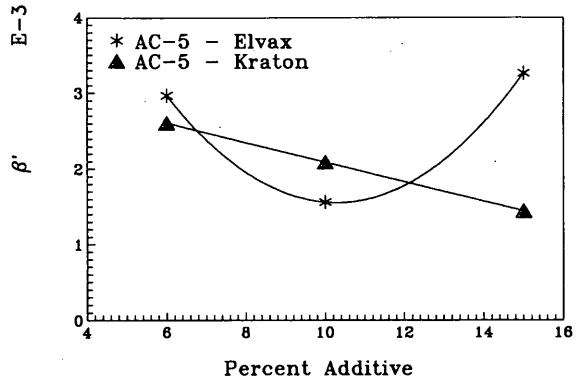

FIGURE 3 Relationship between β' and percent additive loading.

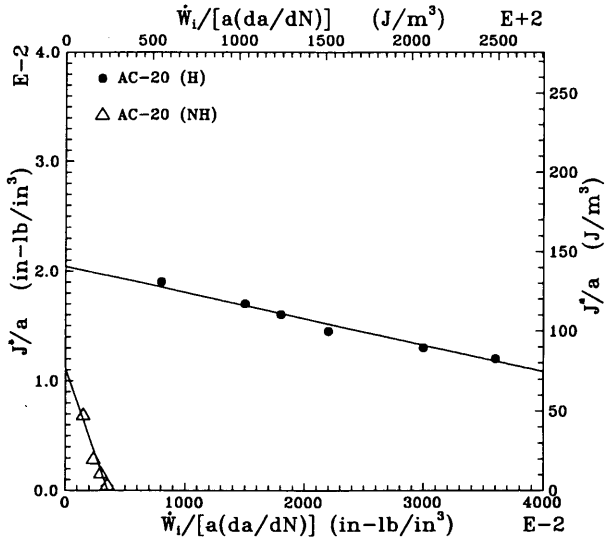

FIGURE 4 FCP behaviors of dynamically/statically (*H*) and statically (*NH*) compacted AC-20 asphalt concrete mixtures plotted in form of MCL model to obtain γ' and β'.

indicate that a higher value of γ' and lower value of β' can be associated with a tougher mixture.

Regarding the effect of additive loading, it was found that the fracture resistance of the Kraton-modified AC-5 mixture as reflected by γ' increases with the increase in the additive loading. Within the range of Kraton percentages tested (6 to 15 percent) it appears that both the polystyrene end blocks and butadiene rubbery midblocks are working together to improve the fracture toughness γ' of the Kraton-modified asphalt mixtures. On the other hand the Elvax-modified AC-5 asphalt concrete mixture showed a maximum fracture resistance at 10 percent additive loading. This can be attributed to the competing effects of the softer ethylene phase and the harder vinyl acetate phase in the Elvax modifier.

Thus, establishing structure-γ' relationships can serve an important role in asphalt mixture design. Such relationships can guide the development of asphalt mixtures with superior resistance to crack propagation (fracture toughness) and assessment of the lifetimes of these mixtures in service.

Relationships Between Processing Conditions and γ'

The effect of processing conditions on γ' was studied by changing the method of compaction of the beams. Beams made from an AC-20 mixture were compacted statically and with a static-dynamic combination method. An optimum asphalt content of 8 percent by weight, as determined from maximum stability and unit weight analysis, was used along with gradation requirements according to ODOT item 403 (*25*). The same procedure described previously was used to compact the statically compacted beams. The air void content for the conventionally compacted specimens was 1.3 percent.

The equipment required for the dynamic-static compaction includes a modified Marshall compaction hammer with a 44.48-N (10-lb) weight and an 0.457-m (18-in.) drop. The compaction face was modified to accept a 152.4 by 50.8 mm (6 × 2 in.) rectangular plate instead of the usual 98.4 mm ($3\frac{7}{8}$-in.)-diameter circular tamping base. The base of the compaction hammer was also preheated by using a bath of boiling water as a convenient method. The heated mold placed on a compaction pedestal was filled with the heated asphalt-aggregate mixture to about half of the depth of the mold. The layer was compacted at three positions by applying 10 blows at each position. The remaining heated asphalt-aggregate mixture was added to the mold as in the first stage, and another series of 30 blows was applied. Following the dynamic compaction procedure, the beam was subjected to a pressure of 13.79 MPa (2,000 lb/in^2) in a hydraulic press for 1 min. The compacted beam was then allowed to cool off in the mold before it was removed, and it was usually tested 7 days after preparation and curing. Curing was the same as that for the conventionally compacted specimens. The air void content was about 1.24 percent.

In Figure 4 the average results from three beams tested by each of the two processing methods are shown in the form of Equation 7. As can be seen the data from each set of the processing conditions form very good straight lines. The average values of γ' and β' for each mixture are shown in Table 1. It is observed from Table 1 that the average value of γ' for the dynamically and statically compacted AC-20 (*H*) mixture is about 1.8 times greater than that for the statically compacted AC-20 (*NH*) mixture, whereas the average value of β' for the statically compacted AC-20 mixture is about 13 times greater than the average value for the dynamically and statically compacted AC-20 (*H*) mixture. A larger value of γ' indicates that more energy is required to cause a unit volume to change from undamaged to damaged material, whereas a higher value of β' reflects the larger percentage of energy expended on dissipative processes and damage growth within the active zone. These two observations indicate that the dynamically and statically compacted AC-20 (*H*) mixture is more resistant to crack propagation than the statically compacted AC-20 (*NH*) one. This finding is in accord with the fatigue lifetime of each mixture. The dynamically and statically compacted specimens have an average fatigue lifetime of 14,000 cycles, whereas the statically compacted specimens have an average lifetime of 2,500 cycles. Thus, γ' has demonstrated its capability of reflecting the increase in the fracture toughness of the mixture, as enhanced by the dynamic-static compaction method.

TABLE 1 Average γ' and β' for AC-20 Mixtures

Mixture	γ' (J/m^3)	β'
AC-20 Stat/Dyn	141 ± 20	$2.40\pm0.15 \times 10^{-4}$
AC-20 Stat	77 ± 15	$3.14\pm0.20 \times 10^{-3}$

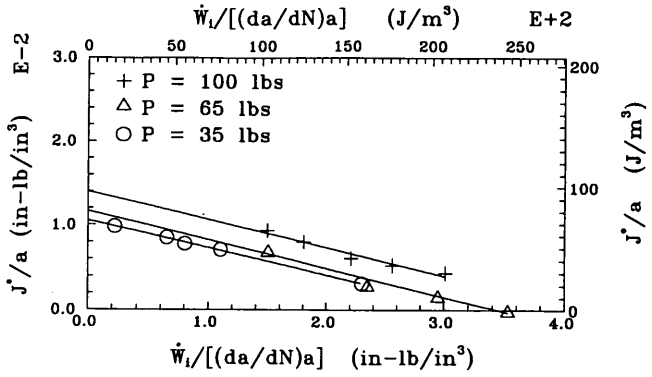

FIGURE 5 FCP behavior of AC-20 asphalt concrete mixture tested at three different maximum stress levels plotted in form of MCL model to obtain γ' and β'.

Relationships Between Stress Level and γ'

In this section the dependence of γ', as extracted from the MCL model, on the level of stress during fatigue loading is examined. The study was designed to verify the invariant nature of γ', which is proposed as a material parameter characteristic of the asphalt concrete mixture's resistance to crack propagation. The consistency of β' is also to be assessed in view of the level of loading or stress.

An AC-20 asphalt concrete mixture was prepared for the study by using gradation requirements corresponding to ODOT specification item 403 (*25*). An optimum asphalt cement content of 8 percent was used, as evaluated from maximum stability and unit weight. The beams were prepared by the same methods described in the previous section for the structure-γ' relationship. Four point flexural FCP tests were performed on three geometrically identical notched beams at three levels of stress. Tests were conducted in a laboratory environment at room temperature [21°C (70°F)] by using an invert haversine waveform. The load application period was 0.2 sec; this was followed by a 2-sec rest period between repeated loads. The notch depth was 6.35 mm (0.25 in.). Maximum loads of 444.8, 289, and 155.7 N (100, 65, and 35 lb) were used with continuous cycle load applications from zero to the maximum load. These levels correspond to approximately 29, 19, and 10 percent of the ultimate bending stress, respectively. All other experimental conditions were kept constant.

The average results for the three tested specimens at each stress level are plotted, on the basis of the MCL model, in Figure 5. It is evident from Figure 5 that the experimental points for all of the specimens at different stress levels make a good straight line, in which γ' is the intercept and β' is the slope. The average values of γ' and β' on the basis of three identical specimens at each stress level are given in Table 2.

In Figure 6 the experimental data are plotted, with the straight line based on the average values of γ' and β'. It can be seen that the average line represents the data at the different stress levels reasonably well. Bearing in mind the severe heterogeneity of the asphalt concrete mixture, the variations in γ' and β' can be tolerated and it is probably safe to conclude that the values of γ' and β' are independent of the stress level.

The consistency of γ' can be understood by examining Equation 7 and assuming that the term $\dot{W}_i/(da/dN)a$ is equal to 0 to obtain γ' at the intercept. It can be seen that γ' is dependent on the ratio J^*/a. As can be seen in Figure 6 this ratio, which is simply the slope of the curves, is almost constant at any given crack length for the three stress levels shown, and hence, γ' is independent of stress level. By a similar analysis, now assuming that the terms J^*/a and γ' are constant, it can be seen that β' is dependent on the ratio $\dot{W}_i/(da/dN)a$. It has been observed that both $\dot{W}_i$ and (da/dN) increase with the increased stress level, and it appears that they have increased proportionally since β' has remained constant.

Analysis of stress-controlled FCP experiments on the basis of the MCL theory revealed that the parameters controlling the fracture process, namely, γ' and β', appear to be independent of the stress level of fatigue loading.

Relationships Between Temperature and γ'

In this section the effect of temperature on the fracture and fatigue behaviors of Kraton-modified AC-5 asphalt concrete mixture is studied. Specimens were tested at three temperatures [1.67, 21.1, and 29.4°C (35, 70, and 85°F)]. The stress level and all other experimental conditions were kept constant as described in the section on the structure-γ' relationship. The Kraton loading was 6 percent by weight of the 8 percent asphalt cement binder. Beams were again prepared in the same manner as described previously in the section on the structure-γ' relationship.

The results for typical specimens tested at the three temperatures (1.67, 21.1, and 29.4°C) are plotted, on the basis of the MCL theory, in Figures 7, 8, and 9, respectively. It is evident from Figures 7 to 9 that the experimental points in each case make a good straight line in which γ' is the intercept and β' is the slope. The relationship between γ' and temperature is given in Figure

TABLE 2 Average γ' and β' for AC-20 Mixture Tested at Three Different Maximum Stress Levels

Maximum Load (N)	Percent Ultimate Bending Stress	γ' (J/m³)	β' E-3
444.8 (100 lbs)	29%	96.6	3.33
289.1 (65 lbs)	19%	77.6	3.18
155.7 (35 lbs)	10%	72.8	3.22
average values		82.3	3.24

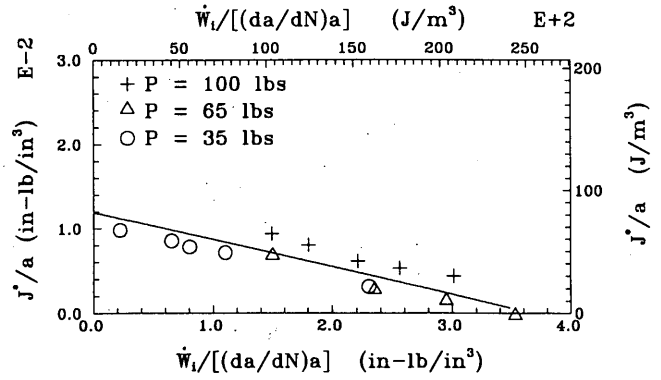

FIGURE 6 FCP data for AC-20 asphalt concrete mixture tested at three different maximum stress levels plotted in form of MCL theory along with the straight line representing average values of γ' and β'.

10. As seen from Figure 10, the value of γ' is almost independent of temperature. Thus, it is safe to conclude that γ' is a material constant that reflects the material's resistance to crack propagation because it has been found to be independent of testing conditions (stress level and temperature).

On the other hand, the value of β', which reflects the dissipative character of the material, depends strongly on temperature. This was not the case for the stress level tests described previously. There is a sharp increase in β' as the test temperature increases from 1.67 to 21.1°C (35 to 70°F). At temperatures greater than 21.1°C (70°F), β' appears to have less dependency on temperature. The consistency of γ' with temperature and the increase in β' with temperature have been reported independently (*26*) during fatigue crack propagation studies on PEEK. This lends support to the proposed approach by verifying it independently on other materials.

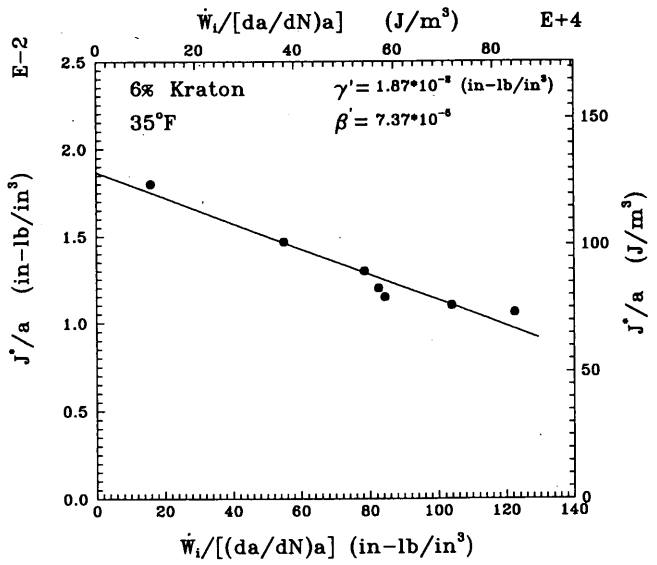

FIGURE 7 FCP behavior of 6 percent Kraton-modified AC-5 asphalt concrete mixture tested at 35°F plotted in form of MCL model to obtain γ' and β'.

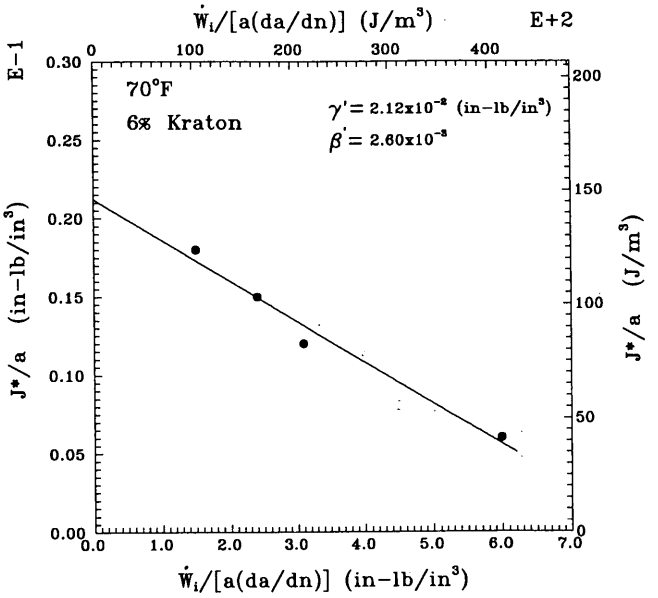

FIGURE 8 FCP behavior of 6 percent Kraton-modified AC-5 asphalt concrete mixture tested at 70°F plotted in form of MCL model to obtain γ' and β'.

CONCLUDING REMARKS

γ' is proposed as a material parameter characteristic of an asphalt mixture's resistance to crack propagation (fracture toughness). It is based on a constitutive equation, the MCL model, which is derived from the thermodynamics of irreversible processes. The validity of the approach was demonstrated through several case studies. It discriminated the subtle effects introduced by different loadings of two polymer modifiers, namely, Elvax and Kraton, to

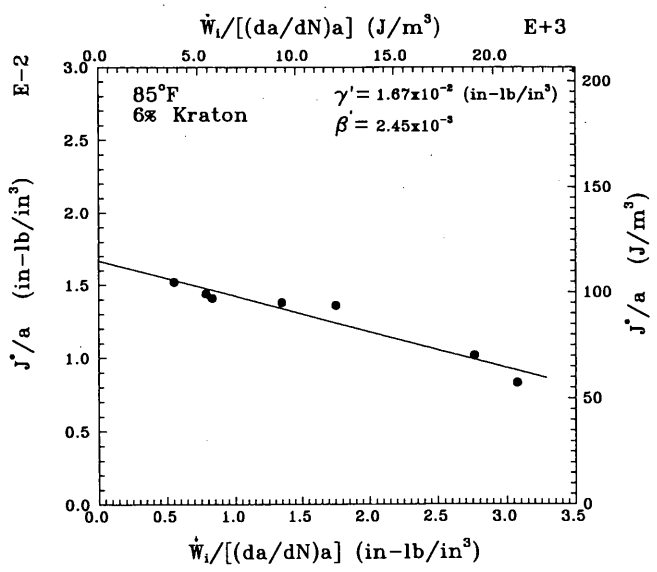

FIGURE 9 FCP behavior of 6 percent Kraton-modified AC-5 asphalt concrete mixture tested at 85°F plotted in form of MCL model to obtain γ' and β'.

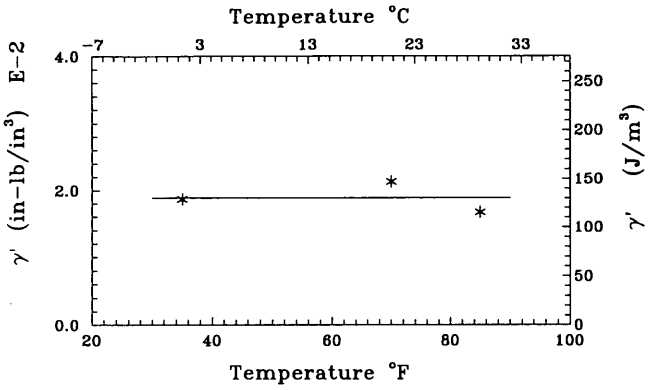

FIGURE 10 Relationship between γ' and temperature for 6 percent Kraton-modified AC-5 asphalt concrete mixture.

an AC-5 asphalt concrete mixture. The validity of the approach was further tested by studying the effects of processing conditions on the value of γ'. Again γ' successfully reflected the superior toughness of an AC-20 mixture that had been subjected to both dynamic and static compaction to that of an AC-20 mixture that had only been statically compacted. The usefulness of γ' as a material parameter was shown with studies on the effects of both maximum stress level during fatigue testing and testing temperature. In both cases the specific energy of damage was found to be consistent, showing very little change over the range of stress levels and temperatures considered. On this basis it is safe to conclude that γ' can be viewed as a material constant that reflects changes in material composition and processing but that has little dependency on testing conditions.

ACKNOWLEDGMENTS

This work was sponsored by the U.S. Army Corps of Engineers Waterways Experiment Station, Vicksburg, Miss. The direction of R. Rollings of the U.S. Army Corps of Engineers is gratefully appreciated.

REFERENCES

1. Wohler, A. *English Abstract in Engineering,* Vol. II, 1871, p. 199.
2. Monismith, C. L., K. E. Secor, and E. W. Blackmer. Asphalt Mixture Behavior in Repeated Flexure. *Proc., Association of Asphalt Paving Technology,* Vol. 30, 1961, p. 188.
3. Monismith, C. L., and J. A. Epps. *Asphalt Mixture Behavior in Repeated Flexure.* Report TE 69-6. University of California, Berkeley, 1969.
4. Pell, P. W., and I. F. Taylor. Asphalt Road Materials in Fatigue. *Proc., Association of Asphalt Paving Technology,* Vol. 37, 1969, pp. 423–458.
5. Pell, P. S. Fatigue Characteristics of Bitumen and Bituminous Mixes. *Proc., International Conference on the Structure and Design of Asphalt Pavements,* 1962, p. 310.
6. Clyton-Cave, J., R. J. Taylor, and E. Ineson. *Journal of Iron and Steel Instruments,* Vol. 180, 1955, p. 161.
7. McClintock, F. A. M., and A. S. Argon, eds. *Mechanical Behavior of Materials.* Addison Wesley, New York, 1966.
8. Rao Tangella, S. C. S., J. Craus, J. A. Deacon, and C. L. Monismith. *Summary Report on Fatigue Response of Asphalt Mixtures.* Report ASHRP-A/IR-90-011. National Research Council, Washington, D.C. 1990.
9. Paris, P., and F. Erdogan. *Journal of Basic Engineering,* in *Transactions of ASME,* Vol. 85, 1963, p. 528.
10. Schapery, R. A. A Theory of Crack Initiation and Growth in Viscoelastic Media. I. Theoretical Development. *International Journal of Fracture,* Vol. 11, 1975, pp. 141–159.
11. Schapery, R. A. A Theory of Crack Initiation and Growth in Viscoelastic Media. II. Approximate Methods of Analysis. *International Journal of Fracture,* Vol. 11, 1975, pp. 369–388.
12. Schapery, R. A. A Theory of Crack Initiation and Growth in Viscoelastic Media. III. Analysis of Continuous Growth. *International Journal of Fracture,* Vol. 11, 1975, pp. 549–562.
13. Majidzadeh, K., E. Kauffmann, and C. Saraf. *Analysis of Fatigue of Paving Mixtures from the Fracture Mechanics Viewpoint.* Report ASTM-STP 508. ASTM, Philadelphia, 1972, pp. 67–83.
14. Germann, P. F., and R. L. Lytton. Methodology for Predicting the Reflection Cracking Life of Asphalt Concrete Overlays. Report TT-2-8-75-207-5. Texas Transportation Institute, College Station, 1979.
15. Little, D. N., J. W. Button, et al. *Investigation of Asphalt Additives.* Report FHWA-R-D87/001. U.S. Department of Transportation, November 1986.
16. Rice, J. R. A Path Independent Integral and the Approximate Analysis of Strain Concentrations by Notches and Cracks. *Journal of Applied Mechanics,* Vol. 35, 1968, p. 379.
17. Eshelby, J. D. *Solid State Physics,* Vol. 3, 1956, pp. 79–144.
18. Begley, J. A., and J. D. Landes. *The J-Integral as a Fracture Criterion.* ASTM STP 514. ASTM, Philadelphia, 1972, p. 1.
19. Aglan, H. Evaluation of the Crack Layer Theory Employing a Linear Damage Evolution Approach. *International Journal of Damage Mechanics,* Vol. 2, 1993, pp. 53–72.
20. Aglan, H., I. Shehata, L. Figueroa, and A. Othman. Structure-Fracture Toughness Relationships of Asphalt Concrete Mixtures. In *Transportation Research Record 1353,* TRB, National Research Council, Washington, D.C., 1992, pp. 24–30.
21. Aglan, H., and J. L. Figueroa. A Damage Evolution Approach to Fatigue Cracking in Asphalt Concrete Mixtures. *Journal of Engineering Mechanics,* Vol. 119, 1993, pp. 1243–1259.
22. Aglan, H. Polymeric Additives and Their Role in Asphaltic Pavements. Part I. Effect of Additive Type on the Fracture and Fatigue Behavior. *Journal of Elastomers and Plastics,* Vol. 25, 1993, pp. 307–321.
23. Chudnovsky, A. Crack Layer Theory. In *10th U.S. Conference on Applied Mechanics* (J. P. Lamb, ed.). ASME, Houston, 1986, p. 97.
24. Aglan, H., A. Chudnovsky, et al. Crack Layer Analysis of Fatigue Crack Propagation in Rubber Compounds. *International Journal of Fracture,* Vol. 44, 1990, p. 167.
25. Department of Transportation Specification. *Construction and Materials Specifications.* Ohio Department of Transportation, Columbus, January 1989, p. 112.
26. Brillhart, M., and J. Botsis. Fatigue Fracture Behavior of PEEK. *Proc. Society of Plastics Engineering Annual Technical Conference,* 1992, pp. 136–139.

Publication of this paper sponsored by Committee on Flexible Pavement Design.

Optimizing Design Standards for New Pavements Using Highway Design and Maintenance Standards Model (HDM-III)

MIKE J. RILEY, CHRISTOPHER R. BENNETT, DAVID R. SAUNDERS, AND ANDY KIM

A set of new pavement design standards for highways in Thailand derived by using a life-cycle costing approach is presented. The analysis was conducted with the World Bank's Highway Design and Maintenance Standards Model (HDM-III), which simulates the total transport costs of a pavement under different design and maintenance standards. Before the analysis was undertaken, the HDM-III vehicle operating cost and pavement deterioration models were calibrated for Thailand. The analysis was undertaken by first establishing the optimum long-term periodic maintenance policies. This was done by considering a combination of treatments and triggers, with the optimum policy being that which minimized the total transport costs. These periodic maintenance policies were used in conjunction with different initial pavement designs to determine the optimum initial pavement strength by traffic volume. This pavement strength was expressed in terms of the modified structural number. Sensitivity analyses were conducted by using patching only and suboptimal periodic maintenance strategies. These indicated that the current Thailand design standards are appropriate for pavements with traffic of more than 2,000 vehicles per day, given the uncertainties over future maintenance levels and traffic loading. At fewer than 2,000 vehicles per day the current design standards are overdesigning pavements, and a more economical design was recommended. A comparison was made to establish the optimum traffic volume for upgrading asphalt concrete pavements to cement concrete. It was found that unless the time between cement concrete pavement construction and reconstruction is sufficiently long, asphalt concrete pavements are a more economical choice even at higher traffic volumes.

The Highway Design and Maintenance Standards Model (HDM-III) was produced by the World Bank to perform economic appraisals of different road design and maintenance standards (*1*). The program predicts the pavement deterioration and vehicle operating costs over an extended analysis period in which these are dependent on the pavement design standards and the maintenance policies applied to the pavement. It is therefore possible to use HDM-III to determine the optimum new pavement design standards on the basis of economic principles.

This paper presents the results of such an analysis for Thailand. The work was undertaken as part of the Asian Development Bank Technical Assistance Project 1106-THA: Thailand Road Maintenance Project (*2*).

M. J. Riley, Riley Partnership, P.O. Box 177, Kumeu, Auckland 1250, New Zealand. C. R. Bennett, N.D. Lea International. P.O. Box 177, Kumeu, Auckland 1250, New Zealand. D R. Saunders and A. Kim, N.D. Lea International, 251 Consumers Road, Suite 1200, Toronto, Ontario, Canada.

METHODOLOGY

HDM-III Calibration

HDM-III was calibrated for the conditions in Thailand as described previously (*2*). The calibration consisted of modifications to the vehicle operating costs (VOCs) and also changes to the pavement deterioration model. The VOC calibration will be briefly described, and since this paper deals with pavement design standards, the pavement deterioration model calibration will be described in more detail.

A new mechanistic fuel model was supplied for HDM-III. Parameter values for trucks were derived from Thailand data, whereas those for other vehicle classes were based on overseas values. The tire consumption model was modified so that the predictions under average conditions were the same as the observed tire life. On the basis of local studies the Thailand repair and maintenance costs were much lower than those predicted by HDM-III. The HDM-III predictions were reduced by a fixed amount to make the predictions similar to the known values. This approach meant that the roughness effects were not changed from the default effects. The speed prediction model was calibrated on the basis of limited free speed data.

Data on a number of pavement test sections were collected over a 7-year period as part of the Thailand Road Deterioration Study. These data were used to investigate the relevance of the HDM-III pavement deterioration model and to make whatever changes were necessary to it.

It was found that the roughness progression model adequately reflected the observed roughness progression, as did the crack initiation model. However, the rate of observed crack progression was much higher than that predicted by HDM-III. In the Thailand context, HDM-III appeared to be significantly underpredicting crack progression.

HDM-III predicts crack progression only as a function of time. Paterson (*3*) notes:

> The time based models will satisfy most demands of a management system . . . because they represent a good average for typical standards of pavement strengths and loadings. However, when the effects of different loading rates or of pavement strength on cracking are to be evaluated then the traffic based models are preferred.

By using appropriate equations from Paterson (*3*), the traffic-based crack progression models were replaced with time-based

ones. Comparison of these predictions with the available crack progression data gave much closer predictions to those observed than the time-based models did. Because the traffic-based model gives unreasonably low predictions for volumes below 1,000 vehicles per day (veh/day), the time-based model was used for volumes below this traffic level.

HDM-III was further modified to take into account the area of previous cracking on postoverlay crack progression. Pavements that have substantial wide cracking before maintenance will suffer from reflective cracking, and thus higher postmaintenance crack progression rates. The annual incremental crack progression was modified by applying the factor

$$\text{INCRFC} = \left(1 + \frac{\text{PCRW}}{100}\right)$$

where INCRFC is a factor to increase the postoverlay crack progression, and PCRW is the percentage of the area with wide cracks before the overlay.

The INCRFC factor indicates that with no wide cracking before the overlay the postoverlay crack progression will be at the standard rate; with 100 percent cracking it will be at twice the standard rate. These rates were not based on any field studies but were selected on the basis of the judgments of the analysts.

A further modification to the pavement deterioration model was in the form of a new equation for predicting the effects of overlays on roughness. A study was conducted at 26 sites in Thailand to investigate the effects of roughness on overlays. Data were collected before and after the overlay by using a TRRL Bump Integrator, calibrated to the international roughness index (in meters per kilometer). The data were analyzed and the following linear equation was developed to predict the impact of 50-mm overlays on roughness (*2*):

$$\text{IRI}a = 1.87 + 0.25\ \text{IRI}b$$

where IRI*a* is the roughness after an overlay (in IRI m/km) and, IRI*b* is the roughness before an overlay (in IRI m/km).

This equation predicts that below 6 IRI m/km an overlay will not reduce the roughness as much as that predicted by the default HDM-III equations (*1*). It was assumed that the relative effects of different overlay thicknesses on roughness embodied in the HDM-III equations were correct, so these effects were used to develop a Thailand model for various overlay thicknesses (*2*). This Thailand model was used to replace the default HDM-III equations.

Analysis Approach

The analysis of alternative pavement designs was undertaken for eight traffic ranges. These ranges were <200, 201 to 500, 501 to 1,000, 1,001 to 2,000, 2,001 to 4,000, 4,001 to 6,000, 6,001 to 10,000, and >10,000 veh/day. The optimum pavement design standard was considered to be that which minimized the total transport costs (i.e., initial construction, periodic maintenance, and road user costs) over a 30-year analysis period.

For flexible pavements the following five surfacing types and thicknesses were evaluated:

- Double bitumen surface treatment (DBST),
- 25-mm asphalt concrete,
- 50-mm asphalt concrete,
- 75-mm asphalt concrete, and
- 100-mm asphalt concrete.

Pavements representing a range of strengths were designed by varying the thickness of different layers (i.e., surface, base and subbase). The strength was expressed in terms of the modified structural number (MSN). This is the traditional AASHO structural number increased to reflect the contribution of the subgrade to pavement strength (*1*).

Pavement Designs

HDM-III simulates the deterioration of a pavement because of the effects of environment and traffic loading. The pavement design parameters used in this simulation are MSN and the thickness of surfacing courses. Of these, MSN largely determines the time required for cracks to appear and the progression of rutting and roughness. Surfacing thickness reduces the rate of cracking through its contribution to pavement strength.

To achieve a specified MSN the least-cost theoretical solution is to put as much of the strength contribution as possible into the lower pavement layers, which, as shown in Table 1, have the highest strength-to-cost ratio.

HDM-III simulates failure because of only aging and fatigue. To guard against shear failure under occasional heavy wheel loads, minimum course thicknesses need to be applied. There are also minimum practical construction thicknesses, normally 100 mm for a granular base or subbase. The thinnest surfacing course is 15 mm for DBST, whereas 150 mm is widely considered to be a safe minimum thickness for a base course. Therefore, the minimum practical MSN for a pavement with a subgrade CBR of 6 percent is 2.21, as shown in Table 2.

The above is based on TRRL Road Note 31 (*4*) and allows some safeguard against heavily loaded trucks on low-volume roads. For higher-strength designs the base thickness should range from 150 to 200 mm and the subbase thickness should range from 100 to 300 mm. Additional select fill should be used to increase pavement strength since the most economical design is to maximize the use of the least-expensive material.

Initial pavement costs vary with subgrade strength since additional material is required to achieve the same MSN. To evaluate the implications of construction on weak subgrades two subgrade strengths were analyzed: a CBR of 6 percent, which is appropriate for most of Thailand, and a CBR of 2 percent, which is found in the soft clay region of central Thailand.

The thickness of various layers required to achieve a specified MSN were established. It was not possible to use all surface types and thicknesses with each MSN because of engineering limitations. Also, some surfacings were unsuitable for certain traffic ranges. The matrix of feasible MSN and surfacing types and thicknesses developed is shown in Table 3.

The cement concrete pavement evaluated was a standard 230-mm concrete slab constructed on a 100-mm base and a 150-mm subbase. Since HDM-III does not contain any cement concrete pavement deterioration relationship, it was decided to simulate the performance of a cement concrete pavement as a strong asphalt concrete pavement (MSN of 7.0) with reduced roughness progression and cracking. Such a pavement was found to have rough-

TABLE 1 Comparison of Relative Costs and Strengths of Pavement Materials

	Asphaltic Concrete	Base	Subbase	Select Fill
Cost (Baht/m^3)[A]	2,500	600	150	100
Cost Index[B]	1.00	0.24	0.06	0.04
Strength coefficient	0.30	0.14	0.10	0.08
Strength index[C]	1.00	0.47	0.30	0.27
Strength/cost[D]	1.00	1.96	5.00	6.75

Notes: [A]/ 1 $U.S. = 25 Baht.
[B]/ The cost of each pavement material divided by the asphaltic concrete surfacing cost.
[C]/ The strength of each pavement material divided by the asphaltic concrete surfacing strength.
[D]/ The strength index divided by the cost index.

TABLE 2 Calculation of Minimum MSN

Course	Thickness	MSN Contribution
DBST	15 mm	0.18
Base	150 mm	0.84
Subbase	100 mm	0.40
Subgrade Support		0.79
Total MSN		2.21

TABLE 3 Pavement Surfacing Evaluated in Analysis

Traffic Volume in veh/day	Pavement Modified Structural Number						
	2.2	2.5	3.0	3.5	4.0	5.0	6.0
1 - 200	DBST; 25	DBST; 25; 50	DBST; 25; 50	DBST; 25; 50	DBST; 25; 50		
201 - 500	DBST; 25	DBST; 25; 50	DBST; 25; 50	DBST; 25; 50	DBST; 25; 50		
501 - 1000	DBST; 25	DBST; 25; 50	DBST; 25; 50	DBST; 25; 50	DBST; 25; 50		
1,001 - 2,000		DBST; 25; 50	DBST; 25; 50; 75	DBST; 25; 50; 75	DBST; 25; 50; 75	50; 75	
2,001 - 4,000		DBST; 25; 50	DBST; 25; 50; 75	DBST; 25; 50; 75	DBST; 25; 50; 75	50; 75	
4,001 - 6,000		DBST; 25; 50	DBST; 25; 50; 75	DBST; 25; 50; 75	DBST; 25; 50; 75	50; 75	
6,001 - 10,000			50; 75	50; 75; 100	50; 75; 100	50; 75; 100	75; 100
10,001 - 16,000			50; 75	50; 75; 100	50; 75; 100	50; 75; 100	75; 100

NOTES: DBST - Double Bitumen Surface Treatment
25 - 25 mm Asphaltic Concrete
50 - 50 mm Asphaltic Concrete
75 - 75 mm Asphaltic Concrete
100 - 100 mm Asphaltic Concrete

ness progression similar to that observed on Thailand cement concrete test sections (*2*).

Construction Costs

By using the layer thicknesses from the various pavement designs, the costs of a pavement were calculated by multiplying each layer thickness by the appropriate unit cost.

In Thailand the width of a pavement varies by traffic volume (*2*). The new pavement costs were expressed per meter of carriageway width. Multiplying the per meter costs by the appropriate carriageway width for each traffic volume range produced a series of costs for each traffic volume, surface type and thickness, and MSN. These costs are plotted in Figure 1 for the subgrade with a CBR of 6 percent.

Periodic Maintenance

To determine the optimum initial flexible pavement strength the impact of future maintenance must be taken into account. Thus, the HDM-III evaluations included both the initial design strength of the pavement and the periodic maintenance required over the analysis period.

The optimum periodic maintenance standards were determined by using HDM-III for each of the traffic ranges (*2*).

Since cracking is a major factor influencing overlays in Thailand, it was deemed necessary to trigger overlays as a function of cracking. However, the standard HDM-III triggers overlays only as a function of roughness. The HDM-III source code was therefore modified to include a switch for triggering overlays as a function of cracking, and changes were made to the input routines.

HDM-III was used to determine the total transport costs over a 30-year analysis period in each of the eight traffic ranges. These costs comprised the construction, maintenance, and vehicle operating costs for each pavement surface type-strength combination. By comparing the total transport costs of each pavement for a given traffic volume range the optimum periodic maintenance standards were established. These optimum standards are presented in Table 4. In addition to the optimum periodic maintenance policy, suboptimum and patching only policies were also tested.

Given the competing demands for capital and the insufficient budgets that are available, it is unwise to select projects that are only marginally economically viable. It is not prudent to assume that the VOC estimates are absolutely correct. Although the construction and maintenance costs will be much more accurate, there will still be errors with these costs as well. Thus, were one to select a project with a marginal incremental benefit to cost ratio, there is a possibility that the project is in fact uneconomical.

After assessing various estimates of the accuracy of the VOC and the construction and maintenance cost estimates, the value of 2.5 as a cutoff for the incremental benefit to cost ratio was selected. Thus, the optimum pavement strength was defined as the design that minimized the total transport costs subject to a limiting incremental benefit to cost ratio of 2.5.

Figure 2 is an example of the total transport costs for a pavement with a traffic volume of 2,001 to 4,000 veh/day.

RESULTS OF ANALYSES

Flexible Pavement Strengths

The optimal design standards for both surface treatment and asphaltic pavements are shown in Figure 3 for the eight traffic categories. The optimal design is expressed in terms of the pavement strength by using the MSN.

For low traffic volumes (fewer than 1,000 veh/day) the analyses indicate that the optimum pavement strength is the minimum tested, an MSN of 2.2. With increasing traffic volume the optimum MSN increases steadily up to a value of 4.0 for pavements carrying more than 10,000 veh/day.

The only difference between a pavement with a CBR of 2 percent and one with a CBR of 6 percent is a constant cost increment because of the additional select fill or subbase required to attain the required MSN. Therefore, the optimum MSNs for the two subgrade conditions are the same.

Surface Course Thicknesses

For traffic volumes of fewer than 1,000 veh/day the results indicated that the preferred surfacing is either a DBST or a 25-mm asphalt concrete, with marginal differences between the two. For higher traffic volumes the optimum surface thickness was the thinnest tested for the traffic range. However, HDM-III simulates only the long-term effects of fatigue on surfacing performance and does not allow for shear failure because of small numbers of exceptionally heavy axle loads, loads that are common in developing countries. Therefore, it was recommended that the results of this analysis regarding surfacing thickness should be treated with caution.

When sensible maintenance policies are assumed, the HDM-III pavement deterioration model favors thin surfacings. Consequently, the total transport costs for thin surfacings are less than those for thicker surfacings. The bias toward thin surface courses should therefore be treated with caution. However, it should be recognized that with proper design thin surfaces can offer significant economic benefits over thicker surfacings, particularly for low-volume roads.

Asphalt Concrete Versus Cement Concrete Pavements

The total transport costs of asphalt concrete and cement concrete pavements were compared to determine at what traffic volume roads should be upgraded to cement concrete. The results of this analysis demonstrated the importance of the service life of cement concrete pavements in establishing the volume for upgrading to concrete.

As shown in Figure 4 the total transport costs of constructing a cement concrete pavement are dependent on the length of the time period that extends from when the pavement is first constructed to when it must be reconstructed. For roads forecast to initially carry 6,000 to 10,000 veh/day, a design life of 28 years must be achieved before cement concrete should be selected instead of asphalt concrete. For roads forecast to carry more than 10,000 veh/day initially, the period between reconstruction drops to about 18 years. Thus, unless a suitably long service life can be

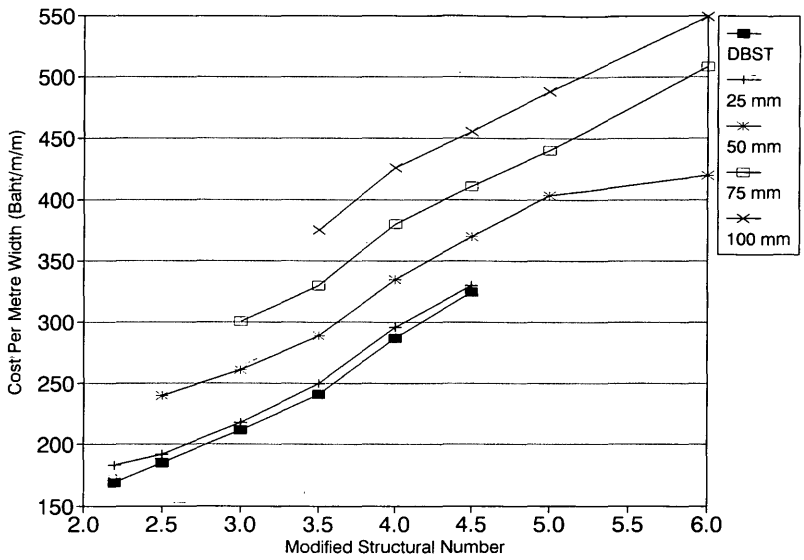

NOTES: A/ All costs are economic costs in 1992 Baht ($1 U.S. = 25 Baht)
B/ Costs were calculated by establishing standard designs with combinations of various layer thicknesses to achieve a target MSN. The unit costs of each layer were multiplied by the layer thickness to get the total cost. For each traffic volume, the total cost was divided by the pavement width and these were averaged for all traffic volumes.

FIGURE 1 Pavement costs versus MSN for CBR of 6 percent.

guaranteed, asphalt concrete pavements should be preferred to cement concrete pavements at these volumes.

SENSITIVITY TESTS

The analysis of the optimal flexible pavement design for each traffic range was repeated for two different maintenance policies:

- a suboptimal periodic maintenance policy that over the network would amount to 60 percent of the budget requirements of the optimum standards (Table 4), and
- a minimum maintenance policy of patching only, with no periodic treatments.

For low-traffic-volume roads (fewer than 1,000 veh/day) the results of the suboptimal maintenance policy analysis indicated no change to the optimal designs; that is, a minimum-strength pavement was still the best solution. With higher volumes the optimum MSN increased by about 0.5 compared with the optimum maintenance case.

The results of the "patching only" sensitivity analysis indicated that the strength requirement was unchanged up to 500 veh/day (i.e., an MSN of 2.2). Thereafter, the required MSN increased rapidly to 6.0 for the highest traffic range. This is illustrated in Figure 3. However, except for very low volume roads, this is an unlikely maintenance scenario for Thailand.

COMPARISONS WITH CURRENT PRACTICE

At present the Thailand Department of Highways (DOH) uses the Asphalt Institute (AI) design method and a 10-year design life for

TABLE 4 Optimum Periodic Maintenance Standards

Traffic Volume in veh/day	Reseal at % All Cracks	Overlay at % Wide Cracks	Overlay at IRI Roughness
< 200	10	-	5.0
201 - 500	10	-	5.0
501 - 1,000	10	-	4.5
1,001 - 2,000	10	-	4.0
2,001 - 4,000	10	5	3.5
4,001 - 6,000	10	5	3.5
6,001 - 10,000	10	5	3.5
> 10,000	10	5	3.0

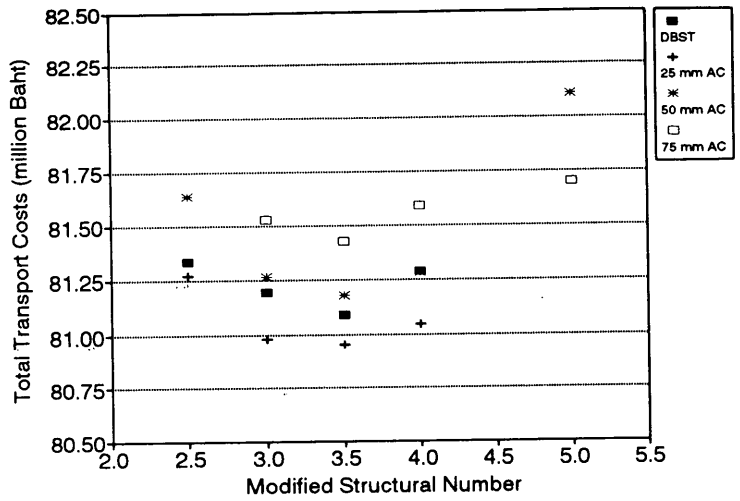

(a)

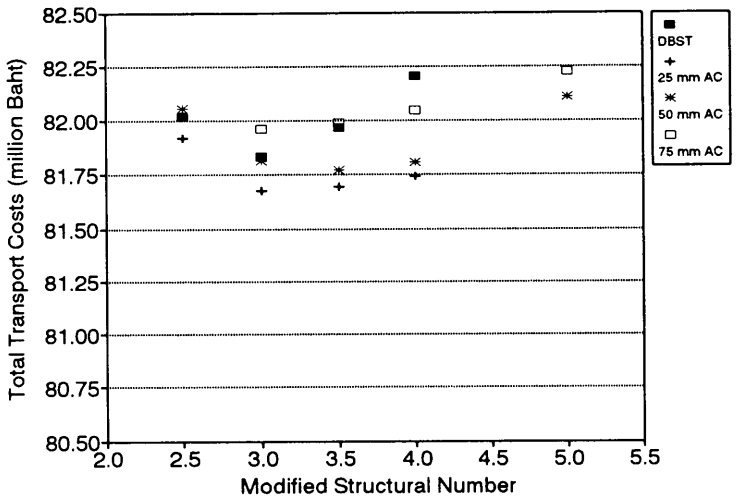

(b)

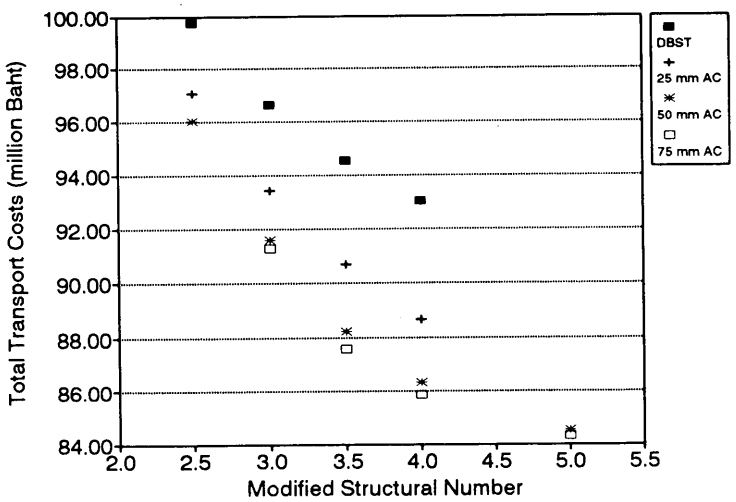

(c)

FIGURE 2 Total transport costs for different pavement designs at 2,001 to 4,000 veh/day: (*a*) optimum periodic maintenance, (*b*) suboptimum periodic maintenance, (*c*) routine maintenance (patching potholes).

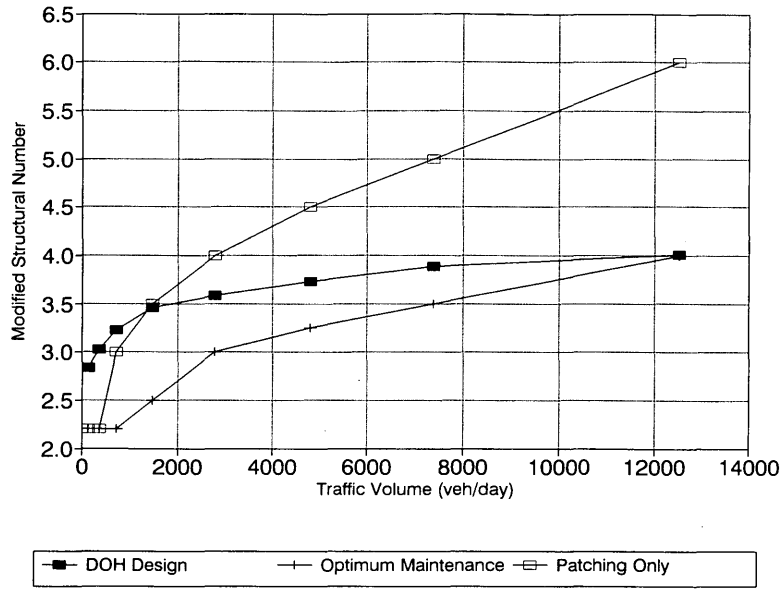

NOTES: A/ There is no direct conversion between traffic volume and ESAL since the percentage of heavy traffic varied with traffic volume.

FIGURE 3 New pavement strength comparison.

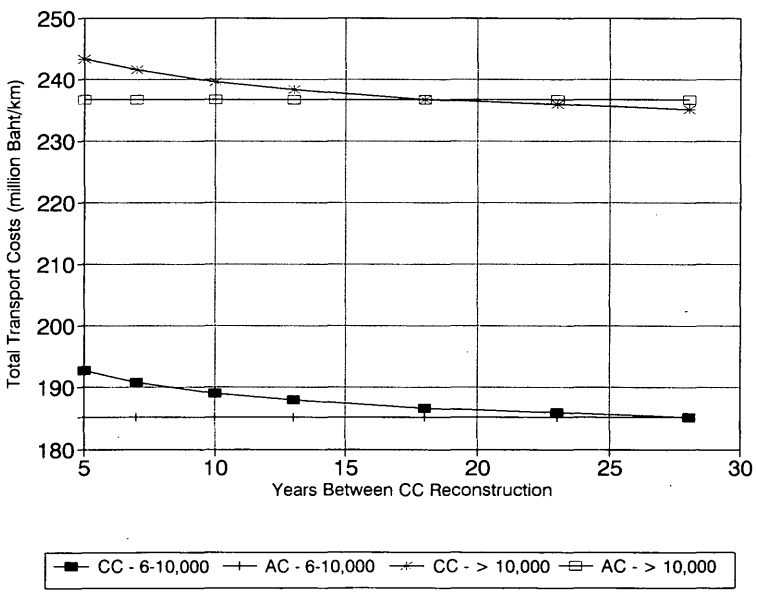

NOTES: A/ The term "CC" in the legend pertains to cement concrete; "AC" to asphaltic concrete.

FIGURE 4 Total transport costs of cement concrete (CC) and 50-mm asphalt concrete (AC) pavements.

new pavements. The optimum strengths determined from AI designs are shown in Figure 3, along with the results from the present study for optimal periodic maintenance and patching only. Figure 3 illustrates that there is a large difference between the Thailand optimum with periodic maintenance and the AI design methods at low traffic ranges and that the lines converge at 10,000 veh/day. Making allowance for the risk of substandard maintenance and a future increase in axle loading, it is considered that the present DOH design method is entirely appropriate at traffic volumes of more than 2,000 veh/day.

Below this level it appears that the DOH method produces higher designs than are economically warranted and that the use of TRRL Road Note 31 (*4*) would be more appropriate.

The present practice of using DBST surfacings for roads carrying fewer than 2,000 veh/day is not contradicted by the analyses. For roads carrying traffic above this volume the analyses offer little guidance on surface course thickness for the reasons given earlier.

CONCLUSIONS

This paper has presented the optimum new pavement design standards on the basis of economic principles for highways in Thailand. The analysis was conducted with HDM-III of the World Bank, which simulates the total transport costs of a pavement under different design and maintenance standards.

The economic consequences of different initial pavement designs were established and compared to determine the optimum initial pavement strength. Since the long-term maintenance policies will have a significant impact on the optimal initial pavement design standards the analysis incorporated a regular periodic maintenance policy.

Sensitivity analyses were conducted by using patching only and suboptimal periodic maintenance strategies. These indicated that the current Thailand design standards are appropriate for pavements with traffic volumes of more than 2,000 veh/day, given the uncertainties over future maintenance levels and traffic loadings. At fewer than 2,000 veh/day the current design standards are overdesigning pavements and a more economical design such as that embodied in TRRL Road Note 29 (*4*) is more appropriate.

Unless the time between construction and reconstruction is sufficiently long, asphalt concrete pavements are more economical than cement concrete pavements.

ACKNOWLEDGMENTS

The work described in this paper was funded by the Asian Development Bank. The authors would like to acknowledge the assistance of the Thailand Department of Highways in undertaking the work. This paper is presented with the permission of the Asian Development Bank, Thailand Department of Highways, and N.D. Lea International Ltd.

REFERENCES

1. Watanatada, T., et al. *The Highway Design and Maintenance Standards Model: Description of the HDM-III Model.* World Bank Publications, Washington, D.C., 1987.
2. *Thailand Road Maintenance Project Final Report: Asian Development Bank T.A. No. 1106-THA.* N.D. Lea International Ltd., Vancouver, British Columbia, Canada, 1992.
3. Paterson, W. D. O. *Road Deterioration and Maintenance Effects: Models for Planning and Management.* World Bank Publications, Washington, D.C., 1987.
4. TRRL. *A Guide to the Structural Design of Pavements for New Roads.* Road Note 29, 3rd ed. Her Majesty's Stationery Office, London, 1977.

The views presented in this paper are those of the authors and do not represent the opinions of the Asian Development Bank or the Thailand Department of Highways.

Publication of this paper sponsored by Committee on Flexible Pavement Design.

Mechanistic Evaluation of AASHTO Flexible Pavement Design Equations

GILBERT Y. BALADI AND ANTHONY THOMAS

A total of 243 pavement sections with various layer properties, roadbed moduli, and traffic volumes was designed using the 1986 AASHTO design guide. Mechanistic analyses of each pavement section were also conducted, and the mechanistic responses in terms of deflection, stresses, and strains were calculated and are presented and discussed. Mechanistic evaluation of the AASHTO design procedure was conducted. The evaluation addressed three features of the AASHTO design method: the structural number, the layer coefficient, and the main design equation. It is shown that the role of the roadbed resilient modulus in the AASHTO design process is not accurate and that, for any pavement layer, its layer coefficient is not a simple function of the modulus value of that layer. It is a function of all layer thicknesses and properties.

The outputs (structural number and layer thicknesses) of the AASHTO design procedure are affected by numerous variables. These variables can be separated into three categories, as follows:

1. Primary material variables that have a significant impact on the AASHTO design outputs. These include the resilient moduli or layer coefficients, the resilient modulus of the roadbed soil, and the traffic volume in terms of an 18-kip single axle load (ESAL) (*1–3*).
2. Secondary material and environmental variables (e.g., drainage coefficients and loss of serviceability because of environmental factors) that have an impact on the AASHTO design outputs (*1,3–9*). Their impacts can be addressed after analyzing the effects of the primary material variables.
3. Other variables, including reliability level, the overall standard deviation, performance period, analysis period, economic factors, initial serviceability index, and terminal serviceability index (*1*).

This paper addresses the impact of the primary material variables on the AASHTO design and mechanistic outputs. The impacts of the other variables are presented under different titles (*9*). Furthermore, a mechanistic evaluation of the AASHTO design procedure was also conducted by using the following four-step procedure.

1986 AASHTO DESIGN PROCEDURE

Step 1: Full Factorial Experiment Design Matrix

Figure 1 depicts the full factorial experiment design matrix. As can be seen the matrix consists of 243 cells (for convenience and easy reference the cells are numbered from 1 to 243). Each cell represents one pavement section. For each cell (pavement section) the resilient moduli assigned to the asphalt surface, base and subbase layers, and roadbed soil and the traffic volume in terms of an 18-kip ESAL are shown in Figure 1.

Department of Civil Engineering, Michigan State University, East Lansing, Mich. 48824-1226.

Step 2: Secondary Material and Environmental Variables

For each cell in Figure 1 the following constant values of the secondary material and environmental variables, design reliability, and standard deviation values were assigned:

1. Loss of serviceability because of environmental factors. It is assumed that the pavement materials experience no loss of serviceability because of frost heave or swelling soil. The evaluation of the concept of loss of serviceability because of frost heave has been presented previously (*9*).
2. Drainage coefficient. A value of the drainage coefficients of the base and subbase materials of 1.0 was assumed. The evaluation of the concept of drainage coefficient has been presented previously (*9*).
3. An analysis and a performance period of 20 years each.
4. A desired level of reliability of 95 percent and an overall standard deviation of 0.45.
5. Initial and terminal serviceability indexes of 4 and 2.5, respectively.
6. A discount rate of zero, a salvage value of $0.0, and material costs of $0.0.
7. No maintenance or rehabilitation cost is allowed.

Step 3: AASHTO Design Parameters (Layer Coefficients)

In step 3 the 1986 AASHTO guide (*3*) was used to convert the resilient modulus of each pavement layer to an equivalent layer coefficient as follows:

1. Figure 2.5 of the 1986 AASHTO guide (*3*) was used to convert the resilient modulus of the asphalt concrete (AC) layer to an equivalent layer coefficient (a_1).
2. The layer coefficients of the base (a_2) and subbase (a_3) materials were calculated by using the following AASHTO equations [see page II-18 of the AASHTO guide (*3*)]:

$$a_2 = 0.249[\log_{10}(E_{base})] - 0.977 \text{ and}$$

$$a_3 = 0.227[\log_{10}(E_{subbase}) - 0.839$$

AC (ksi)	Base (ksi)	Subbase (ksi)	ESAL (10^6)	Roadbed (ksi)																										
					100									300									500								
					10			25			40			10			25			40			10			25			40		
					10	15	25	10	15	25	10	15	25	10	15	25	10	15	25	10	15	25	10	15	25	10	15	25	10	15	25
			5	1	1 0	1 9	2 8	3 7	4 6	5 5	6 4	7 3	8 2	9 1	1 0 0	1 0 9	1 1 8	1 2 7	1 3 6	1 4 5	1 5 4	1 6 3	1 7 2	1 8 1	1 9 0	1 9 9	2 0 8	2 1 7	2 2 6	2 3 5
		1	10	2	1 1	2 0	2 9	3 8	4 7	5 6	6 5	7 4	8 3	9 2	1 0 1	1 1 0	1 1 9	1 2 8	1 3 7	1 4 6	1 5 5	1 6 4	1 7 3	1 8 2	1 9 1	2 0 0	2 0 9	2 1 8	2 2 7	2 3 6
			20	3	1 2	2 1	3 0	3 9	4 8	5 7	6 6	7 5	8 4	9 3	1 0 2	1 1 1	1 2 0	1 2 9	1 3 8	1 4 7	1 5 6	1 6 5	1 7 4	1 8 3	1 9 2	2 0 1	2 1 0	2 1 9	2 2 8	2 3 7
			5	4	1 3	2 2	3 1	4 0	4 9	5 8	6 7	7 6	8 5	9 4	1 0 3	1 1 2	1 2 1	1 3 0	1 3 9	1 4 8	1 5 7	1 6 6	1 7 5	1 8 4	1 9 3	2 0 2	2 1 1	2 2 0	2 2 9	2 3 8
		5	10	5	1 4	2 3	3 2	4 1	5 0	5 9	6 8	7 7	8 6	9 5	1 0 4	1 1 3	1 2 2	1 3 1	1 4 0	1 4 9	1 5 8	1 6 7	1 7 6	1 8 5	1 9 4	2 0 3	2 1 2	2 2 1	2 3 0	2 3 9
			20	6	1 5	2 4	3 3	4 2	5 1	6 1	6 9	7 8	8 7	9 6	1 0 5	1 1 4	1 2 3	1 3 2	1 4 1	1 5 0	1 5 9	1 6 8	1 7 7	1 8 6	1 9 5	2 0 4	2 1 3	2 2 2	2 3 1	2 4 0
			5	7	1 6	2 5	3 4	4 3	5 2	6 1	7 0	7 9	8 8	97	1 0 6	1 1 5	1 2 4	1 3 3	1 4 2	1 5 1	1 6 0	1 6 9	1 7 8	1 8 7	1 9 6	2 0 5	2 1 4	2 2 3	2 3 2	2 4 1
		10	10	8	1 7	2 6	3 5	4 4	5 3	6 2	7 1	8 0	8 9	9 8	1 0 7	1 1 6	1 2 5	1 3 4	1 4 3	1 5 2	1 6 1	1 7 0	1 7 9	1 8 8	1 9 7	2 0 6	2 1 5	2 2 4	2 3 3	2 4 2
			20	9	1 8	2 7	3 6	4 5	5 4	6 3	7 2	8 1	9 0	9 9	1 0 8	1 1 7	1 2 6	1 3 5	1 4 4	1 5 3	1 6 2	1 7 1	1 8 0	1 8 9	1 9 8	2 0 7	2 1 6	2 2 5	2 3 4	2 4 3

FIGURE 1 Full factorial experiment design matrix for mechanistic analysis of AASHTO flexible pavement design procedure.

where E_{basc} is the resilient modulus of the base material, and $E_{subbasc}$ is the resilient modulus of the subbase material.

In addition, for the thickness design of all pavement sections of Figure 1, the layered design analysis found on pages II-37 and II-38 of the AASHTO guide (*3*) was used. Hence, unique layer thicknesses were obtained for each of the 243 pavement sections of Figure 1 [i.e., subjective solution of the AASHTO structural number (SN) equation was not allowed].

Step 4: AASHTO Thickness Design

In step 4 the 1986 AASHTO design procedure (DNPS86 computer program) was used for the design of each of the 243 pavement sections of Figure 1. The outputs of the AASHTO design (layer thicknesses and SN) were then tabulated [for details regarding the thicknesses and the SN values, the reader is referred to work by Baladi and McKelvey (*9*)].

MECHANISTIC ANALYSIS

Given the material properties listed in Figure 1 and the layer thicknesses obtained from the AASHTO design procedure for the 243 pavement sections, a mechanistic analysis of each section was conducted by using the linear option of MICHPAVE (a finite-element computer program). Some of the results of the mechanistic analysis were verified by using the CHEVRON5 computer program. It should be noted that in all mechanistic analyses, Poisson's ratios of 0.3, 0.35, 0.4, and 0.45 for the AC, base, subbase, and roadbed soils, respectively, were used. The mechanistic responses (compressive vertical stresses and strains at the top and bottom of the AC, base, and subbase layers and at the top of the roadbed soil, the tensile stress and strain at the bottom of the AC layer, and the deflections at the top of the AC, base and subbase layers, and roadbed soil) were tabulated (*9*).

MECHANISTIC EVALUATION OF AASHTO DESIGN EQUATIONS

To avoid unnecessary repetitions the mechanistic evaluation of the AASHTO design method was accomplished by using the results for nine pavement sections. Table 1 provides a list of the nine pavement sections along with their SN values, total thicknesses, layer thicknesses, and material properties. The nine sections are grouped, relative to the material variables, into four categories, as follows:

1. Sections 60, 141, and 222, in which the only material variable is the AC modulus.

TABLE 1 Structural Number, Layer Thicknesses, and Layer Moduli of Nine Pavement Sections of Figure 1 (Performance Period of 20 years and 20,000,000 18-kip ESAL)

Cell Number	Structural Number	Total Thickness (inch)	Layer Thicknesses (inches)			Layer Modulus (ksi)			
			AC	Base	Subbase	AC	Base	Subbase	Roadbed
141	6.51	38.50	8.41	12.09	18.0	300	40	10	5
114	6.51	39.98	10.04	11.94	18.0	300	25	10	5
87	6.51	31.80	13.8	0.0	18.0	300	10	10	5
141	6.51	38.5	8.41	12.09	18.0	300	40	10	5
150	6.51	34.09	8.41	8.18	17.50	300	40	15	5
159	6.51	28.87	8.41	3.66	16.80	300	40	25	5
141	6.51	38.5	8.41	12.09	18.0	300	40	10	5
60	6.51	47.84	17.75	12.09	18.0	100	40	10	5
222	6.51	37.03	6.94	12.09	18.0	500	40	10	5
156	10.3	52.46	8.41	3.66	40.40	300	40	25	1
159	6.51	28.90	8.41	3.66	16.80	300	40	25	5
162	5.25	21.03	8.41	3.66	8.96	300	40	25	10

2. Sections 87, 114, and 141, in which the only material variable is the base modulus.
3. Sections 141, 150, and 159, in which the only material variable is the subbase modulus.
4. Sections 156, 159, and 162, in which the only material variable is the roadbed modulus.

Furthermore, for the purpose of mechanistic evaluation of the AASHTO design procedure, an engineering criterion was developed and is presented in the next section.

Engineering Criteria for Evaluation of AASHTO Design Equations

Recall that the 243 pavement sections were designed by using the AASHTO design procedure for a total loss of serviceability during the performance period of 1.7 PSI where PSI is present serviceability index. This implies that the 243 pavement sections will receive the same level of protection against damage because of their respective traffic volumes and loads. On the basis of this AASHTO concept, an engineering evaluation criterion was developed. The criterion can be stated as follows: Pavement sections designed by the AASHTO method to carry the same traffic level, to be supported on the same roadbed soil, and to have the same performance period should also experience the same magnitude of stresses, strains, and deflections caused by an 18-kip ESAL. Otherwise, the level of protection is different and the pavements will have variable performance periods. This criterion implies that the magnitude of the mechanistic responses (stresses, strains, and deflections) delivered to a pavement section can be used as a measure of pavement damage. Higher responses cause higher levels of damage. Likewise, higher mechanistic responses indicate a lower protection level from damage because of traffic loading.

Observations of AASHTO Design Outputs

Examination of the AASHTO design outputs (SN and layer thicknesses) of the nine pavement sections listed in Table 1 indicates that the AASHTO design method produces

1. A constant structural number that is independent of the layer properties but dependent on the roadbed soil resilient modulus and the number of 18-kip ESALs.
2. A constant AC thickness that is independent of the moduli of the subbase layer and the roadbed soil.
3. A constant base thickness that is independent of the moduli of the AC layer and the roadbed soil.
4. A constant subbase thickness that is independent of the moduli of the base and AC layers.

Evaluation of AASHTO Design Equations

As stated earlier the 243 pavement sections were analyzed by using the linear option of the MICHPAVE computer program, and the mechanistic responses were obtained and tabulated. The mechanistic responses of the nine pavement sections of Table 1 are summarized in Table 2. For those pavement sections with the same roadbed modulus, the data are plotted in Figures 2 through 9. For those pavements (sections 156, 159, and 162) with different roadbed soil moduli, Figure 10 depicts the variations in the pavement peak deflection. Nevertheless, examination of the range of the AC, base, and subbase layer properties listed in Table 1 and the mechanistic responses (listed in Table 2 and shown in Figures 2 to 9) indicates that for a constant traffic level and for one type of roadbed soil the AASHTO design method produces pavement sections (layer thicknesses) such that

1. The peak surface deflection is almost constant (Figure 2). Hence, the amount of the overall damage delivered to the pavement section (or the overall protection level) is constant and independent of the material properties.
2. The amount of compression and the resulting compressive strains experienced by any one pavement layer vary from one section to another (Figures 3 through 8). These variations are favorable (provide a better protection of the layer in question) for some pavement sections and unfavorable for other sections. Hence, the amount of damage delivered to each layer of the pavement sections varies. This implies that although the AASHTO design procedure ensures that the overall damage of the pavement

TABLE 2 Mechanistic Responses of Nine Pavement Sections of Table 1 Owing to 18-kip ESAL

Cell Number	Deflection at the Top of (mills)				Vertical Compressive Stress at the Top of (psi)			Vertical microstrain at top/bottom of layers				Tensile Stress at the Bottom of the AC layer (psi)
	AC	Base	Subbase	Roadbed	Base	Subbase	Roadbed	AC	Base	Subbase	Roadbed	
141	21.26	20.13	17.10	13.25	15.91	2.88	1.01	30/81	426/198	324/167	201	64.10
114	20.87	19.57	16.54	13.02	9.39	2.52	0.97	42/160	406/195	282/159	191	64.54
87	19.64	N/A	18.03	14.30	N/A	3.20	1.12	68/115	N/A	315/168	201	52.04
141	21.26	20.13	17.10	13.25	15.91	2.88	1.02	30/181	426/198	324/167	201	64.10
150	21.70	20.58	18.22	14.37	15.25	4.58	1.21	26/184	421/238	348/181	240	66.58
159	21.83	20.71	19.43	15.66	14.84	8.59	1.46	25/186	417/309	377/195	283	68.47
141	21.26	20.13	17.10	13.25	15.91	2.88	1.01	30/181	426/198	324/167	201	64.10
60	21.14	15.31	13.58	11.05	7.24	1.71	0.70	63/134	214/123	199/115	138	10.30
222	21.14	20.60	17.51	13.50	16.27	3.02	1.05	28/159	423/206	337/175	209	105.50
156	35.19	34.07	32.79	27.00	15.34	9.44	0.2	31/179	4.16/3.11	3.79/1.09	1.82	64.05
159	21.83	20.71	19.43	15.66	14.71	8.59	1.46	46/186	4.17/3.09	3.77/1.95	2.83	68.47
162	16.93	15.79	14.52	12.03	14.38	8.23	3.25	27/188	4.15/3.07	3.75/2.46	3.14	69.81

N/A = Not applicable, the AASHTO design produced zero thickness for this layer.

sections is the same, the relative damage delivered to each layer is not.

3. The tensile stress induced at the bottom of the AC layer varies from one section to another (Figure 9). Hence, the amount of fatigue damage delivered to each layer of the pavement sections varies. This implies that the performance (or the rate of deterioration) of the various pavement sections is not the same.

For pavement sections 156, 159, and 162 (all variables have a constant value except the roadbed soil resilient modulus) examination of the data listed in the last three rows of Tables 1 and 2 and shown in Figure 10 indicates that the peak pavement deflection at the top of each layer, the compressive stresses and strains, and the tensile stresses are variables. They are a function of the roadbed soil resilient modulus.

On the basis of these observations three features of the AASHTO design procedure are discussed next.

DISCUSSION OF RESULTS

Several important aspects relative to the mechanistic evaluation and calibration of the AASHTO flexible design equations can be inferred from the mechanistic analysis of those equations. These aspects are divided (according to the features of the AASHTO

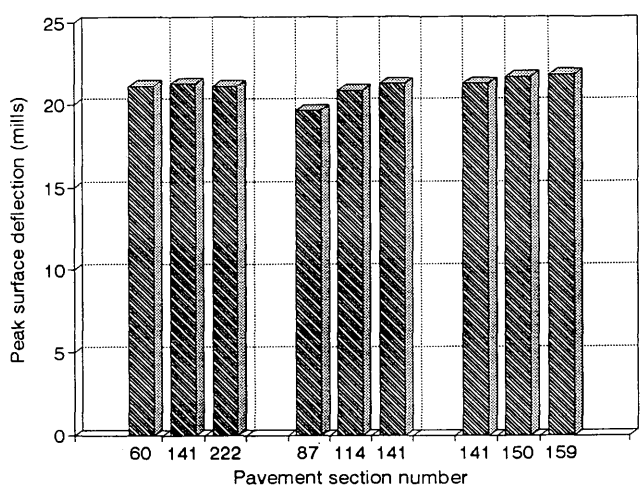

FIGURE 2 Peak pavement surface deflections of pavement sections having same roadbed soil modulus and traffic volume and load.

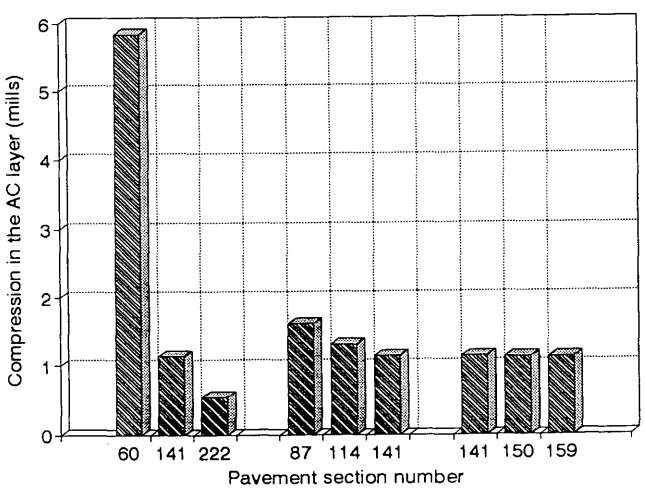

FIGURE 3 Amount of compression in AC layer of pavement sections having same roadbed soil modulus and traffic volume and load.

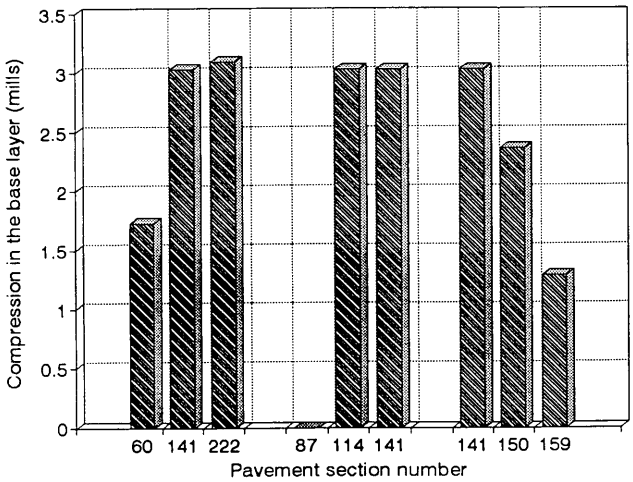

FIGURE 4 Amount of compression in base layer of pavement sections having same roadbed soil modulus and traffic volume and load.

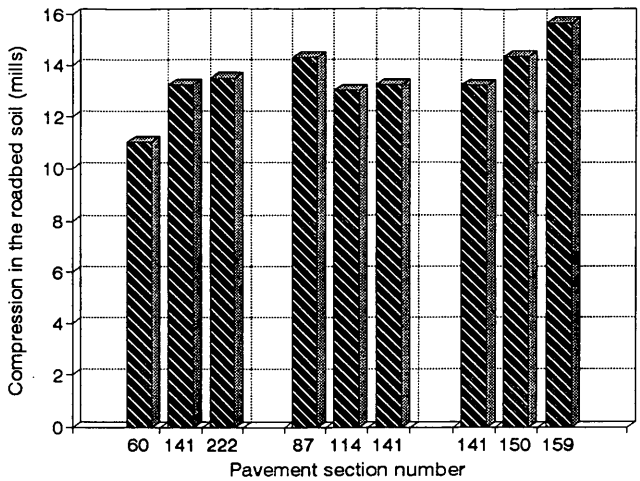

FIGURE 6 Amount of compression in roadbed soil of pavement sections having same roadbed soil modulus and traffic volume and load.

equation) into three categories and are discussed in the following sections.

Features Related to SN Equation

The AASHTO SN equation (the effects of drainage are excluded) can be in two forms, as follows:

$$SN = a_1D_1 + a_2D_2 + a_3D_3 \quad \text{or} \quad SN = SN_1 + SN_2 + SN_3$$

The AASHTO concept embedded into the SN equation is that the total SN of any flexible pavement section is the sum of the SNs of its layers. The outputs of the mechanistic analysis support this AASHTO concept. The reason for this is that for pavement sections supported on the same roadbed soil, variations in the layer coefficients or moduli are offset by varying the layer thicknesses, which minimizes their impacts on the pavement peak deflection. Hence, the total structural capacity is the same.

Features Related to AASHTO Layer Coefficient Equations or Nomographs

The AASHTO layer coefficients are related to the layer modulus through nomographs or equations, as follows:

$$a_2 = 0.249[\log(E_{BS})] - 0.977 \quad \text{and}$$

$$a_3 = 0.227[\log(E_{SB})] - 0.839$$

On the basis of the SN and layer coefficient equations, the second AASHTO concept can be written as follows: the structural number

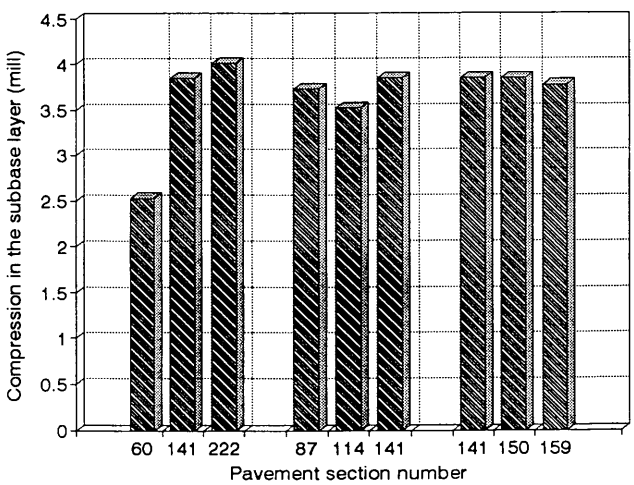

FIGURE 5 Amount of compression in subbase layer of pavement sections having same roadbed soil modulus and traffic volume and load.

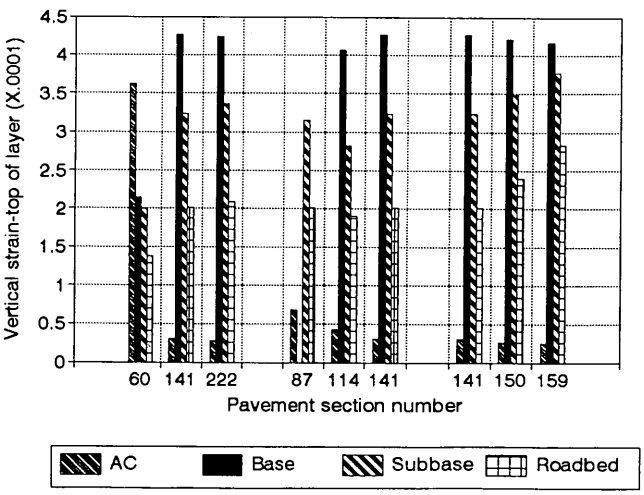

FIGURE 7 Vertical strains induced at top of each layer of pavement sections having same roadbed soil modulus and traffic volume and load.

of any pavement layer is the product of its layer coefficient and thickness, and the layer coefficient is a simple function of the modulus of that layer. The outputs of the mechanistic analysis do not support this AASHTO concept. The reason for this is that (see Figures 2 through 9) the amount of damage delivered to each layer (or the mechanistic response) varies from one pavement section to another. Given that the mechanistic response (amount of damage) in each pavement layer is a function of the properties and thicknesses of all layers, one can conclude that the AASHTO layer coefficient equations and nomographs need to be calibrated so that the amount of damage delivered to each layer because of an 18-kip ESAL remains constant. Such a calibration is a function of the type of distress (damage) being considered and the properties and thicknesses of all pavement layers. Stated differently, for any pavement layer the value or values of its layer coefficients are distress mode dependent. For example, the layer coefficient values required to ensure equal rutting may not be the same as those required to ensure equal fatigue cracking or equal roughness (ride quality).

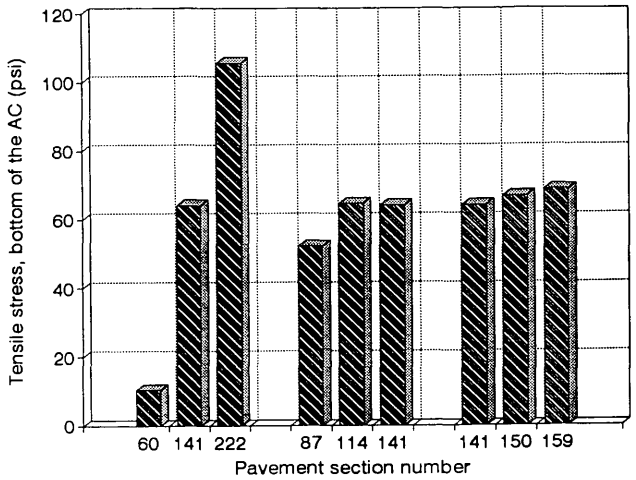

FIGURE 9 Tensile stress at bottom of AC layer of pavement sections having same roadbed soil modulus and traffic volume and load.

Features Related to Main AASHTO Design Equation

The AASHTO main design equation is written in terms of an 18-kip ESAL, design reliability and standard deviation, resilient modulus of the roadbed soil, the serviceability loss, and the required SN of the pavement, as follows:

$$\log(W_{18}) = (Z_R)(S_0) + 9.36[\log(SN + 1)] - 0.20 + \frac{\log[(\Delta PSI)/(4.2 - 1.5)]}{[0.4 + 1{,}094/(SN + 1)^{5.19}]} + 2.32[\log(MR)] - 8.07$$

Typically, the number of 18-kip ESALs is used as an input to the equation, and the required SN is calculated. Hence, the AASHTO concept herein is that, for a constant number of 18-kip ESALs and for the same design reliability, standard deviation, and serviceability loss, the required SN of any pavement section is a function of the resilient modulus of the roadbed soil. The results of the mechanistic analysis do not support this AASHTO concept. In reference to Figure 10 pavement sections 156, 159, and 162 were designed by using the AASHTO flexible pavement design procedure. The material properties of the AC, base, and subbase layers for all three sections are the same. All sections were designed to carry 20 million ESALs. The only difference between the three sections is the resilient modulus of the roadbed soil. The layer moduli, the resilient modulus of the roadbed soil, and the AASHTO design outputs (layer thicknesses) for those sections are listed in Table 1. Their mechanistic responses are summarized in Table 2. The mechanistic responses (listed in Table 2 and shown in Figure 10) indicate that

1. The pavement peak surface deflection varies from 35.19 mils for pavement section 156 to 16.93 mils for pavement section 162.

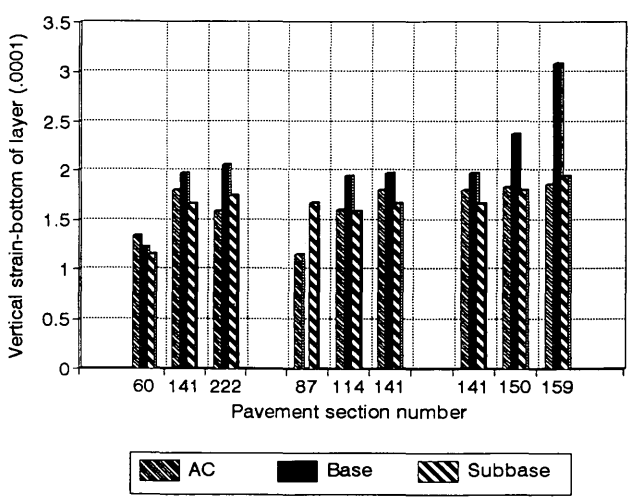

FIGURE 8 Vertical strain induced at bottom of each layer of pavement sections having same roadbed soil modulus and traffic volume and load.

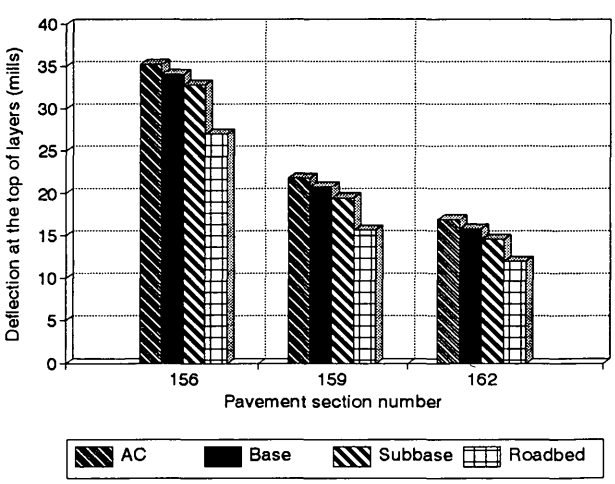

FIGURE 10 Deflection at top of each pavement layer for pavement sections 156, 159, and 162 with roadbed resilient moduli of 1, 5, and 10 ksi, respectively.

This indicates that the overall damage delivered to the pavement sections because of traffic load varies from one section to another. Previously, it was stated that for the same type of roadbed soil and traffic level the AASHTO design procedure produces pavement sections (on the basis of their SN) such that the peak pavement deflection is almost constant. This finding, however, is not true when the roadbed soil is changed from one type to another. The implication here is that the SNs produced by the AASHTO method do not provide the same level of protection to the roadbed soil. Because in the AASHTO main design equation the only factor affecting the calculation of the SN is the resilient modulus of the roadbed soil, one can conclude that the AASHTO main design equation for flexible pavements does not properly account for the effects of the resilient modulus of the roadbed soil on the SNs of the pavement. Hence, its role needs to be calibrated.

2. The values of the deflections at the top of the base and subbase layers and at the top of the roadbed soil (see the last three rows of Table 2 and the data depicted in Figure 10) indicate that the amount of damage received by the pavement sections because of traffic load varies from one section to another. This observation is similar to that reported earlier and confirms the finding that the AASHTO layer coefficient values need to be calibrated.

3. The tensile stress delivered at the bottom of the AC layer also varies from one pavement section to another, indicating various levels of fatigue damage. This is also similar to an earlier observation and confirms the finding that for any pavement layer its coefficient is a function of the thicknesses and moduli of all pavement layers.

One important point that should be noted here is that the AASHTO flexible pavement design procedure is empirical in nature. Its inherent distress mode is serviceability (ride quality). The accuracy of the AASHTO method relative to this mode of distress (pavement serviceability) cannot be verified by using mechanistic analysis at this time. Long-term pavement performance data must be used to address the adequacy of the AASHTO procedure. The observations stated above are related to other distress modes that are not inherent in the AASHTO design procedure. Simply stated, the present form of the AASHTO design procedure cannot be used to design a pavement section with high rut and fatigue cracking resistance.

SUMMARY AND CONCLUSIONS

A full factorial experiment design matrix containing 243 flexible pavement sections was established. Each section was designed by using the AASHTO design procedure. Mechanistic analyses were then conducted, and the mechanistic responses in terms of deflection, stresses, and strains were calculated. On the basis of the analyses, the following conclusions relative to the AASHTO design method are drawn:

1. The impact of the roadbed resilient modulus on the structural number and layer thicknesses is not accurate and needs to be calibrated.
2. For a constant subgrade modulus, pavement sections designed by the AASHTO procedure would have similar peak deflections independent of layer properties.
3. The AASHTO layer coefficients are not accurate and need to be calibrated as a function of the thicknesses and moduli of all pavement layers.

ACKNOWLEDGMENTS

The authors would like to thank the Strategic Highway Research Program (SHRP) for providing financial support for the study and SHRP staff and members of the Advisory Committee of the Long-Term Pavement Performance program for providing continuous support.

REFERENCES

1. Baladi, G. Y., and M. B. Snyder. *Highway Pavements,* Vol. I and II. National Highway Institute, Washington, D.C., 1990.
2. Yoder, E. J., and M. W. Witczak. *Principles of Pavement Design,* 2nd ed. John Wiley & Sons, Inc., New York, 1987.
3. *Guide for Design of Pavement Structures.* AASHTO, Washington, D.C., 1986.
4. Baladi, G. Y. In-Service Performance of Flexible Pavements, Vol. II. *Proc., International Air Transportation Conference.* American Society for Civil Engineering, New Orleans, 1979.
5. Baladi, G. Y. Fatigue Life and Permanent Deformation Characteristics of Asphalt Concrete Mixes. In *Transportation Research Record 1227,* TRB, National Research Council, Washington, D.C., 1989.
6. Ruth, B. E., A. K. Bloy, and A. A. Avital. Prediction of Pavement Cracking at Low Temperatures. *Proc., AAPT,* Vol. 51, 1982.
7. Fromm, H. J., and W. A. Phang. A Study of Transverse Cracking of Bituminous Pavements. *Proc., AAPT,* Vol. 41, 1972.
8. Chan, Y. T. Analysis of Subgrade Rutting in Flexible Airfield Pavements. In *Transportation Research Record 616,* TRB, National Research Council, Washington, D.C., 1976.
9. Baladi, G. Y. and F. X. McKelvey. *Mechanistic Evaluation and Calibration of the AASHTO Design Equations, and Mechanistic Analysis of the SHRP Asphalt Surfaced Pavement Sections.* SHRP Final Report P-678. Strategic Highway Research Program, National Research Council, Washington, D.C., March 1993.

Publication of this paper sponsored by Committee on Flexible Pavement Design.

Dynamic Finite-Element Analysis of Jointed Concrete Pavements

KARIM CHATTI, JOHN LYSMER, AND CARL L. MONISMITH

A new dynamic finite-element computer program, DYNA-SLAB, for the analysis of jointed concrete pavements subjected to moving transient loads is presented. The dynamic solution is formulated in both the time and the frequency domains. The structural model for the slab system is the one used in the static computer program ILLI-SLAB. The foundation support is represented by either a damped Winkler model with uniformly distributed frequency-dependent springs and dashpots or a system of semi-infinite horizontal layers resting on a rigid base or a semi-infinite half-space. An important contribution from the study is a new analytical method for determining the stiffness and damping coefficients to be used in the Winkler foundation model. The accuracy of DYNA-SLAB has been verified by comparing the results produced by the program with those from theoretical closed-form solutions and from a powerful dynamic soil-structure interaction computer program called SASSI as well as with field data. The analytical results indicate that dynamic analysis is generally not needed for the design of rigid pavements and that it usually leads to decreased pavement response. Thus, it appears that a quasistatic analysis is sufficient and that the results from this type of analysis will generally be conservative, provided that the wheel loads used in the analysis have been adjusted for the effects of vehicle velocity, truck suspension characteristics, and pavement roughness.

The problem of truck-pavement dynamics and its importance in the analysis and design of rigid pavements has been an increasing concern in the field of pavement engineering in recent years. The questions of (a) how important dynamic considerations are in affecting rigid pavement response and (b) which characteristics of the truck-pavement system are the most significant are yet to be answered. Today there are a number of finite-element methods available for analyzing jointed concrete pavements (*1–5*). However, these methods are restricted to static analysis. Recently, a few dynamic methods have been presented (*6–8*). These new methods are, however, confined to the analysis of continuous flexible pavements. A dynamic finite-element method for rigid airport pavements has just been published (*9*). The method, however, is not directly suited for incorporating realistic truck loads. Furthermore, the method is limited to representing the subgrade by a standard damped Winkler foundation.

This paper presents a new dynamic method for analyzing jointed concrete pavements subjected to moving dynamic truck loads. These loads are obtained by using truck simulation programs and are subsequently introduced to the pavement model as transient loads with arbitrary time histories. The method, which was implemented in a computer program called DYNA-SLAB, is an improvement over state-of-the-art procedures because it allows for moving transient loads and uses improved foundation support models. An additional important contribution from this study is a new analytical method for determining the stiffness and damping coefficients to be used in the Winkler foundation model.

The paper first describes the models and methods of analysis used in DYNA-SLAB. Later, an attempt to answer the questions raised above is made through the use of some application examples.

K. Chatti, Department of Civil and Environmental Engineering, A349 Engineering Building, Michigan State University, East Lansing, Mich. 48824. J. Lysmer, Department of Civil Engineering, University of California, Berkeley, 400 Davis Hall, Berkeley, Calif. 94720. C. L. Monismith, Institute of Transportation Studies, Department of Civil Engineering, University of California, Berkeley, 215 McLaughlin Hall, Berkeley, Calif. 94720.

DESCRIPTION OF MODEL

Structural Model

The structural model for the concrete slab system and load transfer mechanisms used in DYNA-SLAB is a modification of the model used in the well-known computer program ILLI-SLAB (*3*). The modified program accounts for inertial and viscous effects. In brief, the concrete slab is modeled by rectangular medium-thick plate elements that were independently developed by Melosh (*10*) and Zienkiewicz and Cheung (*11*). Each node contains three degrees of freedom: A vertical translation in the z-direction and two rotations about the x and y axes, respectively. Load transfer across joints is modeled either by a vertical spring element, to represent aggregate interlock or keyway, or by a bar element, to represent dowel bars. ILLI-SLAB's capability of handling the effects of stabilized bases or overlays on the stresses and deflections in concrete pavements, among other features, has been maintained. A description of the static model has been given previously (*3*). Figure 1 shows a schematic view of the DYNA-SLAB model.

Foundation Support Models

The subgrade is modeled by either a damped Winkler foundation with frequency-dependent springs and dashpots, uniformly distributed underneath the slabs, or a viscoelastic layered system on a rigid or deformable half-space.

In the Winkler foundation option the values for the springs (k) and dashpots (c) are determined by equating elastic and viscous forces, respectively, from steady-state force-displacement relationships of a massless slab supported by a layered medium and subjected to a harmonic unit load. To the best of the authors' knowledge, this method is the first attempt to determine the values of k and c analytically. The method is described next.

In the layered-solid foundation option, the subgrade dynamic stiffness matrix is obtained by inverting the dynamic flexibility matrix corresponding to the layered medium (Figure 2). At each frequency the ith non-zero column of the flexibility matrix is

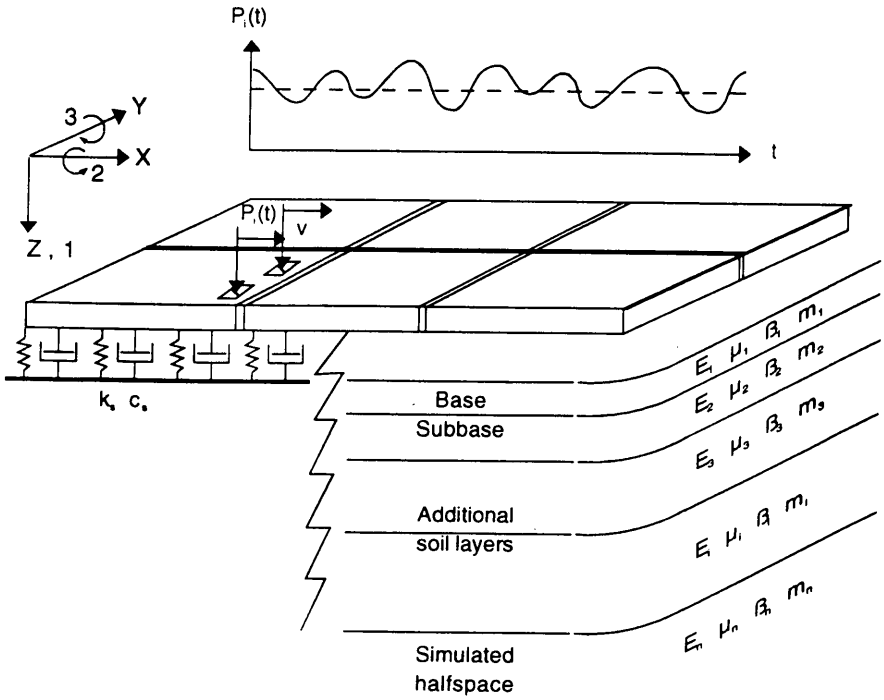

FIGURE 1 Schematic view of the DYNA-SLAB model, with damped Winkler foundation (LHS) and layered solid foundation (RHS).

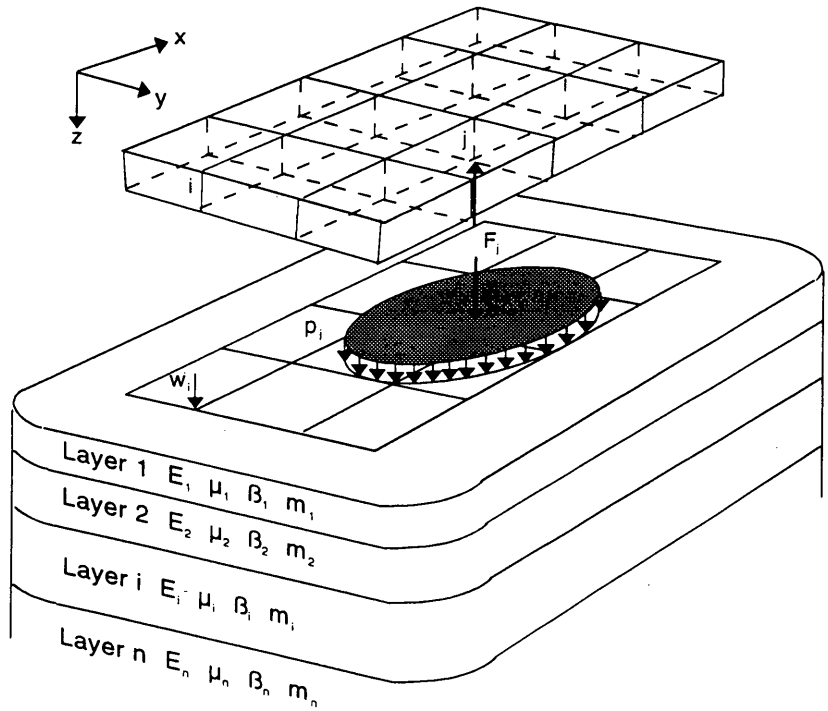

FIGURE 2 Interaction between concrete slab and multilayered system.

formed by calculating the vertical (complex) displacements, at all nodes, because of a vertical harmonic disk load of unit amplitude acting at Node *i*. The radius of the disk load is chosen equal to the distance between two adjacent nodes to establish compatibility with plate element displacements.

For both foundation types the displacement basin underneath the slab system is computed by using a computer program called SAPSI, developed at the University of California, Berkeley (*6*). This program solves for the response of a layered medium subjected to stationary dynamic surface disk loads. The accuracy of the SAPSI program has been verified by using available "exact" solutions (*6*) and more recently by comparing SAPSI results with extensive field data obtained using nondestructive test equipment for airfield pavements (*12*).

Method for Determining Dynamic Subgrade Stiffness and Damping Coefficients

Consider a massless slab resting on a layered soil profile over a half-space or a rigid boundary. If the layered foundation is equated to an analog system consisting of distributed springs and dashpots, then the internal forces in the system will be the elastic and viscous forces, which are represented by the springs, k, and the dashpots, c, respectively. The inertial forces in the slab are zero since the slab is massless. The only external force is the exciting force (Figure 3). The dynamic equilibrium of the system is satisfied by the following equation:

$$P(t) = k \int_A u(r,t)dA + c \int_A \dot{u}(r,t)dA \tag{1}$$

where k and c are the real elastic and viscous forces, averaged over the displaced volume, respectively, and the integrals represent the volume of the displacement basin, or its time derivative. For the steady-state case with circular frequency ω, the exciting force and the displacement response are both harmonics. By substituting these into Equation 1, equating the real and imaginary parts separately, and solving for k and c, one obtains (*13*):

$$k = P_0 \cdot \frac{\int_A ReU\, dA}{\left(\int_A ReU\, dA\right)^2 + \left(\int_A ImU\, dA\right)^2} \tag{2}$$

$$c = -\frac{P_0}{\omega} \cdot \frac{\int_A ImU\, dA}{\left(\int_A ImU\, dA\right)^2 + \left(\int_A ImU\, dA\right)^2}$$

These expressions will not work for edge/corner loadings.

Moving Load Representation

A moving load is represented by using local displacement shape functions from the finite-element formulation at successive time-dependent positions of the load as it moves from one plate element to the next. Thus, at each instant of time the global load vector is composed of zero entries except at the nodes of those elements on which the load is positioned. This block of nonzero values will

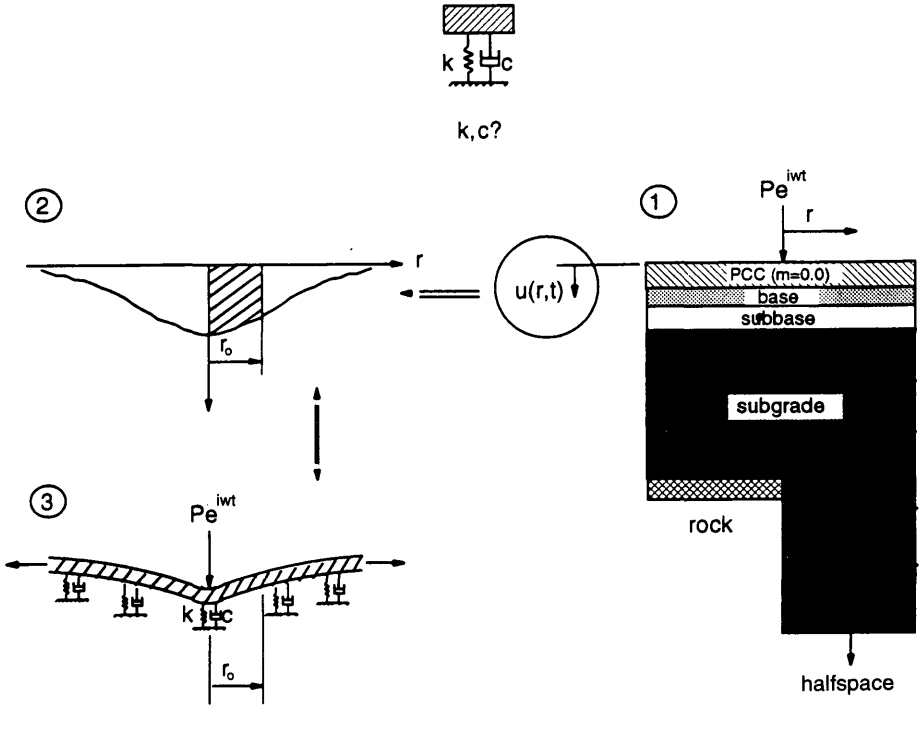

FIGURE 3 Determination of foundation parameters *k* and *c*.

be moving to other parts of the load vector as the load moves along the slab system. For a load distributed over a small area within an element, the block of nonzero values is composed of equivalent nodal forces expressed by

$$\{\bar{P}\}_e = \int_{b_1}^{b_2} \int_{a_1(t)}^{a_2(t)} [N(x,y)]^T p(t)\, dx\, dy \tag{3}$$

where

$a_1(t) = [v_0 t - (a/2)]$,
$a_2(t) = [v_0 t + (a/2)]$,
$[N]$ = shape function matrix for the element on which the distributed load is acting,
b_1 and b_2 = constant local y-limits of the loaded area,
$a_1(t)$ and $a_2(t)$ = local x-limits of the loaded area, and
a = length of the loaded area.

For multiple loads the overall load vector is obtained by superposing the effects of the individual loads.

METHOD OF ANALYSIS

The equation of motion governing the linear dynamic response of the pavement system is

$$[M]\{\ddot{U}\} + [C]\{\dot{U}\} + [K]\{U\} = \{P(t)\} \tag{4}$$

where $\{U\}$ is the vector of nodal displacements and $\{P(t)\}$is the external load vector acting at the nodal points. $[M]$, $[C]$, and $[K]$ are the total mass, damping, and stiffness matrices, respectively. The stiffness and damping matrices include the contributions from the slab system and the subgrade. The matrices for both stiffness and damping of the subgrade are based on the consistent mass formulation. The matrices can be written as

$$[M] = \sum_{e=1}^{n} [M]_e = \sum_{e=1}^{n} \rho_e \int \int_{A_e} [N]_e^T [N]_e dA_e \tag{5}$$

$$[K] = \sum_{e=1}^{n} ([K]_{\text{plate}} + [K]_{\text{subgrade}})_e$$

$$= \sum_{e=1}^{n} \left(\int \int_{A_e} [B]_e^T [D]_e [B]_e dA_e + k_e \int \int_{A_e} [N]_e^T [N]_e dA_e \right) \tag{6}$$

$$[C] = \sum_{e=1}^{n} [C]_{\text{subgrade}_e} = \sum_{e=1}^{n} c_e \int \int_{A_e} [N]_e^T [N]_e dA_e \tag{7}$$

where

$[N]_e$ = element shape function matrix,
$[B]_e$ = operator matrix expressing strains as a function of displacements, and
$[D]_e$ = constitutive matrix expressing stresses as a function of strains.

In the frequency-domain solution damping can be conveniently introduced by the use of complex stiffness matrices, which are formed exactly like real-valued matrices $[K]$ except that real coefficients are replaced by the corresponding complex values.

Two methods were used to solve the equation of motion (Equation 4), depending on the foundation support model. For the frequency-independent Winkler foundation. Newmark's constant acceleration method was chosen among the different time integration methods because the procedure is unconditionally stable and does not introduce artificial numerical damping (*14*). The method is based on satisfying the equation of motion at successive discrete time points that define a solution time interval, Δt, and assuming the acceleration to be constant within Δt and equal to the average of the end values. The complete algorithm is given elsewhere (*14*).

For both the frequency-dependent Winkler and the layered system foundations the complex response method was used. This method uses a complex representation for harmonic oscillations to solve for the steady-state response at several frequencies and obtains the transient response by superposition by using Fourier transforms. A more complete discussion of the complex response method can be found elsewhere (*15*).

VERIFICATION

To verify the moving load algorithm, DYNA-SLAB results were compared with the results obtained from two limiting theoretical solutions:

1. An approximate solution for the case of a point load moving on an infinite plate supported by an elastic Winkler foundation (*16*). The solution, which assumes that the displacement depends only on the radial variable, is valid only at speeds less than approximately half the critical speed of wave propagation (the velocity of flexural waves in the slab). As shown in Figure 4(*a*), good agreement was observed within the range of validity of the approximate solution.
2. An exact solution for the case of a transient load moving on a beam of finite length supported by a viscoelastic Winkler foundation (*13,17*). As shown in Figure 4(*b*), DYNA-SLAB predictions agree closely with this "closed-form" solution.

To verify the foundation models, deflection amplitudes due to harmonic loading for both interior and edge load cases were calculated at several frequencies by using DYNA-SLAB, with both foundation models, and compared with the results obtained by using a powerful three-dimensional dynamic soil-structure interaction computer program called SASSI (*15*) for three different soil profiles: a "typical" layered pavement profile [Figure 5(*a*)], a weak homogeneous half-space [Figure 5(*b*)], and a strong soil layer resting on a stiff rock formation [Figure 5(*c*)]. The values of k and c were calculated by the new method described above. The results show that sites with deep soil profiles will exhibit very strong damping ($\beta > 2.0$) because of the dissipation of energy through wave propagation (radiation or geometric damping). This observation is significant because it confirms analytically what several researchers have observed in field measurements of pavement deflections (*8,18*). Furthermore, the values of β obtained analytically herein fall within the range of values that these same researchers had to use to fit field measurements to theory.

Figures 6 to 8 show that DYNA-SLAB gives excellent results for all cases when the layered foundation system is coupled with the slab system. When the damped Winkler foundation is used there is very good agreement for center deflections; this further verifies the proposed method for determining k and c. However,

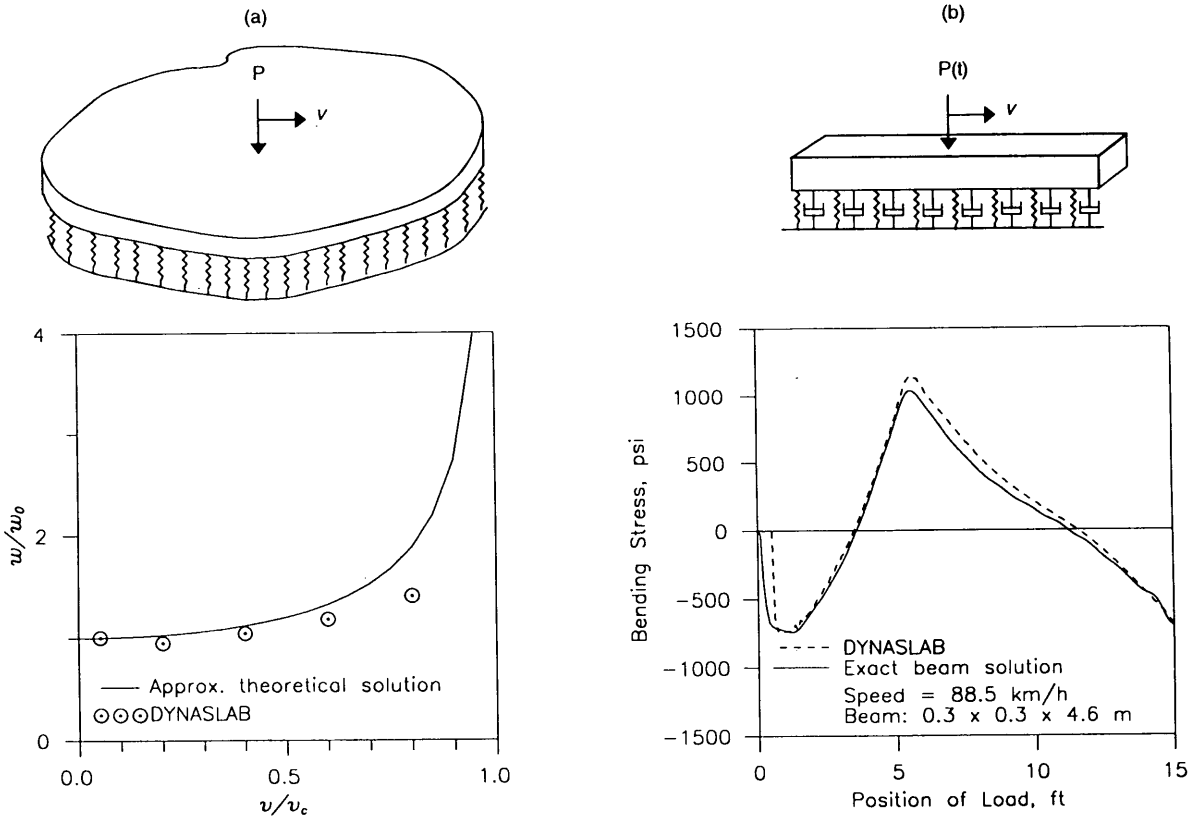

FIGURE 4 Theoretical verification of DYNA-SLAB: (*a*) comparison of dynamic to static deflection ratios of an infinite plate on a Winkler foundation; (*b*) comparison of bending stress influence lines for a finite beam on a damped Winkler foundation.

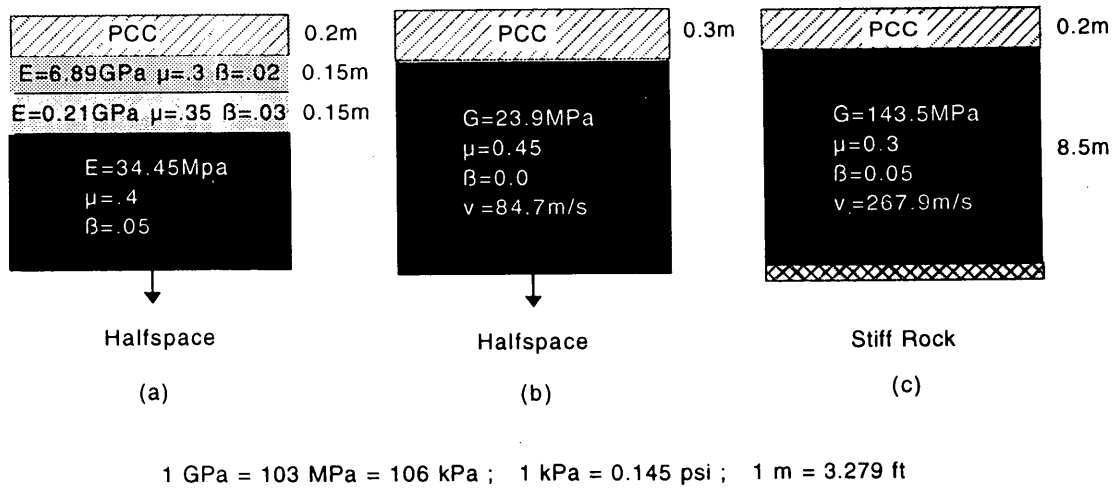

1 GPa = 103 MPa = 106 kPa ; 1 kPa = 0.145 psi ; 1 m = 3.279 ft

FIGURE 5 Pavement profiles used in the verification of DYNA-SLAB foundation models: (*a*) Profile 1; (*b*) Profile 2; (*c*) Profile 3.

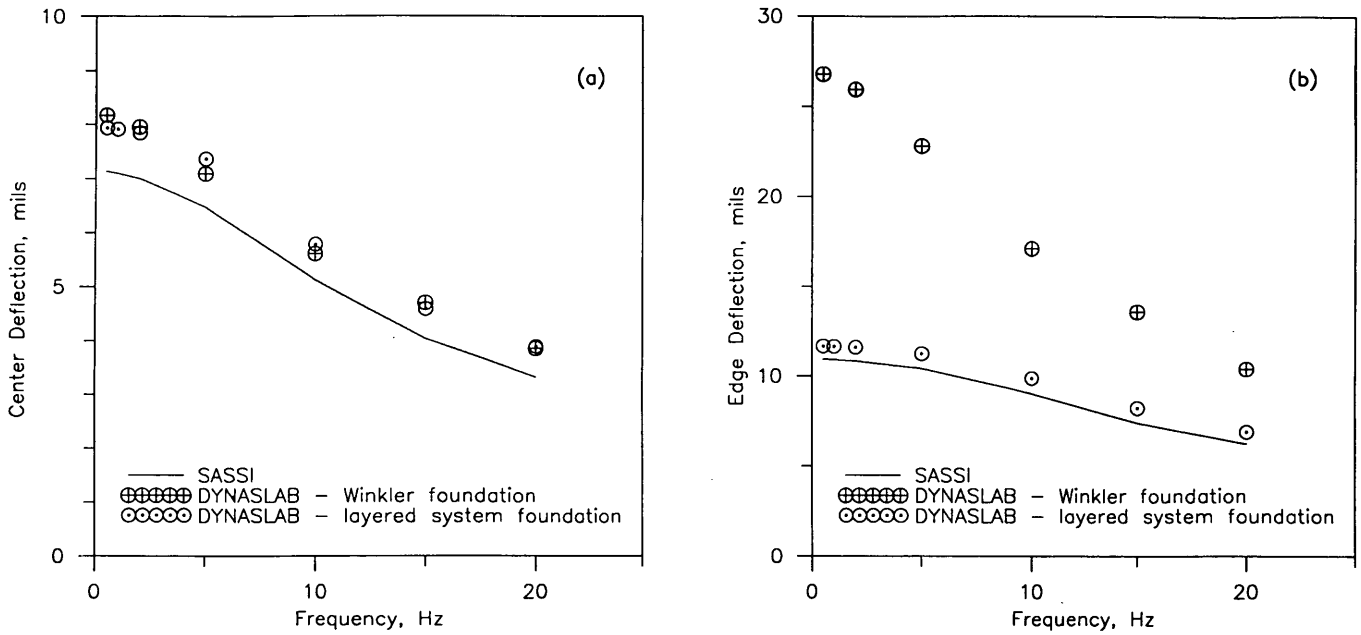

FIGURE 6 Verification of foundation models for Profile 1: (*a*) center loading; (*b*) edge loading.

edge deflections that are too high are predicted by DYNA-SLAB when the Winkler foundation is used. This is especially so at lower frequencies. This error is due to the Winkler assumption that implies that soil elements beyond slab edges do not provide any support. Overpredictions also occurred in the case in which there was a stiff layer at a relatively shallow depth (Figure 8). This is because a shallow rigid base may cause a wider deflection basin, suggesting that use of the equivalent radius of the slab as the radius of the deflection basin to compute k and c may not be appropriate in this case. Much better agreement was obtained when the equivalent radius of a rigid slab was used (*13*).

Further verification of the accuracy of DYNA-SLAB was made by using experimental results from a study conducted by the U.S. Army Corps of Engineers. The purpose of that study was to evaluate a number of nondestructive testing devices for use in airfield pavements (*19*). Results from three of the four rigid pavement sites (Sites 3, 7, and 11) measured by the WES 16-kip Vibrator were compared with DYNA-SLAB predictions. The results,

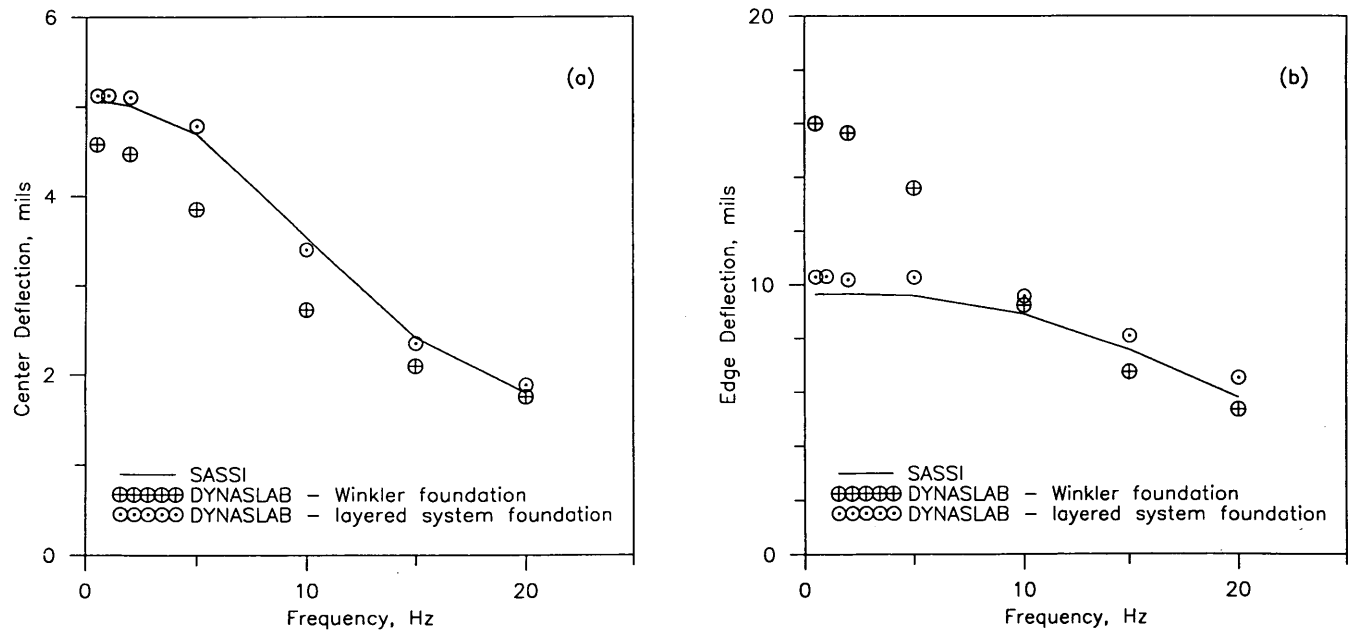

FIGURE 7 Verification of foundation models for Profile 2: (*a*) center loading; (*b*) edge loading.

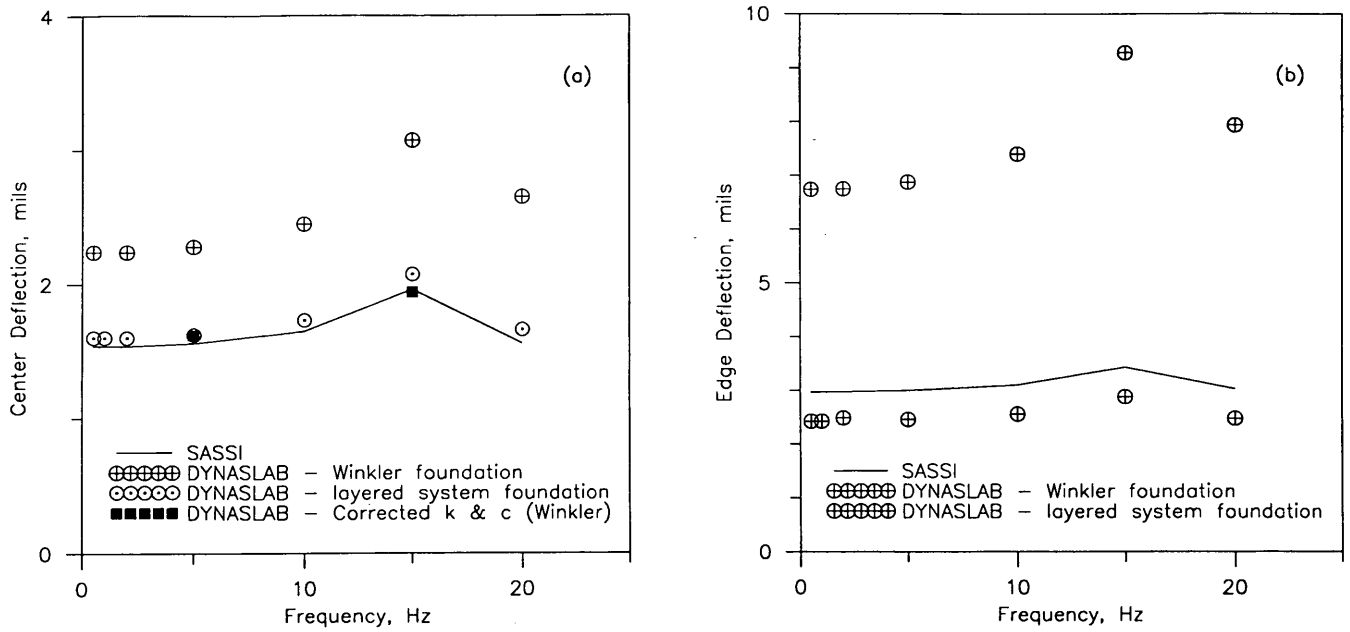

FIGURE 8 Verification of foundation models for Profile 3: (*a*) center loading: (*b*) edge loading.

shown in Table 1, indicate that DYNA-SLAB predicts very well the dynamic deflection at the joint, whereas the static ILLI-SLAB agrees well only for the case when the foundation support is stiff [81.4 MPa/m (300 pci) for Site 3 versus 21.7 MPa/m (80 pci) for Sites 7 and 11]. The discrepancy is probably due to a poor choice of the static coefficient of subgrade reaction as well as to the fact that the frequency of interest (15 Hz) departs considerably from the static case (0 Hz). Thus, dynamic effects may be significant.

PRACTICAL CONSIDERATIONS

The possible applications of DYNA-SLAB are numerous since it extends all of the capabilities of the original static ILLI-SLAB into the dynamic range. In the present study, however, the new computer program was used mainly to investigate whether dynamic analysis is really needed to predict the response of jointed concrete pavements subjected to moving dynamic truck loads. This was done through the use of some numerical examples.

Effects of Vehicle Speed

Figures 9 and 10 show the bending stress influence lines for points near the transverse joint and at midslab, respectively, due to a constant load moving at zero speed (quasistatic) and at 88.5 km/hr (55 mph) across a series of three 4.6-m (15-ft)-long slabs with

TABLE 1 Comparison of DYNA-SLAB Predictions with WES Experimental Results

Site No.	Foundation Parameters: Dynamic (15 Hz) Stiffness Coeff., k (MPa/m)	Damping Coeff., c (sec.MPa/m)	Damping Ratio, β	Static Coeff. Subgrade Reaction, k_s (MPa/m)	Maximum Deflection (mm) Measured	DYNASLAB	ILLISLAB
1[a]	-	-	-	-	-	-	-
3[b]	20.3	0.36	1.33	81.3	0.132 0.212	0.137 0.197	0.146 0.209
7[c]	8.9	0.34	2.74	22.2	0.203 0.329	0.238 0.349	0.509 0.748
11[d]	42.5	0.48	1.03	21.9	0.070 0.099	0.055 0.078	0.121 0.172

1 mm = 39.37 mil 1 MPa/m = 3.69 pci

[a] - unavailable data
[b] Pensacola NAS: 10in PCC + 4in Base
[c] Birmingham: 7in PCC
[d] Sheffard AFB: 21in PCC + 6in Base

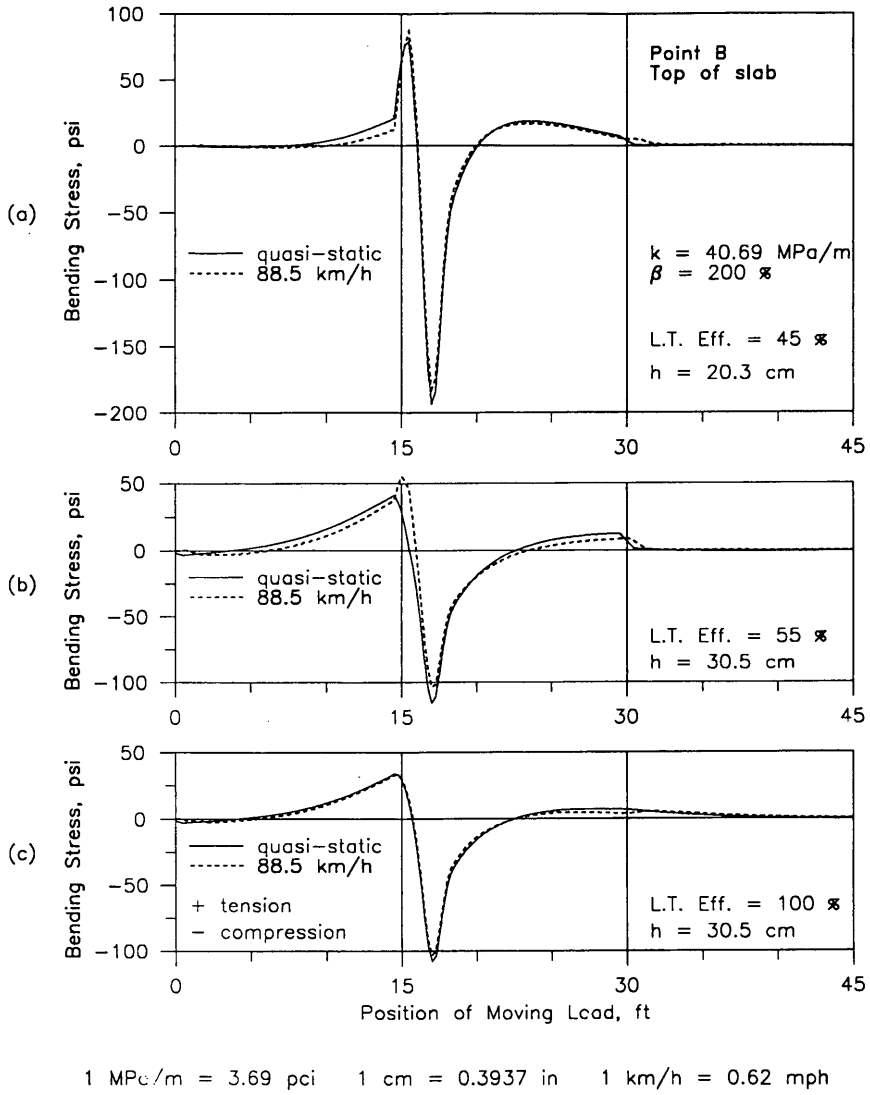

FIGURE 9 Bending stress influence lines at Point B located along the top edge of the slab at 0.6 m from the transverse joint: (*a*) weak aggregate interlock; (*b*) dowel bars; (*c*) strong aggregate interlock.

different load transfer mechanisms and different thicknesses. A comparison between graphs (*a*) and (*b*) in both figures confirms that the effect of slab thickness is most important, whereas comparison of graphs (*b*) and (*c*) indicates that the effect of load transfer efficiency is minimal. More important for the present study, however, is the fact that both Figures 9 and 10 clearly show that the effect of vehicle velocity on bending stress response is negligible.

Figure 11 indicates that the effects of both vehicle velocity and load transfer efficiency on the deflection response are somewhat more pronounced than those on bending stress. In contrast, the effect of slab thickness on the deflection response is less noticeable than the effect on the bending stress response.

Effects of Pavement Roughness

Dynamic wheel loads are caused by vibrations of the vehicle as it is excited by the roughness of the pavement surface. The dynamic forces generate additional stresses and strains in the pavement, which in turn may accelerate pavement deterioration and lead to increased truck "wear."

In the present study a truck simulation program termed VESYM, developed by Hedrick et al. (*20*), was used to generate axle loads. A typical 3-S2 18-wheel truck moving at 88 km/hr (55 mph) was assumed, and load time histories were generated for several surface profiles; these included faulting, day- and nighttime warping, and breaks of different levels of severity. Breaks caused the most severe load increases and joint faulting produced larger peak dynamic axle loads than did warping, for realistic distress levels (*13*).

Figure 12 shows computed bending stress influence lines at critical points in the slab for different pavement roughnesses. The stress pulses caused by the five different axles have basically the same shape irrespective of the axle number or the distress type. This suggests that the response pulses are basically independent

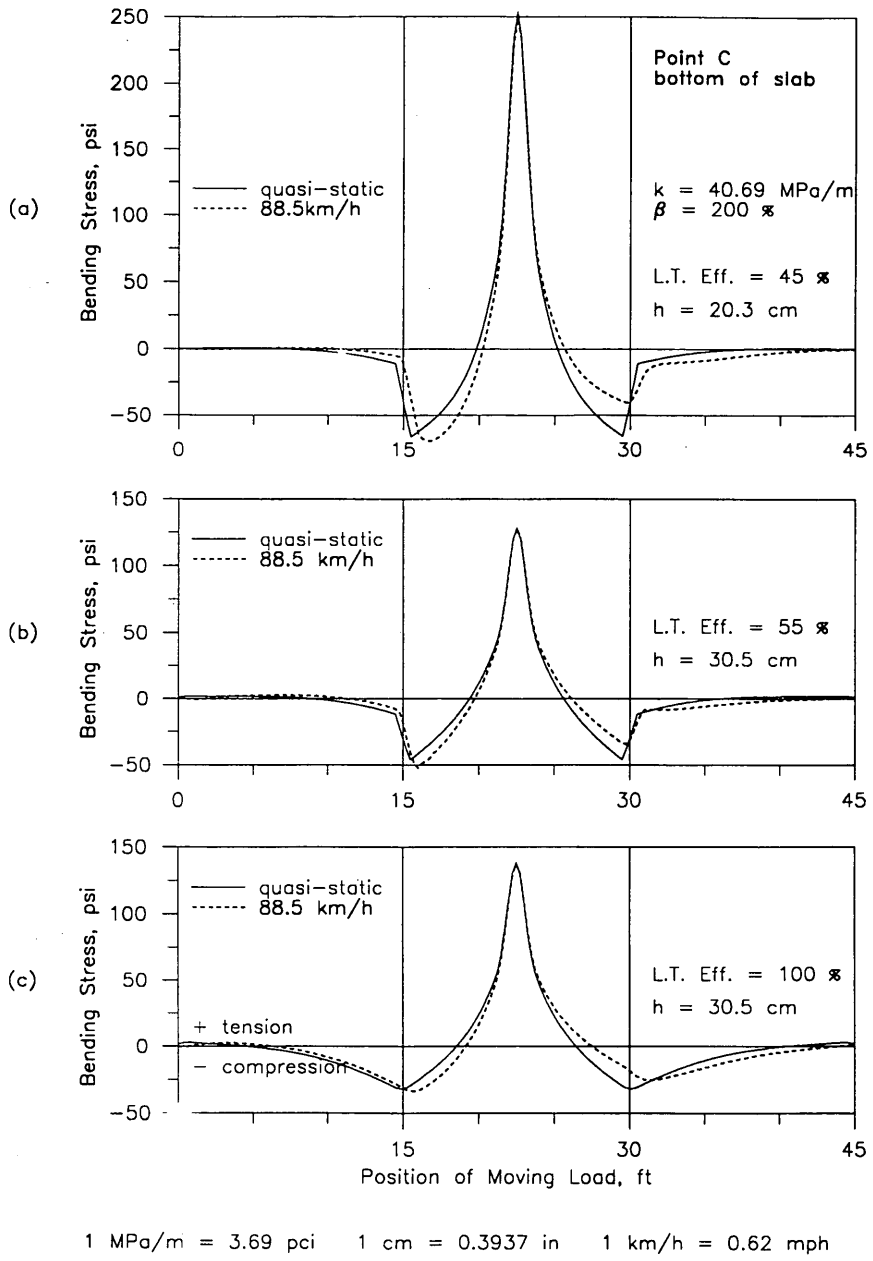

FIGURE 10 Bending stress influence lines at Point C located along the bottom edge of the slab at midslab: (*a*) weak aggregate interlock; (*b*) dowel bars; (*c*) strong aggregate interlock.

of the shape (frequency content) of the time histories of the axle loads. The frequency content of these pulses depend mainly on truck speed and other pavement factors such as the location of the response point, slab flexibility, or the load transfer mechanism. Furthermore, the quasistatic response curves are nearly identical to the dynamic curves (for β values of both 0.6 and 2.0). This is because the truck speed is considerably lower than the critical wave propagation velocity of the pavement.

These results clearly indicate that although it is important to correctly predict dynamic truck load histories in terms of their magnitudes and the locations of peaks (using truck simulation programs such as VESYM and appropriate pavement roughness profiles), dynamic analysis is generally not needed to determine the response of concrete pavements. Instead, once the dynamic loads have been determined it is sufficient to use a quasistatic analysis in which moving loads have different time-dependent values at different positions on the pavement, but are otherwise assumed to be stationary and constant at each instant of time.

Possibility of Dynamic Amplification due to Special Site Conditions

The existence of a stiff layer (e.g., bedrock) at a relatively shallow depth [e.g., within 10 m (33 ft)] may amplify the pavement re-

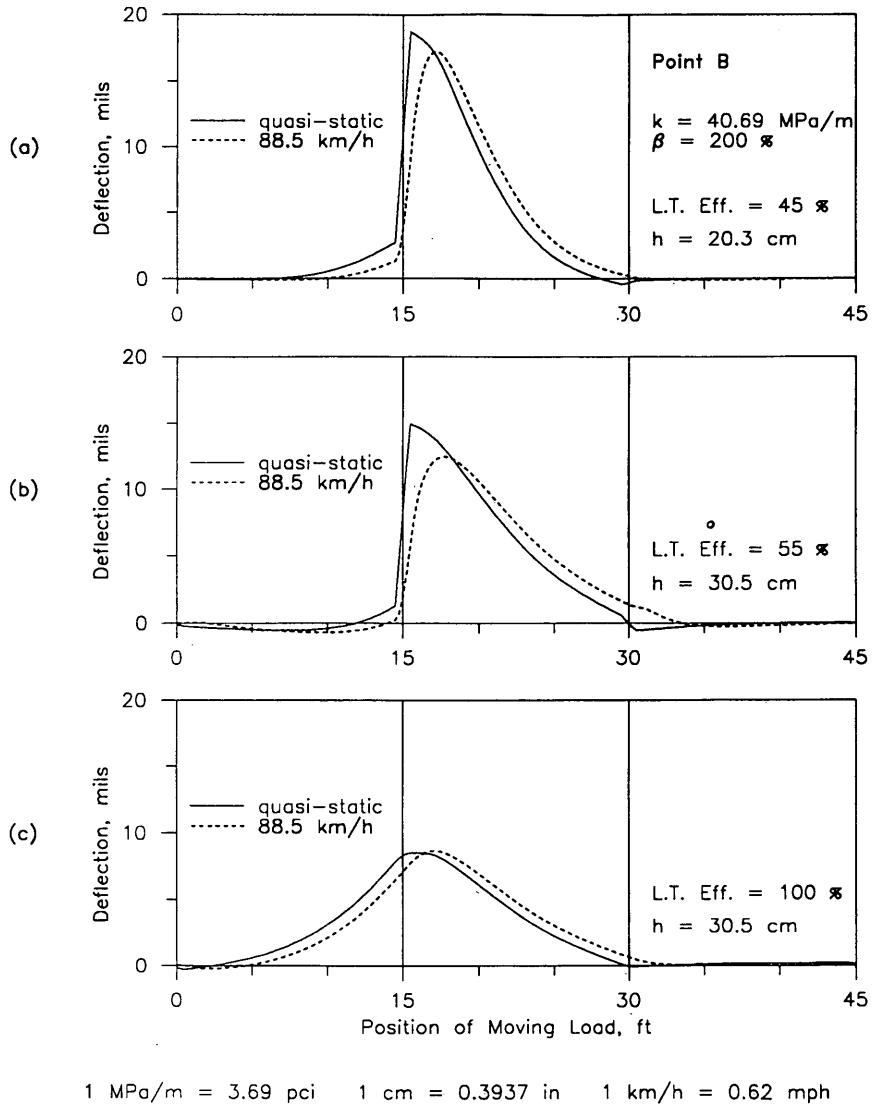

FIGURE 11 Deflection influence lines at Point B located along the edge of the slab at 0.6 m from the transverse joint: (*a*) weak aggregate interlock; (*b*) dowel bars; (*c*) strong aggregate interlock.

sponse at certain site-dependent frequencies as waves propagating away from the pavement slab reflect at the soil-bedrock interface and return back to the surface, interfering with downward propagating waves and, thus, increasing slab motions (resonance). In terms of foundation impedance coefficients, resonance occurs when the real part of the impedance (stiffness) is at or near a minimum. The possibility of resonant response because of a moving transient load was investigated in the present study for the hypothetical case in which both stiffness and damping vanish at a certain frequency. It was found that severe dynamic amplification (dynamic to static magnification factor higher than 5) will occur if the speed at which the load is moving causes a predominant frequency of the response that is nearly equal to the critical frequency (*13*). Further studies are needed to assess the practical significance of this finding.

SUMMARY AND CONCLUSIONS

A new dynamic linear finite-element method has been presented for the analysis of jointed Portland cement-concrete pavements with different foundation supports and subjected to moving loads with arbitrary time histories. The method is formulated either in the time domain by using Newmark's constant average acceleration method (Winkler foundation only) or in the frequency domain by using the complex response method (both Winkler and layered viscoelastic solid foundations). A rational method for determining the dynamic foundation stiffness and damping coefficients for the Winkler foundation has been developed by using layered continuum theory. The models and methods used were verified by comparing computed results with available theoretical solutions and experimental results. Several examples have been presented to il-

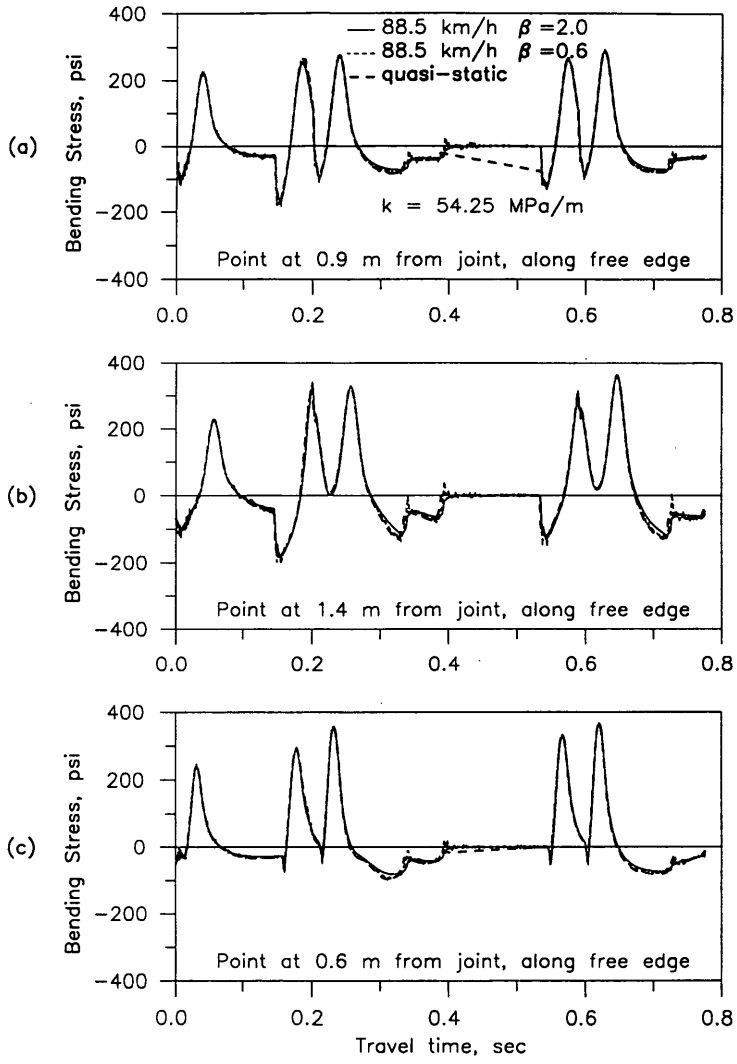

1 MPa/m = 3.69 pci 1 cm = 0.3937 in 1 km/h = 0.62 mph

FIGURE 12 Bending stress time histories at critical points in slab for different surface roughness profiles: (*a*) 0.5-cm warping; (*b*) 1-cm faulting; (*c*) 2.5-cm break.

lustrate the capabilities of the DYNA-SLAB computer program. The following conclusions were reached:

1. The major dynamic effect of moving traffic relates to the influence of vehicle speed and pavement roughness on the wheel loads that act on the pavement. Realistic time histories of wheel loads that consider pavement roughness and truck suspension characteristics can be determined by a truck simulation computer program. As far as the response of the pavement is concerned, only the peak values of the wheel loads and the velocity with which the loads traverse the pavement are important, with the latter being significant only in determining the durations and rise times of an individual pavement response pulse. The detailed frequency content of the wheel loads may be of importance for the truck and its suspension system, but it appears to have little effect on the behavior of the pavement.

2. Once the dynamic wheel loads have been determined, there is generally little to gain from a complete dynamic analysis of the pavement and its foundation. It appears that a quasistatic analysis, in which the time histories of wheel loads are treated as sequences of stationary static loads, is sufficient and that results from this type of analysis will generally be slightly on the conservative side as far as design is concerned.

3. There exists a possibility that an amplifying resonance phenomenon would occur in pavements founded on sites with a reflecting rock surface at a relatively shallow depth. Additional studies will be required to establish the conditions under which this may occur. For these conditions dynamic analyses may be required for pavement design.

ACKNOWLEDGMENTS

This research was made possible through funding provided by the University of California Transportation Center in collaboration with the U.S. Department of Transportation and the California Department of Transportation.

REFERENCES

1. Tayabji, S. D., and B. E. Colley. *Analysis of Jointed Concrete Pavements.* Interim Report FHWA/RD-86/041. FHWA, U.S. Department of Transportation, Feb. 1986.
2. Chou, Y. T. *Structural Analysis Computer Programs for Rigid Multi-Component Pavements with Discontinuities—WESLIQUID and WESLAYER.* Technical Reports 1, 2, and 3. Waterways Experiment Station, U.S. Army Corps of Engineers, Vicksburg, Miss., May 1981.
3. Tabatabaie, A. M., and E. J. Barenberg. Finite-Element Analysis of Jointed or Cracked Concrete Pavements. In *Transportation Research Record 671,* TRB, National Research Council, Washington, D.C., 1978, pp. 11–19.
4. Huang, Y. H. Finite Element Analysis of Slabs on Elastic Solids. *Journal of Transportation Engineering,* ASCE, Vol. 100, No. 2, 1974, pp. 403–416.
5. Huang, Y. H., and S. T. Wang. Finite Element Analysis of Concrete Slabs and Its Implications for Rigid Pavement Design. In *Highway Research Record 466,* HRB, National Research Council, Washington, D.C., 1973, pp. 55–69.
6. Chen, S. S. *The Response of Multi-Layered Systems to Dynamic Surface Loads.* Ph.D. dissertation. University of California, Berkeley, 1987.
7. Hanazato, T., K. Ugai, M. Mori, and R. Sakaguchi. Three-Dimensional Analysis of Traffic-Induced Ground Vibrations. *ASCE Journal of Geotechnical Engineering,* Vol. 117, No. 8, Aug. 1991.
8. Cebon, D. *An Investigation of the Dynamic Interaction Between Wheeled Vehicles and Road Surfaces.* Ph.D. dissertation. University of Cambridge, Cambridge, United Kingdom, 1985.
9. Kukreti, A. R., M. R. Taheri, and R. H. Ledesma. Dynamic Analysis of Rigid Airport Pavements with Discontinuities. *ASCE Journal of Transportation Engineering,* Vol. 118, No. 3, 1992, pp. 341–360.
10. Melosh, R. J. Basis for Derivation of Matrices for the Direct Stiffness Method. *Journal of the AIAA,* Vol. 1, No. 7, 1963, pp. 1631–1637.
11. Zienkiewicz, O. C., and Y. K. Cheung. The Finite Element Method for Analysis of Elastic Isotropic and Orthotropic Slabs. *Proc., Institution of Civil Engineers,* Vol. 28, Aug. 1964, pp. 471–488.
12. Tabatabaie, A. M. Dynamic Analysis of Pavement Systems-Model Evaluations. Presented at 70th Annual Meeting of the Transportation Research Board, Washington, D.C., 1991.
13. Chatti, K. *Dynamic Analysis of Jointed Concrete Pavements Subjected to Moving Transient Loads.* Ph.D. dissertation. University of California, Berkeley, 1992.
14. Bathe, K., and E. L. Wilson. *Numerical Methods in Finite Element Analysis.* Prentice-Hall, Englewood Cliffs, N.J., 1976.
15. Lysmer, J., M. B. Tabatabaie, R. Tajirian, S. Vahdani, and F. Ostadan. *SASSI—A System for Analysis of Soil-Structure Interaction.* Report 81-02, UCB/GT. University of California, Berkeley, April 1981.
16. Fryba, L. *Vibration of Solids and Structures Under Moving Loads.* Noordhoff International Publishing, Groningen, The Netherlands, 1972.
17. Boquenet, D., and D. Le Houedec. Comportement d'une Chaussée Reposant sur un Matelas Antivibratile et Soumise à des Charges Roulantes Vibratoires se Déplaçant à Vitesse Constante (in French). *Annales de l'Institut Technique du Bâtiment et des Travaux Publics, Paris, Série: Essais et Mesures,* March 1979, pp. 33–56.
18. Harr, M. E. Influence of Vehicle Speed on Pavement Deflections. In *Proc., Highway Research Board 41st Annual Meeting,* HRB, National Research Council, Washington, D.C., 1962, pp. 77–82.
19. Bentsen, R. A., A. J. Bush III, and J. A. Harrison. *Evaluation of Nondestructive Test Equipment for Airfield Pavements—Phase I: Calibration Test Results and Field Data Collection.* Technical Report GL-89-3. Waterways Experiment Station, U.S. Army Corps of Engineers, Vicksburg, Miss., Jan. 1989.
20. Hedrick, J. K., M. J. Markow, B. D. Brademeyer, and E. Abbo. *The Simulation of Vehicle Dynamics Effects on Road Pavements.* Final Report DTRS5684-C-0001. Office of University Research, U.S. Department of Transportation, Dec. 1988.

Publication of this paper sponsored by Committee on Rigid Pavement Design.

Sawcut Depth Considerations for Jointed Concrete Pavement Based on Fracture Mechanics Analysis

DAN G. ZOLLINGER, TIANXI TANG, AND DAPENG XIN

The efficient control of slab cracking that develops in concrete pavements is important to pavement performance. From the viewpoint of engineering analysis and the design of pavements it is desirable to control pavement cracking to joint locations at desirable intervals to decrease the possibility of uncontrolled cracking. An approach for estimating appropriate sawcut depths and placement timing by using fracture mechanics for jointed concrete systems is suggested. Early-age sawcutting, as one form of crack induction, has been applied to concrete pavement surfaces at specific contraction joint locations. A mechanics-based approach to the determination of sawcut depth and spacing requirements by fracture mechanics analysis is presented. The stress field in a concrete slab induced by thermal and shrinkage gradients is based on curling and warping analysis, which also leads to sawcut spacing criteria. The fracture parameters K_{If} and C_f defined by the size effect law are obtained from laboratory notched beam fracture tests for specific coarse aggregate types. Modified linear elastic fracture mechanics is applied to determine a sufficient notch or sawcut depth to ensure controlled cracking. Preliminary field results show that early-age sawcutting with appropriately determined joint spacing and depth can be used for the positive control of cracking in jointed plain concrete pavements. The theoretical sawcut depth, as determined by fracture analysis, that can be used in pavement construction practice, is significantly less than the conventional $d/3$ or $d/4$, where d is the slab thickness. Recent pavement surveys have verified this conclusion.

In newly paved concrete pavements the temperature rise caused by the hydration process can be considerable. If unrestrained the concrete pavement can expand and contract during the heating and subsequent cooling process without stresses being induced. Similar displacements may result because of shrinkage as the pavement dries and expands when it is wetted. However, actual pavements in the field are nearly always restrained to some degree by either an external restraint such as friction, the slab weight, tied adjoining lanes, or a combination of these. The interaction of the induced temperature and drying shrinkage gradients and the slab restraint can induce tensile stresses that lead to slab cracking. Field experiments have indicated that many sawcut joints in the concrete pavement typically break within the first few days after placement when concrete is poured under hot weather conditions. It is evident that an understanding of the mechanism related to early-age cracking in concrete pavements should provide a basis for making improvements in current pavement sawcutting practices with respect to an appropriate combination of sawcut timing and sawcut depths. The sawcut should be deep enough such that a crack initiated at a sawcut surface notch will propagate in an unstable manner from the sawcut tip to the slab bottom under stresses caused by temperature and shrinkage gradients or variations. Since this cracking consumes the elastic energy that developed within the concrete slab, stress and the incidence of cracking elsewhere are reduced in the slab. The controlled cracks reduce the restraint in the concrete pavement slab and therefore lower the maximum tensile stress. Since the early 1950s one-third of the pavement thickness ($d/3$) has been accepted and assumed to be the necessary depth of cut to induce cracking. However, literature reviews reveal little technical justification for this assumption other than field experience in isolated instances of uncontrolled cracking in which engineers may have assumed that deeper sawcuts would solve the problems with random cracking that they were experiencing. It will be shown later that the depth of the sawcut is dependent on the fracture strength of the concrete and that the most significant factor in the effective control of random cracking is the time of sawcut placement. In this sense the use of a sawcut depth of $d/3$ or $d/4$ in all instances without respect to aggregate type, concrete properties, or pavement thickness characteristics is technically unjustified. The conventional analysis of crack development in sawcut concrete pavement typically assumes a flawless beam or plate, although crack formation and development are of primary interest. In this paper fracture mechanics is applied to determine sawcut depth requirements on the basis of the stresses that develop during the first few days after concrete placement. Since the use of fracture mechanics to analyze sawcut depth criteria in jointed concrete systems constitutes a new approach to the analysis of crack development (and basically a rational approach to accurately account for the factors pointed out above), sufficient mathematical derivation will be provided to adequately document and justify the approach.

Texas Transportation Institute, Texas A&M University, College Station, Tex. 77843-3135.

THEORETICAL APPROACH: CLIMATIC STRESSES

Environmental stresses in concrete pavements can be attributed to both temperature and drying shrinkage effects and are particularly important at an early age. Stresses caused by both of these effects are discussed subsequently.

Thermal Stresses

Because of exposure to ambient conditions a concrete pavement may cool to a minimum temperature after cycling through a maximum temperature such that tensile stresses can be induced in the slab. The tensile stress distribution through the pavement thick-

ness can be assumed to be linear for the sake of simplicity, but others (*1,2*) have indicated that the distribution may be decomposed into three parts: axial stress, curling stress, and nonlinear stress. The stress distribution is caused not only by a temperature effect but may also be caused by moisture effects. Therefore, a complete analysis of early-age stresses will include curling, warping, and frictional stresses in which the axial stress component may be primarily due to subbase/subgrade frictional effects. Stress development may become significant very soon after placement, perhaps even before the concrete has attained a certain degree of stiffness (which may not occur until 18 to 24 hr after placement) has developed. Crack development in concrete pavements has been noted to be sensitive to diurnal temperature effects. The tendency to curl is restrained by the slab weight, in which the resulting level of stress development is a function of the stiffness of the subbase layer as reflected in the radius of relative stiffness (*l*). When the slab curls in an upward configuration, tensile stresses are induced in the upper part of the slab, whereas compressive stresses are induced in the lower part. Analysis of induced stresses by a linear temperature gradient in rigid pavements was developed by Westergaard (*3*) and others (*4*).

The Westergaard solution for slab stresses under temperature gradients will not be elaborated here. However, a similar approach for slab stresses caused by moisture gradients will be presented later. Westergaard presented solutions that considered curling stresses in a slab of infinite and semi-infinite dimensions on the basis of the following governing equations:

$$l^4 \frac{d^4w}{dy^4} + kw = 0 \tag{1}$$

where

$$l = \left[\frac{Eh^3}{12(1 - \nu^2)k}\right]^{1/4}$$

E = Young's modulus (psi),
ν = Poisson's ratio,
k = foundation modulus (psi/in.),
h = slab thickness (in.), and
w = slab deflection (in.).

Equation 1 encompasses a spring model that was proposed for the base reaction with the k value as the spring modulus. Although the slab weight restrains the curling, the weight is not included in the equation. However, the displacement (w) caused by curling can be considered only part of the slab displacement (*5*). In addition to w, the slab weight causes a uniform subsidence (w_s). The total displacement w_t is the sum of w_s and w. So long as $w_t = w_s + w \geq 0$, the spring model is valid even if $w < 0$.

The solution to Equation 1 indicates a negative w or upward displacements at or near the slab edge in concave curling, which should not be interpreted that the slab is pulled down there by the base (i.e., the Winkler spring should be released). Whenever w is less than 0, part of the slab weight is supported by the base, whereas the rest of it is supported by the slab itself, which contributes to the stresses in the slab. The total displacement w_t must be positive, otherwise Equation 1 is not valid. Further explanation is provided elsewhere (*5*).

Nonetheless, from Westergaard's analysis the maximum curling stress (σ_0) far away from the slab edge boundary is

$$\sigma_0 = \sigma' = \frac{E_c \alpha t}{2(1 - \nu)} = \frac{E_c}{2(1 - \nu)} \epsilon' \tag{2}$$

where

α = thermal coefficient of expansion (/°F),
t = temperature change or drop, and
$\epsilon' = \alpha t$.

Bradbury (*4*) developed coefficients on the basis of the Westergaard solution as applied to slabs of practical dimensions. The coefficients are used in the following equations:

Edge stress:

$$\sigma = \frac{CE_c\alpha t}{2} = C(1 - \nu)\,\sigma' \tag{3}$$

Interior stress:

$$\sigma = \frac{E_c\alpha t}{2}\left(\frac{C_1 + \nu C_2}{1 - \nu^2}\right) = \left(\frac{C_1 + \nu\, C_2}{1 - \nu^2}\right)\sigma'(1 - \nu)$$

$$= \sigma'\left(\frac{C_1 + \nu C_2}{1 + \nu}\right) \tag{4}$$

If $C_1 = C_2 = C$, then $\sigma = C\sigma'$.

The coefficient C_1 is the desired direction, whereas C_2 is for the direction perpendicular to this direction. L_x and L_y are the free length and width, respectively.

Shrinkage Stresses

Similarly, the interaction of drying shrinkage (ϵ^{sh}) of concrete and pavement restraint can induce stresses in a concrete slab. According to Bažant and Wu (*6*), the shrinkage of concrete can be described by the following function of humidity:

$$\epsilon^{sh} = \epsilon^{sh\infty}\,(1 - h^3)\ \text{(microstrain)} \tag{5}$$

where h (or rh to avoid confusion with slab thickness) in this and following expressions is the relative humidity, and $\epsilon^{sh\infty}$ is a material parameter, which is the ultimate concrete shrinkage at the reference rh of 50 percent. A formula from the model of Bažant and Panula (*7*) for calculating $\epsilon^{sh\infty}$ is applied here:

$$\epsilon^{sh\infty} = 1{,}330 - 970y \tag{6}$$

$$y = (390z^{-4} + 1)^{-1} \tag{7}$$

$$z = 0.381\sqrt{f'_{28}}\left[1.25\left(\frac{a}{c}\right)^{1/2} + 0.5\left(\frac{g}{s}\right)^2\right]^{1/3}\left(\frac{1 + \frac{s}{c}}{\frac{w}{c}}\right) - 12 \tag{8}$$

where

a/c = total aggregate/cement ratio,
g/s = coarse aggregate/fine aggregate ratio,
s/c = fine aggregate/cement ratio,
w/c = water/cement ratio, and
f'_{28} = 28-day cylinder compressive strength (psi).

In the middle portion of an infinitely large concrete slab where $(\partial^2w/\partial x^2) = (\partial^2w/\partial y^2) = 0$, the curling or warping strain is totally

restrained. Therefore, the shrinkage-induced stress at this location (σ^{sh}) is

$$\sigma_x = \sigma_y = \frac{E_c}{1 - \nu} \epsilon^{sh} \tag{9}$$

Moisture measurements in actual field slabs obtained by using instrumentation described by others (*8*) have indicated that the drying process tends to occur to some extent vertically through the slab. These measurements have also indicated the nonlinearity of the humidity profile vertically through a pavement slab during wetting and drying cycles. One would expect that such variations would result in similar profiles or distributions of moisture-induced warping stresses. The representation of these distributions numerically in an analysis may well require sophisticated methods such as the finite-element or finite-difference approaches. However, for the purpose of introducing an approach to the analysis of moisture-induced warping, the moisture-induced stress distribution in a concrete slab is simplified (as was done for temperature gradient-related stresses) to vary linearly along the thickness with the maximum tensile stress σ^{sh} at the top surface as shown in Figure 1. If it is assumed that the shrinkage stress distributes linearly through the thickness of the slab, varying from σ^{sh} at the top to zero at the bottom, the solutions provided by Westergaard (*3*) and Bradbury (*4*) can be implemented only by replacing ϵ' in all of the equations (e.g., Equations 2 to 4) by ϵ^{sh}. Another simplification results in no shrinkage-related stresses within $-H/2 < z < h/2$ ($0 < H < h$, as defined in Figure 1) and that the shrinkage-induced normal stress σ^{sh} linearly decreases from $z = -h/2$ to 0 at $z = -H/2$. Work is under way at the Texas Transportation Institute to model and verify the nonlinear temperature and moisture stress distributions in jointed concrete pavement by numerical analysis techniques.

The following mathematical expressions are provided to lend an adequate explanation for the inclusion of moisture-induced stresses in curling and warping analysis, since analysis of this nature has received little attention in the published literature. The moment caused by the shrinkage-induced, linearly distributed stress when the slab is fully restrained is calculated as follows:

$$M_y^{sh} = -\int_{-\frac{b}{2}}^{-\frac{H}{2}} \frac{\sigma^{sh}}{\frac{h - H}{2}} \left(z + \frac{H}{2}\right) z dz = \tag{10}$$

$$-\frac{\sigma^{sh}}{24(h - H)} \left(2h^3 - 3Hh^2 + \frac{1}{24} H^3\right)$$

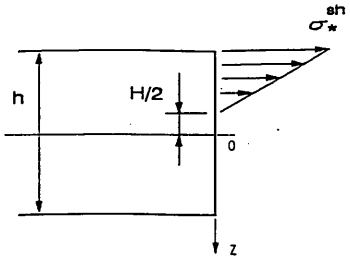

FIGURE 1 Shrinkage-induced stresses.

$$\sigma^{sh} = \frac{E}{1 - \nu} \epsilon^{sh} \tag{11}$$

where ϵ^{sh} is the free shrinkage at the top surface of the pavement, which may be estimated with Equations 6 to 8.

For the warping caused by shrinkage the following equations (in addition to Equation 1) result, corresponding to Westergaard's analysis for the thermal curling case:

$$M_y = D\left[-\frac{d^2w}{dy^2} - \frac{(1 + \nu)(2h^3 - 3Hh + H^3)\epsilon^{sh}}{2(h - H)h^3}\right] \tag{12}$$

$$\frac{d^2M_y}{dy^2} = -kw \tag{13}$$

Therefore, for a slab that has an edge along the x-axis and extends infinitely far in the positive y-axis direction and positive and negative x-axis directions the tensile stress at the top of the slab is

$$\sigma_y = \sigma^{sh}\left[1 - \frac{\sqrt{2}}{4} \frac{(2h^3 - 3Hh^2 + H^3)}{(h - H)h^2} \times \sin\left(\frac{y}{l\sqrt{2}} + \frac{\pi}{4}\right) e^{-\frac{y}{l\sqrt{2}}}\right] \tag{14}$$

$$\sigma_x = \sigma^{sh} + \nu(\sigma_y - \sigma^{sh}) \tag{15}$$

For an infinitely long strip of slab of finite width b with two edges $y = \pm b/2$

$$\sigma_y = \sigma^{sh}\left\{1 - \frac{1}{2} \frac{(2h^3 - 3Hh^2 + H^3)}{(h - H)h^2} \times \frac{\cos\lambda\cosh\lambda}{\sin2\lambda + \sinh2\lambda} \times \left[(\tan\lambda + \tanh\lambda)\cos\frac{y}{l\sqrt{2}} \cosh\frac{y}{l\sqrt{2}} + (\tan\lambda - \tanh\lambda)\sin\frac{y}{l\sqrt{2}} \sinh\frac{y}{l\sqrt{2}}\right]\right\} \tag{16}$$

and σ_x is found from Equation 15.

As seen, the difference between Westergaard's solution and Equation 14 is a factor of the second term in the braces. The numerical solution listed in Tables IV and V in Westergaard's paper can be easily modified for Equation 14. For example, $\sigma_c/\sigma_0 = 1.084$ for $\lambda = b/l\sqrt{8} = 3$ in Table V, but for the shrinkage case with $H = 0$

$$\sigma_y = \sigma^{sh}\left[1 - \frac{\cos\lambda\cosh\lambda}{\sin2\lambda + \sinh2\lambda} (\tan\lambda + \tanh\lambda) \cos\frac{y}{l\sqrt{2}} \frac{\cosh y}{l\sqrt{2}} + (\tan\lambda - \tanh\lambda) \sin\frac{y}{l\sqrt{2}} \sinh\frac{y}{l\sqrt{2}}\right] \tag{17}$$

Comparing Equation 17 with Westergaard's solution results in the following:

$$\frac{\sigma_y}{\sigma^{sh}} = 1 + \frac{(1.084 - 1)}{2} = 1.042$$

Maximum frictional stresses (σ_f) at the midslab area of a concrete pavement may be calculated from the traditional expressions elaborated by Yoder and Witczak (*9*). If the unit weight of concrete is taken as 144 lb/ft^3 then

$$\sigma_f = \frac{L}{2}\mu \tag{18}$$

where μ is the coefficient of subbase friction, and L is the length of the slab. Equation 18 suggests that σ_f will vary directly with L (for a given value of μ); however, a practical limit does exist for σ_f when it equals the maximum frictional stress (σ_m) that results from complete restraint at the bottom of the slab of the climate-induced strains:

$$\sigma_m = E(\epsilon^t + \epsilon^{sh}) \tag{19}$$

Therefore:

$$\frac{L}{2} = L' \leq \frac{1}{\mu} E(\epsilon^t + \epsilon^{sh})$$

where L' represents the length of pavement (from a construction joint) where $\sigma_f = \sigma_m$. Note in Equation 19 that as the friction coefficient increases, the distance to where $\sigma_f = \sigma_m$ decreases.

Friction coefficients depend on the type of subbase and typical coefficients and are listed by others (*10*). The variation in frictional stress along the slab length as it approaches the maximum frictional stress (σ_f) was found to vary nonlinearly by numerical analysis as suggested by McCullough (*10*) and Palmer et al. (*11*). Accordingly, the frictional stress at any point (x) from a construction joint (up to L') of a newly placed pavement may be only linearly approximated by Equation 19 if x is substituted for L' in Equation 19.

Creep Analysis

Creep can generally be defined as a time-dependent deformation of a material subjected to a sustained stress. When deformation is kept constant the creep reduces the stress. This process is defined as relaxation. As suggested by Grzybowski (*12*), stresses that result from relaxation under various strains such as restrained thermal expansion and shrinkage can be calculated by the rate of flow method (*13*). In this method the stress increment $\Delta\sigma_i = \sigma_{i+1} - \sigma_i$ caused by the strain increment $\Delta\epsilon_i = \epsilon_{i+1} - \epsilon_i$ can be obtained as follows:

$$\Delta\sigma_i = \frac{E(t_i)}{1 + \phi(t_{i+1}, t_i)} \Delta\epsilon(t_i) = R(t_{i+1}, t_i)\Delta\epsilon(t_i) \tag{20}$$

where

t = time
$R(t_{i+1}, t_i)$ = relaxation function, and
$\phi(t_{i+1}, t_i)$ = creep coefficient.

From Equation 20 the stress increment $\Delta\sigma_i = \sigma_{i+1} - \sigma_i$ caused by the strain increment $\Delta\epsilon_j = \epsilon_{j+1} - \epsilon_j$, which is imposed at time j before time i, can be calculated as follows:

$$\Delta\sigma = \frac{E(t_j)}{\phi(t_{i+1}, t_i) - \phi(t_i, t_j)} \Delta\epsilon(t_j) \tag{21}$$

The total stress increment that occurs during the ith time interval is the sum of the stress increments $\Delta\sigma_i$ caused by every strain increment $\Delta\epsilon_j (j \leq i)$ and the stress increment caused by the strain increment $\Delta\epsilon_i$:

$$\Delta\sigma_{i,tot} = \sum_{j=1}^{i=1} [R(t_{i+1}, t_j) - R(t_i, t_j)]\, \Delta\epsilon(t_j) + R(t_{i+1}, t_i)\, \Delta\epsilon(t_i) \tag{22}$$

Thus, the stress at the end of the ith time interval can be written as

$$\sigma(t_{i+1}) = \sigma(t_i) + \Delta\sigma_{i,tot} \tag{23}$$

A creep coefficient of the two time instants t and t_0 is suggested in American Concrete Institute (ACI), Standard 209R as

$$\phi(t, t_0) = \frac{(t - t_0)^{0.6}}{10 + (t - t_0)^{0.6}} \phi_\infty(t_0) \tag{24}$$

where

t = actual age of concrete,
t_0 = age of concrete at which the strain increment is imposed, and
$\phi_\infty(t_0)$ = ultimate creep coefficient, depending on the load age, $(t - t_0)$, concrete properties, and environmental conditions.

In the absence of specific creep and shrinkage data for the aggregates and conditions, ACI Standard 209R suggests:

$$\phi_\infty(t_0) = 2.35\, \gamma_c \tag{25}$$

where γ_c is the correction factor, which is the product of correction factors for the load age, ambient relative humidity, the average thickness of the concrete structure, and the cement content, fine aggregate content, and air content in the concrete.

Calculation of Climatic Stresses

The calculation of climatic stresses in a pavement slab at an early age will require the determination of Young's modulus and Poisson's ratio for the concrete. Oluokum et al. (*14*) examined the existing formula for Young's modulus of concrete at an early age proposed by ACI Standard 318. Their investigation showed that the ACI Standard 318 relation for Young's modulus evaluation is essentially valid at concrete ages 12 hr and greater:

$$E = 57{,}000\sqrt{f'_c} \tag{26}$$

where f'_c is compressive strength of concrete (in psi).

Klink (*15*) and Higginson (*16*) observed that Poisson's ratio of concrete varied little at different ages and curing conditions. According to their observations Poisson's ratio is insensitive to the mixture content as well as age and it may be taken as 0.15.

For discussion purposes the climatic stresses in a 13-in. concrete slab constructed in Texarkana, Tex., placed directly on subgrade were calculated. It was assumed that the test pavement,

during the period of crack development, behaved as an infinitely long slab of finite width b (assuming a 24-ft-wide, two-lane pavement). The frictional subbase stresses (σ_f) are calculated according to Equation 18 on the portion of the pavement segment where curling and warping stresses are a maximum. This was shown by Westergaard to be 4.44l from a free edge (the construction joint for new pavements) or greater. The computation of frictional stresses is based on the temperature and moisture changes that occur at the bottom of the slab and the appropriate coefficient of friction for an untreated clay subgrade (μ = 1.5).

Information from one of the concrete mix designs used in experimental pavement sections referred to previously is used in demonstrating the development of early-age stresses in jointed concrete pavements. The following data show the mix design ratios relevant to Equation 6: a/c = 7.36, w/c = 0.51, g/s = 1.36, and s/c = 2.80.

For this mix design the correction factor relevant to the equation for relaxation analysis is the product of all of the correction factors listed in Table 1.

Field data collected during the first 5 days after construction and placement of the concrete consisted of the slab temperature and the humidity profile. From these data the history of the maximum stresses in the slab was determined over the 5-day period; however, the history is not illustrated here because of space requirements. Maximum curling (σ^t) and warping (σ^{sh}) stresses over the first few days of construction require the determination of the time-dependent properties (compressive strength, modulus of elasticity, and l-value) of the concrete that vary during and for a period of time after hardening. The variation in the compressive strength (f'_c) of the concrete is shown in Figure 2. Noting how these parameters vary with time, it is no surprise to see a variation in the maximum σ^t and σ^{sh} values (as determined at the surface in the longitudinal direction). Since the pavement under consideration was placed directly on subgrade, the subgrade k-value was taken as 100 psi/in. Frictional stresses are calculated, as pointed out previously, on the basis of the temperature and moisture changes at the slab bottom; depending on the magnitude and direction of change, the total stresses may be tensile or compressive. The shrinkage stresses were calculated by using Equations 6 to 8 and the ratios tabulated previously. Equation 16 yields the warping stresses in the longitudinal direction. The warping stresses in the longitudinal direction include σ^{sh} (= σ_0 in this case) because of a shrinkage-caused gradient. The Bradbury expressions (Equations 3 and 4) are used to find similar thermal stresses. The combination of or total stresses discussed above were determined at a distance of 90 ft from the pavement end. The stresses were found at this distance because this is approximately where maximum restraint occurred in the paved segment, which approaches the center of the paved segment.

The sum of the combination of curling, warping, and friction will vary along the longitudinal axis of the paved segment. The maximum combination of these stresses, which occurs near the center of any paved segment, may be dominated by the frictional component. However, curling and warping stresses may dominate near the free edge of the paved segment. By considering the process of relaxation, the resultant of these two stress components is calculated by using Equations 20 to 25. The maximum friction-caused stress at 90 ft from the pavement free edge (where a first crack was found near the center of the paved segment) is 141 psi for a pavement thickness of 12 in., a unit weight of concrete of 150 lb/ft^3, and a friction coefficient of 1.5. The total longitudinal stress at the top of the pavement is the sum of the curling, warping, and friction-caused stresses at that location. Figure 3 shows the superposition of these three stresses at 90 ft from the pavement free edge. The dashed line includes only the combination of the curling and warping stresses. When the contribution caused by curling and warping is less than 141 psi the subbase friction dominates the restraint to slab movement and causes stresses that are equal to the value of the combination or exceeds them. The bold solid line in Figure 3 is the result of the superposition, the total longitudinal stress at the top of the pavement (which includes creep). Cracking appears to occur initially in the portion of the paved segment of maximum restraint and then proceeds from this point at intervals of 4.44l.

SAWCUT SPACING DEPTH REQUIREMENTS

To determine the spacing of the transverse joint locations or sawcuts for a newly placed concrete pavement for the purpose of stress analysis, the assumption that a newly paved pavement is infinitely long applies. Therefore, the maximum total climatic stress (as described previously) is calculated at approximate intervals of 4.44l as predicted by Westergaard analysis. The position of maximum stress may vary for early-age concrete because l changes during this period of time. As the concrete ages, maximum stress locations typically stabilize at 13- to 16-ft intervals, depending on the subbase type, which provides some guidance as to the recommended joint spacing for design and construction purposes.

The same analysis may apply to the spacing of the longitudinal sawcut locations; however, the focus in this instance is normally examination of the suitability of using standard joint locations, which often serve as lane dividers. In a two-lane pavement the longitudinal tensile stress at the pavement top is calculated at the longitudinal joint location (such as along the center line, where the pavement is divided into two 12-ft-wide strips) and the total tensile stress σ_x is reduced by a factor of 50 percent according to

TABLE 1 Correction Factors for Ultimate Creep Coefficient

variable	load age $(t-t_0)$	ambient R.H.=75%	pavement thickness h=12in	Slump s=1.5in	Cement Content c=521 lb/yard^3	air content α=5%	fine aggregate percentage ψ=35.9%
Correction factor	$1.25(t-t_0)^{-0.118}$	0.768	0.864	0.92	0.938	1	0.966

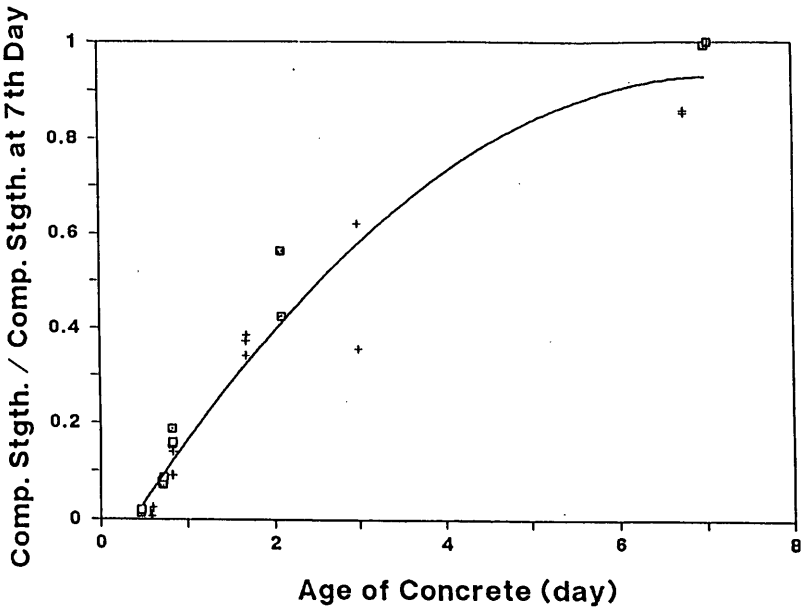

FIGURE 2 Variation in compressive strength of early-age concrete.

Equation 16, which in this case is below the tensile strength of concrete.

THEORY AND APPLICATION OF FRACTURE MECHANICS

The analysis of a notched concrete pavement slab on the basis of fracture mechanics incorporates the stresses generated by temperature and shrinkage effects, which are applied as loads. Important material parameters identified by the Size Effect Law (*17*) are determined on the basis of notched beam tests. The notch depth is great enough such that the crack will develop quickly and extend to the slab bottom under the applied stress. Through fracture tests the fracture parameters K_{If} and C_f have been obtained for early-age concretes made up of different coarse aggregates (*18*). The K_{If} is the critical stress intensity factor for a specimen of infinite dimension (in depth), in which linear elastic fracture mechanics (LEFM) applies to the analysis thereof. With respect to the application of K_{If} to a concrete slab, LEFM can still be applied to determine a sufficient notch depth, even though a concrete slab is not infinitely large. This is because the nominal strength of a specimen of infinite dimension is lower than the nominal strength that is predicted for the specimen of finite dimension by LEFM on the basis of K_{If} as the failure criterion.

As in linear mechanics the superposition principle can be used for the stress intensity when a specimen or structure is subjected to more than one load. The stress intensity factor caused by any load can always be expressed as follows:

$$K_I = \sigma \sqrt{\pi a}\, N(\omega) \tag{27}$$

where

σ = nominal stress,
a = crack length, and
$N(\omega)$ = nondimensional function of the ratio, ω, of the crack length a to the specimen dimension d.

$N(\omega)$ is called the nominal stress intensity factor. The beam depth (pavement thickness h) is usually taken as the dimension d. $N(\omega)$ is dependent on the specimen geometry but is independent of the specimen size. The nominal stress intensity factor $N(\omega)$ for the simple tension (*19*) is

$$N(\omega) = 1.122 - 0.231\omega + 10.550\omega^2 - 21.710\omega^3 + 30.382\omega^4 \tag{28}$$

where $\omega = a/h$ [Figure 4(*a*)] and the nominal stress σ is the load intensity. For the pure bending (*19*)

$$N(\omega) = 1.122 - 1.40\omega + 7.33\omega^2 - 13.08\omega^3 + 14.0\omega^4 \tag{29}$$

where $\omega = a/h$ [Figure 4(*b*)] and the nominal stress σ is the maximum stress in the distributed load. Note that these two formulas are for the geometry with top and bottom surfaces free from external forces. Because of the tendencies of curling and warping caused by the temperature gradient and shrinkage, Equation 29 is approximately valid. A double edge notched test specimen can be used to develop the fracture analysis because this specimen is somewhat representative of a slab configuration since the centerline in this symmetrical specimen is assumed not to move in the vertical direction. The following equation is valid for $\omega = (a/h) < 0.7$:

$$N(\omega) = 1.12 + 0.203\omega - 1.197\omega^2 + 1.930\omega^3 \tag{30}$$

where the nominal stress σ is the load intensity. Equations 8 and 9 are useful in applying the stress field induced by climatic effects to the determination of the stress intensity given in Equation 27

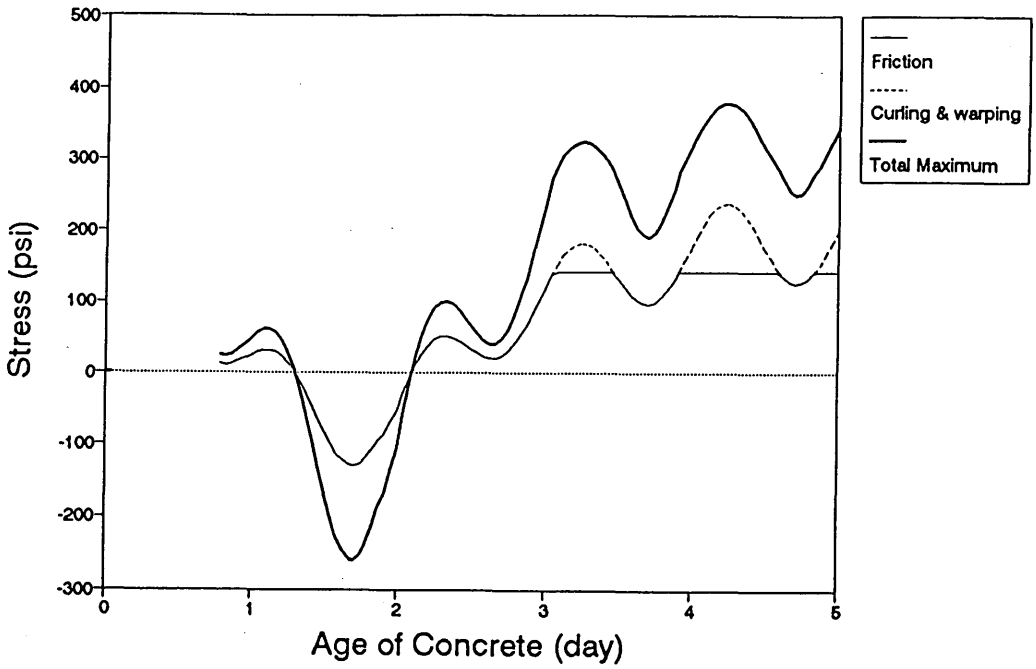

FIGURE 3 Development of stress at concrete pavement surface.

by dividing the stress field into components of tensile forces and bending moments. The finite-element analysis in this study has shown that replacement of the distributed load on a specimen by its resultant does not yield significant change in the K_I value, particularly when the specimen length is four times the thickness. Equation 29 can be applied to pure bending loads other than that shown in Figure 4(*b*) by substituting $\sigma = 6M/h^2$. Equation 30 can be applied to tensile loads on a single edge notched specimen whose unnotched edge remains straight. Accordingly, the shrinkage-induced stresses are transformed to a tensile force and a bending moment. For instance, if $H = h/2$, the resultant tensile force is $h\,\sigma^{sh}/8$, and then Equation 30 can be used in Equation 27 by substituting $\sigma = \sigma^{sh}/8$ (the resultant force). The bending moment $M = (5/96)\,\sigma^{sh}h^2$ yields $\sigma = (5/16)\,\sigma^{sh}$, in which case Equation 29 can be used. K_I results from the sum of Equations 29 and 30.

Determination of the stress intensity given in Equation 27 can be accomplished for a given set of climatic conditions at the anticipated sawcut location to generate the sawcut depth guidelines shown in Figure 5. The K_I values with different notch (sawcut) depths under temperature and shrinkage stresses are determined by Equations 29 and 30. Figure 5 also gives the K_I values for temperature differences t of 10, 20, 40, and 50°F between the pavement top and bottom with the same shrinkage-induced stresses.

The type of coarse aggregate is also important. When the critical stress intensity factor K_{If} equals or exceeds the fracture tough-

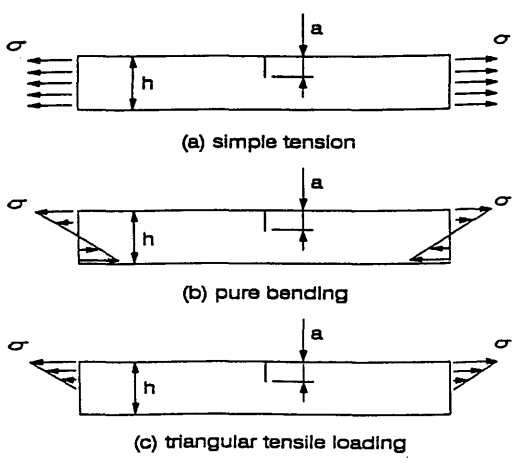

FIGURE 4 Notched specimens under loading.

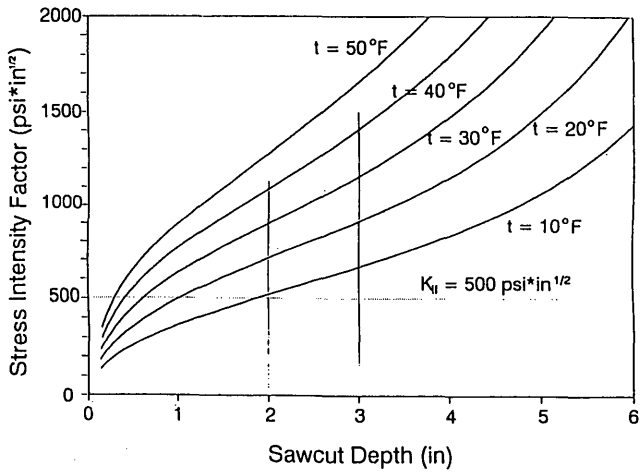

FIGURE 5 Determination of sawcut depths.

ness, K_{If} = 500 psi $\sqrt{\text{in.}}$ (typical for river gravel concrete at an age of 12 hr), a sawcut depth of 1 in. is enough if the temperature difference is not less than 20°F. When K_{If} = 800 psi $\sqrt{\text{in.}}$ (typical for limestone concrete at an age of 12 hr), a sawcut depth of 1.7 in. is enough if the temperature difference is not less than 30°F. Noting the change in stress intensity in comparison with the fracture toughness for the given climatic conditions, one can develop a sense for the appropriate sawcut timing to control cracking at the sawcut notches.

FIELD INVESTIGATION OF CRACK CONTROL

As pointed out previously, the factors that affect the behavior of concrete pavement as they relate to joint formation and crack control were monitored in a field study undertaken at test sections in Texarkana, Tex., for a 13-in. jointed plain concrete pavement placed directly on subgrade soils. Several factors were considered in these test sections such as different types of coarse aggregate, different curing methods, and different sawcut techniques and are elaborated further elsewhere (*9,20*) along with the type of concrete mixtures that were placed on subgrade soils. These mixtures consisted of different coarse aggregate types and blends. However, some results of the crack survey for the observation of joint and crack formation are provided here and coincide with the calculations given previously. Ambient and pavement temperatures and relative humidities were measured as indicated previously. The development of K_I and K_{If} is calculated and is shown in Figure 6. This analysis suggests that cracking initiated 4 to 5 days after placement.

The joints in the test section pavement in Texarkana were sawcut by two different techniques at 15-ft intervals. One method consisted of conventional sawcut techniques that used water to cool the saw blade. By this technique the pavement was cut 3-in. deep ($d/4$). The other method consisted of early-age sawcut techniques. By this technique a light and portable sawcutting machine was used so that a pavement surface notch could be placed early in the pavement life (typically less than 2 to 3 hr after placement). This was achieved without noticeable joint raveling. Typical sawcut depths were 1 in., and no cooling water was used in the process. Crack surveys conducted from October 1991 to July 1992 indicated that of all the transverse cracks that developed, only two occurred in between the sawcut joints. These two uncontrolled cracks were initiated from the corners of blockouts (i.e., inlet drainage structures), where stress concentration would have existed. It is speculated that these stress concentrations at the sharp corners could be avoided by placing joint locations so that they coincided with any sharp corners to guide cracking such that uncontrolled transverse cracks would not occur.

Although the pavement test section in Texarkana was paved on November 8, 1991, no visible cracks were found until November 26, 1991. Cracks at the sawcut tip were observed through the bottom of the pavement slab in later surveys. Earlier cracks occurred at a distance from the pavement construction joint since sufficient stresses needed to develop because of pavement restraint. It should be noted that on June 4, 1991, more joints had been formed at the early-age sawcuts than at the conventional sawcuts. One month later, three more cracks were found at the conventional sawcuts. A significant amount of cracking developed after the pavement was subjected to a greater temperature cycle range. Since the strength of the concrete increased prior to the increase in cracking, it is speculated that cracking at the sawcuts, although observed much later after construction, initiated early in the life of the pavement, which may be indicative of the fact that a certain level of damage is necessary to ensure that cracking will occur at the sawcut joint.

A closer look at the evolution of cracking indicated that the initial crack interval was on the order of 90 ft or more. Apparently, it is intervals of this magnitude at which the combination of curl, warping, and frictional stresses was enough to initiate cracking (Figure 6). The frictional stress may have been the significant contributor to crack development given the climatic conditions under

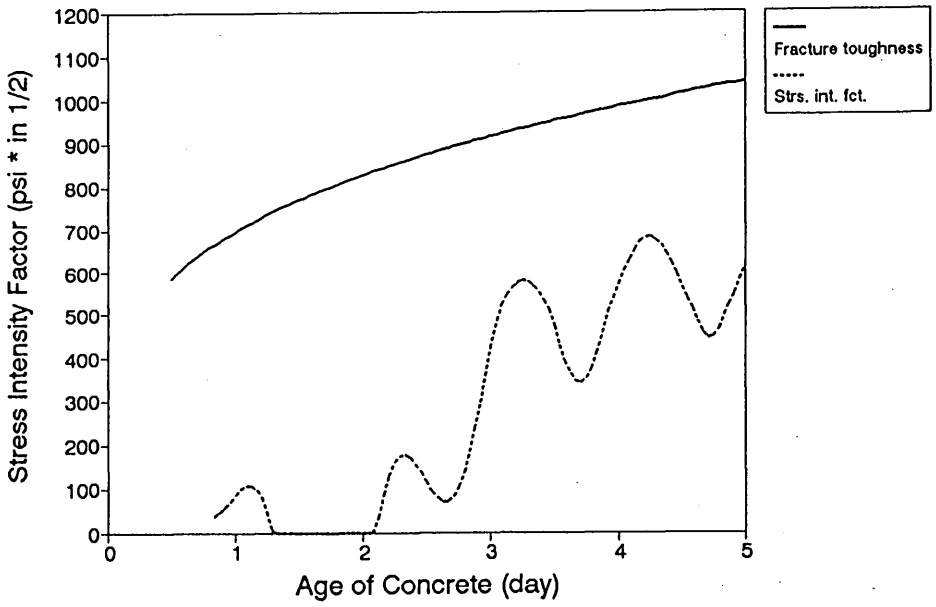

FIGURE 6 Development of stress intensity and fracture toughness.

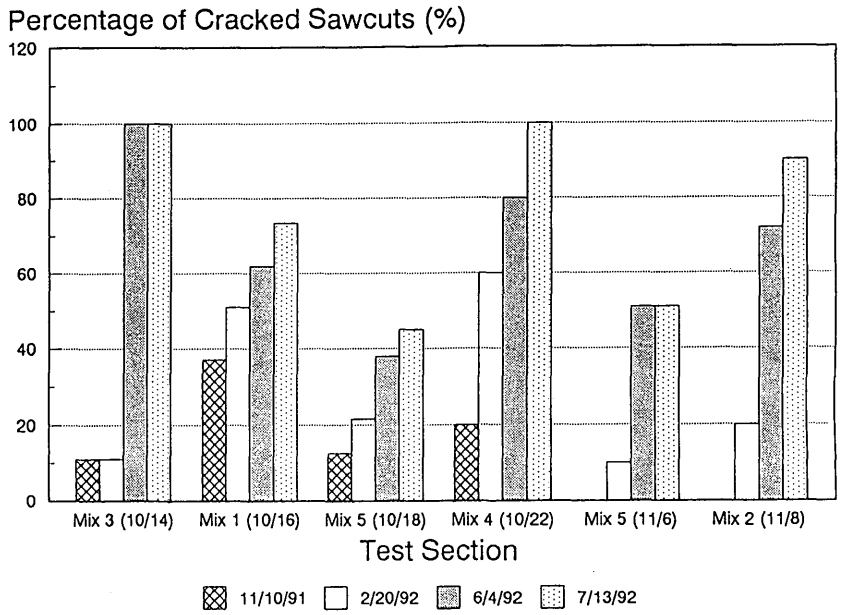

FIGURE 7 Percentage of sawcuts with cracks observed at different dates in test sections paved at different dates (in parentheses) with different concrete mix designs.

which the paving was accomplished, although a much improved crack pattern developed the following summer. The disadvantage of a crack pattern developing in this manner is that some joints open wider than they were designed to, which may damage the joint sealant material. It should be pointed out this characteristic was prevalent whether conventional or early-age cutting techniques were used. This situation deserves further consideration in future cracking studies.

It is interesting to note that different types of aggregate affect the fracture properties and crack development of concrete pavement, as shown in Figure 7. Cracking at the sawcut tip occurred more frequently when the concrete coarse aggregate type was river gravel than when it was crushed limestone. This was also the case in the subsection paved with the concrete that used a blend of crushed limestone and river gravel as the coarse aggregate in comparison with that in the subsection paved with the concrete that used crushed limestone only as the coarse aggregate. Laboratory tests showed that concrete of crushed limestone had a higher fracture strength than that of concrete of river gravel at early ages (*10,18*). These field results tend to confirm the validity of using early-age sawcutting techniques. Although not expressly addressed in this paper, it appears that sawcut timing is much more significant than sawcut depth. A shallow notch placed early in the pavement surface can take advantage of the greater change in temperature and moisture in the vicinity of the pavement surface (in comparison with the changes at a greater depth), which results in a greater amount of crack damage and subsequent incidence of cracking at the shallow surface notches.

CONCLUSIONS

Modified linear fracture mechanics is applicable for determining sawcut depth for cracks that develop early. The sawcut depth is dependent on the spacing of the transverse sawcut, the material fracture parameters K_{If} and C_f, and the stress level in the concrete slab with given geometrical conditions. The material fracture parameters vary with time, especially at early ages of concrete. Field observations have found that late-appearing cracks are also initiated by shallow (1 in.) sawcut notches. However, the propagation of these cracks may be caused by long-term fluctuating thermal and moisture loads, for which further research is needed.

The reduction of the sawcut depth (less than $d/3$ or $d/4$) at concrete joints by early-age sawcut or placement techniques can take advantage of the greater change in moisture and temperature in the concrete at the pavement surface (in comparison with the change at $d/3$ or $d/4$) to initiate a greater incidence of cracking at the notches than would otherwise be the case. Therefore, the control of cracking of concrete pavement should be improved. Field surveys indicate that under some circumstances (such as paving under cool weather conditions) transverse cracks at the sawcut notches may initiate much later after placement. On a preliminary basis this study indicates that it is reasonable to use notch depths at an early concrete age on the order of 1 in. to initiate cracking at the pavement surface, which is significantly less than the traditional $d/4$ or $d/3$.

ACKNOWLEDGMENTS

Appreciation is extended to the Texas Department of Transportation and FHWA for financial support under Project 1244. This paper is based on portions of the results of the study.

REFERENCES

1. Emborg, M. *Thermal Stresses in Concrete Structures at Early Ages.* Doctoral thesis. Luleå University of Technology, Luleå, Germany, 1989.

2. Richardson, J. M., and J. M. Armaghani. Stress Caused by Temperature Gradient in Portland Cement Concrete Pavements. In *Transportation Research Record 1121*, TRB, National Research Council, Washington, D.C., 1987.
3. Westergaard, H. M. Analysis of Stresses in Concrete Pavements Due to Variations of Temperature. *HRB*, Vol. 7, HRB, National Research Council, Washington, D.C., 1927.
4. Bradbury, R. D. *Reinforced Concrete Pavements*. Wire Reinforcement Institute, Washington, D.C., 1938.
5. Tang, T., D. G. Zollinger, and S. Senadheera. Analysis of Concrete Curling in Concrete Slabs. *Journal of Transportation Engineering*, July/September 1993, pp. 618–633.
6. Bažant, Z. P., and S. T. Wu. Creep and Shrinkage Law for Concrete at Variable Humidity. *Journal of the Engineering Mechanics Division*, Vol. 100, 1974.
7. Bažant, Z. P., and L. Panula. Practical Prediction of Time-Dependent Deformation of Concrete. Part 3: Drying Creep. Part 4: Temperature Effect on Basic Creep. *Matériaux et Constructions*, Vol. 11, No. 66, 1978.
8. Buch, N., and D. G. Zollinger. Preliminary Investigation on the Effect of Moisture on Concrete Pavement Strength and Behavior. In *Transportation Research Record 1382*, TRB, National Research Council, Washington, D.C., 1993.
9. Yoder, E. J., and M. W. Witczak. *Principles of Pavement Design*, 2nd ed. John Wiley & Sons, Inc., New York, 1975.
10. McCullough, B. F. *Mechanistic Analysis of Continuously Reinforced Concrete Pavements Considering Material Characteristics, Variability, and Fatigue*. Research Report 1169-2. Center for Transportation Research, University of Texas at Austin, April 1990.
11. Palmer, R. P., M. Olsen, and R. L. Lytton. *TTICRCP—A Mechanistic Model for the Prediction of Stresses, Strains, and Displacements in Continuously Reinforced Concrete Pavements*. Research Report 371-2F. Texas Transportation Institute, Texas A&M University, College Station, Aug. 1987.
12. Grzybowski, M. *Determination of Crack Arresting Properties of Fiber Reinforced Cementitious Composites*. Royal Institute of Technology, Stockholm, Sweden, 1989.
13. England, G. L., and J. M. Illston. Methods of Computing Stress in Concrete from a History of Measured Strain. *Civil Engineering and Public Works Review*, Vol. 60, No. 705, No. 706, and No. 707, 1965.
14. Oluokum, F. A., E. G. Burdette, and J. H. Deatherage. Elastic Modulus, Poisson's Ratio, and Compressive Strength Relationship at Early Ages. *ACI Material Journal*, Vol. 88, No. 1, 1991.
15. Klink, S. A. Aggregates, Elastic Modulus, and Poisson's Ratio of Concrete. *ACI Journal, Proceedings*, Vol. 83, No. 6, Nov.–Dec. 1985.
16. Higginson, I. L. Effect of Steam Curing on the Important Properties of Concrete,'' *ACI Journal, Proceedings*, Vol. 58, No. 3, 1961.
17. Bazant, Z. P., and M. T. Kazemi. Determination of Fracture Energy Process Zone Length and Brittle Number from Size Effect, with Application to Rock and Concrete. *International Journal of Fracture*, Vol. 44, 1990.
18. Zollinger, D. G., T. Tang, and R. H. Yoo. Fracture Toughness of Concrete at Early Ages. *ACI Material Journal*, Vol. 90, No. 5, Sept.–Oct. 1993.
19. Tada, H., P. C. Paris, and G. R. Irwin. *The Stress Analysis of Cracks Handbook*. Paris Productions Inc., St. Louis, Mo., 1985.
20. Tang, T., D. G. Zollinger, and F. McCullough. *Concrete Pavement Field Tests in Texarkana and La Porte*. Research Report 1244-7. Texas Transportation Institute, Texas A&M University, June 1994.

Publication of this paper sponsored by Committee on Rigid Pavement Design.

Loading and Curling Stress Models for Concrete Pavement Design

YING-HAUR LEE AND MICHAEL I. DARTER

Determination of the edge loading tensile bending stress in a concrete slab due to individual and combination effects of wheel loading and thermal curling is important to a mechanistic-based design procedure. The recent discovery of two additional dimensionless mechanistic variables, such that the problems encountered in previous investigations that have used dimensional analysis for thermal-related curling problems are resolved, is described. A new regression technique (projection pursuit regression) together with traditional linear and nonlinear regressions are utilized to develop prediction models. These prediction models provide an accurate representation of the finite-element model. They are simple, easy to comprehend, dimensionally correct, may be extrapolated to wider ranges of other input parameters, and are ready for implementation in a spreadsheet or computer program. Examples of practical applications showing the use of the new models are also provided.

Cracking of slabs can be caused by three different repeated loading positions: transverse joint, longitudinal joint midway between transverse joints, and at the corner. Given certain design, construction, and loading conditions, any of these load positions could lead to fatigue cracking over time. This paper focuses on the longitudinal joint edge location, which could lead to transverse cracking. Determination of the maximum bending stress at the edge is important to a mechanistic-based design procedure (the other positions are also important and should be evaluated). The analysis of longitudinal edge stress due to the individual and combination effects of wheel loading and thermal curling is presented in this paper. Critical stresses from the corner loading is being pursued as part of continuing research at the University of Illinois.

Finite-element models have been successfully used to account for the effects of a finite slab size as well as the possible loss of support due to a linear temperature differential more realistically than theoretical solutions basded on infinite slab and full contact assumptions. However, because of the required run time and complexity of the finite-element model, finite-element analysis cannot easily be implemented as a part of a design procedure. Therefore, a series of finite-element runs were performed over a wide range of pavement designs. The resulting edge stresses were compared with theoretical Westergaard solutions, and adjustment factors were introduced to account for this discrepancy. Statistical regression techniques were utilized to develop predictive models for each adjustment factor. These predictive models were then used as an alternative to finite-element analysis to estimate stresses for pavement design with sufficient accuracy.

Previous predictive models (*1,2*) were based on a series of input parameters by using multiple regression and stepwise regression techniques. Thus, the resulting models contain only arbitrary linear combinations of variables, with few insights in describing their actual physical relationships. The results of the prediction are also limited to the ranges of the cases analyzed.

This paper presents a more mechanistic-based approach in developing such predictive models. Through the use of the principles of dimensional analysis, the dominating mechanistic variables were first identified on the basis of previous research. In addition, two newly discovered additional dimensionless mechanistic variables were necessary such that the problems encountered in previous investigations that used dimensional analysis for thermal-related curling problems are resolved. A new regression technique (projection pursuit regression) together with traditional linear and nonlinear regressions were used to develop prediction models.

Consequently, three closed-form mechanistic design models that have been carefully validated and that are ready for implementation in a spreadsheet or computer program are presented as a result of the present study. In contrast to those earlier predictive models, the new models not only used the dominating mechanistic variables identified herein but they were also properly formulated to satisfy applicable engineering boundary conditions. These stress models turned out to be accurate representations of the finite-element model. They are simple, easy to comprehend, and dimensionally correct and can be extrapolated to wider ranges of other input parameters. The parameter estimates of each model have their own physical meanings as well. Examples of practical applications showing the use of the new models are also provided.

This paper not only provides more complete coverage of the solutions to the cases analyzed but it also demonstrates the advantages of incorporating subject-related engineering knowledge and selecting proper functional forms for the predictive models. It will be of interest to those working on mechanistic pavement design and pavement prediction modeling.

IDENTIFICATION OF IMPORTANT MECHANISTIC VARIABLES

Primary Structural Responses Due to Loading

In the analysis of a slab-on-grade pavement system, Westergaard (*3*) and others (*4,5*) have presented closed-form solutions for three primary structural response variables, that is, slab bending stress, slab deflection, and subgrade stress, owing to a single wheel load. On the basis of the assumptions of an infinite or semi-infinite slab over a dense liquid foundation (Winkler foundation), three different loading conditions (interior, edge, and corner) were analyzed.

Y.-H. Lee, Department of Civil Engineering, Tamkang University, E725, #151, Ying-Chuan Road, Tamsui, Taipei, Taiwan 25137, Republic of China. M. I. Darter, Department of Civil Engineering, University of Illinois, NCEL #1212, 205 North Mathews Avenue, Urbana, Ill. 61801.

The Westergaard solutions for a circular edge loading based on medium-thick plate theory are given as follows:

$$\sigma_w = \frac{3(1+\mu)P}{\pi(3+\mu)h^2}\left[\log_e \frac{Eh^3}{100ka^4} + 1.84 - \frac{4\mu}{3} + \frac{1-\mu}{2} + 1.18(1+2\mu)\frac{a}{l}\right] \quad (1)$$

$$\delta_w = \frac{\sqrt{2+1.2\mu}\,P}{\sqrt{Eh^3k}}\left[1 - (0.76 + 0.4\mu)\frac{a}{l}\right] \quad (2)$$

$$l = \sqrt[4]{\frac{Eh^3}{12(1-\mu^2)k}} \quad (3)$$

where

σ_w = Westergaard's edge stress (FL^{-2}),
δ_w = Westergaard's edge deflection (L),
P = total applied wheel load (F),
a = radius of the applied circular load (L),
E = modulus of elasticity of the concrete slab (FL^{-2}),
h = thickness of the slab (L),
μ = Poisson's ratio of the concrete,
k = modulus of subgrade reaction (FL^{-3}), and
l = radius of relative stiffness of the slab subgrade system (L).

(Note that primary dimensions are represented by F for force and L for length.) The subgrade stress was not explicitly specified; however, it can easily be determined by multiplying the slab deflection by the modulus of subgrade reaction.

Through the use of the principles of dimensional analysis, earlier investigators (*4*) have demonstrated that theoretical Westergaard solutions for these three primary structural responses can be reduced to three dimensionless terms, shown as follows, which all depend on the normalized load radius alone for a constant Poisson's ratio (usually $\mu \approx 0.15$).

$$\frac{\sigma h^2}{P}, \frac{\delta k l^2}{P}, \frac{q l^2}{P} = f\left(\frac{a}{l}\right) \quad (4)$$

where σ and q are equal to slab bending stress and subgrade vertical stress (FL^{-2}), respectively, and δ is equal to slab deflection (L).

By doing so the relationships between the primary structural responses and the external wheel loading are concisely defined. The dependent variables are $\sigma h^2/P$, $\delta k l^2/P$, and $q l^2/P$, whereas the independent variable is the dominating factor a/l, rather than the other input parameters (E, h, μ, k, and a). These relationships are not only simple to understand but they also provide a dimensionally correct form for further analysis on a more complicated problem.

The analysis of finite slab length and width effect owing to an external wheel load is not possible until the introduction of finite-element models. According to previous research (*4,5*), the normalized slab length and width (L/l and W/l, respectively) are the dominating mechanistic variables for the finite extent of slab condition, where L and W are the finite slab length and width, respectively. In fact, theoretical treatments on the effect of thermal curling (rather than wheel loading), which can be traced back as early as Westergaard (*6*) and Bradbury (*7*), have already shown that the finite extent of slab condition is simply a function of these two dimensionless terms. Thus, the following expression can concisely describe the above relationships:

$$\frac{\sigma h^2}{P}, \frac{\delta k l^2}{P}, \frac{q l^2}{P} = f\left(\frac{a}{l}, \frac{L}{l}, \frac{W}{l}\right) \quad (5)$$

Primary Structural Responses Due to Thermal Curling

Considering the curling stresses caused by a linear temperature differential on a concrete slab over a dense liquid foundation, Westergaard (*6*) developed equations for three slab conditions (i.e., an infinite, a semi-infinite, and an infinitely long strip). For the case of an infinitely long strip that had a finite width W and an infinite length along the x-axis, the deflection and bending stress solutions along the y-axis are given as follows:

$$\sigma_y = \sigma_0\left\{1 - \frac{2\cos\lambda\cosh\lambda}{\sin 2\lambda + \sinh 2\lambda}\left[(\tan\lambda + \tanh\lambda)\cos\frac{y}{l\sqrt{2}}\cosh\frac{y}{l\sqrt{2}} + (\tan\lambda - \tanh\lambda)\sin\frac{y}{l\sqrt{2}}\sinh\frac{y}{l\sqrt{2}}\right]\right\} \quad (6)$$

$$\delta_y = -\delta_0\frac{2\cos\lambda\cosh\lambda}{\sin 2\lambda + \sinh 2\lambda}\left[(-\tan\lambda + \tanh\lambda)\cos\frac{y}{l\sqrt{2}}\cosh\frac{y}{l\sqrt{2}} + (\tan\lambda + \tanh\lambda)\sin\frac{y}{l\sqrt{2}}\sinh\frac{y}{l\sqrt{2}}\right] \quad (7)$$

$$\sigma_0 = \frac{E\alpha\Delta T}{2(1-\mu)},\ \delta_0 = \frac{(1+\mu)\,\alpha\,\Delta T\,l^2}{h},\ \lambda = \frac{W}{l\sqrt{8}} \quad (8)$$

where

σ_y = bending stress along the y-axis (y is equal to $\pm W/2$ at the slab edges) (FL^{-2}),
δ_y = deflection along the y-axis (L),
α = thermal expansion coefficient of the concrete slab (T^{-1}), and
ΔT = linear temperature differential through the thickness of the slab (T).

Bradbury (*7*) later expanded Westergaard's bending stress solutions for a slab with finite dimensions in both the x and the y directions. Thus, considering a narrow and long strip of slab, the curling stress along the edge of the slab could be determined by the following equation:

$$\sigma_c = \frac{CE\alpha\Delta T}{2} = \frac{E\alpha\Delta T}{2}\left[1 - \frac{2\cos\lambda\cosh\lambda}{\sin 2\lambda + \sinh 2\lambda}(\tan\lambda + \tanh\lambda)\right] \quad (9)$$

where σ_c is equal to bending stress at the edge of the slab due to thermal curling (FL^{-2}).

Similarly, the closed-form solutions derived for slab bending stress, slab deflection, and subgrade stress owing to a linear temperature differential can be summarized in the following expression by using dimensional analysis for a constant Poisson's ratio:

$$\frac{\sigma}{E}, \frac{\delta h}{l^2}, \frac{qh}{kl^2} = f\left(\alpha\Delta T, \frac{L}{l}, \frac{W}{l}\right) \quad (10)$$

Identification of Two Additional Dimensionless Parameters

For thermal-related curling problems, Westergaard's and Bradbury's analytical solutions are based on an assumption of full contact between the pavement slab and the subgrade. However, experimental data by Teller and Sutherland (*8*) have clearly shown that parts of the pavement slab were found without subgrade support when a temperature or moisture differential existed through the slab thickness. Thus, the effect of the loss of subgrade support owing to a temperature differential must be considered to account for the actual pavement condition more realistically. The ILLI-SLAB finite-element model (*9–11*), which has implemented this effect through an iterative procedure and which has been developed over the years at the Univesity of Illinois, was selected for this study.

Because of the above theoretical difference, attempts by earlier investigators (*12*) to relate the actual structural response due to the combination effect of a single wheel load and a temperature influence using only the aforementioned dimensionless parameters were not very successful. Thus, it was necessary to search for other possible mechanistic variables to describe this difference adequately. Particular attention was focused on the effect of the self-weight of the concrete slab on the thermal-induced curling stress. Westergaard (*6*) did not explicitly consider the self-weight effect in his deflection equation, since the center of the slab was assumed to be flat and the deflection was zero. On the other hand, the effect of self-weight is included in the ILLI-SLAB model. The deflection at the center is determined by

$$\delta_\gamma = \frac{\gamma h}{k} \quad (11)$$

where γ is equal to the unit weight of the concrete slab (FL^{-3}).

Considering Westergaard's analytical solution for deflection as shown in Equation 7, the deflection due to thermal curling alone may be described by normalized slab length and width (L/l and W/l, respectively), the dimensionless product of $\alpha\Delta T$, and the deflection factor (l^2/h). All these parameters are dimensionless except the last one, l^2/h, which has the same dimension as length and can be used as an indicator for the extent of loss of subgrade support. By taking the ratio of self-weight deflection versus l^2/h, the following dimensionless parameter, D_γ, was defined to represent the relative deflection stiffness due to the self-weight of the concrete slab and the possible loss of subgrade support:

$$D_\gamma = \frac{\gamma h^2}{kl^2} \quad (12)$$

It was hypothesized that the resulting ILLI-SLAB edge strain due to curling alone may be well characterized by L/l, W/l, $\alpha\Delta T$ as well as by this additional parameter (D_γ). To validate this hypothesis, 16 ILLI-SLAB runs were performed by keeping the above four parameters constant while changing any individual input variables. The resulting edge stress was numerically confirmed to be proportional to the elastic modulus of the concrete slab as summarized in Table 1. In other words the resulting edge strains are equal to each other.

By the same token this "deflection ratio" concept was applied again in searching for another dimensionless parameter for the effect of an applied wheel loading on a curled slab due to a linear temperature differential. On the basis of Westergaard's analytical solution for deflection shown in Equation 2, the edge deflection can be represented by two parameters, a/l and $P/(Eh^3k)^{1/2}$. The second one is a deflection factor that is analogous to P/kl^2 and that has the same dimension as length. By taking the ratio of this deflection factor versus l^2/h, the following dimensionless parameter, D_P, can be used as an indicator to represent the relative deflection stiffness due to the external wheel load and the loss of subgrade support:

$$D_P = \frac{Ph}{kl^4} = 12(1 - \mu^2)\frac{P}{Eh^2} \quad (13)$$

Thus, it was also hypothesized that six dimensionless parameters, a/l, L/l, W/l, $\alpha\Delta T$, D_γ, and D_P, would adequately describe the primary structural responses for the combination effect of loading plus thermal curling. To numerically validate this hypothesis, 16 ILLI-SLAB runs were performed and are summarized in Table 2. Keeping these six parameters constant and changing any individual input variables result in ILLI-SLAB edge stresses proportional to the elastic modulus of the concrete slab. Thus, a unique edge strain was obtained as well.

Equations 14 and 15 summarize the above relationships due to the effects of thermal curling alone and loading plus curling, respectively:

$$\frac{\sigma}{E}, \frac{\delta h}{l^2}, \frac{qh}{kl^2} = f\left(\alpha\Delta T, \frac{L}{l}, \frac{W}{l}, \frac{\gamma h^2}{kl^2}\right) \quad (14)$$

$$\frac{\sigma}{E}, \frac{\delta h}{l^2}, \frac{qh}{kl^2} = f\left(\frac{a}{l}, \alpha\Delta T, \frac{L}{l}, \frac{W}{l}, \frac{\gamma h^2}{kl^2}, \frac{Ph}{kl^4}\right) \quad (15)$$

Factorial Finite-Element Runs

A series of factorial finite-element runs were performed on the basis of the dominating variables identified previously. Small personal computer programs were written to generate the finite-element grids and input files to facilitate routine finite-element analyses. The finite-element mesh was designed according to the guidelines established in earlier studies (*10*). With the assistance of a file of batch commands, these factorial runs were performed as a background job on the HP/Apollo network. The desired results were automatically summarized to avoid untraced human errors.

NEW PREDICTIVE MODELING PROCEDURES

The proper selection of regression techniques is one of the most important factors to the success of prediction modeling. Tradi-

TABLE 1 ILLI-SLAB Runs: An Additional Parameter (D_γ) for Curling Only

ΔT °F	h in.	E Mpsi	k pci	L in.	W in.	α x10^{-6}	γ pci	σ_i psi
16	8.47	39.94	51	398.94	398.94	6.88	0.136	1156.576
16	21.18	2.56	51	398.94	398.94	6.88	0.022	74.405
40	8.47	39.94	51	398.94	398.94	2.75	0.136	1156.132
40	21.18	2.56	51	398.94	398.94	2.75	0.022	74.376
16	8.47	19.97	102	282.09	282.09	6.88	0.136	578.046
16	21.18	1.28	102	282.09	282.09	6.88	0.022	37.179
40	8.47	19.97	102	282.09	282.09	2.75	0.136	577.815
40	21.18	1.28	102	282.09	282.09	2.75	0.022	37.164
16	8.47	4.99	409	141.05	141.05	6.88	0.136	145.151
16	21.18	0.32	409	141.05	141.05	6.88	0.022	9.339
40	8.47	4.99	409	141.05	141.05	2.75	0.136	145.095
40	21.18	0.32	409	141.05	141.05	2.75	0.022	9.335
16	8.47	2.22	920	94.03	94.03	6.88	0.136	64.563
16	21.18	0.14	920	94.03	94.03	6.88	0.022	4.139
40	8.47	2.22	920	94.03	94.03	2.75	0.136	64.539
40	21.18	0.14	920	94.03	94.03	2.75	0.022	4.138

Note:

1. L/l = 5.0, W/l = 5.0, $\alpha\Delta T$ = 1.1E-04, D_γ = 3.0E-05, μ = 0.15.
2. 1 °F = (F - 32) / 1.8 °C, 1 inch = 2.54 cm, 1 psi = 6.89 kPa, 1 pci = 0.27 MN/m^3

tional "parametric" regression techniques such as linear and nonlinear regressions require the imposition of a parametric form on the functions, and then the parameter estimates are obtained afterward. With the multidimensional pavement engineering problems in mind, several unresolved deficiencies in the use of traditional stepwise regression and nonlinear regression were frequently identified. These include problems in the selection of correct functional form, violations of the embedded statistical assumptions, and failure to satisfy some engineering boundary conditions.

In situations in which little knowledge about the shape and the form of a function exists, several new "nonparametric" regression techniques developed over the past 10 years have gradually gained popularity. Without imposing an unjustified parametric assumption, nonparametric regression techniques strive to estimate the actual functional form that best fits the data through the use of scatter plot smoothers (*13*).

The projection pursuit regression (PPR or "projection") algorithm introduced by Friedman and Stuetzle (*14*) appears to have the most favorable features because of its capability of handling variable interactions when suggesting transformations to improve the fit. The projection algorithm strives to model a multidimensional response surface as a sum of several projected curves through the use of a local smoothing technique. The projected curves are essentially two-dimensional curves, which can be graphically displayed, easily visualized, and properly formulated. The relative importance of each projected curve can be determined by measuring the absolute value of each coefficient associated with them as well.

A new statistical package named S-PLUS that has been widely used by statisticians for data analysis (*15–18*) was selected because of the availability of this new regression technique. As a result the following two-step modeling procedure was adopted (*19*):

1. Use the projection algorithm to break down the multidimensional response surface into a sum of several smooth projected curves, and
2. Use traditional linear and nonlinear regression techniques to obtain the parameter estimates of each individual projected curves and the overall regression statistics.

PREDICTIVE MODELS FOR LOADING ONLY

The effects of an external wheel loading subjected to a finite slab length and a finite slab width were analyzed separately. Adjustment (multiplication) factors for each individual effect were developed. Their combination effects can be approximately represented by multiplying both adjustment factors together.

Effect of Finite Slab Length

An adjustment factor (R_L) for the finite slab length effect was developed on the basis of the following relationship:

$$R_L = \frac{\sigma_i}{\sigma_w} = f\left(\frac{a}{l}, \frac{L}{l}\right) \quad (16)$$

TABLE 2 ILLI-SLAB Runs: Two Additional Parameters (D_γ) and (D_P) for Loading Plus Curling

c in.	P lbs	ΔT °F	h in.	E Mpsi	k pci	L in.	W in.	α x10^{-6}	γ pci	σ_i psi
2.5*	1833	16	8.47	9.99	204.35	119.68	159.58	6.88	0.136	172.266
2.5*	733	16	21.18	0.64	204.35	119.68	159.58	6.88	0.022	11.039
2.5*	1833	40	8.47	9.99	204.35	119.68	159.58	2.75	0.136	172.239
2.5*	733	40	21.18	0.64	204.35	119.68	159.58	2.75	0.022	11.038
5.0	3666	16	8.47	19.97	102.17	169.26	225.68	6.88	0.136	344.294
5.0	1466	16	21.18	1.28	102.17	169.26	225.68	6.88	0.022	22.063
5.0	3666	40	8.47	19.97	102.17	169.26	225.68	2.75	0.136	344.239
5.0	1466	40	21.18	1.28	102.17	169.26	225.68	2.75	0.022	22.060
7.5	8248	16	8.47	44.93	45.41	253.89	338.51	6.88	0.136	773.457
7.5	3299	16	21.18	2.88	45.41	253.89	338.51	6.88	0.022	49.565
7.5	8248	40	8.47	44.93	45.41	253.89	338.51	2.75	0.136	773.335
7.5	3299	40	21.18	2.88	45.41	253.89	338.51	2.75	0.022	49.557
10.0	14663	16	8.47	79.88	25.54	338.51	451.35	6.88	0.136	1360.855
10.0	5865	16	21.18	5.11	25.54	338.51	451.35	6.88	0.022	87.211
10.0	14663	40	8.47	79.88	25.54	338.51	451.35	2.75	0.136	1360.642
10.0	5865	40	21.18	5.11	25.54	338.51	451.35	2.75	0.022	87.197

Note:

1. Load dimensions are c x c, except those starred cases use 2c x c. L/l = 3.0, W/l = 4.0, $\alpha\Delta T$ = 1.1E-04, D_γ = 3.0E-05, D_P = 3.0E-05, μ = 0.15.
2. 1 °F = (F - 32) / 1.8 °C, 1 lb = 4.45 N, 1 inch = 2.54 cm, 1 psi = 6.89 kPa, 1 pci = 0.27 MN/m^3.

where σ_w is Westergaard's edge stress solution given in Equation 1 (FL^{-2}), and σ_i is the edge stress determined by the finite-element model (FL^{-2}). On the basis of a previous investigation (*7*), the maximum edge stress condition or Westergaard's infinite slab assumption may be achieved by selecting a value of 5.0 or more for the normalized slab length term (L/l). Thus, a more conservative value of 7.0 for both the normalized slab length and the normalized slab width (W/l) was selected to ensure an infinite slab condition. The following factorial finite-element runs were performed:

a/l: 0.05, 0.10, 0.20, and 0.30 and

L/l: 2.0, 2.5, 3.0, 3.5, 4.0, 4.5, 5.0, 6.0, and 7.0.

Note that W/l was kept at a constant value of 7.0 for all runs. The pertinent input parameters of these factorial runs regarding load size, total wheel load, slab thickness, concrete modulus, and subgrade reaction are given in Table 3. The resulting ILLI-SLAB edge stresses when L/l was equal to 7.0 and W/l was equal to 7.0 were used to approximate Westergaard's solution in calculating adjustment factors. A three-dimensional perspective plot providing a very clear picture of the relationship among R_L, a/l, and L/l is shown in Figure 1(*a*).

By using the aforementioned predictive modeling approach, the following one-term projection model was developed:

$$R_L = 0.9399 + 0.07986\Phi_1(ATX1) \tag{17}$$

$$\Phi_1(ATX1) = -4.0308 + \frac{1}{0.2029 + 0.0345ATX1^{-3.3043}} \tag{18}$$

$$ATX1 = -0.9436\frac{a}{l} + 0.3310\frac{L}{l} \tag{19}$$

Statistics: N = 36, R^2 = 0.994, SEE = 0.0063, CV = 0.67 percent
Limits: $2 \le L/l \le 7$, $0.05 \le a/l \le 0.3$
(note that N is the number of datum points, R^2 is the coefficient of determination, SEE is the standard error of estimates, and CV is the coefficient of variation.)

Effect of Finite Slab Width

The effect of finite slab width was often neglected in practice, since it is not as significant as the slab length effect. However, this effect as represented by the following adjustment factor (R_W) was considered in the present study to have a more complete coverage on this topic:

$$R_W = \frac{\sigma_i}{\sigma_w} = f\left(\frac{a}{l}, \frac{W}{l}\right) \tag{20}$$

TABLE 3 Pertinent Input Parameters for Loading and Loading Plus Curling

a/l	c	*a*	E	k	h	*l*	P	DG	DP
	in.	in.	Mpsi	pci	in.	in.	lbs		
0.05	2.5*	1.995	5	200	10.59	39.89	1250	3.07	2.61
0.10	5.0	2.821	4	300	8.23	28.21	2500	2.47	10.82
0.20	10.0	5.642	3	400	9.97	28.21	10000	2.72	39.34
0.30	10.0	5.642	2	500	7.16	18.81	10000	2.52	114.40

Note:

1. Load dimensions are c x c, except those starred cases use 2c x c. α = 5.5E-06 /°F, μ = 0.15, γ = 0.087 pci, p = 100 psi, DG = D_γ x 10^5, DP = D_p x 10^5.
2. 1 °F = (F - 32) / 1.8 °C, 1 lb = 4.45 N, 1 inch = 2.54 cm, 1 psi = 6.89 kPa, 1 pci = 0.27 MN/m^3.

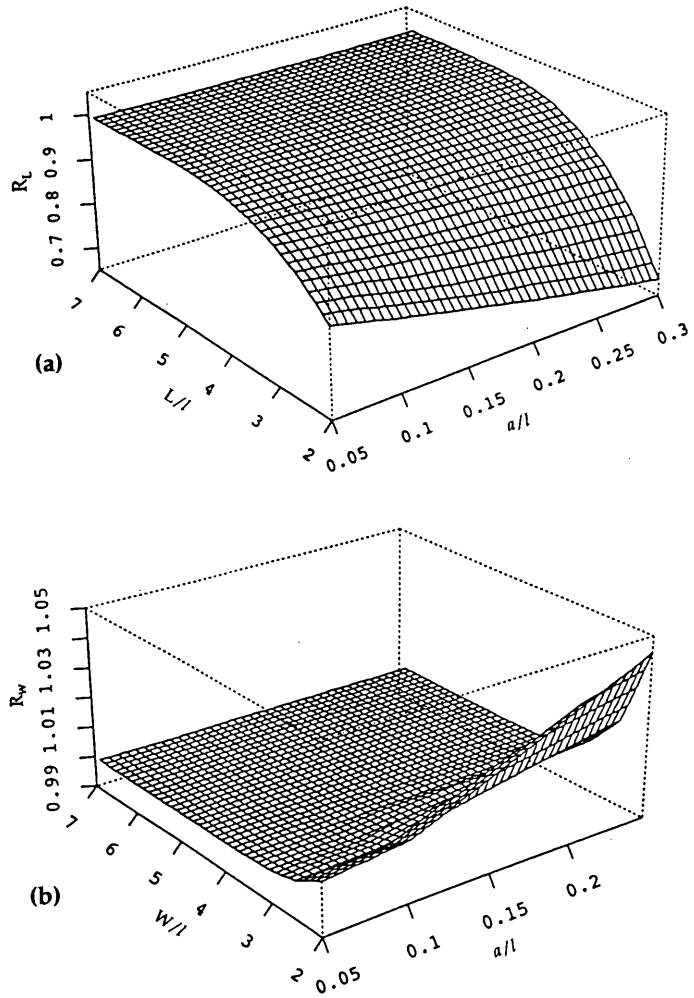

FIGURE 1 Finite slab size effects: (*a*) length and (*b*) width.

Thus, the following factorial ILLI-SLAB runs were performed:

a/l: 0.05, 0.10, 0.20, and 0.30 and

W/l: 2.0, 2.5, 3.0, 3.5, 4.0, 4.5, 5.0, 6.0, and 7.0.

Note that L/l was kept at a constant value of 7.0 for all runs. The pertinent input parameters were the same as before. A three-dimensional perspective plot for the relationship of R_w, a/l, and W/l is shown in Figure 1(*b*). As expected the slab width effect is not very significant. In fact this effect is negligible when W/l is greater than 3 or 4. Besides, this effect is more pronounced for a pavement slab with a smaller W/l but a larger a/l.

Similarly, the following one-term projection model was developed:

$$R_W = 1.00477 + 0.01214\Phi_1(ATX1) \quad (21)$$

$$\Phi_1(ATX1) = -0.5344 + 1.6540(1 - ATX1)^{-10.7412} \quad (22)$$

$$ATX1 = 0.9951\,\frac{a}{l} - 0.09856\,\frac{W}{l} \quad (23)$$

Statistics: $N = 36$, $R^2 = 0.947$, SEE = 0.00299, CV = 0.30 percent

Limits: $2.0 \leq W/l \leq 7.0$, $0.05 \leq a/l \leq 0.3$

Because of the limited number of runs performed and the narrow range of the adjustment factors obtained, this projection model was not as accurate as expected. However, it is relatively adequate for practical pavement design. With finer grids and more finite-element runs performed, the above equations can easily be improved by using the same modeling approach to achieve a higher degree of accuracy if necessary.

EFFECT OF THERMAL CURLING ONLY

The effect of a linear temperature differential and the finite extent of slab sizes must be considered together, since the principles of superposition cannot be applied here. To account for the theoretical difference between Westergaard's solution and the finite-element model, an adjustment factor (R_c) for curling may be defined as:

$$R_c = \frac{\sigma_i}{\sigma_c} = f\left(\alpha\Delta T, \frac{L}{l}, \frac{W}{l}, \frac{\gamma h^2}{kl^2}\right) \quad (24)$$

where σ_c is Westergaard's and Bradbury's edge stress solution given in Equation 9 (FL^{-2}).

Note that the adjustment factor introduced here is undefined when there is no temperature differential across the slab thickness. If temperature differentials are small, the ILLI-SLAB results caused by daytime curling are approximately equal to those caused by nighttime curling. The difference between them becomes substantial because of the combination effects of the self-weight of the concrete slab and the different extent of the loss of subgrade support caused by higher temperature differentials. Therefore, predictive models were separately developed for each daytime (positive ΔT) and nighttime (negative ΔT) curling condition.

Preliminary Analysis

To investigate the combination effects of a linear temperature differential, a finite slab length, and a finite slab width, the following full factorial ILLI-SLAB runs were performed:

L/l: 3, 5, 7, 9, 11, 13, and 15;

W/l: 3, 5, 7, 9, 11, 13, and 15; and

ΔT: ±10, ±20, ±30, and ±40°F.

The symmetry option of the program was used to allow finer grids generated for the ILLI-SLAB runs. A constant slab thickness of 10.59 in. with an elastic concrete modulus of 5×10^6 psi over a subgrade with a k-value of 200 pci was also chosen for these runs. The coefficient of thermal expansion α was 5.5×10^{-6}/°F, and the slab Poisson's ratio was 0.15. The unit weight of concrete slab (γ) was set to 0.087 pci because it is approximately constant in practice. [Note that 1°F = (°F − 32)/1.8°C, 1 in. = 2.54 cm, 1 lb/in.^{2} = 6.89 kPa, 1 pci = 0.27 MN/m^3.]

The relationships among these variables and adjustment factors for the daytime curling condition are displayed in Figure 2. Through the assistance of graphical displays the overall trend and the individual adjustment factor can be easily identified. In this manner any extraordinary behavior of the data may be located as well. As expected, the L/l requirement for an infinite slab condition is higher for higher temperature differentials. The theoretical discrepancy is higher for a shorter slab with a large negative temperature differential. On the basis of this investigation, those shorter slabs having both L/l and W/l equal to 3.0 were decided to be excluded from later predictive model development. It is mainly because numerical difficulties might arise while taking the ratio of small ILLI-SLAB results and small theoretical Westergaard solutions. Any approximation that resulted from the ILLI-SLAB program might adversely affect the accuracy of the adjustment factors.

Attempts to develop predictive models with only these three important variables were not very successful. This was also the main reason that prompted the authors to search for an additional mechanistic variable, as previously discussed.

Predictive Models for Thermal Curling Only

Additional ILLI-SLAB runs were apparently necessary since D_γ was unintentionally kept at a constant value in the previous factorial runs, that is, D_γ was equal to 3.07E-05. Thus, the following full factorial finite-element runs were performed:

W/l: 3, 7, and 11;

L/l: 3, 5, 7, 9, 11, 13, and 15;

ΔT: ±20 and ±40°F; and

D_γ: 0.78E-05, 6.13E-05, and 11.03E-05.

This was done by simply changing the unit weight of the concrete slab from the previous 0.087 pci to 0.022, 0.174, and 0.313 pci (1 pci = 0.27 MN/m^3) while keeping all the rest of the input parameters the same as before. Together with those 392 cases previously analyzed, a total of 644 ILLI-SLAB runs that repre-

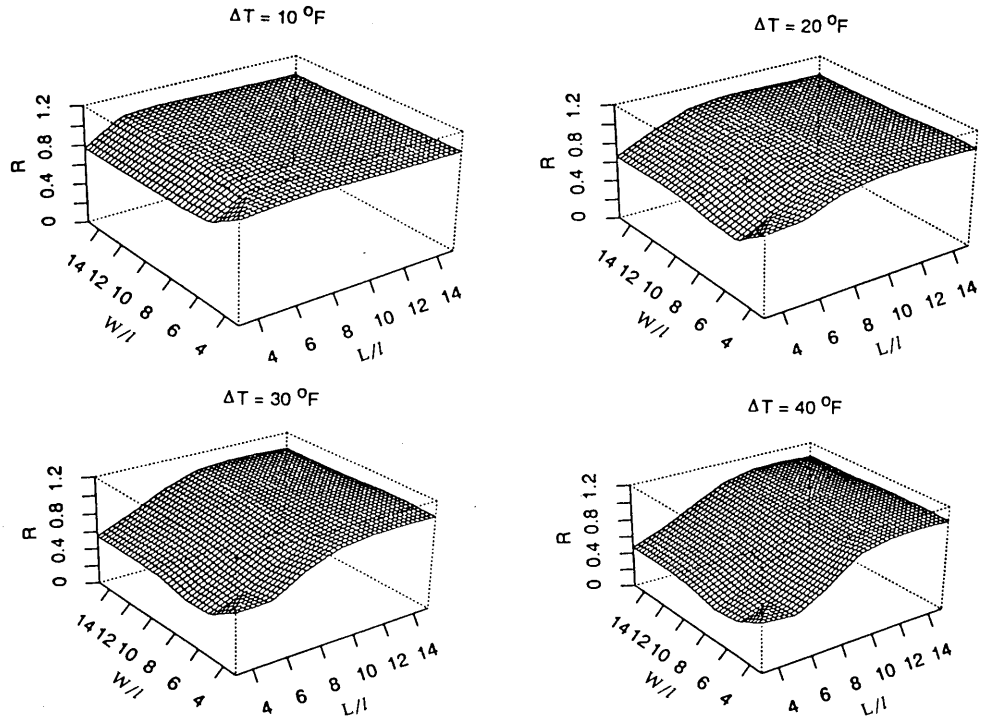

FIGURE 2 Effects of a positive temperature differential and finite slab size.

sented a partial factorial of these four dimensionless parameters were obtained to develop the following predictive models.

In general, the adjustment factor may be adequately defined by the sum of a series of projected curves by using only these dimensionless parameters as independent variables. However, it was decided not to rely only on the projection algorithm for modeling variable interactions to obtain the least number of projected curves for this high dimensional response surface (five dimensions). Some highly probable interaction terms were tested and included during the modeling process as well. By doing so, only a limited number of projected curves, which are more comprehensible to the user and which can be easily formulated, are necessary for the model.

For the daytime curling condition the following two-term projection model was developed (note that a piecewise linear model was chosen to represent these projected curves):

$$R_c = 0.88369 + 0.22005\Phi_1(ATX1) + 0.02383\Phi_2(ATX2) \quad (25)$$

$$\Phi_1(ATX1) = \begin{cases} -2.8903 + 2.7825ATX1 + 1.2565ATX1^2, \\ \qquad \text{if } ATX1 \le 0.85 \\ -2.4275 + 4.9285ATX1 - 1.9459ATX1^2, \\ \qquad \text{if } 0.85 < ATX1 \le 1.5 \\ 0.8111 - 0.1409ATX1, \text{ if } ATX1 > 1.5 \end{cases} \quad (26)$$

$$\Phi_2(ATX2) = \begin{cases} 2.3228 - 3.8187ATX2 - 52.8964ATX2^2, \\ \qquad \text{if } ATX2 \le -0.2 \\ -0.1891 - 0.2237ATX2 + 6.3312ATX2^2, \\ \qquad \text{if } -0.2 < ATX2 \le 0.6 \\ 25.7909 - 58.8336ATX2 + 32.4322ATX2^2, \\ \qquad \text{if } ATX2 > 10.6 \end{cases} \quad (27)$$

$$ATX1 = 0.00656\frac{W}{l} + 0.09886\frac{L}{l} - 0.02621ADT - 0.01857DG + 0.99456\log_{10}DG + 0.00129DG\frac{L}{l} \quad (28)$$

$$ATX2 = -0.00306\frac{W}{l} + 0.01649\frac{L}{l} + 0.02163ADT + 0.01336DG - 0.99953\log_{10}DG + 0.00413DG\frac{L}{l} \quad (29)$$

Statistics: $N = 312$, $R^2 = 0.987$, SEE = 0.0248, CV = 2.81 percent

Similarly, the following two-term projection model was developed for the nighttime curling condition:

$$R_c = 0.69811 + 0.36425\Phi_1(ATX1) + 0.03841\Phi_2(ATX2) \quad (30)$$

$$\Phi_1(ATX1) = \begin{cases} -1.5663 + 1.3093ATX1 + 0.7435ATX1^2, \\ \qquad \text{if } ATX1 \le 0.5 \\ -2.3037 + 3.6569ATX1 - 1.0298ATX1^2, \\ \qquad \text{if } 0.5 < ATX1 \le 2 \\ 1.0017 - 0.0272ATX1, \text{ if } ATX1 > 2 \end{cases} \quad (31)$$

$$\Phi_2(ATX2) = \begin{cases} -0.5836 + 1.0057ATX2 + 0.9323ATX2^2, \\ \qquad \text{if } ATX2 \le 1 \\ -0.9296 + 2.2040ATX2, \text{ if } ATX2 > 1 \end{cases} \quad (32)$$

$$ATX1 = -0.02688\frac{W}{l} + 0.13185\frac{L}{l} + 0.04738ADT - 0.02553DG + 0.98938\log_{10}DG + 0.01089DG\frac{L}{l} \quad (33)$$

$$ATX2 = -0.14612\frac{W}{l} + 0.01252\frac{L}{l} - 0.10378ADT - 0.01890DG - 0.98355\log_{10}DG + 0.00053DG\frac{L}{l} \quad (34)$$

Statistics: N = 312, R^2 = 0.986, SEE = 0.0431, CV = 6.17 percent
Where: $ADT = \alpha\Delta T \times 10^5$, $DG = D_\gamma \times 10^5$.
Limits: $3 \le L/l \le 15$, $3 \le W/l \le 15$, $5.5 \le ADT \le 22$, $0.78 \le DG \le 11.03$

EFFECT OF LOADING PLUS THERMAL CURLING

The combination effects of loading and thermal curling cannot be adequately described by simply superimposing the individual effects of loading and thermal curling alone, since the assumption of a condition of full contact between the slab and subgrade is often violated. Thus, the following adjustment factor (R_T) was introduced to quantify this difference (*20*):

$$\sigma_i = \sigma_L + R_T\sigma_c \quad (35)$$

Together with knowledge of the dominating mechanistic variables involved, the adjustment factor can be determined by the following expression:

$$R_T = \frac{\sigma_i - \sigma_L}{\sigma_c} = f\left(\frac{a}{l}, \alpha\Delta T, \frac{L}{l}, \frac{W}{l}, \frac{\gamma h^2}{kl^2}, \frac{Ph}{kl^4}\right) \quad (36)$$

where σ_L is the edge stress determined by the finite-element model because of loading alone, which may be estimated by $(R_L \cdot R_W \cdot \sigma_w)$ (FL^{-2}).

Preliminary Analysis

A preliminary analysis was conducted by using the following four parameters: a/l, L/l, W/l, and $\alpha\Delta T$. The following full factorial ILLI-SLAB runs were performed:

a/l: 0.05, 0.1, 0.2, and 0.3;

L/l: 3, 5, 7, 9, 11, 13, and 15;

W/l: 3, 5, 7, 9, and 11; and

ΔT: 0, ±20, and ±40°F.

The pertinent input parameters are given in Table 3. Extreme difficulties were encountered while using only these four dimensionless parameters to develop a predictive model for the adjustment factor. The addition of more interaction terms and more projected curves did not resolve this model inadequacy either. This problem also prompted us to search for the additional dimensionless mechanistic variables as discussed previously.

Predictive Models for Loading Plus Thermal Curling

To assess the effect of all six parameters on edge stress it was necessary to perform additional ILLI-SLAB runs. However, a complete full factorial of these six parameters, which requires a tremendous amount of computer time, is not feasible. Thus, it was decided to generate a smaller supplemental factorial that could be added to the previous data base to form a partial factorial for later model development. The data previously presented gave four D_γ values (3.07E-05, 2.47E-05, 2.72E-05, and 2.52E-05) and four D_P values (2.61E-05, 10.82E-05, 39.34E-05, and 114.40E-05) corresponding to four a/l values of 0.05, 0.1, 0.2, and 0.3. In other words, a/l and D_P were correlated with each other. To randomize the relationship among a/l, D_γ, and D_P, a smaller full factorial on the basis of the following parameters was performed:

a/l: 0.05, 0.1, 0.2, and 0.3;

L/l: 3, 5, 7, 9, 11, 13, and 15;

W/l: 3, 7, and 11; and

ΔT: 0, ±10, and ±30°F

This was done by changing the unit weight of the concrete slab and the total wheel load (or tire pressure) while keeping the other input parameters the same as before for different a/l values. The pertinent input parameters are given in Table 4.

For the case of daytime curling plus loading the following three-term projection model was developed:

$$R_T = 0.94825 + 0.15054\Phi_1(ATX1) + 0.03724\Phi_2(ATX2) + 0.03395\Phi_3(ATX3) \quad (37)$$

$$\Phi_1(ATX1) = \begin{cases} -2.5575 + 0.8003ATX1, & \text{if } ATX1 \le 3 \\ -2.6338 + 1.1038ATX1 - 0.0914ATX1^2, & \text{if } 3 < ATX1 \le 7 \\ 0.7564 - 0.0155ATX1, & \text{if } ATX1 > 7 \end{cases} \quad (38)$$

$$\Phi_2(ATX2) = \begin{cases} -0.6788 + 0.0107ATX2, & \text{if } ATX2 \le 3 \\ 3.7674 - 2.2970ATX2 + 0.2963ATX2^2, & \text{if } 3 < ATX2 \le 7 \\ -7.0337 + 1.2945ATX2, & \text{if } ATX2 > 7 \end{cases} \quad (39)$$

$$\Phi_3(ATX3) = \begin{cases} 4.0843 + 4.8241ATX3, & \text{if } ATX3 \le -1 \\ 0.1815 + 0.0541ATX3 - 1.0899ATX3^2, & \text{if } -1 < ATX3 \le 0.5 \\ 0.0453 + 0.0383ATX3, & \text{if } ATX3 > 0.5 \end{cases} \quad (40)$$

$$ATX1 = -0.04724\frac{W}{l} + 0.56954\frac{L}{l} - 0.08408ADT + 0.20033\frac{a}{l} - 0.26647DG + 0.00375DP + 0.73881\frac{a}{l}\frac{L}{l} - 0.01142ADT\frac{L}{l} + 0.09530DG\frac{L}{l} + 0.01121DG\frac{W}{l} \quad (41)$$

TABLE 4 Pertinent Input Parameters for Loading Plus Curling (Additional Runs)

a/l	c	a	E	k	h	l	γ	p	P	DG	DP
	in.	in.	Mpsi	pci	in.	in.	pci	psi	lbs		
0.05	2.5*	1.995	5	200	10.59	39.89	0.030	5000	62500	1.06	130.74
0.10	5.0	2.821	4	300	8.23	28.21	0.350	600	15000	9.93	64.94
0.20	10.0	5.642	3	400	9.97	28.21	0.170	250	25000	5.31	98.34
0.30	10.0	5.642	2	500	7.16	18.81	0.300	10	1000	8.69	11.44

Note:

1. Load dimensions are c x c, except those starred cases use 2c x c. α = 5.5E-06 /°F, μ = 0.15, DG = D_γ x 10^5, DP = D_P x 10^5.
2. 1 °F = (F - 32) / 1.8 °C, 1 lb = 4.45 N, 1 inch = 2.54 cm, 1 psi = 6.89 kPa, 1 pci = 0.27 MN/m^3.

$$ATX2 = 0.03869\frac{W}{l} + 0.35781\frac{L}{l} + 0.09078ADT - 0.04054\frac{a}{l} + 0.86388DG + 0.01635DP - 0.31246\frac{a}{l}\frac{L}{l} + 0.00552ADT\frac{L}{l} - 0.12677DG\frac{L}{l} - 0.01765DG\frac{W}{l} \quad (42)$$

$$ATX3 = 0.58567\frac{W}{l} + 0.25804\frac{L}{l} + 0.14784ADT + 0.14984\frac{a}{l} + 0.12743DG - 0.05012DP + 0.72295\frac{a}{l}\frac{L}{l} - 0.01310ADT\frac{L}{l} - 0.01304DG\frac{L}{l} - 0.06591DG\frac{W}{l} \quad (43)$$

Statistics: N = 432, R^2 = 0.970, SEE = 0.0280, CV = 2.95 percent

Similarly, the following three-term projection model was developed for the case of nighttime curling plus loading:

$$R_T = 0.76068 + 0.28490\Phi_1(ATX1) + 0.10707\Phi_2(ATX2) + 0.10048\Phi_3(ATX3) \quad (44)$$

$$\Phi_1(ATX1) = \begin{cases} -2.5301 + 0.3866ATX1, & \text{if } ATX1 \le 6 \\ -4.0938 + 0.8799ATX1 - 0.0395ATX1^2, & \text{if } 6 < ATX1 \le 12 \\ 0.3181 + 0.0435ATX1, & \text{if } ATX1 > 12 \end{cases} \quad (45)$$

$$\Phi_2(ATX2) = \begin{cases} -1.4980 - 1.1359ATX2, & \text{if } ATX2 \le -1 \\ -0.4956 - 0.0892ATX2 + 0.0174ATX2^2, & \text{if } -1 < ATX2 \le 5 \\ -1.1278 + 0.1075ATX2, & \text{if } ATX2 > 5 \end{cases} \quad (46)$$

$$\Phi_3(ATX3) = \begin{cases} 3.6341 + 0.6512ATX3, & \text{if } ATX3 \le -7 \\ -0.2683 - 0.6808ATX3 - 0.1116ATX3^2, & \text{if } -7 < ATX3 \le -1 \\ 0.1966 - 0.2061ATX3, & \text{if } ATX3 > -1 \end{cases} \quad (47)$$

$$ATX1 = -0.13971\frac{W}{l} + 0.85779\frac{L}{l} + 0.07003ADT + 0.19562\frac{a}{l} + 0.36589DG + 0.05950DP - 0.24211\frac{a}{l}\frac{L}{l} + 0.07242DG\frac{L}{l} - 0.00482DP\frac{L}{l} + 0.00797ADT\frac{L}{l} + 0.01220ADT\frac{W}{l} \quad (48)$$

$$ATX2 = -0.15106\frac{W}{l} + 0.08443\frac{L}{l} + 0.28234ADT - 0.48812\frac{a}{l} + 0.17449DG - 0.03194DP - 0.78445\frac{a}{l}\frac{L}{l} - 0.01999DG\frac{L}{l} + 0.00206DP\frac{L}{l} - 0.06949ADT\frac{L}{l} - 0.00419ADT\frac{W}{l} \quad (49)$$

$$ATX3 = 0.10960\frac{W}{l} - 0.60315\frac{L}{l} - 0.26836ADT + 0.06965\frac{a}{l} - 0.71547DG - 0.12704DP + 0.02846\frac{a}{l}\frac{L}{l} + 0.13364DG\frac{L}{l} + 0.01088DP\frac{L}{l} + 0.02248ADT\frac{L}{l} + 0.00260ADT\frac{W}{l} \quad (50)$$

Statistics: N = 432, R^2 = 0.961, SEE = 0.0546, CV = 7.17 percent

Where: $ADT = \alpha\Delta T \times 10^5$, $DG = D_\gamma \times 10^5$, $DP = D_P \times 10^5$
Limits: $0.05 \leq a/l \leq 0.30$, $3 \leq L/l \leq 15$, $3 \leq W/l \leq 11$, $5.5 \leq ADT \leq 22$, $1.06 \leq DG \leq 9.93$, $2.61 \leq DP \leq 140.74$

VALIDATION OF PROPOSED PREDICTIVE MODELS

To further validate the applicability of the developed predictive models, a series of ILLI-SLAB factorial runs were performed on the basis of a wide range of input parameters. These factorial runs were totally independent of the previous modeling process. The following input parameters covering most of the practical cases found in the field were selected:

Elastic modulus of the concrete, E = 3.0, 5.5, and 8.0 Mpsi;
Modulus of subgrade reaction, k = 50, 250, and 500 pci;
Slab length, L = 10, 20, and 30 ft;
Slab thickness, h = 8, 12, and 16 in.; and
Temperature differential, $\Delta T = \pm 20$ and ± 40°F.
[Note: 1 psi = 6.89 kPa, 1 pci = 0.27 MN/m^3, 1 ft = 30.48 cm, 1°F = (F − 32)/1.8°C.]

The above factorial runs (324 runs) were performed for the case of curling only without an external wheel load being applied. The width of the slab was 12 ft, the slab Poisson's ratio was 0.15, the coefficient of thermal expansion was 5.5×10^{-6}/°F, and the unit weight of concrete slab was set to 0.087 pci.

For the case of loading only, a wheel load of 9,000 lb (40 KN) was applied to the 10-ft slabs, whereas an 18,000-lb (80-KN) load was applied to the other 20- and 30-ft slabs. The tire pressure was set to 90 psi. Thus, a single loaded rectangle of the size of 10×10 or 20×10 in.^{2} was used for the 10-ft slabs or the 20- and 30-ft slabs, respectively. Therefore, only 81 ILLI-SLAB runs were performed. As for the case of loading and curling, a total of 324 runs similar to the case of curling only but with the wheel loads were performed.

Thus, the above factorials essentially result in a group of pavement slabs whose data ranges are a/l = 0.07 to 0.35, L/l = 1.4 to 15.9, W/l = 1.7 to 6.4, $\alpha\Delta T = -0.00022$ to 0.00022, D_γ = 1.3E-05 to 9.7E-05, and D_P = 5.2E-05 to 110.0E-05. To examine the applicability of the predictive models to pavement slabs with any other input parameters, some of the datum points that are outside the specified limits of the proposed predictive models were not considered.

The adequacy of the proposed predictive models for the effects of loading alone, thermal curling alone, and loading plus curling were further validated by using the above factorial data. The predicted edge stresses are plotted against the actual values as shown in Figure 3(*a*), (*b*), and (*c*), respectively. Clearly, these predictive models were able to make fairly good predictions for these data. Thus, it further reconfirmed the applicability of the proposed predictive models.

CALCULATED VERSUS MEASURED STRESSES

The edge stresses computed by the proposed predictive models were compared with the actual measured stress from the AASHO Road Test (*21*) and the Arlington Road Test (*8*). Favorable agreements (*19*) have also been achieved for the three cases analyzed.

NUMERICAL EXAMPLES

Consider a pavement slab with the following characteristics: E = 5.5 Mpsi, k = 250 pci, L = 10 ft, W = 12 ft, h = 12 in., γ = 0.087 pci, μ = 0.15, and $\alpha = 5.5 \times 10^{-6}$/°F. A single wheel load of 9,000 lb with a loaded rectangle of the size of 10×10 in.^{2} is applied. A linear temperature differential of +20°F (daytime condition) exists through the slab thickness. Determine the critical edge stresses due to loading alone, curling alone, and loading plus curling. [Note: 1 psi = 6.89 kPa, 1 pci = 0.27 MN/m^3, 1 ft = 30.48 cm, 1 in. = 2.54 cm, 1°F = (F − 32)/1.8°C, 1 lb = 4.45 N.]

The equivalent radius of the loaded area is a = 5.64 in., and the radius of relative stiffness of the slab-subgrade system is l = 31.20 in. Therefore, the actual dominating mechanistic variables are a/l = 0.18, L/l = 3.83, W/l = 4.60, $\alpha\Delta T$ = +11.0E-05, D_γ = 2.27E-05, and D_P = 29.99E-05. The theoretical Westergaard's solutions on the basis of Equations 1 and 9 are σ_w = 345.75 psi and σ_c = 118.25 psi for loading only and curling only, respectively.

For the case of loading only the adjustment factors for finite slab length and width are R_L = 0.968 and R_W = 1.000 by using Equations 17 and 21, respectively. Thus, the edge stress determined by the proposed models is $0.968 \times 1.000 \times 345.75 = 334.7$ psi. (Note that the actual ILLI-SLAB edge stress was 344.36 psi.)

For the case of curling only, the adjustment factor is R_c = 0.570, which is determined by Equation 25. This gives a predicted edge stress of $118.25 \times 0.570 = 67.40$ psi. (Note that the actual ILLI-SLAB edge stress was 68.4 psi.)

For the case of loading plus curling the adjustment factor is R_T = 0.732 based on Equation 37. Thus, the predicted total edge stress determined by the proposed model is $334.7 + 0.732 \times 118.25 = 421.3$ psi by using Equation 35. (Note that the actual ILLI-SLAB edge stress was 436.42 psi for this case.)

CONCLUSIONS

The edge stress of a concrete pavement due to the individual and combination effects of a single wheel load and a linear temperature differential across the slab thickness was conducted in the present study. The subgrade was assumed to act as a dense liquid foundation.

On the basis of previous research using dimensional analysis, the major independent variables were normalized load radius (a/l), normalized slab length (L/l), normalized slab width (W/l), and a dimensionless product ($\alpha\Delta T$) of a temperature differential and thermal expansion coefficient. However, by using only these four parameters the actual structural response to a temperature influence could not be described adequately. Fortunately, two additional dimensionless parameters (D_γ and D_P) representing the relative deflection stiffness due to the self-weight of the concrete slab, the applied load, and the possible loss of support were recently identified. With this discovery the problems encountered in previous investigations (*12*) in which dimensional analysis was used for thermal-related curling problems are now resolved.

A new predictive modeling procedure proposed by Lee (*19*), which makes use of the projection pursuit regression (PPR or projection) algorithm and traditional linear and nonlinear regression techniques, was used to develop the proposed models. The new models use only the dominating mechanistic variables, as opposed to earlier attempts, which used an arbitrary linear combination of input parameters with few insights into the actual re-

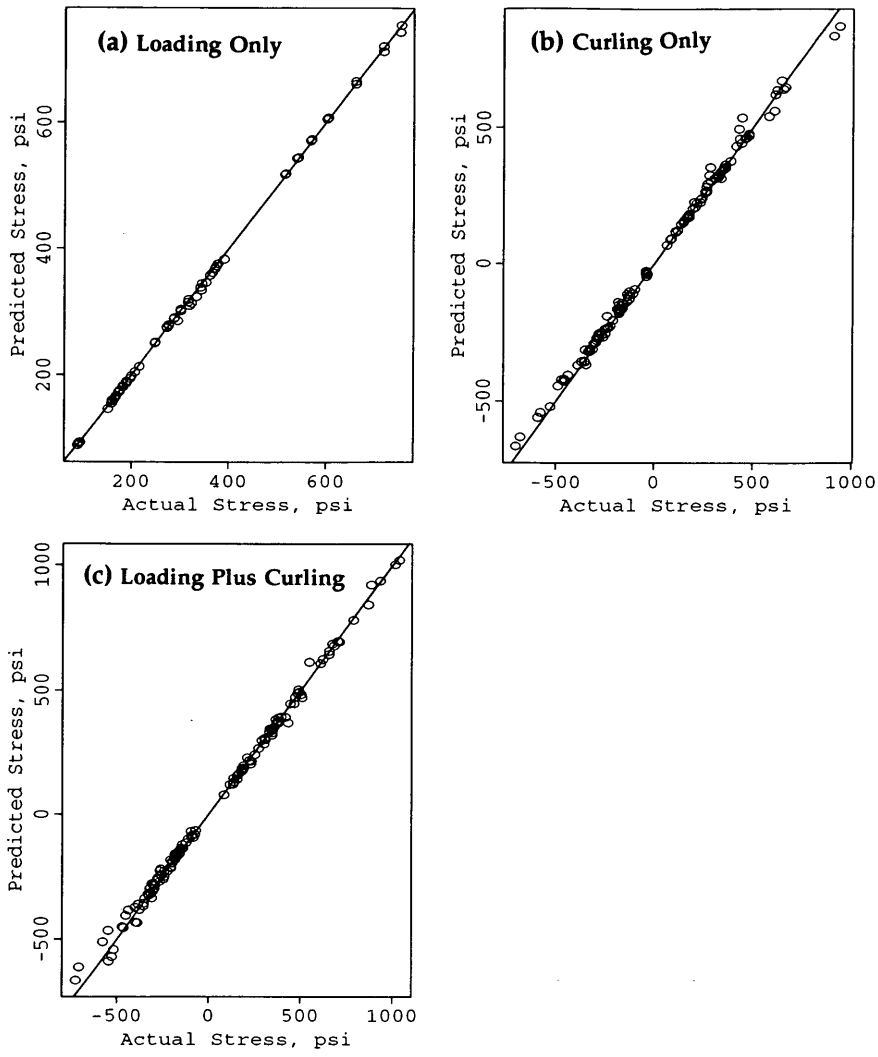

FIGURE 3 Validation of the proposed models for: (*a*) loading only, (*b*) curling only, and (*c*) loading plus curling.

lationships among the variables. Consequently, three closed-form mechanistic design models that have been carefully validated and that are ready for implementation on a spreadsheet or computer program were presented. These stress models turned out to be very accurate representations of the finite-element model.

The new models were also properly formulated to satisfy applicable engineering boundary conditions. They are also simple, easy to comprehend, and dimensionally correct and may be extrapolated to wider ranges of other input parameters. Practical numerical examples showing the use of the new models are also provided.

The predictive models cover almost all practical ranges of pavement designs. Because they are dimensionally correct they can be used in any other unit systems as well. However, extrapolation outside the specified ranges of these dominating parameters is not recommended. Practical pavement design guidelines for edge stress analysis may be easily developed on the basis of these predictive models, together with the use of some reliability concepts. Besides, the predictive modeling procedures and the deflection ratio concept can be used in other pavement-related modeling problems as well.

ACKNOWLEDGMENTS

This research work was sponsored by the Illinois Department of Transportation. The authors are grateful to James Hall for assistance in this project.

REFERENCES

1. Westergaard, H. M. Computation of Stresses in Concrete Roads. In *HRB Proc.*, Vol. 5, Part I, HRB, National Research Council, Washington, D.C., 1926, pp. 90–112. Also in "Stresses in Concrete Pavements Computed by Theoretical Analysis." *Public Roads*, Vol. 7, No. 2, April 1926, pp. 25–35.
2. Westergaard, H. M. Stress Concentrations in Plates Loaded over Small Areas. *Transactions*, Vol. 108, 1943, pp. 831–886. Also in *ASCE Proc.*, Vol. 68, No. 4, April 1942.

3. Westergaard, H. M. New Formulas for Stresses in Concrete Pavements
of Airfields. *Transactions*, Vol. 113, 1948, pp. 425–444. Also in *ASCE Proceedings*, Vol. 73, No. 5, May 1947.
4. Ioannides, A. M., and R. A. Salsilli-Murua. Temperature Curling in Rigid Pavements: An Application of Dimensional Analysis. In *Transportation Research Record 1227*, TRB, National Research Council, Washington, D.C., 1989.
5. Ioannides, A. M., M. R. Thompson, and E. J. Barenberg. The Westergaard Solutions Reconsidered. In *Transportation Research Record 1043*, TRB, National Research Council, Washington, D.C., 1985.
6. Westergaard, H. M. Analysis of Stresses in Concrete Pavements due to Variations of Temperature. *HRB Proc.*, Vol. 6, HRB, National Council, Washington, D.C., 1926, pp. 201–217. Also in *Public Roads*, Vol. 8, No. 3, May 1927.
7. Bradbury, R. D. *Reinforced Concrete Pavements*. Wire Reinforcement Institute, Washington, D.C., 1938.
8. Teller, L. W., and E. C. Sutherland. The Structural Design of Concrete Pavements, Part 2. *Public Roads*, Vol. 16, No. 9, Nov. 1935.
9. Tabatabaie-Raissi, A. M. *Structural Analysis of Concrete Pavement Joints*. Ph.D. thesis. University of Illinois, Urbana, 1978.
10. Ioannides, A. M. *Analysis of Slabs-on-Grade for a Variety of Loading and Support Conditions*. Ph.D. thesis. University of Illinois, Urbana, 1984.
11. Korovesis, G. T. *Analysis of Slab-on-Grade Pavement Systems Subjected to Wheel and Temperature Loadings*. Ph.D. thesis. University of Illinois, Urbana, 1990.
12. Salsilli-Murua, R. A. *Calibrated Mechanistic Design Procedure for Jointed Plain Concrete Pavements*. Ph.D. thesis. University of Illinois, Urbana, 1991.
13. Hastie, T. J., and R. J. Tibshirani. *Generalized Additive Models. Monographs on Statistics and Applied Progability* 43. Chapman & Hall, 1990.
14. Friedman, J. H., and W. Stuetzle. Projection Pursuit Regression. *Journal of the American Statistical Association*, Vol. 76, 1981, pp. 817–823.
15. Becker, R. A., J. M. Chambers, and A. R. Wilks. *The New S Language—A Programming Environment for Data Analysis and Graphics*. The Wadsworth & Brooks/Cole Computer Science Series, AT&T Bell Laboratories, 1988.
16. *S-PLUS for DOS: Reference Manual*, Versiòn 2.0. Statistical Sciences, Inc., Seattle, Wash., Nov. 1991.
17. *S-PLUS for DOS: User's Manual*, Version 2.0. Vol. 1 and 2, Statistical Sciences, Inc., Seattle, Wash., Nov. 1991.
18. Chambers, J. M., and T. J. Hastie. *Statistical Models in S*. Wadsworth & Brooks/Cole Computer Science Series, AT&T Bell Laboratories, 1992.
19. Lee, Y. H. *Development of Pavement Prediction Models*. Ph.D. thesis. University of Illinois, Urbana, 1993.
20. Darter, M. I. Design of Zero-Maintenance Plain Jointed Concrete Pavement, Vol. I. Development of Design Procedures. Report FHWA-RD-77-111. FHWA, U.S. Department of Transportation, 1977.
21. *Special Report 61E: The AASHO Road Test, Report 5: Pavement Research*. Publication 954. HRB, National Research Council, Washington, D.C., 1962.

Publication of this paper sponsored by Committee on Rigid Pavement Design.

Framework for Incorporation of Spalling in Design of Concrete Pavements

SANJAYA P. SENADHEERA AND DAN G. ZOLLINGER

A framework that can be used to incorporate crack spalling in the design of concrete pavements is proposed. Crack spalling is a common form of distress in concrete pavements. However, available literature on the modeling of spalling is limited to some regression-based models developed for jointed concrete pavements. On the basis of comprehensive field surveys and results from analysis of pavement condition survey data for continuously reinforced concrete pavements, several factors have been identified as excellent predictors of spalling, allowing the proposal of the design framework leading to a mechanistic spalling model to predict crack spalling. The design framework presented incorporates survival analysis, which is a statistical technique based on failure-time theory and reliability. The results obtained by the use of this technique provide the pravement engineer with the information required to assess the survivability of the pavement from spalling and the predicted level of spalling at a certain age, both simply and succinctly. Because the proposed statistical technique can be effectively used for other forms of pavement distress as well, a detailed description of the mathematical development of the model is also included for better understanding of the principles involved.

Spalling, which is an often encountered form of distress in concrete pavements, has not received the same attention in pavement design as the other distresses such as cracking and punch-outs in continuously reinforced concrete pavements (CRCPs) and joint failure in jointed concrete pavements (JCPs). It is a very important distress in concrete pavements from the standpoint of the road user because it results in a rough ride and gives a negative perception, that is, a lack of structural integrity in the pavement. From a technical standpoint, because spalling takes place at the transverse joints or random cracks in the pavement, it may take away from the load transfer efficiency that is important for minimizing stress levels in the pavement. Unless adequate load transfer is maintained, spalls may develop into more serious forms of distress such as punch-outs in CRCPs or joint failure in JCPs.

The lack of attention given to the spalling distress on a fundamental basis may have been caused by a lack of understanding of the mechanisms involved. At the Texas Transportation Institute (TTI) of the Texas A&M University System, research is currently under way to identify the mechanisms of spalling that would enable the modeling of spalling in concrete pavements by incorporating a number of factors that appear to influence spalling significantly.

The available literature on the modeling of spalling is limited to JCPs, and they indicate attempts to model spalling as a function of age. Field observations on CRCPs undertaken at TTI have indicated that spalling is not necessarily a function of age, but it is the culmination of the accumulation of fatigue damage starting with early-age delaminations that are extended by vehicle tire loads and repeated changes in pavement temperature. It is likely that this mechanism is applicable to JCPs as well.

In this paper a framework for mechanistically incorporating crack spalling as a design criterion for concrete pavements is introduced by incorporating the factors observed to influence spalling. The influences of these factors were further investigated by analyzing the available spalling data on CRCPs in Texas. The survival analysis technique, which is commonly used in medical research (*1*) and other industrial disciplines, is introduced, and its usefulness to pavement design is emphasized. Because of limitations in the currently available field data, a comprehensive spalling model can be only suggested at this point, but an illustrative model is developed to introduce the results that will be available to the pavement designer by using this technique.

OVERVIEW OF PRIOR RESEARCH

Several researchers have previously investigated spalling in concrete pavements. One definition defines spalling as the breakdown of the pavement along the cracks leading to the loss of concrete and the disintegration of the load transfer mechanism (*2*). Another definition indicates spalling in JCPs as any type of fracture or deterioration of the transverse joints, excluding corner breaks (*3*).

In CRC pavements spalling can take place on either one or both sides of a transverse crack (*4*). Spalls are generally categorized by their depth as either deep or shallow, with a depth greater than 2.5 cm generally being considered deep (Type II and Type III spalls; Figure 1). Spalls are also categorized as either minor or severe. In the CRCP spalling data base used for the development of spall models in this paper (*5*), minor spalling was defined as "edge cracking in which the loss of material has formed a spall of 0.5 in. wide or less."

It would be appropriate at this point to note some observations indicated in previous work on spalling.

1. Aggregate type may have some influence on spalling (*6*).
2. Concretes made with coarse limestone aggregate showed less spalling than concretes with siliceous gravel aggregates (*7*).
3. Primary causes of spalling are entrapment of road debris in cracks, which causes a buildup of compressive stresses, a combination of shear and tensile stresses under wheel load, and poor concrete at the surface of the pavement, presumably because of overworking during the finishing process (*8*).
4. Minor spalling increases with age and traffic. Severe spalling does not seem to have a correlation to minor spalling or crack spacing (*8*).
5. Spalling increases with increasing crack width (*8*).

Texas Transportation Institute, Texas A&M University System, College Station, Tex. 77843.

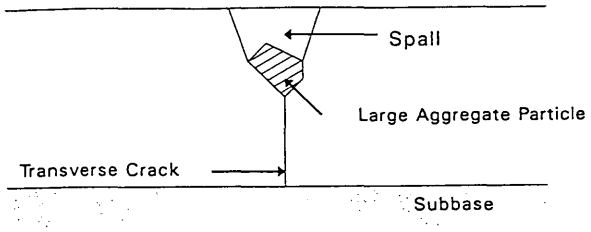

(a) Type I-Deep Spall caused by Large Aggregate Particle

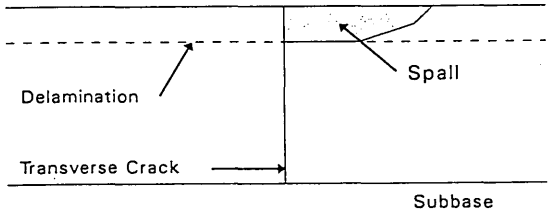

(b) Type II-Shallow,Wide Spall by Delamination & Traffic

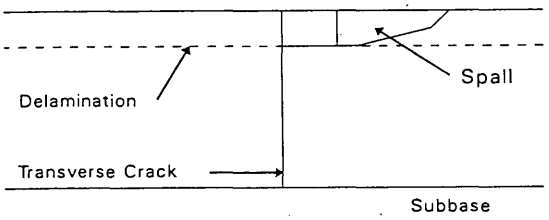

(c) Type III-Shallow Spall, Initial Spalling away from Crack

FIGURE 1 Types of spalling in concrete pavements.

6. Severe spalling is usually a result of construction operations and is influenced by traffic, pavement age, and the location of the spall (*7*).

7. Spalling generally occurs in the wheelpath regions of the pavement (*9*).

8. Surface spalling associated with reinforcement results from the pressure exerted by corrosion products when the steel rusts. However, spalling over reinforcement is not a widespread problem in CRC pavements (*2*).

9. Deep spalls are generally related to structural weaknesses, and shallow spalls are related to weakened horizontal planes in the concrete (*10*).

10. Spalling is a result of discontinuities developed during propagation of cracks as the crack propagates along a path of least resistance (*11*).

11. Spalling develops because of restraint to volume change resulting from temperature variation through the slab depth (*12*).

12. Subgrade support conditions can influence spalling (*2*).

13. Crack width and depth to steel reinforcement have an influence on the stiffness and consequently will influence the spall stresses (*2*).

Except for Item 11 above, all other observations come from studies on CRC pavements.

A spalling model was first proposed for jointed pavements in the PEARDARP program in which spalling was modeled as a function of time (*13,14*). It was later found that the PEARDARP spalling model tended to overpredict transverse joint spalling for spalling data from certain environmental regions (*15*). Analysis of spalling data by Smith et al. (*15*) further indicated that in general spalling was observed on pavements of all ages and with different joint spacings in which material problems such as nondurable aggregates under harsh climates existed or the dowel bars had corroded or locked up the joints. On the basis of the analysis of the Michigan road test spalling data, Smith et al. (*15*) proposed spall models for jointed plain concrete pavements (JPCPs) and jointed reinforced concrete pavements (JRCPs) incorporating factors such as D-cracking, type of joint sealant, freezing index, and aggregate reactivity.

The model for JPCP had a coefficient of determination (R^2) of 0.59 and a standard error of estimate of 5 joints/mi. The model for JRCP had an R^2 of 0.47 and a standard error of estimate of 3 joints/mi. Smith et al. (*15*) believed that incompressible material inside the transverse joints is the major cause of joint spalling and postulated that preformed seals that seemed to reduce spalling at joints do so because of their ability to keep incompressible material away from the joints for a significant period of time.

FIELD SURVEYS

Extensive field surveys or spalling have been undertaken in concrete pavements in the state of Texas for a long period of time. Initial field surveys recorded the level of spalling in a large number of concrete pavement survey sections throughout the state. Recently, more field studies were undertaken by TTI with the idea of establishing the mechanisms involved in spalling (*4*). These field surveys have indicated the presence of several types of spalls (Figure 1). Types II and III appear to be the most widespread and to have the same type of distress development, that is, formation of delaminations that eventually lead to spalling because of fatigue loading from both traffic- and temperature-induced stresses.

Several important observations were noted from the field surveys conducted by TTI (*4*). These were that

1. Spalling is an extended form of delaminations at the transverse cracks.
2. Delaminations originate at transverse cracks (Figure 1).
3. Delaminations may be forming very early in the life of a concrete pavement, as early as when cracks initiate. This could be a matter of hours or days after the concrete is paved, depending on the environmental and curing conditions.
4. Most delaminations usually occur at depths ranging from 2.5 to 5.0 cm from the surface of the pavement, and they eventually propagate toward the surface, causing a visible spalling distress.
5. Most spalling distresses occur along the wheelpaths.
6. Higher levels of spalling were observed primarily in pavement sections constructed with siliceous river gravel coarse aggregate (Table 1 and Figure 2). Also at the spalling failure planes there is a high percentage of failure at the aggregate-cement paste interface (*4*).
7. Particularly in rural highways, inside lanes display more spalling than outside lanes.

These factors indicate that any design framework for spalling should be a two-tiered process. In Step 1 delaminations occur very early in the pavement life, most likely because of differential moisture loss across the depth of the pavement, and are accentuated by the low interfacial strength between the aggregate and the

TABLE 1 Summary of Observations on Sample Survey Sections

Highway	Coarse Aggregate Type	Modes of Distress	Remarks
SH-6	Siliceous River Gravel	Spalling	Extensive spalling. More spalling in the inside lane. 75 % of spalls downstream of crack. Spalling on wheel path. Plane of weakness at 2.5 cm depth at most transverse cracks.
BW-8	Siliceous River Gravel	Spalling	Isolated areas of extensive spalling. Spalling distributed among all 3 lanes. Concrete cores from pavement had planes of weakness at 2.5 cm depth.
US-59	Siliceous River Gravel	Spalling	Extensive spalling. More spalling in the inside lane. Most spalls were downstream of crack. Spalling in wheel path.
IH-10 Houston	Siliceous River Gravel	Spalling	Extensive spalling. Almost all spalling in 2 inside lanes.
IH-45	Crushed stone /siliceous gravel blend	Punchouts	Virtually no spalling.
IH-10 Gonzales	Crushed stone	Punchouts	Virtually no spalling.

cement paste at early ages. In Step 2 the subsequent development of the delaminations into spalls would be a process based on the accumulation of fatigue damage because of the action of vehicle tire load-induced stresses (*4*) and temperature change-induced stresses (*12*).

Spalling data for this analysis were obtained from the concrete pavement data base compiled by the Center for Transportation Research of the University of Texas at Austin. The condition surveys for spalling were performed in 1974, 1978, 1980, 1982, and 1984 (*16*). In this CRCP data base, each pavement section constructed at the same time is identified as a control unit. Each one of these control units is then divided into a number of survey sections, each of which is 305 m (1,000 ft) long, and spalling data are collected on each of these survey sections. Therefore there is a distribution of spalling data values for each control unit and for each survey period.

The spalling data base indicated minor and severe spalling for each pavement section surveyed. Minor spalling was defined in the data base as "edge cracking in which the loss of material has formed a spall of 0.5 in. wide or less" (*5*). All other spalling was considered severe. Because minor spalling as defined is not likely to fall into the Type II and III spalling, only severe spalling from the data base was considered in this analysis. The CRCP data base does not distinguish between the different types of spalls mentioned in this paper; however, because Type I spalls are few and far between, it is expected that they will not cause any significant bias in the analysis of the data.

The survey sections included in the data base had information such as pavement thickness, coarse aggregate type in the concrete, subbase treatment, type of subgrade soil (likelihood of swelling or shrinkage), average annual rainfall, and the estimated average daily traffic and its projected rate of growth.

Preliminary analysis of spalling data (*16*) indicated the following:

1. Eighty-five percent of survey sections were more than 5 years old at the time of the first survey.
2. Seventy-two percent of survey sections displayed no spalling whatsoever.

Field studies undertaken by TTI aimed at understanding the mechanism of spalling have revealed that there are a number of CRCP sections in the Houston area alone that have spalled within the first 2 to 4 years of service. Even though the development of spalls is caused by fatigue damage, the origins of these spalls (i.e., the presence of delaminations) are greatly influenced by the environmental conditions at the time of paving and immediately afterward (*17*). These conditions include the temperature and relative humidity profile during the first few days after the placing of concrete, wind velocity, and the method of curing. It is possible that these conditions dictate the number of delaminations in the pavement that are likely to develop into spalls, provided that the subsequent fatigue damage so dictates.

Typical spalling curves plotted against time for six survey sections in the data base are shown in Figure 3. An interesting feature

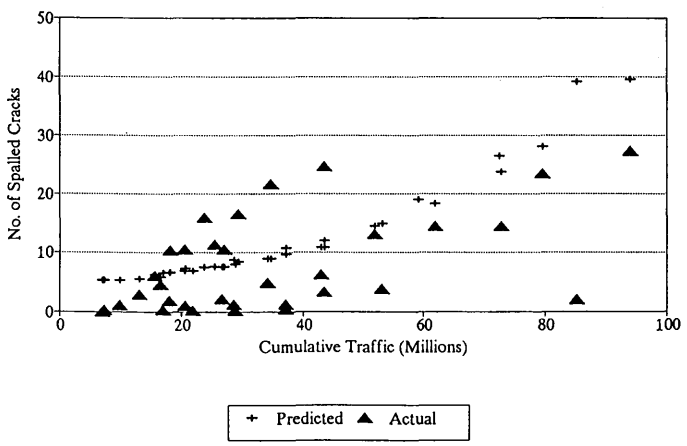

FIGURE 2 Actual and predicted spalling at 50th percentile level for pavements made with siliceous gravel.

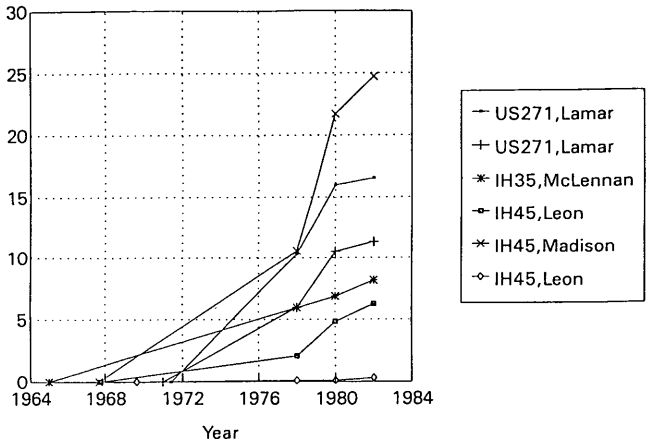

FIGURE 3 Typical spall development curves from survey sections.

about these curves is that they all have an S shape, which indicates a maximum asymptotic level of spalling, which these curves approach, in spite of a continuing increase in traffic volume. The shapes of these spalling curves are important criteria in selecting the mathematical distribution for representing spalling in the proposed spalling model. This maximum asymptotic level of spalling would be the level of delaminations present in the pavement.

A further analysis of a correlation of the spalling data was performed on some selected variables that were already identified as factors that influence spalling as a result of the TTI field survey (Table 1). The coarse aggregate type had the best correlation with the spalling data. Because of the unavailability of data on aggregate characteristics in the data base, separate correlation analyses were performed for the two primary aggregate types. These indicated that the following factors have the best correlation.

1. Cumulative traffic at the time of the survey,
2. Cumulative rainfall at the time of the survey, and
3. Interaction between the age of the pavement and subbase type.

FRAMEWORK FOR A SPALLING MODEL

To establish good design practices and maintenance strategies for spalling, it is important to estimate the time at which spalling first takes place and the level of spalling at different times during the service life of the pavement. If spalling were to be eliminated from concrete pavements, it would be necessary to make sure that no delaminations occur in the first place. This calls for extremely effective curing practices based on the ambient temperature and humidity profiles at the time of paving and immediately afterward. However, further study is required to assess the economic feasibility of such considerations associated with highway construction. In the meantime it may be important to predict the occurrence of spalling and its development with time on the basis of the factors identified to be the best predictors of spalling.

A design framework for spalling is proposed in this paper on the basis of a statistical method called the failure-time theory (*18*). In this method the failure time is a random variable and the dependence of failure time is assessed by using explanatory variables (covariates).

For pavements under the same conditions, the time that it takes for the pavement to spall will vary from one section of pavement to the other because of the random nature of spalling. Therefore the time to failure (spalling) can be represented by a probability density function. This is a situation in which extreme values of such a random variable (largest or smallest value, but in this case the smallest value for failure time) are of interest. These extreme values from samples with different numbers of datum points are also random variables nad have probability distributions of their own. These extreme values may be derived from the distribution of the initial variate.

Failure Time Theory and Concept of Survivability

Let T be a nonnegative random variable representing the failure time of a pavement section from a homogeneous population. The probability distribution of the failure time T can be specified by using one of three different functions, namely, the survivor function, the probability density function, and the hazard function.

The survivor function $S(t)$ is defined as

$$S(t) = P(T \geq t),\ 0 < t < \infty \tag{1}$$

The survivor function can be described as the probability of failure at time t provided that the pavement did not fail up to that time. Because of the aging of pavement, the survivability of the pavement should gradually decrease with time.

If the failure time T is a continuous variable, the probability density function $f(t)$ of the failure time T is given by

$$f(t) = \lim_{\Delta t \to 0} \frac{P(t \leq T \leq t + \Delta t)}{\Delta t}$$

$$= -\frac{dS(t)}{dt} \tag{2}$$

In words, it is the proportion of pavements failing near time t within a very small time interval per unit time. $f(t)$ is a nonnegative function.

Also,

$$S(t) = 1 - F(t) \tag{3}$$

where $F(t)$ is the cumulative probability at time t.

The hazard function $h(t)$ of the failure time is defined as the probability of failure during a very small time interval (Δt) assuming that the pavement has survived up to the beginning of the time interval. Therefore, this gives the conditional failure rate.

$$h(t) = \lim_{\Delta t \to 0} \frac{P(t \leq T \leq t + \Delta t | T \leq t)}{\Delta t} \tag{4}$$

The hazard function for a pavement is positive and increases with time.

Selection of a mathematical distribution to represent failure data is an important step in the survival analysis. There can be many

different causes that lead to the failure of a pavement. It would be difficult, if not impossible, to isolate all of these causes and mathematically account for all of them. Therefore, selecting a theoretical distribution to approximate failure data needs to be done carefully by considering the type of hazard or survival function characteristics of the application at hand.

Commonly used mathematical distributions in failure-time theory are exponential distribution, lognormal distribution, and Weibull distribution. The simplest of these, the exponential distribution, provides a constant rate of hazard in which no aging effects are involved. If this distribution were to be used, failure (spalling) would be a random event independent of age. This is not suitable for representing spalling in a pavement in which the aging effect should be reflected by a monotonically increasing hazard.

The lognormal distribution shows an initially increasing and then decreasing hazard rate. This decrease takes place almost as soon as the median is passed and approaches zero as time approaches infinity. Therefore, it is unsuitable for modeling pavement distress.

The two-parameter Weibull distribution is a generalized form of the exponential distribution. It is characterized by two parameters, shape and scale. This distribution can be used to model the survival distribution of a population with increasing, decreasing, or constant risk. It can provide a mnotonically increasing hazard and a Type III extreme value distribution. A Type III extreme value distribution is one in which its largest value has a finite upper bound and the smallest value has a finite lower bound, which is similar to the spalling distributions shown in Figure 3. Therefore, this is suitable for determining the minimum of a series of minima (i.e., failure times).

The survivor function $S(t)$ and the hazard function $h(t)$ of the two-parameter Weibull distribution are given by

$$S(t) = e^{-(\lambda t)^{\gamma}} \tag{5}$$

$$h(t) = \lambda\gamma(\lambda t)^{\gamma-1} \tag{6}$$

where γ is the shape parameter, and λ is the scale parameter.

These distributions can be generalized to incorporate a number of covariates. For illustrative purposes the case of a single covariate represented by Z is considered. Usually, the scale function selected is $\exp(Z\,\beta)$, where β is an unknown parameter.

If the effect of covariates is to act multiplicatively on the Weibull hazard, the conditional hazard may be taken as

$$h(t; Z) = \lambda\gamma(\lambda t^{\gamma-1} \exp(Z\beta) \tag{7}$$

A characteristic feature of the failure time data is that the response variable (such as the failure time) cannot be negative. This enables the use of a transformation such as log transformation before standard statistical methods can be applied. Log transformation is advantageous because it will reduce the presence of extremely large values in the distribution that can otherwise have a strong influence on the final fitting of the extreme value.

The survival functino $S(Y)$ and the hazard function $h(Y)$ for the natural logarithm of failure time Y are given by

$$S(Y) = \exp\left[-\exp\left(\frac{Y-\alpha}{\sigma}\right)\right] \tag{8}$$

$$h(Y) = \frac{1}{\sigma}\exp\left(\frac{Y-\alpha}{\sigma}\right) \tag{9}$$

where σ equals $1/\gamma$ and α equals $-\ln\lambda$.

With the addition of covariates, the survival function $S(Y)$ is given by

$$S(Y) = \exp\left[-\exp\left(\frac{Y-\alpha}{\sigma} + Z\beta\right)\right] \tag{10}$$

From Equation 10 the linear model can be obtained

$$Y = \alpha - (\sigma\beta)Z + \sigma \ln\left[\ln\left(\frac{1}{1-F(y)}\right)\right] \tag{11}$$

and for n number of covariates $Z_1, Z_2, \ldots Z_n$, the linear regression model

$$Y = \alpha + \sum_{i=1}^{n} Z_i\beta_i^* + \sigma W_p \tag{12}$$

where

n = number of covariates,
$\alpha = -\ln\lambda$,
$\sigma = 1/\gamma$,
$\beta^* = -\sigma\beta$, and
W_p = pth percentile of the extreme value distribution.

Although the failure-time theory and the survivability concept previously explained were in terms of the actual time response of failure time, often other variables can be used as the responsible variable. In spalling, for instance, the number of spalled cracks can be used as the response variable. This would enable the pavement engineer to perform the analysis without defining the level of failure in a pavement. Thus a prediction model that includes both the level of spalling and reliability can be developed. Because the spalling distress is being considered in this paper, the response variable is the natural logarithm of the number of spalled cracks. The *LIFEREG* procedure of the statistical analysis package SAS (*19*) can be used to obtain the regression parameters described in Equation 12.

Development of Spalling Model

On the basis of the previous discussions in this paper, the following factors can be earmarked for the modeling process.

Factors Influencing Formation of Delaminations

1. Ambient relative humidity and temperature during early days after paving.
2. Aggregate-cement paste interfacial strength in concrete.
3. Curing conditions.

Factors Relating to Strain Development Causing Fatigue Damage

1. Cumulative traffic volume.
2. Periodic fluctuations in temperature in the pavement.
3. Type of subbase, which influences the stresses in the pavement slab.

Factors Causing Restraint Necessary for Generation of Stresses

1. Cumulative rainfall as a means by which the restraint at the crack or joint faces are altered.
2. Tensile strength of concrete or the interfacial strength between the aggregate and cement paste, which influences the cohesion at crack faces.

All of this information is not available in the current data base. Only cumulative traffic volume and cumulative rainfall at the time of each condition survey can be calculated from the available data. Because these factors show a high correlation with the spalling data and the mechanisms of spalling identify these as two primary factors that affect spalling, a satisfactory spalling model can still be obtained by using them.

The importance of rainfall in this model is reflected in two ways. First, as mentioned earlier, in rural highways the debris inside cracks on the outside lane can get splashed along with the rainwater onto the inside lane. This will make spalling in the outside lane subject only to stresses from the vehicle tires. Now, with more debris inside the cracks in the inside lane, it can be subject to both the traffic-induced stresses and the temperature change-induced stresses. Second, the rainfall provides lubrication at the crack faces inside transverse cracks and delaminations. This will reduce or eliminate the cohesion between the crack faces, which plays an important role in reducing the stresses. When friction across the delamination faces are low, it will result in higher stresses (*4*).

The spalling model can be represented in the form of Equation 13:

$$\ln(\text{number of spalled cracks}) = \alpha + \beta_1^* \cdot CUMTR + \beta_2^* \cdot CRAIN + \sigma W_p \quad (13)$$

where *CUMTR* is cumulative traffic in millions, and *CRAIN* is cumulative rainfall (in centimeters) at the time of the condition survey.

Using the *LIFEREG* procedure in the SAS statistical analysis package (*19*), the following linear regression models were obtained separately for pavements made with siliceous river gravel and crushed limestone. Because the natural logarithm of the number of spalled cracks per survey section was considered the response variable, to validate the model, left censoring was performed on the large number of sections that had not spalled at the time of the survey.

For pavements with siliceous river gravel coarse aggregate:

$$Y = 2.01 + 0.027 \cdot CUMTR - 5.3E{-}04 \cdot CRAIN + 1.34 \ln\left[\ln\left(\frac{1}{1 - F(t)}\right)\right] \quad (14)$$

For pavements with crushed limestone coarse aggregate:

$$Y = 0.31 + 0.009 \cdot CUMTR - 2.31E{-}04 \cdot CRAIN + 0.85 \ln\left[\ln\left(\frac{1}{1 - F(t)}\right)\right] \quad (15)$$

where Y is the natural logarithm of the number of spalled cracks.

Statistical data for spalling models in Equations 14 and 15 is provided in Table 2.

Illustrated in Figure 2 are the actual and predicted levels of spalling for pavements made with siliceous river gravel coarse aggregate. There is a certain amount of scatter evident in Figure 2. This scatter in the data may be a result of different initial conditions at the time of paving, variations in aggregate properties, and differences in temperature changes between pavements. It is hoped that more refinement, as discussed later in this paper, would eliminate this scatter.

Results from Proposed Spalling Model

The results from the models in Equations 14 and 15 are illustrated in Figures 4 and 5. These illustrations are given for a specific case of average daily traffic of 20,000, an annual traffic growth rate of 1 percent, and an average annual rainfall of 100 cm.

How the survivability (probability of survival) changes with time for pavements made with siliceous river gravel and crushed limestone coarse aggregates, respectively, is illustrated in Figures 4(*a*) and 4(*b*). As expected they display the aging effect of the pavement by giving probabilities of survival that decrease with time. It can clearly be seen from these curves how the probability of survival would change depending on the failure criterion selected. The failure criterion is the number of spalled cracks per survey section (305 m) that the pavement engineer would consider as failure. Therefore the pavement engineer need not decide beforehand what the failure criterion for spalling should be. Different design curves can be developed for different failure criteria (as shown in Figure 4), or the probability of survival can be directly calculated by using the model for each failure criterion. A survivability curve during the lifetime of a pavement that has a steep drop during the first few years would be inappropriate because it is an indication of possible fast deterioration (spalling) of the pavement.

TABLE 2 Statistical Parameters Pertaining to Model Development

Statistical Parameter		Model for Siliceous Gravel	Model for Crushed Limestone
Log Likelihood		2241	1019
α	Parameter Estimate	2.01	0.31
	Standard Error	0.14	0.12
	Chi-Square	201.0	6.3
	Pr>Chi	0.0001	0.0121
β_1	Parameter Estimate	0.027	0.009
	Standard Error	0.002	0.0046
	Chi-Square	176.7	3.39
	Pr>Chi	0.0001	0.0655
β_2	Parameter Estimate	-0.00053	0.000231
	Standard Error	0.0001	0.00027
	Chi-Square	15.73	0.75
	Pr>Chi	0.0001	0.39
σ	Parameter Estimate	1.34	0.85
	Standard Error	0.029	0.02

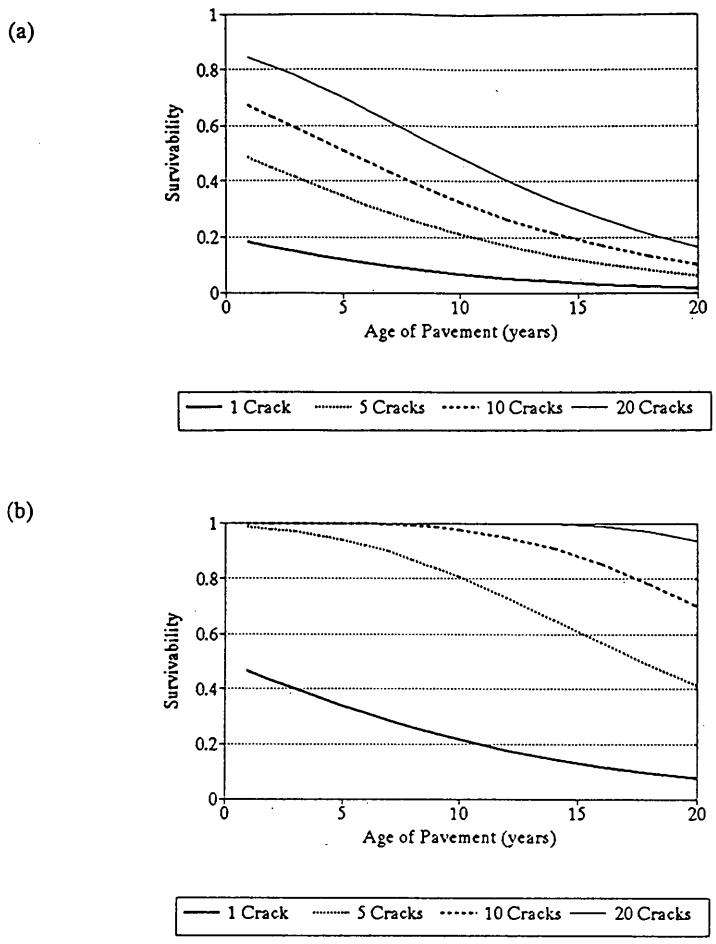

FIGURE 4 Survivability curves for different failure criteria for concrete pavements made with (*a*) siliceous river gravel and (*b*) crushed limestone coarse aggregate.

Shown in Figures 5(*a*) and 5(*b*) are the predicted number of spalls per survey section for pavements with siliceous river gravel and crushed limestone coarse aggregate types, respectively. Different curves are provided for three levels of reliability (50, 90, and 99 percent). It should be noted that a 90 percent reliability would mean that 90 percent of the original field data would fall below this level.

CONCLUSION

Preliminary analysis of spalling data identified the coarse aggregate type, level of traffic, rainfall, and subbase type as the best predictors of the level of spalling. Parameters such as ambient relative humidity and temperature, periodic temperature fluctuations, and concrete strength are not available in the data base but are nevertheless considered important predictors of spalling. Even though this lack of available data prevents the use of all of these parameters in the modeling process, a more complete model could be developed by accommodating all of these variables.

The proposed modeling method that uses survival analysis appears to be a promising tool for predicting the occurrence of spalling and the level of spalling at a certain time. This technique can be used not only for spalling but for other pavement distresses as well.

The proposed mechanistic model can be extended to incorporate damage as a covariate instead of having separate covariates in the form of cumulative traffic and temperature change. This can be achieved by developing a method of calculating fatigue damage primarily from the application of wheel loads and restraint stresses because of daily temperature changes while incorporating the effects of rainfall and subbase type as well.

Once damage is included in the spalling prediction model, two other important steps need to be taken. First, calibration of the model to account for local pavement conditions is important. The scatter visible in Figure 5 is an indication that more refinement of the data, particularly the calibration of the data to relate design parameters to local conditions, is necessary. This can be done once data such as initial environmental conditions at the time of paving are known. Also allowance must be made for variability in the design parameters by using statistical techniques (Lyton, R. L., and D. G. Zollinger. Modeling Reliability in Pavement. Presented at 72nd Annual Meeting of Transportation Research Board, Washington, D.C., 1993).

The design framework proposed in this paper incorporates data that can be easily measured or that are readily available. Thus,

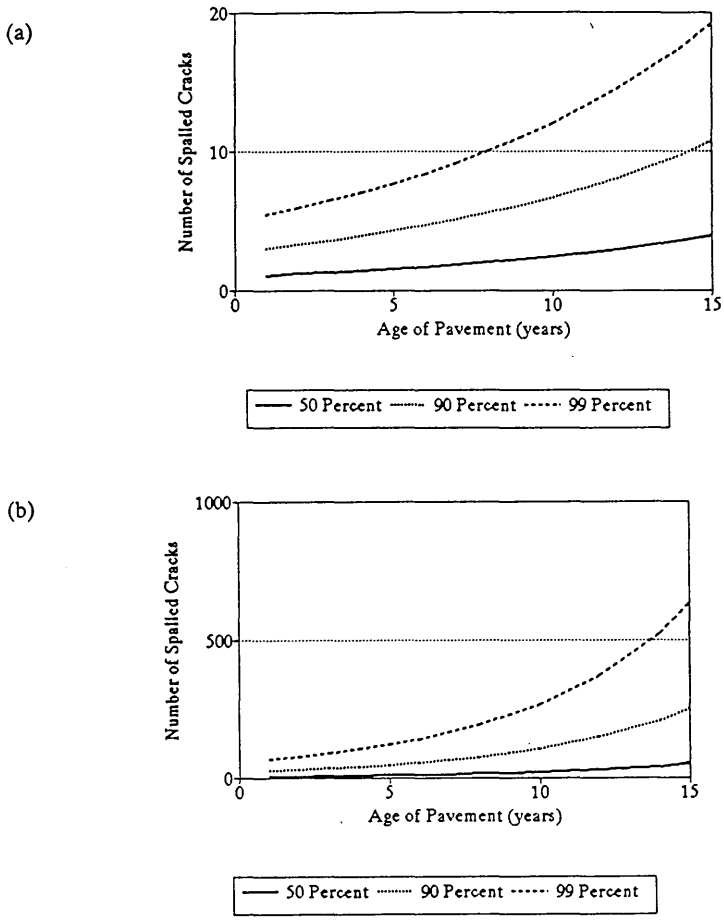

FIGURE 5 Predicted number of spalled cracks for different levels of reliability in pavements made with (*a*) siliceous river gravel and (*b*) crushed limestone coarse aggregate.

models such as those in Equations 14 and 15 can be developed for different localities and climatic conditions.

ACKNOWLEDGMENTS

This paper is based on the results of a cooperative study between the Texas Department of Transportation and the Texas Transportation Institute of the Texas A&M University System. The study is sponsored by the Texas Department of Transportation and FHWA.

REFERENCES

1. Lee, E. T. *Statistical Methods for Survival Data Analysis*, 2nd ed., John Wiley & Sons, Inc., New York, 1992.
2. Zollinger, D. G., and E. J. Barenberg. *Continuously Reinforced Pavements: Punch-outs and Other Distresses and Implications for Design.* Research Report FHWA/IL/UI 227. Department of Civil Engineering, Illinois Department of Transportation, University of Illinois, Urbana, March 1990.
3. Darter, M. I., and K. T. Hall. *Structural Overlay Strategies for Jointed Concrete Pavements*, Vol. IV. *Guidelines for the Selection of Rehabilitation Alternatives.* Report FHWA-RD-89-145. FHWA, U.S. Department of Transportation, Jan. 1990.
4. Zollinger, D. G., S. P. Senadheera, and T. Tang. Spalling in Continuously Reinforced Concrete Pavements. *Journal of Transportation Engineering, ASCE*, Vol. 120, No. 3, May–June 1994.
5. Dossey, T., and A. Weissmann. *A Continuously Reinforced Concrete Database.* Research Report 472-6. Center for Transportation Research, University of Texas at Austin, Nov. 1989.
6. Shelby, M. D., and B. F. McCullough. Experience in Texas with Continuously Reinforced Concrete Pavement. *Bulletin 274*, HRB, National Research Council, Washington, D.C., 1960.
7. Gutierrez de Velasco, M., and B. F. McCullough. *Summary Report for 1978 CRCP Condition Survey in Texas.* Research Report 177-20. Center for Transportation Research, University of Texas at Austin, Jan. 1981.
8. McCullough, B. F., J. C. M. Ma, and C. S. Noble. *Limiting Criteria for the Design of CRCP.* Research Report 177-17. Center for Transportation Research, University of Texas at Austin, 1979.
9. Tracy, R. G. *Deterioration of Continuously Reinforced Concrete Pavement in Minnesota—An Overview.* Research and Development Section, Minnesota Department of Transportation, Aug. 1978.
10. *NCHRP Synthesis of Highway Practice 60: Failure and Repair of Continuously Reinforced Concrete Pavement.* TRB, National Research Council, Washington, D.C., 1979.
11. McCullough, B. F., A. Abou-Ayyash, W. R. Hudson, and J. P. Randall. *NCHRP Report 1-15: Design of Continuously Reinforced Concrete Pavements for Highways.* TRB, National Research Council, Washington, D.C., Aug. 1975.
12. Tayabji, S. D., and B. E. Colley. *Improved Rigid Pavement Joints.* FHWA Research Report FHWA/RD-86/040. Construction Technology Laboratories, Skokie, Ill., 1986.

13. van Wijk, A. J. *Purdue Economic Analysis of Rehabilitation and Design Alternatives for Rigid Pavements: A User's Manual for PEARDARP*, FHWA Contract DTFH61-82-C-00035. Final Report. FHWA, U.S. Department of Transportation, Sept. 1985.
14. Kopperman, S., G. Tiller, and M. Tseng. *JCP-1: Interactive Microcomputer Version, User's Manual: IBM-PC and Compatible Version.* Report FHWA-TS-87-205. FHWA, U.S. Department of Transportation, Jan. 1986.
15. Smith, K. D., A. L. Mueller, M. I. Darter, and D. G. Peshkin. *Performance of Jointed Concrete Pavements*, Vol. II. *Evaluation and Modification of Concrete Pavement Design and Analysis Models.* Research Report FHWA-RD-89-137. ERES Consultants, Savoy, Ill., 1990.
16. Dossey, T., and W. R. Hudson. *Distress Curves for CRCP Crack Spalling.* Technical Memorandum 1908-12. Center for Transportation Research, University of Texas at Austin, Oct. 1992.
17. McCullough, B. F., and D. G. Zollinger. *Compendium of Research Activities To-Date: Evaluation of the Performance of Texas Concrete Pavements Made with Different Coarse Aggregates.* Texas Department of Transportation, Center for Transportation Research of the University of Texas at Austin, and Texas Transportation Institute of the Texas A&M University System, May 1993.
18. Kalbfleisch, J. D., and R. L. Prentice. *The Statistical Analysis of Failure Time Data.* John Wiley & Sons, Inc., New York, 1980.
19. *SAS/STAT® User's Guide*, Release 6.03 Edition. SAS Institute Inc., Cary, N.C., 1988.

Publication of this paper sponsored by Committee on Rigid Pavement Design.

Evaluation of Heavy Load Damage Effect on Concrete Pavements Using Three-Dimensional, Nonlinear Dynamic Analysis

SAMEH M. ZAGHLOUL, THOMAS D. WHITE, AND THOMAS KUCZEK

A study on the effects of heavy loads on Indiana highways was conducted. Available load equivalency factor (LEF) concepts were found to be inadequate for the study. An analytical approach was used to develop LEFs for concrete pavement. These LEFs are based on the total surface deformation. A three-dimensional dynamic finite-element method (3D-DFEM) was used in the analysis. The 3D-DFEM was verified for static, linear elastic, and dynamic nonlinear analyses. The 3D-DFEM predictions were compared with actual field measurements. There was good agreement between predicted and measured pavement responses. A comparison was made between the AASHTO LEFs and the Purdue LEFs for conditions similar to those of the AASHO Road Test, and no significant difference was found. Purdue LEFs consider different load and cross-section parameters, whereas the AASHTO LEFs do not. Also, Purdue LEFs were developed on the basis of an analytical model that can be extended in the future to cover a wider range of pavement thicknesses, layer materials, and load variables.

Accommodation of mixed traffic with a wide variety of axle loads and configurations is a critical step in pavement design. During the last 50 years a number of load equivalency concepts have been used to transform complex load configurations into a single standard load that can be used for the design of concrete pavements. These load equivalency concepts include equivalent single wheel load, equivalent single axle load (ESAL), and equivalent single axle radius (*1*). ESAL is the most commonly applied concept for highway pavements and was introduced by AASHO in the 1972 interim design guide (*2*). Load equivalency factors (LEFs) that use the ESAL concept are based on equal loss of serviceability. Empirical/statistical LEF sets were developed from analysis of the AASHO Road Test (*3*) results.

Westergaard analysis (*4,5*) and two-dimensional finite-element analysis (2D-FEM) are widely used to predict the structural response of rigid pavements to loads. These types of analyses assume static loading conditions and linear elastic material properties (*6*). Realistically, pavements are subjected to moving loads. Also paving materials may be characterized as elastic, elastic-plastic, visco-elastic, or plastic. The inability of the Westergaard analysis and currently used 2D-FEM analysis to represent actual loading conditions and paving material characteristics is significant. This reflects on the predicted pavement response and hence on any LEFs based on these predictions.

A study was conducted at Purdue University to develop a procedure for permitting overloaded trucks in Indiana. Funding was provided by the Indiana Department of Transportation (INDOT) and FHWA. The study addresses the permissibility of overloaded trucks as well as recommendations of vehicle configuration for various load levels. Both bridges and pavements were considered. However, the pavement part of the study only is addressed in this paper.

A 1-year sample of overload permit applications was reviewed to determine the configurations of the trucks being permitted. This sample revealed that permits were requested for trucks with up to nine axles in one group as well as trucks with single axle loads of 72 kips (32,668 kg). The AASHO Road Test included only single and tandem axle loads of up to 30 kips (13,612 kg) and 48 kips (21,779 kg), respectively. LEFs on regression analysis of the AASHO Road Test results are valid only for these numbers of axles and load ranges. Simple extrapolation of such regression relations beyond the range of factors for which data have been collected is questionable unless there is a basis of realistic material and structural models. This appears to be a deficiency in the AASHTO *Guide for Design of Pavement Structures* (*7*), in which LEFs are presented for single and tandem axle loads higher than those in the Road Test as well as for tridem axles, which were not used at all. These extrapolations are made by using the original serviceability-based regression equations for performance.

In the Load Equivalency Workshop, sponsored by FHWA (*8*), Barenberg emphasized the importance of using validated mathematical models in predicting pavement response and developing LEFs. He said, "A validated mathematical model is a model that accurately predicts pavement response to load and environment." He defined pavement response as deformation and strain.

In this paper LEFs for concrete pavements are presented. These LEFs were developed for the study addressing the permissibility of overloads and are based on equal maximum surface deflection (the elastic deformation of all layers and the plastic deformation of the bound and unbound layers under the concrete slabs, if any). A three-dimensional dynamic finite-element method (3D-DFEM) was used to analyze concrete pavements (*9*). This 3D-DFEM has the capability to simulate truck loads moving at different speeds. Also, it can realistically model paving materials as elastic, elastic-plastic, plastic, and viscoelastic materials. The 3D-DFEM predicts both the elastic and plastic pavement responses for one or more load applications. The 3D-DFEM was verified in two steps: first for static linear elastic analysis and then for dynamic nonlinear analysis (*10*).

School of Civil Engineering, Purdue University, West Lafayette, Ind. 47907.

AVAILABLE LEF APPROACHES

There are several approaches to evaluating the effect of loads on pavements, and therefore to determining LEFs. Two examples of LEF concepts for concrete pavement are equal loss of pavement serviceability and equal pavement distress (e.g., fatigue).

Loss of Serviceability Approach (AASHTO LEFs)

In 1959 and 1960 the AASHO Road Test was conducted in Ottawa, Ill. (*3*). Two types of truck loading were used: single and tandem axles. The results of the AASHO Road Test and the concept of present serviceability index (PSI) were used as a measure of pavement performance in the AASHTO Interim Design Guide (*2*). The PSI of concrete pavement is a function of pavement slope variance (roughness), cracking, and patching. Pavement failure was defined in terms of terminal serviceability instead of strict structural failure. Empirical relationshps were developed to correlate PSI, as a measure of pavement performance, to the number of load repetitions. On the basis of these two factors, PSI and load repetitions, the AASHTO LEFs were developed. In the AASHO Road Test the maximum axle loads were 30 and 48 kips (13,612 and 21,779 kg) for single and tandem axles, respectively. In the 1986 AASHTO design guide (*7*) LEFs for higher loads and tridem axle configuration are presented by using the same statistical models.

Analytically Based LEFs

As another approach to determining LEFs, Westergaard analysis (*4,5*) or a 2D-FEM analysis (*11*) was used to predict the elastic pavement response for different load parameters, such as axle load and spacing. The pavement damage owing to different load parameters is estimated by using correlations of various types of distress, such as cracking, and pavement response, such as tensile stress. Several relationships are available to correlate fatigue failure to maximum tensile stress. A frequently used relationship was developed by Vesic and Saxena (*12*):

$$N_{2.5} = 225{,}000\left(\frac{M_R}{\sigma}\right)^4$$

where

$N_{2.5}$ = load repetitions to a serviceability index of 2.5,
M_R = modulus of rupture of concrete (lb/in.^{2}), and
σ = tensile stress (lb/in.^{2}).

In an analysis reported by Hallin et al. (*13*), tensile stress was taken as the combined load and warping stresses. The load stress was determined by using ILLI-SLAB, a two-dimensional finite-element program (*11*), whereas the warping stress was based on regression equations developed by Darter (*14*). The combined stress was determined at the maximum load-related stress position. The LEF for load (i) is represented as (*13*)

$$(\text{LEF})_i = \frac{[N_f]_{18}}{[N_f]_i}$$

where $[N_f]_{18}$ and $[N_f]_i$ are the number of repetitions of the standard 18-kip (8,167-kg) load and any load (i), respectively, resulting in a serviceability index of 2.5.

COMPARISON BETWEEN DIFFERENT LEF METHODS

A comparison between the AASHTO LEFs (*2*) and LEFs based on fatigue analysis (*13*) for a single axle load configuration is presented in Figure 1. LEFs based on fatigue analysis are significantly different from the AASHTO LEFs. The fatigue analysis LEFs were found to underestimate the pavement damage caused by any axle load. This was expected because the fatigue analysis LEFs are based on the elastic response of pavements, whereas the AASHTO LEFs are based on slope variance (roughness), which is a function of permanent pavement deformation or loss of support. Not accounting for or incorrectly accounting for other factors such as temperature curling or moisture warping may also contribute to the poor correlation of fatigue analysis.

THREE DIMENSIONAL-DYNAMIC FINITE ELEMENT ANALYSIS

Features of Finite-Element Model

A jointed reinforced concrete pavement cross section similar to that of the AASHO Road Test was modeled in the present analysis as two 12-ft (365.76-cm) lanes plus 8-ft (243.84-cm) shoulders on either side. The pavement structure consists of three layers: concrete slab, granular subbase, and subgrade. Granular shoulders were used in the analysis to be consistent with the AASHO Road Test. Three-dimensional finite-element meshes (3D-FEMs) with variable openings were created to model the pavement structures. Meshes with variable size openings were used to reduce the computer memory requirements and computational time. A smaller mesh spacing was used to provide detailed response predictions when they were needed. Pavement structures were modeled as a

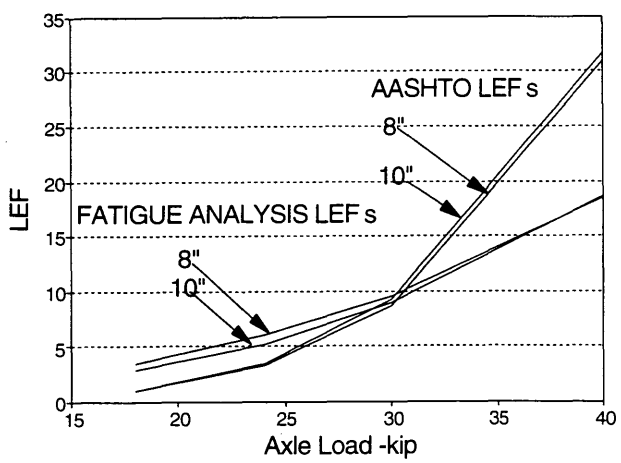

FIGURE 1 Comparison between AASHTO LEFs and fatigue analysis-based LEFs (single axle configuration).

set of layers. Shown in Figure 2 is one of the 3D-FEMs used in the analysis. In this example the subgrade thickness was represented by five elements; the concrete slab and the granular subbase thicknesses were represented by single elements. Longitudinal and transverse joints were modeled by using gap elements with an initial opening of 3/8 in. (9.53 mm). Depending on the deformed shape of the slabs after loading, the slabs might come into contact and develop friction. Dowel bars were modeled and located in the midthickness of the slab. The bond stress of one-half of the dowel bar was set equal to zero. Details of the finite-element features used in the analysis have been reported previously (*12,14*). Loads were sequentially applied at surface nodes. The time rate of loading from one node to the next simulated vehicle speeds. From previous studies (*10,15*), vehicle speed was found to have a significant effect on pavement response. Therefore, a speed similar to the average speed of the AASHO Road Test, 35 mph (50 km/hr) (*16*), was used in developing the LEFs.

Material Models

In the analysis pavement materials were divided into three groups: portland cement concrete, granular materials, and cohesive soils. Details of these material models were reported by Zaghloul and White (*17*).

Portland cement concrete behavior was divided into three stages: elastic, plastic, and after-failure stages. The stress-strain curve used to model portland cement concrete is shown in Figure 3. In this model if the concrete slab is subjected to a stress level less than its yield stress it will behave as an elastic material. When the stress level exceeds the yield stress of the concrete, behavior is elastic-plastic until the stress reaches the failure limit. At that point the after-failure stage starts (*18*).

Granular materials, base, subbase and subgrade in some cases were modeled by using the Drucker-Prager model (*20,21*). This is an elastic-plastic model in which granular materials are assumed to behave elastically for low stress levels. When the stress reaches a certain yield stress the material will subsequently behave as an elastic-plastic material. The assumed stress-strain curve for a granular material is shown in Figure 3*a*.

The Cam-Clay model (*18,21,22*) was used to model clays. This model uses a strain rate decompositoin in which the rate of deformation of the clay is decomposed additively into an elastic and a plastic part. The assumed soil response in pure compression is shown in Figure 3*b*.

Other material and layer characteristics required in the analysis include modulus of elasticity, Poisson's ratio, damping coefficient, and bulk density. Listed in Table 1 are the material properties used in the analysis.

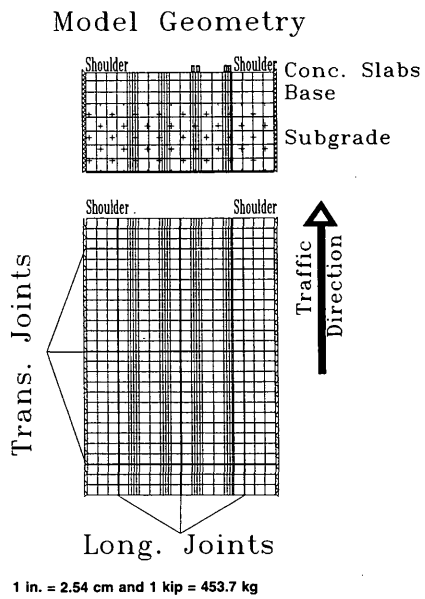

FIGURE 2 Example of 3D-FEMs used in analysis.

Finite-Element Model Verification

The 3D-DFEM was verified for static, linear elastic analysis as well as for dynamic, nonlinear analysis.

Static Analysis Verifications

A design of experiment (DOE) was developed to determine if the 3D-DFEM predictions of pavement response agree with those calculated by using the Westergaard equations (*4,5*). Three factors were included in the DOE: slab thickness, subgrade type, and load position. Three levels for the slab thickness, 6, 10, and 14 in. (15.24, 25.4, and 35.56 cm), and two subgrade types, sand and clay, were included in the analysis. Values of modulus of elasticity (E) and modulus of subgrade reaction (k) were selected on the basis of the correlation of soil type with the Unified Soil Classification system (*23*). Assuming a static loading condition and linear elastic material properties, the maximum tensile stress in the concrete slab for three loading positions, center, edge, and corner, were predicted by using the 3D-DFEM and the Westergaard equations (*4,5*). An analysis of variance of the results was made to test if there was a linear correlation between the deflections predicted by the 3D-DFEM and those calculated from the Westergaard equations. It was found that there is a very high linear correlation between the pavement responses predicted by the 3D-DFEM and those calculated from the Westergaard equations (R^2 = 97.7 percent).

In another study (*24*), the 3D-DFEM predictions, assuming linear elastic material properties and static loads, were compared with the predictions of a multilayer analysis by using the computer program Bitumen Structures Analysis in Roads (BISAR) (*25*). There was good agreement between the predictions of deflection by the two models at different depths and offset distances from the loaded area (R^2 = 96.0 percent).

Dynamic Analysis Verification

To evaluate the dynamic analysis capabilities of the 3D-DFEM, a comparison was made of its predictions with actual pavement deflections measured under moving trucks. In a study by the Portland Cement Association (*26*), a field testing program was conducted at six sites; three of these sites were located in Wisconsin and the other three sites were located in Pennsylvania. The surface

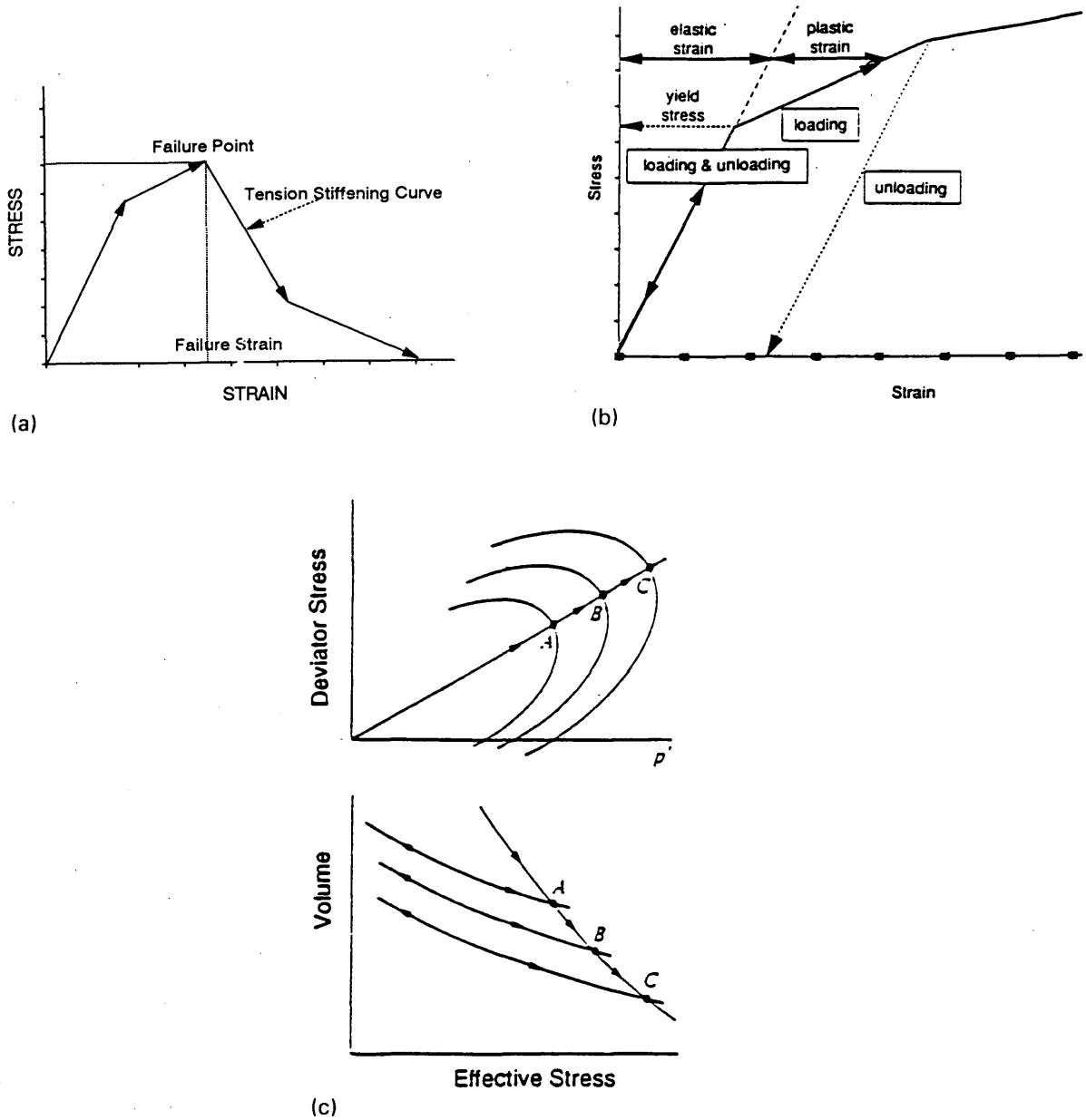

1 in. = 2.54 cm and 1 kip = 453.7 kg

FIGURE 3 Material models used in analysis: (*a*) concrete model (*18*), (*b*) Drucker-Prager Model (*18*), and (*c*) Cam-Clay model (*18,19*).

deflection was measured at these sites under single and tandem axles moving at creep speed, 2 mph (3 km/hr). The three pavement sections located in Wisconsin were incorporated into the verification study. Finite-element meshes were created to match these cross sections, and reasonable material properties were assumed. Moving axle loads similar to those used in the field test were considered in the analysis, and the total surface deflection from these loads was predicted by using the 3D-DFEM. The measured and predicted pavement deflections are shown in Figure 4. A linear correlation analysis between the measured and predicted deflections showed an excellent correlation between the 3D-DFEM predictions and the field measurements (R^2 = 99.64 percent).

This dynamic verification study was conducted for pavement response to loads moving at creep speed, 2 mph (3 km/hr). No field data for concrete pavement response to loads moving at higher speeds were available at the time of the study. However, other dynamic verification studies were conducted by using the 3D-DFEM for asphalt pavements. These studies included comparisons of pavement response to loads moving at speeds of 4 and 35 mph (6 and 50 km/hr) (*24*) and comparison of pavement response to falling-weight deflectometer loading (*15*).

TABLE 1 Example of Material Properties Used in Analysis

Material Name	Material Property	Typical Value
Concrete Slabs	Modulus of Elasticity - psi(GPa)	4,000,000 (27.62)
	Poisson's Ratio	0.15
	Initial Yield Stress - psi (MPa)	2670 (18.4)
	Failure Plastic Strain	1.3E-03
	Density - pcf (gm/cm^3)	150 (2.403)
	Damping Coefficient (%)	5
Granular Subbase	Modulus of Elasticity - psi (GPa)	40,000 (0.276)
	Poisson's Ratio	0.3
	Initial Yield Stress - psi (MPa)	19.29 (0.133)
	Initial Plastic Strain	0.0
	Angle of Friction - degree	33
	Density - pcf (gm/cm^3)	135 (2.1625)
	Damping Coefficient (%)	5
Lean Clay (CL) Subgrade	Shear Modulus - psi (MPa)	2750 (18.964)
	Poisson's Ratio	0.3
	Logarithmic Hardening Modulus	0.174
	Initial Overconsolidation Parameter - psi (KPa)	8.455 (58.306)
	Permeability - ft/sec (cm/sec)	0.000021 (0.00064)
	Initial Void Ratio (%)	8
	Initial Stress psi (MPa)	weight of the pavement layers
	Density - pcf (gm/cm^3)	130 (2.0824)
	Damping Coefficient (%)	5

PURDUE LEFs

An LEF set was developed for concrete pavement with granular subbase (Purdue LEFs) on the basis of equal maximum surface deflection (MSD). MSD deflection consists of the elastic deformation of different layers and the plastic deformation of the unbound layers under the concrete slabs, if any. For a given load and speed the plastic deformation in the unbound layers increases with the number of load applications until an asymptotic value is reached. This asymptotic value and the rate of deflection increase with the number of load applications and are a function of load magnitude, speed, and slab thickness. The elastic deformation of the slab increases because of reduced support from the accumulating permanent deformation. Shown in Figure 5 is the effect of load repetitions on an unbound layer with a permanent deformation and on the total surface deflection for two slab thicknesses, 8 and 14 in. (20.32 and 35.56 cm).

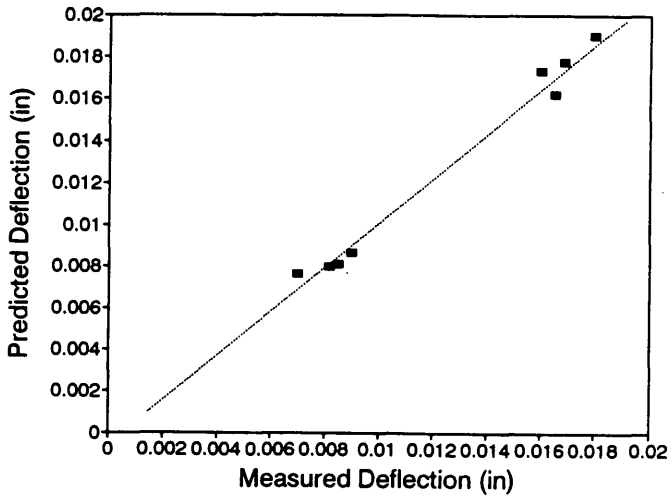

1 in. = 2.54 cm and 1 kip = 453.7 kg

FIGURE 4 Dynamic analysis verification.

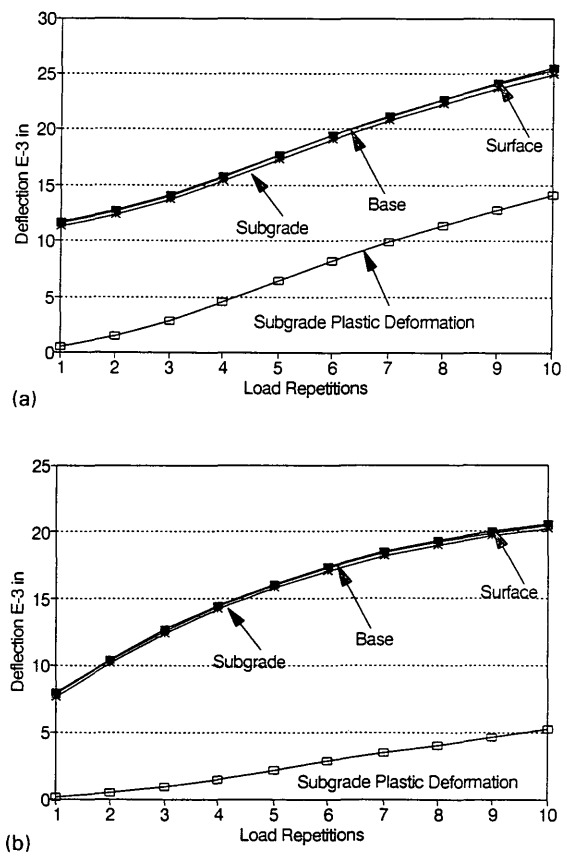

1 in. = 2.54 cm and 1 kip = 453.7 kg

FIGURE 5 Effect of load repetitions on total surface deformation: (*a*) 8-in. concrete slab and (*b*) 14-in. concrete slab.

Use of MSD was arrived at after evaluating the results of a number of sensitivity studies (*10*). There is a logic as to why the MSD of concrete pavements would correlate so effectively with the AASHO Road Test serviceability concept. Fatigue of concrete pavements is related to elastic defection, whereas roughness is related to permanent deformation. Therefore, it takes the combined MSD to provide a scale for rigid pavement serviceability. In application, the LEF of any load j is the number of 18-kip (8,167-kg) single axle loads required to develop the same MSD developed by one pass of the road j on the same pavement cross section.

Two statistical models were developed for Purdue LEFs. The first model predicts the MSD developed by one pass of any axle load configuration, including the 18-kip (8,167-kg) single axle load, on a range of rigid pavement cross sections. The second model predicts the MSD owing to repetitions of the 18-kip (8,167-kg) single axle load. LEFs are developed by using the two models. The first model predicts the MSD owing to load j on cross section i, and then the predicted MSD is used as an input to the second model to estimate the number of the 18-kip (8,167-kg) single axle load repetitions required to develop the same MSD in cross section i, which is LEF_{ij}. Figure 6 provides a graphical representation of the Purdue LEF concept for rigid pavements.

Design of Experiments

Two DOEs were implemented to develop the rigid pavement LEFs. The factors in Table 2 were included in the first DOE (DOE1). In a study concerned with developing LEFs for flexible pavements (*27*), the subgrade type was found to be insignificant for flexible pavement LEFs at a speed of 35 mph (50 km/hr). On the basis of this experience and because of the surface rigidity of the concrete pavement, a decision was made not to include subgrade type in DOE1. A 4-in. (10.16-cm) granular subbase was assumed for all cross sections included in this analysis. The sample of overload permit applications showed that the average axle spacing is 4 ft (121.92 cm); therefore, a 4-ft (121.92-cm) axle spacing was assumed for n axle configurations.

A partial factorial design was used to develop the first model. Different load-cross section combinations were analyzed by using the 3D-DFEM. An analysis of variance was used to test the significance of different factors included in DOE1. The significant main effects and two-way interactions were used to develop a regression model to predict the MSD for various axle load configurations. From this analysis it was found that speed is a significant factor. The MSDs for high speeds [>20 mph (32 km/hr)] are small compared with those for low speeds [<20 mph (32 km/hr)]; therefore, two regression models were developed to predict MSD, one model for low speeds and the other for high speeds. Both models showed high correlations, R^2 = 98.4 and 99.5 percent, respectively.

Low-speed model (LSM) (R^2 = 98.4 percent):

$$MSD = 5.6E\text{-}6 \cdot D^4 + 18.402 \cdot N - 1.036 \cdot T - 2.416 \cdot N^2$$

where

D = axle load (kip per single axle),
T = slab thickness (in.), and
N = number per axles.

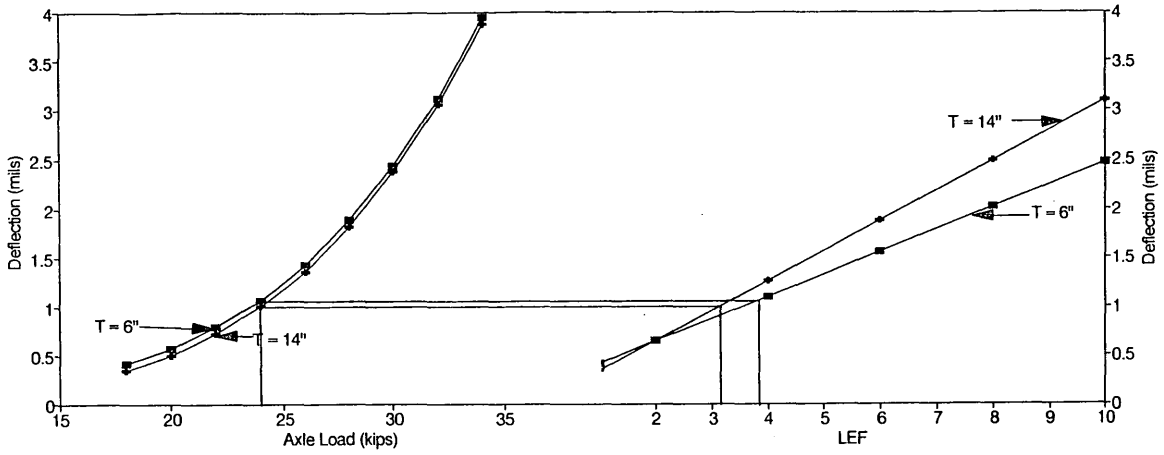

1 in. = 2.54 cm and 1 kip = 453.7 kg

FIGURE 6 Purdue LEFs.

TABLE 2 Factors in DOE1

Factor	Levels		
	1	2	3
Axle Load - kip (kg)	18 (8,167)	24 (10,889)	36 (16,334)
No. of Axles	1	2	4
Slab Thickness - in (cm)	6.0 (15.24)	12.0 (30.48)	18.0 (45.72)
Speed - mph (km/h)	1.75 (2.6)	20.0 (32.0)	40.0 (65.0)

High-speed model (HSM) (R^2 = 99.5 percent):

$$MSD = 2.98E\text{-}6 \cdot D^4 + 0.3051 \cdot N + 0.0088 \cdot T - 0.0057 \cdot S \cdot N - 3.3E\text{-}9 \cdot S \cdot D^4 + 5E\text{-}5 \cdot S^2$$

where S is speed (in mph).

Two LEF sets were developed, one for low and one for high speeds. A comparison between these two sets and the AASHTO LEFs is presented in Figure 7. As can be seen from Figure 7, LEFs based on HSM agree with AASHTO LEFs. This is because the mean speed at the AASHO Road Test was approximately 35 mph (50 km/hr) (*16*). Subsequent analysis is made by using HSM. To extend the validity of HSM more cases were analyzed to cover a wider range of factor levels, and the results were compared with the extrapolated predictions of this model.

A second DOE (DOE2) was implemented to consider the effect of 18-kip (98,167-kg) single axle load repetitions. Two factors were included in DOE2, slab thickness (T) and number of 18-kip (8,167-kg) single axle load repetitions (C). Three levels for slab

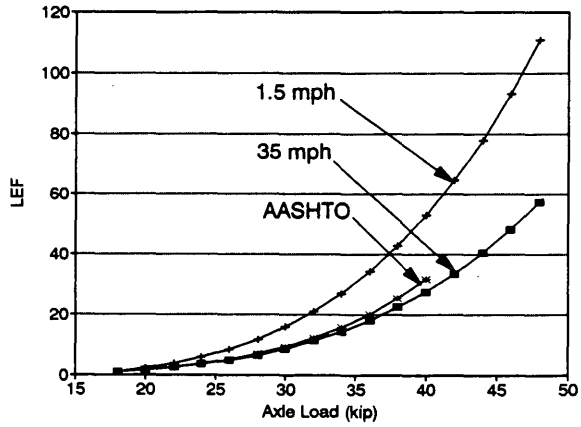

1 in. = 2.54 cm and 1 kip = 453.7 kg

FIGURE 7 Effect of speed on Purdue LEFs.

thickness 6 in. (15.24 cm), 12 in. (30.48 cm), and 18 in. (45.72 cm), were included in the analysis, and the 18-kip (8,167-kg) single axle load was repeated up to 30 times. A regression analysis was made on the results obtained by using the 3D-DFEM, and the following regression model was developed (R^2 = 97.8 percent):

$$MSD = (0.17 + 0.0096 \cdot T) \cdot C$$

Comparison Between Purdue LEFs and AASHTO LEFs

Purdue LEFs for different slab thicknesses were compared with the corresponding AASHTO LEFs for single and tandem axle configurations. Figures 8 and 9 show the results of this comparison. Purdue LEFs were found to agree with the AASHTO LEFs for both single and tandem axle configurations.

Examples

A permit request is made for an overloaded truck having two single axles in addition to the steering axle. Each single axle will carry a load of 72 kips (32,668 kg). The LEF of the 72-kip single axle is determined for a pavement section consisting of a 10-in. (25.4-cm) concrete slab and a 4-in. (10.16-cm) granular base course. The truck was assumed to travel at a speed of 30 mph (50 km/hr).

1. Total surface deformation for the 72-kip (32,668-kg) single axle load j and the 18-kip (8,167-kg) single axle load on section i:

$$TSD_{ij} = 2.98E\text{-}6(72^4) + 0.3051(1) - 0.00877(10) - 0.005678(30)(1) - 3.3E\text{-}9(30)(72^4) + 5.5E\text{-}5(30)(30) = 77.52014 \text{ mils } (1.968 \text{ mm}).$$

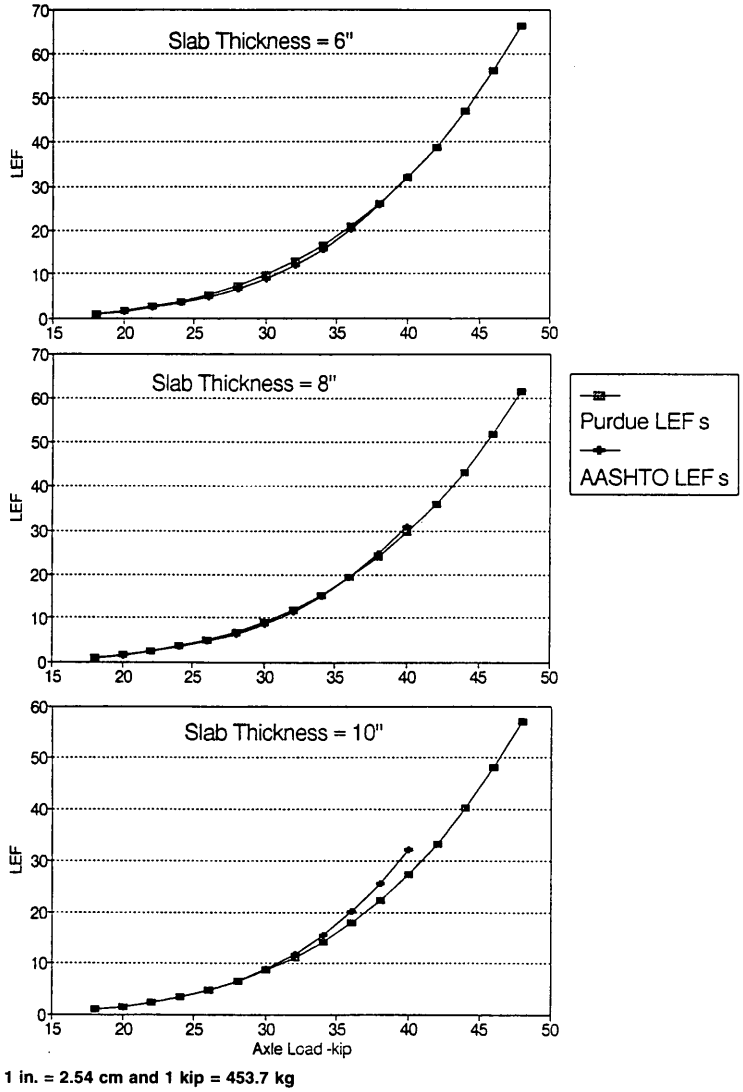

FIGURE 8 Comparison between AASHTO LEFs and Purdue LEFs for single axle configuration.

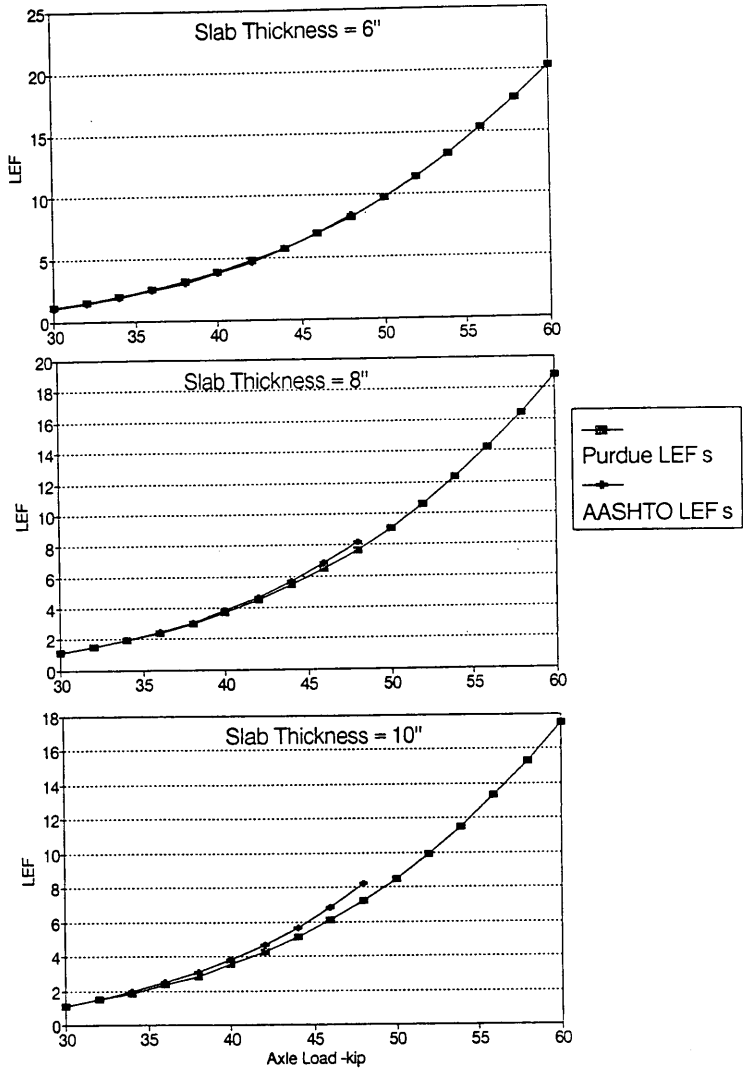

FIGURE 9 Comparison between AASHTO LEFs and Purdue LEFs for tandem axle configuration.

$$TSD_{18} = 2.98E\text{-}6(18^4) + 0.3051(1) - 0.00877(10) - 0.005678(30)(1) - 3.3E\text{-}9(30)(18^4) + 5.5E\text{-}5(30)(30)$$

$$= 0.398996 \text{ mils } (0.0101 \text{ mm}).$$

2. Number of 18-kip (8,167-kg) single axle loads required to develop the same total surface deformation from one pass of load j on cross section i (LEF_{ij}):

$$LEF_{72} = 1 + \frac{77.52014 - 0.398996}{0.17 + 0.00959(10)} = 454.654$$

The LEF of a 30-kip (13,612-kg) single axle load on the same pavement section is as follows:

$$TSD_{30} = 2.98E\text{-}6(30^4) + 0.3051(1) - 0.00877(10) - 0.005678(30)(1) - 3.3E\text{-}9(30)(30^4) + 5.5E\text{-}5(30)(30)$$

$$= 2.43017 \text{ mils } (0.0617 \text{ mm})$$

$$LEF_{30} = 1 + \frac{2.43017 - 0.398996}{0.17 + 0.00959(10)} = 12.9$$

The corresponding AASHTO LEF is 12.17.

Sensitivity Analysis

The effect of slab thickness on LEFs is shown in Figure 10 for single and tandem axle configurations. With an increase in slab thickness the pavement damage because of the loads decreases and therefore the LEFs decrease. As can be seen from Figure 10 the LEFs decrease as slab thickness increases, as expected. The same is true for the AASHTO LEFs for thin slabs [6 to 8 in. (15.24 to 20.32 cm)]. For thicker slabs [>8 in. (20.32 cm)] the AASHTO LEFs increase with an increase in slab thickness. This could be associated with surface defects such as spalling and joint faulting.

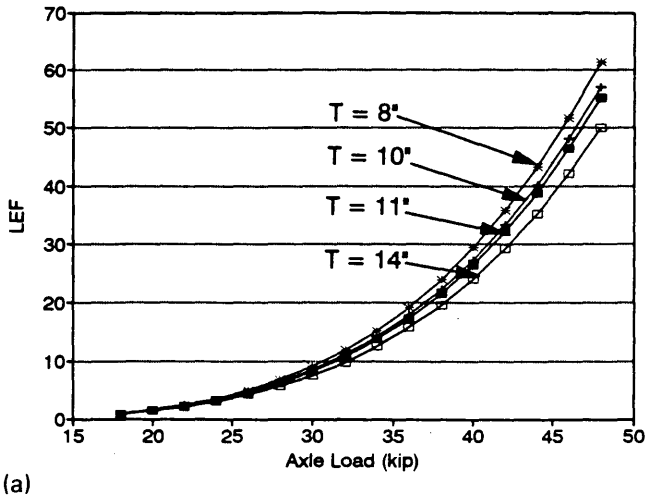

(a)

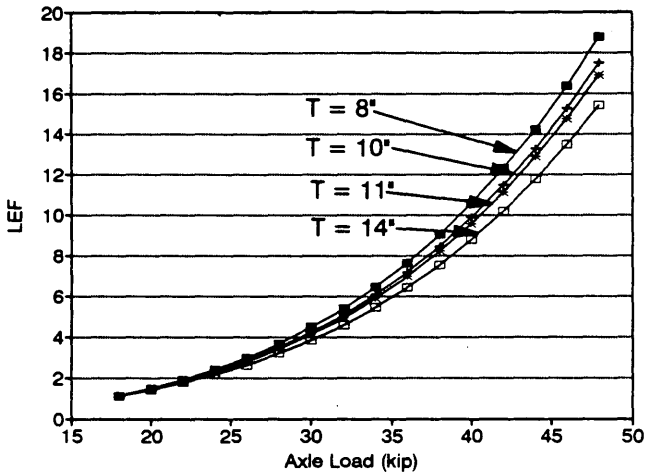

(b)

1 in. = 2.54 cm and 1 kip = 453.7 kg

FIGURE 10 Effect of slab thickness on Purdue LEFs: (*a*) single axle configuration and (*b*) tandem axle configuration.

The effect of the number of axles on LEFs is shown in Figure 11. As expected for the same axle group load magnitude, the LEFs decrease with the increase in the number of axles.

Advantages of Purdue LEFs

Purdue LEFs can be considered serviceability-based LEFs. The reason there is such a good correlation between the AASHTO LEFs and Purdue LEFs is that subgrade permanent deformation is related to the potential accumulation of roughness, and roughness is a large component of serviceability. Purdue LEFs have the following advantages:

1. Purdue LEFs are based on dynamic analysis in which moving loads at different speeds were considered. Also realistic material properties and models were inlcuded in the analysis.
2. The 3D-DFEM analysis used to develop these LEFs has been verified for static, linear elastic analysis and dynamic, nonlinear analysis.

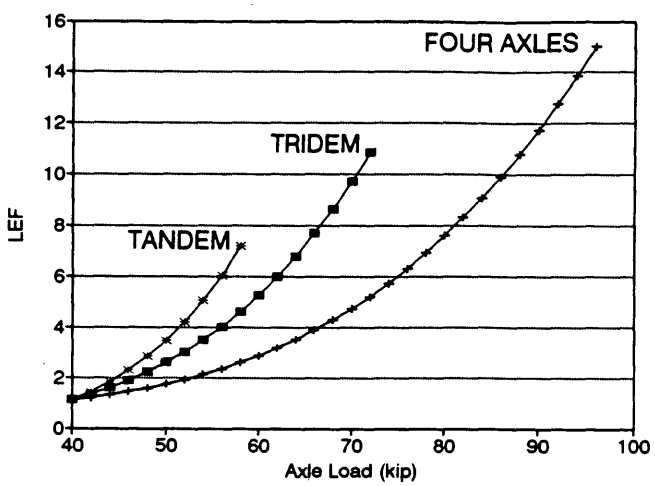

1 in. = 2.54 cm and 1 kip = 453.7 kg

FIGURE 11 Effect of number of axles on Purdue LEFs.

3. The concept presented here is different from those concepts that assume that the pavement response is a linear function in the number of load applications.
4. Both elastic and plastic deformations were included in the analysis. This cannot be done using a closed-form solution, which predicts the elastic pavement response only. Regardless of how accurately the elastic response is predicted, these methods do not provide a comprehensive measure of pavement performance.
5. Purdue LEFs are based on an analytical model. As a result they can be updated or extended to cover other factors not already included.

REFERENCES

1. Ioannides, A., and L. Khazanovich. *Load Equivalency Concepts: A Mechanistic Reappraisal.* In *Transportation Research Record 1388*, TRB, National Research Council, Washington, D.C., Jan. 1993, pp. 42–51.
2. *Interim Guide for Design of Pavement Structures—1972.* AASHO, Washington, D.C., 1972.
3. *Special Report 61E: AASHO Road Test, Report 5: Pavement Research.* HRB, National Research Council, Washington, D.C., 1962.
4. Westergaard, H. M. Stresses in Concrete Pavements Computed by Theoretical Analysis. *Public Roads*, April 1926.
5. Westergaard, H. M. New Formulas for Stresses in Concrete Pavements of Airfields. *Transactions, ASCE*, Vol. 113, pp. 425–444.
6. *Rigid Pavement Analysis and Design.* Report FHWA-RD-88-068. FHWA, U.S. Department of Transportation, June 1988.
7. *Guide for Design of Pavement Structures.* AASHTO, Washington, D.C., 1986.
8. *Load Equivalency Workshop Synthesis.* Publication FHWA-RD-89-117. FHWA, U.S. Department of Transportation, April 1989.
9. *ABAQUS, Finite Element Computer Program, Version 4.9.* Hibbitt, Karlsson and Sorensen, Inc., 1989.
10. Zaghloul, S., and T. D. White. Non-Linear Dynamic Analysis of Concrete Pavements. *Proc., 5th International Conference on Concrete Pavement Design and Rehabilitation*, Vol. 1. Purdue University, West Lafayette, Ind., 1993, pp. 277–292.
11. Tabatabaie-Raissi, A. *Structural Analysis of Concrete Pavement Joints.* Ph.D. thesis. University of Illinois, Urbana, 1977.
12. Vesic, A., and S. Saxena. *NCHRP Report 97: Analysis of Structural Behavior of AASHO Road Test Rigid Pavements.* HRB, National Research Council, Washington, D.C., 1970.
13. Hallin, J., J. Sharma, and J. Mahoney. Development of Rigid and Flexible Pavement Load Equivalency Factors for Various Widths of

Single Tires. In *Transportation Research Record 949*, TRB, National Research Council, Washington, D.C., 1983.
14. Darter, M. I. *Design of Zero Maintenance Plain Jointed Concrete Pavement*, Vol. 1. *Development of Design Procedures*. Report FHWA-RD-77-111. FHWA, U.S. Department of Transportation, 1977.
15. Zaghloul, S. M., T. D. White, V. P. Drnevich, and B. Coree. Dynamic Analysis of FWD Loading and Pavement Response Using a Three-Dimensional Dynamic Finite Element Program. In *Nondestructive Testing of Pavements and Backcalculation of Moduli*, Second Volume. ASTM STP 1198 (H. L. Von Quintas, A. J. Bush, and G. Y. Baladi, eds.). ASTM, Philadelphia, Pa., 1994.
16. Coree, B., and T. White. *Layer Coefficients in Terms of Performance and Mixture Characteristics*. Joint Highway Research Project. Report FHWA/IN/JHRP-88/13. Purdue University, West Lafayette, Ind., 1988.
17. Zaghloul, S. M., and T. D. White. *Guidelines for Permitting Overloads, Part 1: Effect of Overloaded Vehicles on the Indiana Highway Network*. Joint Highway Research Project. Report FHWA/IN/JHRP/93/5. Purdue University, West Lafayette, Ind., 1993.
18. *ABAQUS, Finite Element Computer Program, Version 4.9, Theory Manual*. Hibbitt, Karlsson and Sorensen, Inc., 1989.
19. Wood, D. *Soil Behavior and Critical State Soil Mechanics*. Cambridge University Press, Cambridge, United Kingdom, 1990.
20. Drucker, D. C., and W. Prager. Soil Mechanics and Plastic Analysis or Limit Design. *Quarterly of Applied Mathematics*, Vol. 10, 1952, pp. 157–165.
21. Schofield, A., and C. P. Worth. *Critical State Soil Mechanics*. McGraw-Hill, New York, 1968.
22. Parry, R. H., ed. *Stress-Strain Behavior of Soils*. G. T. Foulis and Co., Henley, England, 1972.
23. Yoder, E. J., and M. W. Witczak. *Principles of Pavement Design*, 2nd ed. John Wiley & Sons, Inc., New York, 1975.
24. Zaghloul, S., and T. D. White. Use of a Three-Dimensional Finite Element Program for Analysis of Flexible Pavement. In *Transportation Research Record 1388*, TRB, National Research Council, Washington, D.C., 1993, pp. 60–69.
25. *Bitumen Structures Analysis in Roads (BISAR)*, Computer Program. Koninlilijke/Shell-Laboratorium, Amsterdam, July 1972.
26. Okamoto, P., and R. Packard. Effect of High Tire Pressures on Concrete Pavement Performance. *Proc., 4th International Conference on Concrete Pavement Design and Rehabilitation*. Purdue University, West Lafayette, Ind., April 1989.
27. Zaghloul, S. M., and T. D. White. Load Equivalency Factors for Flexible Pavements. *Proc., 1994 Annual Meeting of the Association of Asphalt Paving Technologists*, St. Louis, Mo., Feb. 1994, and *Journal of the Association of Asphalt Paving Technologists*, in press.

Publication of this paper sponsored by Committee on Rigid Pavement Design.

Factors Affecting Crack Width of Continuously Reinforced Concrete Pavement

YOUNG-CHAN SUH AND B. FRANK MCCULLOUGH

Crack width is an important factor affecting the behavior and performance of continuously reinforced concrete pavement (CRCP). Wide cracks can lead to various pavement distresses, including spalling, punchouts, and steel rupture. Various factors affecting CRCP crack width were evaluated on the basis of the width measurements of 208 transverse cracks randomly selected from a series of experimental test sections constructed in Houston, Tex. The crack widths were measured at various times and slab temperatures by using a microscope with a graduated eyepiece. It was found from a statistical analysis of the collected data that the factors that significantly affect crack width are construction season, coarse aggregate type, amount of steel, and time of crack occurrence. Thus, hot weather placement produced much wider cracks than cool weather placement. The use of siliceous river gravel resulted in cracks wider than those associated with the use of limestone, and the difference was larger at lower temperatures. The greater the amount of longitudinal steel, the narrower the crack width. Cracks occurring during the first 3 days of construction were significantly wider than those that occurred later. Finally, the effect of crack spacing on crack width was found to be insignificant.

Crack width is an important factor affecting the behavior and performance of continuously reinforced concrete pavement (CRCP). For effective performance crack width should be narrow enough to provide sufficient aggregate interlocking and to avoid infiltration of appreciable amounts of water through the crack.

Excessive crack openings can lead to the loss of load transfer, causing excessive flexing of the concrete slab under traffic (with the resultant spalling of the concrete). They can also lead to punchouts, steel rupture, the infiltration of incompressible material (causing spalling and blowups), and water seepage that can reduce roadbed support and that can cause rusting of the steel (*1*). A maximum allowable crack width of 0.04 in. was suggested by AASHTO (*2*) on the basis of the consideration of spalling and water penetration.

Crack width varies with temperature; cracks are wider in cold weather when the concrete slab has contracted than in hot weather when the individual concrete slabs have expanded. Crack width also changes with age. Drying shrinkage (which occurs after the initial crack formation) and incompressible foreign material entering the crack both contribute to the increase in crack width (*3,4*). The rate of increase, however, decreases with time (*1*). Many literature sources (*1,5,6*) have indicated that the crack width varies with the depth of the crack, being greatest at the surface and progressively smaller with increasing depth. It is a well-accepted fact that the crack width is a function of the amount of longitudinal steel, in which the greater the amount of longitudinal steel, the smaller the crack width (*1,7*). This is true because crack width is a function of steel stress and the effectiveness of the bond between the concrete and steel near the crack. In this paper various design and construction factors affecting crack width are evaluated on the basis of field measurements of crack widths taken from a series of experimental test sections.

Y. C. Suh, Korea Institute of Construction Technology, Seoul, Republic of Korea. B. F. McCullough, Center for Transportation Research, University of Texas, Austin, Tex. 78712.

EXPERIMENTAL TEST SECTIONS

The experiment included CRCP test projects constructed at four locations in Houston (*8*). They were placed during two different seasons (summer and winter). For convenience the following abbreviations for the projects will be used in this paper:

SH6-summer:	These test sections were placed on State Highway 6 in the summer (June 1989).
BW8-winter:	These test sections were placed on Beltway 8 in the winter (November 1989).
SH6-winter:	These test sections were placed on State Highway 6 in the winter (January 1990).
IH45-winter:	These test sections were placed on Interstate Highway 45 in the winter (January 1990).

With each project, 1,840 ft of CRCP was placed; one-half of the length (920 ft) used siliceous river gravel (SRG) and the other half used limestone (LS) as the coarse aggregate. Each of these lengths was subdivided into four test sections so that each section was 230 ft long (*8*).

One of the four sections for each coarse aggregate type used the same quantity of longitudinal steel specified in the Texas design standard (*8*), CRCP(B)-89B (hereafter termed *medium steel*). Two other test sections used about 0.1 percent higher quantity and lower quantity, respectively, of longitudinal steel than the medium steel (hereafter termed *high steel* and *low steel*, respectively). These three test sections used a 3/4-in.-diameter bar (No. 6 bar). The fourth test section used medium steel with a larger-size bar (a 7/8-in.-diameter or No. 7 bar) for investigating the interactive effect of bond area and concrete volume ratio.

EXPERIMENTS

A total of 208 transverse cracks was selected: sixty-four cracks (8 cracks from each of eight sections) were selected from SH6-summer, and 48 cracks (6 cracks from each of eight sections) were

selected from each of the BW8-winter, SH6-winter, and IH45-winter projects. The cracks were randomly selected within a section by using a random number table (*9*).

The crack widths were measured at various times and slab temperatures by using a microscope with a graduated eyepiece (Figure 1). The microscope contained a vernier scale and was capable of measuring to the closest 0.001 in. Measurements were performed by one operator so as to reduce measurement error caused by operator variance. Slab temperatures were measured at three positions along the thickness of the slab: top (1 in. from the surface), middle (center of the slab), and bottom (1 in. from the bottom).

The temperatures at these three positions were correlated with the crack width, which was measured under various time and temperature conditions, to select the position at which the temperatures most nearly identified with the crack width. The typical plots of correlations are given in Figure 2. These plots indicate that the slab temperatures at the top give the best correlation with the crack widths. Accordingly, the slab temperatures at the top were used to represent the slab temperature in this crack width study. Summarized in Table 1 are the time of crack width measurements and the corresponding slab temperature.

It should be noted that the crack widths were measured near the center of the traffic lane. At first, three locations along the crack, near both ends and at the center of the traffic lane, were measured and were averaged to represent the width of the crack. But because there was no significant difference between the average of the crack widths measured at three locations and the crack width measured at the center, the crack width at the center location was therefore used.

The averages and standard deviations of the crack widths collected from the test sections are shown in Figures 3 through 6 for the four different steel reinforcement designs. The *T* marks on the columns in the figures represent the standard deviations of the crack widths. It is apparent that a difference in average crack width exists between the pavements with different types of coarse aggregate; sections with SRG showed greater crack widths than those with LS in all the cases except for the high steel sections placed on State Highway 6 in the summer (Figure 3), in which the order is opposite but the difference is negligible, considering the standard deviation.

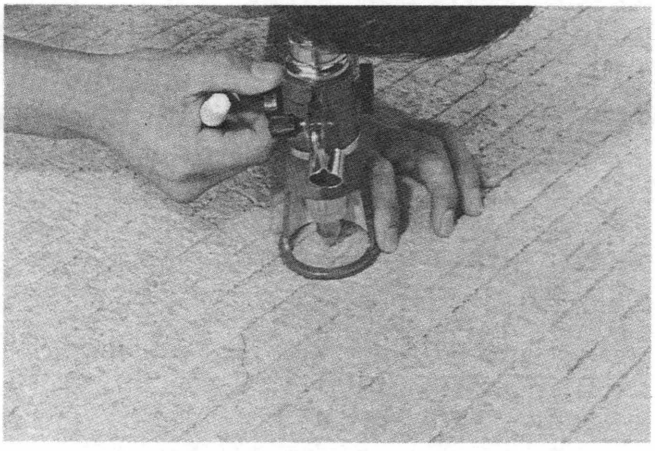

FIGURE 1 Crack width measurement with a measuring microscope.

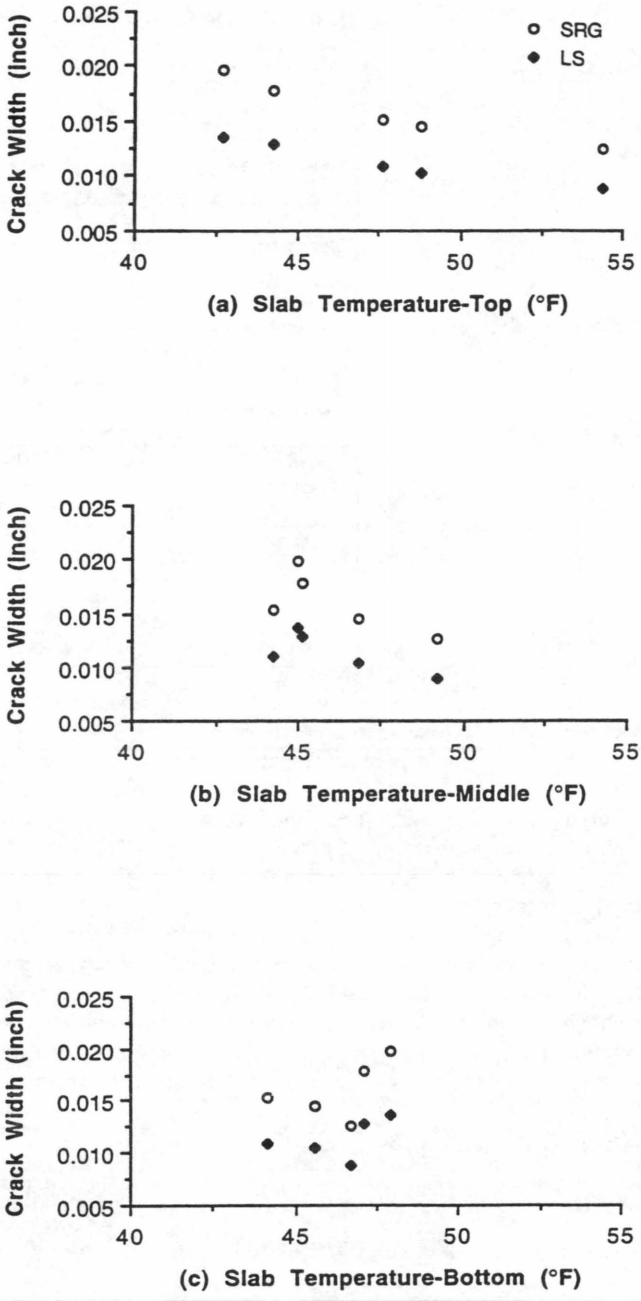

FIGURE 2 Correlation of slab temperature at various positions with corresponding crack width.

FACTORS AFFECTING CRACK WIDTH

Because the measurements of the crack widths were conducted at different conditions in terms of slab temperature and pavement age, it was difficult to extract additional information from Figures 3 through 6. To identify and evaluate the factors affecting the crack width, the crack width data were statistically analyzed by using the General Linear Model (GLM) procedure in the SAS.

The variables considered in that analysis included project (with two different seasons), coarse aggregate type, amount of longitudinal steel, time of crack occurrence, crack spacing, pavement age, and slab temperature. Some of the two-factor interactions were

TABLE 1 Time of Crack Width Measurements and Corresponding Slab Temperature

		TEST SECTION			
		SH6-summer	BW8-winter	SH6-winter	IH45-winter
1st Measurement	Date	6/28/89	12/20/89	2/1/90	1/31/90
	Time	6:12 AM	1:14 PM	10:42 AM	9:00 AM
	Slab temp.	73.3	54.4	65.8	58.2
2nd Measurement	Date	6/28/89	12/21/89	2/1/90	1/31/90
	Time	1:54 PM	6:50 AM	3:50 PM	11:30 AM
	Slab temp.	79.4	42.7	64.2	61.3
3rd Measurement	Date	6/29/89	12/21/89	2/13/90	1/31/90
	Time	1:28 PM	9:50 AM	12:00 NOON	3:05 PM
	Slab temp.	76.5	44.2	69.9	62.2
4th Measurement	Date	7/6/89	12/21/89	2/13/90	2/14/90
	Time	6:30 AM	12:50 PM	2:00 PM	4:30 PM
	Slab temp.	76.1	47.6	73.4	70.2
5th Measurement	Date	7/19/89	12/21/89	2/14/90	2/15/90
	Time	3:05 PM	2:00 PM	7:55 AM	8:57 AM
	Slab temp.	96.3	48.8	63.5	65.7
Construction Date	SRG sections	6/16/89	11/24/89	1/10-11/90	1/14/90
	LS sections	6/19/89	11/25/89	1/11-12/90	1/21/90

also investigated in the analysis. They include crack spacing-coarse aggregate type, amount of steel-coarse aggregate type, and slab temperature-coarse aggregate type.

In theory there is a nonlinear relationship between pavement age and crack width that is mainly a result of the nonlinearities of drying shrinkage and creep. However, because the range of pavement ages at the time of crack width measurements represented a relatively short time period (9 to 35 days after construction), a linear relationship was assumed.

The GLM analysis indicated that the significant factors affecting crack width at the 0.05 level included project, coarse aggregate type, amount of longitudinal steel, time of crack occurrence, pavement age, slab temperature, and the interaction between slab temperature and coarse aggregate type. (They were significant even at the significance level of 0.0001.) Crack spacing and the interactions of crack spacing-coarse aggregate type and amount of steel-coarse aggregate type were not significant at the 0.05 level. The R^2 value of the model was 0.82, indicating a good fit. The model can be expressed as:

$$CW = 34.1 + PROJ + CAT + STL + TCR + 0.15 \cdot AGE - 0.50 \cdot TEMP + TEMP \cdot CAT$$

where

CW = crack width in 0.001 in.;
PROJ = project and season of placement:
14.9 for SH6-summer,
1.5 for BW8-winter,
0.0 for SH6-winter, and
0.7 for IH45-winter;

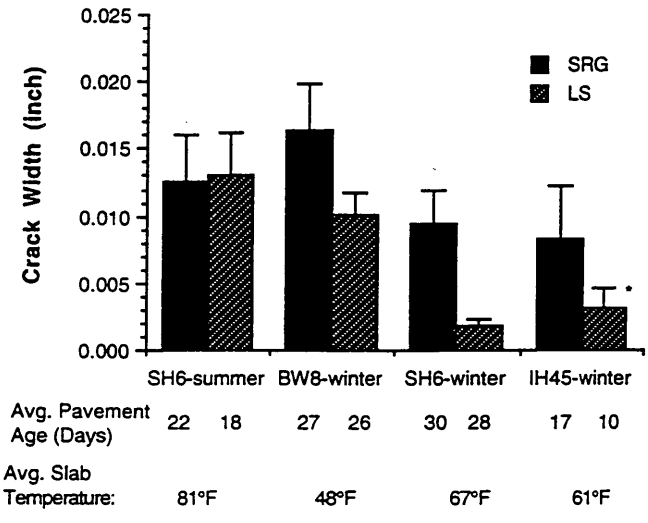

* 'T' marks on the columns represent the standard deviations.

FIGURE 3 Average crack width of each test section (high steel).

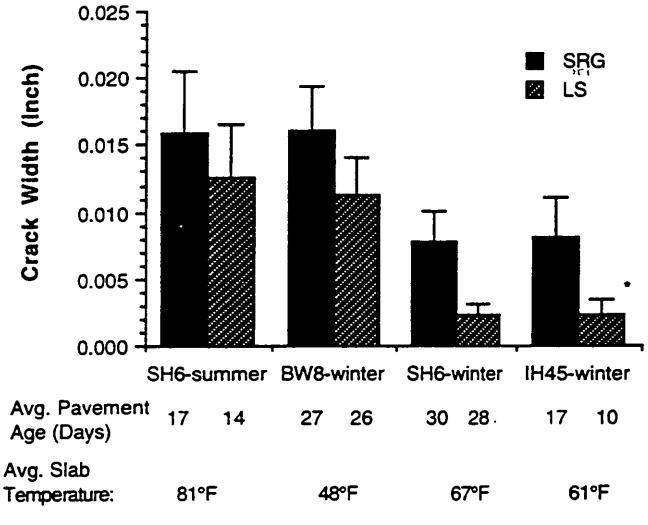

* 'T' marks on the columns represent the standard deviations.

FIGURE 4 Average crack width of each test section (medium steel).

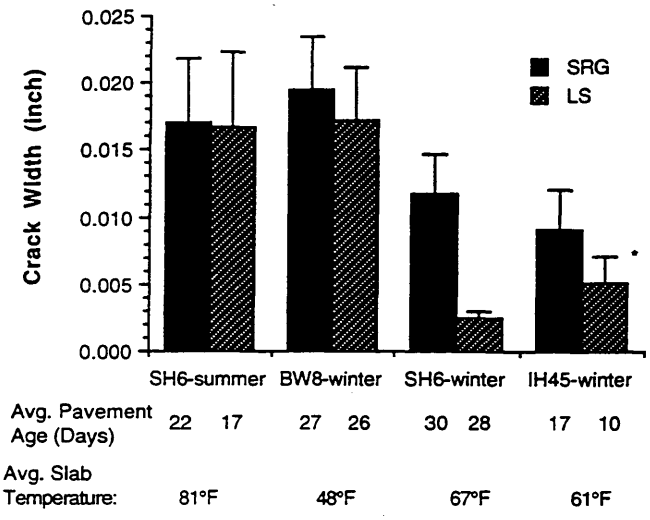

* 'T' marks on the columns represent the standard deviations.

FIGURE 5 Average crack width of each test section (low steel).

CAT = coarse aggregate type:
0.0 for SRG, and
−10.0 for LS;
STL = amount of longitudinal steel:
−0.3 for high steel with No. 6 bar,
0.0 for medium steel with No. 6 bar,
2.9 for low steel with No. 6 bar, and
0.4 for medium steel with No. 7 bar;
TCR = time of crack occurrence in terms of pavement age:
4.0 for 1 day,
3.3 for 2 days,
3.4 for 3 days, and
from −1.4 to 1.4 for 4 days or later (see Figure 10);

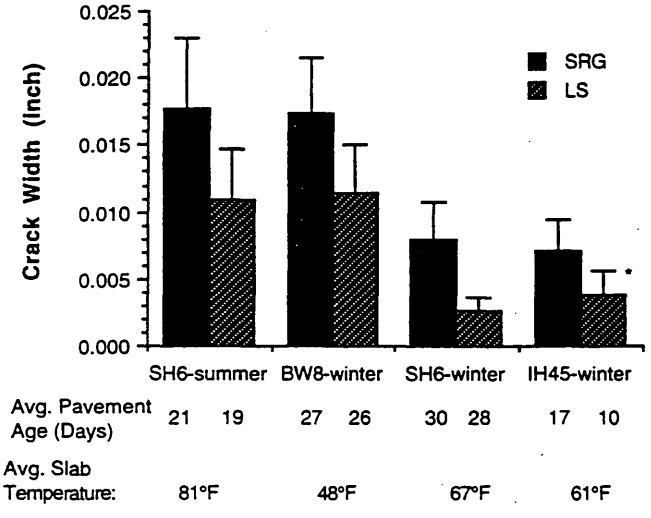

* 'T' marks on the columns represent the standard deviations.

FIGURE 6 Average crack width of each test section [medium steel with larger size (No. 7) bar].

AGE = age of the pavement at the time of crack width measurement (days) (note that the inference space of the pavement age is 9 to 35 days);
TEMP = slab temperature (°F); and
TEMP · CAT = interaction between slab temperature and coarse aggregate type:
0.0 for SRG, and
0.097 times slab temperature for LS.

It can be seen from this model that the placement season and coarse aggregate type were the two most significant factors affecting the crack width for a given age and temperature. Another important factor was the time of crack occurrence. Any of these three factors was more dominant than the amount of longitudinal steel. Therefore, more attention should be given to these three factors than to steel design in the control of crack width. Also, controlling these factors could prove less expensive than controlling the amount of steel.

The following sections discuss each factor considered in this analysis. It should be noted that, for the fair comparison of the levels in each factor, the levels of other factors (except the factor under discussion) were fixed.

Season of Year of Placement

Test sections were placed in two opposite seasons: summer and winter. The effect of placement season on the crack width when all other conditions are the same is shown in Figure 7. As can be seen summer placement (SH6-summer) resulted in much greater crack width than winter placement. This might be mainly because of the high curing temperature of the summer placement. Crack width is a function of temperature differential, which is the difference between the curing temperature and the temperature at the time of crack width measurement; the higher the temperature differential, the wider the crack. Consequently, the higher the curing temperature, the greater the crack width at a given temperature (*8*).

Coarse Aggregate Type and Slab Temperature

Because there exists an interaction between the factors of coarse aggregate type and slab temperature at the time of the measurements, the effect of coarse aggregate type should be interpreted along with the effect of slab temperature.

The effect of coarse aggregate type on the crack width is shown in Figure 8. The use of SRG resulted in wider cracks than the use of LS, and the difference was larger at lower temperatures (note the difference in the slopes in Figure 8). This difference may be caused by the higher thermal coefficient of SRG.

Steel Reinforcement

The effect of the amount of longitudinal steel on the crack width was statistically significant. In general, the greater the amount of longitudinal steel, the narrower the crack width (Figure 9). This effect occurs because the heavier steel holds the cracks more tightly, a result of the larger bond area between steel and concrete.

It was noted from Figure 9 that the difference in crack width between the high steel and the medium steel was much less than

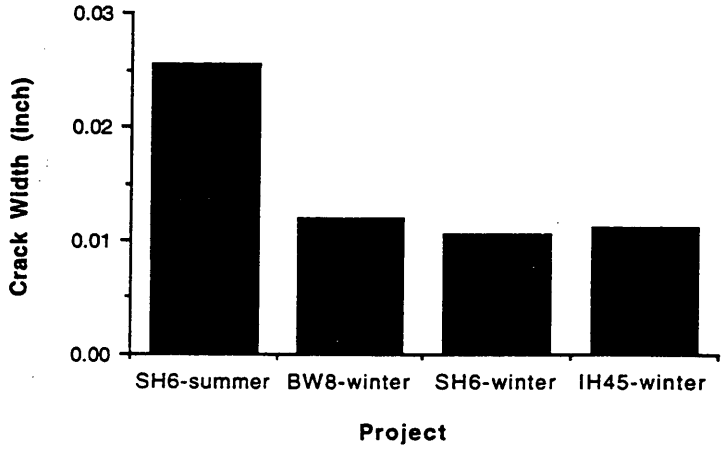

FIGURE 7 Effect of placement season on crack width.

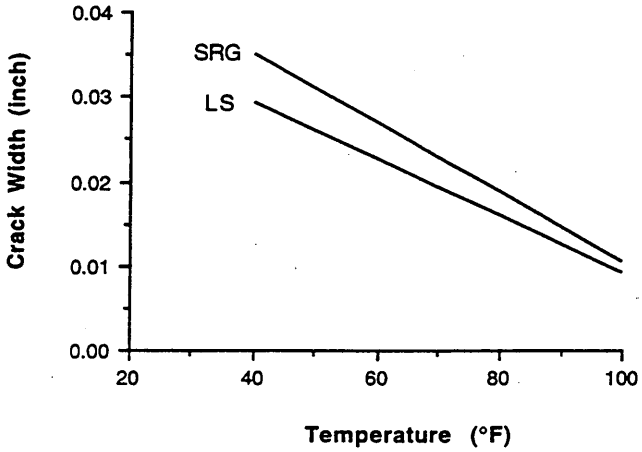

FIGURE 8 Effect of coarse aggregate type and slab temperature on crack width.

that between the low steel and the medium steel, even though the differences in the amount of steel were about the same.

The effect of the size of the steel bar on crack width is also shown in Figure 9. The use of a larger bar (one having the same total amount of steel) resulted in slightly greater crack width; the use of No. 7 bars (7/8 in. in diameter) instead of No. 6 bars (3/4 in. in diameter) resulted in a slightly wider crack. This might be because of the smaller total bond area between steel and concrete of the larger-size bar (crack width is minimized by the bond between steel and concrete). It should be noted, however, that the increase in crack width by use of No. 7 bars instead of No. 6 bars was very small.

Time of Crack Occurrence

One of the unique findings of the study was the effect of the time of crack occurrence on the crack width. The cracks that occurred during the first 3 days after construction were significantly wider than those that occurred later (Figure 10).

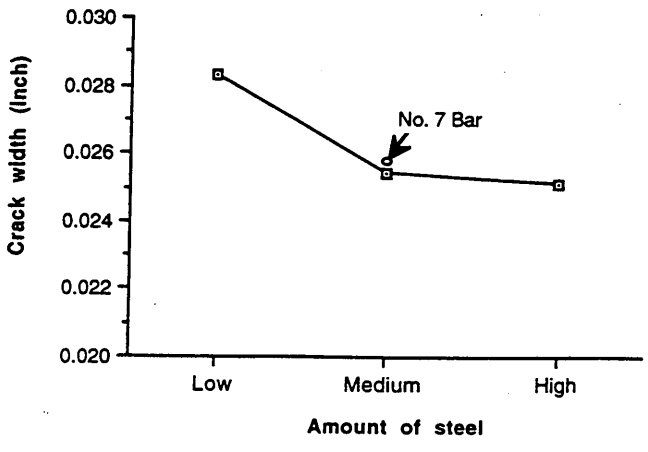

FIGURE 9 Effect of longitudinal steel design on crack width.

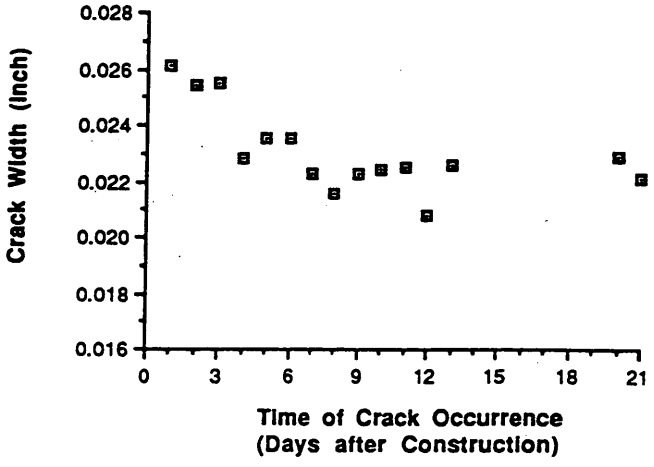

FIGURE 10 Effect of time of crack occurrence on crack width.

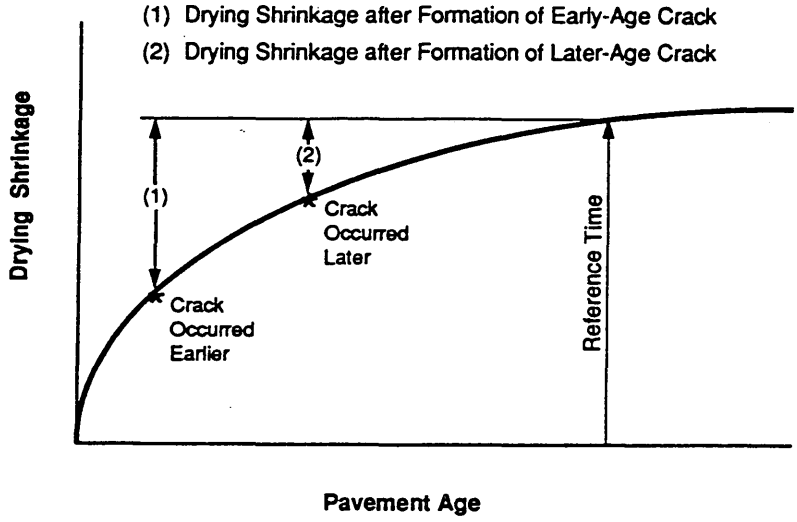

FIGURE 11 Conceptual explanation of wider crack width of early-age cracks by difference in residual shrinkage.

As mentioned previously, drying shrinkage serves to explain the greater crack width of early-age cracks. Once a crack occurs its width increases as a result of the drying shrinkage of the concrete (*3*). It is believed that the increase in crack width is a function of the residual shrinkage (drying shrinkage after formation of the crack), and an early-age crack will have higher residual shrinkage than a later-age crack (Figure 11), consequently resulting in greater crack width.

Crack Spacing

It is generally believed that the greater the crack spacing, the greater the crack width. But the effect of crack spacing (slab length between the adjacent two cracks) on crack width was not statistically significant at the significance level of 0.05. Shown in Figure 12 is the plot of the crack width versus the crack spacing, indicating no significant correlation between crack spacing and crack width. Each point on the graph has not standardized other variables (e.g., temperature). It should also be recognized that the process of selecting a specific crack to study had an impact on the observations. Previous studies have always found a correlation between the average crack width for a given temperature and the average crack spacing.

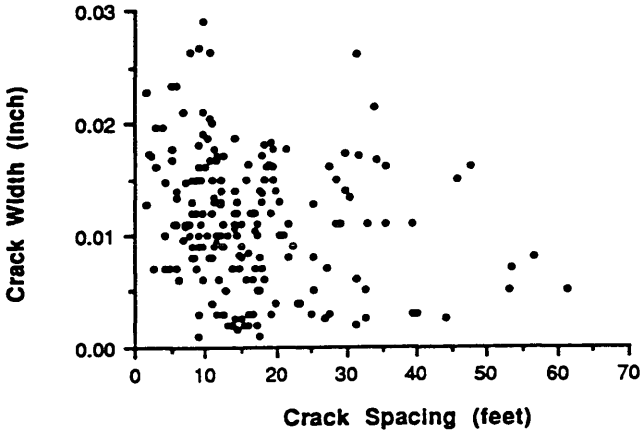

FIGURE 12 Relationship between crack spacing and crack width, showing no significant correlation.

SUMMARY OF FINDINGS

Various factors affecting crack width have been discussed on the basis of a statistical analysis conducted on the crack width data collected from the experimental test sections. Findings from the statistical analysis can be summarized as follows:

1. Hot weather placement resulted in much wider cracks than cool weather placement.
2. The use of SRG resulted in greater crack width than the use of LS, and the difference was larger at lower temperatures. This difference might be caused by the different thermal coefficients of the two coarse aggregate types used in the concretes.
3. The larger the amount of longitudinal steel, the narrower the crack width. However the difference in crack width between the high steel and the medium steel was less than that between the low steel and the medium steel.
4. Cracks occurring during the first 3 days of construction were significantly wider than those occurring later. Because early-age cracks are more prevalent with summer placement than with winter placement (*8*), special care should be taken during hot weather placement to reduce early-age cracks.
5. The effect of crack spacing on crack width was not significant owing to the nature of the data collection and analysis.
6. In the control of crack width, more attention should be given to the placement season, coarse aggregate type, and the time of crack occurrence (rather than to steel design). Controlling these factors could prove less expensive than controlling the amount of steel.

REFERENCES

1. Burke, J. E., and J. S. Dhamrait. A Twenty-Year Report on the Illinois Continuously Reinforced Concrete Pavements. In *Highway Research Record 239*, HRB, National Research Council, Washington, D.C., 1968.
2. *Guide for Design of Pavement Structures*, AASHTO, Washington, D.C., 1986.
3. Hughes, B. P., and T. Mahmood. An Investigation of Early Thermal Cracking in Concrete and the Recommendations in BS 8007. *The Structural Engineer*, Vol. 66, No. 4/16, Feb. 1988.
4. Russell, H. W., and J. D. Lindsay. Three-Year Performance Report on Experimental Continuously Reinforced Concrete Pavement in Illinois. *Highway Research Board Proceedings*, HRB, National Research Council, Washington, D.C., 1950.
5. Zollinger, D. G. *Investigation of Punchout Distress of Continuously Reinforced Concrete Pavement.* Ph.D. dissertation. University of Illinois, Urbana-Champaign, 1989.
6. *NCHRP Synthesis of Highway Practice 16: Continuously Reinforced Concrete Pavement.* HRB, National Research Council, Washington, D.C., 1973.
7. Lindsay, J. D. A Ten-Year Report on the Illinois Continuously Reinforced Pavement. *Bulletin 214*, HRB, National Research Council, Washington, D.C., 1959.
8. Suh, Y. C. *Early-Age Behavior of CRC Pavement and Calibration of the Failure Prediction Model in CRCP-7.* Ph.D. dissertation. The University of Texas, Austin, May 1991.
9. Anderson, V. L., and R. A. McLean. *Design of Experiments: A Realistic Approach.* Marcel Dekker, Inc., New York.

Publication of this paper sponsored by Committee on Rigid Pavement Design.

Mechanistic-Empirical Rigid Pavement Design for New York State

LUIS JULIAN BENDAÑA, DAN MCAULIFFE, AND WEI-SHIH YANG

In 1993 New York published a new *Thickness Design Manual for New and Reconstructed Pavements* based on the 1986 AASHTO design guide. The AASHTO equation for rigid pavement performance was calibrated with performance data for 225-mm rigid pavements in New York, and the calibrated equation was then used to design rigid pavements. Because New York does not have experience with thicknesses greater than 225 mm, the modified AASHTO equation could not be verified for thicker pavements. The development of a mechanistic-empirical (M-E) design procedure for verifying the designs presented in the new thickness manual is described. First, a nondimensional fatigue model was established on the basis of New York's past pavement performance, environmental conditions, and traffic loadings. The study was then extended to develop design curves for thicknesses of 225, 250, 275, 300, and 325 mm (5-m slab lengths for 225- to 275-mm thicknesses and 5.5-m slab lengths for 300- to 325-mm thicknesses). Finally, the M-E design curve was compared with the modified AASHTO equation. The results indicate that for thicknesses greater than 275 mm, AASHTO predicts up to 40 percent more equivalent single axle loads than the M-E approach.

In New York State an empirical procedure has been used since early in the 20th century to design highway pavements. It was formalized about two decades ago when it was incorporated into the state's *Highway Design Manual* (*1*). This procedure had evolved from New York's past experience, but was not based on pavement performance data from specific projects and was last revised in 1979. It provides a simplified pavement-thickness selection system based on highway classification, design hourly traffic, and two truck weight categories (heavy or light). It does not consider such other variables as reliability, drainage, soil and material properties, joint load transfer, or failure criteria. The cross section required in designing a rigid pavement carrying truck traffic is 225-mm portland cement concrete over a minimum 300-mm granular subbase course, independent of the number of load repetitions or the magnitude and configuration of the axle loads.

With the 1972 publication of the AASHO *Interim Guide for Design of Pavement Structures* (*2*), the New York State Department of Transportation (NYSDOT) recognized an opportunity to adopt a more rational rigid pavement design procedure. In-house evaluation of the 1972 guide was considered but was set aside without affecting the state's design procedure because of the lack of agreement with New York's experience. In 1986 AASHTO finally published its comprehensive *Guide for Design of Pavement Structures* (*3*). FHWA urged the states to review and adopt all or portions of it. In 1987 the Engineering Research and Development Bureau initiated Research Project 202 (Relating the AASHTO Guide to New York State Procedures) to evaluate the guide, anticipating that this could be a major undertaking. Then in 1989 FHWA issued a pavement policy mandating that each state develop a process for pavement design and type selection that was acceptable to FHWA. Although FHWA would recognize design procedures based on local experience, the AASHTO guide procedure was cited as an example that it would accept. In 1989 the NYSDOT Pavement Management Steering Committee recommended that appropriate portions of the 1986 guide be adopted as a framework for design selections.

In March 1992 the NYSDOT Technical Services Division organized a task force to prepare a departmental pavement design procedure for new and reconstructed pavements by January 1993 on the basis of the 1986 AASHTO guide. In their work the findings of Research Project 202 were to provide a basis for implementation. The AASHTO rigid pavement performance equation was calibrated with performance data for 225-mm New York rigid pavement, and the calibrated equation was then used to predict the number of load repetitions to failure in the state's *Thickness Design Manual for New and Reconstructed Pavements* (*4*). Because New York did not have actual performance data for thicknesses other than 225 mm, performance predicted with the modified AASHTO equation could not be verified for greater thicknesses. To verify that the manual was reasonable, an independent mechanistic-empirical (M-E) fatigue analysis was conducted, relating a nondimensional parameter (stress ratio σ_{cr}/M_r, where σ_{cr} is the critical stress under center slab loading near the free edge and a daytime gradient, and M_r is the concrete modulus of rupture) to load applications to failure. For New York this study and adoption of the new *Thickness Design Manual for New and Reconstructed Pavements* are the first steps in incorporating M-E structural analysis into future design procedures.

EMPIRICAL DESIGN PROCEDURES

Historically, the most important full-scale experimental design study in the United States was the AASHO Road Test in the 1950s at Ottawa, Ill. The 1986 AASHTO guide is based on in-service performance of the Road Test pavements and takes into account numerous design and behavioral factors under test loads, such as soil conditions, material properties, load transfer devices, and axle loading and configuration. The AASHTO approach is empirical and is based on the ability of the pavement to serve traffic over the design period—that is, its functional performance. This is measured by the present serviceability index (PSI), which is a numerical value ranging from 5 (representing the best possible pavement) to 0 (representing no pavement at all). Test data on pavement serviceability were obtained in the Road Test, and for each test section a serviceability-time history was plotted from the start of traffic operation until its PSI dropped to a minimum

Engineering Research and Development Bureau, New York State Department of Transportation, Albany, N.Y. 12232.

tolerance level—typically 2.5. A decrease in PSI over the serviceability-time history was then used to develop performance equations for flexible and rigid pavements.

In the AASHTO guide the performance equations were derived for dual-tire single and tandem axle trucks, with a maximum single axle load of 133.5 kN and maximum tandem axle load of 214 kN, for about 10 million 80-kN equivalent single axle loads (ESALs) under the environmental conditions prevailing only at the AASHO site. These equations thus were limited to conditions at Ottawa, Ill., and to those axle configurations and load ranges. As a result of trends in the trucking industry toward heavier gross vehicle weights, pavement problems related to multiple wheel loads have developed. Higher axle loads and varying axle spacings were not considered in the AASHO Road Test—thus, performance for heavier and different axle configurations must be extrapolated from the Road Test performance data outside the boundaries for which the equations were developed. Moreover, the trucking industry has adopted various axle spacings to meet the limitations of vehicle size and weight subsequently imposed by legislative action. These new configurations allow increased load-carrying capacity without violating the law, but they introduce complications in fatigue loading that were not considered in developing the AASHTO guide.

Obviously, problems arise when the functional method is used in predicting pavement performance without experimental data to support its use. To update the AASHTO guide to current conditions, various approaches have been suggested. One is to develop a test track similar to that at Ottawa in the 1950s to test current configurations (loads and numbers of adjacent axles). However, prototype pavement studies involving new axle load configurations would be time consuming and very costly. An alternative approach used nationally for more than 30 years has been reevaluation of AASHO Road Test data in conjunction with information obtained from state satellite tests. Finally, theoretical solutions have also been used; these are based on mechanistic parameters calibrated with pavement fatigue distress.

MECHANISTIC-EMPIRICAL DESIGN PROCEDURES

Pavements are very complicated structures, with performance depending on the interaction of such factors as climate, traffic conditions, support conditions, physical dimensions, and material properties. Developing a purely analytical prediction model thus is also extremely complex. To overcome this difficulty numerous simplifications must be made to predict long-term pavement performance. An M-E procedure is the solution most commonly used. M-E analysis and design methods evolved in the 1970s on the basis of known relationships between material behavior under stressed conditions (stress, strain, deflection) and the corresponding empirical performance of the pavement structure for all important combinations of loading and environmental conditions. The M-E approach is based on the hypothesis that pavement distress is related to states of strain or deflection. Performance models thus can be developed from theoretical computations of these pavement response parameters, calibrated with serviceability-time histories of pavement structures. The M-E approach uses the principles of engineering mechanics to calculate pavement responses and relate them to rates of deterioration. Then, Miner's hypothesis is used to sum the damage caused by traffic and environmental loading.

For rigid pavements two models are used to predict fatigue life: fatigue cracking and faulting. For the fatigue cracking model, the M-E procedure uses critical stresses at the bottom of the concrete slab to estimate total wheel load applications before cracks begin, propagate, and ultimately fracture the pavement. For the faulting model the performance evaluation relates faulting rate to a mechanistic parameter—maximum concrete bearing stress. Fatigue life is the number of stress repetitions, at a magnitude less than its strength, required for the pavement to fail structurally for a given failure criterion. In addition to fatigue cracking, faulting is also considered in determining fatigue life. This is considered because (as shown in NCHRP Project 1-26) faulting is a function of loadings and concrete bearing stress, and thus can be considered a mode of structural failure. New York's new design does not expect any failures because of faulting for the following reasons: (*a*) provisions to ensure a well-drained base (the stabilized base has been shown to provide drainage of 915 m/day), (*b*) sufficient load transfer devices, and (*c*) the added support of full-depth concrete shoulders and widened outer lanes.

NONDIMENSIONAL PERFORMANCE MODEL FOR NEW YORK STATE RIGID PAVEMENTS

The nondimensional performance model for New York State rigid pavements was developed by using pavement response to the combined effects of temperature and traffic loading, calibrated with actual pavement performance and 90 percent reliability. Miner's hypothesis was used to sum the damage caused by traffic and environmental loading. Pavement response (that is, critical stresses) was determined with actual physical dimensions, material properties, soil support, temperature gradients, and traffic from New York pavements.

Past Performance of New York Rigid Pavements

NYSDOT periodically collects pavement condition data for all sections of its highway network. These data consist of sufficiency ratings and dominant distress features that together are used to classify uniform highway sections. The rating scale is 1 to 10—1 for a pavement having a very high distress frequency and severity and 10 for a pavement with no distress. To compare the AASHTO design to New York's design, it was necessary to approximate the PSI by dividing the New York sufficiency rating by 2.

In the present study the actual fatigue life of rigid pavements in New York was assumed to be the number of cumulative 80-kN ESAL applications from the time that the pavement was opened to traffic to the time that it reached a sufficiency rating of 5. This was done by examining the state's *Highway Sufficiency Ratings* (*5*) to determine the cumulative 80-kN ESALs at a sufficiency rating of 5 or when the pavements were overlaid. The next step was to examine contract plans to determine when the pavements were placed and the details of their cross sections. The pavements considered had a 225-mm concrete layer on a 300-mm granular subbase. The failure criterion used in selecting these pavements was fatigue cracking; pavements that failed because of faulting or D-cracking were not included, both of these problems

having been previously considered in New York and the suggested solutions implemented.

Next, pavement condition surveys were examined to determine the sufficiency rating at the time of overlay for each pavement that had been overlaid before reaching a sufficiency rating of 5. The surveys showed that about 60 percent of the pavements were overlaid at a sufficiency rating of 6. The next step was to calculate the additional traffic that the pavement would have carried to reduce the sufficiency rating from 6 to 5. This additional traffic was estimated for the average time that a rigid pavement took to go from a condition rating of 6 to one of 5. It was found that an average of 3 years or about 3 million ESALs are required to produce a drop of 1 in the sufficiency rating. The additional time and traffic were then added to each of the performance curves. Because all the data were for pavements with similar cross sections and the number of load applications to failure ranged from 21 million to 54 million ESALs, a representative fatigue life had to be chosen.

In the present study reliability was defined as the probability that the service rating would remain above 5 during the design life. It was decided that the number of load applications to failure would be based on a 90 percent design reliability. The first attempt to determine this life was to try to fit the data to a normal distribution, but it was found that the normal distribution did not fit well, and a distribution-free confidence interval for percentiles (*6*) was used instead. By this method it was found that 24.4 million ESALs was the fatigue life giving the desired reliability. In Figure 1 the actual number of ESALs on rigid pavements in New York is shown and their performance is compared with 90 percent reliability to the AASHTO rigid pavement prediction equation with 50 and 90 percent reliability. It also shows that the AASHTO prediction equation with 50 percent reliability correlates well with performance at 90 percent reliability.

Pavement Response

The Illi-Con program (*7*) was used to analyze the combined effects of temperature (curling stresses) and traffic loading. This is a data base program based on output from the Illi-Slab finite-element program (*8*). Critical stresses found by using Illi-Con were checked with those from Illi-Slab to ensure equivalence. The comparison showed that they were about equal (within ±4 percent), which confirmed that Illi-Con was adequate to calculate the stresses resulting from thermal and traffic loads for various slab thicknesses. Illi-Con was used instead of Illi-Slab because of its ease of data input and the speed with which it generated results. Input parameters to determine critical stresses in New York rigid pavements were physical properties, temperature gradients, and traffic.

Physical Properties

The previous New York State pavement design consisted of a single cross section for interstate pavements with the following design values: dowel bars were solid 28-mm-diameter steel bars with a modulus of elasticity of 200 GPa and spacing beginning 150 mm from the pavement edge and then every 300 mm on center across the transverse joint. The rigid pavement had a modulus of elasticity of 25 GPa, a thickness of 225 mm, a coefficient of thermal expansion of 1.0×10^{-5} (1/°C), a lane width of 3.6 m, and 3-m-wide asphalt shoulders.

Because of its high modulus and rigidity, rigid pavement behaves as a rigid body—that is, a wheel load is distributed over a relatively large area of soil. Rigid pavement flexural capacity is provided primarily by flexural strength of the concrete—its modulus of rupture (M_r). In New York concrete modulus of rupture has been estimated on the basis of the results of split-cylinder tensile testing on two experimental projects—in 1965 on Route 23 between Catskill and Cairo and in 1975 on I-88 near Otego (*9*). Testing on core centers was performed in accord with AASHTO Method T-198, and M_r was estimated by using Hammit's equation (*10*). The results indicated that the mean M_r is 5.2 MPa, with a standard deviation of 572 kPa and a 90 percent lower confidence limit of 4.25 MPa. Also, the NYSDOT Materials Bureau tested concrete beams for 28-day flexural strength and found that it was approximately equal to 15 percent of concrete compressive strength. For the present study M_r was estimated by using a factor of 15 percent of the compressive strength. For Class C concrete with a compressive strength of 27.58 MPa, a value of 4.14 MPa was used for M_r.

Temperature Gradients

Thermal gradients between the top and bottom on a rigid pavement slab are the cause of slab curling and also determine the direction and size of this curling. When temperatures at the top and bottom of a slab are equal, it is flat (level). A positive gradient (the top warmer than the bottom) causes the free edge to curl downward, and a negative gradient (the top cooler than the bottom) will cause an upward curl. The greater these gradients, the more the slabs curl. Large stresses are created when downward curl is restrained by the weight of the slab itself. As observed by the Department of Civil Engineering of the University of Illinois at Urbana-Champaign (*7*):

> Because the warping stresses occur early in the concrete aging cycle, and the stresses are long term, it follows that much of the warping stress is relieved by concrete creep. Thus the residual stress due to warping is highly speculative

For this reason warping stresses were not included in this study.

New York has been collecting temperature gradients on two roads (I-87 and Route 29) as part of Research Project 188 (Effect of Overlays on Faulted Concrete Pavements) (*11*). Temperatures were gathered to determine how a bituminous overlay affects stresses within an overlaid concrete slab (the test section) in comparison with the stresses and pressures within a concrete slab without an overlay (the control section). Data collected for the control section are discussed here. Temperatures were collected for about 2 years for periods of 2 to 4 days each month. Ambient (air) temperatures were also recorded by thermocouples situated on two 0.8-m wooden stakes and covered with small wooden squares to prevent exposure to direct sunlight.

Information from analyses of these data included temperature variations for various depths within the slab, temperature differences between various depths, and temperature differentials (gra-

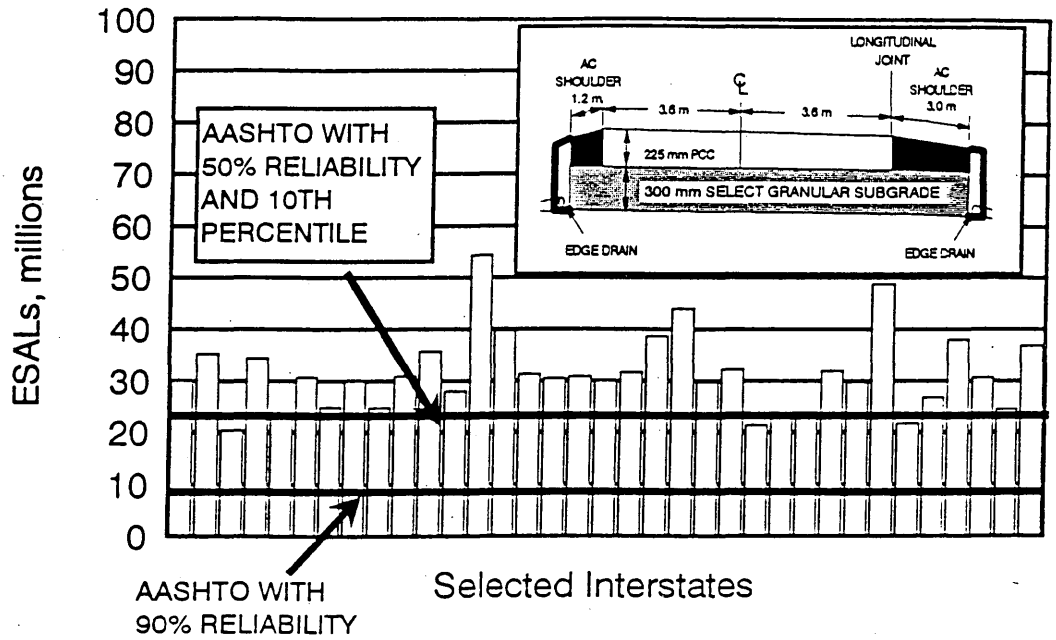

FIGURE 1 ESALs to failure (inset shows former cross-section).

dients) through the slabs. Thermal gradients were computed by subtracting the temperature reading at a 200-mm depth from that at the slab surface.

Shown in Figure 2 are typical seasonal variations of thermal gradients over a 24-hr period, indicating that positive gradients occur during daylight hours and negative gradients occur at night. Frequency of various gradients over an entire year are shown in Figure 3. That study (*11*) indicated that the greatest variation in thermal gradient occurs during hot months, when the daily air temperature also varies the most. It showed that the greatest thermal gradients also occurred during the summer months. For the combined effects of temperature and loading, the critical condition occurred with a daytime temperature gradient and design truck loading.

Critical tensile stresses were then taken from the output of the Illi-Con program (*7*) and analyzed. Input files for the program were also created for critical loading and temperature conditions. Other analyses were performed to determine which variables directly affected the critical stress. All analyses showed that daytime gradient was a determining factor for maximum tensile stress. This was expected, because the nighttime gradient would produce compressive stresses opposing the tensile stresses produced by the load.

Traffic

Vehicle weight and traffic profile information is necessary to calibrate the fatigue model accurately. To determine hourly traffic

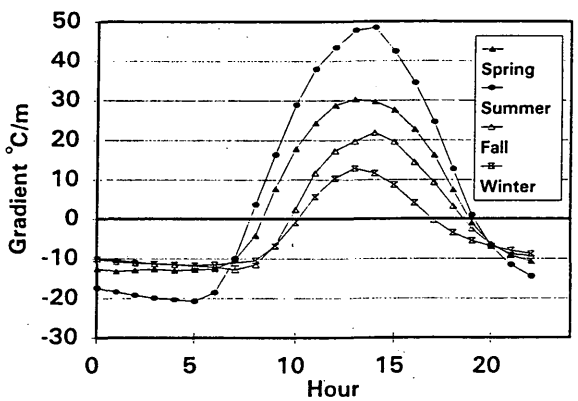

FIGURE 2 Thermal gradient versus time of day.

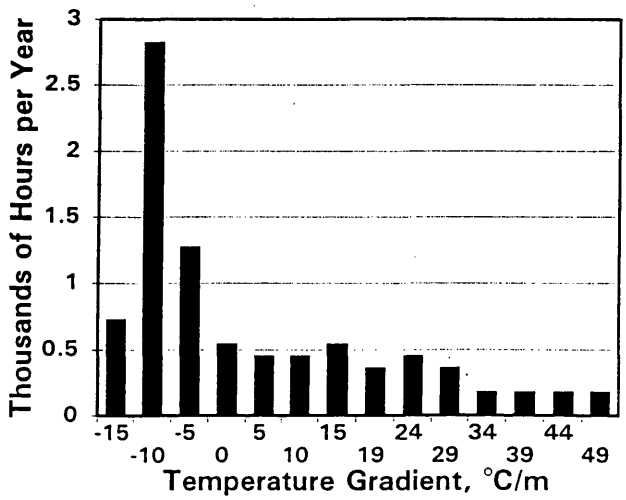

FIGURE 3 Frequency versus gradient.

profile, the percentage of truck traffic must be determined throughout the day. The values presented in Figure 4 are taken from *New York State Truck Weight and Vehicle Classification Reports* (*12*), converting the number of trucks each hour on a typical Interstate to the total percentage of trucks. The next step was to select what design trucks and axle loadings produced the greatest cumulative damage—that is, the highest combination of weights and load repetitions. It was found that the most numerous and heaviest trucks were 3S-2 tractor semitrailers (five-axle trucks). This was chosen as the design truck, whose loads would be converted to ESALs as a basis for traffic predictions. Figure 4 is a profile of the hourly percentage of traffic on a typical day for five-axle trucks. This profile was necessary because damage caused by a truck depends on both its weight and the thermal gradient at which the load is applied. These factors are combined later in this paper. The traffic data analyzed to determine the profile and weight measurements were based on more than 25,000 heavy vehicles.

It was necessary to develop a representative method to convert from load applications to ESALs for two reasons: (a) traffic predictions generally are given in ESALs, and (b) the fatigue model used is based on load applications, not ESALs. One pass of the design truck consists of a single 35-kN axle and two 160-kN tandem axles (a five-axle truck with 355-kN gross vehicle weight). Next, load equivalency factors (LEFs) were determined by using the tables provided in the 1986 AASHTO guide. LEFs were used only for the comparison of traffic between the M-E model and the AASHTO model. In addition, ESALs were the only available measure of performance for existing sections and had to be converted to design truck loading for the M-E model. In that model traffic was accounted for by the number of passes of the design truck, not ESALs. The design truck was found to account for 80 percent of all traffic, and only 5 percent of the trucks were heavier (most of those were trucks with more than five axles). After the LEFs were found, the total number of ESALs for the design truck was determined by multiplying the LEF for each axle load by the percentage of time that axle would cross a given point; that is, 33.3 percent for a single 35-kN axle and 66.7 percent for a 160-kN tandem axle (Table 1). The number of ESALs per truck for the design truck was found to be 4.86. This was used to convert the number of passes of the design truck with a total fatigue of 1 to ESALs.

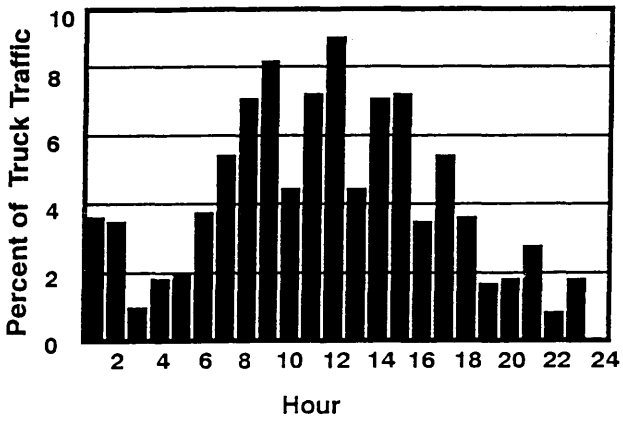

FIGURE 4 Hourly five-axle truck traffic on typical day.

TABLE 1 ESALs per truck and anticipated load applications

Total Axles	Load/Axle, kN	Mixed Traffic	LEF	ESALs/Truck
1 (Single)	35.0	33.33	0.032	0.032
2 (Tandem)	160.0	66.67	2.430	4.860
			=	4.892

Model Formulation

Various fatigue models were examined to determine if they could match actual New York rigid pavement performance; that is, for a 225-mm concrete slab with 300-mm granular base, asphalt shoulders, and traffic, material properties, and environmental conditions representative of New York pavements, the model would have to predict about 24.4 million ESALs. No model that produced results comparable to actual performance was found. Those examined were by Liddle, Vesic, and Hudson and Scrivener, discussed by Treybig et al. (*13*), and by Darter (*14*). Finally, a model was selected and calibrated to match the actual data—that is, the fatigue curve had the same shape but a different location. The model chosen was that developed by Hudson and Scrivener (*13*), because it was the only one that could be calibrated to fit New York's performance. To further improve the M-E procedure, New York has planned projects to establish data requirements, collect the appropriate pavement performance data for new pavements, improve or develop better fatigue models, and integrate the new data and models into its performance model (*15*).

Determination of Anticipated Total Axle Load Applications

The 24.4 million ESALs for the standard cross-section were converted to the total applications of the design truck and to the total number of 160-kN tandem axle applications, as shown in Table 2. Then, the anticipated load applications at each gradient were determined by finding the product of the percentage of traffic occurring at a given gradient and the total 160-kN tandem axle applications.

Determination of Total Permissible Axle Load Applications

Critical stress and stress ratios (σ_{cr}/M_r) were computed for each load-gradient combination. These ratios were used to determine the permissible (noncalibrated) load applications by using the Hudson and Scrivener model (*13*). The anticipated load applications at each load-gradient combination were divided by the noncalibrated permissible load applications. A curve of stress ratios (σ_{cr}/M_r) versus noncalibrated permissible load applications was plotted, and total damage was computed by using Miner's hypothesis. The nondimensional curve was then translated until the total accumulated damage was equal to 1. At this point the calibrated Hudson and Scrivener model became the New York rigid pavement model. The end product was Figure 5—a nondimensional curve for rigid pavement design in New York. Figure 5 was developed by plotting the number of permissible load applications against the stress ratios (σ_{cr}/M_r).

TABLE 2 Calibrated fatigue analysis (24.4 million ESALs/4.96 million 160-kN tandem axle loads) for 225-mm pavement thickness

Temperature Gradient, deg C/m	% Traffic At Gradient	Anticipated Total Applications	Critical Stress, kPa	Stress Ratio, σ_{cr}/M_r	Permissible Load Applications	Damage
0	10.31	510,872	1627	0.39	21,455,099	0.02
10	5.00	247,755	2089	0.51	7,252,832	0.03
15	7.13	353,299	2303	0.56	4,752,356	0.07
19	6.41	317,622	2496	0.60	3,350,992	0.09
24	6.23	308,703	2682	0.65	2,452,378	0.13
29	5.95	294,829	2854	0.69	1,871,488	0.16
34	2.76	136,761	3006	0.73	1,494,849	0.09
39	2.08	102,947	3158	0.76	1,207,292	0.09
44	3.22	159,760	3289	0.80	1,012,043	0.16
49	2.76	136,693	3413	0.83	861,752	0.16
					Total	1.00

Note: M_r = 4137 kPa.

DEVELOPMENT OF DESIGN CURVES

The nondimensional curve (Figure 5) was used as a fatigue model to predict probable fatigue lives for the pavement cross sections, slab lengths, shoulders, and materials properties used in the *Thickness Design Manual for New and Constructed Pavements* (*4*). First, the stress ratio was computed for each load-gradient combination. Second, the anticipated load applications were calculated. Damage at each gradient was then determined by dividing the anticipated applications by the allowable applications. Finally, total damage was computed by summing the damage at each gradient. To determine ESALs to failure, an arbitrary ESAL total was selected, and the damage owing to this total was then calculated. If this sum differed from 1.0, then total ESALs were divided by total damage, resulting in the ESALs to failure for the given pavement thicknesses. Predicted performance by both the M-E model and the manual (*4*) is indicated in Table 3. The design curve used in the manual (*4*) and that developed by using the M-E model is shown in Figure 6. This graph suggests that the *Thickness Design Manual* is more conservative for thicknesses of less than 275 mm and is less conservative for greater thicknesses.

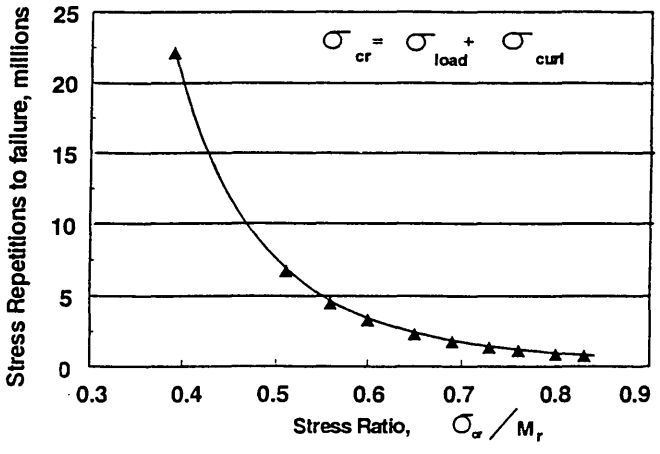

FIGURE 5 Stress repetitions versus stress ratio.

CONCLUSIONS

1. The study described in this paper has demonstrated that it is feasible and practical to develop M-E pavement design procedures, even with limited performance data, as in New York.
2. A nondimensional performance model was developed by using pavement response to the combined effects of temperature and traffic loading, and reliability was calibrated with actual life. For this paper New York's actual environmental data, materials properties, and traffic data were used to develop this nondimensional performance model.
3. Nondimensional models and M-E design procedures can be developed and adopted by other states and agencies, provided that the necessary data are available. These concepts in developing new pavement design procedures, however, are more broadly based (use of mechanistic parameters allows application of the M-E model to any pavement thickness in which the critical stresses are within the range of those used in calibrating the model) than the traditional empirical approach, which is based on full-scale road tests.
4. The pavement community is moving toward M-E design procedures, and state agencies cannot wait 30 or more years to collect new data to develop those procedures. The present study provides a step toward a true M-E process that will be recalibrated when more data become available.
5. The M-E and AASHTO models (after both were calibrated with the same performance data) predicted different performances for identical input values. In the present study the M-E model predicts more ESALs than AASHTO for pavement thicknesses under 275 mm and fewer ESALs for thicker pavements.

TABLE 3 Design results

Pavement Thickness, mm	ESALs to Failure, millions	
	M-E Analysis	Thickness Design Manual
225	91.5	50
250	126.0	90
275	172.0	165
300	216.0	290

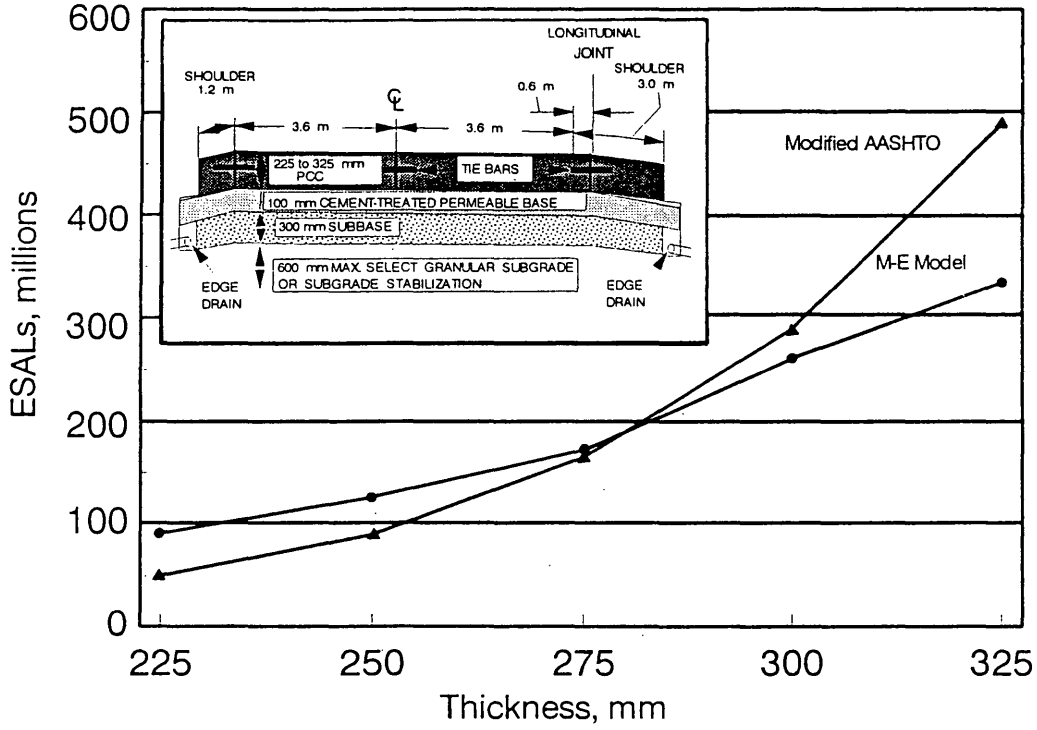

FIGURE 6 Traffic related to rigid pavement thickness (inset shows current cross-section).

REFERENCES

1. Pavement Selection Guide, Table 4–1. In *Highway Design Manual.* Facilities Design Division, New York State Department of Transportation, June 1979.
2. *Interim Guide for Design of Pavement Structures.* AASHO, Washington, D.C., 1972.
3. *Guide for Design of Pavement Structures.* AASHTO, Washington, D.C., 1986.
4. *The New York State Thickness Design Manual for New and Reconstructed Pavements.* Technical Services Division, New York State Department of Transportation, Sept. 1993.
5. *Highway Sufficiency Ratings.* Data Services Bureau, Planning Division, New York State Department of Transportation, published periodically.
6. Hahn, G. J., and W. Q. Meeker. *Statistical Intervals: A Guide for Practitioners.* John Wiley & Sons, 1991.
7. Calibrated Mechanistic Structural Analysis Procedures for Pavements: Phase 2, Vol. 1. Final Report on National Cooperative Highway Research Program Project 1-26. Construction Technology Laboratories, University of Illinois at Urbana-Champaign, Dec. 1992. Unpublished.
8. Tabatabaie, A. M., E. J. Barenberg, and R. E. Smith. Analysis of Load Transfer Systems for Concrete Pavements. In *Longitudinal Joint Systems for Slip-Formed Rigid Pavements*, Vol. II. Report RAA-RD-79-4, II. University of Illinois, Urbana-Champaign, 1979.
9. Smith, K. D., H. T. Yu, E. Owasu-Antwi, D. G. Peshkin, M. I. Darter, and R. Ahmad. *Performance Evaluation of Rigid Pavements—Data Collection and Analysis: Interim Report.* FHWA Contract DTGH61-91-C-00053. ERES Consultants, Savoy, Ill., April 1993.
10. Hammit, G. M., II. Concrete Strength Relationships. Miscellaneous Paper. Waterways Experiment Station, U.S. Army Corps of Engineers, 1974.
11. Morgan, R. L., H. J. Chen, I. Chengalur-Smith, and D. E. McAuliffe. *Overlays on Faulted Concrete Pavements.* Final Report on Research Project 188, in preparation.
12. *New York State Truck Weight and Vehicle Classification Reports.* Data Services Bureau, Planning Division, New York State Department of Transportation, published periodically.
13. Treybig, H. J., B. F. McCullough, P. Smith, and H. VonQuintus. Development of New Design Criteria. In *Overlay Design and Reflection Cracking Analysis for Rigid Pavements*, Vol. I. Report FHWA-RD-77-66. Austin Research Engineers, Inc., Austin, Tex., Aug. 1977.
14. Darter, M. I. Development of Design Procedures. In *Design of Zero-Maintenance Plain Jointed Concrete Pavement*, Vol. 1. Report FHWA-RD-77-111. Department of Civil Engineering, University of Illinois, Urbana-Champaign, June 8, 1977.
15. *Pavement Management Systems Plan Update.* Pavement Management Unit, Office of Operations, New York State Department of Transportation, July 1992.

Publication of this paper sponsored by Committee on Rigid Pavement Design.

Influence Function Approach to Analysis of Jointed Portland Cement Concrete Pavement

C. R. BYRUM AND W. HANSEN

A technique for analyzing the interactions between typical highway loads and jointed rigid pavements by using influence functions is presented. Influence functions are generated by using a modified version of the ILLI-SLAB finite-element model. These influence functions can be used to estimate the minimum and maximum responses caused by moving wheel loads for any point of interest on the slab. A parametric study of the model is presented showing the effects of various key input parameters on the influence functions and stress distributions in the slab. A field model validation case study is presented for M-14, a 229-mm pavement built in Michigan in 1965. Traffic distributions were broken down into equivalent single axle loads per hour. Temperature and moisture gradient effects were estimated for a typical day. These factors were then reduced to obtain the daily fatigue loss. The results of the study indicate that the upward curled or nighttime temperature condition is prevalent and most severe. This results in the peak tensile stresses being located in the top of the slab. Results from the study compare well with field distress surveys for the test pavement.

Recently there has been a large push to develop more mechanistic approaches for pavement analysis and design that are based primarily on sound engineering principles. Most design methods in use are largely empirical and are often based on small data bases. Many question their accuracies and validities. An accurate mechanistic determination of the stresses and strains in a pavement caused by moving vehicle loads is complicated. The problem falls into the broad study of soil-structure interaction problems.

The problem begins immediately after the slab is placed. This is typically done with slip-form paving machines, which require the use of concrete that is fairly workable and has resulting high levels of shrinkage. The concrete begins to undergo drying shrinkage during curing. It does not shrink uniformly, however. The top of the slab, which is exposed to air, typically shrinks more and faster than the bottom. This results in a curled or warped upward condition (Figure 1). The top of the slab will be in tension because of the self-weight of the lifted corners. The pavement will immediately begin to go through daily and annual cycles of moisture and temperature gradients and subgrade strength fluctuations. As the top surface of the slab expands or contracts relative to the bottom, curling results. Friction forces develop along the bottom of the slab because of foundation restraint as the slab undergoes changes in length because of temperature fluctuation. When the slab contracts, tensile stress develops because of the friction. When it expands compression results. Contraction joints are used to minimize the stresses resulting from these phenomena and to control cracking. The contraction joints are typically saw cut to one-third of the pavement thickness as soon as possible after the slab is placed. A joint sealant is then used to prevent water from infiltrating the cracks. The joints are typically doweled by using 25.4- to 38.1-mm steel dowel bars. Coatings are used on the dowels to prevent corrosion and to debond them from the concrete such that expansion and contraction is allowed to occur while wheel loads are transferred from slab to slab. In dry, nonfreezing environments, joints without dowels are often used. They rely on aggregate interlock for load transfer. Cracks that form between planned joints also use this mechanism. These discontinuities cause the stresses in the slab to increase near the joint because of the larger deflections and curvatures in the slab when the load is on or near the joint. The consequences of curling and warping are residual stresses present in the pavement before loading. It can be shown that these stresses are significant and that they must be included in any rationally based mechanistic design procedure. Current empirically based methods typically ignore these aspects.

Traffic is the next part of the problem. The only vehicles of concern are the large trucks because of their large axle loads. Although passenger cars make up most of the traffic volume, they induce very little stress in the pavement. Another concern is the time of day that the trucks are traveling. This is a highly variable site-specific parameter.

Axle spacing, allowable static wheel loads, and tire configurations vary from vehicle to vehicle and also geographically. As the pavement ages and becomes more rough the static axle loads get magnified to a greater extent as the vehicle travels over the surface irregularities, inducing higher stresses. They are velocity, suspension, tire, and road profile dependent.

When all of the coupled effects previously mentioned are reviewed and the variables counted, it is easy to understand the complexity of the problem of estimating the state of stress for different points on the pavement. Presented in this paper is a method for estimating the stress distributions in jointed rigid pavements. This is accomplished by generating influence functions (Figure 2) by using a modified version of the ILLI-SLAB finite-element computer model. Because an influence function represents a continuous response of any point of interest versus load position, it is a powerful tool for determining the location of the load relative to the point of interest that causes the maximum response, even in the presence of residual stresses.

MODIFIED ILLI-SLAB

One of the most promising mechanistic tools currently being developed is the finite-element method (FEM). The computer pro-

C. R. Byrum, Michigan Department of Transportation, Lansing, Mich. 48909. W. Hansen, Department of Civil and Environmental Engineering, University of Michigan, Ann Arbor, Mich. 48109.

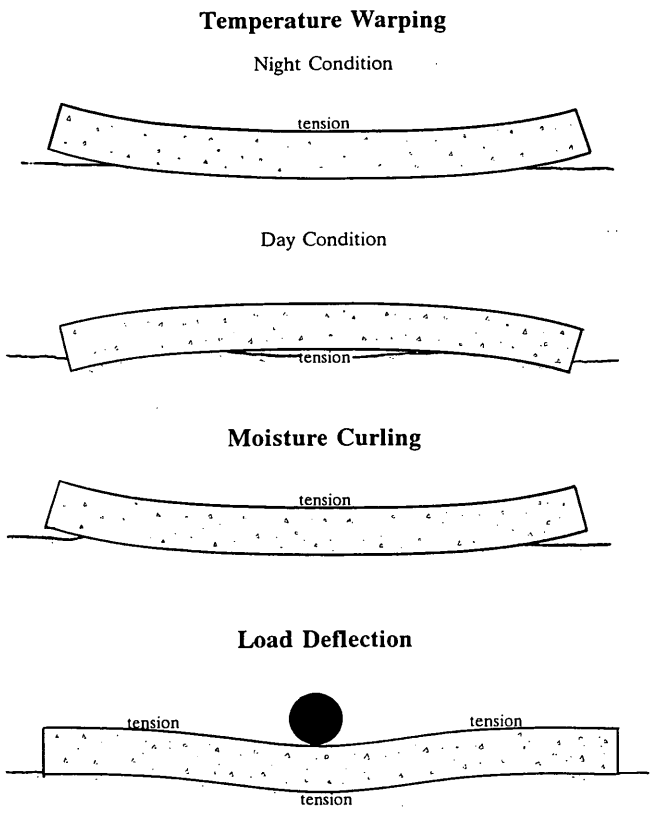

FIGURE 1 Temperature-, moisture-, and load-related curvatures.

gram ILLI-SLAB is an FEM model based on linear elasticity. It was developed at the University of Illinois for analyzing load transfer systems for jointed rigid pavements (*1*). FEM attempts to model the nonlinear response by dividing the problem into small interconnected elements that respond linearly. It uses what is referred to as plate elements to model the concrete slabs in bending. The slabs are connected by beam elements that transmit shear and moment for the doweled joints or spring elements that transmit shear only for the aggregate interlock joints. It can estimate the bending stresses caused by loads in the vertical direction and temperature gradients. A number of subgrade models are available.

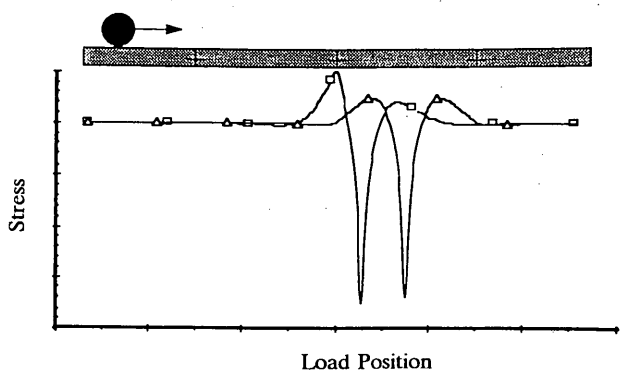

FIGURE 2 Typical shapes for pavement influence functions.

This study focuses on the region from the central joint to the center of a slab along the wheelpath.

In a previous study on the effects of heavy vehicle characteristics on pavement response and performance (*2*) the ILLI-SLAB program was modified to generate influence functions. Influence functions are a way of showing the response (stress, strain, or deflection) at a point of interest versus load position as the load approaches and passes over the point. Shown in Figure 2 are influence functions for stress at the bottom of the slab along the wheelpath caused by a 40-kN wheel load passing over points in the center and near a joint of a 7.62-m-long by 3.65-m-wide, doweled, 229-mm-thick slab with no temperature gradient. In this study only the stress along the wheelpath is examined. The wheelpath is defined as 838 mm from the edge of the pavement for a 3.65-m lane. As the tire approaches the point of interest there is a point at which the deflection basin (Figure 1) caused by the load begins to influence the stresses. Initially the bottom of the slab goes into compression and the top goes into tension. This corresponds to the initial curved downward portion of the deflection basin. The point of maximum compressive stress shown in Figure 2 would correspond to the point of maximum downward curvature in the deflection basin shown in Figure 1. Then as the tire moves on top of the point of interest the slab is curved upward and the bottom of the slab is in tension. As the tire moves away from the point of interest the bottom of the slab once again undergoes compression and then goes back to zero stress as shown or to its residual stress level if temperature or moisture gradients exist. There are two compression peaks and one tension peak at the bottom of the slab per passing wheel. The stress condition at the top of the slab is always assumed to be of equal magnitude but opposite sign compared with that at the bottom of the slab.

In a previous study by Nasim et al. (*3*) instrumented slabs were used to compare strain histories predicted by the modified ILLI-SLAB with strain gauge response. The curved upward response, or tension on the bottom of the slab, showed a very good correlation. For the curved downward response, or tension on the top of the slab, the correlation was adequate but not as good. This may be because of hairline cracks from shrinkage that appear on the top of the slab (*4*) affecting the bending response. When the slab goes into downward curvature (tension on top) these cracks would open up, affecting the neutral axis in bending. The cracks would close during curved upward bending and the slab would behave more as it is modeled, with the neutral axis at midslab.

In a modified ILLI-SLAB run the wheel load is moved across the pavement model at 76.2-mm intervals so that its center rests on a nodal point of the mesh. The response for each node along the wheelpath is recorded for each load position. The result is that influence functions can be generated for points at intervals of every 76.2 mm along the pavement by plotting load position versus response at a given node. Notice that in Figure 2 the maximum tensile and compressive stresses are shown to be higher for a point near the transverse joint. This is because of the higher curvature and deflections caused by the load in the presence of the discontinuity or joint.

When the minimum and maximum stresses from each influence function are plotted versus distance from the transverse joint, it is observed that at some distance away from the joint the stresses reach a maximum. The stresses drop to a stable value as the load moves away from the joint and toward the middle of the slab, where the stresses are no longer affected by the discontinuity (Figure 3).

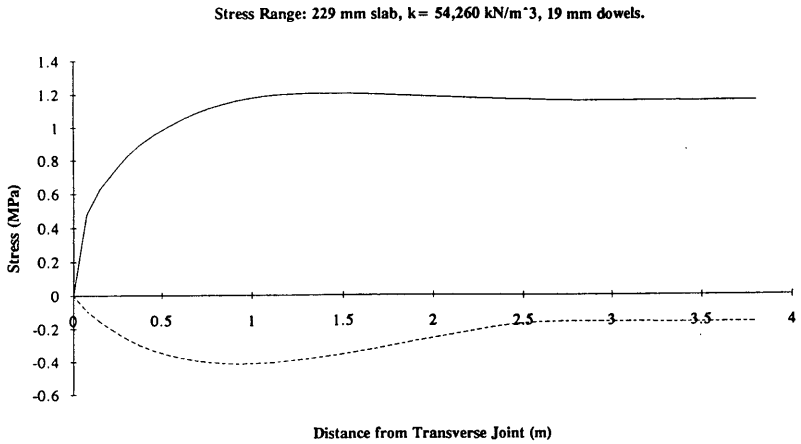

FIGURE 3 Resulting stress range for points along wheelpath as tension on top of slab/compression on bottom of slab.

PARAMETRIC STUDY OF MODIFIED ILLI-SLAB

A parametric study of the modified ILLI-SLAB model was performed to show how the input parameters affect the shapes of the influence functions and the resulting stress ranges in the slab. Some of the variables studied and their relative effects are described below.

Temperature Gradients

By far the most interesting and severe effects observed in the study were those caused by curling and warping. Shown in Figure 4 is the effect of slab length on residual stresses along the wheelpath caused by nighttime temperature gradients. In this situation the top of the slab is in tension and the bottom is in compression. It shows the concept of critical slab length (*5*). For this pavement-subgrade combination the critical slab length is between 7.62 and 9.14 m. It can be seen that as the slab length is increased beyond 9.14 m the tensile stresses caused by the slab's self-weight in response to thermal warping do not increase in the interior of the slab.

How varying the temperature gradients in a 279-mm slab of 6.1 m in length affects the stress range along the bottom of the slab caused by a passing 40-kN wheel load is shown in Figure 5. Remember that on the basis of this model a compressive stress on the bottom of the slab is accompanied by a tensile stress of equal magnitude at the top of the slab. The residual stress caused by the temperature gradient is not shown in Figure 5, but the coupled response of a temperature gradient and a 40-kN wheel load is shown. During the nighttime gradient condition for portions toward center slab, the bottom of the 279-mm slab will never experience tension as the 40-kN load passes. For these portions the top of the slab is in a constant state of tension. As the load approaches a point of interest the tension at the top of the slab increases as the curved down portion of the deflection basin passes over the point. Then the stress goes almost to zero as the load is directly above the point of interest. The tensile stress at the bottom of the slab caused by the wheel is not as large as the residual compressive stress caused by the temperature gradient. The stress then increases above the residual stress level as the trailing curved downward portion of the deflection basin passes over the point of interest and eventually returns to its residual stress level. In a 178-mm slab the deflections and curvature caused by the load are great enough to cause the top of the slab to go from residual tension to compression and then back to tension.

Moisture and shrinkage gradients that behave similarly to nighttime temperature gradients can completely cancel the effect of the daytime temperature gradients. The result is that the slabs are predominantly in a curled upward condition or nighttime gradient condition. This results in the critical tensile stresses being located on the top of the slab when the curved down portion of the deflection basin passes over the point of maximum residual stress, and there are two of these tensile peaks for each pass of a wheel load.

It must be pointed out that during periods of high afternoon temperature gradients the slab is expanding and foundation restraint friction forces are inducing compressive stresses, reducing the effect. During the night, however, the slab is contracting and the foundation restraint is inducing tensile stresses, increasing the effect. Also, the location of the maximum residual stress is not on the wheelpath. However, the stress range is at a maximum along the wheelpath. Thus it is here that the loading is most cyclic in nature and load repetitions become a more important consideration.

Temperature gradients typically vary from 0.087 to 0.109°C/mm in the daytime to 0.044 to 0.065°C/mm in the nighttime (*6,7*).

Moisture and Shrinkage Gradients

Work by Tremper and Spellman (*8*) has shown that upward curvature is the predominant condition for highway pavement slabs

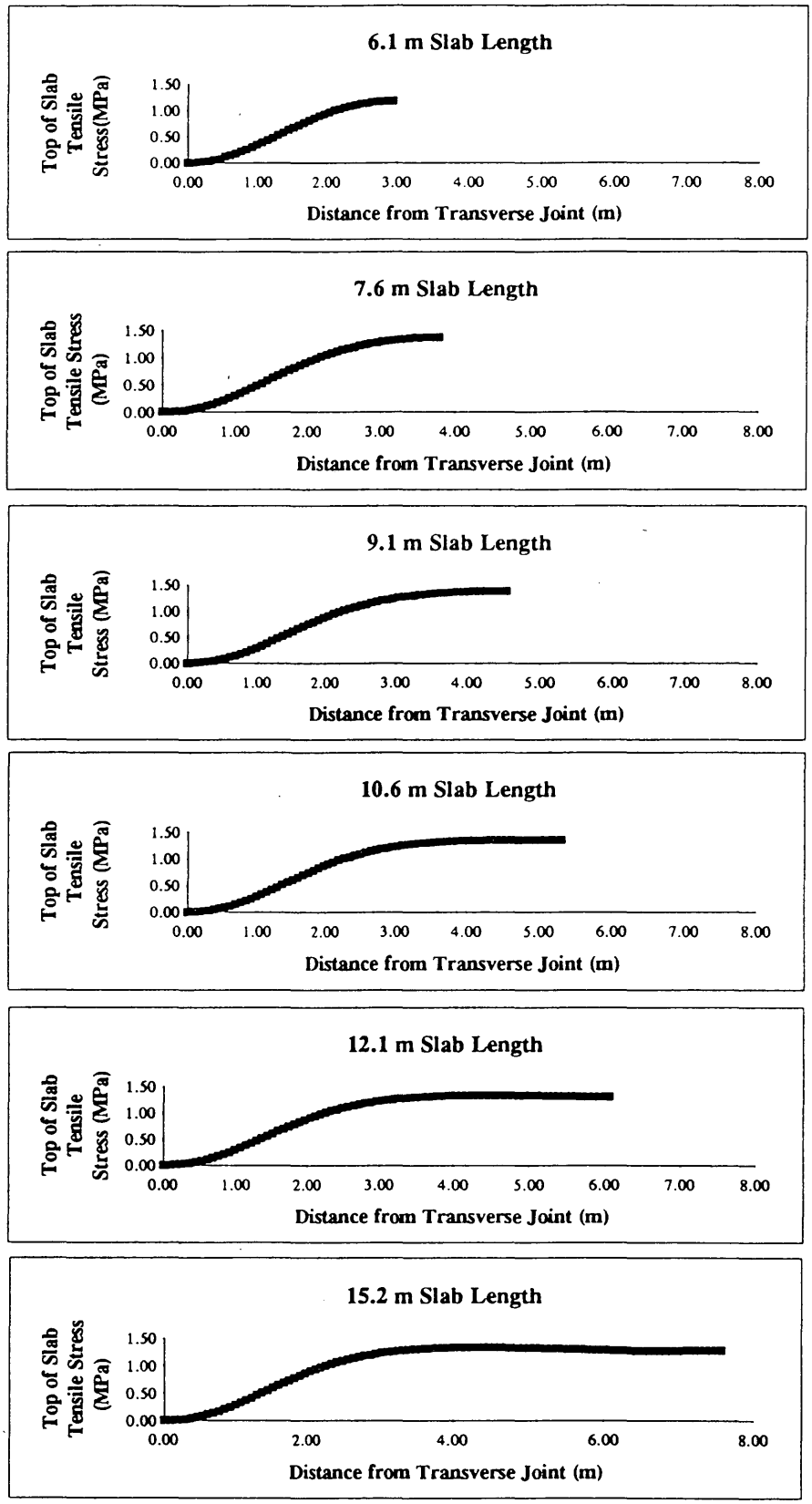

FIGURE 4 Residual stresses caused by nighttime temperature differential (tension on top of slab) along wheelpath for various slab lengths from joint to center of slab.

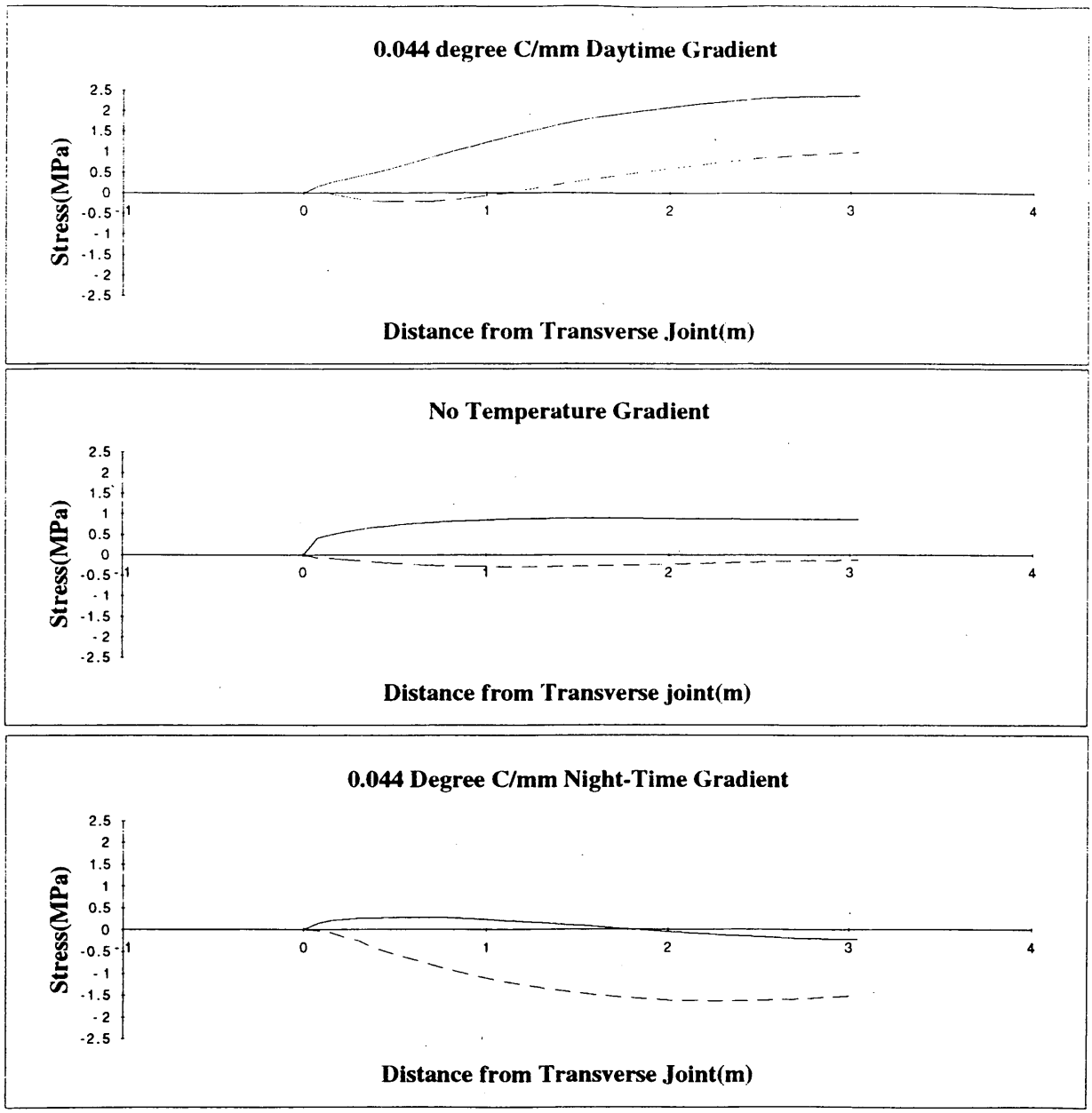

FIGURE 5 Stress variations for different temperature gradients for a 40-kN single tire as tension on bottom of slab (279-mm slab, 6.1-m slab length, 25.4-mm dowels at 305 mm; k = 54, 260 kN/m^3).

and that highway slabs are typically drier on the top than the bottom. They showed that the afternoon gradients were seldom great enough to cause the slab to go into downward curvature. They also point out that the state of California has shown that slabs constructed with concrete that exhibits higher levels of shrinkage have greater curling.

Janssen (*4*) has studied moisture profiles in highway pavements and has shown that the moisture gradient is nonlinear over the depth of the pavement. He estimates that the resulting movement owing to typical moisture gradients is not enough to fail the slab in bending but is enough to cause cracking in the top 19 mm of the slab because of the locally high level of shrinkage that causes high tensile stresses.

All of the factors described previously are typically modeled as equivalent nighttime temperature gradients (i.e., curved upward). Reddy et al. (*9*) have estimated that the moisture gradients encountered have equivalent nighttime temperature gradients of 0.065 to 0.13°C/mm of slab thickness. This combined with the average range of temperature gradients indicates that the slab will be curled upward, with effective temperature gradients varying between 0.022°C/mm in the daytime to 0.13°C/mm in the nighttime.

Results from a study of pavements in Chile (*10*) show that the curved upward condition dominates. During periods with high levels of rainfall the upward curvature is reduced, and in dry periods it is most extreme.

Load Magnitude

The stress variation in the pavement is nonlinear with respect to load magnitude. This is because for small loads the pavement slab, which is much stiffer than the Winkler subgrade, carries most of the load. As the load magnitude is increased and deflections increase, a larger and larger fraction of the load is carried by the subgrade. The increase in stress in the pavement slab for each load increase is reduced accordingly.

The shape of the deflection basin, that is, the locations of points of maximum curvature and stress, does not change much as the load magnitude is increased. This results in changes in the influence functions and stress range functions essentially only in magnitude but not in shape.

Joint Opening

Stress distributions are largely affected by the size of the joint opening. The effects of various joint openings on the range of stresses in the slab are shown in Figure 6. When the joint opening is very small the stress is distributed uniformly in the slab. As the joint opening increases larger deflections occur, resulting in the distribution of the load over a greater area. This results in higher curvatures and bending stresses in the slab that move farther away from the joint as the joint opening increases.

Joint opening is affected by slab length, the coefficient of thermal expansion, and the foundation restraint.

Dowel Size

Dowel size has an interesting effect. The results for dowels of various diameters are shown in Figure 7. When 19.1-mm dowels were analyzed the maximum stress in the slab was predicted to be far from the joint. In this case the joint is relatively flexible and the ends of the slabs at the joint are more free to deflect. This pushes the points of maximum curvature away from the joint.

When 38.1-mm-diameter dowels were analyzed an interesting phenomenon became apparent. The stresses were concentrated near the joint and the magnitude of the stresses increased sharply. These results indicate that there is an optimum dowel size for a given slab thickness. In this case it is the 31.75-mm bars.

Other Input Variables

All of the other input parameters studied had very little effect on the resulting magnitude of the estimated stresses and little effect on the locations of the resulting stresses.

MODEL VALIDATION CASE STUDY

Analysis of M-14 Ann Arbor, Mich.

M-14 is a 229-mm portland cement concrete pavement constructed in 1965. It has two 3.66-m lanes with 30.5-m joint spacing and 31.75-mm dowel bars spaced at 3.66 m. The slab rests on 102 mm of select gravelly sand compacted in place and underlain by 76.2 mm of compacted sand subbase. The local geology can be classified as glacial end moraine. The modulus of subgrade reaction for this section was estimated to be 67 825 kN/m^3, but in this environment support would be expected to be quite variable.

Shown in Figure 8 is the distribution of what will be referred to as medium and heavy trucks and the resulting equivalent single axle loads (ESALs) per hour. The data are based on a 1992 weigh-in-motion (WIM) survey of the design lane. The ESALs per hour were estimated by using a truck factor of 1.39 for heavy trucks and 0.41 for medium trucks (G. Siwek, Method of Calculating 18-kip Axle Equivalencies, unpublished position paper). It is interesting to note that most of the ESALs occur when the worst possible nighttime gradient conditions exist.

Crack surveys have been performed at 5-year intervals since the time of construction. Shown in Figure 9 is the distribution of cracks at 5 and 15 years after construction. Shown in the plot at 5 years is the number of cracks as a function of distance from the transverse joint. In the plot for 15 years is shown the number of cracks as a function of distance from cracks that existed at 5 and 10 years. Once a crack forms in one of the 30.5-m slabs it behaves as two slabs of shorter lengths connected by an aggregate interlock joint. At 5 years the greatest numbers of cracks occur at 4.6 to 4.9 m, 10.1 to 10.4 m, and 14.6 to 15.2 m from the transverse joint. The majority of the cracks that appeared in the 15-year survey were 4.6 to 4.9 m from previous cracks.

Analysis Method

An ILLI-SLAB model of the pavement was established. Influence functions were obtained for 40-kN loads passing over the slabs with temperature gradients of −0.044°C/mm for daytime conditions and 0, 0.044, 0.087, and 0.131°C/mm for nighttime conditions. The daily traffic was divided up into three ranges representing daytime (10 a.m. to 6 p.m.), average (6 a.m. to 10 a.m. and 6 p.m. to 10 p.m.), and nighttime (10 p.m. to 6 a.m.) conditions. It was assumed that the combined moisture and temperature effects resulted in effective temperature gradients of 0°C/mm for the daytime condition, 0.044°C/mm for the average condition, and 0.087°C/mm for the nighttime condition. The stress and ESAL distributions for each condition were analyzed with available fatigue models to roughly estimate the damage versus distance from the transverse joint that would occur for each condition. The results for the three conditions were added together to yield damage per day.

M-14 Analysis Results

Shown in Figure 10 is the response of a 15.2-m slab model of M-14 to a 40-kN load for various temperature gradients. Since the critical slab length for this pavement model is about 9.1 m the model response for a 15.2- or a 30.5-m slab will be the same beyond about 4.6 m from the joint. When the slab is curled upward the location of maximum stress varies only slightly for the different temperature gradients and occurs at 4.6 to 5.1 m from the joint. The maximum stress occurs during the nighttime condition, on the top of the slab, after the tire has gone by the point of interest and the trailing curved downward portion of the deflection basin is passing through the point. Each point of the re-

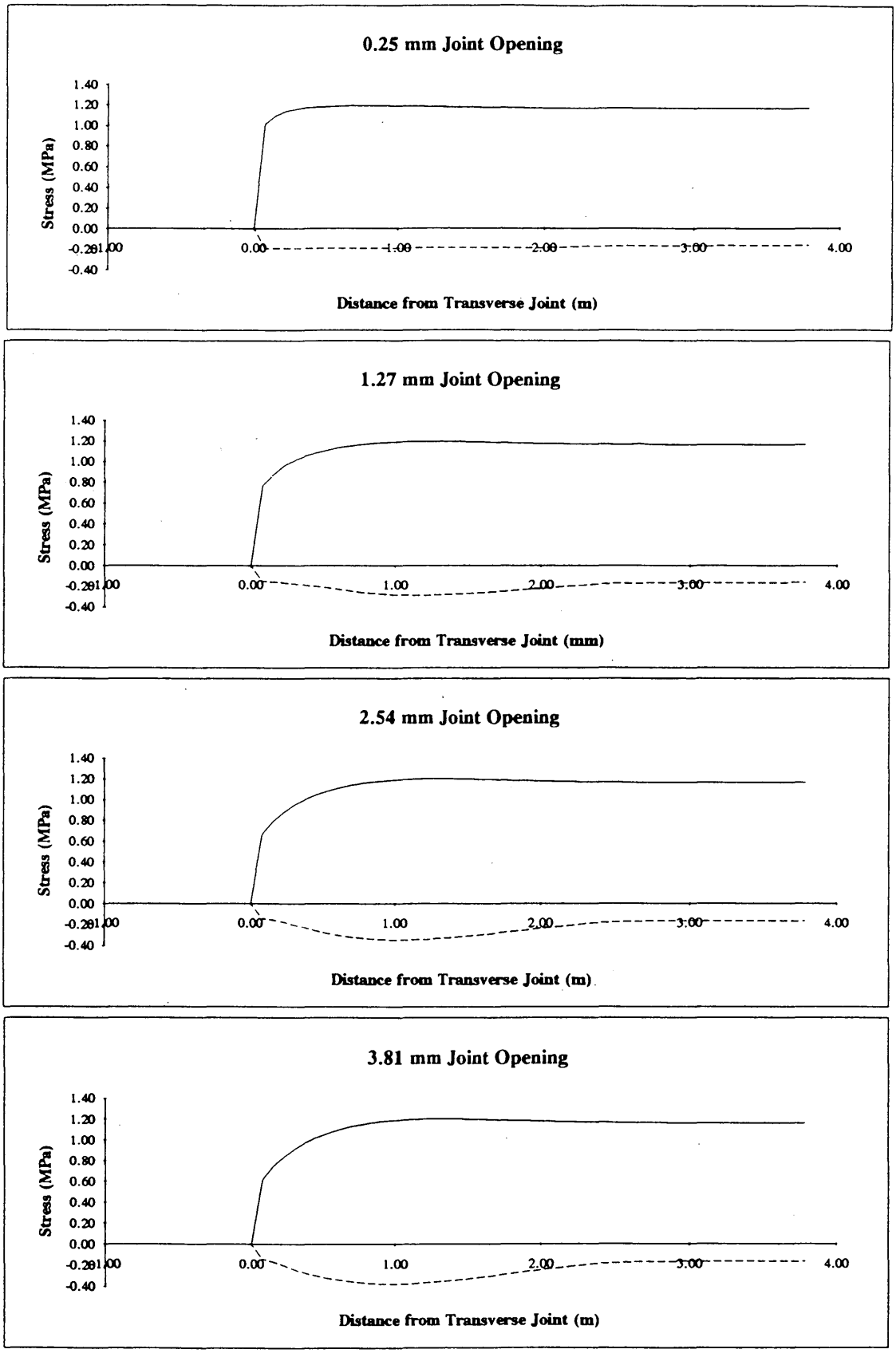

FIGURE 6 Relationship between joint opening and longitudinal stress.

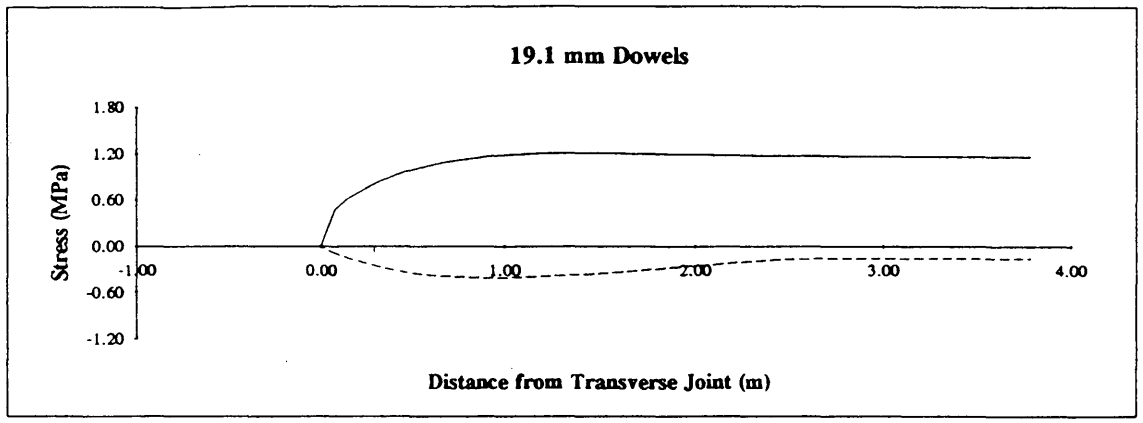

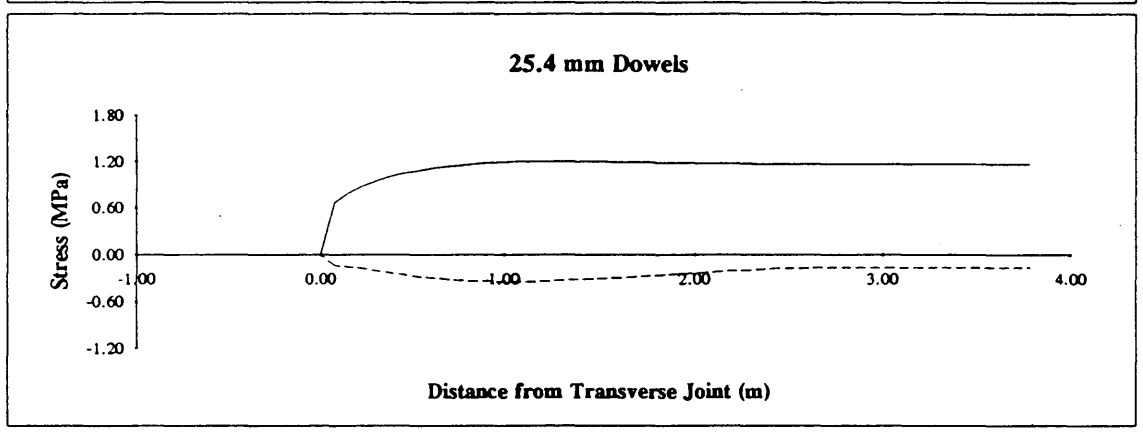

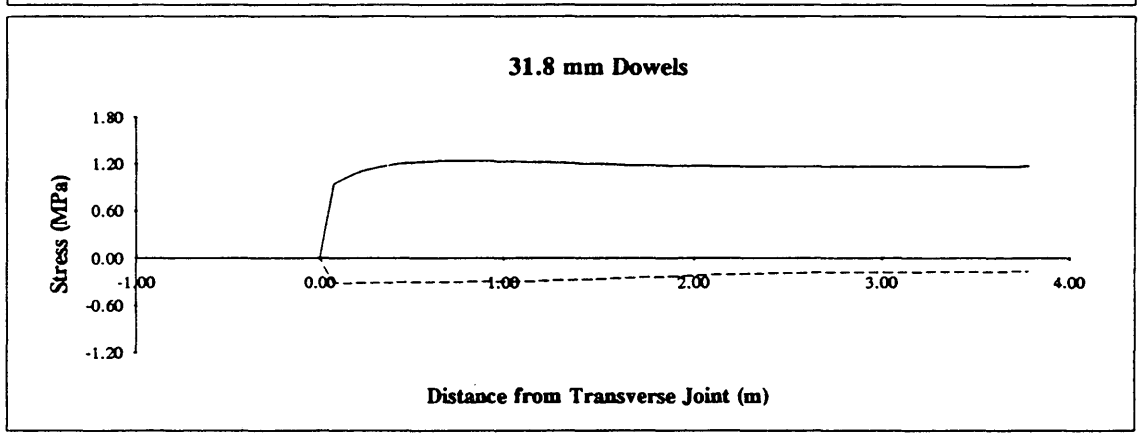

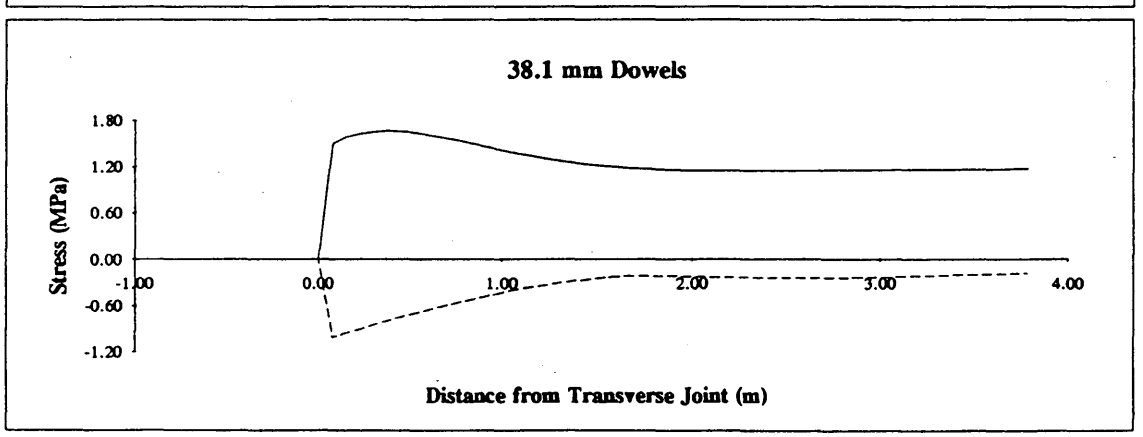

FIGURE 7 Relationship between dowel size and longitudinal stress.

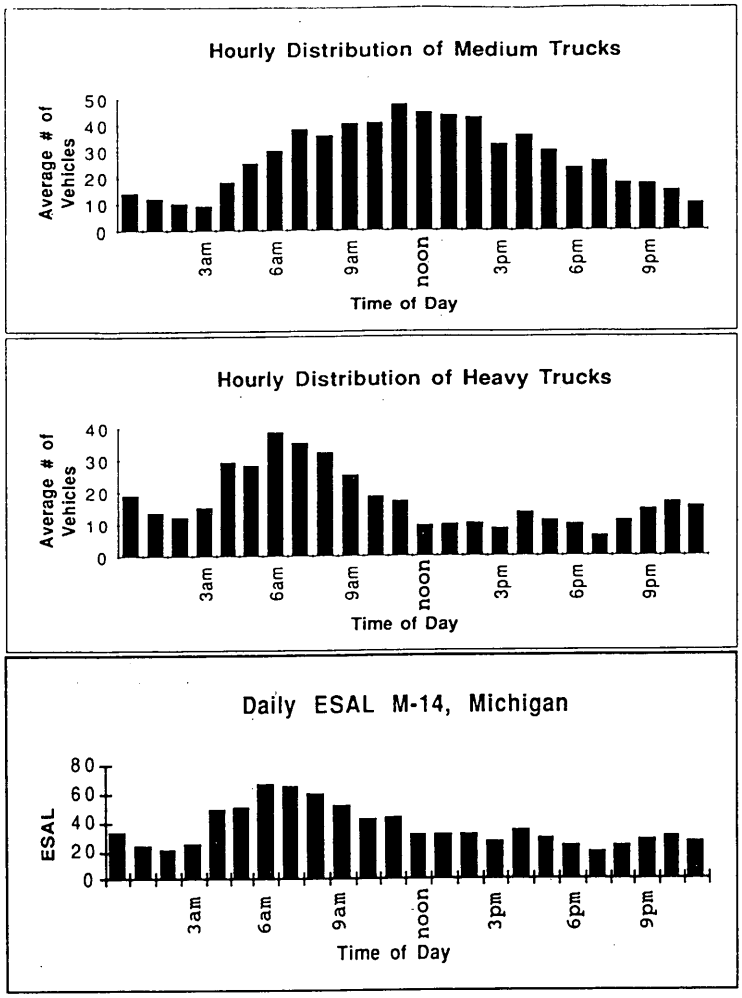

FIGURE 8 Average hourly truck distribution for M-14 in Ann Arbor, Mich., on the basis of a 1993 WIM study.

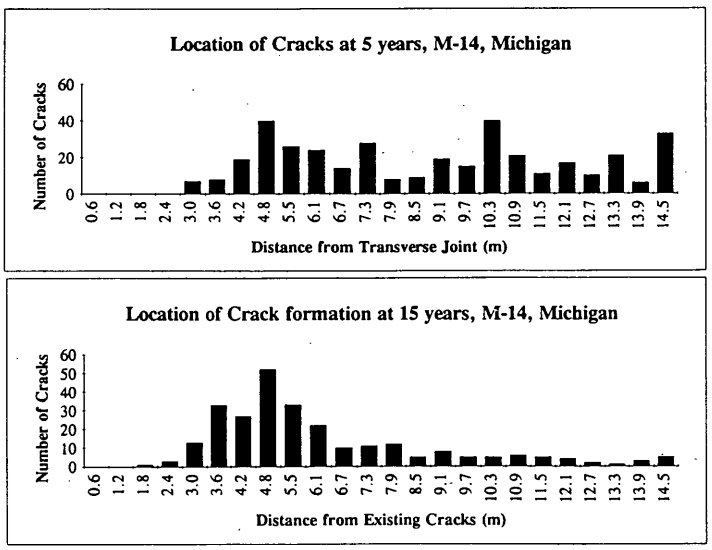

FIGURE 9 Crack distribution from M-14 distress surveys.

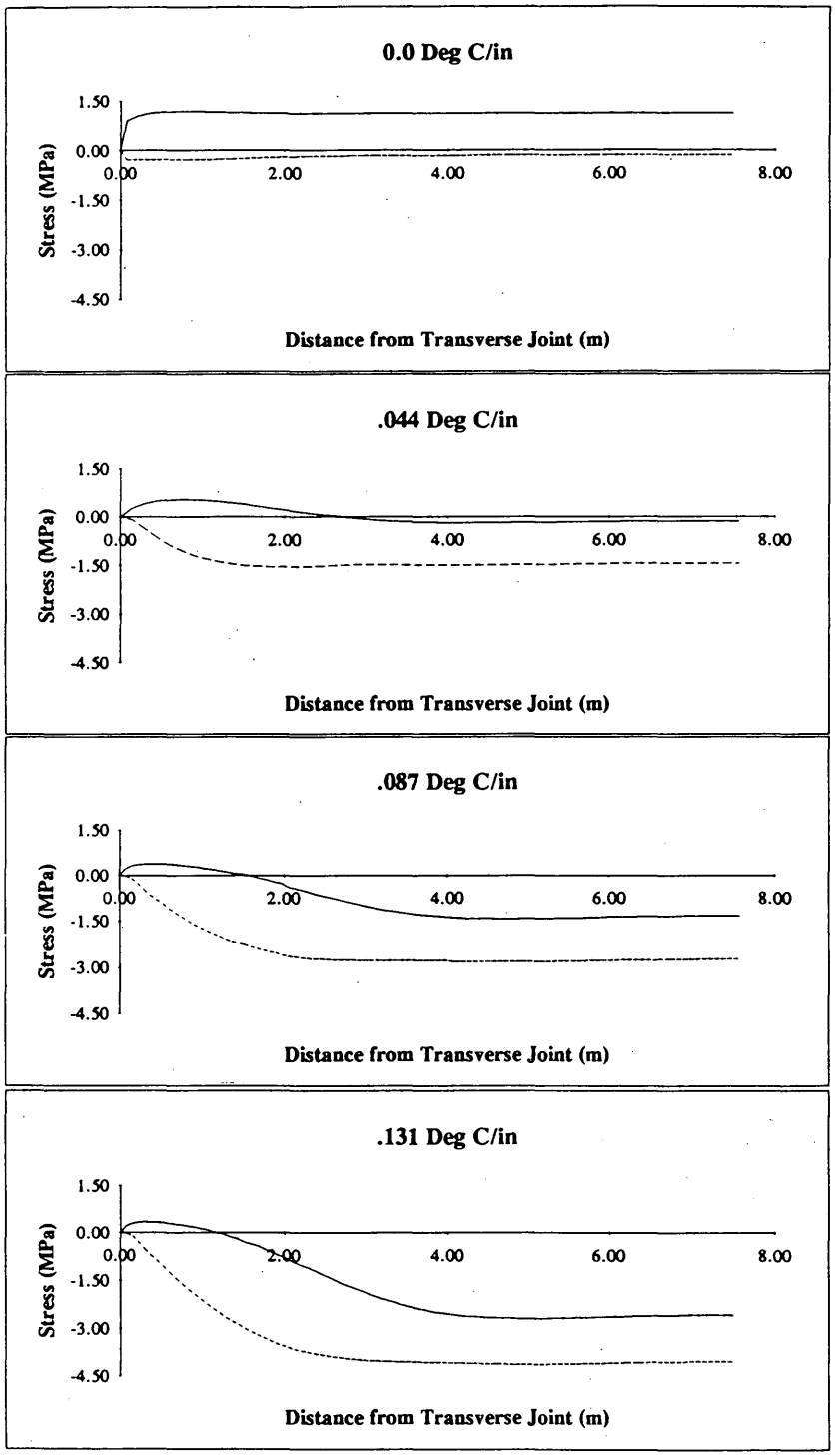

FIGURE 10 Response of M-14 model to nighttime gradients.

sulting stress distributions was analyzed with the PCA, Vesic, and Darter fatigue models (*2*) to estimate its daily fatigue loss. Shown in Figure 11 are the results based on a 4.48-MPa modulus of rupture. None of the models was developed on the basis of load patterns similar to those shown in an influence function. Hence they are not considered to be accurate. Qualitatively, however, they all predict that the maximum distress will occur at about 4.6 m from the joint. When this is compared with the crack locations from the distress surveys the match is very good.

CONCLUSIONS

Described in this paper has been an influence function approach to rigid pavement analysis. The influence function approach, de-

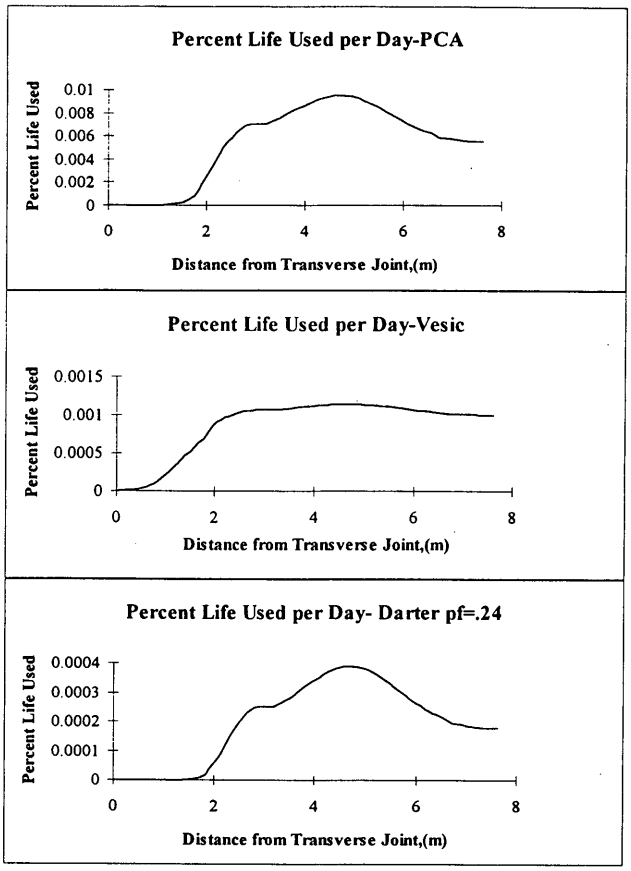

FIGURE 11 Estimated damage from various fatigue models for described method.

veloped at the University of Michigan Transportation Research Institute (*2*), is demonstrated to be a very powerful tool for pavement analysis. The recent studies cited on thermal, moisture, and shrinkage gradients have all shown that they have a significant effect on the residual stresses and that the highway slabs are predominantly in the upward curled condition, placing the top of the slab in tension. When this condition exists the peak tensile stresses are on the top of the slab when the curved downward portions of the deflection basin pass over the point of interest. There are two of these peaks for each pass of a tire. It is the combined residual stresses caused by the curling, warping, and load that have the most significant effects. When all of these factors are modeled with the modified ILLI-SLAB and the resulting stresses are analyzed with existing fatigue models, the estimated location of the maximum damage per day matches well with the observed crack locations from M-14.

The influence functions can also be used to compare different joint properties. It was demonstrated that there was an optimum dowel size and that the stress distribution around the joint is sensitive to joint opening.

This influence function approach can help in the development of greater understanding of the problem of vehicle-pavement interaction and shows good potential as a mechanistic-empirical design approach. Before this, work must be done in the areas of fatigue models based on the type of stress histories described here, determination of regional moisture and temperature conditions, specific mix design factors and their impacts in the context of this model, and determination of how to handle the load magnitude distribution (i.e., ESAL concept). This will allow engineers to more effectively design pavements and for the more effective regulation of the trucking industry.

ACKNOWLEDGMENTS

The authors wish to thank the Great Lakes Center for Truck and Transit Research Scholars Program for supporting the project entitled Life Expectancy of Rigid Pavements. Thanks are given to Tom Gillespie and Steve Karamihas at the University of Michigan Transportation Research Institute for developing and providing the modified ILLI-SLAB model and guidance in its use. Thanks are given to D. Mark Danzig for assisting in the enormous amount of computer time that was required to conduct the study. Thanks are given to Michigan Department of Transportation employees Ed Novak, Gloria Siwek, and Steve Purdy for comments and assistance in obtaining the traffic information and pavement distress data.

REFERENCES

1. Tabatabaie, A. M., et al. *Longitudinal Joint Systems in Slip Formed Rigid Pavements*, Vol. 2. *Analysis of Load Transfer Systems for Concrete Pavements*. Report FAA-RD-79-4(II). U.S. Department of Transportation, Nov. 1979.
2. Gillespie, T. D., et al. *NCHRP Report 353: Effects of Heavy-Vehicle Characteristics on Pavement Response and Performance*. TRB, National Research Council, Washington, D.C., 1993.
3. Nasim, M. A., et al. Behavior of Rigid Pavement Under Moving Dynamic Loads. In *Transportation Research Record 1307*, TRB, National Research Council, Washington, D.C., 1991.
4. Janssen, D. J., Moisture in Portland Cement Concrete. In *Transportation Research Record 1121*, TRB, National Research Council, Washington, D.C., 1987.
5. Ioannides, A. M., and G. T. Korovesis. Aggregate Interlock: A Pure Shear Load Transfer Mechanism. In *Transportation Research Record 1286*, TRB, National Research Council, Washington, D.C., 1990.
6. Saxena, S. K., and G. T. Dounias. Mechanical and Environmental Stresses in Continuously Reinforced Concrete Pavements. In *Transportation Research Record 1099*, TRB, National Research Council, Washington, D.C., 1986.
7. Croney, P., and D. Croney. *The Design and Performance of Road Pavements*, 2nd ed. McGraw-Hill, New York.
8. Tremper, B., and D. L. Spellman. Shrinkage of Concrete—Comparison of Laboratory and Field Performance. In *Highway Research Record 3*, HRB, National Research Council, Washington, D.C., 1963.
9. Reddy, A., G. A. Leonards, and M. E. Harr. Warping Stresses and Deflections in Concrete Pavements: Part III. In *Highway Research Record 44*, HRB, National Research Council, Washington, D.C., 1963.
10. Poblete, M., et al. Model of Slab Cracking for Portland Cement Concrete Pavements. In *Transportation Research Record 1307*, TRB, National Research Council, Washington, D.C., 1991.

Publication of this paper sponsored by Committee on Rigid Pavement Design.

Evaluation and Rehabilitation Design of I-495 in Delaware

SHIRAZ D. TAYABJI, PETER J. STEPHANOS, AND W. PRESTON DAVIS

In 1991 the Delaware Department of Transportation initiated a comprehensive study to evaluate the performance of a portion of the Delaware Interstate highway system (including the turnpike). The highway systems evaluated included I-495 and associated ramps, including ramps to and from I-495 and I-295. A primary objective of the evaluation was to develop maintenance and rehabilitation strategies for the studied pavements. The pavements consisted of 228.6-mm (9-in.)-thick continuously reinforced concrete (CRC) pavement along most of I-495 and 254-mm (10-in.)-thick jointed reinforced concrete (JRC) pavement along the remaining portion of I-495 and the ramps. A major concern with the pavements of I-495 was the extensive occurrence of alkali-silica reactivity (ASR) and extensive joint deterioration along many of the jointed pavements. As part of the evaluation process, a field investigation was conducted to determine the current condition of I-495 and the associated ramps. The field investigation consisted of visual condition survey, nondestructive deflection testing with a falling-weight deflectometer (FWD), coring and boring, and laboratory testing. The field and laboratory data were evaluated to identify the current condition of the pavements, considering the widespread existence of ASR. The manifestation of the ASR along the CRC pavement was in the form of longitudinal cracking, that is, parallel cracks spaced generally about 50.8 to 304.8 mm (2 to 12 in.) apart along the width of the pavement. Spalls existed along the wheelpath at the intersection of the "normal" transverse cracking and the ASR-related longitudinal cracking. The FWD data were used to backcalculate concrete modulus of elasticity and the modulus of subgrade reaction values. In addition, joint load transfer analysis was performed for the JRC pavements. On the basis of the FWD test data and condition survey results, the pavements were delineated into several uniform projects. Maintenance and rehabilitation needs were then identified for each project, and rehabilitation priorities were assigned for each project. Several rehabilitation strategies were developed for each project to improve the structural and functional condition of the existing pavement to an acceptable serviceability level for the duration of the specified design/analysis period. Life cycle cost analyses were performed for each rehabilitation alternative for each project, and final rehabilitation designs were recommended. In 1993 and 1994 the I-495 section and the associated ramps were overlaid with a 304.8-mm (12-in.)-thick unbonded plain jointed concrete overlay. The details of the field investigation, data analysis, and the rehabilitation design process used to arrive at the final designs are presented.

In 1986 the Delaware Department of Transportation (DelDOT) initiated a study to evaluate the performance of the Delaware Interstate highway system (including the turnpike) and to identify at the network level future rehabilitation needs for the system. The systems studied included I-95, I-495, and associated ramps including ramps to and from I-95 and I-495 to I-295. The study areas were divided into 32 sections, and specific recommendations were prepared for future rehabilitation strategies for each section on the basis of present condition, future anticipated condition, and cost analysis. In 1990 DelDOT initiated evaluation of maintenance and rehabilitation strategies for I-495 and several associated ramp sections. As part of this evaluation a visual condition survey of I-495 and the ramp sections was performed in the fall of 1990 to update the data from the 1986 study. In March 1991 a project-level rehabilitation design study for I-495 and selected ramp sections was initiated.

A major concern with I-495 was the occurrence of alkali-silica reactivity (ASR) in the continuously reinforced concrete (CRC) pavement of I-495 and the presence of reactive aggregates in jointed reinforced concrete (JRC) pavement of the ramps. ASR appeared to be extensive in terms of extent and severity along the northern portions (both directions) of I-495. ASR did not appear to be as severe along the southern portions of I-495. There did not appear to be other significant design- or construction-related deficiencies in the CRC pavements of I-495, and these pavements would have undoubtedly been considered adequate for many more years of traffic if not for the ASR problem.

This paper presents a background on I-495 and the associated ramps under study and details of a field investigation conducted to evaluate the condition of the existing pavements. Finally, rehabilitation design alternatives including unbonded concrete overlays are discussed for each study section and life cycle cost estimates are presented.

OBJECTIVES AND SCOPE OF WORK

The objective of this study was to develop rehabilitation design alternatives for portions of I-495 and I-295 (associated ramp sections). Specifically, the study area consisted of the sections listed in Table 1. The section numbers were designated during the 1986 pavement rehabilitation study. As discussed the scope of work consisted of field investigation of the designated pavements to evaluate the condition of the existing pavement and development of rehabilitation strategies for those pavements.

BACKGROUND

The pavements along I-495 were constructed between 1972 and 1977 and were opened to traffic in 1978. The ramp sections associated with I-295 (Sections 4, 7, and 8) were constructed between 1964 and 1967 and were opened to traffic in 1967. Except for a small section along I-495N, none of these pavement sections had been overlaid.

Most pavements along I-495 consisted of 228.6-mm (9-in.)-thick CRC pavement constructed over a 101.6-mm (4-in.)-thick

S. D. Tayabji, Transportation Technologies USA, Inc., 9030 Red Branch Road, Suite 210, Columbia, Md. 21045. P. J. Stephanos, PCS/Law Engineering, 12240 Indian Creek Court, Suite 120, Beltsville, Md. 20705. W. P. Davis, Whitney, Bailey, Cox, and Magnani, 1850 York Road, Timonium, Md. 21093.

TABLE 1 Rehabilitation Study Sections

Section No.	Roadway	Ramp Route	Beginning Station	Ending Station	Pavement Surface	Length, ft
13a, b	495N	-	3147+51	3267+10	CRCP	11,959
14a, b	495N	-	3311+00	3413+30	CRCP	10,230
15	495N	-	3415+80	3668+95	CRCP	25,315
16	495N	495N-95N	3668+95	3713+00	JRCP	4,405
17	495S	95S-495S	4100+00	4164+17	JRCP	6,417
18a	495S	-	4164+17	4415+20	CRCP	25,133
18b, c	495S	-	4418+35	4521+57	CRCP	10,322
19a, b	495S	-	4563+03	4623+65	CRCP	6,062
20	495S	-	4626+80	4631+68	JRCP	488
21	495S	-	4633+58	4684+28	CRCP	5,070
4	295	295W-95S	5400+00	5437+78	JRCP	3,778
7	295	495S-295E	5507+12	5529+97	JRCP	2,258
8	295	495S-295E	5531+65	5560+08	JRCP	2,843

cement-treated base (CTB) placed over a select subbase material. The ramps and one section of pavement along I-495 consisted of 254-mm (10-in.)-thick JRC pavement over CTB placed over select subbase material. The JRC consists of 13.7-m (45-ft)-long slab panels reinforced with 152.4 × 15.4-mm (6 × 6-in.) welded wire fabrics. The shoulders along I-495 are typically asphalt concrete (AC), with an AC surface thickness of about 76.2 to 101.6-mm (3 to 4 in.). The study pavements were constructed in or near marshland areas and required considerable preconstruction soil stabilization and removal efforts. These activities included much excavation, subgrade removal, construction of sand blankets, and the use of sand wick drains to move, consolidate, or drain undesirable soils.

A considerable amount of information was collected during the 1986 rehabilitation study (*1*). The maintenance information collected indicated that maintenance along I-495 consisted primarily of crack sealing and repair of expansion joints at bridges. The longitudinal cracking (now confirmed to be related to ASR) was becoming more frequent and wider. As for the ramp sections, Section 8 was noted as having full-depth joint repairs at some joints. These repairs were noted to have been necessitated because of joint deterioration caused by reactive aggregates. Since 1986 more spalling had been reported along Sections 15 and 18 as a result of the extensive ASR-related longitudinal cracking, and these spalls had generally been patched with AC. One small section of the CRC pavement along Section 15 (northbound I-495) had been overlaid with 76.2-mm (3-in.) of AC a few years before. In addition, more full-depth joint repair had been made along the ramps of I-295. The 1986 rehabilitation study included field investigation consisting of the following:

1. Nondestructive deflection testing (NDT) with a Phoenix falling-weight deflectometer (FWD),
2. Pavement condition survey by a modified pavement condition index (PCI) procedure,
3. AASHTO pavement serviceability rating (PSR) survey, and
4. Roughness survey with a portable universal roughness device (PURD).

On the basis of the analysis of the field data and projected traffic data, a comprehensive evaluation was made of each roadway section, and future maintenance and rehabilitation needs were identified.

1990 Pavement Condition Study

In the fall of 1990 a visual condition survey along sections of I-495 and I-295 ramps was performed. The survey was conducted to determine whether the rehabilitation recommendations made during the 1986 study were still applicable because only limited maintenance and repair activities had been performed along the study sections. On the basis of that survey, Sections 4, 17, 15, and 18a were rated as requiring rehabilitation within the next 0 to 5 years, and rehabilitation was rated high priority. For the CRC pavement Sections 15 and 18a, the primary distresses were ASR-related longitudinal cracking, spalling at cracks, and many patches. Section 4 had numerous full-depth repairs. For Sections 13, 14, 18b, 19, and 21 it was recommended that these sections be monitored over the next 3 to 5 years and that the rehabilitation needs confirmed at that time. All these sections were exhibiting low-severity ASR-related longitudinal cracking. However, the longitudinal cracking at these sections was not considered to be a cause for concern at that time.

On the basis of the results of that study a full-scale project-level field investigation was recommended to identify rehabilitation needs for the study pavements.

ASR Problem

The most significant distress along the CRC pavements of I-495 and the I-295 ramps was the longitudinal cracking related to ASR. This problem had apparently been identified just a few years before. As noted previously ASR occurs when silica or silicates in aggregates react with alkali in the cement to form a gel-like substance. The gel absorbs water and expands. Within a few years

this expanding gel can crack the concrete. The process is irreversible and can lead to severe deterioration of the concrete. The ASR phenomenon has been known since the 1940s, and extensive studies have been conducted in the affected central states of, for example, Colorado, Nebraska, and Kansas to minimize or eliminate the risks of ASR. Some of these states have reportedly not constructed ASR-affected pavements since the early 1960s and have rehabilitated or reconstructed most of their ASR-affected pavements. Recognition of the ASR problem was slower along the East Coast states of the United States, and the problem has been recognized only in recent years. The I-495 problem is an example of the nonrecognition of reactive aggregates within Delaware. Although techniques for retarding the ASR process (which can continue for a long time) have been proposed, techniques for correcting the damage from ASR are not yet available. The ASR process can be arrested or retarded if moisture is kept from entering the ASR-affected concrete.

The ASR-affected concrete pavements have generally been overlaid with hot-mix asphalt concrete to temporarily extend the service life of the pavements. In most cases it has been reported that these pavements are reconstructed after the AC overlay has served its purpose. Bonded concrete overlays cannot be used to rehabilitate ASR-affected pavements. However, unbonded concrete pavements can be used without any problems. Also, ASR-affected concrete pavement cannot be recycled as aggregate for concrete. Recently, as part of the Strategic Highway Research Program, extensive studies of the ASR problem and its mitigation have been conducted.

1991 FIELD INVESTIGATION

During early 1991 a field investigation was conducted to determine the current condition of the I-495 and I-295 ramp sections designated by DelDOT for possible rehabilitation. The field investigation consisted of visual condition survey, nondestructive deflection testing, and coring and boring.

Visual Condition Survey

The visual condition survey was conducted by a two-person team riding in a car. The objective of the survey was primarily to identify the extent and severity of ASR and to note areas exhibiting other distresses that would require localized repairs during future rehabilitation of the pavements. No attempt was made to determine a numerical index such as the PCI or the PSR.

The general observations made on the basis of the condition survey are given as:

1. The CRC and JRC pavements generally provided a smooth ride, even though many of these pavements exhibited ASR-associated cracking.
2. The primary distresses observed included longitudinal cracking in CRC pavements (ASR related), spalling, midslab cracking in JRC pavements, and joint deterioration/patching (reactive aggregate related) in JRC pavements. The transverse cracking in CRC pavements per se was not considered a distress. Only the severity of the transverse cracking was considered when evaluating the condition of CRC pavements.
3. The AC shoulders were rated in poor to fair condition. Only areas recently replaced were in very good to excellent condition.

One interesting phenomenon observed along I-495 was the variability in the severity of ASR between the northern portions (Sections 15 and 18; high-severity ASR) and the southern portions (Sections 13, 14, 19, and 21; low-severity ASR). Interstate 495 was constructed over a period of many years, and portions were constructed under different contracts. Thus, the difference in the ASR activity may have been a result of age or different sources of aggregate and cement. The longitudinal cracking caused by ASR along the northern portions of I-495 was more pronounced because of truck traffic loadings and was more damaging in the CRC pavement because of the closely spaced transverse cracking. The wheelpaths in the outside lanes of I-495 exhibited numerous spalls and patch areas as a result of accelerated concrete deterioration in these areas. These spalls and patch areas generally occurred at intersections of longitudinal and transverse cracks along the wheelpaths.

A review of available construction data indicated that Sections 15, 16, 17, and 18a, which exhibited the high-severity ASR, were placed the earliest, during 1972 and 1973. Also, Sections 15, 16, 17, and 18a constructed by one contractor exhibited a unique combination of coarse aggregates, fine aggregate, and cement suppliers, resulting in a different (higher) rate of ASR development in the CRC pavement than for the other contracts/sections.

The concrete deterioration in the I-495 CRC pavements as a result of the ASR-related longitudinal cracking was expected to continue. However, the rate of deterioration could not be predicted. This deterioration would necessitate a continuing need for repairs such as patching along the northern portions of I-495, and these repairs could be considered temporary only because such repairs have low useful service life. On the basis of the condition survey it was clear that corrective action would soon be needed for Section 15 and Section 18 (northern half portion of I-495). A visual condition survey of the interchange ramps along I-495 was also conducted. The survey indicated that these ramps were in generally good condition and required only minor patch repair and resealing of some joints.

Nondestructive Deflection Testing

An NDT program was conducted along the study sections to evaluate the structural condition of the pavements. The NDT was conducted with a Dynatest 8002E FWD.

For the CRC pavement deflection basin testing was conducted, and for the JRC pavement deflection basin testing and joint load transfer testing were conducted. All testing was conducted along the outside lane. Load levels of 4081.5, 5442.0, and 7256.0 kg (9,000, 12,000, and 16,000 lb) were used. For the CRC pavements the basin testing was conducted at a spacing of 30.5 m (100 ft). For the JRC pavements basin testing was conducted at the midslab of every third slab panel. Joint testing was conducted at every third joint at corner locations.

Coring and Boring

To ascertain the actual thicknesses of the various pavement layers and to characterize the base, subbase, and subgrade materials, a

coring and boring program was conducted by DelDOT staff. Cores were 101.6 to 152.4 mm (4 to 6 in.) in diameter. Borings were made at each core location and went to a depth of about 1.5 m (5 ft) from the pavement surface. The CTB was generally recovered intact and appeared to be in excellent condition. A total of 28 concrete cores were tested for splitting tensile strength. Also, subbase and subgrade characterization was performed by DelDOT staff by using materials recovered from the borings.

OTHER DATA COLLECTION

Although a significant amount of data was available from the 1986 study reports, additional data were also collected to update that information. These data types included traffic data and unit cost data.

Traffic Data

Updated traffic data for a 40-year period were requested from DelDOT. DelDOT had asked that the rehabilitation designs be prepared to provide a 40-year service life. Early discussions with DelDOT staff indicated that there was no reliable way of projecting traffic for 40 years because the common practice was to project traffic for only 20 years. It was suggested that the 20-year projections be used and that these projections be doubled to provide the 40-year traffic projections. The average annual daily traffic (AADT) projected for 2010 for various sections of the study area was available, and these data also indicated the level of service (LOS) at Level C for these sections for 2010. For 2010 most of I-495 and many of the ramp sections were projected to approach LOS C. The AADT data and LOS traffic data are summarized:

- AADT along I-495 Projected year 2010 ranged from 59,000 to 84,000 vehicles.
- LOS capacity along I-495 Projected year 2010 ranged from 44,000 to 69,000 vehicles per day.

For computing traffic over a 40-year period it was assumed that the roadway sections would not be able to accommodate traffic beyond the LOS C. The 40-year traffic projections in terms of 18-kip equivalency single axle loads (ESALs) (from 1990) are summarized in the in-text table.

Period (years)	*Cumulative 18-kip ESAL*
8	12,000,000
15	34,000,000
20	59,000,000
40	166,000,000

For developing the rehabilitation designs by using various pavement schemes, the following initial design periods were used in estimating design traffic (PCC is portland cement concrete):

Pavement Scheme	*Initial Design Life*
AC overlay	8
AC reconstruction	15
PCC reconstruction	20
PCC unbonded overlay	20

Unit Cost Data

Typical pavement construction-related unit costs were compiled by using current bid tabulations from recent Delaware and Maryland highway construction projects and consultant's in-house files. These costs were used in developing cost estimates for the various proposed pavement rehabilitation strategies.

Bridge Clearances

Bridge clearance data were tabulated to identify possible constraints in the development of specific rehabilitation designs. Information on bridge clearance is critical since bridge clearance is a critical item for overlay alternatives. The designed bridge clearance was 4.9 m (192 in.) for I-495.

ANALYSIS OF DATA

Analysis of the results of the field investigations are presented in this section. The data were analyzed to evaluate the extent and severity of the distresses in the existing pavements and to estimate material properties for use as input in developing rehabilitation designs.

Visual Condition Survey

The visual condition survey data indicated that the CRC pavements along Section 15 and the northern portion of Section 18 were exhibiting high-severity ASR-related longitudinal cracking. The condition of the transverse cracking was not considered unusual considering that the pavements were opened to traffic in 1978. The pavements of the other CRC sections exhibited ASR-related longitudinal cracking but at a very low to low level of severity. The CRC pavements were providing a good ride, and a rough ride was encountered generally only at expansion joints near bridge structures. As noted previously the CRC pavements would be considered to be performing in accordance with the design if it had not been for the ASR-related longitudinal cracking.

The JRC pavements of Sections 16 and 17 were also exhibiting reactive aggregate problems, and this was noticeable at joints within the southern portions of Sections 16 and 17. The northern portions of Sections 16 and 17 did not exhibit this problem and were apparently constructed under a different contract.

Section 4 had numerous full-depth joint repairs because of joint deterioration caused by reactive aggregate. The repaired joints appeared to be performing satisfactorily. Section 7 appeared to be performing well, with no indication of reactive aggregates. Mid-slab cracking was nonexistent and joints looked good. On the other hand, the adjacent Section 8 was exhibiting extensive reactive aggregate-related deterioration at joints. Many of the joints had been replaced full depth, and AC patches were applied to joints not so repaired. Section 8 also rode poorly.

Nondestructive Deflection Testing

The NDT data were used to backcalculate concrete modulus of elasticity and the modulus of subgrade reaction values. In addition, joint load transfer and void analyses were performed for the JRC pavements. No significant presence of voids was detected along the JRC pavement sections. Load transfer at joints of the JRC pavements ranged from 65 to 85 percent. Load transfer for

Sections 4, 8, and 20 was poor. A review of the deflection basin data and the extent and severity of ASR indicated that the study areas could be delineated into several uniform projects. The project delineation is summarized in Table 2.

Projects A, B, C, and D were designated primarily on the basis of the extent and severity of ASR. Project A was the better-performing project and Project D was the worst-performing project along I-495.

The backcalculated effective concrete modulus of elasticity value for Project D of 21,760 MPa (3,200,000 psi) was considerably lower than the values obtained at other projects. This reflected the poor condition of the pavements in Project D. Project C also exhibited lower modulus of elasticity values for the concrete. Projects C and D were most affected with ASR, and the extent of concrete deterioration was clearly reflected in the backcalculated concrete modulus of elasticity values. Projects A and B, on the other hand, exhibited high modulus of elasticity values for the concrete, indicating that the concrete in these projects was not deteriorated or not deteriorated to the extent as in Projects C and D.

For the JRC projects the backcalculation also provided high concrete modulus of elasticity values. These values were high, even though these pavements had reactive aggregates. This was because the deflection basin testing was conducted in the midslab locations of the slab panels where there was little damage caused by the reactive aggregates.

The characteristics of the CTB, subbase, and subgrade were modeled as a composite modulus of subgrade reaction value. The modulus of subgrade reaction was generally lower in the southern portions of I-495. The backcalculated modulus of subgrade reaction values ranged from about 150 to 270 pci.

Core Testing

Concrete cores obtained from the study sections were tested for splitting tensile strength. Cores were cut into top and bottom portions, and one or both portions were tested depending on the presence of steel reinforcement within the core. Cores were maintained in a soaked state for about 40 hr before testing. The splitting tensile strength ranged from 1,482 to 3,827 kPa (215 to 555 psi) for top portions of the cores and ranged from 1,758 to 5,068 kPa (255 to 735 psi) for the bottom portions of the cores.

Although no clear trend could be determined from the core testing, it appeared that the north portions of I-495N and I-495S had relatively lower strength concrete. No petrographic studies were conducted directly as part of the field investigation because the presence of reactive aggregates in the I-495 pavements had been established by previous studies.

TABLE 2 Project Delineation

Project	Roadway	1986 Study Section No.	Design Section Limits
A	495N	13	3147-3267
		14 (part)	3379-3413
	495S	18b (part)	4406-4453
B	495N	14 (part)	3311-3379
	495S	19	4563-4623
		20	4626-4631
		21	4633-4684
		18b (part)	4453-4497
		18c	4497-4521
C	495N	15 (part)	3415-3476
	495S	18a part)	4256-4406
D	495N	15 (part)	3476-3669
	495S	18a part)	4164-4256
E	495N	16	3669-3713
	495S	17	4100-4164
F	295W-95S	4	5400-5437
	495S-295E	7	5507-5529
	495S-295E	8	5531-5560

Materials Characterization

As part of the coring and boring effort DelDOT also performed laboratory analysis and characterization of the subbase and subgrade samples obtained from the study pavements. The subbase and subgrade sampling was conducted only to a depth of 1.5 m (5 ft). The subbase material was typically coarse to fine sand: AASHTO Classification A-1-a, A-1-b, A-2-4, and A-2-6. The sand layer at some locations had silt and traces of gravel. The nominal 101.6-mm (4-in.)-thick CTB under the CRC pavement was in excellent condition, and intact cores were recovered from the soil cement layer. In a few instances the CTB was bonded to the surface concrete layer. Also, in a few instances an A-6 (silty clay) layer was encountered within the upper 1.5 m (5 ft) of the pavement and was considered to be the natural subgrade material. No water was encountered within the 1.5-m (5-ft) depth of the boring.

The materials study indicated that the existing CRC pavement was constructed on a sound CTB and a relatively free-draining layer of coarse to fine sand. Lack of adequate drainage did not appear to be a matter of concern along the I-495 pavements. This was also evidenced by lack of drainage-related distresses in the CRC pavement.

Summary

The field investigation indicated that sections of I-495 and the ramps to and from I-295 were exhibiting extensive distresses resulting from ASR. It was considered that Projects D, E, and some of the I-295 ramp projects would need to be rehabilitated in the near future. Without major rehabilitation, an increased level of maintenance would be needed along these projects in the future.

On the basis of the discussions presented the following levels of priorities were assigned for rehabilitation of the study area:

Priority Level	*Projects*	*Rehabilitation Time*
Very high	C, D, E, F	0–3 years
Medium	A, B	5 years

It was realized that other extrinsic factors such as future traffic control and traffic disruptions may dictate the need to select rehabilitation strategies on the basis of minimizing future traffic disruptions along the heavily used I-495. Thus, even though Projects A and B were not in immediate need of rehabilitation, serious consideration was given to including Projects A and B with the other projects in need of immediate rehabilitation.

REHABILITATION DESIGN ALTERNATIVES

The primary objective of the study was to develop and identify rehabilitation alternatives for the pavements of I-495 and I-295 ramps. Under normal circumstances the development of practical rehabilitation strategies is a complex process because the forecasting of pavement performance is not an exact science. For the present study the task was further complicated because of the presence of ASR and the lack of knowledge of rate of deterioration of concrete structures affected by ASR. As indicated previously Projects C, D, E, and F (I-295 ramp sections) were designated as requiring rehabilitation in the near future, whereas the remaining projects were not in urgent need of rehabilitation. However, it was considered a prudent alternative strategy to perform rehabilitation of all projects together on the basis of administrative decisions related to minimizing multiple traffic control operations within a short time. Therefore, design alternatives were prepared for all projects.

The rehabilitation of concrete pavements can be performed by using concrete pavement restoration (CPR), resurfacing (overlays), and reconstruction.

Because of extensive ASR-related deterioration, the CPR technique was not considered feasible. With respect to overlays and reconstruction both AC and PCC were considered equally acceptable construction materials. As part of the rehabilitation design process numerous overlay design procedures were reviewed and considered for use. In addition, some preliminary analyses were perfromed by using both the layer elastic method and the finite-element method of analysis. The reviews provided some preliminary guidance on possible overlay thicknesses and other design features to be considered. However, the final rehabilitation designs were based on the 1986 *Guide for Design of Pavement Structures* (*2*) and the June 1990 proposed *Revision of AASHTO Pavement Overlay Design Procedures* (*3*). Eight design strategies were evaluated for rehabilitation of each project, as applicable. These included

1. AC overlay,
2. Unbonded jointed plain concrete (JPC) overlay,
3. Unbonded CRC overlay,
4. Reconstruct with AC pavement,
5. Rubblize with AC overlay (JRC pavement sections only),
6. Reconstruct with JPC pavement,
7. Reconstruct with CRC pavement, and
8. Maintain the existing condition of the pavement.

A brief description of some of the key design parameters used for development of required pavement thicknesses is presented in the following section.

Design Period

For the AC overlay design an initial design period of 8 years was selected for analysis. For the new AC design and rubblize design an initial design period of 15 years was selected for analysis. For the new rigid design and rigid overlay design an initial design period of 20 years was selected for analysis.

Condition Factor

Revised (1990) AASHTO Overlay Design

The condition factor was selected on the basis of the level of the ASR and the number of existing and new repairs required in the pavement. A parametric study of required thickness was performed by selecting a maximum and minimum condition factor for design.

1986 AASHTO Overlay Design

The condition factor was selected on the basis of the visual condition of the pavement and the backcalculated "cracked" modulus of elasticity. A required thickness was determined for each condition factor.

Overlay Designs

Rigid and flexible overlay designs were based on the effective structural capacity of the existing pavement. For rigid pavements the effective structural capacity was defined as the effective concrete thickness and for flexible pavements as the effective structural number. Both of these values were determined on the basis of the original material characteristics and the existing condition factor as described in the AASHTO design guide (*3*).

New Construction Designs

The AC and rigid pavement designs and the design for the rubblized section were based on the expected ESAL loadings over a specified design period. The required AC design thicknesses including that for the rubblized section were determined from the 1986 AASHTO flexible design equation. The required concrete thickness was determined from the 1986 AASHTO rigid design equation.

Design Thicknesses

The overlay and pavement design thicknesses were calculated for each rehabilitation design for each project. A sensitivity analysis was also performed for each design alternative to identify the effect of the various design inputs. The final thicknesses were based on the results of the sensitivity study. It should be noted that the designs were for an initial design life, which varied on the basis of the rehabilitation design selected. In the life cycle cost analysis presented later, details are provided on the assumed future maintenance and rehabilitation needs for each rehabilitation strategy on the basis of a 40-year analysis period. A summary of future rehabilitation activities for each pavement type is listed in Table 3.

The computed pavement and overlay design thicknesses were critically reviewed in light of the various assumptions made for the input parameters. On the basis of this review it was determined that Projects A and B could be considered together because the rehabilitation design requirements were similar. Also, Projects C and D were found to require similar rehabilitation and were therefore considered together. The final selected design thicknesses are

TABLE 3 Estimated Key Construction and Maintenance Activities

Year	AC Overlay	PCC Overlay	JPC Recon	CRC Recon	AC Recon
0	Initial Construction	Initial Construction	Initial Construction	Initial Construction	Initial Construction
5		Clean & Seal 5% Trans, 25% Long	Clean & Seal 5% Trans, 25% Long	Clean & Seal Shoulder 5% Trans, 25% Long	
8	Mill 3 in., 3% Patch Replace 4 in., AC +1 in. FC				3% AC Patching, Mill 3 in., Replace 2 in., +1 in. FC
10		Clean & Seal 5% Trans, 25% Long	Clean & Seal 5% Trans, 25% Long	Clean & Seal Shoulder 5% Trans, 25% Long	
14					
15		Clean & Seal 10% Trans, 25% Long	Clean & Seal 10% Trans, 25% Long	Clean & Seal Shoulder 10% Trans 25% Long	
16	Mill 5 in., 3% Patch Replace 7 in., AC +1 in. FC				Mill 3 in., 3% Patch Replace 2 in., +1 in. FC
20	1% AC Patching	Clean & Seal; 100% Trans & Long; 1% Spall Repair; 5% PCC Patching; Grinding	Clean & Seal; 100% Trans & Long; 1% Spall Repair; 5% PCC Patching; Grinding	5% PCC Patching; Grinding	1% AC Patching
24	Mill 5 in., 3% Patching Replace 4 in., +1 in. FC				Mill 3 in., 3% Patching Replace 2 in., +1 in. FC
25		Clean & Seal 5% Trans, 25% Long	Clean & Seal 5% Trans, 25% Long	Clean & Seal Shoulder 5% Trans, 25% Long	
29					
30		.5% Spall Repair; 2.5% PCC Patching;4" AC Overlay, +1 in. FC	.5% Spall Repair; 2.5% PCC Patching;4" AC Overlay, +1 in. FC	.5% Spall Repair; 2.5% PCC Patching; 4 in. AC Overlay, +1 in. FC	
32	Mill 3 in., 3% Patching Replace 4 in., +1 in. FC				Mill 3 in., 3% Patching Replace 2 in., +1 in. FC
34		1% AC Patching	1% AC Patching	1% AC Patching	
38		Mill 3 in., 3% Patching Replace 2 in., +1 in. FC	Mill 3 in., 3% Patching Replace 2 in., +1 in. FC	Mill 3 in., 3% Patching Replace 2 in., +1 in. FC	

NOTE: FC = open graded friction course

summarized later for each design project. Portions between adjacent bridges within Projects A and B were too short to allow construction of either AC or PCC overlays. For these projects reconstruction was the only practical rehabilitation option.

Asphalt Concrete Overlay

Minimum AC overlay thicknesses were selected for each design project. This thickness was required to maintain a functional serviceability level over an initial design life of 8 years.

- Projects A and B: 50.8-mm (2-in.) Type "C" AC over 101.6-mm (4-in.) Type "B" AC;
- Projects C and D: 50.8-mm (2-in.) Type "C" AC over 152.4-mm (6-in.) Type "B" AC; a thinner overlay was specified at the Myrtle Avenue bridge overpass to allow for minimum clearance;
- Project E: 50.8-mm (2-in.) Type "C" AC over 76.2-mm (3-in.) Type "B" AC; and
- Project F: 50.8-mm (2-in.) Type "C" AC over 127-mm (5-in.) Type "B" AC; a thinner overlay was specified at the I-95 North bridge overpass to allow for minimum clearance.

Rigid Overlay (JPC and CRC Pavements)

Minimum concrete overlay thicknesses were selected for each design project. This thickness was required to maintain a functional serviceability level over an initial design life of 20 years. It was assumed that CPR activities at 20 years would provide an additional 10 years of acceptable level of serviceability before an overlay would be required.

For Projects A, B, C, D, and E, a 254-mm (10-in.) concrete overlay with tied-concrete shoulders over 38.1- to 50.8-mm (1.5- to 2-in.) Type "C" AC bond breaker is required. The thicknesses are applied to both JPC and CRC pavement, although the CRC pavement was not recommended for Project E.

It should be noted that, because of the need to maintain grade at bridge approaches and to maintain vertical clearances under

overpasses, it was considered necessary to require removal of sections of the existing CRC pavement at these locations and in effect reconstruct the pavement. This would require elimination of the terminal anchorages at bridge approaches and loss of continuity in the existing CRC pavement at critical overpasses.

It should also be noted that, although a 254-mm (10-in.) thickness was determined to be the minimum thickness for the PCC overlay, the use of thickness required for reconstructed PCC was considered appropriate for the concrete overlays. Thus, up to 304.8-mm (12-in.)-thick concrete overlay was considered an acceptable solution. The use of the larger thickness would provide significantly improved pavement performance with only a minimal increase in overall cost. Joint spacing of 4.6 m (15 ft) was recommended for the JPC pavement.

For I-295 ramps (Project F), a 228.6-mm (9-in.) concrete overlay over 38.1- to 50.8-mm (1.5- to 2-in.) Type "C" AC bond breaker is required.

New Asphalt Concrete Pavement

Minimum AC pavement thicknesses were selected for each design project. This thickness was required to maintain a functional serviceability level over a design life of 15 years. For all projects 101.6-mm (4 in.) of Type "C" AC over 279.4 mm (11 in.) of Type "B" AC is required.

New Concrete Pavement

Minimum concrete pavement thicknesses were selected for each design project. This thickness was required to maintain a functional serviceability level over an initial design life of 20 years. It was assumed that CPR activities at 20 years would provide an additional 10 years of acceptable level of serviceability before an overlay would be required. For all projects 304.8 mm (12 in.) of concrete pavement with tied-concrete shoulders is required. This thickness applied to JPC and CRC pavements, although the CRC pavement was not recommended for Projects E and F. A joint spacing of 4.6 m (15 ft) was recommended for the JPC pavement.

Rubblize with Asphalt Concrete Overlay

Minimum AC pavement thicknesses were selected for each design project. This thickness was required to maintain a functional serviceability level over a design life of 15 years. For all JRC pavement projects 2 in. of Type "C" AC over 6 in. of Type "B" AC is required. This rehabilitation method was recommended only for Project E and Project F (I-295 ramps). A thinner thickness was specified at the I-95 North overpasses to allow for minimum clearance.

Maintain Without Overlay or Reconstruction

Projects A and B exhibited very low to low-severity ASR and other distresses and therefore were not considered to require immediate structural rehabilitation. Under this rehabilitation design initial improvements would include only localized repairs. As noted previously structural rehabilitation could be delayed for at least 5 years.

LIFE CYCLE COST ANALYSIS

An economic analysis incorporating life cycle cost was performed to evaluate the feasibility of the various rehabilitation strategies. This analysis enabled selection of preferred design alternates on the basis of the cost of the rehabilitation over a specified analysis period. This was done because the benefit of a particular rehabilitation strategy solely on the basis of initial cost may often be misleading if future costs were not considered. For this study each rehabilitation type was evaluated for its respective life cycle costs over a 40-year analysis period.

A discount rate of 2 percent was used for the life cycle cost analysis. The discount rate is the difference between the interest rate and inflation rate. The difference between interest and inflation rates, that is, the discount rate, stays within a narrow range over the long term even if the individual rates may experience changes with time. For highway construction projects a discount rate of between 2 and 4 percent is typically used to estimate the present cost of future construction. On the basis of discussions with DelDOT staff a discount rate of 2 percent was selected for this analysis.

Life cycle costs were determined for each rehabilitation design for each design project. These analyses resulted in a set of life cycle cost values for each project. Several project rehabilitation strategies that incorporated one rehabilitation design and life cycle cost values from each design project were then developed. A total life cycle cost for each project rehabilitation strategy was determined. In the life cycle cost analysis the costs considered included initial cost, maintenance cost, rehabilitation cost, civil costs, and maintenance of traffic cost. No user costs were incorporated. User costs would be higher for strategies requiring more frequent maintenance and rehabilitation activities.

The format for establishing future maintenance activities was based on Chapter 2 of the Pennsylvania Department of Transportation's *Roadway Management Manual* (*4*). The AC overlay, AC reconstruction, and rubblize rehabilitation design strategies included AC patching at 4-year cycles. The concrete overlay and concrete reconstruction design strategies included cleaning and sealing of joints at 5-year cycles. The timing and thickness of future structural rehabilitation activities were based on fatigue life consumption as determined by the AASHTO rigid and flexible design equations.

The rehabilitation designs for each project were grouped to develop overall rehabilitation strategies for all projects. Twelve distinct strategies were identified and summarized in Table 4.

STUDY FINDINGS AND RECOMMENDATIONS

The primary objective of the study was to identify immediate pavement rehabilitation needs along I-495 and I-295 ramps. As noted previously the primary reason that there was a concern about the need for rehabilitation was that there was extensive ASR-related deterioration along projects of the study areas. As discussed previously Projects C, D, E, and F were in need of major rehabilitation, possibly within the next 3 years, to ensure that adequate levels of service were maintained along these projects.

TABLE 4 Summary of Rehabilitation Strategies

Rehabilitation Strategy	Project				Total LCC Cost, Millions $
	A & B	C & D	E	F	
I	Maintain Recon in 2000	AC Overlay	AC Overlay	AC Overlay	30.9
II	AC Overlay/PCC Recon	AC Overlay	AC Overlay	AC Overlay	30.9
III	Maintain Recon in 2000	PCC Overlay	PCC Overlay	PCC Overlay	33.8
IV	PCC Overlay/PCC Recon	PCC Overlay	PCC Overlay	PCC Overlay	33.5
V	Maintain Recon in 2000	AC Recon	AC Recon	AC Recon	36.2
VI	AC Recon	AC Recon	AC Recon	AC Recon	40.0
VII	PCC Recon	PCC Recon	PCC Recon	PCC Recon	39.9
VIII	Maintain Recon in 2000	PCC Recon	PCC Recon	PCC Recon	36.3
IX	Maintain Recon in 2000	1. AC Overlay 2. Reconstruct in 8 years with AC	1. AC Overlay 2. Reconstruct in 8 years with AC	1. AC Overlay 2. Reconstruct in 8 years with AC	38.4
X	1. AC Overlay/ PCC Reconstruct in 8 years 2. Reconstruct AC Overlays in 8 years	1. AC Overlay 2. Reconstruct in 8 years with AC	1. AC Overlay 2. Reconstruct in 8 years with AC	1. AC Overlay 2. Reconstruct in 8 years with AC	41.0
XI	1. AC Overlay/ PCC Reconstruct in 8 years 2. Reconstruct AC Overlays in 8 years	1. AC Overlay 2. Reconstruct in 8 years with PCC	1. AC Overlay 2. Reconstruct in 8 years with PCC	1. AC Overlay 2. Reconstruct in 8 years with PCC	39.8
XII	1. AC Overlay 2. PCC Reconstruct in 8 years	1. AC Overlay 2. PCC Reconstruct in 8 years	1. AC Overlay 2. PCC Reconstruct in 8 years	1. AC Overlay 2. PCC Reconstruct in 8 years	43.8

It should be noted that the I-495 pavements did provide a good ride, but this was primarily because of the CRC design of the pavement. In the northern portions of I-495 the good ride gave a false sense of security; actually the pavements were severely distressed and required constant attention to repair spalled concrete. An analysis of projected traffic data for I-495 indicates that traffic volumes were expected to grow at a high rate and truck traffic would continue to be a high percentage of the total traffic. In fact the projected traffic volumes indicated that an additional traffic lane would be needed soon.

Design Recommendations

In the evaluation of pavement rehabilitation alternatives several were studied. Pavement rehabilitation designs were prepared for the different sections of I-495 and for the ramps. Basically the I-495 roadway was divided into two sections: the northern portion (north of the Edgemore interchange) and the southern portion. The following were the primary design alternatives recommended:

1. AC overlay: 152.4-mm (6-in.) thickness for southern sections of I-495 and 203.2-mm (8-in.) thickness for northern sections of I-495;
2. Reconstruction with AC: 381-mm (15-in.) thickness;
3. Concrete overlay: 254-mm (10-in.) thickness but up to 304.8-mm (12-in.) thickness recommended; and
4. Reconstruction with concrete: 304.8-mm (12-in.) thickness.

Overlay Alternatives Compared with Reconstruction

The overlay strategies offer several important advantages over reconstruction strategies. These are listed below:

1. Overlay construction would require a shorter construction period.
2. No reconstruction of soil cement base or subbase would be required.
3. No drainage system changes would need to be made.

A major disadvantage of overlays was related to maintaining grade at bridge approaches and at overpasses (for vertical clearance). Removal of the existing CRC pavement would be required at these locations.

Asphalt Concrete Overlay Compared with Concrete Overlay

1. The AC overlay option would need more frequent traffic disruptions for future rehabilitation activities (normally resurfac-

ing was needed after about 8 years). In the case of I-495's northern sections it was possible that the pavement would need to be reconstructed after about 8 to 10 years if the ASR continued to deteriorate the existing CRC pavement.

2. The AC overlay would require extensive preoverlay repair of distressed areas.

3. The performance of a concrete overlay would not depend on the future condition of the existing CRC pavement.

4. The concrete overlay would provide 25 to 30 years of low-maintenance pavement before there would be a need for any rehabilitation activity.

SUMMARY

On the basis of the field investigation and the rehabilitation design evaluation the northern sections of I-495 and the associated ramps were recommended for rehabilitation soon, possibly within 3 years. The southern sections of I-495 were not considered in urgent need for rehabilitation, but if the ASR continued these sections would also need to be rehabilitated in the future, possibly within 5 years.

The northern portions of I-495 pavements were rehabilitated during 1993 with an unbonded concrete overlay. The overlay thickness selected by DelDOT was 304.8 mm (12 in.) to ensure a longer-lasting pavement with minimum maintenance needs over the first 20 to 25 years of service life. Also, a 3.7-m (12-ft)-wide tied concrete shoulder was constructed to serve as a travel lane in the future. The southern portions were rehabilitated in 1994.

ACKNOWLEDGMENTS

The study reported here was funded by the Delaware Department of Transportation. The support and cooperation provided by various units of the department are gratefully acknowledged.

REFERENCES

1. *Delaware Interstate Concrete Pavement Rehabilitation Study—Executive Summary.* Whitney, Bailey, Cox, and Magnani and Pavement Consultancy Services, Inc., May 1987.
2. *Guide for the Design of Pavement Structures.* AASHTO, Washington, D.C., 1986.
3. Proposed Revisions to Chapter 5 of the AASHTO Guide for the Design of Pavement Structures. Draft version. AASHTO, Washington, D.C., Dec. 1991.
4. *Roadway Management Manual.* Publication 242. Bureau of Bridge and Roadway Technology, Pennsylvania Department of Transportation, July 1989.

The views and opinions expressed in this paper are those of the authors.

Publication of this paper sponsored by Committee on Rigid Pavement Design.

Performance of Unbonded Concrete Overlay Project in Canada

T. J. KAZMIEROWSKI AND HARRY STURM

The rehabilitation of concrete freeways has challenged highway authorities for many years. This challenge has been met with the use of various techniques such as full- and partial-depth repairs, diamond grinding, and unbonded overlays. In 1989 the Ontario Ministry of Transportation constructed a project to demonstrate the feasibility of using these techniques on the freeways in its jurisdiction and to monitor the long-term performance of the freeways rehabilitated by these various techniques. The project incorporated the use of full-depth and partial-depth repairs, which was followed by diamond grinding and joint sealant replacement on the northbound lanes. The southbound lanes received a 180-mm-thick undoweled plain-jointed unbonded portland concrete cement overlay, which is the focus of this study. Design of the overlay was undertaken by using PCA design guides, which used the familiar Corps of Engineers square root equation. During the design phase falling-weight deflectometer (FWD) testing was undertaken to assess the pavement condition. Following construction an extensive program was implemented to systematically monitor long-term performance. The program included FWD testing for corner-to-center deflection ratios and joint load transfer efficiencies, along with roughness and skid resistance testing and condition surveys. Roughness and skid resistance measurements have been completed on an annual basis, with FWD testing and condition surveys carried out as needed. The design and construction of the unbonded overlay are highlighted, and the results of the performance monitoring program carried out on this 4-year-old project are detailed.

The rehabilitation of concrete pavements has undergone significant development in recent history and has provided options that were previously not realized. One such technique is the use of unbonded concrete overlays. Construction of a concrete overlay is not significantly different from that of conventional concrete pavements; however, design of these structures has not been as thoroughly researched as conventional designs.

The project described here was initiated to assess the feasibility of constructing a concrete overlay and to monitor the long-term performance of such a design in the wet-freeze environment of Ontario, Canada.

BACKGROUND

Highway 126, now Highbury Avenue following transfer to the city of London, is approximately 200 km west of Toronto. The road is a 4-lane divided arterial, with volumes ranging from 22,000 to 30,000 average annual daily traffic in 1992, of which 3,000 are commercial vehicles.

T. J. Kazmierowski, Pavement Design, Evaluation and Management Section, Ministry of Transportation of Ontario, 1201 Wilson Avenue, Downsview, Ontario M3M 1J8, Canada. H. Sturm, Ontario Region, Canadian Portland Cement Association, 1500 Don Mills Road, Suite 501, Toronto, Ontario M3B 3K4, Canada.

The original pavement was constructed in 1963 with 225 mm of mesh-reinforced portland concrete cement (PCC) on 300 mm of granular base and subbase materials placed full width. The pavement was constructed with a 21.3-m joint spacing and load transfer dowel bars. The joints were sealed with preformed neoprene seals. The pavement on the southbound lanes (SBLs) showed significant distress, with full- and partial-width transverse cracks in each slab, severe D-cracking, spalling of all joints throughout, and moderate pavement edge distress. Deterioration had advanced to the stage in which routine maintenance activities could no longer preserve a safe riding service.

The northbound lanes (NBLs) were in much better condition and as such were rehabilitated by using full- and partial-depth concrete repairs and diamond grinding.

The variation in pavement performance was attributed to the two types of aggregate used in the concrete for the opposing lanes. The quarried aggregate used on the SBLs exhibited absorptive characteristics and was highly susceptible to D-cracking under freeze/thaw conditions. A pit run gravel source was used for the coarse aggregate on the NBLs.

Three rehabilitation strategies were considered for use on the SBLs and included crack and seat with an asphalt overlay, repair of the PCC pavement with hot mix and placement of a multiple-lift asphalt overlay, and overlay with concrete. Because of the extensive deterioration of the concrete on the SBLs it was believed that the unbonded concrete overlay would provide the highest level of long-term performance and would provide the opportunity to assess this type of rehabilitation technique.

DESIGN

The thickness design of the overlay was completed by using PCA guidelines, which used the Corps of Engineers square root equation. This formula requires the user to determine the thickness of a single slab, from which the existing pavement thickness is deducted after correcting for the condition and deterioration. In this case it was determined that a slab thickness of between 220 and 240 mm would be required in an initial design. By using an existing pavement condition coefficient of 0.35 for badly cracked pavements, the existing slab was deducted to arrive at an overlay thickness of 180 to 200 mm. An overlay thickness of 180 mm was selected. The selection of a condition coefficient has a significant influence on the overlay thickness. By using a condition coefficient for a pavement with corner cracking as the major distress, an overlay thickness of 115 mm is required; if an intermediate value of 0.55 is input an overlay thickness of 160 mm is estimated. This indicates that selection of this coefficient is critical in determining the overlay thickness. Correlation of the coefficient

with nondestructive test [falling-weight deflectometer (FWD)] information as well as visual data would be of value for future designs.

The design included a bond breaker of compacted asphaltic sand hot mix with a maximum aggregate size of 4.75 mm. This was placed to prevent bonding between the new and old PCC pavements and minimize reflection cracking in the overlay. Other design features were the use of undoweled skewed randomized joints, short slab lengths, a burlap drag/tined surface texture, and improved joint sealing procedures. Typical lane widths were 3.65 m for a total width of 7.3 m in the two lane sections. Tie bars were specified in the longitudinal joints. The 7.3-m-wide overlay typically matched the width of the underlying concrete pavement.

The addition of partial-width concrete shoulders was evaluated during design; however, the decision was made not to incorporate them. One reason for this decision was the underlying rigid nonerodible base, which would provide significant edge support and minimize the risk of long-term faulting. It was concluded that performance would be adequate without concrete shoulders, and the additional expense could not be justified. Typical sections and other design details have been provided previously (*1*).

Drainage of the existing and proposed pavement structure was evaluated, and investigations indicated that the existing full-width granular materials were providing adequate drainage. This was further substantiated by the absence of any joint or crack faulting or staining. On the basis of this assessment no retrofitted drainage measures were incorporated into the rehabilitation design.

CONSTRUCTION

Before placement of the concrete overlay, loosely spalled materials were removed by hand from the existing badly cracked pavement. The spalled areas (427 m^2) were then patched with conventional hot mix, and a compacted 20-mm asphaltic sand mix bond breaker (884 metric tons) was placed over the existing pavement surface. Following placement of the bond breaker, the 180-mm-thick unreinforced plain-jointed concrete pavement (38,200 m^2) was placed. This was the first concrete highway pavement to be placed in Ontario since 1982. Slipforming of the unbonded overlay was carried out by using Ontario's revised specifications and drawings for concrete pavement. The revisions were based on experience gained on the experimental concrete pavement sections on Highway 3N (*2,3*).

Construction of the unbonded concrete overlay went smoothly following a few initial breakdowns with the slip-form paver. The two lanes were slipformed simultaneously, with longitudinal tie bars being inserted every 600 mm on the center line. The plastic concrete surface was dragged longitudinally with a burlap mat and tined transversely to achieve the specified surface texture. Speed change lanes were then slipformed and tied onto the outside of the core lanes when required.

Skewed joints were sawcut into the overlay at random intervals that varied from 3.7 to 5.8 m. No uncontrolled transverse cracking of the pavement occurred with revision of the specification to require sawcutting within 12 hr after placement rather than the 24 hr specified previously. No effort was made to match or avoid matching the original pavement joints.

The pavement ride was somewhat better than that in the previous slipforming project, which was in part because of a requirement for stringline control on both sides of the slip-form paver. Pavement ride is discussed in further detail in the following section.

PAVEMENT PERFORMANCE

Roughness Measurements

The motoring public is generally most concerned with the ride of a pavement; therefore, monitoring of ride condition or roughness was initiated. Roughness was measured just after construction and before opening to traffic and has been measured yearly since construction. The California profilograph was used immediately after construction, and the portable universal roughness device (PURD) was used for ongoing monitoring.

The profilograph measurements were taken on the new concrete overlay, with readings taken in both wheelpaths of the driving and passing lanes. The average profilograph reading, the profile index, for the length of the project was 11.1 in./mi in the driving lane and 10.7 in./mi in the passing lane. These readings were taken before diamond grinding at 21 locations where the roadway did not meet the surface tolerance specifications of 3 mm in 3 m. These values compare reasonably well with the numbers obtained by other authorities constructing considerably larger quantities of concrete pavement. Postgrinding profilograph measurements were not completed because a ride specification was not being used at the time.

Ongoing postconstruction roughness measurements have been completed by using the PURD, a trailer-mounted, accelerometer-based, response-type device. It is operated at constant highway speed and uses the root mean square vertical acceleration, in mil*lig*'s, of the trailer axle to measure roughness. PURD measurements are converted into a ride comfort rating (RCR) by using a transfer function for application in Ontario's Pavement Management system. RCR is based on a scale from 0 to 10, with 10 being a smooth and pleasant ride.

An RCR level of 7.7 to 7.8 for the driving and passing lanes, respectively, was achieved following construction, which is only slightly rougher than generally attained on a new asphalt surface. Since construction the ride values have shown little change and are now at 7.5 and 7.7 for the driving and passing lanes, respectively (see Figure 1 for details). This is a relatively small change over 4 years and would appear to point to acceptable short-term performance.

Load Response Characteristics

A nondestructive load testing program was set up to evaluate the condition of the pavement before rehabilitation and to assess long-term performance of the project. Before rehabilitation slabs were randomly selected for testing of corner-to-center slab deflection ratio and load transfer efficiency across joints. This information was used in the design to determine the presence of voids beneath the slabs and to establish the need for stabilization of the joints.

Deflection testing was completed by using the Dynatest 8000 FWD. Most testing was performed early in the day to minimize the influence of slab curl resulting from differential slab temperatures.

After rehabilitation deflection testing was undertaken at the same locations or at the nearest point to the preconstruction test-

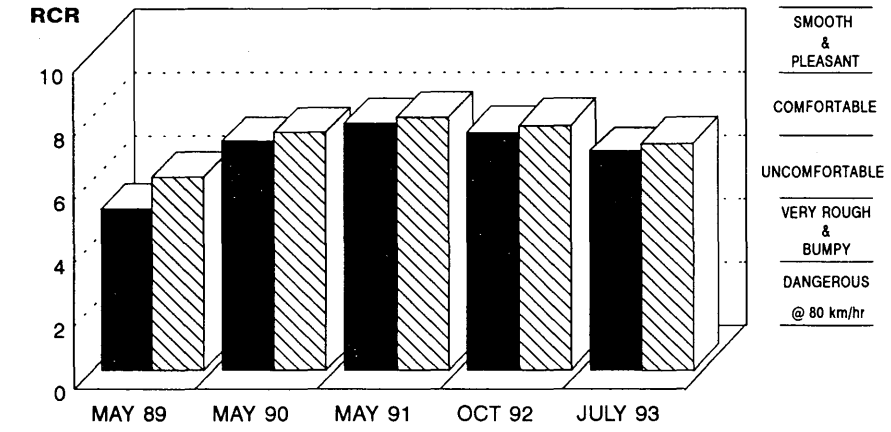

	MAY 89	MAY 90	MAY 91	OCT 92	JULY 93
SDL	5.1	7.7	7.9	7.8	7.5
SPL	6.1	7.8	8	7.9	7.7

FIGURE 1 Summary of PURD roughness survey.

ing. Testing was again undertaken in the summers of 1992 and 1993 to evaluate performance of the overlay. Postconstruction deflection testing yielded some significant improvements in corner-to-center deflection ratios and a slight improvement in load transfer efficiencies over the original pavement as noted previously (*4*). Data from the 4-year monitoring program have complemented information from the more limited program completed in year 3 and substantiates the visual performance of the pavement.

The load transfer results showed very high values, with mean values in the 95 to 97 percent range (Figure 2). The range of values has remained constant after exposure to traffic. The old concrete pavement, which is functioning as a base for the overlay, appears to be providing necessary support for the undoweled joints that have not lost aggregate interlock. In similar pavements constructed on lean concrete bases on the Highway 3N test project (*5*), load transfer efficiencies had generally fallen to below 60 percent after 3 years of service. In a thicker (300-mm) section built on subgrade, the load transfer had fallen to 80 percent.

The resulting increase in pavement strength after overlay placement was also affirmed by the corner-to-center deflection ratios, with mean values of 1.8 and 1.3 in the driving and passing lanes, respectively (Figure 3). These are low values and would indicate that the overlay has a high level of stiffness and is well seated on the underlying concrete base. The high load transfer efficiencies also contribute to the stiffness of the slab and ensure low deflection ratios. Performance numbers achieved on this project are similar to the center edge deflection ratios measured on 200- to 325-mm continuously reinforced concrete pavements constructed

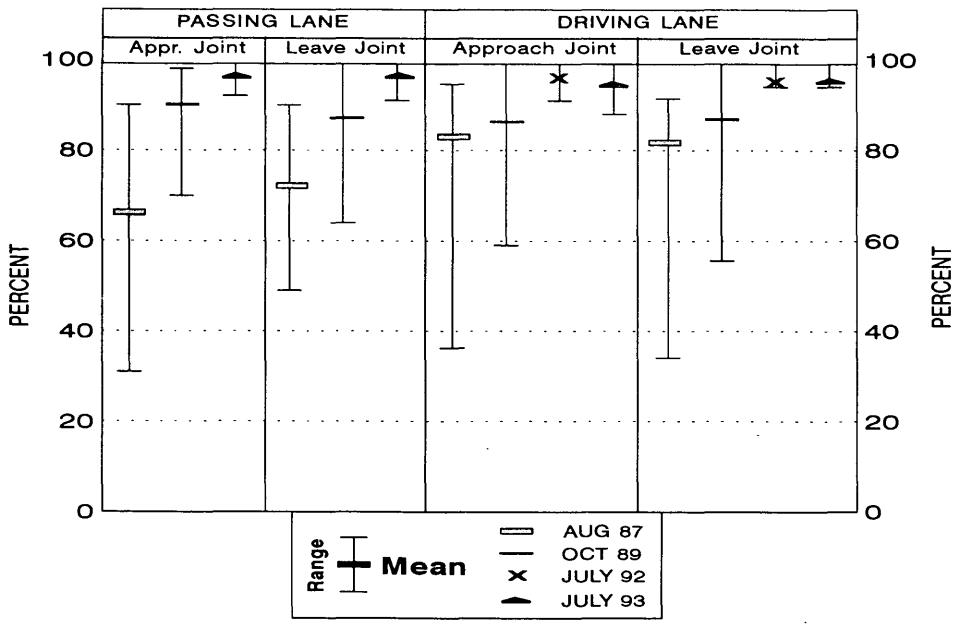

FIGURE 2 Load transfer results.

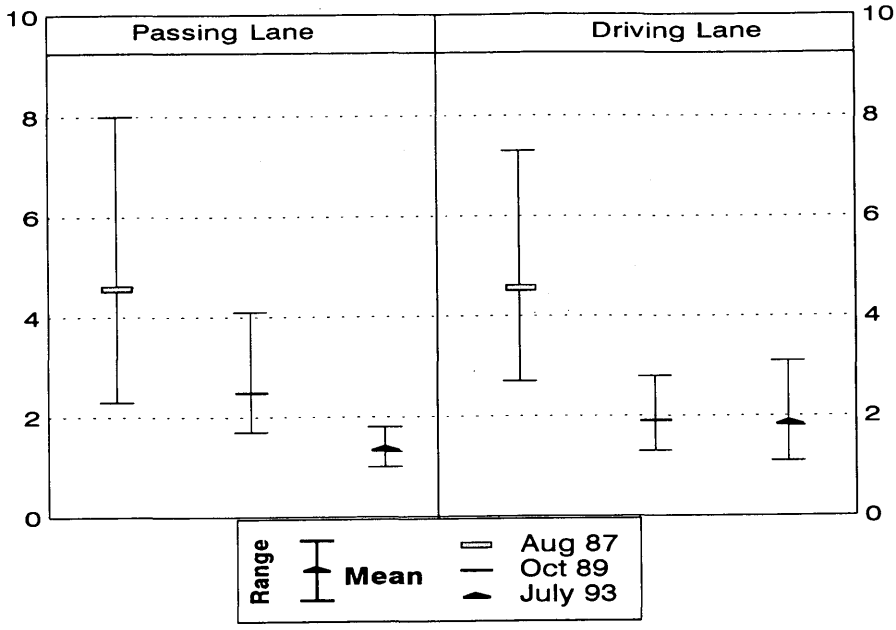

FIGURE 3 Corner-to-center deflection ratios.

in Texas (*6*). Center-to-edge deflection ratios ranged from 1.2 to 1.8 for asphalt shoulder sections in that project.

In 1993 center deflection measurements yielded mean values in the range of 0.03 and 0.05 mm for the driving and passing lanes, respectively. These values again indicate a very stiff and stable slab and compare favorably with numbers on the order of 0.04 to 0.05 for other concrete pavements of a similar age that are generally equal in effective thickness. These center deflection values have not changed significantly from the postconstruction mean values of 0.04 for both lanes in 1989.

Pavement Distress Survey

The visible distresses in the pavement surface were surveyed to provide an overall indication of performance. Generally a high level of performance has been maintained with the unbonded overlay. The only distress observed is very slight longitudinal cracking in 11 driving lane slabs. This cracking can probably be attributed to inadequate longitudinal joint construction because the cracks were visible soon after construction. One of the cracked slabs is now beginning to exhibit more severe distress in the form of spalling along the crack face where it crosses the right wheelpath.

No transverse or reflection cracking was observed, which correlates with the experiences of other agencies (*7*). Some transverse cracking is anticipated in the future because the longest slabs in the randomized pattern are 5.5 and 5.8 m, which are somewhat longer than the recommended maximum of 4.6 m. No faulting of joints has been observed to date.

Skid Testing

Skid resistance was measured by using the skid trailer conforming to ASTM Standard E274. The measured friction force is described as a skid number (SN) at a specific speed; for example SN 80 is the skid number at 80 km/hr.

Results of skid resistance testing are detailed in Figure 4. The test results indicate a substantial increase in skid resistance immediately after rehabilitation, as one would expect. The skid numbers in the SBLs increased to an average SN 80 of 54 for both lanes from SN 80 values of 18 and 21 in the driving and passing lanes before rehabilitation, respectively. Skid numbers of this magnitude indicate a good friction factor and are similar to numbers obtained on premium hot-mix surface courses (*8*).

As anticipated, after the first year the initial sharp projections of the drag/tined surface have been worn, polished, or sheared off by traffic and snow removal operations. This elimination of sharp projections reduced SN 80 values from values in the mid-50s to the values in the mid-30s for the driving lane and low 40s for the passing lane. On the basis of previous experience this trend was anticipated. However, it would appear that skid resistance levels have stabilized at these acceptable levels for the present time.

CONCLUSIONS

The 4-year performance review of this unbonded concrete overlay project warrants the following general conclusions.

1. Initial pavement roughness was somewhat better than that experienced on previously constructed concrete pavements in Ontario. Subsequent PURD readings indicate that an acceptable level of ride is being maintained.
2. Load deflection testing verifies the substantial increase in pavement section strength with low deflections and high load transfer efficiencies across all joints.
3. The distress surveys have indicated no cracking other than the few slight longitudinal cracks observed immediately after construction. No transverse cracking has been observed in the longer 5.5- and 5.8-m slabs.

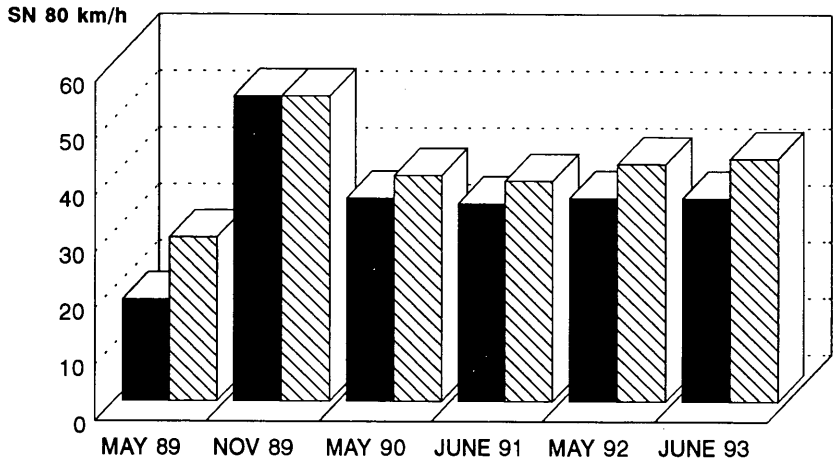

SDL ■	18	54	36	35	36	36
SPL ▨	29	54	40	39	42	43

FIGURE 4 Summary of skid survey.

4. Skid resistance has stabilized at an acceptable level and is displaying performance similar to other exposed concrete pavement surfaces in Canada.

5. Overall the 4-year results indicate that a high level of performance has been maintained. Mid- to long-term performance results will continue to be monitored. The short-term results support the adequacy of the design procedure used.

REFERENCES

1. Kazmierowski, T. J., and H. J. Sturm. Concrete Pavement Rehabilitation and Overlay: Ontario's Experience. *70th Annual Meeting, 1991.* In *Transportation Research Record 1307*, TRB, National Research Council, Washington, D.C., 1991.
2. Kazmierowski, T. J., and G. A. Wrong. Six Years Experience with Experimental Concrete Pavement Sections in Ontario. *Proc., 4th International Conference on Concrete Pavement Design and Rehabilitation*, Purdue University, West Lafayette, Ind., 1989.
3. Chojnacki, B. *Development of Special Provisions for the Acceptance of Lean Concrete Base and Concrete Pavement.* Report M-76. Ministry of Transportation of Ontario.
4. Kazmierowski, T. J., and H. J. Sturm. Performance of Ontario's First Major Rehabilitation and Overlay Project. *Proc., 5th International Conference on Concrete Pavement Design and Rehabilitation*, Purdue University, West Lafayette, Ind., 1993.
5. Kazmierowski, T. J., and A. Bradbury. Ten Years Experience with Experimental Pavement Sections in Ontario. *Proc., 5th International Conference on Concrete Pavement Design and Rehabilitation*, Purdue University, West Lafayette, Ind., 1993.
6. McCullough, B. F., and E. D. Moody. Development of Load Transfer Coefficients for Use with the AASHTO Guide Based on Field Measurements. *Proc., 5th International Conference on Concrete Pavement Design and Rehabilitation*, Purdue University, West Lafayette, Ind., 1993.
7. Hall, K. T., M. I. Darter, and R. P. Elliott. Revision of AASHTO Pavement Overlay Design Procedures. Presented at 71st Annual Meeting of the Transportation Research Board, Washington, D.C., 1992.
8. Ryell, J., J. T. Corkill, and G. R. Musgrove. *Skid Resistance of Bituminous Pavement Test Sections—Highway 401, Toronto Bypass.* Report IR67. Ministry of Transportation of Ontario, 1978.

Publication of this paper sponsored by Committee on Rigid Pavement Design.

Structural Analysis of Unbonded Concrete Overlays Under Wheel and Environmental Loads

LEV KHAZANOVICH AND ANASTASIOS M. IOANNIDES

At present it is common to treat an overlaid concrete pavement system as a multilayered Kirchhoff plate. A number of finite-element computer programs use this idealization, which assumes that the original slab and the overlay have the same deflection profile, that is, that the two act as an effective, homogeneous plate. Environmental loads, however, are among the most significant factors, making the assumption of equality of the deflection profiles of slab and overlay unacceptable. A formulation proposed by Totsky is implemented into an existing finite-element program to account for the effects of layer separation and compressibility. The effects of combined traffic loading and temperature differentials on the stresses and deflections in the pavement system when the overlay curls away from the existing slab are examined. The product is a finite-element code, abbreviated ILSL2, which represents an extension of the ILLI-SLAB program. Practical illustrative examples of the use of ILSL2 pertaining to typical pavements are presented. When appropriate these results are compared with existing analytical or numerical solutions, including those obtained by using an earlier version of ILLI-SLAB. It was found that both layer compressibility and separation effects need to be accommodated in a reliable mechanistic model for unbonded concrete overlays. If these effects are neglected, significant errors may result.

Structural analysis of portland cement concrete (PCC) overlays is a complex engineering problem. A valid mechanistic model should accommodate the overlaid pavement as a multilayered system subjected to traffic and environmental loads. The model should also take into account pavement joints, which may be mismatched between layers, as well as the possibility of through-the-thickness compression and layer separation. At present it is common to treat a concrete pavement slab overlaid with a PCC or an asphalt concrete overlay as a multilayered Kirchhoff plate. A number of finite-element computer programs use this idealization, which assumes that the original PCC slab and the overlay have the same deflection profile, that is, that the two act as an effective, homogeneous plate.

In a previous paper (*1*) an attempt was made to eliminate one of the plate theory assumptions, namely the requirement of incompressibility for both placed layers (i.e., slab and base or overlay). The authors considered, however, only the case of applied wheel load without environmental loading, such as temperature curling and moisture warping. Environmental loads are among the most significant factors making the assumption of equality of the deflection profiles of slab and overlay unacceptable. This problem has been raised by several investigators (*2,3*). This paper presents a finite-element formulation that accommodates the effects of layer compressibility and the potential for layer separation in concrete pavement systems incorporating two placed layers, for example, slab and overlay or slab and stabilized base. The proposed methodology is well-suited for analysis of partial separation of unbonded PCC overlays.

Department of Civil Engineering, University of Illinois at Urbana-Champaign, 205 North Mathews Avenue, #2230C, Urbana, Ill. 61801.

MECHANICAL MODEL FOR MULTILAYERED CONCRETE PAVEMENTS

The finite-element formulation presented is based on an interesting suggestion first made by Totsky (*4*). This treats a multilayered pavement system resting on a Winkler foundation as a series of alternating plate elements and springs. The plate elements model the bending, whereas the springs accommodate the direct compression occurring in such a system. The contact pressure, q, between two consecutive plates is related to the relative deflection of the two plates, $(\Delta_j - \Delta_{j+1})$, through

$$q = k_I(\Delta_j - \Delta_{j+1}) \tag{1}$$

in which k_I denotes the interlayer spring stiffness.

In the study described here a practical approach has been developed for calculating the interlayer spring stiffness. The following assumptions are made:

1. Compression through the thickness of each placed layer remains independent of the respective bending deformations.
2. Compression of the layers causes only vertical deflections $w(x,y,z)$. Thus, horizontal deflections, $u(x,y,z)$ and $v(x,y,z)$, and therefore horizontal strains, $\epsilon_{xx}(x,y,z)$ and $\epsilon_{yy}(x,y,z)$, are set equal to zero.
3. Vertical strains, $\epsilon_{zz}(x,y)$, are constant (or zero) between any layer surface and the corresponding neutral axis, but they can be different between layers as well as between the upper and lower portions of the same layer. For the case of unbonded PCC overlays it is reasonable to assume in addition that $\epsilon_{zz}(x,y)$ is nonzero only between the two neutral axes.

Denoting the structural characteristics of the upper and lower placed layers by Subscripts 1 and 2, the difference between the vertical deflections of the neutral axis of the upper layer and its bottom surface, $\Delta_1(x,y)$, may be written as

$$\Delta_1(x,y) = \epsilon_{zz1}(x,y)\frac{h_1}{2} = \frac{q(x,y)}{E_1}\frac{(1 - \mu_1 - 2\mu_1^2)}{(1 - \mu_1)}\frac{h_1}{2} \tag{2}$$

where

$\epsilon_{zz1}(x,y)$ = constant value assigned to the vertical strain between the neutral axis of the upper layer and its bottom surface,
$q(x,y)$ = contact pressure arising between the upper and lower layers, and
h_1 = upper layer thickness.

Equation 2 may be rewritten in the form

$$q(x,y) = k_1\Delta_1(x,y) \tag{3}$$

where

$$k_1 = \frac{2E_1(1 - \mu_1)}{h_1(1 - \mu_1 - 2\mu_1^2)} \tag{4}$$

Similarly, for the lower slab

$$q(x,y) = k_2\Delta_2(x,y) \tag{5}$$

where

$$k_2 = \frac{2E_2(1 - \mu_2)}{h_2(1 - \mu_2 - 2\mu_2^2)} \tag{6}$$

and $\Delta_2(x,y)$ is the corresponding difference between the vertical deflections of the neutral axis of the lower layer and its top surface. Accordingly, k_l in Equation 1 can be determined from

$$k_l = \frac{1}{\frac{1}{k_1} + \frac{1}{k_2}} \tag{7}$$

Parameter k_l can be interpreted as an effective stiffness for two springs in series with stiffnesses k_1 and k_2.

This approach for determining k_l can be adapted to accommodate a bituminous interlayer, which is often placed on top of an existing pavement slab before constructing a PCC overlay, for the purpose of providing a leveling course and arresting reflective cracking. Because the eleastic modulus of such a bituminous interlayer, E_b, is much lower than that of either PCC layer, it may be expected that the interlayer will act as a bed of springs whose stiffness, k_b, can be defined as follows:

$$k_b = \frac{2E_b(1 - \mu_b)}{h_b(1 - \mu_b - 2\mu_b^2)} \tag{8}$$

Here h_b and μ_b are the thickness and Poisson's ratio, respectively, for the bituminous interlayer. In this case Parameter k_l in Equation 1 can be considered as an effective stiffness for three springs in series, where

$$k_l = \frac{1}{\frac{1}{k_1} + \frac{1}{k_2} + \frac{1}{k_b}} \tag{9}$$

with k_1 and k_2 given by Equations 4 and 6, respectively.

FINITE-ELEMENT IMPLEMENTATION

Implementation of Totsky's approach in a finite-element code requires the introduction of a special eight-noded (24 degree-of-freedom) element (Figure 1). The first four nodes are placed at the neutral axis of the upper plate, whereas the other four nodes are placed at the neutral axis of the lower plate. The stiffness matrix for this element is

$$[K] = \begin{bmatrix} [K_{PL1}] + [K_{KDI}] & -[K_{DLI}] \\ -[K_{DLI}] & [K_{DLI}] + [K_{PL2}] + [K_{DLS}] \end{bmatrix} \tag{10}$$

where

$[K_{PL1}]$ and $[K_{PL2}]$ = stiffness matrices for the upper and lower plates, respectively;
$[K_{DKI}]$ = stiffness matrix for the interlayer springs; and
$[K_{DLS}]$ = stiffness matrix for the dense liquid (DL) subgrade.

The stiffness matrix in Equation 10 has been incorporated into the library of elements of computer program ILLI-SLAB (1989 version) (*5*). The resulting extended version of the code is abbreviated here as ILSL2. In view of the potential for separation under temperature loading, the proposed formulation in ILSL2 assumes for simplicity that the stiffness matrices for both the spring interlayer and the subgrade are dependent only on nodal deflections and not on modal rotations. The interlayer stiffness k_l may be specified by the user. Alternatively, the program will calculate it from the plate parameters by using Equation 7.

The following iterative scheme is adopted in ILSL2 for analyzing an unbonded three-layer system with applied external and temperature loads.

1. Formulate individually the stiffness matrices for the two plates, the spring interlayer, and the subgrade.
2. Combine these matrices as indicated by Equation 10 to form the global stiffness matrix.
3. Formulate individually the load vectors for the external applied load (upper plate), the self-weight (both plates), and the tem-

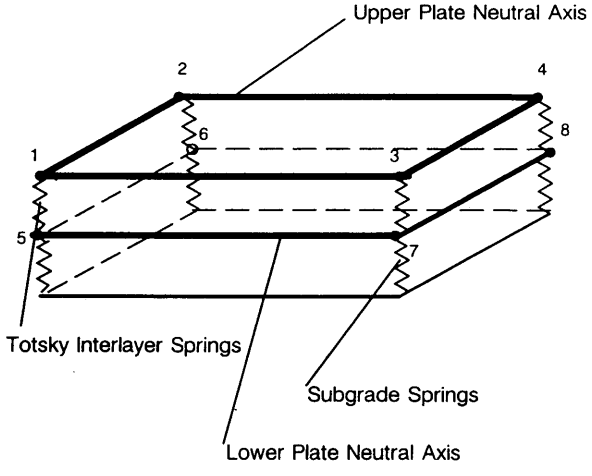

FIGURE 1 Finite-element idealization for two plates with Totsky interlayer springs resting on dense liquid foundation.

perature differentials (both plates) (*6*). In this paper a positive temperature differential, ΔT, indicates that the top surface is warmer than the bottom surface.

4. Combine these load vectors into the corresponding global load vector.

5. Solve the resulting system of equations to determine the nodal deflections and rotations.

6. Check the vertical deflection at each node to determine whether contact is maintained along the two interfaces, that is, between the upper and lower plates and between the lower plate and the subgrade.

7. If the deflection of the lower plate is negative (upward) contact with the subgrade has been lost. Therefore, set the corresponding subgrade spring equal to zero.

8. Similarly, if the difference in deflections at corresponding nodes in the two plates is negative, then the two plates are no longer in contact. In this case set the corresponding interlayer spring equal to zero.

9. Return to Step 1 and perform another iteration, continuing the process until the contact condition at all nodes remains unchanged during two consecutive iterations.

VERIFICATION OF PROPOSED FINITE-ELEMENT FORMULATION

Two series of finite-element runs detailed elsewhere (*7*) have verified that for certain special cases Totsky's approach implemented in ILSL2 gives the same results as the earlier ILLI-SLAB (1989 version) code, as expected. In addition, these runs have shown that for inputs close to these special points ILSL2 solutions are reasonably different and exhibit no abrupt jumps. For example, decreasing the flexural stiffness of the lower placed layer (e.g., the existing slab) leads to a reduction in its influence on the deformation of the upper placed layer (e.g., the overlay slab). In the limit, as the thickness of the lower layer tends to zero, subgrade and interlayer work together as a springs-in-series foundation, whose effective stiffness, k_e, is given by

$$k_e = \frac{1}{\frac{1}{k_I} + \frac{1}{k}} \tag{11}$$

On the other hand, increasing the flexural stiffness of the lower layer results in greater resistance to the bending offered by this layer. Consequently, the deflection profile of the lower layer becomes flatter, and in the limit this layer experiences only a rigid body motion because of the compressibility of the subgrade and the self-weight of the upper layer. At that extreme the lower layer acts like a rigid (no bending) base for the upper layer and the interlayer, and the subgrade adds a constant increment to the deflection of the upper layer at all points.

In addition, ILSL2 runs show that when the interlayer spring stiffness k_I is very high ($k_I \approx 2.71 \times 10^6$ to 2.71×10^8 MPa/m, or 10^7 to 10^9 psi/in.), the bending stresses at the bottom of both the upper and lower layers are practically identical to those calculated by using the earlier version of ILLI-SLAB or using the DL "closed-form" plate theory method proposed by Ioannides et al. (*1*). The latter method employs Westergaard's well-known equation (*8*), into which an equivalent plate thickness is introduced. In all cases the two placed layers were assumed to be unbonded. Such close agreement is to be expected, because very high k_I values denote that neither placed layer experiences compression through its thickness, in accordance with plate theory. It was also observed that as k_I decreases the bending stress in the upper layer increases quite significantly, whereas the corresponding stress in the lower layer decreases, albeit much less dramatically. Both stresses are particularly sensitive to the value of k_I if the latter drops below 2.71×10^5 MPa/m (10^6 psi/in.). The proposed Equation 7 yields a k_I value of 9.97×10^4 MPa/m (3.673×10^5 psi/in.), at which value both stresses are significantly different from those predicted by conventional plate theory applications.

From these observations it can be concluded that Totsky's approach provides a useful enhancement of conventional finite-element analysis of concrete pavements and can be used to account for through-the-thickness compressibility neglected in conventional plate theory applications. Good agreement with available numerical and analytical solutions verifies the robustness of the finite-element formulation introduced in this paper.

PRACTICAL EXAMPLES

To investigate the effects of separation between an existing slab (SL) and its overlay (OL) and of the compressibilities of these two placed pavement layers, a typical airport pavement loaded with a Boeing 727 (B-727) aircraft at the edge or corner was considered. Results are presented in Tables 1 to 3. The thicknesses of SL and OL were 406 mm (16 in.) and 178 mm (7 in.), respectively. The modulus of the subgrade reaction was assumed to be 54 MPa/m (200 psi/in.), whereas the stiffness of the interlayer springs, calculated according to Equation 7, was set equal to 9.97×10^4 MPa/m (3.673×10^5 psi/in.). Linear temperature variations, which could be different through the thicknesses of SL and OL, were also imposed. All pavement system parameters employed are given in Table 1. Several runs were conducted, in which the temperature gradient ($\Delta T_j/h_j$) in the overlay, g_{OL}, and in the existing slab, g_{SL}, was varied. Differences between the results from ILLI-SLAB and ILSL2 were also examined.

Edge Loading

For conventional analysis of airport pavements, edge loading is considered critical. To study this type of loading, a series of nine runs was performed, as shown in Table 1. A rather broad range of temperature gradients was assumed here to highlight temperature loading effects and to permit inferences with respect to the consequences of less severe conditions. Table 1 shows the magnitude of maximum tensile bending stresses arising at the top and bottom of OL and SL, σ_{OL}, σ_{OLb}, σ_{SL}, and σ_{SLb}, respectively. Results obtained indicate that maximum tensile bottom stresses occur under the load, whereas maximum tensile top stresses occur at some radial offset from the load, typically on the order of 1.8 to 2.4 m (6 to 8 ft).

A detailed examination of the stresses in Table 1 can begin with the baseline case of no-curling conditions for both OL and SL (i.e., $g_{OL} = g_{SL} = 0$). For this case a qualitative coincidence of results from ILSL2 and ILLI-SLAB is noted. Both codes show that the maximum tensile top and bottom stresses in SL exceed those in OL. Furthermore, the maximum tensile bottom stresses

TABLE 1 MPa Under Edge Loading with B-727

g_{OL}	g_{SL}	σ_{OLt}		σ_{OLb}		σ_{SLt}		σ_{SLb}	
(°C/cm)		ILSL2	ILLI-SLAB	ILSL2	ILLI-SLAB	ILSL2	ILLI-SLAB	ILSL2	ILLI-SLAB
-0.66	-0.66	1.05	1.05	1.40	0.72	2.41	2.41	1.54	1.66
0.00	-0.66	0.21	0.	2.88	2.32	2.65	1.97	1.33	1.41
+0.66	-0.66	0.72	0.	5.35	3.92	2.96	2.90	1.12	1.17
-0.66	0.00	2.14	2.15	1.29	0.	1.01	1.02	2.87	3.14
0.00	0.00	0.53	0.53	1.98	1.31	1.21	1.21	2.86	2.99
+0.66	0.00	0.21	0.	3.50	2.94	1.41	1.41	2.76	2.84
-0.66	+0.66	3.50	3.47	2.12	0.	0.58	0.13	4.72	5.05
0.00	+0.66	1.94	1.90	1.90	0.42	0.44	0.65	4.59	4.85
+0.66	+0.66	0.32	0.33	2.70	2.03	0.75	0.75	4.52	4.65

Notes: P=2x178 kN; p=1.17 MPa.; L=6 m x 6 m
h_{OL}=178 mm, h_{SL}=406 mm; $E_{OL}=E_{SL}=2.76\times10^4$ MPa; $\mu_{OL}=\mu_{SL}=0.15$;
$\alpha_{OL}=\alpha_{SL}=9\times10^{-6}$ ε/°C; $\gamma_{OL}=\gamma_{SL}=23.6$ kN/m
k=54 MPa/m, $k_I=9.97\times10^4$ MPa/m
Finite Element Mesh: 325 elements (half slab), 21.6 to 25.4 cm on side; Element Aspect Ratio = 1 to 1.2

TABLE 2 MPa Under Edge Loading of Bare Slab with B-727 Using ILSL2

g_U	g_L (°C/cm)	σ_{SLb}	σ_{SLt}
-0.66	0.00	4.30	0.048
0.00	0.00	3.20	0.400
+0.66	0.00	2.21	0.765

Notes: All parameters same as in Table 1, except h_{OL}=0. The 406-mm SL is analyzed as two bonded plates, 178 mm and 228 mm thick, respectively. No interface springs are used.

TABLE 3 MPa Under Corner Loading with B-727

g_{OL}	g_{SL}	σ_{OLt}		σ_{OLb}		σ_{SLt}		σ_{SLb}	
(°C/cm)		ILSL2	ILLI-SLAB	ILSL2	ILLI-SLAB	ILSL2	ILLI-SLAB	ILSL2	ILLI-SLAB
-0.66	-0.66	1.47	1.48	1.43	0.88	3.36	3.36	1.90	2.01
0.00	-0.66	0.32	0.	2.94	2.45	3.59	3.61	1.62	1.70
+0.66	-0.66	1.01	0.	5.63	4.02	3.80	3.86	1.15	1.40
-0.66	0.00	2.73	2.72	0.94	0.	2.32	2.31	2.19	2.36
0.00	0.00	1.11	1.11	1.48	0.92	2.53	2.53	1.99	2.09
+0.66	0.00	0.28	0.	3.02	2.50	2.71	2.76	1.72	1.81
-0.66	+0.66	4.16	3.96	1.83	0.	1.24	1.26	2.32	2.77
0.00	+0.66	2.50	2.37	0.88	0.	1.53	1.53	2.28	2.46
+0.66	+0.66	0.86	0.79	1.54	0.94	1.80	1.79	2.05	2.15

Notes: All pavement system parameters same as in Table 1.
Finite Element Mesh: 325 elements (full slab), 19.5 to 76.2 cm on side; Element Aspect Ratio = 1 to 3.9

are higher than those at the top for both SL and OL. As was also the case for interior loading, however, Totsky's approach in ILSL2 results in a significantly higher σ_{OL_b} than the conventional approach in ILLI-SLAB (1.98 cf. 1.31 MPa, or 287 cf. 190 psi).

To investigate the cause for this difference an additional no-curling run with ILSL2 was conducted in which the interface spring stiffness k_i was set to a very high value (2.71×10^7 MPa/m, or 10^8 psi/in.). Thus, SL and OL were assumed to be free to separate but not to possess any compressibility. A value of σ_{OL_b} = 1.42 MPa (206 psi) was obtained in this case, indicating that layer separation is responsible for only one-sixth of the increase predicted by ILSL2, the bulk of this change being attributable to layer compressibility. It is therefore imperative to account for compressibility in the analysis and design of unbonded concrete overlays.

Consider next the two cases with g_{SL} equal to 0 and g_{OL} varying, which are also very important from a practical point of view. Field measurements suggest that daily cycle temperature changes result in a high temperature gradient near the top surface of a concrete pavement and that the value of this gradient decreases with depth (*9,10*). Table 1 shows that as g_{OL} changes from −0.66 to +0.66°C/cm (−3 to +3°F/in.) a significant increase in σ_{OL_b} is observed, whereas σ_{OL_t} decreases considerably. Indeed, for g_{OL} equal to +0.6°C/cm (+3°F/in.), σ_{OL_b} from ILSL2 is almost twice the corresponding value obtained for no-curling conditions (3.50 cf. 1.98 MPa, or 507 cf. 287 psi). The difference in σ_{OL_t} is even more dramatic: decreasing g_{OL} from 0 to −0.66°C/cm (0 to −3°F/in.) causes a fourfold increase in σ_{OL_t} predicted by ILSL2 (from 0.53 to 2.14 MPa, or from 77 to 311 psi). Similar comparisons can be made by using results from ILLI-SLAB.

It is therefore apparent that as far as OL is concerned, critical stress conditions (i.e., overall maximum values of bending stress for the three g_{OL} values considered) arise at the bottom when a positive g_{OL} is introduced (3.50 MPa or 507 psi), whereas a negative g_{OL} causes a critical stress at the top (2.14 MPa, or 311 psi). Although for these three cases critical stress at the bottom of OL is higher than that at the top (3.50 cf. 2.14 MPa, or 507 cf. 3311 psi), the latter is still appreciable and should not be disregarded. Recall that the upper portion of OL is more susceptible to freeze thaw or other environmental damage and may therefore be more prone to rapid crack propagation, even at moderate stress levels.

By comparison stresses in SL are influenced to a much lesser degree by changes in g_{OL}. Critical stress arises at the bottom of SL for a negative g_{OL} (2.87 MPa or 416 psi), and at the top of SL for a positive g_{OL} (1.41 MPa or 204 psi). The larger of these two stresses is practically the same as that for no-curling conditions (2.87 cf. 2.86 MPa, or 416 cf. 415 psi). In fact, it is important to note that for the three cases considered here this value is about 20 percent smaller than the overall maximum stress in OL (2.87 cf. 3.50 MPa, or 416 cf. 507 psi). This observation suggests that under temperature loading it is inappropriate to assume that stresses in SL will always be higher than those in OL. This is only the case in the absence of curling, when it can be attributed directly to the lower flexural stiffness of OL. A fairly thin unbonded overlay may still be subjected to excessive stresses. This justifies the 150-mm (6-in.) minimum thickness recommended by the Portland Cement Association for such overlays (*11*).

The remaining six cases in Table 1 examine the influence of several combinations of temperature gradients in SL and OL. It is again observed that stresses in SL are considerably more sensitive to changes in g_{SL} than to changes in g_{OL}. This does not imply, however, that the response of SL is unaffected by the presence of OL. Under field conditions the thermal properties of OL may influence the development of g_{SL} considerably by slowing down any cooling and warming in SL. For example, in the early afternoon, OL will provide thermal insulation for SL, thus preventing g_{SL} from rising to high positive values. This will reduce the probability of high stresses at the bottom of SL. Consequently, the ILSL2 prediction for σ_{SL_b} for g_{OL} equal to 0.66°C/cm (+3°F/in.) and g_{SL} equal to +0.22°C/cm (+1°F/in.) would be only 3.43 MPa (498 psi), compared with a value of 4.52 MPa (656 psi) for g_{OL} equal to g_{SL} equal to +0.66°C/cm (+3°F/in.) given in Table 1. Additional comments with regard to this important thermal blanket function of unbonded overlays are made in a subsequent paragraph.

On the other hand, OL stresses are sensitive to changes in both gradients. A worst-case scenario arises when the external load is combined with gradients of opposite signs in SL and OL. The combination of a negative g_{OL} with a positive g_{SL} is critical for SL, whereas for OL the critical pair is a positive g_{OL} and a negative g_{SL}. Both extremes occur at the respective bottom surfaces. These trends may have been expected, because under these environmental conditions separation between OL and SL, as well as between SL and subgrade, is most pronounced.

It is also observed that the conventional approach in ILLI-SLAB may significantly underestimate stresses in OL [e.g., σ_{OL_b} = 3.92 cf. 5.35 MPa (568 cf. 776 psi), for g_{OL} = +0.66°C/cm (+3°F/in.) and g_{SL} = −0.66°C/cm (−3°F/in.)]. In several cases ILLI-SLAB predicts that the entire top or bottom surface of OL experiences only compression (the entry in Table 1 is zero). In contrast, ILSL2 indicates the presence of significant tensile stresses as well. Such results underscore the effects of separation and compressibility introduced in ILSL2. On the other hand, ILLI-SLAB predictions for both the top and bottom of SL are reasonably close to those from ILSL2, being slightly higher for σ_{SL_b} and slightly lower for σ_{SL_t}. For typical PCC pavements, in which the flexural stiffness of SL exceeds that of OL, the response of SL will be largely insensitive to separation and compressibility effects.

The thermal blanket effect of unbonded PCC overlays identified above deserves some additional exploration. Conventional analysis usually suggests that the effectiveness of such overlays in reducing the bending stresses in the existing slab is severely limited. Three additional finite-element runs were conducted to reexamine this assertion, as shown in Table 2. In these runs the same existing slab was considered as in Table 1, but without the overlay. The 406-mm (16-in.) SL is subdivided into two bonded plates, 178 mm (7 in.) and 229 mm (9 in.) thick, respectively. Furthermore, the gradient in the lower plate, g_L, is assumed to be zero. Thus, SL responses in Table 2 are comparable to those in Table 1 with g_{SL} equal to 0. The gradient in the upper plate, g_U, was allowed to vary between −0.66 and +0.66°C/cm (−3 and +3°F/in.), as would be the case if the pavements in Tables 1 and 2 were in the same general climatic region. For the case of no curling, Table 2 shows that the maximum tensile stress at the bottom of the slab (lower plate), σ_{SL_b}, is 3.20 MPa (464 psi). This value is only 7 percent higher than 2.99 MPa (434 psi), the stress predicted for the overlaid slab by the conventional approach in ILLI-SLAB (see Table 1). Note that both these stress values ignore compressibility effects. This justifies earlier observations about the small contribution of OL in reducing σ_{SL_b} on the basis of the flexural stiffnesses of the two placed layers alone. When an upright gradient of −0.66°C/cm (−3°F/in.) is considered, however, the bare slab

experiences 4.30 MPa (623 psi), compared with 2.87 MPa (416 psi) in the overlaid slab of Table 1. The latter value is obtained by using the proposed, more realistic ILSL2 model. Therefore, the overlay effectively reduces $\sigma_{SL,b}$ by 50 percent through its impact on g_{SL} (i.e., by preventing a negative gradient in SL). Given the thermal protection that the overlay provides to the slab, the only way to increase $\sigma_{SL,b}$ while maintaining g_{OL} at −0.66°C/cm (−3°F/in.) is to allow g_{SL} to assume a high positive value. Yet even under the extremely severe combination of g_{OL} equal to 0.66°C/cm (−3°F/in.) and g_{SL} equal to +0.66°C/cm (+3°F/in.), Table 1 shows that $\sigma_{SL,b}$ from ILSL2 is 4.72 MPa (684 psi), that is, only 10 percent higher than the bare slab value of 4.30 MPa (623 psi) in Table 2. Thus, the presence of the overlay mitigates significantly what could have been disastrous temperature loading on the bare slab.

It should also be pointed out in Table 2 that for such a thick slab, daytime conditions (g_U = −0.66°C/cm or +3°F/in.) can be less severe (2.21 MPa or 320 psi) than no-curling conditions (3.20 MPa or 464 psi) or nighttime conditions (g_U = −0.66°C/cm or −3°F/in.; 4.30 MPa or 623 psi). This finding is in agreement with earlier investigations into the effect of nonlinear (or bilinear) temperature distributions (*5,9,10*).

Corner Loading

Corner cracking is one of the most common forms of distress exhibited by unbonded concrete overlays. To examine this phenomenon a series of nine runs was performed by using the same pavement system parameters given in Table 1. Results obtained under corner loading indicate that maximum tensile bottom stresses occur under one of the tire prints. Maximum tensile top stress location varies, most frequently occurring at some radial offset from the load, typically on the order of 1.5 to 2 m (5 to 7 ft). The magnitudes of maximum tensile bending stresses arising at the top and bottom of OL and SL, $\sigma_{OL,t}$, $\sigma_{OL,b}$, $\sigma_{SL,t}$, and $\sigma_{SL,b}$, respectively, are shown in Table 3.

For the baseline case of no curling, ILSL2 and ILLI-SLAB results in Table 3 show that maximum tensile top and bottom stresses in SL exceed those in OL, consistent with the relative flexural stiffnesses of SL and OL. Furthermore, $\sigma_{SL,t}$ is higher than $\sigma_{SL,b}$, as expected for corner loading. Yet ILSL2 predicts that $\sigma_{OL,b}$ is higher than $\sigma_{OL,t}$, whereas ILLI-SLAB suggests the reverse. As discussed above for edge loading, the conventional approach in ILLI-SLAB significantly underestimates $\sigma_{OL,b}$ in comparison with Totsky's approach in ILSL2 (0.92 cf. 1.48 MPa, or 133 cf. 215 psi). The primary contributor to this discrepancy is the effect of layer compressibility.

Examination of results obtained for the three cases of g_{SL} equal to 0 and g_{OL} varying reveals that the influence of g_{OL} on maximum tensile stresses is similar to that observed under edge loading. Table 3 demonstrates that as g_{OL} changes from −0.66 to +0.66°C/cm (−3 to +3°F/in.), a significant increase in $\sigma_{OL,b}$ is observed, whereas $\sigma_{OL,t}$ decreases considerably. For g_{OL} equal to +0.66°C/cm (+3°F/in.), $\sigma_{OL,b}$ from ILSL2 is more than twice the value obtained for no-curling conditions (3.02 cf. 1.48 MPa, or 438 cf. 215 psi). For g_{OL} equal to +0.66°C/cm (−3°F/in.), the same is true for $\sigma_{OL,t}$ (2.73 cf. 1.11 MPa, or 396 cf. 161 psi). These trends suggest that conclusions reached for edge loading are valid for corner loading as well. Critical OL stress conditions (i.e., overall maximum values of bending stress for the three g_{OL} values considered) occur at the bottom when a positive g_{OL} is acting, whereas a negative g_{OL} may produce a critical stress at the top. Comparing corresponding cases in Tables 1 and 3 for g_{SL} equal to 0 shows that $\sigma_{OL,b}$ is higher under edge loading, whereas corner loading causes a higher $\sigma_{OL,t}$. As mentioned earlier, even a moderate level of top stresses in OL can cause significant damage. Therefore, it can be concluded that corner loading may be critical under conditions of severe negative g_{OL}, leading to considerable OL cracking.

The remainder of the cases in Table 3 illustrate the effect of several combinations of temperature gradients in SL and OL. It is again observed that stresses in SL are considerably more sensitive to changes in g_{SL} than to changes in g_{OL} and that OL stresses are sensitive to changes in both gradients. As might have been anticipated following the discussion of Table 1, critical conditions arise when the external load is combined with gradients of opposite signs in SL and OL. Under corner loading the combination of a positive g_{OL} with a negative g_{SL} is critical for SL, with the overall maximum stress occurring at the top.

As far as OL is concerned, the combination of a positive g_{OL} with a negative g_{SL} is critical under corner loading, just as it was for edge loading. Under these conditions, $\sigma_{OL,b}$ from ILSL2 is 5.63 MPa (817 psi), the overall highest stress among all cases considered, including those for edge loading. This high level of stress can be attributed to widespread separation between OL and SL. This assertion may be verified by reanalyzing this case by using ILSL2 with k_l set to a very high value [e.g., 2.71×10^7 MPa/m (10^8 psi/in.)]. In contrast, ILLI-SLAB predicts a significantly lower value for $\sigma_{OL,b}$ (4.02 MPa or 583 psi). The combination of a negative g_{OL} with a positive g_{SL} leads to critical $\sigma_{OL,t}$ (4.16 MPa or 604 psi), but this stress is smaller than the $\sigma_{OL,b}$ quoted above. Top OL stress predictions from both ILSL2 and ILLI-SLAB are comparable for this temperature gradient combination. This suggests that neither layer separation nor compressibility has much influence on critical bending stresses in this case, contrary perhaps to intuitive expectations.

Stress and Deflection Profiles

Examination of critical bending stresses in the preceding paragraphs revealed that layer compressibility and separation effects can be quite significant in a number of cases. On the other hand, agreement between ILSL2 and ILLI-SLAB in several cases was quite good, even surprisingly so. Consider, for example, the case of corner loading with g_{OL} equal to −0.66°C/cm (−3°F/in.) and g_{SL} equal to +0.66°C/cm (+3°F/in.), for which the $\sigma_{OL,t}$ values predicted by ILLI-SLAB and ILSL2 were 3.96 and 4.16 MPa (574 and 604 psi), respectively. For this case it would have been reasonable to expect that separation between OL and SL would have produced a much higher stress at the top fiber of OL than that predicted by ILLI-SLAB, because OL would be essentially responding as an unsupported cantilever. The implications of the closeness of the results from the two codes are therefore worth examining in some more detail. In the process it becomes apparent that correct interpretation of pavement behavior may often require consideration of the distributions of stresses and deflections instead of mere identification of maximum responses. For airport pavements in particular it is pertinent to recall that the estimation of the pass-to-coverage ratio for various aircraft may require the entire stress profile, not merely the maximum stress value. The

finite-element method is well-suited for response distribution determination.

For the aforementioned corner loading case, Figure 2 presents deflection profiles for SL and OL, obtained by using ILSL2 and ILLI-SLAB, along the edge at which the two B-727 tire prints were applied. Because it allows no separation the latter code shows that the more flexible OL follows the deflection profile of the stiffer SL. All three deflection profiles shown are practically coincident in the neighborhood of the loaded corner. ILSL2 predicts deflections of OL and SL within 2 percent of those from ILLI-SLAB for about 1.2 m (4 ft) from the loaded corner. This can be explained by the observation that the heavy applied load enforces contact between OL and SL in this region. Furthermore, the interlayer spring stiffness k_i is much higher than the subgrade modulus k, thereby contributing little to total OL deflection. Nevertheless, OL and SL deflection profiles from ILSL2 become significantly different at greater offsets from the loaded corner, where the effects of curling and separation become predominant. In this region ILSL2 predicts separation between OL and SL, allowing the unloaded OL corner to curl upward in response to the imposed negative g_{OL}. It is apparent that the ILLI-SLAB deflection profile for OL in this region is unrealistic. The deflection profile of the stiffer SL, on the other hand, remains practically unaffected by separation and is close to the corresponding profile obtained by using ILLI-SLAB.

Figure 3 presents a similar comparison of OL bending stresses for the same corner loading case. Both ILLI-SLAB and ILSL2 predict stress distributions of similar shape, if not of similar magnitude. To interpret these trends it may be recalled that according to Westergaard's theory a maximum tensile stress may be expected at about 1.8 m (6 ft) from the loaded corner (*12*). In this case, however, the second heavy tire print in ILSL2 causes a localized stress reversal, in a manner characteristic of edge loads, before the stress attains the expected maximum. This stress reversal is considerably more pronounced when compressibility effects are taken into account. It appears that, because of their respective assumptions, ILLI-SLAB treats the second tire print as a corner load, causing a much milder stress reversal.

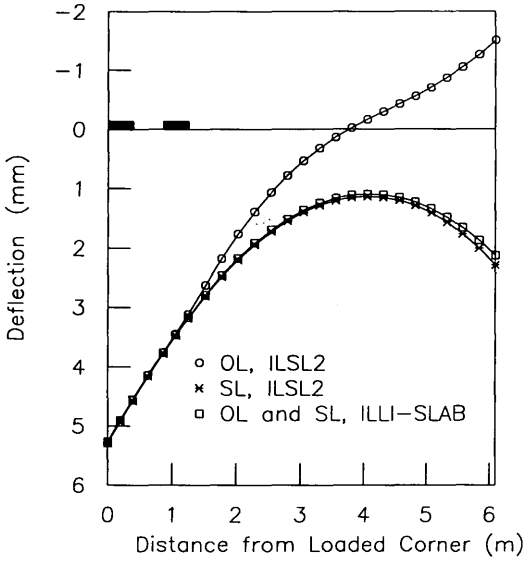

FIGURE 2 Deflection profiles from ILLI-SLAB and ILSL2 under corner loading and curling.

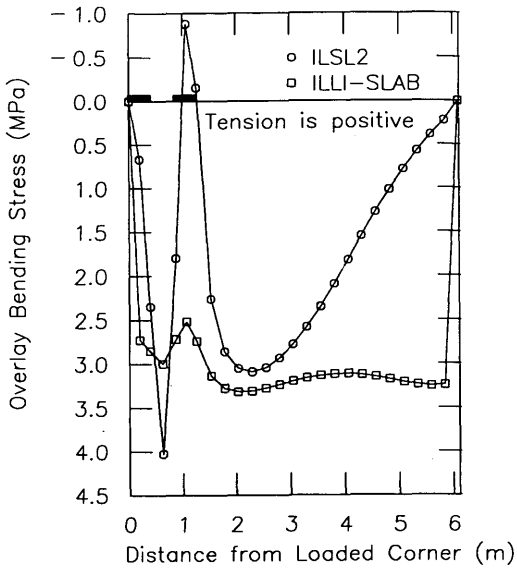

FIGURE 3 Overlay bending stress profiles from ILLI-SLAB and ILSL2 under corner loading and curling.

Interestingly, ILSL2 predicts that at greater offsets the tensile stress in OL decreases rapidly and smoothly to zero at the unloaded corner. For its part ILLI-SLAB suggests that OL stresses remain uniformly high until they are forced to return to zero by the boundary condition imposed at the unloaded corner. The higher stress level predicted by ILLI-SLAB for offsets greater than 2.5 m (100 in.) is attributable to the requirement that the OL follow the deflected shape of SL. The abrupt discontinuity observed in this case is evidence of the shortcomings of the conventional approach in ILLI-SLAB. It can therefore be concluded that agreement between the two codes with respect to maximum responses does not guarantee that response profiles predicted by each will be similar.

CONCLUSIONS

The study described here was undertaken in the context of a broader investigation into the behavior of multilayered concrete pavements. The specific objective was to develop a mechanistic tool for analysis of PCC pavements incorporating an unbonded PCC overlay and to use this in assessing the practical significance of the effects of layer compressibility and separation, as are likely to arise under conditions of dissimilar temperature gradients acting through the thicknesses of the existing slab and overlay.

The product of the study is a finite-element code, abbreviated herein as ILSL2, which represents an extension of the ILLI-SLAB program (1989 version). Numerous ILSL2 runs have been conducted for the purpose of verifying the new code. Practical illustrative examples pertaining to typical pavements are presented, and where appropriate these results are compared with existing analytical or numerical solutions, including those obtained by using ILLI-SLAB. It is found that both layer compressibility and separation effects need to be accommodated in a reliable mecha-

nistic model for unbonded PCC overlays. Although ILLI-SLAB often predicts maximum tensile stresses close to those predicted by ILSL2, stress and deflection profiles produced by the latter are more representative of actual pavement behavior. Furthermore, the conventional approach represented by ILLI-SLAB may sometimes underestimate significantly the maximum tensile stresses in the unbonded overlay in comparison with those estimated by ILSL2.

It has been found that combinations of temperature gradients through the slab and overlay having opposite signs are most detrimental to the pavement. When a heavy edge load is applied a positive temperautre gradient through the overlay and a negative gradient through the existing slab define the critical conditions for the existing slab; a negative gradient through the overlay acting together with a positive gradient through the existing slab is critical for the overlay. Under corner loading conditions, undesirable combinations of temperature gradients may create more critical conditions in the overlay than edge loading does. Therefore, ILSL2 can be especially helpful in assessing the potential for corner failures.

An unbonded overlay often contributes little to the flexural stiffness of the existing slab. Its beneficial effect on the performance of the pavement, however, is shown to be the result of thermal protection provided to the underlying slab. In addition, results obtained suggest that the overlay itself may be called on to carry a significant level of stress under certain severe combinations of temperature and external loadings. In fact even relatively thin overlays may experience tensile stresses higher than those developing in the existing slab. In contrast, conventional analysis, which ignores layer compressibility and separation effects, predicts lower stresses in the overlay if its flexural stiffness is lower than that of the existing slab. As a result the possibility of underdesigning unbonded PCC overlays is an issue that deserves serious reconsideration in conventional design approaches.

ACKNOWLEDGMENTS

This study was funded by the University of Illinois Campus Research Board (Grant 1-2-68437). The comments and suggestions of Arthur R. Robinson and Rami M. Hajali are greatly appreciated.

REFERENCES

1. Ioannides, A. M., L. Khazanovich, and J. L. Becque. Structural Evaluation of Base Layers in Concrete Pavement Systems. In *Transportation Research Record 1370*, TRB, National Research Council, Washington, D.C., 1992, pp. 20–28.
2. Van Dam, T., E. Blackmon, and M. Y. Shahin. Effect of Overlay Debonding on Pavement Performance. In *Transportation Research Record 1136*, TRB, National Research Council, Washington, D.C., 1987, pp. 119–132.
3. Hall, K. T., M. I. Darter, and W. J. Seiler. Improved Design of Unbonded Concrete Overlays. *Proc., 5th International Conference on Concrete Pavement Design and Rehabilitation*, Vol. 2, Purdue University, West Lafayette, Ind., April 20–22, 1993, pp. 227–240.
4. Totsky, O. N. Behavior of Multi-Layered Plates and Beams on Winkler Foundation (in Russian). *Stroitel'naya Mekhanika i Raschet Sooruzhenii*, No. 6, Moscow, 1981, pp. 54–58.
5. Korovesis, G. T. *Analysis of Slab-on-Grade Pavement Systems Subjected to Wheel and Temperature Loadings*. Ph.D. thesis. University of Illinois, Urbana, 1990.
6. Przemieniecki, J. S. Theory of Matrix Structural Analysis. McGraw-Hill, New York, 1968.
7. Khazanovich, L. *Structural Analysis of Multi-Layered Concrete Pavement Systems*. Ph.D. thesis. University of Illinois, Urbana, 1994.
8. Westergaard, H. M. New Formulas for Stresses in Concrete Pavements of Airfields. *Transactions, ASCE*, Vol. 113, 1948, pp. 425–439.
9. Mirambell, E. Temperature and Stress Distributions in Plain Concrete Pavements Under Thermal and Mechanical Loads. *Proc., 2nd International Workshop on the Design and Rehabilitation of Concrete Pavements*, Sigüenza, Spain, Oct. 1990, pp. 121–135.
10. Choubane, B., and M. Tia. Nonlinear Temperature Gradient Effect on Maximum Warping Stresses in Rigid Pavements. In *Transportation Research Record 1370*, TRB, National Research Council, Washington, D.C., 1992, pp. 11–19.
11. Tayabji, S. D., and P. A. Okamoto. Thickness Design of Concrete Resurfacing. *Proc., 3rd International Conference on Concrete Pavement Design and Rehabilitation*, Purdue University, West Lafayette, Ind., April 23–25, 1985, pp. 367–379.
12. Ioannides, A. M., M. R. Thompson, and E. J. Barenberg. Westergaard Solutions Reconsidered. In *Transportation Research Record 1043*, TRB, National Research Council, Washington, D.C., 1985, pp. 13–23.

Publication of this paper sponsored by Committee on Pavement Rehabilitation.

Effect of Pavement Variables on Average Joint Deflections in Experimental Concrete Pavement

ANDREW BODOCSI, ISSAM A. MINKARAH, RAJAGOPAL S. ARUDI, MAHESH BHUPALAM, AND ANURAG KAK

Knowledge of the magnitude of joint deflections in a concrete pavement caused by truck traffic is important because the larger the deflection the larger the stresses and the lower the fatigue life of the pavement. For improved design of concrete pavements it is important to evaluate the effects of various factors on pavement joint deflections. For this purpose an experimental concrete pavement was built in 1972 in Chillicothe, Ohio, by the Ohio Department of Transportation. The variables built into the pavement included two types of bases, different joint spacings, one section with skewed joints, and joints with no dowels, standard dowels, and plastic-coated dowels. The University of Cincinnati researchers have investigated this pavement for several years, first in the middle 1970s and then between 1989 and 1991. This last phase included a thorough investigation of vertical joint deflections. The deflections were produced by a two-axle truck moving at 80 km/hr and were measured by an electronic transducer. The ways in which the type of base, season, joint spacing and crack patterns, presence of dowels, type of dowels, and time of day affected the joint deflections of the experimental pavement are described. The test procedures and measuring methods used are discussed, and the results, analysis, and conclusions are presented.

Among other factors the magnitude of the vertical joint deflection in a concrete pavement depends on the degree of support that the pavement receives from its base and subgrade. The magnitude of vertical joint deflection is important because the larger the deflection of the pavement under an applied wheel load the larger its strains and stresses and the lower its fatigue life.

In 1972 the Ohio Department of Transportation (ODOT) built a 983-m-long experimental jointed reinforced concrete pavement segment in southbound State Route Ros 23 in Chillicothe, Ohio. This test pavement was divided into 12 sections. Nine sections were built on a 190.5-mm-thick granular base, and the remaining three were built on a 101.6-mm-thick asphalt-treated base. Other variables included joint spacing and type of dowel. This test section was studied from 1972 to 1980 by Minkarah and Cook (*1,2*) and Cook et al. (*3*) and again from 1989 to 1992 by Minkarah et al. (*4*) for joint behavior, such as vertical joint deflection and horizontal joint movements, and for various signs of deterioration.

In the latest test phase eight joints were tested for vertical joint deflection. Each joint was tested both in the morning and in the afternoon and in each of the four seasons during the years 1990 and 1991. Table 1 lists the joints tested, with information on joint spacing, type of base, and type of dowels.

To conduct the tests a fully loaded two-axle dump truck with a rear axle load of approximately 80 kN moving at 80 km/hr was used. The resulting vertical joint deflections were measured by a linear variable differential transducer (LVDT).

The fundamental purpose of the test program was to compare vertical joint deflections at the various sections of the test pavement to establish the effect of the time of day of testing, type of base, season of testing, type of dowel, and joint spacing.

This paper presents a summary of the instrumentation, test methods, the results, a detailed analysis, and conclusions.

Department of Civil and Environmental Engineering, University of Cincinnati, 741 Baldwin Hall, ML 71, Cincinnati, Ohio 45221-0071.

INSTRUMENTATION AND TESTING

LVDT and Its Placement

The LVDT is a proven device used to measure relative displacements. Its drawback is that it requires a fixed reference point. The LVDT yields a voltage-time history directly proportional to the displacement-time history of its core-to-coil position. The only error that the manufacturer's specification lists is that due to nonlinearity. The transducer used in this test phase had an error band of ± 0.0635 mm. This being a bias error, it could be reduced by proper calibration techniques to yield an accuracy of ± 0.0152 mm. Calibration of the LVDT was performed before each test sequence to determine the appropriate calibration factor.

Before testing a joint an LVDT was placed on the approach side of the joint, as shown in Figure 1. The required fixed reference point for the LVDT measurement was provided by driving a 3.048-m-long, 34.9-mm-diameter steel rod approximately 101.6 mm away from the pavement in a 228.6-mm-deep cutout hole adjacent to each of the eight joints tested. The top of each rod was kept approximately level with the bottom of the 228.6-mm-thick pavement slab. One joint was selected to represent the respective group in each subsection, because it was not practical to provide fixed reference points for all the joints. For each test sequence the coil assembly of the LVDT was attached to the side of the pavement at a point directly above the reference rod. The core of the LVDT was attached to the top of the reference rod. Deflection of the pavement at the approach side of the joint caused the coil assembly to move in relation to the fixed core. An output voltage proportional to the pavement deflection was produced and recorded. Power to the LVDT was supplied by a 12-V battery. The LVDT signals were recorded by an HP35660 Signal Analyzer.

Test Procedure

A total of 140 dynamic tests (including repeated runs) with a fully loaded two-axle ODOT truck driven at a speed of 80 km/hr were

TABLE 1 Joint Designation and Test Pavement Information

Joint #	Joint Spacing (m)	Type of Base	Type of Dowel
4	12.2	Granular	Standard (Uncoated)
21	6.4	Stabilized	Standard (Uncoated)
29	12.2	Stabilized	Standard (Uncoated)
40	5.18	Stabilized	No dowels
49	6.4	Granular	Coated
59	12.2	Granular	Coated
69	12.2	Granular	Standard (Uncoated)
89	6.4	Granular	Standard (Uncoated)

performed on the test pavement, and deflections under both front and rear axles were recorded. The front and real axle loads were approximately 40 and 80 kN, respectively, for each run. These deflections were then linearly normalized for an 80-kN axle load, resulting in a total of 280 readings. The tests were conducted on eight selected joints during four seasons in 1990 and 1991 and, typically, over a 4-day period in each season.

For each of the eight joints measurements were taken twice, in the morning on a cool pavement and later in the afternoon when the pavement had warmed up. These measurements were taken during summer and fall of 1990 and winter and spring of 1991. At each joint the truck was driven across the joint and the vertical deflection of the pavement on the approach side of the joint was measured. Usually a sequence of three runs was made for each measurement. Lines were placed on the pavement to guide the truck in maintaining a distance of 304.8 mm ± 50.8 mm from the pavement edge. Runs outside this range were repeated.

The data recorded were uncalibrated LVDT voltages. These were converted to displacements by multiplying the data by a constant scale factor that was obtained earlier from the calibration procedure.

Dynaflect readings were also taken on all joints in the test pavement to check the validity of using deflection data from one joint in each subsection to represent that group of joints. Also, the edge of the pavement was inspected at all joints to check the condition of the slab and the base. The investigation revealed uniform conditions at all joints with full support of the slab and only minor spalling of the concrete surface.

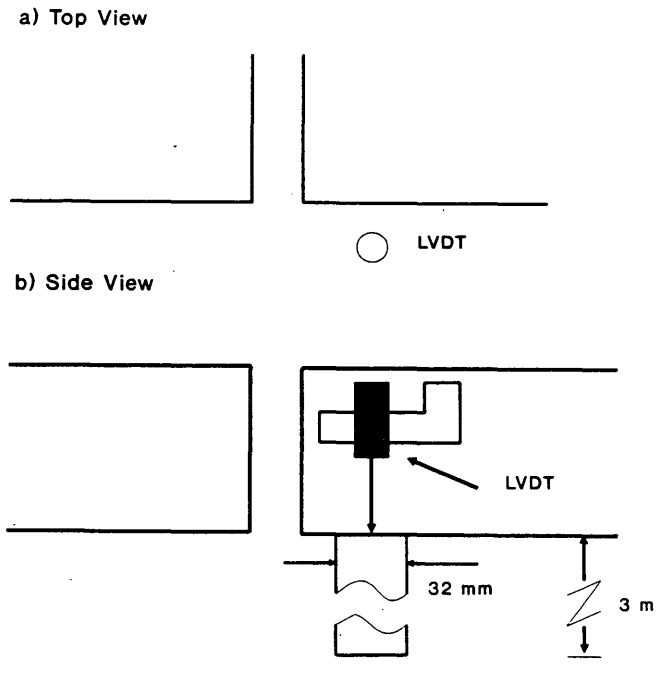

FIGURE 1 Placement of LVDT on pavement.

RESULTS

The averages of the peak LVDT deflection measurements for eight joints in the experimental concrete pavement are summarized in Table 2. The values provided are the averages of six measurements under the front and rear axles of the test truck.

The LVDT data were analyzed, digitized, and plotted for each of the eight joints, for each one of the test runs, and for each of the four seasons. As an example, Figure 2 gives the LVDT plot of deflections for a typical joint caused by the fully loaded two-axle truck moving across the joint at a speed of 80 km/hr. As can be seen in Figure 2 there are two peaks on the curve, the first caused by the passing of the front axle of the truck over the joint and the second caused by the passing of its rear axle. The net deflection of the joint caused by either of the axles can be obtained by reading the deflection at the peak point and adjusting this reading by the zero offset at the beginning of the plot.

All the data collected were entered into a data base. The data were then sorted according to the type of base, type of dowel, time of day when each test was conducted, the span of the slabs, and typical number of cracks. All the readings were then adjusted by the zero offset and linearly normalized for a standard 80.1-kN axle load for further analysis. A separate data base was also established for the Dynaflect readings.

ANALYSIS

The Dynaflect data from each group were analyzed, and the results are shown in Table 3. As seen in Table 3 the Dynaflect deflections for the joints selected for LVDT measurements are a good representation of the mean vertical deflections for each group.

From LVDT measurements, as shown in Table 2, the absolute maximum measured deflection was 0.3990 mm. The maximum deflection was measured on Joint 4, on November 15, 1990, during the morning hours (no temperature data were available for this measurement.) The overall average deflection from all LVDT measurements was found to be 0.1226 mm. Seasonally, the average deflections were 0.1088 mm in the summer, 0.1395 mm in the fall, 0.1303 mm in the winter, and 0.1169 mm in the spring.

The variations in joint deflections caused by variables such as time of day, type of base, season, presence of dowels, type of dowels, joint spacing, and number of cracks are presented in Figures 3 through 14. Also presented in Table 4 is a statistical summary of joint deflections were reference to these variables. Table 4 gives the results of a hypothesis test performed on each of the variables. The null hypothesis (H_0) tested was the difference in means equal to 0 at a level of significance of α equal to 0.05.

TABLE 2 Average Vertical Joint Deflections as a Result of Moving an 80.1-kN Axle Load Measured by LVDT at 80 km/hr

DATE	JOINT #							
	4	21	29	40	49	59	69	89
July 10, 1990	0.074 PM							
July 11, 1990		0.075 AM		0.079 AM	0.109 PM			
July 31, 1990	0.145 AM	0.074 PM			0.130 AM			
August 1, 1990						0.064 PM	0.323 AM 0.109 PM	0.104 AM
August 8, 1990			0.038 PM			0.175 AM	0.125 PM	0.069 PM
August 9, 1990			0.114 AM	0.043 AM				
Oct 31/Nov. 1, 1990		0.091 PM	0.114 AM		0.104 PM	0.155 AM	0.084 PM	0.081 PM
Nov. 14, 1990		0.056 PM	0.053 PM	0.191 AM 0.081 PM	0.173 AM			
Nov. 15, 1990	0.399 AM 0.135 PM						0.203 AM	0.173 AM
Feb. 14, 1991	0.379 AM		0.012 PM					
Feb. 21, 1991				0.064 AM	0.112 PM	0.079 PM	0.104 PM	
Feb. 22, 1991	0.053 PM		0.172 PM					0.198 AM
April 16, 1991	0.079 AM		0.033 PM	0.022 PM	0.048 PM			
April 17, 1991				0.074 AM	0.074 AM	0.038 PM	0.051 PM	
April 23-24, 1991	0.315 AM	0.208 AM 0.046 PM	0.089 PM			0.102 PM	0.132 PM	0.391 AM 0.168 PM

Note: All deflection values are average of three runs

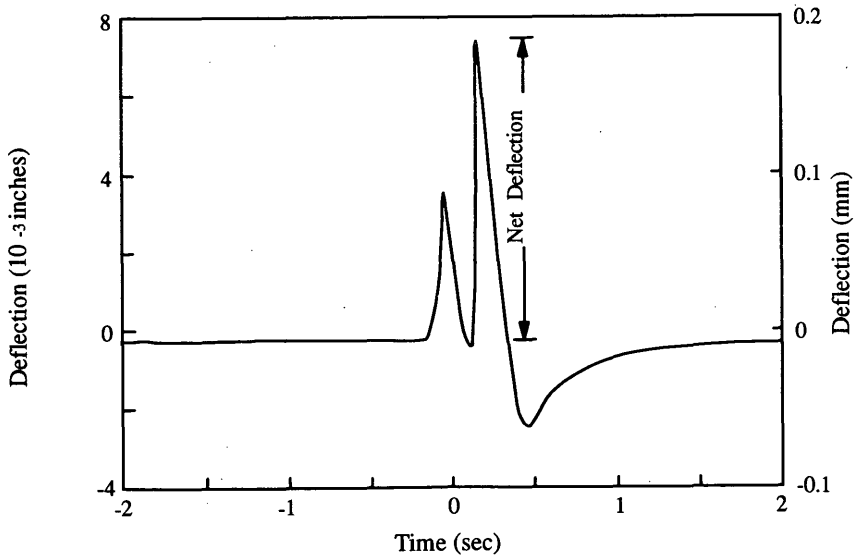

FIGURE 2 LVDT deflections for Joint 59.

TABLE 3 Analysis of Dynaflect Deflection Data

Group #	# of Joints	Mean Vertical Joint Deflection, mm	Standard Deviation, mm	Coeff. of Varn. = (SD/MEAN) X 100, (%)	Joint Selected for Detailed Studies	Deflection at Joint Selected, mm
1	7	23.876	4.826	20.6	4	25.908
2	8	10.414	1.27	11	21	10.16
3	12	9.652	1.27	14.1	29	10.16
4	10	12.446	1.27	9.6	40	11.684
5	10	23.114	8.89	38.8	49	22.352
6	11	22.352	5.588	24.6	59	20.32
7	9	22.860	4.826	21.1	69	No Data
8	10	19.812	7.366	36.4	89	16.51

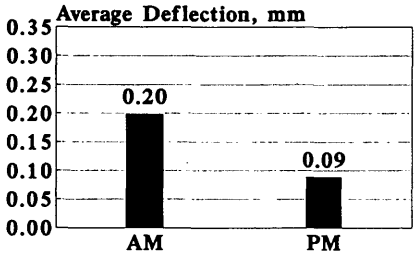

FIGURE 3 Effect of time of day (a.m. versus p.m. deflections).

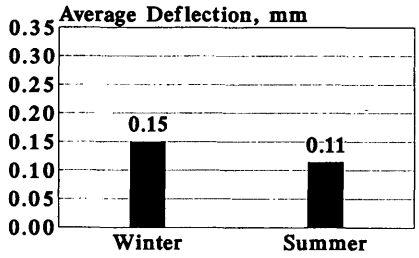

FIGURE 6 Effect of seasons (winter versus summer deflections).

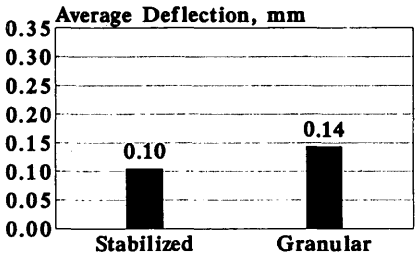

FIGURE 4 Effect of base (stabilized versus granular deflections.)

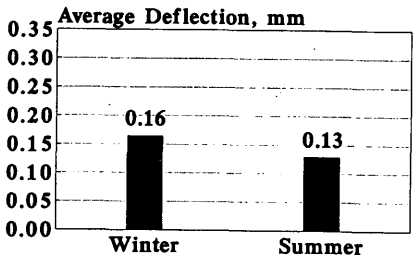

FIGURE 7 Effect of seasons (winter versus summer, granular base only).

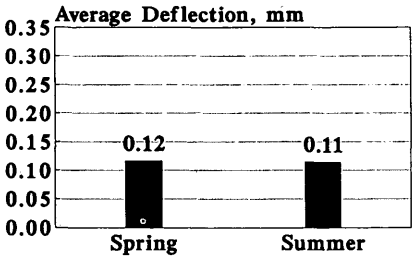

FIGURE 5 Effect of seasons (spring versus summer deflections).

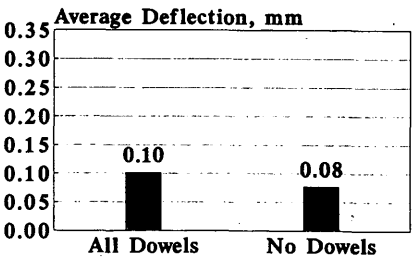

FIGURE 8 Effect of dowels (stabilized base).

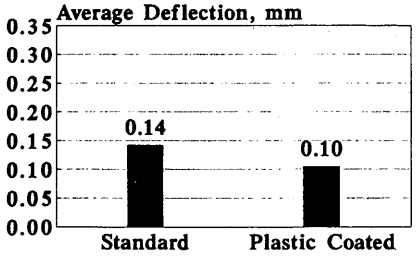

FIGURE 9 Effect of dowels (standard versus plastic coated).

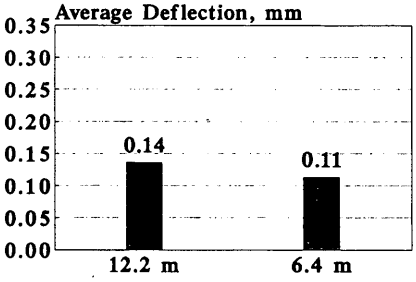

FIGURE 10 Effect of joint spacing (12.2 versus 6.4 m).

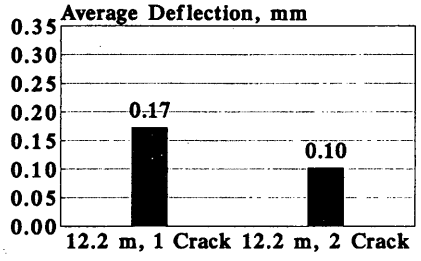

FIGURE 11 Effect of joint spacing (12.2 m, one crack versus 12.2 m, two cracks on granular base).

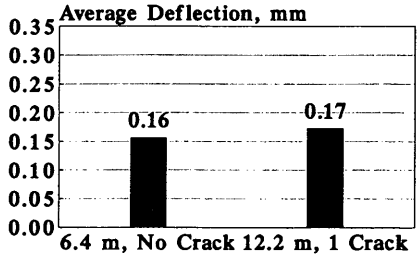

FIGURE 12 Effect of joint spacing (6.4 m, no crack versus 12.2 m, one crack on granular base).

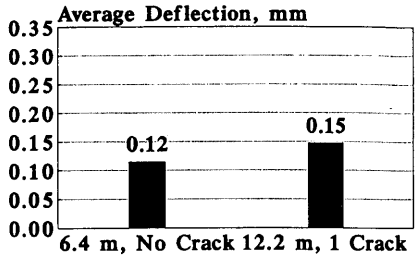

FIGURE 13 Effect of joint spacing (6.4 m, no crack versus 12.2 m, one crack on granular and stabilized base).

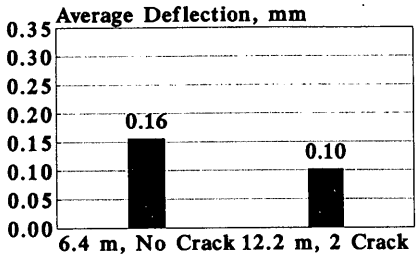

FIGURE 14 Effect of joint spacing (6.4 m, no crack versus 12.2 m, two cracks on granular base).

Figure 3 shows joint deflection results in a bar-chart format comparing average morning (a.m.) and afternoon (p.m.) deflections, regardless of season or type of base. The average a.m. deflection of 0.1984 mm was more than twice the average p.m. deflection of 0.0889 mm. This agrees well with the observations of Minkarah and Cook (*1,2*) and Cook et al. (*3*). In the morning the top surface temperature of the pavement is usually colder than its bottom, causing the pavement slab to curl upward. When the wheel load is applied a curled pavement deflects more because it is poorly supported near the joint. The statistical test performed to compare the averages of the two groups reveals that time of day (a.m. versus p.m.) has a significant effect on joint deflections (Table 4).

The effect of the type of base on joint deflection is shown in Figure 4. Figure 4 compares the average joint deflection on asphalt-stabilized base (0.1049 mm) with that on granular base (0.1435 mm). Clearly, joints supported on asphalt-stabilized base had smaller vertical deflections than those supported on granular base. This observation also agrees well with those of Minkarah and Cook (*1,2*) and Cook et al. (*3*). The statistical test revealed that type of base (granular versus stabilized) has a significant effect on joint deflections (Table 4).

To study the effect of the season on joint deflections, the average joint deflection from all measurements during the spring was plotted versus the average from all deflections during the summer (Figure 5). Similarly, the winter deflections were plotted versus the summer deflections in Figure 6. The average spring deflection of 0.1166 mm was slightly higher than the summer deflection of 0.1143 mm, whereas the winter deflection of 0.1501 mm was higher than both. Furthermore, the average winter joint deflections on granular base only were compared with the summer deflections at the same joints (Figure 7). The difference between winter and summer deflections was even larger than when all joints, regard-

TABLE 4 Effect of Pavement Variables: Summary Statistics

Variable		Sample Size	Mean vertical joint deflection, mm	Significant Difference between Means	Level of Significance (Probability of error)
Time of day	AM PM	41 75	0.1984 0.0889	Yes	3.775E-11
Base	Granular Stabilized	86 49	0.1435 0.1049	Yes	0.0198
Seasons	Spring Summer	32 47	0.1166 0.1143	No	0.907
	Winter Summer	20 47	0.1501 0.1143	No	0.1103
	Winter Summer (Granular Base)	14 29	0.1646 0.1295	No	0.2597
Dowels	Standard Plastic coated	85 33	0.1425 0.1049	Yes	0.0403
	No dowels(skewed) All dowels (Stabilized Base)	17 31	0.0774 0.1017	No	0.1434
Joint Spacing	12.2 m 6.4 m	71 63	0.1361 0.1133	No	0.1318
	12.2 m, 1 crack 12.2 m, 2 cracks (Granular Base)	37 17	0.1725 0.1019	Yes	0.0221
	6.4 m, No crack 12.2 m, 1 crack (Granular Base)	16 37	0.1565 0.1725	No	0.6431
	6.4 m, No crack 12.2 m, 1 crack (Gran. & Stab. Base)	47 54	0.1151 0.1471	No	0.1013
	6.4 m, no crack 12.2 m, 2 cracks (Granular Base)	16 17	0.1565 0.1018	No	0.0546

less of base, were considered. It should be noted that the winter of 1991 was mild and wet in Chillicothe, Ohio, causing larger than typical joint deflections. The statistical tests, on the other hand, do not show any significant effect of season on the mean vertical joint deflections (Table 4). Therefore, it is recommended that more tests be run to investigate this point.

In Figure 8 the effect of dowels on the average joint deflection in the pavement slabs on stabilized base is shown. The bar charts indicate that the joints with no dowels undergo smaller deflections (0.0774 mm) than the ones with dowels (0.1017 mm). The undoweled joints are all skewed, and therefore, as the test truck moves across these joints, the effective load causing the deflection is smaller than for the nonskewed doweled joints. The statistical test indicated that this difference was insignificant (Table 4). In other words, joint deflections on the asphalt-stabilized base are minimally affected by the presence of dowels. The asphalt-stabilized base was still in excellent condition, as seen from cores taken from the pavement and from visual inspection at the edges.

Figure 9 presents bar charts showing the average of all joint deflections as affected by the type of dowel, standard or plastic coated. The joint deflections were somewhat larger with standard dowels (0.1425 mm) than with plastic-coated dowels (0.1049 mm). This difference was statistically insignificant (Table 4). Even though plastic-coated dowels are slightly more effective than standard dowels in reducing joint deflections, the difference is not appreciable.

The above-stated effects of plastic-coated dowels on the vertical deflection of joints was not observed when the test pavement was new in the early 1970s. Then the plastic-coated dowels seemed to have little or no effect on vertical joint deflections (*1–3*). Cores taken through the joints in 1985 and 1990 showed little deterioration of the dowels. To shed more light on this question, ODOT and the researchers are planning to cut out several doweled joints for inspection when this pavement is rehabilitated in the near future.

Another parameter of interest was the effect of joint spacing on joint deflection. The bar charts in Figure 10 show that joint spacing had only a small effect on joint deflections. Specifically, the overall average joint deflection of the 12.2-m slabs (0.1361 mm) was slightly higher than that of the 6.4-m slabs (0.1133 mm). This comparison was done for all joints, on all bases, and with all dowel combinations. The statistical test indicated no significant effect of joint spacing on vertical deflection (Table 4). This was perhaps because many slabs, particularly the 12.2-m slabs, developed midslab cracks that reduced the effective lengths of the slabs. Hence a more detailed analysis of the effect of joint spacing was made by considering the effect of the number and spacing of cracks in each type of slab.

In the first case the average joint deflections of 12.2-m slabs on granular base were compared. From this, the 12.2-m slabs with one crack at midslab showed a greater average joint deflection than the 12.2-m slabs with two cracks at the third points. As

shown by the bar charts in Figure 11 the average deflection of slabs with one crack was 0.1725 mm, whereas it was 0.1018 mm for slabs with two cracks. Similarly, the statistical test showed that the difference in averages was significant. The probable reason for this difference is the greater curl of the slab with the longer span, that is, the one with only one crack.

In the second case the average joint deflection of 12.2-m slabs with one crack at midslab was compared with the average joint deflection of 6.4-m slabs with no crack, both on granular bases (Figure 12). The results indicate no significant difference in the average deflections (Table 4). An explanation for this is that in both cases the curling spans are approximately the same, 6.1 and 6.4 m. Similar results were obtained from comparing the average deflections of these slabs on all bases, both granular and stabilized (Figure 13). However, the average deflections were smaller.

In the third case the average joint deflection of 6.4-m slabs without cracks was compared with that of the 12.2-m slabs with two cracks, with both types again being on a granular base. As shown in Figure 14 the average deflection of the 6.4-m slabs was greater than that of the 12.2-m slabs (0.1565 m versus 0.1018 mm). However, the statistical test indicated that there was no significant difference between the two.

CONCLUSIONS

On the basis of the detailed analysis of the data, the following conclusions can be made:

1. The overall mean vertical joint deflection was found to be 0.1226 mm, which compared very well with the mean deflection measured when the pavement was new. Note that the pavement and the base are still in good condition.
2. The maximum measured deflection was 0.3990 mm. This occurred in the fall in the morning and on granular base.
3. The overall average deflection of the joints in the morning was significantly greater than the overall average deflection in the afternoon. The direction of pavement curl because of a temperature differential was the probable cause.
4. The joints on stabilized base deflected significantly less than the ones on granular base. This was expected, because the stabilized base should provide better support with less deflection. It also minimizes pumping and erosion.
5. Although the average vertical joint deflections during winter and spring were greater than those during summer, the difference was not statistically significant. More tests are recommended for further study.
6. There was no significant difference between the average joint deflections of doweled and undoweled joints on stabilized base.
7. The effect of dowel type, plastic-coated versus standard (uncoated) dowels, on vertical deflection was statistically significant. Joint deflections were somewhat larger with standard dowels. This was not the case in earlier reports on this pavement, when there was no significant difference in vertical deflections between the two types.
8. Slab dimension or joint spacing had little effect on the average vertical joint deflection. However, when the cracks in the pavement were considered, the difference in average deflections was much more noticeable. Specifically, the following observations were made:
   - The 12.2-m slabs with one crack had greater average deflection than the 12.2-m slabs with two cracks;
   - The average deflection of 12.2-m slabs with one crack was close to the average deflection of the 6.4-m slabs with no cracks; and
   - The average deflection of the 12.2-m slabs with two cracks was smaller than the average deflection of the 6.4-m slabs with no cracks, but the difference was not statistically significant.

ACKNOWLEDGMENTS

The funding for this project was provided by ODOT under Contract 5648C, State Job 14451(0), titled Final Evaluation of the Field Performance of ROS 23 Experimental Concrete Pavement.

The authors gratefully acknowledge the assistance of William F. Edwards, ODOT, for support throughout the project. Thanks are also given to the staff of ODOT's District 4 for their able assistance in the field.

REFERENCES

1. Minkarah, I. A., and J. P. Cook. *A Study of the Effect of the Environment on an Experimental Portland Cement Concrete Pavement.* Final Report to the State of Ohio Department of Transportation, Aug. 1976.
2. Minkarah, I. A., and J. P. Cook. The Vertical Movement of Jointed Concrete Pavements. In *Transportation Research Record 990*, TRB, National Research Council, Washington, D.C., 1984, pp. 9–16.
3. Cook, J. P., I. A. Minkarah, and J. F. McDonough. *Determination of Importance of Various Parameters on Performance of Rigid Pavement Joints.* Report to the Ohio Department of Transportation and FHWA, U.S. Department of Transportation, Aug. 1981.
4. Minkarah, I. A., A. Bodocsi, R. Miller, and R. S. Arudi. Final Evaluation of the Field Performance of ROS 23 Experimental Concrete Pavement. Draft Final Report submitted to the Ohio Department of Transportation, Dec. 1992.

Publication of this paper sponsored by Committee on Rigid Pavement Design

Portland Cement Concrete Pavement Rehabilitation in Washington State: Case Study

LINDA M. PIERCE

Washington, like other states, is nearing the completion of the Interstate highway construction program. The pavement design period for this system was only 20 years, and Washington, like all states, is experiencing the need to rehabilitate the pavements constructed in the early years of the Interstate program. A large and ever-increasing proportion of the Interstate system is beyond the design age of 20 years. As of 1993 more than 50 percent (approximately 1,680 lane-km) of all Interstate portland cement concrete (PCC) pavements in Washington State have been in service for 20 or more years. Because of budgeting constraints and user impacts the proper fix to the aging and distressed PCC pavements is not completely obvious. Total reconstruction is costly, successful and documented PCC pavement rehabilitation techniques are few, and all alternatives will result in delays to users of the facility. A general overview of the PCC pavement performance in Washington State is provided. In addition, the construction, analysis, and initial performance of a PCC pavement rehabilitation project that involves the use of retrofitted dowel bars, a tied concrete shoulder, and pavement grinding are discussed. The project was initiated to determine the effectiveness of these methods on the rehabilitation of PCC pavements in Washington. The outcome of the project will determine the viability of using these options for future rehabilitation projects in the state.

Washington is nearing the completion of the Interstate highway construction program. This extensive highway building program has taken over 30 years to complete. The pavement design period for this system was only 20 years, and Washington is experiencing an ever-increasing need to rehabilitate the pavements constructed in the early years of the Interstate program. A large and ever-increasing proportion of the Interstate portland cement concrete (PCC) pavement system is beyond the design age of 20 years. As of 1993 more than 50 percent (approximately 1,680 lane-km) of all Interstate PCC pavements in Washington have been in service for 20 years or more. These pavements have required almost no maintenance or rehabilitation since construction. Even after 25 or more years of service some sections in western Washington exhibit no signs of faulting or cracking. This unusually good performance is probably due to the well-drained subgrade, mild climate, high-quality aggregate, and high-strength PCC pavement.

DESIGN OF AND CONSTRUCTION CONSIDERATIONS FOR EXISTING PAVEMENT

The concrete pavements constructed from 1959 to 1967 typically consisted of unreinforced 230-mm-thick pavements with perpendicular (nonskewed) transverse joints spaced 4.6 m apart. In the 1970s the Washington State Department of Transportation (WSDOT) changed to an unreinforced skewed and random joint spacing (4.3 m, 2.8 m, 3.4 m, 4.0 m). The transverse contraction joints are sawed to a depth of $D/4$, whereas the longitudinal contraction joints are sawed to a depth of $D/3$. The widths for both joints range from 5 to 8 mm.

Most concrete pavements have crushed stone base courses, which have a maximum aggregate size of 16 mm. In some locations the base material consists of asphalt-treated base or cement-treated base. Most shoulders have been constructed with asphalt concrete pavement (ACP).

TYPICAL FORMS OF DISTRESS

To date the main forms of distress for the Interstate PCC pavements in Washington have been in the form of joint faulting and longitudinal cracking in the wheelpaths. Typically, in areas that have base materials consisting of asphalt-treated base or select gravel borrow (pea gravel), the slabs are distressed with longitudinal cracking and no significant faulting (0 to 3 mm). In areas with poor drainage and base materials consisting of cement-treated base or crushed stone, the prevalent form of distress is joint faulting (3 to 22 mm).

Longitudinal Cracking

The longitudinal cracking found in Washington appears to be load related instead of caused by other factors such as improperly sawed longitudinal joints. WSDOT's and California's experiences have shown that this cracking appears frequently in the inner wheelpath as well as the outer wheelpath. In addition, the longitudinal cracking observed in the AASHO road test occurred most often approximately 24 to 42 in. from the slab edge (*1*).

The mechanisms causing longitudinal cracking were investigated as part of a research study conducted by the University of Washington at Seattle and the University of Illinois at Urbana-Champaign (*2*). The first step was to look at the differences between those pavements exhibiting longitudinal cracking and those exhibiting transverse cracking. The most obvious differences between these two sites were the measured load transfer efficiencies. The pavement sections were tested at approximately the same temperature (16°C), but the load transfer efficiency for all transverse joints at the longitudinally cracked sites averaged 91.6 percent, with a coefficient of variation (COV) of 8.0 percent, and at the transversely cracked site the load transfer efficiency averaged

Washington State Department of Transportation, P.O. Box 167, Olympia, Wash. 98507-0167.

67.0 percent, with a COV of 33.8 percent. The tight joints at the longitudinally cracked site indicated that in-plane compressive forces parallel to the pavement centerline may have existed. To investigate whether other data supported this conclusion, the Dynatest 8000 falling-weight deflectometer (FWD) deflection data were further evaluated.

From that evaluation it was found that in several instances the deflection at center slab was greater than those at the joint locations (for the same slab). In addition, the deflection testing at the longitudinally cracked site was conducted when the temperature gradient was negative, causing a convex curvature in the slab (the corners and joints curled up off the underlying supporting layer). This curvature should have resulted in higher transverse joint deflections and larger transverse joint-to-slab center deflection ratios, so the ratios measured at other times of the day may have been lower. There are two possible explanations for this phenomenon: large voids existed under the slab centers or significant in-plane compressive stresses existed. The first alternative was evaluated according to the void detection process (*3*) and showed that voids did not exist under the slab centers. These results tended to support the second alternative. If in-plane compressive stresses did exist, they would have reduced the tensile load-induced and thermal stresses occurring at the pavement edge midway between the transverse joints. This reduction would have been caused by the compressive stresses being parallel to, but of opposite sign of, the load and thermal tensile stresses. In essence, the compressive stresses would have applied a prestressing along the slab length, reducing the effective tensile stress at the critical fatigue damage location (midway between the transverse joints, at the pavement edge). Using the ILLI-SLAB finite-element computer program and a load transfer efficiency equal to 91.8 percent, the results showed that the critical fatigue location for lateral traffic distributions centered at 0.5 and 2.6 m (center of each wheelpath) was under the inner wheel load 2.6 m from the pavement edge. A secondary critical fatigue location existed at 0.8 to 0.9 m from the pavement edge. These results indicated that primary longitudinal cracking should be initiating in the middle of the inner wheelpath, with secondary cracking at 0.8 to 0.9 m from the pavement edge. Field observations have shown that most longitudinal cracking originates in the inner wheelpath, as would be expected from the analysis conducted by this study.

Pavement Faulting

Of the PCC pavements that are fatigued (longitudinal cracked), the cracks developed within 10 to 15 years of construction and have not resulted in any decrease in overall pavement performance. The faulted PCC pavements, on the other hand, have deteriorated at such a rate that rehabilitation of approximately 80 to 160 km is currently required and approximately the same length will need to be rehabilitated within the next 5 to 10 years. Therefore, the main concern for WSDOT for the rehabilitation of PCC pavements has been to better understand the mechanism of faulting and the most appropriate and cost-effective rehabilitation method for the PCC pavements.

JOINT PERFORMANCE

To determine the levels of joint performance it is essential to quantify the slab deflections under an applied load. The FWD was used to determine the deflections of the PCC pavements under a normalized load of 40 kN. Typical pavement testing locations are shown in Figure 1. The deflection data were analyzed to determine joint load transfer and the presence of voids beneath the slabs.

Load Transfer Analysis

When a wheel load is applied at a joint both the loaded slab and adjacent unloaded slab deflect. The amount that the unloaded slab deflects is directly related to joint performance. If a joint is performing perfectly, both the loaded and unloaded slabs deflect equally. The amount that the pavement deflects is important because when deflection occurs tensile stresses are induced in the slab. The magnitude of these tensile stresses has a direct impact on pavement performance (the lower the stress, the longer the

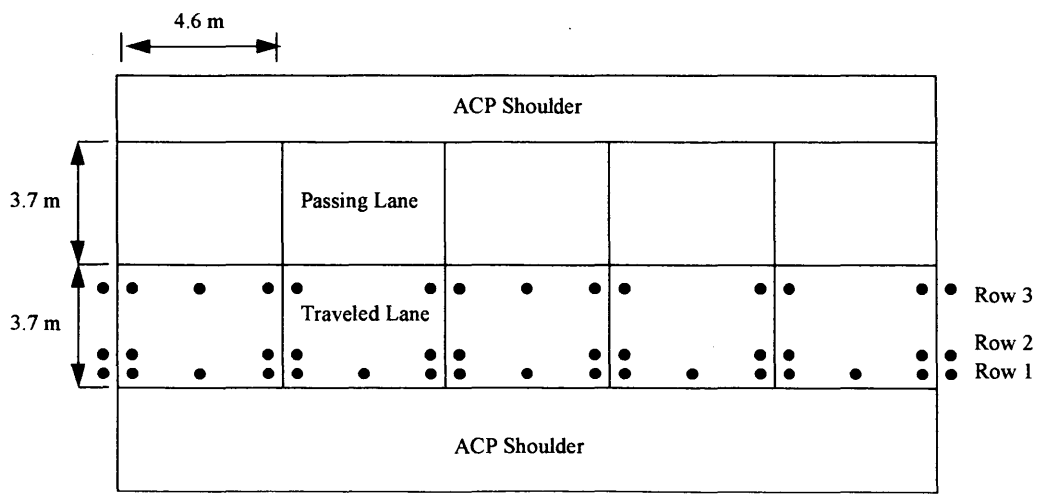

FIGURE 1 Typical FWD testing locations for I-90 PCC pavement rehabilitation test section.

fatigue life) (*4*). If joint performance is perfect and both slabs deflect equally, both slabs experience the same deflection and the same stress. The stresses induced in the loaded slab are thus reduced by 50 percent over what they would have been if there had been no load transfer between adjacent slabs. Besides affecting the magnitude of stress induced in the pavement, joint performance also affects faulting. If joint performance is poor, it is likely that joint faulting will occur.

One method of evaluating joint performance is by calculating load transfer efficiency across a joint or crack by using measured deflection data. Load transfer efficiency across a joint or crack is normally defined as the ratio of deflection of the unloaded side of the joint or crack to the deflection of the loaded side (*5*). The concept of joint load transfer efficiency is shown in Figure 2. Load transfer efficiency can be calculated by the following equation:

$$\text{load transfer} = \frac{\text{deflection of loaded slab}}{\text{deflection of unloaded slab}} \times 100 \quad (1)$$

Corner Slab Deflection Difference (CSDD)

A second measure of joint performance can be viewed by calculating the difference in the corner slab deflection between the approach and leave slabs. This can be viewed as the relative movement of the joint as a wheel load passes over the joint.

$$\text{CSDD} = |\text{deflection of loaded slab} - \text{deflection of unloaded slab}| \quad (2)$$

Void Detection Method

A third way of evaluating joint performance is by determining the voids or loss of support under the jointed concrete pavements (*3*). This procedure was used on several of the Interstate PCC pavements, and from that analysis it was determined that voids existed at most of the joint locations of the PCC pavements tested.

Slab Under View

To verify the results of the FWD testing and void detection method that was outlined, WSDOT lifted (removed) nine slabs at various locations across the state.

Present concrete pavement rehabilitation guides describe the faulting mechanism as a displacement or pumping of fines across the joint from the leave slab (typically) to the approach slab. This action results in the development of a void and increases in size with continued traffic loading. Void development then results in the leave slab being unsupported and generally leads to pavement faulting.

From the WSDOT analysis it was determined that voids developed only at locations where the underlying base material was cement-treated base. At other locations, where the base course is crushed stone, no void could be detected. At these locations it appeared that the fine material mitigated upward as well as horizontally across the joint, resulting in a wedge of fine material directly beneath the slab, presumably causing a reduction in slab support. This hypothesis is supported by gradations taken on either side of the joint for the wedge material and for the crushed stone base. Gradation samples of the crushed stone base were taken from a depth of 70 to 275 mm. Without exception all tests showed that the base material beneath the leave slab was finer than the material beneath the approach slab. In addition, measurements were taken on the topography of the concrete slab and the wedge material; it appeared that the faulting measurement and the height of the wedge material were roughly equal. Measurements were taken when slab temperatures were approximately 16°C, when curling of the slab was improbable.

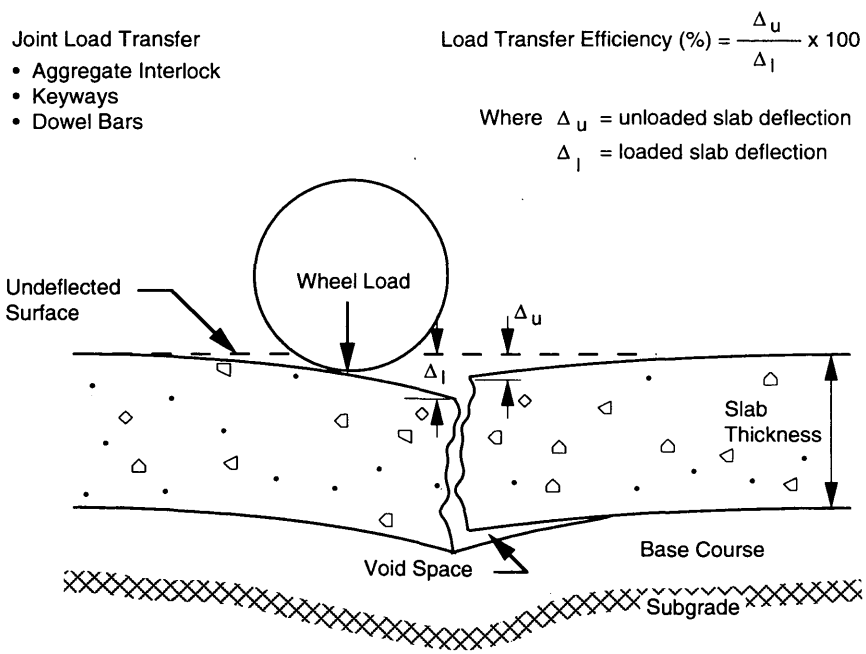

FIGURE 2 Concept of joint load transfer efficiency.

Therefore, since the major distress for the PCC pavements in Washington is in the form of faulting and no voids appear to exist at the joint locations, pavement subsealing, pavement grinding, or both, were viewed to have marginal effectiveness or at best a short-lived performance life.

Subsealing has been performed on several PCC pavement rehabilitation projects and has performed best on PCC pavements that have failed cement-treated base as the base course. Because voids are present beneath the slabs, the subsealing material is capable of filling the void. On the PCC pavements that have crushed stone as the base material (which is the dominant base type in Washington) no void is present and the subsealing material may be forced into the small gaps or channels that exist in the base course and can result in the creation of a larger void. This may cause the raising of the joints, which leaves the middle of the slab unsupported and leads to premature failure of the slab. This actually occurred under a special contract to restore a small test section (approximately 78 m) of faulted PCC pavement. The subsealing material was placed in an area where the base material was crushed stone, and the joints were raised, leaving the middle of the slab unsupported; this resulted in several fatigued (transversely cracked) and settled slabs.

Because pavement grinding does not correct the pavement deficiencies that initially caused the faulting and a reduction in pavement thickness increases the pavement edge stresses, faulting often recurs shortly after grinding has been completed. This rapid faulting recurrence has been noted on several PCC pavement sections on I-5 (Pierce-King County Line) and on I-90 (Snoqualmie Pass) where grinding was completed and joint faulting returned within 2 to 3 years.

National practice tends to support the use of subsealing and pavement grinding for restoring faulted PCC pavements. The results outlined above imply that additional rehabilitation techniques, beyond joint subsealing, pavement grinding, or both, will be required to rehabilitate the faulted PCC pavements in Washington.

PCC PAVEMENT REHABILITATION TEST SECTION

A PCC pavement rehabilitation test section was established on westbound I-90, milepost 77.35 to milepost 78.11 (a total length of 1.2 km), between West Nelson Siding Road and the Little Creek Bridge, approximately 5 km west of Cle Elum, Washington, and approximately 130 km east of Seattle. The climate in this area of Washington is a wet-freeze with approximately 580 mm of annual precipitation. The pavement was constructed in 1964 and has experienced approximately 10,000,000 equivalent single axle loads (ESALs) since its original construction. The pavement is 230 mm of plain jointed concrete on a crushed stone base with a joint spacing of 4.6 m. The shoulders consist of asphalt concrete.

Existing Pavement Distress

The existing distress of the PCC pavement outside lane were a few slabs with single transverse cracks (midpanel) and contraction joint faulting. Cracking and faulting (Table 1) were relatively uniform between Sections A, B, C, and D. The faulting ranged from a minimum of 2 mm to a maximum of 16 mm, with an overall average of about 8 mm. Generally, a fault of 5 mm or more is considered critical.

Test Section Details

The test section is being used to determine the effectiveness of four experimental features in reducing fault development: (a) retrofitted dowel bars, (b) a 1.2-m-wide tied and doweled concrete shoulder, (c) retrofitted dowel bars and a 1.2-m-wide tied and doweled concrete shoulder, and (d) a control section that received no treatment other than pavement grinding. The test section was also included in the diamond grinding project, which was from milepost 69.52 to milepost 102.49 (westbound only). Construction was completed in September 1992. The test section layout is shown in Figure 3.

Retrofit Dowel Bars

Restoration of joint load transfer across a transverse joint is necessary so that joint deterioration, pumping, faulting, spalling, and corner breaks can be minimized. Previous field studies have demonstrated the ability of retrofit load transfer devices to improve deflection load transfer and thereby delay the recurrence of faulting (*6*). Load transfer restoration should be considered for all transverse joints and cracks that exhibit measured deflection load transfers of between 0 and 50 percent (*5*).

Dowels placed in slots cut in the pavement are effective in restoring load transfer across joints or cracks. Dowels should be 457 mm long and at least 32 mm in diameter (*5*). In addition, the

TABLE 1 Pavement Distress

	Number	July 1992				March 1993			
Section	of Slabs	Trans.	Long.	Corner	Fault	Trans.	Long.	Corner	Fault
A	67	8	0	1	10 mm	9	3	1	0 mm
B	69	5	0	3	8 mm	5	0	4	0 mm
C	68	4	0	5	7 mm	4	5	5	1 mm
D	66	10	0	1	7 mm	10	0	1	2 mm

Trans. = Number of slabs that are cracked transversely.
Long. = Number of slabs that are cracked longitudinally
Corner = Number of slabs with corner cracks
Fault = Average faulting (mm) for entire section

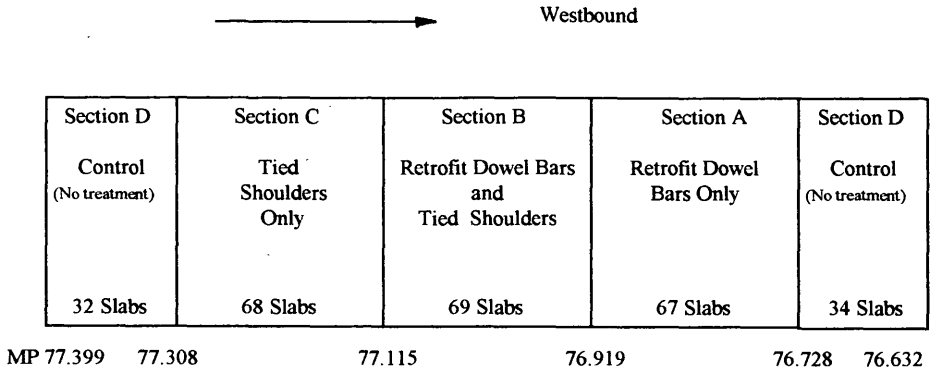

FIGURE 3 Test section layout.

number of dowel bars placed per joint has some significance on the performance of joint load transfer restoration. "In most but not all cases, sections with five dowels per wheelpath had slightly higher load transfer efficiencies than sections with three dowels per wheelpath. Similarly, sections with 38 mm dowels had slightly higher load transfer efficiencies than sections with 25 mm dowels. Dowel length did not appear to affect load transfer efficiency" (*6*). In addition, the AASHTO design guide (1993) (*5*) recommends the placement of two or three 41-mm-diameter dowel bars per wheelpath or four to six 32-mm-diameter dowel bars per wheelpath.

The diameters of the dowels and the numbers placed in the outer wheelpath have a major influence on the prevention of faulting. "Three dowels per wheelpath and five dowels per wheelpath performed equally well in terms of faulting. Dowel length had mixed results on faulting. Dowel diameter appeared to significantly affect faulting: sections with 25 mm diameter dowel bars showed increases in faulting, while sections with 38 mm diameter dowels did not" (*6*).

Therefore, on the basis of a study done in Florida (*6*), the AASHTO design guide, and contacts made by WSDOT personnel, it was determined that a total of eight dowel bars (four per wheelpath) with a diameter of 38 mm and a length of 457 mm would be used per joint to restore load transfer and minimize fault development.

The dowel bar slots were saw cut to a width of 64 mm, a depth of approximately 146 mm or as required to place the center of the dowel at middepth, and the required length for bar placement. Lightweight jackhammers (weight less than 14 kg) were used to loosen the concrete. All exposed surfaces were sandblasted and cleaned before the installation of the dowel bar. Epoxy-coated dowel bars were inserted and held in position by supporting chairs. Dowel bars were placed so that horizontal and perpendicular alignment with the existing slabs and joints was maintained. Dowel bar end caps were not used in this project. A mastic filler was placed in the joint to prevent the backfill material from filling the joint. The slot was then backfilled with Burke Fast Patch 928 grout.

Tied Concrete Shoulders

A major advantage in using tied PCC shoulders or a widened outside lane is the reduction in slab stresses. Reductions in slab stresses have been shown to increase the performance life of the pavement.

A 1.2-m concrete shoulder was tied to the existing outside lane with epoxy coated No. 5 reinforcing bars with a length of 762 mm. The tie bar holes were pneumatically bored into the existing concrete with a backhoe-mounted device that was capable of boring three holes at one time. The tie bars were then epoxy grouted into the existing concrete panels. Three epoxy-coated dowel bars were also placed in the transverse contraction joints. The concrete was placed by using a Gamaco slip-form paver. Other construction considerations are outlined in the following sections.

Section A (Retrofit Dowel Bars Only)

Four dowel bars in each wheelpath were spaced 305 mm apart. The first dowel bar in the outer wheelpath was placed 305 mm from the lane/shoulder edge. The first dowel bar in the inner wheelpath was placed 610 mm from the longitudinal joint with the adjacent lane. The entire section was then diamond ground to remove faulting. The section was approximately 305 m long. See Figure 4 for retrofit dowel bar layout.

Section B (Retrofit Dowel Bars and Tied Shoulders)

The same number and configuration for the dowel bars described for Section A were used. The added PCC shoulders were the same thickness as the existing pavement PCC main lanes (230 to 255 mm thick). The entire section was then diamond ground to remove faulting. This section was approximately 305 m long. See Figures 4 and 5 for retrofit dowel bar and tied shoulder layouts, respectively.

Section C (Tied Shoulders Only)

The tied PCC shoulders were the same as those described for Section B. The entire section was then diamond ground to remove faulting. This section was approximately 305 m long. See Figure 5 for tied shoulder layout.

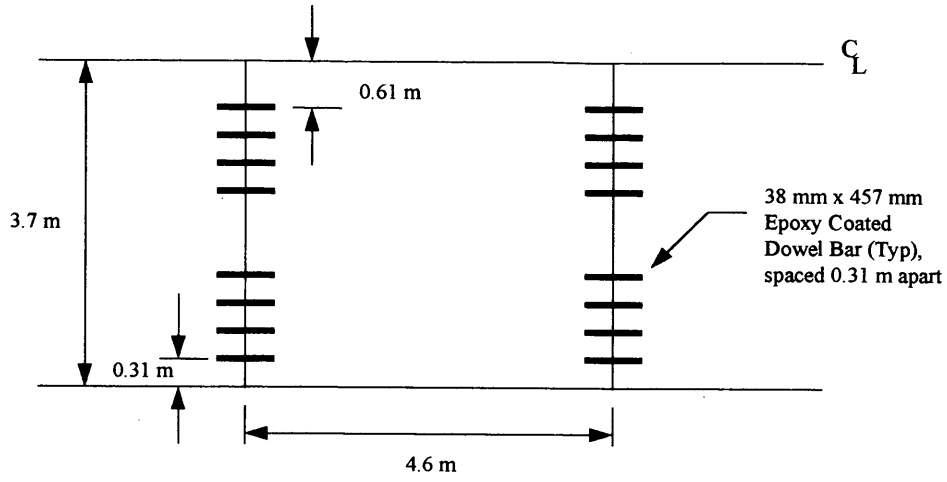

FIGURE 4 Retrofit dowel bar layout.

Section D (Control)

The control section was split into approximately 152-m-long sections at the beginning and end of the experimental features. The entire section was diamond ground to remove faulting.

Load Transfer Analysis

FWD testing was conducted before construction in July 1992, within 2 weeks following construction in September 1992, March 1993, and July 1993. On the FWD test days the deflection measurements were obtained so that large thermal gradients in the slabs [the more critical condition at transverse joints (larger deflections) occurs when the slabs are curled upward, which is due to a lower surface slab temperature and a higher bottom slab temperature] were avoided. This was accomplished by placing a thermometer at the bottom of the slab and at the top of the slab, and the changes in slab temperature were monitored. Testing was conducted such that the air temperature was less than 27°C. Testing was terminated when the limiting (maximum) thermal gradient equaled 17°C between the top and bottom of the slab.

All FWD testing was performed in the outside lane; I-90 has two westbound lanes at this location. As shown in Figure 1, Row 1 was located on the outside edge of the PCC slabs, Row 2 on the outside wheelpath, and Row 3 inside the wheelpath. Four FWD testing locations, each consisting of five continuous slabs, were established for each experimental feature. For each experimental feature these locations occurred at the beginning, at approximately 90 m, at approximately 180 m, and at the end of the section.

As outlined previously, the deflection data were evaluated by determining the load transfer efficiency and the corner slab deflection differences; a summary of these results is shown in Tables 2 and 3 (July 1992 and March 1993), respectively. The retrofitted dowel bars only (Section A) generally increased the load transfer efficiencies from an average of 33 percent and a COV of 46 percent to an average of 82 percent and a COV of 6 percent. The retrofit dowel bars and tied shoulder had results similar to those for Section A. The tied shoulders only (Section C) increased the

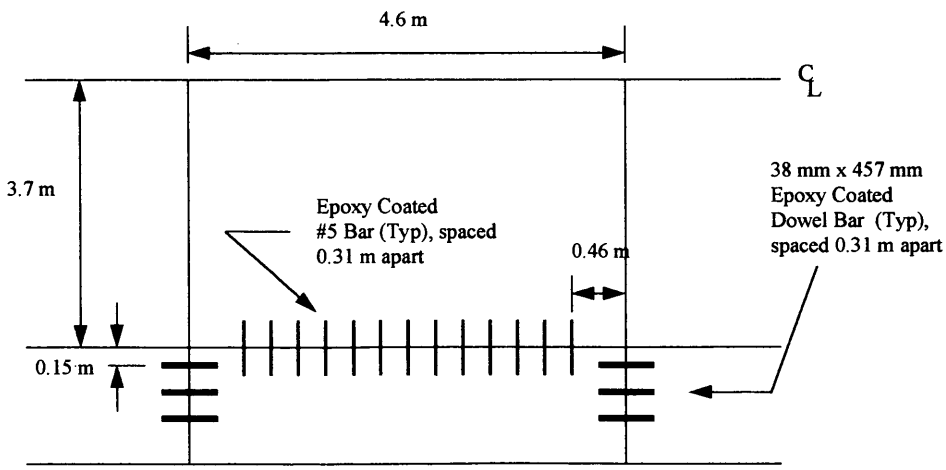

FIGURE 5 Tied shoulder layout.

TABLE 2 Summary of Load Transfer Analysis

TITLE	Row 1 Jul 92	Row 1 Mar 93	Row 2 Jul 92	Row 2 Mar 93	Row 3 Jul 92	Row 3 Mar 93
Dowel Bars Only						
Average	33	82	37	92	29	92
Standard Deviation	15	5	18	3	10	3
Dowel Bars & Shldrs						
Average	41	88	38	90	39	91
Standard Deviation	23	4	25	4	20	3
Shoulders Only						
Average	27	72	22	63	41	81
Standard Deviation	13	17	11	19	24	9
Control						
Average	52	50	45	59	58	79
Standard Deviation	24	15	14	16	24	10

Jul 92 - Pre Construction Mar 93 - In service for 6 months

load transfer efficiencies from an average of 27 percent and a COV of 50 percent to an average of 72 percent and a COV of 23 percent. Similar trends are also noted with the corner deflection differences.

Thus, retrofitted dowel bars appear to be an effective PCC rehabilitation treatment. The addition of tied shoulders only was shown to be of some benefit. On the basis of the FWD data the tied shoulder-only section (Section C) appears to be the worst section on the basis of the lowest average load transfer and the highest average center deflection difference) of all four sections. Although relatively good results were obtained with the tied shoulder, it is believed that a tied shoulder would be better applied in an area that had a load transfer in the range of 50 to 70 percent instead of the 20 to 40 percent range experienced by Section C. It appears that the tied shoulder would be more effective as a preventative measure than as a total load transfer restoration option.

Faulting Analysis

As stated previously, the existing, prerehabilitated PCC pavement had an average fault of 8 mm. Following the grinding operation it was assumed that all faults were removed. On the basis of the fault measurements of March 1993, the average faulting for each of the sections is shown in Table 1. On the basis of an in-service measurement after 7 months and approximately 700,000 ESALs the retrofitted dowel bar sections (Sections A and B) have performed extremely well with an average fault of 0.1 mm, the tied shoulder-only section (Section C) has an average fault of 0.6 mm, and the control section has an average fault of 1.8 mm (Figure 6). A straight-line regression analysis was performed on the average fault measurements for each of the sections (Figure 7). Life to previous (before rehabilitation) fault measurements for the control section (Section D) was used as an ending point. From the regression analysis it was determined that within 28 months Section D would be faulted to the level that it was before rehabilitation (which in this case was only pavement grinding). This tends to support the previous deduction that grinding alone on faulted pavements in Washington is not a cost-effective rehabilitation option.

Cost Comparison

The cost comparison is based on the rehabilitation of two 3.7-m lanes and 4.3 m of total shoulder width (total pavement width of 8.0 m). Rehabilitation considerations include three options: (a) retrofit dowel bars and pavement grinding, (b) 1.2-m tied shoulders and pavement grinding, and (c) 110-mm ACP overlay. All three options include rehabilitation of the ACP shoulders, and for Options a and b pavement grinding is for the right lane only. On

TABLE 3 Summary of Corner Deflection Differences

TITLE	Row 1 Jul 92	Row 1 Mar 93	Row 2 Jul 92	Row 2 Mar 93	Row 3 Jul 92	Row 3 Mar 93
Dowel Bars Only						
Average	2.55	0.46	2.33	0.17	1.60	0.19
Standard Deviation	1.53	0.31	1.98	0.15	1.46	0.13
Dowel Bars & Shldrs						
Average	4.05	0.30	3.48	0.26	1.85	0.20
Standard Deviation	2.96	0.25	2.30	0.16	1.06	0.10
Shoulders Only						
Average	5.40	0.67	4.33	1.09	1.38	0.37
Standard Deviation	4.14	0.68	2.72	0.87	1.69	0.32
Control						
Average	2.13	1.47	1.95	1.01	0.90	0.30
Standard Deviation	1.95	1.33	1.60	0.82	0.98	0.32

Jul 92 - Pre Construction Mar 93 - In service for 6 months

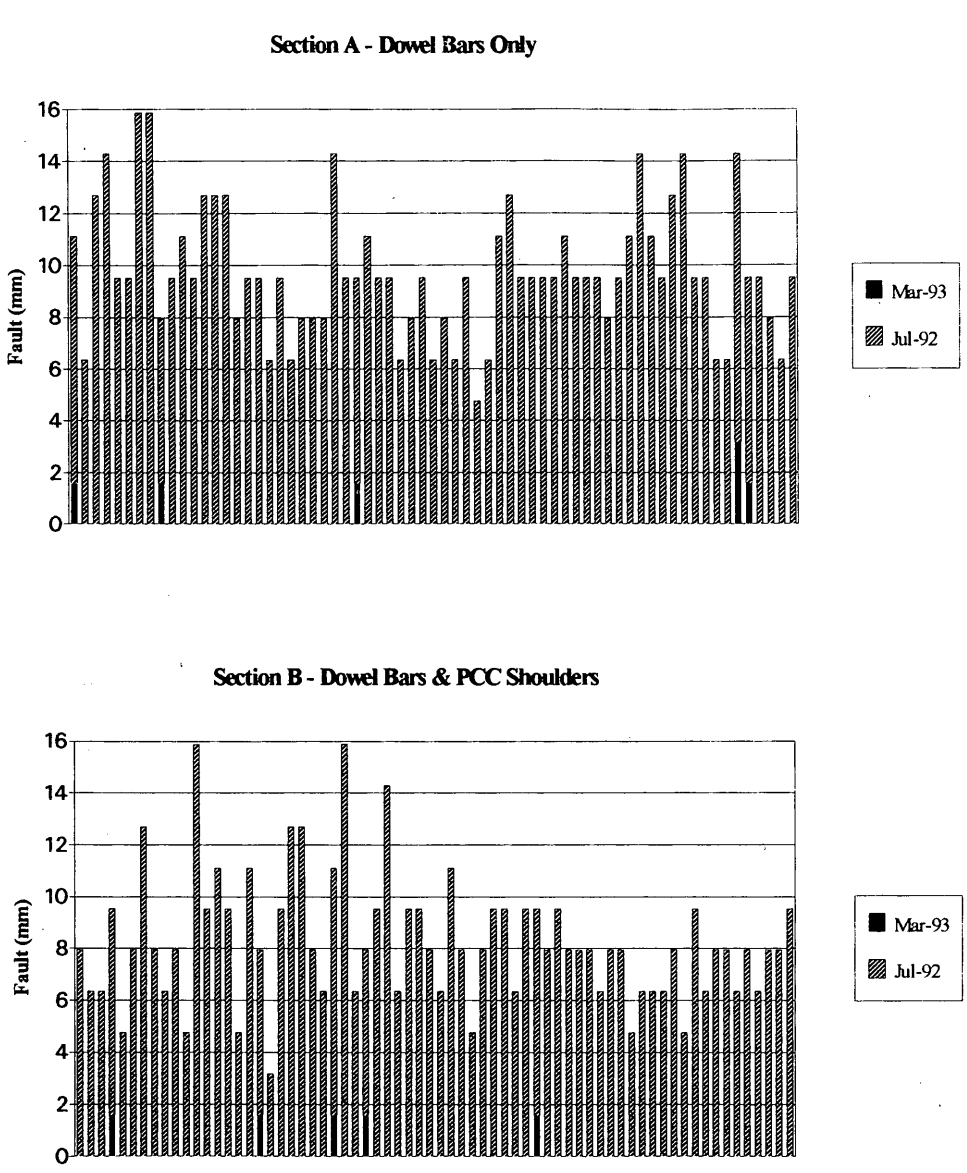

FIGURE 6 Fault measurements.

the basis of material costs, rehabilitation using retrofit dowel bars and pavement grinding is estimated to be $73,800 per lane-km, that using tied shoulders and pavement grinding is estimated to be $69,100 per lane-km, and that using an ACP overlay is estimated to be $118,300 per lane-km.

The costs of materials for the dowel bar retrofit were taken from the WSDOT project currently under construction on the eastbound lanes of I-90 (same vicinity but in the opposite direction of the PCC pavement test section outlined in this paper), tied shoulder material costs are based on the PCC pavement test section and adjusted for anticipated prices for a larger-scale project, and ACP overlay costs are based on statewide average bid prices.

SUMMARY

The performance and evaluation of Interstate PCC pavements in Washington have been discussed. The main concern of many state agencies has been the cause and rehabilitation of the faulted PCC pavements. At this point retrofitted dowel bars appear to be the most cost-effective option for restoring load transfer to the faulted PCC pavements in Washington. The first extensive PCC pavement rehabilitation project in Washington has been in service for approximately 15 months, and initial results support the use of retrofit dowel bars for load transfer restoration. In addition, the use of a tied shoulder appears to have benefits when applied at an early stage of load transfer restoration.

On the basis of an initial analysis of the project and the results of past studies (*6*), the expected performance life of the retrofitted dowel bars is estimated to be 10 years. Of course, this does not account for any early failure of the doweled sections because of improper dowel placement, dowel lockup, or failure of the grout material. Long-term performance may indicate different conclusions. Only time, traffic, and continued pavement monitoring will verify or modify these initial observations.

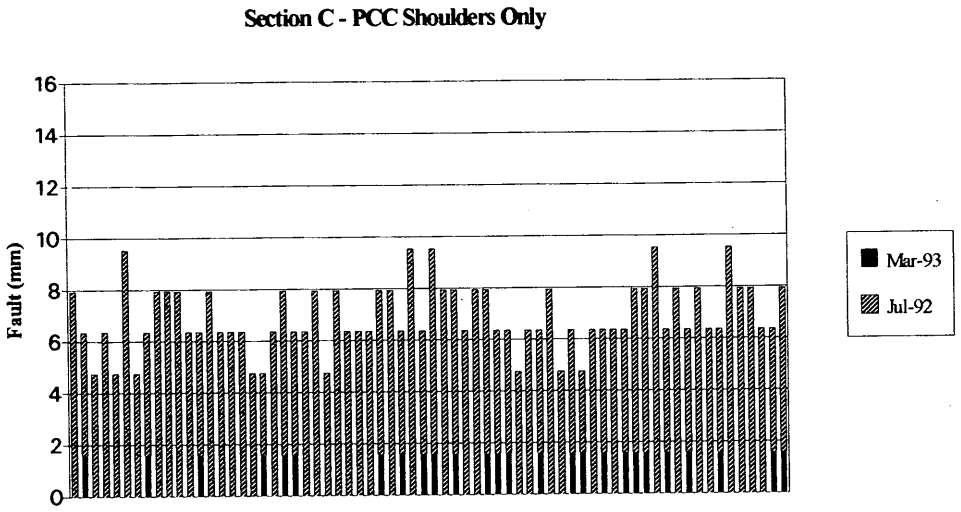

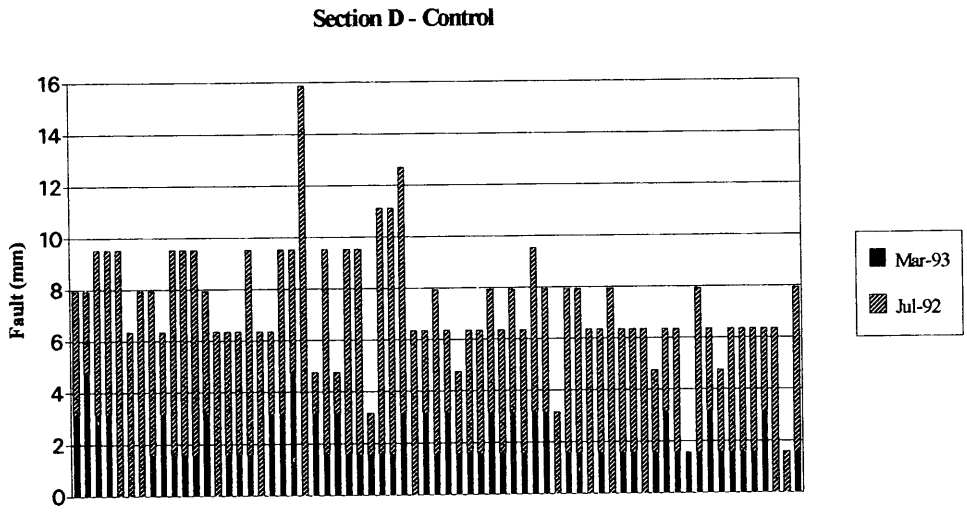

FIGURE 6 *Continued.*

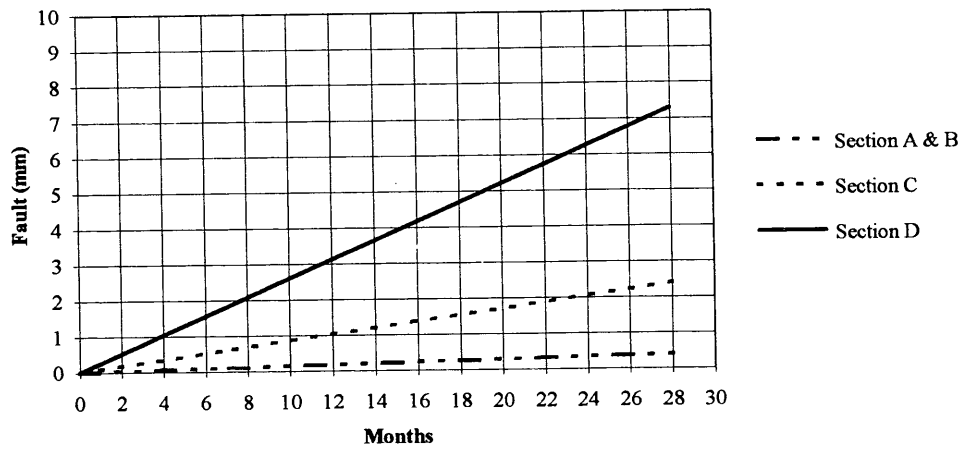

FIGURE 7 Timing for return of original faulting.

ACKNOWLEDGMENTS

The author expresses appreciation to the Research Office of WSDOT for continual support and assistance in the completion of this study. In addition, the author thanks Arnie Korynta (WSDOT), Newt Jackson (formerly of WSDOT), and Joe Mahoney (University of Washington) for technical assistance in the preparation of this paper.

REFERENCES

1. *Special Report 61E: The AASHO Road Test, Report 5: Pavement Research.* HRB, National Research Council, Washington, D.C., 1962.
2. Mahoney, J. P., J. A. Lary, L. M. Pierce, N. J. Jackson, and E. J. Barenberg. Urban Interstate Portland Cement Concrete Rehabilitation Alternatives for Washington State. WSDOT Research Project Y3399, Task 12. Washington State Department of Transportation, April 1991.
3. Crovetti, J. A., and M. I. Darter. Void Detection for Jointed Concrete Pavements. In *Transportation Research Record 1041*, TRB, National Research Council, Washington, D.C., 1985.
4. Mindess, S., and J. F. Young. *Concrete.* Prentice-Hall, Inc., Englewood Cliffs, N.J., 1981.
5. *Guide for Design of Pavement Structures.* AASHTO, Washington, D.C., 1993.
6. Hall, K. T., M. I. Darter, and J. M. Armaghani. Performance Monitoring of Joint Load Transfer Restoration. In *Transportation Research Record 1388*, TRB, National Research Council, Washington, D.C., 1993, pp. 129–139.

Publication of this paper sponsored by Committee on Pavement Rehabilitation.

Use of Three-Dimensional, Dynamic, Nonlinear Analysis To Develop Load Equivalency Factors for Composite Pavements

SAMEH M. ZAGHLOUL, THOMAS D. WHITE, AND THOMAS KUCZEK

Asphalt overlays are frequently used to improve the serviceability of a deteriorated concrete pavement. The asphalt overlay has a significant influence on the concrete pavement's behavior and response to loads. Most highway agencies approximate the behavior of composite pavements to that of asphalt or concrete pavements. In fact the 1993 AASHTO design guide suggests that concrete pavement load equivalency factors (LEFs) be used to assess the effects of traffic on composite pavements. This is an approximation and has not been validated with field measurements or realistic analytical procedures. From a structural point of view an asphalt overlay of a concrete pavement should have a significant effect on the response of the composite pavement. A logical approach for the development of composite pavement LEFs is presented. These LEFs were developed for a study of permissible overloads and are based on total deformation, elastic and plastic, at the pavement surface. A three-dimensional dynamic finite-element mesh (3D-DFEM) method of analysis was used to analyze the composite pavements. The 3D-DFEM was verified in two steps for asphalt and concrete pavements: first for static, linear elastic analysis and then for dynamic, nonlinear analysis. Moving loads and realistic material models were used in the analysis.

Estimating the amount and characteristics of truck traffic is a vital step in pavement analysis, design, and evaluation. Most highway pavement design and evaluation procedures use the concept of load equivalency factors (LEFs) to convert a mixed traffic stream of different axle loads and configurations into a design traffic number. This number represents all of the axle loads expected to use the pavement during the design period converted into an equivalent number of 18-kip (8167-kg) single-axle loads (SAL) (*1*).

The most commonly used LEFs are those published by AASHTO (*2*). These LEFs are based on the AASHO Road Test (*3*) results and the concept of pavement serviceability. In the AASHO Road Test, asphalt and concrete pavement sections were constructed and tested with single and tandem axle loads. The present serviceability index (PSI), which is a function of slope variance (roughness), cracking and patching for concrete pavement, plus rutting for asphalt pavement, was used as a measure of pavement performance. Empirical relationships were developed to correlate PSI to the number of load repetitions for asphalt and concrete pavements. No composite pavement sections of asphalt overlaying concrete were included in the AASHO Road Test, and therefore no LEFs were developed for composite pavements. The 1993 AASHTO design guide (*1*) recommends the use of concrete pavement LEFs for composite pavements, ignoring the asphalt overlay thickness. In this case the effect of traffic on composite pavements is assumed to be similar to that of traffic on concrete pavements.

Other empirical LEFs, such as CanRoad LEFs (*4*), do not address composite pavements. Analytically based LEFs are based on multilayer elastic analysis. The model for this analysis assumes that pavements extend to infinity in the lateral and longitudinal directions and that the subgrade has infinite depth. Assumptions are also made in multilayer analysis that pavement materials are linear elastic and truckloads are static. Previous analysis (*5*) showed a lack of agreement between these types of LEFs and the AASHTO LEFs.

A study funded by the Indiana Department of Transportation (INDOT) and FHWA was conducted at Purdue University to develop a procedure for permitting overloaded trucks in Indiana. In that study the Indiana highway network was categorized into three classes: Interstate and U.S. highways and state roads (SRs). A typical pavement cross section was selected to represent each category in the analysis. Selection of these representative cross sections was made on the basis of the information available in the Road Life data base (*6,7*). The Road Life data base contains information about pavement structures and subgrade materials for more than 50 percent of the total lane miles of highways managed by INDOT. It was found that more than 60 percent of Indiana highways are jointed reinforced concrete pavements (JRCPs) overlaid at least once with asphalt concrete. Four typical pavement cross sections were selected to represent the different highway categories for the overload permit study. Composite cross sections that represented 70 and 77 percent of the total lane miles of Interstate and U.S. highways, respectively, were selected. Two cross sections were selected for the SR category: a composite pavement section representing 55 percent of the total SR lane miles and an asphalt cross section representing 40 percent of the total SR lane miles (*8*). Figure 1 shows typical cross sections of the composite pavements included in the overload permit study. Lean clay (CL) was found to be the predominant soil in Indiana; therefore, a CL subgrade was assumed for the typical sections.

A sample of overload permit applications was reviewed to determine the truck configurations being permitted. This sample revealed that permits were requested for trucks with up to nine axles in one group as well as trucks with axle loads of up to 72 kips (32 668 kg) (*9*). The AASHTO Road Test included only single and tandem axle loads up to 40 kips (18 149 kg) and 48 kips (21

School of Civil Engineering, Purdue University, West Lafayette, Ind. 47907.

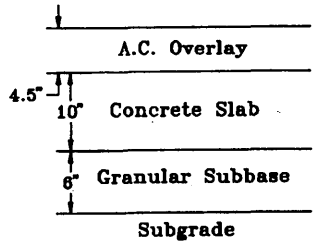

Typical JRCP Cross Section for Interstate Highways

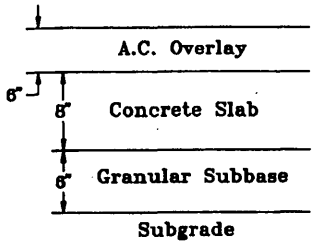

Typical JRCP Cross Section for U.S. Highways

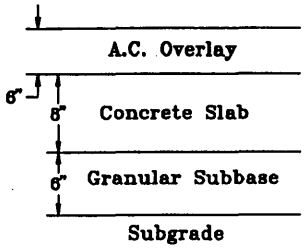

Typical JRCP Cross Section for State Roads

FIGURE 1 Typical composite pavement cross sections. (1 in. = 2.54 cm).

779 kg), respectively. LEFs based on AASHO Road Test results are valid only for these axles and load ranges. Simple extrapolation of regression relations beyond the range of factors for which data have been collected is risky without realistic material and structural models. This appears to be a deficiency of the AASHTO *Guide for Design of Pavement Structures* (*1,10*), in which LEFs are presented for single and tandem axle loads higher than those in the Road Test as well as for tridem axles, which were not used in the Road Test at all. These extrapolations were made by using the original serviceability-based regression equations for performance (*1*).

In this paper LEFs for composite pavements are presented. These LEFs are developed for a study examining permissible overloads and are based on total deformation, elastic and plastic, at the pavement surface [total surface deflection (TSD)]. A three-dimensional dynamic finite-element mesh (3D-DFEM) method was used to analyze the composite pavements (*11*). This 3D-DFEM has the capability of simulating truckloads moving at different speeds. Also, it can model paving materials as elastic, elastic-plastic, plastic, and viscoelastic materials. The 3D-DFEM predicts both the elastic and plastic pavement responses for one or more load applications. The 3D-DFEM was verified in two steps for asphalt and concrete pavements: first for static, linear elastic analysis and then for dynamic, nonlinear analysis (*12,13*). Verification studies for both pavement types showed excellent results.

3D-DFEM ANALYSIS

Model Geometry

The typical composite pavement cross sections for Interstate and U.S. highways and SRs, shown in Figure 1, were modeled in this analysis as two 12-ft lanes plus 8-ft shoulders on either side. The pavement structural model consisted of three layers: asphalt surface, concrete slab, and granular subbase on top of a CL subgrade. Shoulders were modeled to be untied concrete shoulders with the same structure as the traffic lanes. 3D-DFEM with variable openings was created to model the pavement structures. The mesh with variable size openings was used to reduce the computer memory requirements and computational time. A smaller mesh spacing was used to provide detailed response predictions where needed. Pavement structures were modeled as a set of layers. Figure 2 shows one of the 3D-DFEMs used in the analysis. In this example the subgrade thickness was represented by three elements, the concrete slab thickness was represented by two elements, and the granular subbase and the asphalt overlay thicknesses were represented by single elements. Longitudinal and transverse joints were modeled by using gap elements with an initial opening of 3/8 in. (9.53 mm). Depending on the deformed shape of the slabs after loading, the slabs might come into contact and develop friction. Dowel bars were modeled and located in the midthickness of the slab. The bond stress of one-half of the dowel bar was set to zero. Reflected cracks in the asphalt overlay were modeled by using interface elements. Details of the finite-element features used in this analysis are reported by Zaghloul and White (*12,13*). Loads were sequentially applied at surface nodes. The time rate of loading from one node to the next simulated vehicle speeds. From previous studies (*5,14*) vehicle speed was found to have a significant effect on pavement response. Therefore, a speed similar to the average speed of the AASHO Road Test, 35 mph (*15*), was used in developing the LEFs.

Material Models

In the analysis pavement materials were divided into four groups: asphalt concrete, portland cement concrete, granular materials, and

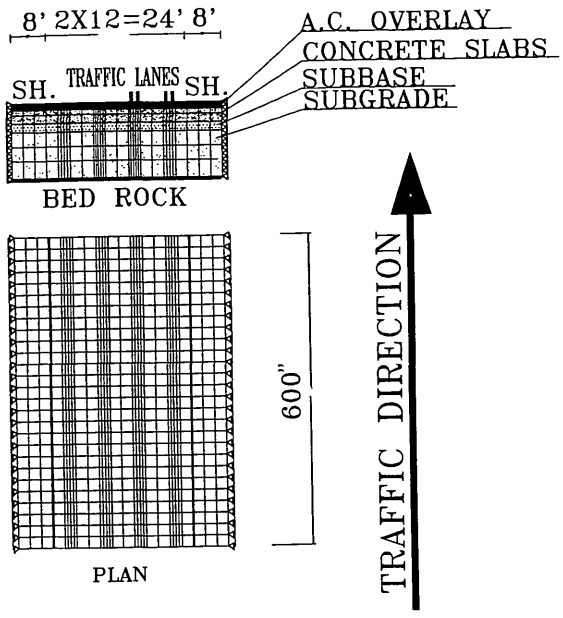

FIGURE 2 Example of a 3D-DFEM used in analysis (1 in. = 2.54 cm and 1 kip = 453.7 kg).

cohesive soils. Details of these material models were reported by Zaghloul in 1993.

Asphalt concrete was modeled as a viscoelastic material. The response of this type of material to loading is time and temperature dependent (*16*). These characteristics were represented by instantaneous and long-term shear moduli (*17*). The instantaneous shear modulus was selected at a loading time of 0.1 sec, and the long-term shear modulus was selected at a loading time of 1.0 sec. These loading times represented speeds of 40 and 1.5 mph, respectively. The temperature effect was considered through the shear modulus values. Figures 3(*a*) shows the effect of loading time and temperature on asphalt mixture stiffness.

Granular materials, base, subbase, and subgrade in some cases were modeled by using the Drucker-Prager model (*17,20*). This is an elastic-plastic model in which granular materials are assumed to behave elastically for low stress levels. When the stress level reaches a certain yield stress, the material will subsequently behave as an elastic-plastic material. Figure 3(*b*) shows the assumed stress-strain curve for a granular material.

The Cam-Clay model (*17,21,22*) was used to model clays. This model uses a strain rate decomposition in which the rate of deformation of the clay is decomposed additively into an elastic and a plastic part. Figure 3(*c*) shows the assumed soil response in pure compression.

Portland cement concrete behavior was divided into three stages: elastic, plastic, and after failure. Figure 3(*d*) shows the stress-strain curve used to model portland cement concrete. If the concrete slab is subjected to a stress level less than its yield stress, it will behave as an elastic material. When the stress level exceeds the yield stress of the concrete, behavior is elastic-plastic until the stress reaches the failure limit. At that point the after-failure stage starts (*17*).

Other material and layer characteristics required in the analysis include modulus of elasticity, Poisson's ratio, damping coefficient, and bulk density. Table 1 shows the typical material properties used in the analysis.

As a general assumption, concrete slabs are assumed to be repaired before construction of the overlay, which is a common technique in Indiana. Longitudinal and transverse joints were modeled in the concrete slab, as were the corresponding reflected cracks in the asphalt overlay. These cracks were extended through the shoulders.

VERIFICATION ANALYSIS

Several studies were conducted to verify the 3D-DFEM predictions.

Static Analysis Verification Studies

Asphalt Pavement

Predictions were compared for a multilayer analysis by using the computer program Bitumen Structures Analysis in Roads (BISAR) (*23*), and the 3D-DFEM assuming linear elastic material properties and static loads. There was good agreement between the two model predictions of deflection at different depths and offset distances from the loaded area (R^2 = 0.96). The factors included in that study were thickness of the asphalt layer, thickness of the granular layers, and subgrade modulus of elasticity (*12*).

Concrete Pavement

A comparison was also made of predictions of concrete pavement response by using Westergaard's equations and the 3D-DFEM assuming linear elastic material properties and static loads. These results also showed good agreement (R^2 = 0.977). The factors included in that study were thickness of the concrete slab, subgrade type, and load position (*13*).

Dynamic Analysis Verification Studies

Asphalt Pavement

Verification of dynamic response was made by comparing field-measured pavement deflections from loads moving at different speeds and the 3D-DFEM predictions for similar conditions (pavement structure, load magnitude and configuration, and speed). The predictions were in good agreement with the measurements (R^2 = 0.999). Figure 4(*a*) shows the result of the comparison (*5*).

Concrete Pavement

Verification of dynamic response was also made for concrete pavements by comparing field-measured pavement deflections from moving loads and the 3D-DFEM predictions for similar conditions (pavement structure, load magnitude and configuration, and speed). There was also excellent agreement between the pre-

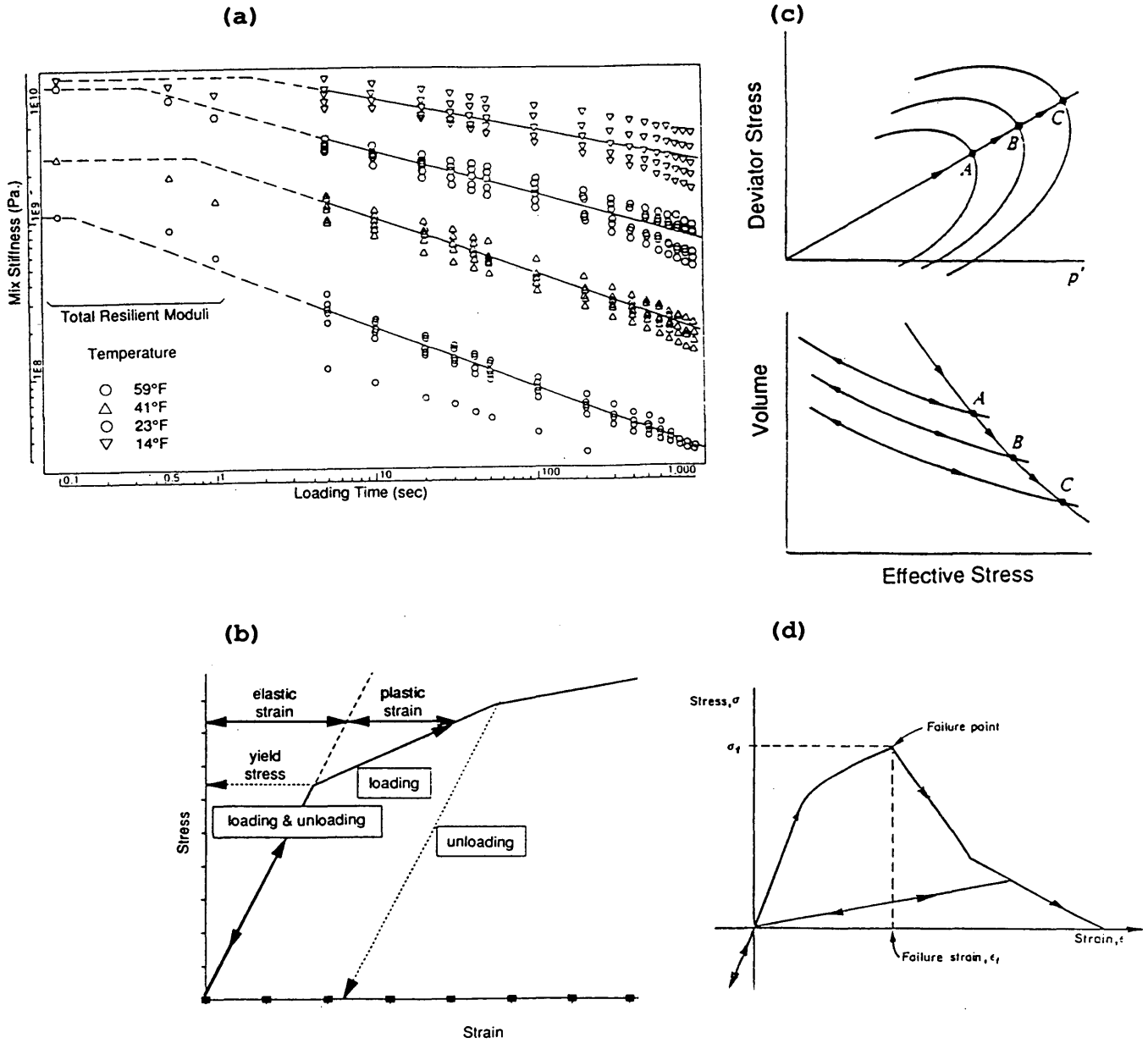

FIGURE 3 Material models used in analysis: (*a*) asphalt mixtures (*18*); (*b*) granular materials (*11*); (*c*) clays (*19*); (*d*) concrete (*11*).

dictions and the measurements (R^2 = 0.996). Figure 4(*b*) shows the result of this comparison (*14*).

Analysis of Falling-Weight Deflectometer Tests

A study was also conducted to verify the dynamic analysis capabilities of the 3D-DFEM by using a falling-weight deflectometer (FWD) data set for a full-depth asphalt section in Indiana. Excellent results were obtained from that study. The predicted peak deflections were found to match the measured ones. Also, the deflection history curves (deflection with time) at different offset distances were found to be in good agreement with the measured ones. The absolute sum of errors between the measured and predicted deflections was 6 percent. Figure 4(*c*) shows the measured and predicted deflection basins (*24*).

LEF Verification Studies

Asphalt Pavement LEFs

Comparisons among the AASHTO LEFs, Purdue LEFs, and other LEFs for single and tandem axle configurations showed excellent agreement between the AASHTO and Purdue LEFs. Conditions similar to those of the AASHO Road Test (layer thicknesses, material properties, and speed) were assumed in the analysis for developing the Purdue LEFs. There was poor agreement between

TABLE 1 Typical Material Properties Used in Analysis

Material Name	Material Property	Typical Value
Asphalt Surface	Modulus of Elasticity - psi	400,000 (2.762 GPa)
	Poisson's Ratio	0.3
	G-Ratio	0.8
	Density - pcf	150 (2.403 gm/cm^3)
	Damping Coefficient (%)	5
Concrete Slabs	Modulus of Elasticity - psi	4,000,000 (27.62 GPa)
	Poisson's Ratio	0.15
	Initial Yield Stress - psi	2670 (18.4 MPa)
	Failure Plastic Strain	1.3E-03
	Density - pcf	150 (2.403 gm/cm^3)
	Damping Coefficient (%)	5
Granular Subbase	Modulus of Elasticity - psi	40,000
	Poisson's Ratio	0.3
	Initial Yield Stress - psi	19.29 (0.133 MPa)
	Initial Plastic Strain	0.0
	Angle of Friction - degree	33
	Density - pcf	135 (2.1625 gm/cm^3)
Material Name	**Material Property**	**Typical Value**
	Damping Coefficient (%)	5%
Lean Clay (CL) Subgrade	Shear Modulus - psi	2750 (18.964 MPa)
	Poisson's Ratio	0.3
	Logarithmic Hardening Modulus	0.174
	Initial Overconsolidation Parameter - psi	8.455 (58.306 KPa)
	Permeability - ft/sec	0.000021 (0.00064 cm/sec)
	Initial Void Ratio (%)	8
	Initial Stress psi	weight of the pavement layers
	Density - pcf	130 (2.0824 gm/cm^3)
	Damping Coefficient (%)	5

the AASHTO and the other LEFs. Results of these comparisons are shown in Figures 5(*a*) and 5(*b*).

Concrete Pavement LEFs

A comparison also shows excellent agreement between the AASHTO and Purdue LEFs for concrete pavements for single and tandem axle configurations. Conditions similar to those of the ASSHO Road Test (layer thicknesses, material properties, and speed) were assumed in the analysis for developing the Purdue

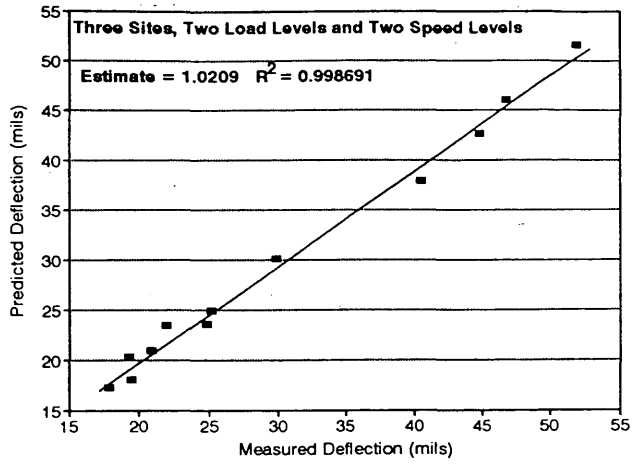

(a)

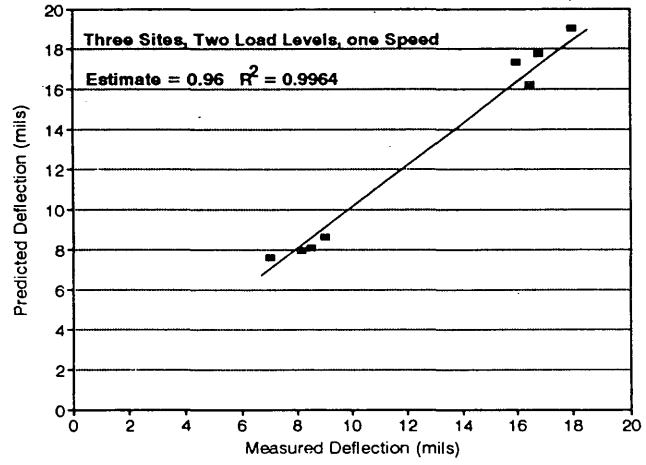

(b)

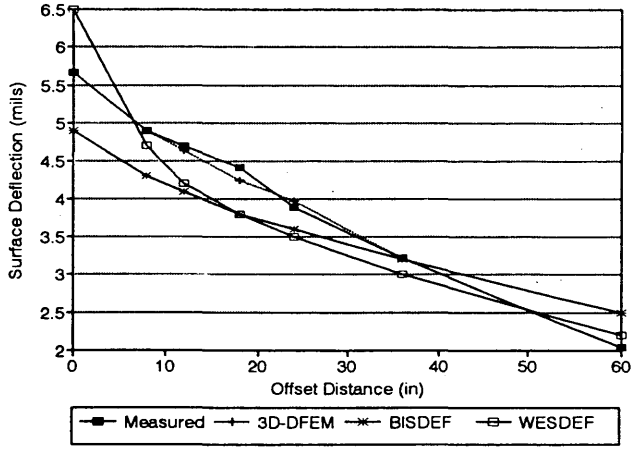

(c)

FIGURE 4 Dynamic analysis verification: (*a*) asphalt pavement, (*b*) concrete pavement, (*c*) FWD—asphalt pavement (1 in. = 2.54 cm and 1 kip = 453.7 kg).

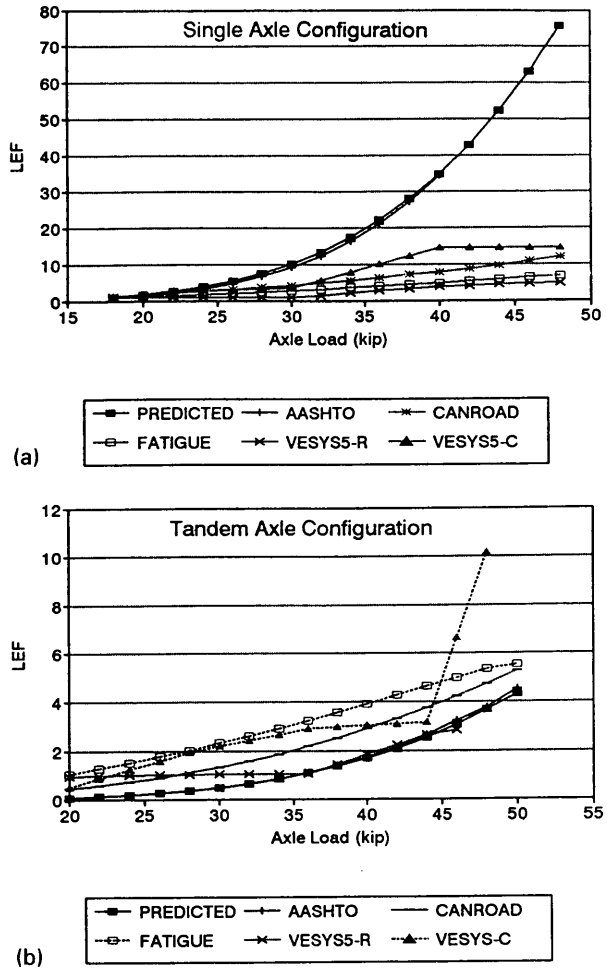

FIGURE 5 Comparison between AASHTO LEFs and Purdue LEFs for asphalt pavements: (*a*) single axle configuration, (*b*) tandem axle configuration (1 in. = 2.54 cm and 1 kip = 453.7 kg).

LEFs. Results of the comparison are shown in Figures 6(*a*) and 6(*b*) (*14*).

PURDUE LEFs

The response, performance, and failure mechanisms of composite pavements are different from those of flexible or rigid pavements. When a very heavy load is applied and repeated on a flexible pavement, some permanent deformation develops in the different layers, including the surface layer. These permanent deformations accumulate at the pavement surface, resulting in a higher pavement roughness. When the roughness reaches a certain value the pavement is considered to be failed.

A similar heavy load applied and repeated on a concrete pavement causes no permanent deformation in the concrete slab itself. Some permanent deformation may be developed in asphalt-bound or unbound layers underneath the concrete slabs, resulting in a void. The development of this permanent deformation occurs if the yield stress of the materials beneath the concrete slab is exceeded. Generally, permanent deformation developed in the layers beneath a concrete slab does not accumulate at the pavement surface because of the concrete slab's rigidity. The total surface permanent deformation under no load in this case is almost zero because the concrete slab returns to its original position when the load is removed. The void under the slab will lead to a larger slab deflection when the load is repeated and to increased pavement roughness. This larger deflection leads to accelerated fatigue and failure (*13*).

The failure mechanism of composite pavements is a combination of those of flexible and rigid pavements. When a heavy load is applied and repeated on a composite pavement, some permanent deformation develops in the asphalt overlay. Permanent deformation may, depending on the stress levels, also develop in asphalt-bound or unbound layers beneath the concrete slab. Permanent surface deformation in this case reflects the permanent deformation of the asphalt overlay only, whereas the total loaded deflection (elastic and plastic) reflects the permanent deformation of the asphalt overlay as well as any permanent deformation in the layers beneath the concrete slab. The total deflection increases with the number of load applications resulting in increased pavement roughness. TSD is used as the basis of a rational equivalency criterion for composite pavements. Simply stated, the LEF of load j on cross section i (LEF_{ij}) is equal to the number of the 18-kip (8167-kg) SAL repetitions on cross section i required to develop the same TSD as one pass of the load j on the same cross section i.

Two statistical models were developed for composite pavement LEFs. The first model predicts the TSD from one pass of load j on cross section i, and then the predicted TSD is used as an input for the second model to estimate the number of 18-kip (8167-kg) SAL repetitions required to develop the same TSD in cross section i, which is the LEF_{ij}. Figure 7 shows the concept of the Purdue LEFs for composite pavements.

Design of Experiments

Two designs of experiments (DOEs) were implemented to develop the composite pavement LEFs. The following factors were included in the first DOE (DOE1):

1. Axle load (D) [three levels: 18, 24, and 36 kips (8167, 10 889, and 16 334 kg)/single axle in an axle group],
2. Number of axles in an axle group (N) (three levels: 1, 2, and 4),
3. Slab thickness (T_{con}) [Two levels: 6 in. (15.24 cm) and 12 in. (30.48 cm)], and
4. Overlay thickness (T_{asp}) [two levels: 4 in. (10.16 cm) and 8 in. (20.3 cm)].

Factor levels for slab and overlay thicknesses represent the range of thicknesses used in Indiana. Subgrade type was not found to be significant in the development of flexible pavement LEFs (*5*). The concrete slab's rigidity would further reinforce this result, and therefore subgrade type would not be expected to be significant for composite pavement LEFs. A subgrade was assumed for all cross sections. The 3D-DFEM analysis was conducted for a speed similar to that of the AASHO Road Test speed, 35 mph (*15*), to be consistent with previously developed flexible and rigid pavement LEFs (*5,14*).

A one-third partial factorial design was used for the above factors and levels. An analysis of different load–cross section com-

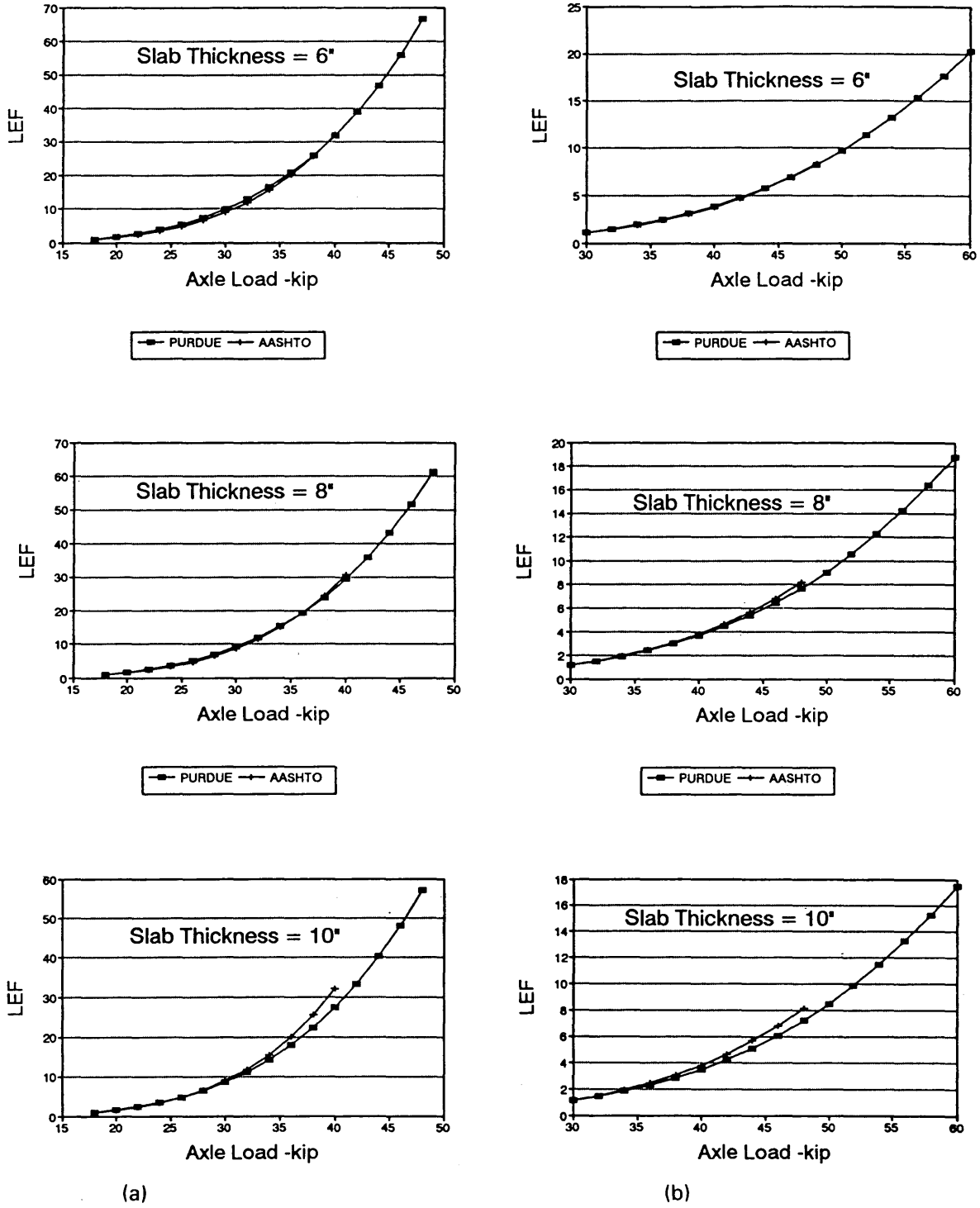

FIGURE 6 Comparison between AASHTO LEFs and Purdue LEFs for concrete pavements: (*a*) single axle configuration, (*b*) tandem axle configuration (1 in. = 2.54 cm and 1 kip = 453.7 kg).

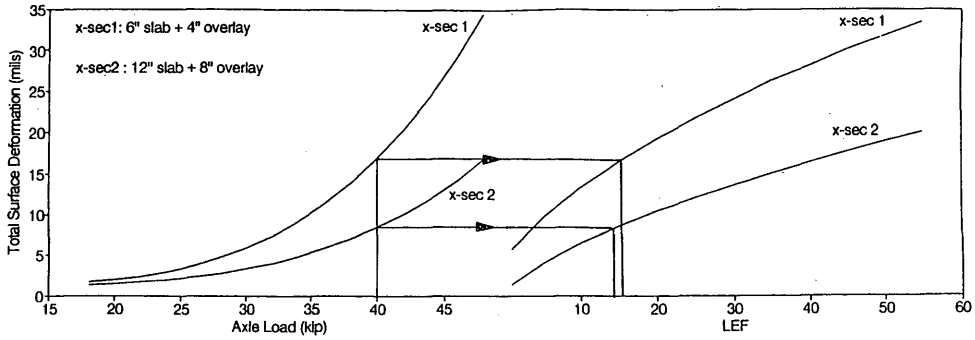

FIGURE 7 Purdue LEFs for composite pavements (SAL) (1 in. = 2.54 cm).

binations was made by using the 3D-DFEM. Analysis of variance (ANOVA) of the results was done to test the significance of the different factors. The significant main effects and two-way interactions were used to develop a regression model for predicting TSD for different loads and axle configurations on different cross sections. The form of the regression model is

$$TSD = 6.556E\text{-}6 \cdot D^4 + 1.0254 \cdot N - 2.28E\text{-}7 \cdot D^4 \cdot (T_{asp} + T_{con}) \quad (R^2 = 98.72 \text{ percent})$$

where

D = axle load (kip/single axle in an axle group),
N = number of axles in an axle group, and
T_{asp} and T_{con} = asphalt overlay and slab thicknesses (in.), respectively.

A second DOE (DOE2) was implemented to consider the effect of the 18-kip (8167-kg) SAL repetitions. Three factors were included in DOE2: slab thickness (T_{con}), 6 in. (15.24 cm) and 12 in. (30.48 cm); asphalt overlay thickness (T_{asp}), 4 in. (10.16 cm) and 8 in. (20.32 cm); and number of 18-kip (8167-kg) SAL repetitions (C), 1 to 30 repetitions. A full factorial design was used to develop this model. Different overlay-slab thickness combinations were analyzed by using the 3D-DFEM. ANOVA of the results was done to test for the significance of the different factors included in DOE2. The significant main effects and two-way interactions were used to develop a regression model to predict TSD as a function of the 18-kip (8167-kg) SAL repetitions. The form of the progression model is

$$TSD = 4.653 + C(1.244 - 0.0502T_{con} - 0.0421T_{asp}) \quad (R^2 = 97.78 \text{ percent})$$

where C is the number of 18-kip (8167-kg) SAL repetitions.

It should be noted that the first model predicts the TSD caused by one pass of any load configuration on any cross section, whereas the second model predicts the TSD caused by one or more passes of the 18-kip (8167-kg) SAL on any cross section. To extend the validity of these models additional cases were analyzed to cover wider ranges of factor levels, and the results were compared with the extrapolated predictions of the models. The extended factors included up to 40 repetitions of the 18-kip (8167-kg) SAL, an overlay thickness of 2 in. (5.08 cm), and a slab thickness of 16 in. (40.64 cm).

Example

A request for a permit is made for an overloaded truck having two single axles in addition to the steering axle. Each single axle will carry a load of 72 kips (32 668 kg) (*9*). The LEF of the 72-kip single axle is determined for the typical Indiana Interstate pavement cross section shown in Figure 1.

1. Total surface deformation of the 72-kip (32 668-kg) SAL j and the 18-kip (8167-kg) SAL on the Interstate typical section i:

$$TSD_{ij} = 6.556E\text{-}06 \cdot (72^4) + 1.025439 \cdot 1 - 2.28E\text{-}07 \cdot (4.5 + 10) \cdot (72^4) = 88.365 \text{ mils } (2.2445 \text{ mm})$$

$$TSD_{18} = 6.556E\text{-}06 \cdot (18^4) + 1.025439 \cdot 1 - 2.28E\text{-}07 \cdot (4.5 + 10) \cdot (18^4) = 1.3666 \text{ mils } (0.0347 \text{ mm})$$

2. Number of 18-kip (8167-kg) SALs required to develop the same damage from one pass of load j on cross section i (LEF_{ij}):

$$LEF_{ij} = \frac{(88.365 - 1.3666) - 4.653}{1.244 - 0.05025 \cdot 10 - 0.042081 \cdot 4.5} = 149.152$$

The AASHTO LEF for this axle load, ignoring the 4.5-in. (11.43-cm) asphalt overlay, cannot be determined! For comparison, the AASHTO LEF for a 40-kip (18 149-kg) SAL, ignoring the 4.5-in (11.43-cm) asphalt overlay, is 31.58.

Sensitivity Analysis

A comparison between the AASHTO LEFs for concrete pavement and Purdue LEFs for composite pavement for single axles in shown in Figure 8. In Figure 8 the maximum and minimum AASHTO LEFs for slab thicknesses in the range of 6 in. (15.24 cm) to 11 in. (27.94 cm) are presented. As can be seen from Figure 8 there is a minimal effect of slab thickness on the AASHTO LEFs (*1*). Four cases were considered for the composite pavement LEFs in this comparison:

1. Thin overlay [4 in. (10.16 cm)] on thin slab [6 in. (15.24 cm)],
2. Thin overlay [4 in. (10.16 cm)] on thick slab [12 in. (30.48 cm)].

3. Thick overlay [8 in. (20.32 cm)] on thin slab [6 in. (15.24 cm)], and
4. Thick overlay [8 in. (20.32 cm)] on thick slab [12 in. (30.48 cm)].

The cases of thin and thick asphalt overlays on thin concrete slabs have total thicknesses in the range represented in the AASHTO LEFs for concrete pavements. As can be seen from Figure 8 the LEFs for the thin and thick asphalt overlays on thin concrete slabs are lower than those of AASHTO. This indicates that the difference between the AASHTO LEFs for concrete pavements and Purdue LEFs for composite pavements is related to differences in layer thicknesses and the differences in the predicted response of composite pavements.

As expected, the thin overlay-thin slab combination showed the highest LEFs, whereas the thick overlay-thick slab combination showed the lowest LEFs. Also, the composite pavement LEFs were lower than the concrete pavement LEFs for the same concrete slab thickness. This was expected because the additional overlay thickness significantly increases the pavement structure stiffness. The effect of slab thickness on LEFs is shown in Figure 9(*a*), whereas the effect of overlay thickness is shown in Figure 9(*b*). As expected, as the slab or the overlay thicknesses increase, the LEFs decrease.

LEFs for tandem, tridem, and four-axle configurations are shown in Figure 10. This analysis was made for a 10-in. (25.4-cm) JRCP with a 4-in. (10.08-cm) asphalt concrete overlay. The sample of overload permit applications discussed above showed that the average axle spacing is 4 ft. Therefore, a 4-ft axle spacing was assumed for *n*-axle configurations.

Advantage of Purdue LEFs

No rational LEFs have been available for composite pavement analysis. The 1993 AASHTO design guide (*1*) recommends that the concrete pavement LEFs be used for composite pavements. In this case the significant contribution of the overlay is ignored.

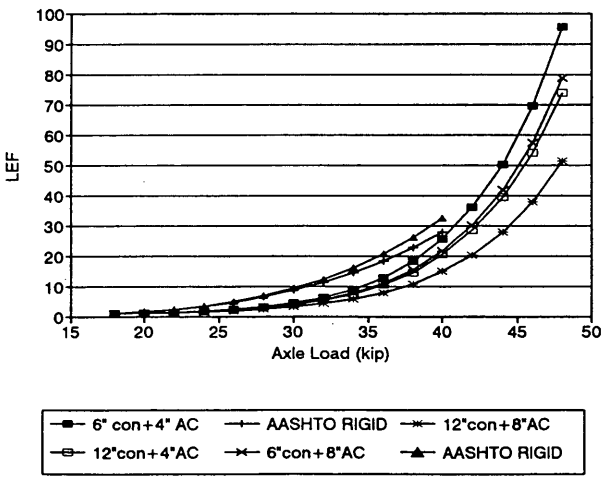

FIGURE 8 Comparison between AASHTO LEFs for concrete pavements and Purdue LEFs for composite pavements (single axle configuration) (1 in. = 2.54 cm and 1 kip = 453.7 kg).

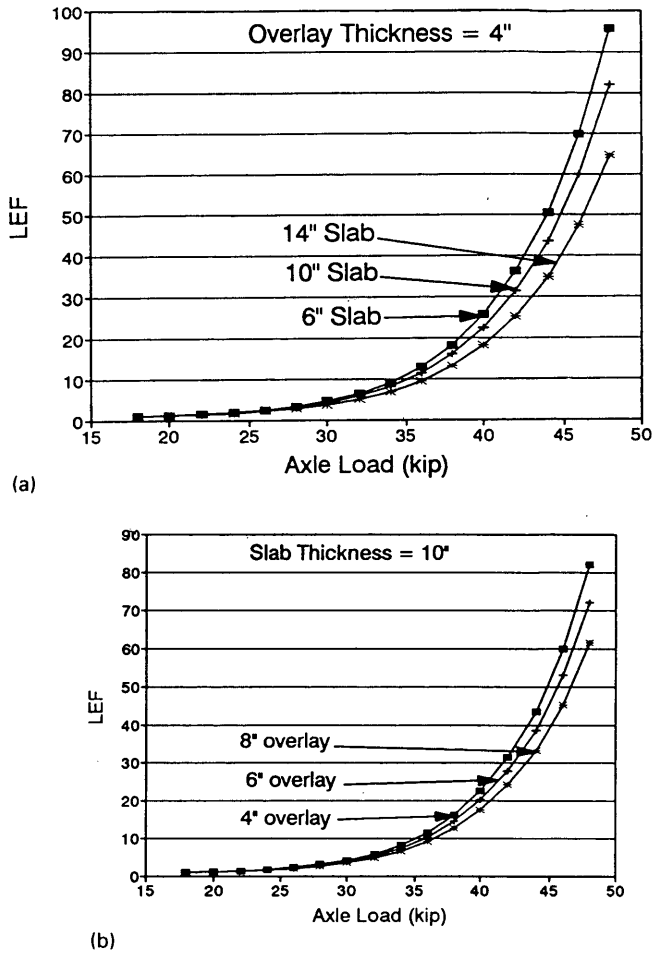

FIGURE 9 Effect of cross section parameters on Purdue LEFs: (*a*) slab thickness, (*b*) overlay thickness (1 in. = 2.54 cm and 1 kip = 453.7 kg).

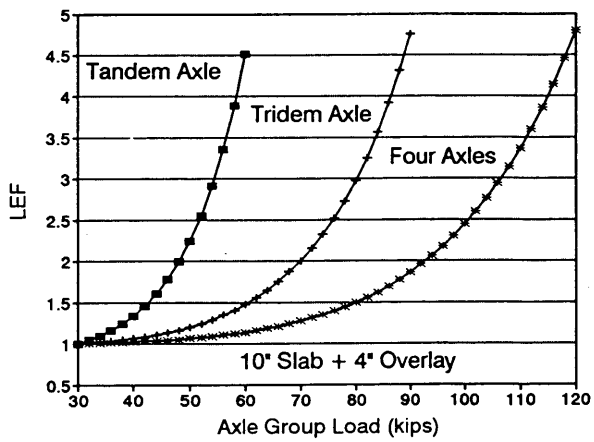

FIGURE 10 Effect of axle configuration on Purdue LEFs (1 in. = 2.54 cm and 1 kip = 453.7 kg).

Purdue LEFs can be considered serviceability-based LEFs and are developed by using TSD. TSD accounts for the permanent deformation developed in the asphalt overlay and unbound layers underneath the concrete slabs. The permanent deformation is related to potential accumulation of roughness, which is a large component of serviceability (*16*). Purdue LEFs have the following advantages:

1. Purdue LEFs are based on dynamic analysis in which moving loads are considered. Also, nonlinear material properties and models are included in the analysis.
2. The 3D-DFEM analysis used to develop these LEFs has been verified for static, linear elastic analysis and for dynamic, nonlinear analysis of both flexible and rigid pavements. Excellent results were obtained in the verification studies and in the comparison of AASHTO LEFs and Purdue LEFs for asphalt and concrete pavements.
3. Purdue LEFs consider the effect of load repetitions and not assume that the pavement response is a linear function of the number of load repetitions.
4. Purdue LEFs are based on an analytical model, which means that they can be easily updated or extended to cover wider ranges of variables, such as pavement thickness, material type, load level, and load configuration.

SUMMARY AND CONCLUSIONS

An asphalt overlay is frequently used to improve the serviceability of deteriorated concrete pavement. The asphalt overlay has a significant influence on the concrete pavement's behavior and response to loads. Most highway agencies approximate the behavior of composite pavements to that of asphalt or concrete pavements. The 1993 AASHTO design guide (*1*) suggests that concrete pavement LEFs be used to assess the effects of traffic on composite pavements. This is an approximation and has not been validated with field measurements or analytical procedures.

A study funded by INDOT and FHWA was conducted at Purdue University to develop a procedure for permitting overloaded trucks in Indiana. In that study the Indiana highway network was categorized into three classes: Interstate and U.S. highways and SRs. Typical pavement cross sections were selected to represent each highway class in the analysis. Four typical pavement cross sections were selected for the study. Three of these four cross sections are JRCPs with an asphalt overlay, composite pavement.

A LEF set was developed for composite pavements. The total surface deformation (elastic and permanent) was used as the equivalency criterion for these LEFs. The total surface deformation includes any permanent deformation developed in the asphalt overlay or the unbound layers underneath the concrete slab.

It was found that the composite pavement LEFs are lower than the AASHTO LEFs for concrete pavement. This is related to the additional stiffness caused by the asphalt overlay as well as to the differences in the responses of concrete and composite pavements.

REFERENCES

1. *Guide for Design of Pavement Structures.* AASHTO, Washington, D.C., 1993.
2. *Interim Guide for Design of Pavement Structures.* AASHO, Washington, D.C., 1972.
3. *Special Report 61E: AASHO Road Test. Report 5, Pavement Research.* HRB, National Research Council, Washington, D.C., 1962.
4. *Vehicle Weight and Dimension Study.* CanRoad Transportation Research Corporation, Ottawa, Ontario, Canada, 1986.
5. Zaghloul, S. M., and T. D. White. Load Equivalency Factors for Flexible Pavements. *Journal of the Association of Asphalt Paving Technologists,* (in press).
6. Lindly, J., and T. D. White. *Development of an Overlay Design Procedure for Flexible Pavements in Indiana.* Joint Highway Research Project, FHWA/IN/JHRP-87/9, 1987.
7. Pumphrey, N., and T. D. White. *Development of Asphaltic Concrete Overlay Design Procedure for Rigid Pavements in Indiana.* Joint Highway Research Project, FHWA/IN/JHRP-89/14, 1989.
8. How Many Miles? *Highway Inventory and Systems Unit Annual Report.* Indiana Department of Highways, 1989.
9. Zaghloul, S. M., and T. D. White *Guidelines for Permitting Overloads. Part 1. Effect of Overloaded Vehicles on the Indiana Highway Network.* Joint Highway Research Project, FHWA/IN/JHRP/93/5, Purdue University, West Lafayette, Ind., 1993.
10. *Guide for Design of Pavement Structures.*, AASHTO, Washington, D.C., 1986.
11. *ABAQUS, Finite Element Computer Program,* Version 4.9. Hibbitt, Karlsson and Sorensen, Inc., 1989.
12. Zaghloul, S., and T. D. White. Use of a Three-Dimensional Finite Element Program for Analysis of Flexible Pavement. In *Transportation Research Record 1388,* TRB, National Research Council, Washington, D.C., 1993, pp. 60–69.
13. Zaghloul, S., and T. D. White. Non-Linear Dynamic Analysis of Concrete Pavements. *Proc., 5th International Conference on Concrete Pavement Design and Rehabilitation,* Vol. 1. Purdue University, West Lafayette, Ind., 1993, pp. 277–292.
14. Zaghloul, S. M., and T. D. White. Evaluation of Heavy Load Damage Effect on Concrete Pavements. Using a Three-Dimensional, Non-Linear Dynamic Analysis. 73rd Annual Meeting of the Transportation Research Board, Washington, D.C., 1994.
15. Coree, B. and T. D. White. *Layer Coefficients in Terms of Performance and Mixture Characteristics.* Joint Highway Research Project, FHWA/IN/JHRP-88/13, Purdue University, West Lafayette, Ind., 1988.
16. Yoder, E. J., and M. W. Witczak. *Principles of Pavement Design* (2nd ed.). John Wiley & Sons, Inc., New York, 1975.
17. *ABAQUS, Finite Element Computer Program, Theory Manual,* Version 4.9. Hibbitt, Karlsson and Sorenson, Inc., 1989.
18. Roque, R., M. Tia, and B. E. Ruth. Asphalt Rheology To Define the Properties of Asphalt Concrete Mixtures and the Performance of Pavements. In *Asphalt Rheology: Relationship to Mixture* (O. E. Briscoe, ed.). ASTM STP 941. American Society for Testing and Materials, Philadelphia, Pa, 1987, pp. 3–27.
19. Wood, D. *Soil Behavior and Critical State Soil Mechanics.* Cambridge University Press, Cambridge, United Kingdom, 1990.
20. Drucker, D. C., and W. Prager. Soil Mechanics and Plastic Analysis or Limit Design. *Quarterly of Applied Mathematics,* Vol. 10, 1952, pp. 157–165.
21. Schofield, A., and C. P. Worth. Critical State Soil Mechanics. McGraw-Hill, New York, 1968.
22. Parry, R. H. (ed.). *Stress-Strain Behavior of Soils.* G. T. Foulis and Co., Henley, England, 1972.
23. *Bitumen Structures Analysis in Roads (BISAR).* Computer program. Koninlilijke/Shell-Laboratorium, Amsterdam, the Netherlands, July 1972.
24. Zaghloul, S. M., T. D. White, V. P. Drnevich, and B. Coree. Dynamic Analysis of FWD Loading and Pavement Response Using a Three-Dimensional Dynamic Finite Element Program. In *Nondestructive Testing of Pavements and Backcalculation of Moduli,* Vol. 2 (H. L. von Quintas, A. J. Bush, and G. Y. Baladi, eds.). ASTM STP 1198. American Society for Testing and Materials, Philadelphia, 1994.

Publication of this paper sponsored by Committee on Pavement Rehabilitation.

Field Investigations of Selected Strategies To Reduce Reflective Cracking in Asphalt Concrete Overlays Constructed over Existing Jointed Concrete Pavements

ERIC D. MOODY

Seven pavement rehabilitation strategies for reducing the extent and severity of reflective cracking of asphalt concrete (AC) overlays constructed over jointed concrete pavements were designed and the effectiveness of the strategies was evaluated. The seven rehabilitation strategies were selected after conducting an extensive literature search of documented attempts to reduce reflective cracking. The general descriptions of the seven strategies selected for this study are (a) full-depth repair; (b) crack and seat; (c) crushed stone base interlayer; (d) open-graded AC interlayer, (e) styrene-butadiene-styrene modified seal coat interlayer; (f) 7.6-cm (3-in.) dense graded, coarse surface AC overlay; and (g) 3.8-cm (1.5-in.) dense graded AC overlay. A technique involving sawing and sealing joints in the AC overlay directly over the transverse joints in the concrete pavement was investigated as well. These seven strategies were constructed under carefully controlled conditions, with continuous documentation of material properties, layer thicknesses, and environmental conditions during construction. The preliminary results of the research project, including early-age performance with respect to reflective cracking, rutting, and pavement profile measurements, are presented.

Reflective cracking has been a major concern of pavement engineers for many years (*1*). Numerous attempts have been made to address this problem, many with only limited success (*2–5*). This paper presents the preliminary results of a research study sponsored by the Texas Department of Transportation aimed at investigating several well-known strategies for reducing reflective cracking of asphalt concrete (AC) overlays placed over jointed concrete pavements (JCPs). The highway selected for constructing the test sections was US 59 located in northeast Texas. This highway was originally constructed in the 1940s as a two-lane, 9-7-9 JCP. The name 9-7-9 JCP comes from the fact that the pavement is 9 in. (22.9 cm) thick along the outside shoulder and 7 in. (17.8 cm) thick along the centerline. Expansion joints were placed in the pavement every 36.5 m (120 ft), and contraction joints where placed every 4.6 m (15 ft). Expanded shoulders were added during the 1960s and 1970s.

This highway is a primary route of the east Texas timber industry, providing direct links to numerous mills in the area and the Port of Houston. The highway has an annual average daily traffic of 16,500 vehicles, with an estimated 2.3 million 18-kip equivalent single axle loads (ESALs) applied to the design lane annually.

Transtec Consultants, 2630 Exposition Boulevard, Suite 10, Austin, Tex. 78703.

DISTRESS HISTORY

Over the years the original JCP has experienced considerable distress because of the extremely heavy traffic and harsh environmental conditions that characterize this highway. The area of east Texas where the test sections are located is characterized as a wet, no-freeze zone. The test site location receives an average of about 127 cm (50 in.) of precipitation per year. The average depth of the water table at the site is 4.0 m (12 ft).

The typical distresses on the test site pavement include pumping, reflective cracking of the AC overlays, joint failures, and some shattering of the original concrete slabs. Figure 1 shows a typical section of this pavement after maintenance crews have sealed both the longitudinal and transverse reflective cracks in the AC overlay.

As a result of the heavy traffic and harsh environmental conditions this JCP has been rehabilitated numerous times over the years. However, because of both inadequate funding and a lack of knowledge regarding the life cycle costs of alternative repair strategies, the typical rehabilitation technique has consisted of simply placing a 3.8-cm (1.5-in.)-thick Type D AC overlay on top of the existing pavement as needed. Table 1 describes the aggregate gradation bands of various Texas Department of Transportation AC mixtures used in the study. The standard rehabilitation

FIGURE 1 Reflective cracking typical of test site location.

TABLE 1 Gradations for Asphalt Mixes Used in the Study

Sieve Size	Type(% Passing) B Fine Graded Base	C Coarse Surface	D Fine Graded Surface	G Open Graded Base
5.1 cm(2.0 in.)				100
3.8 cm(1.5 in.)				50-70
2.5 cm(1.0 in.)	100			30-50
2.2 cm(0.86 in.)	95-100	100		10-20
1.6 cm(0.63 in.)	75-95	95-100		
1.3 cm(0.5 in.)			100	
1.0 cm(0.38 in.)	60-80	70-85	85-100	
0.6 cm(0.25 in.)				
4.75 mm(No. 4)	40-60	43-63	50-70	
2.0 mm(No. 10)	27-40	30-40	32-42	
0.425 mm(No. 40)	10-25	10-25	11-26	
0.178 mm(No. 80)	3-13	3-13	4-14	
0.075 mm(No. 200)	1-6	1-6	1-6	
VMA(% Minimum)	12	13	14	20+

technique described above has been implemented numerous times throughout the history of the highway, and as a result the original JCP is now covered with four AC overlays totaling 17.8 cm (7.0 in.) in thickness. Figure 2 shows the typical cross section of the existing pavement structure.

TEST SECTION DESIGN

After examining deflection data, core samples, and the results of a visual condition survey of US 59, a site was selected for constructing the test sections. The site is located just south of FM 357 in the southbound lanes of US 59, at station 1490+00. Six test sections (R1 to R6), each approximately 305 m (1,000 ft) in length, and a control section (R0) were constructed. Figure 3 shows the general cross section for each test section. The following is a brief description of each test section.

R0: Control

Test section R0 is the control section. In this section a standard 3.8-cm (1.5-in.) Type D AC overlay was placed over the existing AC pavement (ACP). The purpose for this section was to allow for comparison between the performances of the six test sections and the conventional rehabilitation technique used by the Texas Department of Transportation.

R1: Full-Depth Repair

In Test Section R1 the existing ACP was milled, exposing the underlying JCP. Extensive repairs were made to the exposed JCP, including replacing failed joints and repairing cracks in the shattered slabs with high-molecular-weight (HMW) monomer. Deflection testing performed before and after the concrete slabs were repaired confirmed that load transfer was restored across the joints and cracks in the JCP slabs. The inside shoulder of the JCP was extended 2.0 m (6.5 ft) with 22.9 cm (9 in.) of portland cement concrete. After all repairs were made and the shoulder was extended, a one-course surface treatment was applied over the first 152.5 m (500 ft) of the 305-m (1,000-ft) test section. A 10.2-cm (4-in.) Type C AC overlay was then placed in two lifts over the entire test section, completing construction of Test Section R1.

R2: Crack and Seat

In Test Section R2 the existing ACP was again milled and removed. The "crack and seat" technique was then performed on

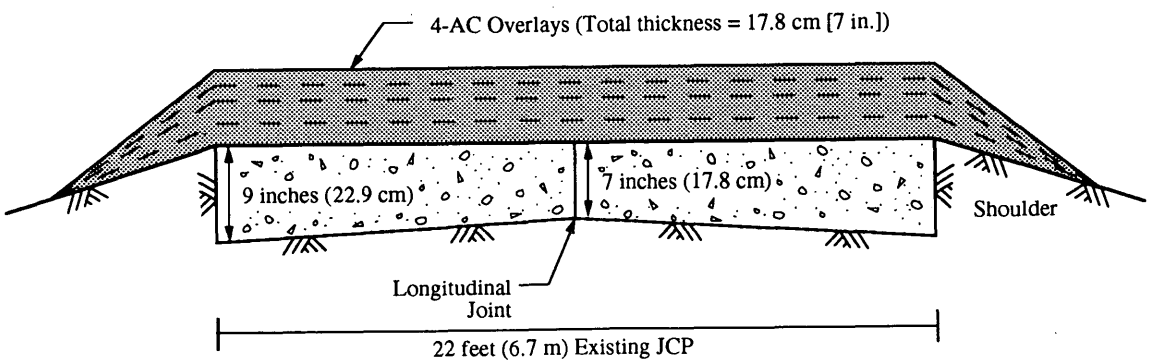

FIGURE 2 Typical cross section of existing 9-7-9 JCP.

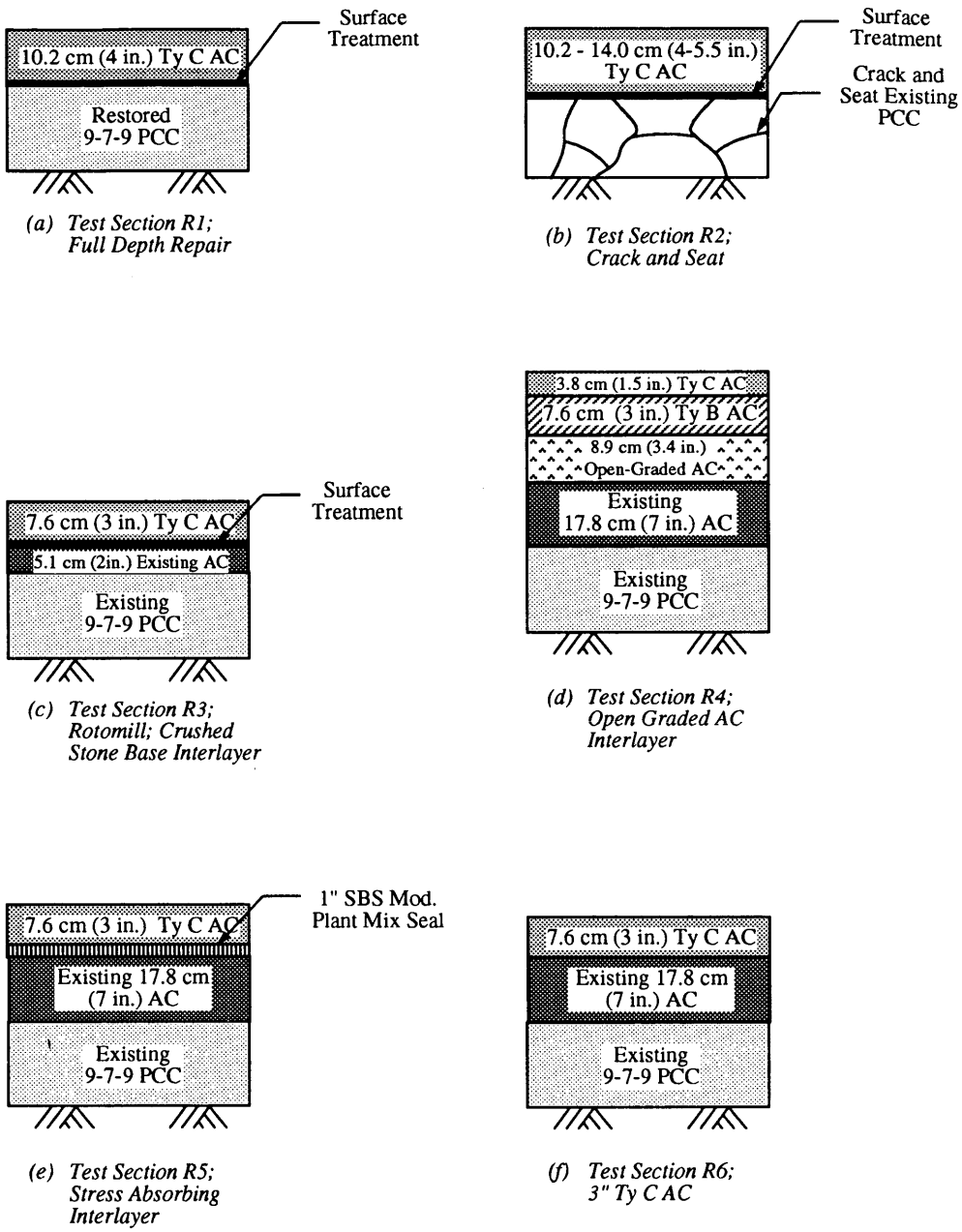

FIGURE 3 General cross sections of test sections.

the exposed JCP. A 5880-kg (13,000-lb) drop hammer was used to break the concrete into 61-cm (24-in.) nominal size pieces. The concrete was then "seated" with a 50-ton pneumatic-tire roller. After the crack and seat operation was complete, a one-course surface treatment was applied to the entire test section. A 10.2-cm (4.0-in.) Type C AC overlay was then placed on the first half of the test section in two lifts. A 14.0-cm (5.5-in.) Type C AC overlay was then placed on the second half in three lifts, completing construction of Test Section R2.

R3: Crushed Stone Base Interlayer

In Test Section R3, 12.7 cm (5 in.) of the existing 17.8-cm (7-in.)-thick ACP was milled and removed. A 20.3-cm (8-in.) crushed stone base (CSB) interlayer was then placed over the remaining 5.1-cm (2-in.)-thick ACP and compacted. A prime coat and a one-course surface treatment were then applied to the CSB. A 7.6-cm (3.0-in.) Type C AC overlay was then placed over the entire test section in two lifts, completing construction of Test Section R3.

R4: Open Graded AC Interlayer

In Test Section R4 the existing pavement was not disturbed. An 8.9-cm (3.5-in.) Type G AC overlay was placed over the existing surface; this was followed by a 7.6-cm (3.0-in.) Type B AC overlay. This was followed by a 3.8-cm (1.5-in.) Type C AC overlay.

R5: SBS Modified Seal Coat Interlayer

In Test Section R5 a 2.5-cm (1-in.)-thick, styrene-butadiene-styrene (SBS) modified plant mix seal coat interlayer was placed over the existing ACP. A 7.6-cm (3-in.)-thick Type C AC overlay was then placed over the entire section in two lifts, completing construction of Test Section R5.

R6: Type C AC

In Test Section R6 a 7.6-cm (3-in.) Type C AC overlay was placed in two lifts over the existing ACP.

MONITORING PLAN

The monitoring plan for these test sections was broken down into three phases: preconstruction, construction, and postconstruction. The focus of this paper is on postconstruction monitoring. However, the contents of each phase are presented.

Preconstruction Monitoring

Preconstruction monitoring consisted of preparing a historical file on each test section. The file included the results from (a) visual condition surveys, (b) high-definition video recording of the pavement surface, (c) deflection testing, (d) material testing, (e) rut depth measurements, (f) profile measurements, and (g) historical records of traffic. The file contains the historical information necessary to correlate the performance of different test sections with their original distress characteristics.

Construction

Several types of data were collected during construction, including the project engineer's daily progress journal, all relevant mix designs, concrete and asphalt test reports, a visual condition survey of the underlying rigid pavement in those sections where the layer was exposed, both videographs and photographs of the various phases of the project and the machinery used, and environmental data. This data file was also necessary to provide insight into the performance of each test section.

Postconstruction

Immediately after construction and before opening the pavement up to traffic several types of data were collected on each test section. These data included visual condition surveys, deflections, rut depth measurements, and profile measurements. The Automatic Road Analyzer (ARAN) was used to document the road condition, and the profilometer was used to document the profile of the pavement before subjecting it to traffic. Twenty-eight cores were taken immediately after construction to test for density, creep, resilient modulus, tensile strength, and other mix characteristics of the various pavement layers. The cores also allowed further verification of layer thickness.

Long-Term Monitoring

A long-term monitoring plan was established to collect performance data on each test section. The long-term monitoring plan activities include monitoring rut depths, reflective cracking, profile, and in situ material properties. These activities were conducted quarterly for the first 6 months, biannually for the following 18 months, and semiannually thereafter. The frequency and extent of this data collection may be modified as time proceeds. A maintenance cost file will also be maintained for each test section. This information is important for calculating the life cycle costs of each test section.

Weigh-in-Motion Installation

An important part of the postconstruction monitoring plan was the installation of state-of-the-art weigh-in-motion (WIM) equipment in the control section, Test Section R0. This equipment will allow engineers to correlate test section performance with the number of 18-kip ESALs applied to the pavement. The installation of the WIM equipment is documented in a research report (987-2) published by the Center for Transportation Research.

The WIM equipment also provides important information on vehicle classification, traffic counts, axle configurations, axle positions, vehicle speed, and pavement temperature. These data will be very valuable for this research project as well as future research related to vehicle-pavement interaction.

TEST SECTION PERFORMANCE

The test sections have been in place for 2 years. Some interesting results regarding their early-age performances are now available. Pavement distress, including reflective cracking and rutting, are evident, and these are being closely monitored as they occur. Some maintenance activities have also been required. Test Section R5, SBS-modified seal coat interlayer, has already reached functional failure. The following is a detailed description of the key performance characteristics of each test section. That section is followed by a brief description of the initial construction and maintenance costs for each test section.

Roughness Profile

Immediately after construction but before allowing traffic on the test sections, an infrared profilometer was used to measure the profile of each test section in the nondimensional international roughness index (IRI). The profile was measured again after 6, 12, 18, and 24 months of continuous traffic. Figures 4 and 5 show the results of these tests for the inside and outside lanes, respectively.

Although the results of the profile measurements of the inside lane included more variability, the IRI values are still relatively low, ranging from 50 to 90, indicating a relatively smooth pavement with high serviceability [present serviceability index (PSI) > 4.0]. The outside lane has shown a considerable increase in roughness, with IRI values increasing from a range of 60 to 75 to a range of 70 to 140. The averages for both the inside and the outside lanes are presented in Figure 6. The most substantial in-

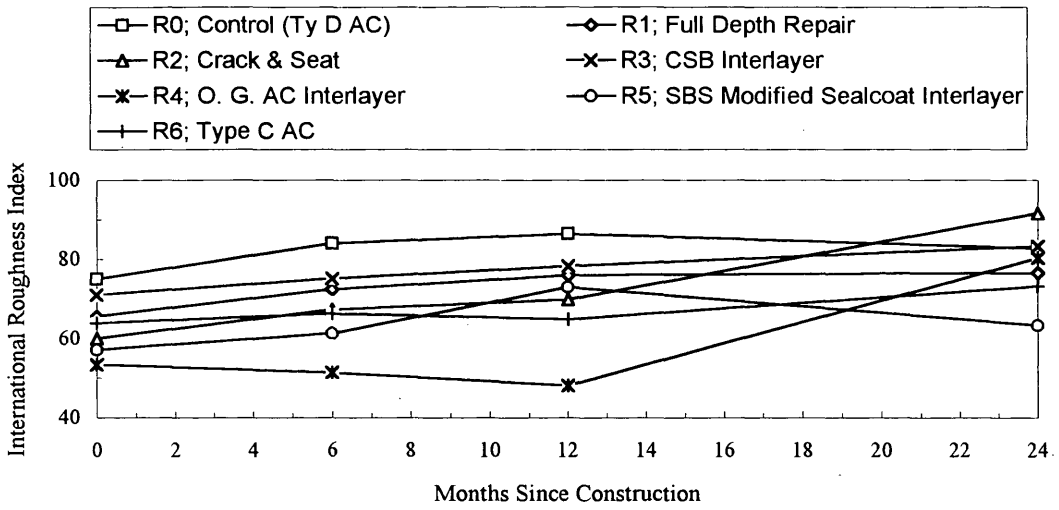

FIGURE 4 International roughness index (inside lane).

creases in roughness have occurred in Test Sections R3 and R4; however, they are still providing good serviceability (PSI > 3.25).

Rutting

In developing the test section designs there was concern that in an attempt to eliminate reflective cracking with various stress relief layers a significant increase in the degree of rutting would result. With the exceptions of Test Section R3, the CSB interlayer, this has not proven to be the case. As shown in Figures 7 and 8 the rut depths have been minimal during the first 18 months of test section performance, ranging from 0.63 to 4.5 mm (0.025 to 0.18 in.). The CSB interlayer test section (Test Section R3) is the exception. Rut depths of 2.5 mm (0.1 in.) were measured in this test section after only 1 month of heavy traffic. These rut depths stabilized during the subsequent 17 months of performance at approximately 4.5 mm (0.17 in.).

Reflective Cracking

Since the primary objective of the present study was to investigate selected strategies for reducing or eliminating reflective cracking, the most important postconstruction data collected have been the periodic condition surveys of reflective cracking. Figure 9 presents the results of surveys collected at 6-month intervals since construction.

Test Section R4, the open graded AC interlayer, and Test Section R3, the CSB interlayer, have shown no reflective cracking. The control section (Test Section R0), crack and seat section (Test Section R3), and the 3-in. Type C AC section (Test Section R6)

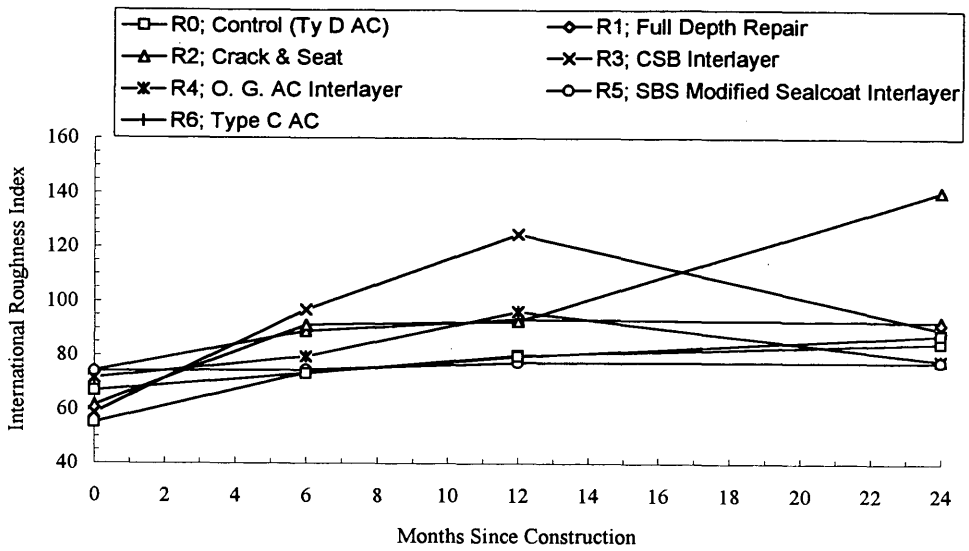

FIGURE 5 International roughness index (outside lane).

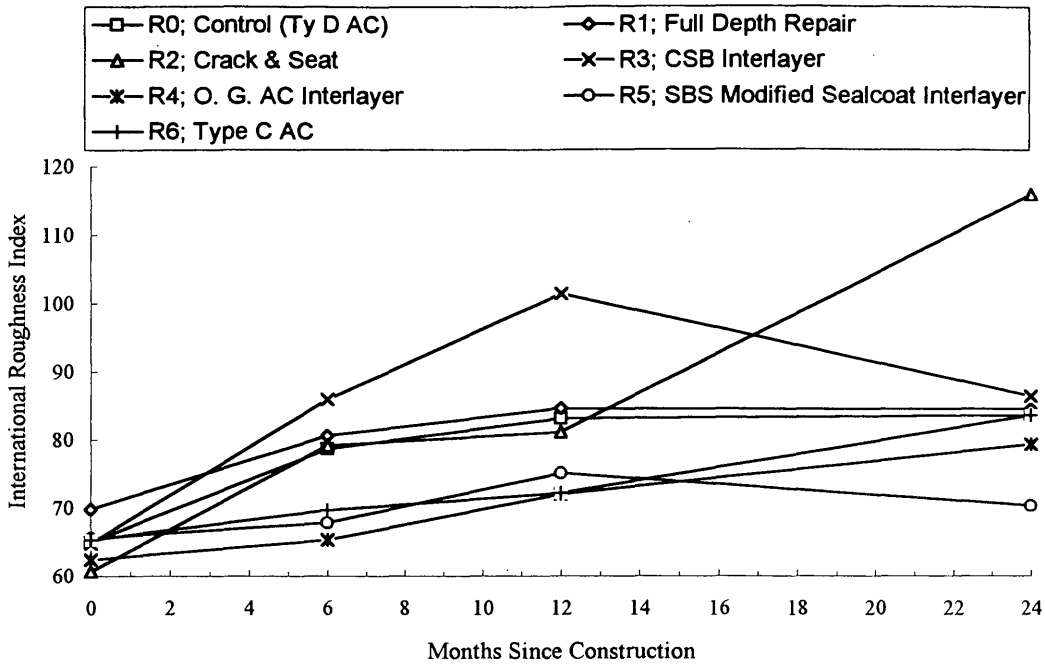

FIGURE 6 International roughness index (average of both lanes).

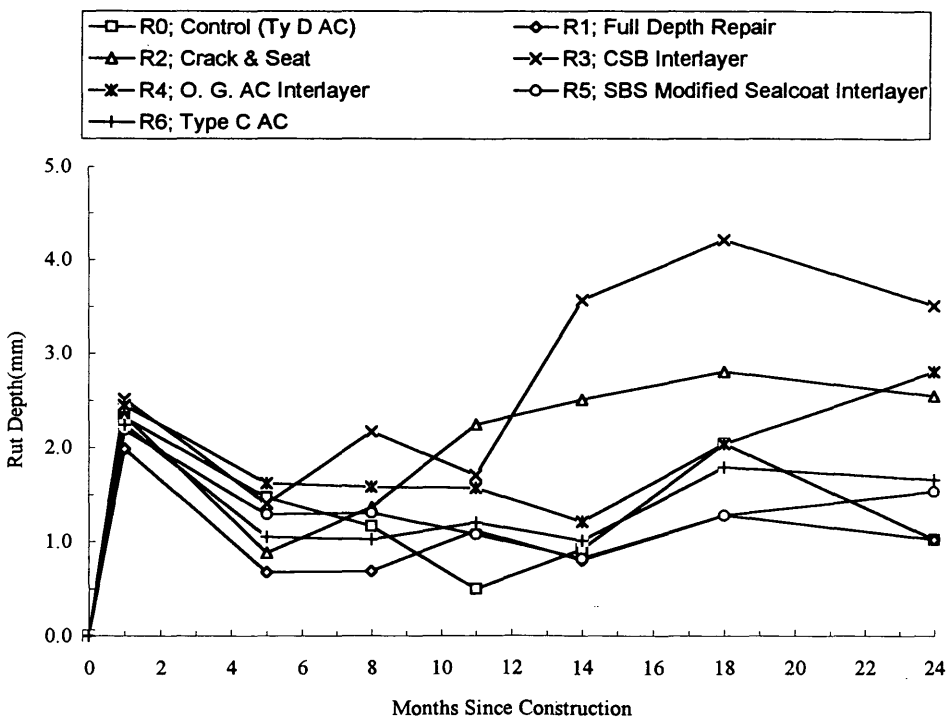

FIGURE 7 Rut depths (inside lane).

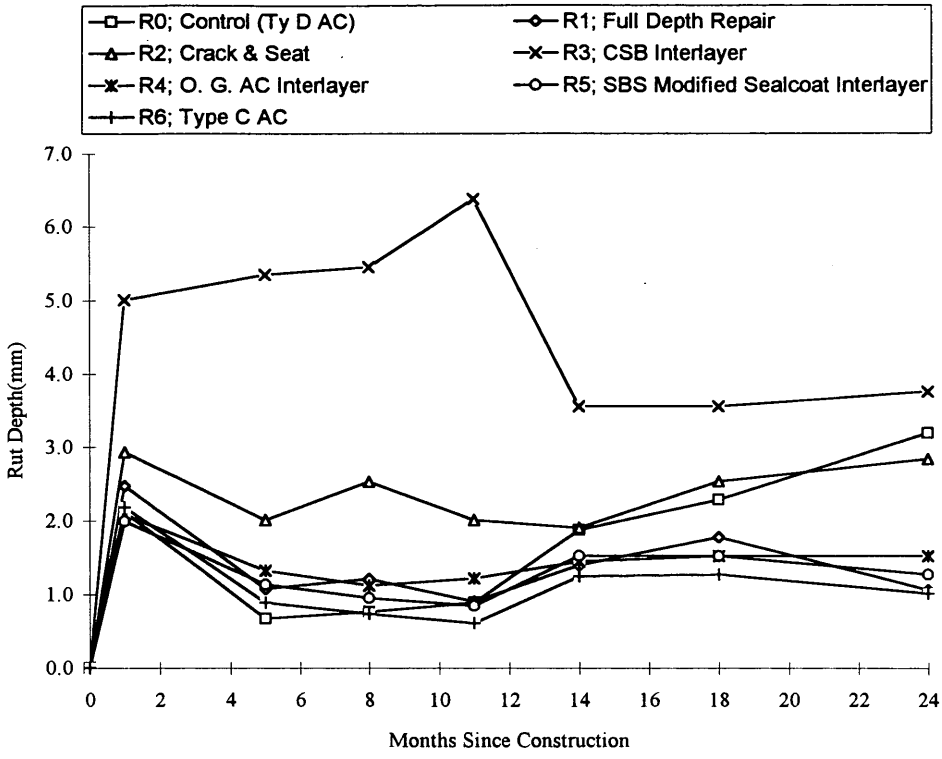

FIGURE 8 Rut depths (outside lane).

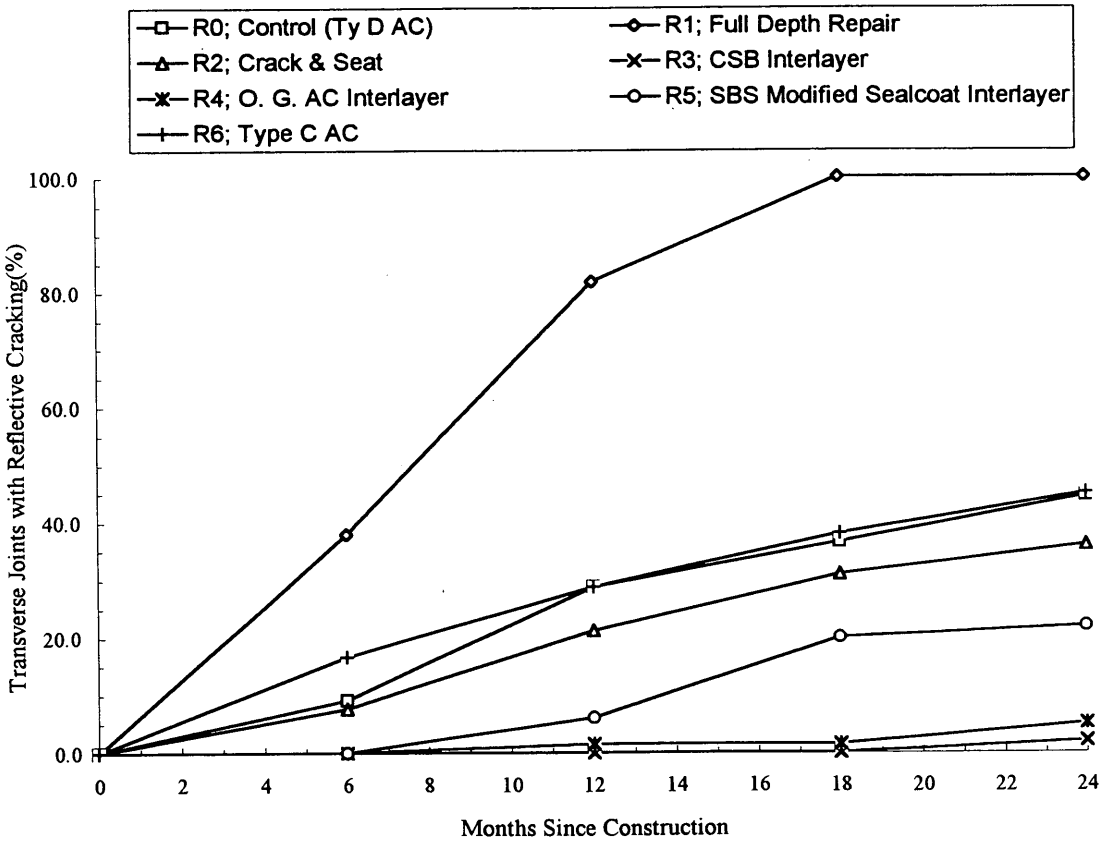

FIGURE 9 Transverse joints showing reflective cracking (percent).

have shown moderate reflective cracking of 20 to 35 percent. The full-depth Repair section (Test Section R1) has shown the most reflective cracking, with 100 percent of the transverse joints reflecting through the Type C AC overlay after 2 years of service. All existing AC was removed on this section prior to placing the AC overlay. This essentially eliminated all stress relief between the existing JCP and the newly placed AC overlay, which has resulted in the extensive reflective cracking.

To date the reflective cracks have not been sealed with hot poured rubber. However, when these cracks are sealed the costs will be documented.

Construction and Maintenance Costs

An important part of the present research effort was to compare test section performance on the basis of life cycle costs. Therefore, a separate cost file has been maintained on each test section. The file includes an estimation of the initial construction costs and all maintenance costs incurred during the life of the test section. Files of each test section can be compared to determine the rehabilitation alternative that provides the lowest life cycle costs. Theoretically, it is the alternative with the lowest life cycle costs that would be adopted by engineers for future rehabilitation efforts on similar pavement sections along US 59.

Since the test sections were relatively short, 305 m (1,000 ft.), only small quantities of certain materials were required to construct the test sections. Because of the relatively small quantities for some bid items, the unit prices bid by the contractor were relatively large. For example, the crack and seat operation for Test Section R3 had a bid quantity of only 275.0 m^2 (330 yd^2) and was bid at \$1.20/m^2. However, most of this cost was in mobilization. Had bid item quantities typical of a regular paving job been used to bid the project, the price for crack and seat would have ranged from \$0.35/m^2 to \$0.42/m^2. Therefore, to compare the construction costs of this test section with those of the others, a value of \$0.36/m^2 was used for estimating the cost of the crack and seat operation. This type of adjustment was necessary for each of the bid items used to let the job. A similar technique was used for administrative, mobilization, and traffic control, which varied significantly between the test sections. Table 2 gives the estimated construction and maintenance costs for each test section.

As would be expected, the control section (Test Section R0) has the lowest costs to date, at \$8.95/m^2. The most expensive test section was the section receiving full-depth repair (Test Section R1), with a total cost of \$29.69. However, since the SBS-modified seal coat interlayer section (Test Section R5) has already reached functional failure, a significant rehabilitative effort was required. This rehabilitative effort included milling and removing the failed layers and placing an AC overlay. These costs are reflected as maintenance costs in Table 2; however, this action was really a

TABLE 2 Construction and Maintenance Costs for Each Test Section

Work Item	R0	R1	R2A	R2B	R3	R4	R5	R6
Administrative	1.50	2.70	2.70	2.70	1.50	1.50	1.50	1.50
Mobilization	1.50	3.00	3.00	3.00	1.50	1.50	1.50	1.50
Barricades, Signing	0.24	1.68	1.20	1.20	0.24	0.24	0.24	0.24
Traffic Control/Conc. Traffic Barrier	0.60	4.20	4.20	4.20	4.20	0.90	0.60	0.60
Const. Pavement Marking	0.10	0.72	0.78.	0.78	0.10	0.10	0.10	0.10
Remove Pavement Markings		0.20	0.20	0.20				
Construct Detours		0.60	0.60	0.60	0.60			
Plane and Remove Existing Asphalt		1.68	1.68	1.68				
Repair Existing Conc. Paving; Includes HMW Monomer		9.00						
Place Concrete Shoulder		1.56						
Clean and Seal Joints			0.36	0.36				
Crack and Seat Existing Concrete			0.36	0.36				
Grade 3 Aggregate					2.10			
Prime Coat and Surface Treatment			0.24	0.24	0.24	0.24		
Prefabricated Underdrains						0.60		
Underdrain Outfall						0.06		
Tack Coat	0.12	0.12	0.24	0.24		0.12	0.12	0.12
Asphalt Concrete Type C		9.98	9.98	13.73	7.49	3.78	7.56	7.56
Plant Mix Seal Coat- SBS Mod.							3.00	
Asphalt Concrete Type D	4.90							
Asphalt Concrete - Type G						2.64		
Asphalt Concrete - Type B						9.24		
Asphalt Concrete						7.24		
Subtotal; Initial Const. Costs(\$/m^2)	8.95.	35.45	25.55	28.93	17.96	28.15	14.62	11.62
Maintenance Costs(PV \$/m^2)		0.18	1.20	1.20			*12.48	
Total Costs(\$/m^2)	8.95	35.63	26.75	30.13	17.96	28.15	15.10	11.62

* Upon reaching terminal serviceability, this section was milled and overlaid.

full-scale rehabilitation. Nevertheless, this caused the total costs to increase dramatically.

CONCLUSIONS AND RECOMMENDATIONS

This section summarizes the advantages and disadvantages of each rehabilitation technique.

The work done on test Section R1 (full-depth repair), which involved milling and removing the existing asphalt and repairing the original JCP slabs and joints before constructing new overlays, is proving to be one of the more expensive techniques, with essentially no success in reducing reflective cracking. In fact the reflective cracking is most extensive in this test section, with 100 percent of the existing JCP joints producing reflective cracks after 2 years of service. The effort to sawcut and seal the AC overlay directly above the existing JCP joints has also proven to be ineffective in reducing reflective cracking.

Test Section R2 (crack and seat), which involved milling and removing the existing asphalt concrete before performing the crack and seat operation, also had a relatively high initial construction cost. During the first year of service of this section two negative performance characteristics have become evident. First, the crack and seat operation did not fracture the JCP slabs enough to eliminate all reflective cracking. At the end of the first year of service approximately 20 percent of the joints in the JCP have caused reflective cracking in the new asphalt concrete layer. The fractured slabs also do not appear to be providing the necessary structural support to carry the heavy traffic loads on this highway, since pumping of subbase materials has also become evident on this test section.

The early indication is that Test Section R2 (crack and seat) is not providing enough benefit through reduced reflective cracking to offset the substantial cost of detouring traffic on this roadway, milling and removing the existing ACP, and performing the crack and seat technique directly on the existing JCP.

As stated previously the crack and seat operation was performed after all of the existing AC was milled and removed, exposing the original concrete pavement. Future research should be performed to evaluate the benefits of performing the crack and seat operation directly on the AC overlay as opposed to milling and removing the overlay first. A correlation between hammer weight, drop height, and thickness of both the asphalt overlays and JCPs should also be developed. These modified techniques would yield the benefit of crack and seat without the expense of milling and removing the existing ACP.

To date no reflective cracking has occurred on Test Section R3 (CSB interlayer). The primary reason for this is that the CSB interlayer is acting as a sufficient stress relief interlayer. However, this section showed excessive rutting during the first 2 months after construction. Since then the rutting has stabilized. It remains to be seen whether the extra cost of this rehabilitation strategy ($28.93/m^2) will be offset by improved pavement performance.

For test Section R4 (open graded AC interlayer) the rerouting of traffic was required during construction. This significantly increased the cost of constructing this section. However, this section has performed well and no maintenance has been required to date. The IRI values and rut depths have also been well below average. Reflective cracking has not occurred in this section.

Test Section R5 (SBS modified plant mix seal coat interlayer) has performed poorly. This section began exhibiting surface distress after 1 year of traffic. The surface distress consisted primarily of an overall deterioration of the pavement. It appeared to be the combined effect of both stripping and inadequate structural support of the surface layer. This section reached terminal serviceability after only 18 months of service life. It has subsequently required milling and an AC overlay.

Test Section R6 (Type D AC overlay) has the lowest life cycle costs of all the test sections with the exception of the control section. It also has performed relatively well, with no rutting occurring and only a minimal increase in IRI. However, it has shown a moderate amount of reflective cracking, with 35 percent of the existing JCP joints reflecting through the ACP surface.

Significant information and knowledge regarding stress relief interlayers have resulted from the project described here. The test sections will continue to be monitored until they reach minimal serviceability. With the knowledge gained in the study engineers will be better informed when making decisions regarding rehabilitation strategies on pavements with similar distress histories.

REFERENCES

1. *NCHRP Synthesis of Highway Practice 144: Breaking/Cracking and Sealing Concrete Pavements*. TRB, National Research Council, Washington, D.C., March 1989.
2. Lorenz, V. M. New Mexico Study of Interlayers Used in Reflective Crack Control. In *Transportation Research Record 1117*, TRB, National Research Council, Washington, D.C., 1987.
3. *Performance Survey of Crushed Stone Crack Relief Layer*. Arkansas State Highway and Transportation Department, April 1983.
4. The Asphalt Institute. Portland Cement Concrete Rehabilitation Crack Relief Layer Incorporated into Asphalt Concrete Overlay. *ASPHALT Magazine*, Spring 1989.
5. *Proc., Association of Asphalt Paving Technologists*, Vol. 49, 1980.

Publication of this paper sponsored by Committee on Pavement Rehabilitation.

Analytical Evaluation of Bituminous Overlays on Flexible Pavements

K. SUDHAKAR REDDY AND B. B. PANDEY

Criteria were developed to predict the performance of bituminous overlays on flexible pavements considering fatigue and modes of distress. Data collected on several pavement sections on national highways in India were correlated to the mechanistic response of the pavement to develop the performance criteria. The theoretical responses of the pavement were calculated by using a computer program developed to solve elastic layered systems. Design charts were prepared to assist field engineers in designing pavement sections that can be expected to perform satisfactorily during the design period without developing excessive fatigue cracking and rutting.

In India flexible pavements are designed by using the subgrade CBR value according to the guidelines of Indian Roads Congress (*1*), with no consideration given to cracking or rutting. The CBR method (*1*), which was developed about 20 years ago, has little relevance for the present-day high volume of traffic coupled with heavy axle loads. It is therefore essential that analytical design methods based on the stress-strain behavior of the pavement materials be developed by correlating the mechanistic response of the pavement with the performance of pavements in the field. The two most important forms of pavement distress that lead to the functional failure of the pavement are fatigue cracking of bituminous and other bound layers and rutting along wheelpaths. Repeated applications of wheel loads, which cause excess tensile strain in the bituminous layer and excess vertical compressive strain on the subgrade, are identified as major reasons for fatigue cracking and rutting, respectively. Hence, to preclude the two modes of distress in a pavement during its design life, any rational design method for flexible pavements must aim at keeping these two strain values within the limits that the pavement materials can withstand. These limits must be determined from laboratory and field tests. Mechanistic design methods with either fatigue cracking or rutting as design criteria have already found application in the United States and several countries in Europe (*2–6*). Efforts have also been made in India in recent years to reduce the empirical content of the pavement design by studying and analyzing the performance of in-service pavements (*7–10*).

As a result of exhaustive research on the fatigue of the bituminous mixes commonly used in India, Pandey (*7,11*) developed performance-based fatigue criteria by calibrating laboratory fatigue results from the field performance of the bituminous pavements. A rutting criterion was developed by the authors (*8*) from the analysis of several in-service pavements that showed failure caused by rutting ranging from 20 to 25 mm along wheelpaths. On the basis of these two criteria, the authors presented charts for the design of flexible pavements with bituminous overlays to preclude the development of excessive cracking and rutting in the pavement within the design period (*10*).

In the present paper several additional pavement sections are considered in developing performance-based fatigue criteria in place of the earlier criteria (*7,10*), which were developed by calibrating a laboratory fatigue curve with limited field performance data. Field engineers in India usually consider a pavement to have failed if the area of cracked surface amounts to about 20 to 30 percent of the total pavement area. Hence, in the present investigation the failure condition considered for fatigue criteria is the development of surface cracking (mean + standard deviation) in excess of 20 percent of the paved area. Similarly, for rutting criteria, development of a rut depth in excess of 20 mm is taken as a failure condition.

Field data collected for several pavement sections on National Highway 5 (NH5) in Orissa, NH2, NH6, and NH41 in West Bengal, NH2 in Bihar, and NH4 in Karnataka states in India were utilized in developing the performance criteria. Structural analysis of the pavements was carried out by using the ELAYER computer program (*12*), which was developed to solve elastic layered pavement systems. Results from laboratory tests conducted on bituminous mixes (*13*) and granular materials and subgrade soils (*14*) and the studies conducted on the lateral placement and axle load characteristics of commercial vehicles (*15–17*) were used in the development of performance criteria. Design charts were developed on the basis of fatigue and rutting criteria to enable field engineers to design pavements to serve during the life period satisfactorily without developing excessive fatigue cracking or rutting.

STRUCTURAL ANALYSIS OF FLEXIBLE PAVEMENTS

The flexible pavement system was idealized as a linear elastic layered system to compute stresses, strains, and deflections in the pavement. Each layer in the pavement is characterized by its elastic modulus (E) and Poisson's ratio (μ). Several field studies (*18–26*) indicated that the use of elastic theory provided a reasonable estimate of pavement response to fast-moving wheel loads if appropriate values of elastic parameters are used in the analysis. Although the behavior of the pavement materials is not linearly elastic in general, this approach can be used by assigning elastic modulus and Poisson's ratio values corresponding to appropriate loading time, pavement temperature, and other field conditions. A computer program, ELAYER, was developed (*12*) on the basis of the solutions presented by Burmister (*27,28*) for elastic layered system. Rough interfaces between layers are assumed in the analysis, which is appropriate for most construction practices. Figure

Department of Civil Engineering, Indian Institute of Technology, Kharagpur, 721 302, West Bengal, India.

1 shows the cross section of a typical three-layer pavement system considered for analysis. As shown in Figure 1 the loading configuration consists of dual wheel loads, each being 20 kN, that are assumed to act over circular areas at 550 kPa of tire pressure. Average center-to-center spacing between the dual wheels was 310 mm.

ELASTIC PROPERTIES OF PAVEMENT MATERIALS

Elastic Modulus Value

Subgrade Soil

The elastic modulus value of subgrade soil (E_3) was estimated from its CBR by using the relationship (*29,30*)

$$E_3 = 10.0 \cdot \text{CBR} \quad (1)$$

where E_3 is in megapascals.

Repeated load triaxial test of various soils indicated that Equation 1 is reasonably correct for CBR values of about 5.0. For stronger subgrades the following relationship, which was found to be closer to the triaxial test results (*6*), was used to estimate the elastic modulus values of subgrade (E_3).

$$E_3 = 17.6 \cdot (\text{CBR})^{0.64} \quad (2)$$

Granular Base Course

A granular layer in a flexible pavement is difficult to characterize. It is a no-tension material, and nonlinear iterative analysis (*31*) is required to determine the stress distribution in such a layer. In the absence of simple mathematical solutions for such granular materials, the Shell relationship (*2*) for the modular ratio given by Equation 3 was used for estimating the elastic modulus value (E_2) of granular base course.

$$E_2 = 0.2(H_2)^{0.45} \cdot E_3 \quad (3)$$

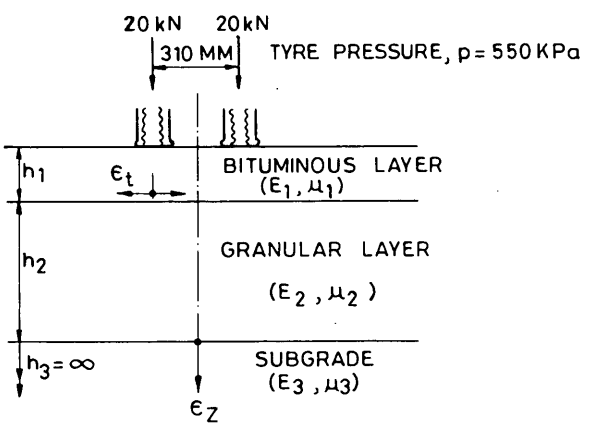

FIGURE 1 Typical three-layer pavement section.

where H_2 is the thickness of granular base (in millimeters). The modular ratio (E_2/E_3) has limits of from 2 to 4.

Bituminous Materials

Bituminous macadam (BM) (*32*), with a wearing course of thin premix bituminous carpet and seal coat (*33*), is the most common type of bituminous construction adopted in India. The gradation of aggregates in BM is close to mix IIe of the Asphalt Institute (*34*). The open-graded mix has a bituminous content of 4-percent by weight of the total mix, and the air void after 6 months of traffic is about 15 percent. All of the pavement sections discussed in this paper contain BM construction with a bituminous wearing surface. The average annual air temperature (AAAT) for the region in which the majority of the pavement sections under consideration are situated was found to range from 27°C to 29°C. In the absence of any data for average annual pavement temperature (AAPT) of bituminous pavements in India, the relationship developed by Brunton et al. (*35*) was used to determine the AAPT from the AAAT. For an AAAT of 28°C, the AAPT was found to be 35°C.

A repeated load test at a rate of 120 repetitions per minute on the open-graded BM specimens 100 mm in diameter and 200 mm in height containing 80/100 bitumen and cast according to the grading of the Ministry of Surface Transport (*32*) resulted in a resilient modulus value of about 200 MPa for a test temperature of 30°C and a loading time of 0.12 sec. Although references on such open-graded materials are scarce, Claessen et al. (*2*) have reported similar values of elastic modulus for lean bituminous macadam. By using Shell's nomograph (*36*), the experimental dynamic modulus value was corrected for a loading time of 0.02 sec and an AAPT of 35°C, and the modified value was 500 MPa. For dense asphalt concrete under similar conditions, the elastic modulus is almost 1000 MPa (*36*) for 80/100 bitumen, with the air void being 3 to 5 percent.

Poisson's Ratio

For the bituminous mix, Poisson's ratio was taken as 0.5, which was considered appropriate for the range of temperatures under consideration (*37,38*). The value of Poission's ratio was taken as 0.40 for granular materials and subgrade soils (*39*).

FIELD PERFORMANCE STUDIES

Performance data collected over several pavement sections on NH2, NH6, and NH41 in West Bengal, NH5 in Orissa, NH2 in Bihar, NH4 in Karnataka, and State Highway 9 in Uttar Pradesh were used in the development of the performance criteria. Tables 1 and 2 show the details for pavement sections considered in developing the fatigue and rutting criteria, respectively. The CBR values were determined after 4 days of soaking of soil specimens cast at the in situ dry density and moisture content. These sections are situated in areas with annual rainfall in the range of 1000 to 1600 mm. Many of the sections considered are part of Research Scheme R-6 sponsored by the Ministry of Surface Transport, Government of India. Performance data on several of the remaining pavement sections were collected as part of a consultancy project

TABLE 1 Details for Pavement Sections Considered for Fatigue Criteria

S NO	LOCATION NH/SH	KM	TRAFFIC (CVPD)	SUBGRADE CBR (%)	LAYER THICKNESS (mm) BITUMINOUS MACADAM	GRANULAR BASE	MAX. HORIZONTAL TENSILE STRAIN (ϵ_t x 10^{-6})	OVERLAY LIFE MONTHS	CSA 10^6
1	4	41.43	3000	30.0	70	320	306.0	36	7.70
2	4	41.50	3000	30.0	95	320	318.3	54	12.1
3	4	41.60	3000	30.0	120	320	297.9	72	16.9
4	2	283.0	3800	3.5	100	540	361.0	18	4.11
5	2	595.3	3650	4.8	95	340	752.7	5	1.07
6	2	607.1	3650	5.5	95	380	659.6	13	2.90
7	2	607.2	3650	5.5	170	380	445.1	21	4.90
8	2	657.7	3650	2.9	150	265	794.4	4	0.86
9	5	256.8	3500	6.7	70	680	493.3	20	4.5
10	5	256.9	3500	6.7	95	680	482.6	20	4.5
11	5	81.60	2280	3.8	95	500	783.7	16	2.0
12	6	128.8	2800	9.8	70	320	465.1	12	2.58
13	6	128.9	2800	9.8	110	320	441.6	11	2.16
14	6	130.0	2800	5.2	70	340	772.8	8	1.98
15	6	131.0	2800	8.9	100	325	572.4	11	2.72
16	9	198.0	1180	5.0	70	600	648.3	50	3.91

CVPD: Commercial vehicles per day in both traffic directions
CSA: Cumulative standard axle repetitions

carried out by the Transportation Engineering Section of the Indian Institute of Technology (IIT), Kharagpur, India (*40,41*). The length of each of the pavement sections of the Research Scheme, which is about 300 m, was subdivided into three parts on which different overlay thicknesses were used. All of the pavement sections have two-lane carriageways 7.0 m in width with two-way traffic.

A thin bituminous wearing course of 20-mm Premix Carpet with a seal coat over a granular base was considered as part of the granular base because the structural strength provided by this layer is negligible. Boulder and brick soling were not considered in the structural layer thicknesses because of their poor load-spreading behaviors, as found by Sivaguru et al. (*42*). The badly cracked bituminous layer on which the overlay was placed was considered part of the granular layer.

Measurement of rut depth along the wheelpaths was made by using a 3-m straight edge at regular intervals in both directions of traffic. The percentage of the area of cracked surface because of fatigue was estimated by visual observation.

TABLE 2 Details for Pavement Sections Considered for Rutting Criteria

S NO	LOCATION NH/SH	KM	TRAFFIC (CVPD)	SUBGRADE CBR (%)	LAYER THICKNESS (mm) BITUMINOUS MACADAM	GRANULAR BASE	MAX. VERTICAL TENSILE STRAIN (ϵ_z x 10^{-6})	OVERLAY LIFE MONTHS	CSA 10^6
1	2	595.1	3650	4.8	--	340	1302.0	16	3.65
2	2	607.0	3650	5.5	--	380	974.30	13	2.90
3	5	81.70	2280	3.8	--	595	667.70	46	6.64
4	6	99.00	2800	4.5	--	200	2368.0	4	0.75
5	6	100.0	2800	3.0	--	395	1668.0	4	0.75
6	6	135.0	2800	1.4	120	560	1257.0	25	5.33
7	6	137.0	2800	4.2	35	425	985.80	48	8.06
8	6	138.0	2800	5.5	30	95	2321.0	4	0.75
9	6	148.0	2800	4.7	80	270	1341.0	48	8.06
10	6	149.0	2800	5.3	45	455	683.3	48	8.06
11	6	150.0	2800	9.7	40	365	707.8	48	8.06
12	6	153.0	2800	10.0	--	390	686.7	4	0.75
13	6	160.0	2800	8.0	--	130	1880.0	4	0.75
14	6	179.0	2800	3.7	50	520	767.40	48	8.06
15	41	46.00	1520	5.0	130	65	1846.0	60	5.26
16	41	48.00	1520	4.0	150	230	1182.0	60	5.26
17	41	49.0	1520	4.0	170	225	1079.0	60	5.26
18	41	50.0	1520	4.5	155	50	1729.0	60	5.26
19	41	51.0	1620	3.2	--	270	2759.0	4	0.43
20	41	52.0	1620	3.6	--	240	2749.0	4	0.43

-- Thin bituminous overlay considered as part of granular base

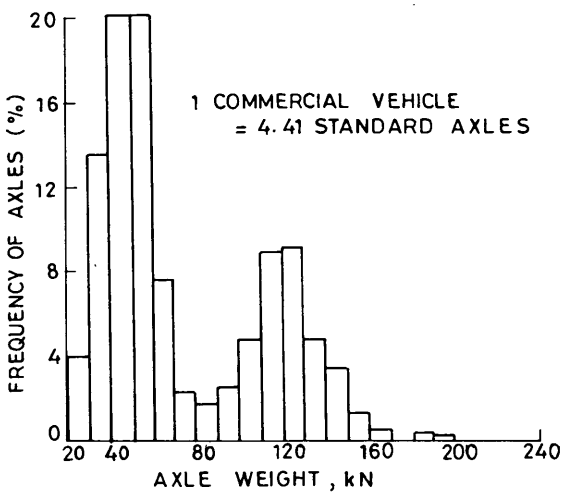

FIGURE 2 Distribution of axle weights (combined data for NH2, NH5, and NH6).

CALCULATION OF EQUIVALENT STANDARD AXLE REPETITIONS

It is necessary to estimate the number of repetitions of 80-kN loads [equivalent single axle loads (ESALs)] from measurements of the axle loads of commercial vehicles. A portable weigh bridge was designed and fabricated by the authors (*16*), and field studies were conducted on NH2, NH5, and NH6 to find the axle load spectrum on the various national highways (*17*) under study. Repetitions of ESAL were determined for different pavement sections by using AASHTO equivalency factors. The average value of the truck factor was found to be 4.40, whereas the value recommended by the Indian Roads Congress (IRC) is 3.0 (*1*). The high truck factor is due to the fact that a very large percentage of commercial vehicles have rear axle loads exceeding 102 kN, which is the legal axle load in India. A typical distribution of axle weights on the national highways under study is shown in Figure 2.

Studies of the lateral placement characteristics of wheel loads of commercial vehicles (*15*) indicated that the inner wheelpaths of commercial vehicles in either direction keep close to the centerline of the two-lane road, and about 50 percent of the wheelpaths of the total two-way commercial vehicles lie within a 1.00-m band. Figure 3 presents a typical distributon of the inner wheelpaths of the rear axles of commercial vehicles on two-lane Indian national highways.

A traffic growth rate of 7.5 percent, as suggested by IRC (*1*), was considered whenever necessary to compute the cumulative standard axle load repetitions.

DEVELOPMENT OF FATIGUE FAILURE CRITERIA

Laboratory Fatigue Relationship

Laboratory investigations of the fatigue behaviors of bituminous mixes were reported elsewhere (*7*). Third-point repeated loading was applied on beams of bituminous mix at a temperature of 20°C. The fatigue relationship for bituminous mixes with 80/100 grade bitumen and 7 percent air voids at a test temperature of 20°C was obtained as

$$N = 7.1140 \cdot 10^{-10} \cdot (1/\epsilon_t)^{3.99} \quad (4)$$

where N is the number of repetitions to fatigue and ϵ_t is the tensile strain.

Bituminous mixtures have longer fatigue lives at higher temperatures because of greater flexibility. Equation 4 was therefore modified to obtain a fatigue relationship for an AAPT of 35°C by using the equations of Rauhut and Kennedy (*43*). The equation is given as

$$N = 1.7564 \cdot 10^{-7} \cdot (1/\epsilon_t)^{3.89} \quad (5)$$

Since fatigue data for bituminous mixes for air voids of 15 percent are not available, the research work of Pell and Taylor (*44*) on the effects of air voids on fatigue life was used in the

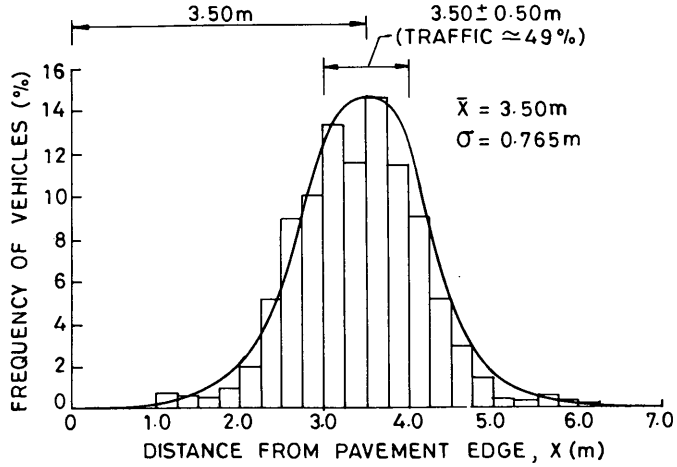

FIGURE 3 Distribution of inner wheelpaths on two-lane roads.

investigation described here. It was found that the fatigue lives of bituminous mixes decreased with an increase in the air voids. Equation 5 was therefore modified to obtain a fatigue curve for BM with 15 percent air void and is shown as line 2 in Figure 4.

Laboratory fatigue relationships do not take into account (a) the healing of the mixes due to the rest periods available in the field because of intermittent traffic, (b) the lateral wander of wheel loads, or (c) changes in the properties of the mixes because of weathering. It is thus necessary to calibrate a laboratory fatigue line with the performance of BM overlays that failed because of fatigue cracking during service.

Calibration of Laboratory Fatigue Relationship

Several pavement sections that failed because of fatigue cracking were analyzed by using the ELAYER program to compute the maximum horizontal tensile strain (ϵ_t) in the bituminous layer. The lives of the bituminous overlays corresponding to the failure of the pavements due to the development of fatigue cracking were computed in terms of cumulative standard axles (CSAs). It was found that the fatigue life computed from the laboratory relationship must be multiplied by an average shift factor of 15.0 to get an estimate of field fatigue life. The laboratory fatigue line (20°C, 7 percent air voids), the extrapolated relationship (35°C, 15 percent air voids), and the fatigue relationship calibrated from field performance are shown in Figure 4. The calibrated fatigue line shown in Figure 4 can be represented by the following relationship.

$$N = 6.6277 \cdot 10^{-7} \cdot (1/\epsilon_t)^{3.89} \quad (6)$$

Errors, if any, introduced while applying corrections for air voids and temperatures are eliminated to a large extent during the calibration.

The authors' fatigue relationship is shown in Figure 5 in comparison with some other fatigue criteria developed elsewhere. The fatigue line developed by the authors is positioned higher on the plot compared with those developed by others mainly because of (a) the higher temperatures in the study area and (b) the lower level of serviceability tolerated before rehabilitation measures are taken.

DEVELOPMENT OF RUTTING FAILURE CRITERIA

Correlation of the computed vertical subgrade strain (ϵ_z) values with observed pavement lives in the rutting mode of failure (N) resulted in the following relationship

$$N = 2.0567 \cdot 10^{-4} \cdot (1/\epsilon_z)^{3.5062} \quad (7)$$

where ϵ_z is the vertical subgrade strain and N is the number of standard axle repetitions.

For 85 percent one-sided confidence limits, the relationship is

$$N = 5.7316 \cdot 10^{-5} \cdot (1/\epsilon_z)^{3.5062} \quad (8)$$

The coefficient of determination (R^2) for these relationships is 0.45. The rutting criterion for an 85 percent one-sided confidence limit was adopted in this paper for developing design charts for BM overlays over flexible pavements. The rutting criterion suggested by the authors is shown in Figure 6 along with some other criteria developed elsewhere. Although the authors' criterion for

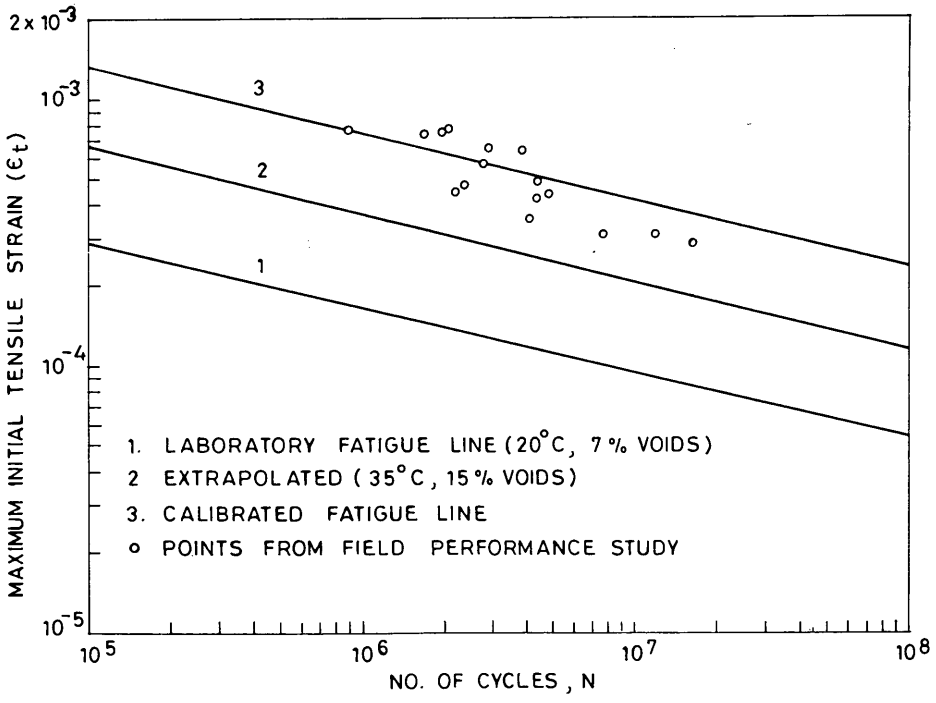

FIGURE 4 Calibration of laboratory fatigue criteria.

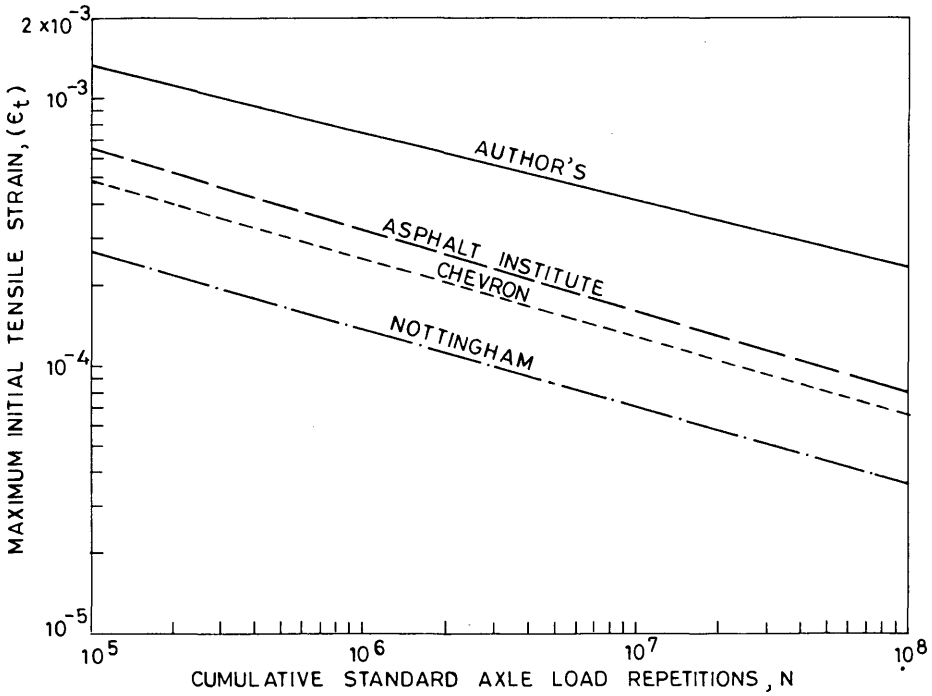

FIGURE 5 Comparison of fatigue criteria.

the 85 percent confidence limit is closer to that of Shell (*2*), it is liberal in comparison with the other two criteria. This is because (a) the allowable rut depth is 20 mm for India in comparison with 10 to 15 mm in, for example, the United Kingdom, the United States, and The Netherlands, and (b) diverse climate and traffic conditions.

DEVELOPMENT OF DESIGN CHARTS

Design charts were developed by analyzing pavement sections for subgrade vertical strain (ϵ_z) and horizontal tensile strain (ϵ_t) under the standard loading conditions discussed earlier in the paper and finding the pavement composition (thickness and elastic proper-

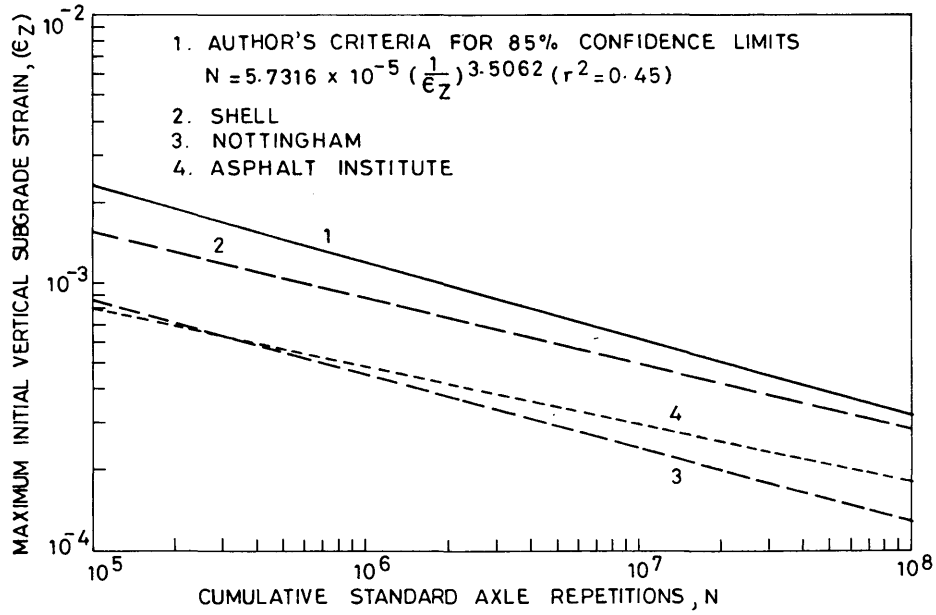

FIGURE 6 Rutting criteria.

ties) that can keep these strain values below the limiting values set by the performance criteria for different values of CSA load repetitions. Several combinations of pavement sections were selected by considering six values of subgrade modulus (30, 40, 50, 60, 100, and 170 MPa), a varying granular base thickness at 20-mm intervals ranging from 150 to 450 mm, and BM thickness ranging from 50 to 350 mm at intervals of 10 mm. Some of the design charts for different levels of traffic prepared for different subgrade modulus values are presented in Figures 7 to 10. These charts were developed to give design thicknesses that can satisfy both the fatigue and rutting failure criteria. The *R* and the *F* noted in Figures 7 to 10 indicate the portions of the curve that correspond to fatigue and rutting criteria, respectively.

By examining the design charts presented in Figures 7 to 10, the following inferences can be drawn with respect to the contribution of the major components of the pavement toward its performance:

1. With an increase in the subgrade modulus value the governing criterion shifts from the rutting to the fatigue mode of failure because pavements with stronger subgrades perform better against rutting failure.
2. Pavements with a lesser thickness of granular base course are likely to fail in rutting early. This in a way signifies the contribution of the granular layer in preventing rutting, as can be seen from the steeper slopes of the rutting criterion portions of the design curves.
3. As is evident from the flatter slopes of the design curves for fatigue criteria, the contribution of the granular base in preventing fatigue cracking is not substantial. Beyond the rutting portion of the design curves, the provision of additional thicknesses of the granular base serves little purpose because the reduction in the thickness of BM is only marginal.
4. The slopes of the design curves give an indication of the equivalence factors for the bituminous layer in terms of the granular base course. As seen from the plots the equivalency factor may vary from a value of as low as 1.2 (for the steepest curve) to a very large value, depending on the combination of subgrade strength and the thicknesses of the granular base course and bituminous layer.

COMPARISON WITH OTHER DESIGN PRACTICES

The design thicknesses obtained from the chart developed by the authors were compared with those obtained from other design methods such as the IRC design method (*1*), the Asphalt Institute method (*45*), the Shell method (*2*), and British practice (*46*). The comparison is shown in Table 3. Although the Asphalt Institute and Shell methods use analytical approaches, the IRC method and British practice are based mostly on field experience. A comparison of design thicknesses has been made for a range of subgrade modulus values, granular and bituminous layer thicknesses, and traffic levels. The IRC method suggests a larger thickness of the granular layer, whose contribution beyond a certain limit has been found to be insignificant. Thus, the pavement sections are in general underdesigned against fatigue cracking because of a low bituminous layer thickness. The suggested design thicknesses differ from others because of the construction practices, traffic, climate, and failure criterion adopted in the preparation of the charts.

CONCLUSIONS

The thickness design charts presented here on the basis of performance studies on several bituminous overlays in India can be

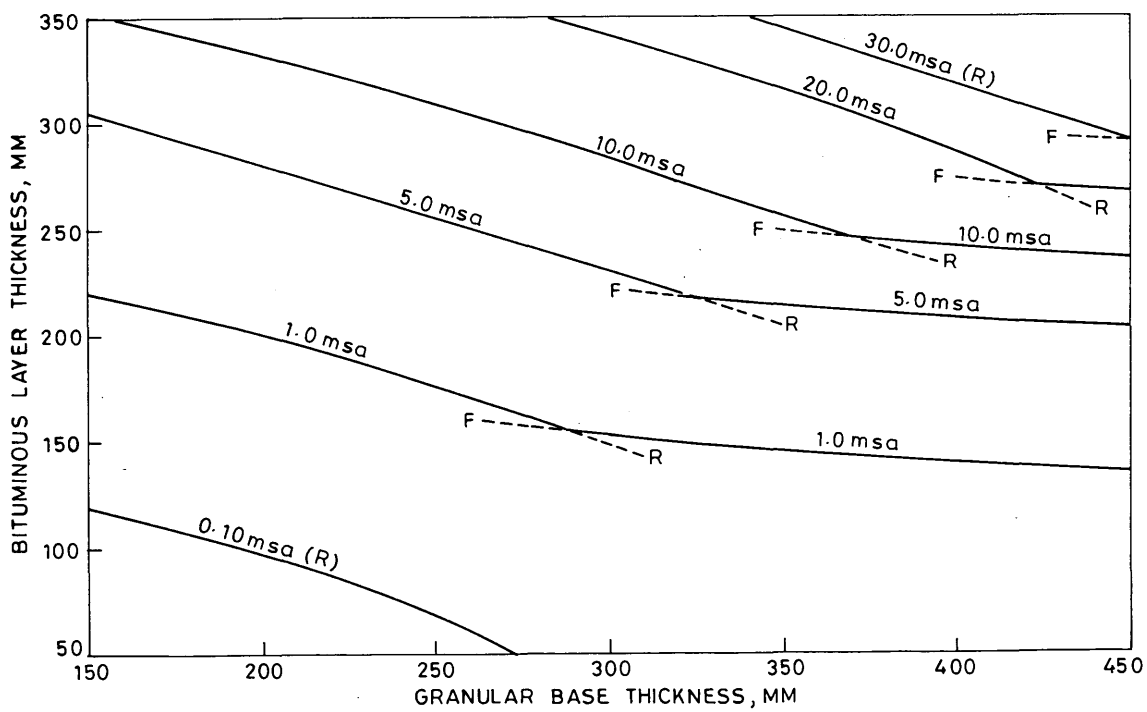

FIGURE 7 Design thickness for different traffic levels (subgrade modulus = 30 MPa).

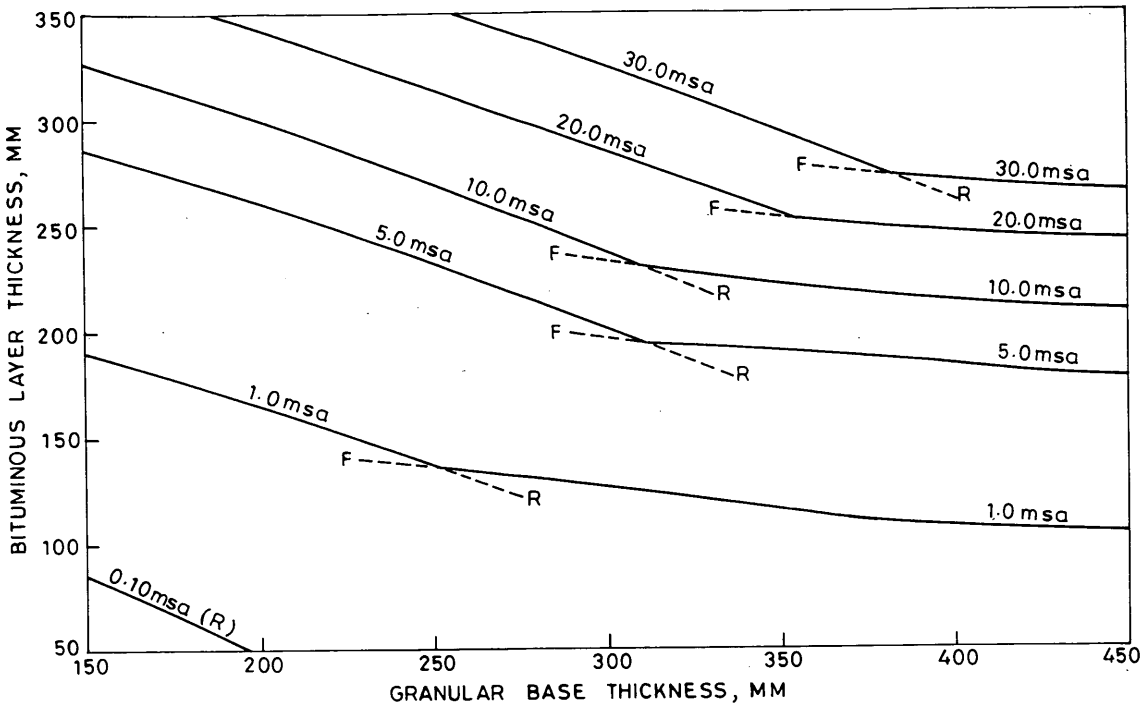

FIGURE 8 Design thickness for different traffic levels (subgrade modulus = 40 MPa).

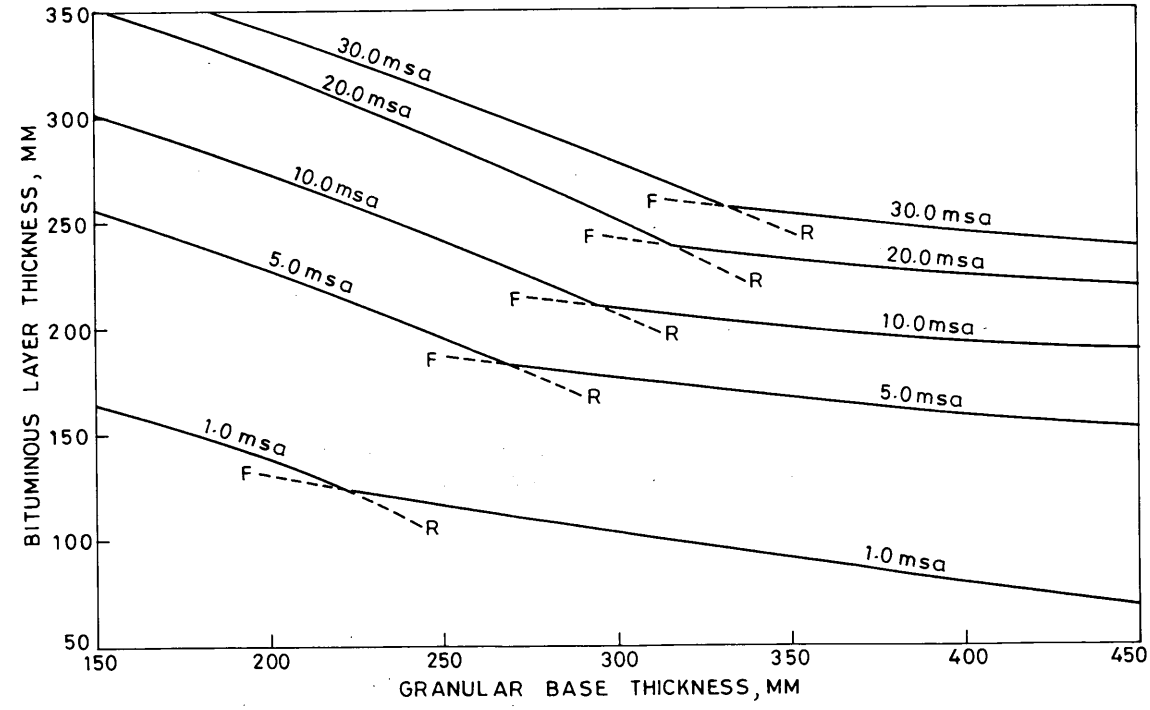

FIGURE 9 Design thickness for different traffic levels (subgrade modulus = 50 MPa).

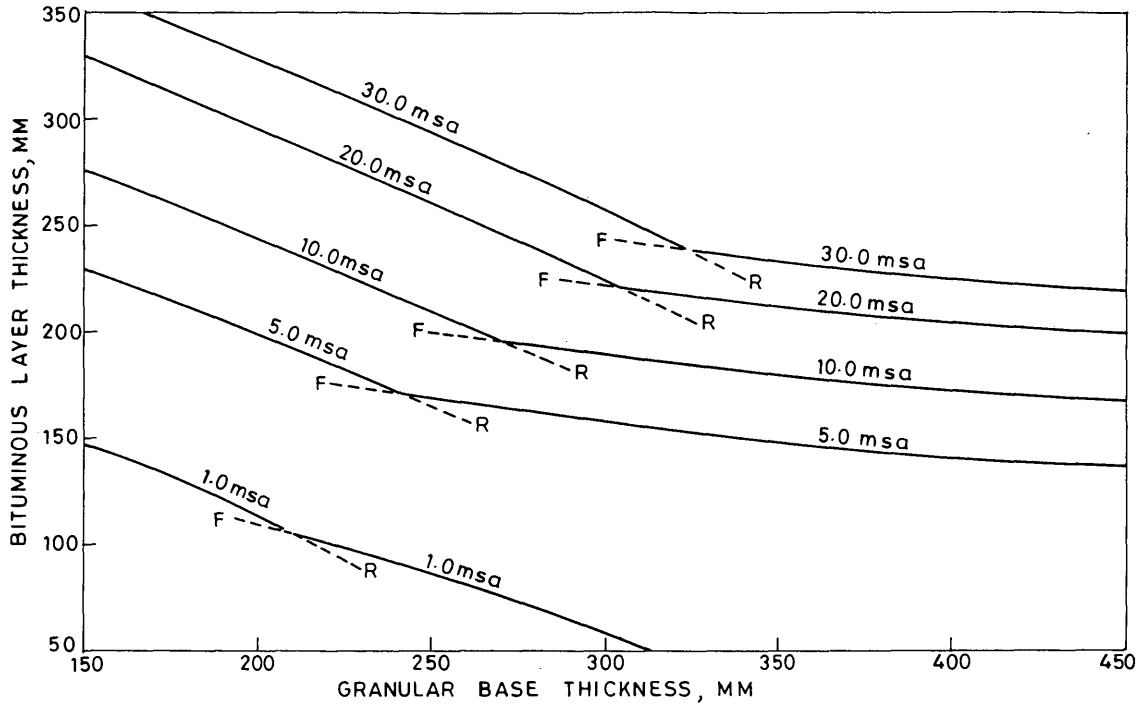

FIGURE 10 Design thickness for different traffic levels (subgrade modulus = 60 MPa).

TABLE 3 Comparison with Other Design Practices

SUBGRADE MODULUS (MPa)	DESIGN LIFE (CSA) (10^6)	GRANULAR BASE THICKNESS (mm)	BITUMINOUS LAYER THICKNESS (mm) ASPHALT INSTITUTE METHOD	SHELL METHOD	IRC METHOD	AUTHORS' CRITERIA
30	1.0	150	275	-	-	220
		300	225	-	-	155
		450	155	-	-	135
50	1.0	150	220	230	-	165
		300	165	150	-	105
		450	125	75	-	70
	10.0	150	350	350	-	300
		300	330	270	-	210
		450	300	180	-	190
60	1.0	370	-	-	20	50
	10.0	395	-	-	105	175
		420	-	-	140	205

- unavailable

used to design BM overlays for the traffic and climatic conditions described in this paper. The proposed fatigue and rutting criteria take into account the seasonal effects, and hence no adjustment to the thickness is necessary.

ACKNOWLEDGMENTS

The authors are grateful to the Ministry of Surface Transport, Government of India, for sponsoring Research Project R-6. The authors acknowledge the cooperation extended by the officers of National Highways of Orissa, West Bengal, and Bihar during field investigations.

REFERENCES

1. *Guidelines for the Design of Flexible Pavements.* 37-1984. Indian Roads Congress, 1984.
2. Claessen, A. I. M., J. M. Edwards, P. Sommer, and P. Uge. Asphalt Pavement Design—The Shell Method. *Proc., 4th International Conference on Structural Design of Asphalt Pavements,* Vol. 1, 1977, pp. 39–74.

3. Brown, S. F., P. S. Pell, and A. F. Stock. The Application of Simplified, Fundamental Design Procedures for Flexible Pavements. *Proc., 4th International Conference on Structural Design of Asphalt Pavements*, Vol. 1, 1977, pp. 327–341.
4. Santucci, L. E. Thickness Design Procedure for Asphalt and Emulsified Asphalt Mixes. *Proc., 4th International Conference on Structural Design of Asphalt Pavements*, Vol. 1, 1977, pp. 424–456.
5. Shook, J. F., F. N. Finn, M. W. Witczak, and C. L. Monismith. Thickness Design of Asphalt Pavements—The Asphalt Institute Method. *Proc., 5th International Conference on Structural Design of Asphalt Pavements*, Vol. 1, 1982, pp. 17–44.
6. Lister, N. W., and W. D. Powell. Design Practice for Bituminous Pavements in the United Kingdom. *Proc., 6th International Conference Structural Design of Asphalt Pavements*, Vol. 1, 1987, pp. 220–231.
7. Pandey, B. B. Fatigue Cracking of Bituminous Pavements. *Indian Roads Congress Journal*, Vol. 51-2, Sept. 1990, pp. 353–386.
8. Sudhakar Reddy, K., and B. B. Pandey. Performance Based Design Criteria for Flexible Pavements. *Indian Roads Congress Journal*, Vol. 52-3, 1992, pp. 383–399.
9. Chandra Tangella, R., and B. B. Pandey. Performance of Flexible Pavements in India. In *Transportation Research Record 1307*, TRB, National Research Council, Washington, D.C., 1991, pp. 51–61.
10. Sudhakar Reddy, K., and B. B. Pandey. Analytical Design of Flexible Pavements. *Highway Research Bulletin*, Indian Roads Congress, New Delhi, in press.
11. *Determination of Elastic Modulus and Fatigue Characteristics of Asphaltic Mixes in Laboratory*. Final Report of Research Scheme R-24. Transportation Engineering Section of IIT, Kharagpur, and the Ministry of Surface Transport, Government of India.
12. Sudhakar Reddy, K., R. Dhanker, and B. B. Pandey. Algorithm for Stresses in Layered Elastic Pavements. *Highway Research Bulletin*, Indian Roads Congress, New Delhi, in press.
13. Pandey, B. B., L. N. Mohan Rao, and A. Kumar. Dynamic Modulus of Asphaltic Mixes. In *Highway Research Bulletin 38*, Indian Roads Congress, 1989, pp. 29–62.
14. Pandey, B. B., and P. K. Naidu. Elastic Moduli of Materials in Flexible Pavement Design. *Highway Research Bulletin*, Indian Roads Congress, 1992.
15. Sudhakar Reddy, K., and B. B. Pandey. Lateral Placement of Commercial Vehicles on National Highways. *Highway Research Bulletin*, Indian Roads Congress, New Delhi, in press.
16. Sudhakar Reddy, K., and B. B. Pandey. Fabrication of a Low Cost Portable Weigh Bridge. *Indian Highways*, Indian Roads Congress, New Delhi, in press.
17. Sudhakar Reddy, K., D. Ray, and B. B. Pandey. Axle Weights and Vehicle Damage Factors on National Highways in Eastern India. *Highway Research Bulletin*, Indian Roads Congress, New Delhi, 1992.
18. Gusfeldt, K. H., and K. R. Dempwolff. Stress and Strain Measurements in Experimental Road Sections Under Controlled Loading Conditions. *Proc., Second International Conference on Structural Design of Asphalt Pavements*, 1967, pp. 663–669.
19. Klomp, A. J. G., and T. W. Niesman. Observed and Calculated Strains at Various Depths in Asphalt Pavements. *Proc., Second International Conference on Structural Design of Asphalt Pavements*, 1967, pp. 671–688.
20. Nijboer, L. W. Testing Flexible Pavements Under Normal Traffic Loadings by Means of Measuring Some Physical Quantities Related to Design Theories. *Proc., Second International Conference on Structural Design of Asphalt Pavements*, 1967, pp. 689–705.
21. Whiffin, A. C., and N. W. Lister. The Application of Elastic Theory to Flexible Pavements. *Proc., International Conference on Structural Design of Asphalt Pavements*, 1962, pp. 499–521.
22. Dempwolf, R., and P. Sommer. Comparison Between Measured and Calculated Stresses and Strains in Flexible Road Structures. *Proc., 3rd International Conference on Structural Design of Asphalt Pavements*, Vol. 1, 1972, pp. 786–794.
23. Thrower, E. N., N. W. Lister, and J. F. Potter. Experimental and Theoretical Studies of Pavement Behaviour Under Vehicular Loading in Relation to Elastic Theory. *Proc., 3rd International Conference on Structural Design of Asphalt Pavements*, Vol. 1, 1972, pp. 521–535.
24. Bleyenberg, W. G., A. I. M. Claessen, F. Van Gorkhum, W. Huekelom, and A. C. Pronk. Fully Monitored Motorway Trials in The Netherlands Corroborate Linear Elastic Design Theory. *Proc., 4th International Conference on Structural Design of Asphalt Pavements*, Vol. 1, 1977, pp. 75–98.
25. Ahlvin, R. G., Y. T. Chou, and R. L. Hutchinson. The Principle of Superposition in Pavement Analysis. In *Highway Research Record 466*, HRB, National Research Council, Washington, D.C., 1973, pp. 153–162.
26. Ahlvin, R. G., Y. T. Chou, and H. H. Ulery. Discussion of paper Implications of Using Layered Theory in Pavement Design. *Journal of Transportation Engineering*, TE4, Vol. 97, ASCE, Nov. 1971, pp. 711–714.
27. Burmister, D. M. The General Theory of Stresses and Displacements in Layered Systems. *Journal of Applied Physics*, Vol. 16, 1945, pp. 89–94, 126–127, 296–302.
28. Burmister, D. M. The Theory of Stresses and Displacements and Applications to the Design of Airport Runways. *Proc., Highway Research Board*, No. 23, 1943, pp. 126–144.
29. Heukelom, W., and A. J. G. Klomp. Dynamic Testing as a Means of Controlling Pavements During and After Construction. *Proc., First International Conference on Structural Design of Asphalt Pavements*, 1962, pp. 667–679.
30. Claessen, A. I. M., C. P. Valkering, and R. Ditmarsch. Pavement Evaluation with the Falling Weight Deflectometer. *Proc., AAPT*, Vol. 45, 1976, pp. 122–157.
31. Doddihal, S. R., and B. B. Pandey. Stresses in Full-Depth Granular Pavements. In *Transportation Research Record 954*, TRB, National Research Council, Washington, D.C., 1984, pp. 94–100.
32. *Specifications for Road and Bridge Works*. Ministry of Surface Transport (Roads Wing), Government of India, 1988.
33. *Recommended Practice for 2 cm Thick Bitumen and Tar Carpet*. 14-1977. Indian Roads Congress, New Delhi, 1977.
34. *The Asphalt Handbook*. MS-4. Asphalt Institute, 1965, p. 66.
35. Brunton, J. M., S. F. Brown, and P. S. Pell. Developments to the Nottingham Analytical Design Method for Asphalt Pavements. *Proc., Sixth International Conference on Structural Design of Asphalt Pavements*, Vol. 1, 1987, pp. 366–377.
36. Van der Poel, C. A General System Describing the Viscoelastic Properties of Bitumens and Its Relation to Routine Data. *Journal of Applied Chemistry*, Vol. 4, Part 5, May 1954, p. 221.
37. Pell, P. S. Pavement Materials. Keynote Address. *Proc., Sixth International Conference on Structural Design of Asphalt Pavements*, Vol. 2, 1987, pp. 36–70.
38. Pell, P. S., and S. F. Brown. The Characteristics of Materials for the Design of Flexible Pavements. *Proc., 3rd International Conference on Structural Design of Asphalt Pavements*, Vol. 1, 1972, pp. 326–342.
39. Treybig, H. J. Mechanistic Method of Pavement Overlay Design. In *Transportation Research Record 700*, TRB, National Research Council, Washington, D.C., 1979, pp. 72–77.
40. *Investigation of Pavement Performance of Selected Sections on NH-41 for Strengthening and Overlay Design*. Transportation Engineering Section, IIT, Kharagpur, India, 1988.
41. *Investigation of Pavement Performance of Selected Sections on NH-6 for Strengthening and Overlay Design*. Transportation Engineering Section, IIT, Kharagpur, India, 1988.
42. Sivaguru, N., K. C. Reddy, A. S. Rajagopal, A. Veeraragavan, and C. E. G. Justo. Studies on New Flexible Pavements. *Indian Roads Congress Journal*, Vol. 47-1, Aug. 1986, pp. 111–156.
43. Rauhut, J. B., and T. W. Kennedy. Characterizing Fatigue Life for Asphalt Concrete Pavements. In *Transportation Research Record 888*, TRB, National Research Council, Washington, D.C., 1982, pp. 47–56.
44. Pell, P. S., and I. F. Taylor. Asphaltic Road Materials in Fatigue. *Proc., AAPT*, Vol. 38, Feb. 1969, pp. 371–422.
45. *Thickness Design Manual* (9th edition). Asphalt Institute, 1981.
46. *A Guide to the Structural Design of Pavements for New Roads* (3rd ed.). Road Note No. 29. Her Majesty's Stationery Office, London, 1970.

Publication of this paper sponsored by Committee on Pavement Rehabilitation.

Evaluation of Highway Undersealing Practices of Portland Cement Concrete Pavements

RAMZI TAHA, ALI SELIM, SA'D HASAN, AND BLAIR LUNDE

Pumping and faulting of undoweled portland cement concrete pavements has become a serious problem in South Dakota. When a pavement becomes faulted the rideability of the pavement becomes objectionable to the traveling public. One of the rehabilitation measures used to reduce the progression of faulting has been undersealing. This process does not correct depressions, increase the design structural capacity, or eliminate faulting, but rather restores the structural integrity of the slab by reducing deflections. The success of an undersealing operation depends on the selection of an acceptable undersealing material, testing of the pavements for voids, estimation of grout quantities, determination of the optimal time in a pavement's life cycle to perform undersealing work, and adequate construction practices. The results of a survey of current undersealing practices in the United States are presented. Of the 33 states that responded to the survey, only 16 are implementing undersealing as a rehabilitation strategy. Areas of concern to highway agencies include cost-effectiveness of undersealing, the adequacy of construction practices, and the long-term performance of undersealed pavements.

Pumping is a load-actuated erosion phenomenon by which material from the pavement foundation or shoulder is moved about by water. When fine material is removed from beneath the slab by pumping action there is a reduction in slab support, which leads to a greater slab deflection and more severe pumping. This process may lead to faulting at joints if positive load transfer is not present. When a pavement becomes faulted the rideability of the pavement becomes objectionable to the traveling public and in some cases can impair the structural integrity of the pavement.

Research (*1*) has shown that four basic conditions must be present simultaneously to create pumping and a faulted slab. They are

1. Free water under the slabs,
2. Frequent heavy axle loads,
3. Cracks or joints in the pavement, and
4. Unstabilized or erodible material under or adjacent to the slabs.

If any of these factors is absent, pumping and faulting will not occur. A combination of visual surveys and nondestructive testing can be used to detect pumping, faulting, and the presence of voids beneath the slab.

The rehabilitation strategies necessary to correct the pumping and faulting of slabs depend on the condition of the pavement and other factors such as available funding and minimum life extension. For each distress type one or more repair or preventative rehabilitation methods can be applied. For example, faulting can be removed or repaired by (a) diamond grinding or (b) placement of a thick overlay. However, faulting of transverse joints can be prevented by (*2*)

1. Undersealing to fill voids and restore support,
2. Reestablishing load transfer across the joint with mechanical devices (this helps to prevent further pumping by reducing deflection),
3. Resealing the transverse and longitudinal joints (this helps to prevent further pumping), and
4. Providing subdrainage (this helps to prevent further pumping).

The successful implementation of an undersealing operation requires the following:

1. The determination of joints or cracks that need undersealing has been a difficult and controversial question. Only those joints or cracks that exhibit loss of support (voids) should be undersealed. Visual surveys, deflection measurements (falling-weight deflectometer), and Benkelman beam, Road Rater, ground-penetrating radar (*3*), and pulsed electromagnetic wave (*4*) technologies can be used to locate and measure voids beneath portland cement concrete (PCC) pavements.
2. The proper undersealing material must be selected. The undersealing material must be capable of penetrating very thin voids, yet it must have sufficient strength and durability to resist loading, moisture, and temperature effects. Asphalt cements (*5*), pozzolanic (fly ash)-cement grouts (*6*), limestone dust-cement grouts (*7*), and polyurethane and silicone rubber foam (*8*) have been used for undersealing.
3. The estimation of grout quantities is extremely difficult, but it can be accomplished by using past experience, the extent of visual distress such as faulting and pumping, and deflection testing for voids or loss of support.
4. The undersealing procedures must be carefully controlled in the field. The success of the operation depends highly on the skill and the knowledge of the contractor and the crew doing the grout injection. Slab lift must be closely controlled to avoid overgrouting, which may result in premature slab breakup. The down force exerted during the drilling of grout injection holes must be controlled to avoid causing deterioration or spalling at the bottom of the slab near the hole. Pumping pressures must be limited to avoid damage to the pavement from excessive slab lift.

R. Taha, Department of Civil and Environmental Engineering, Washington State University, Pullman, Wash. 99164-2910. A. Selim and S. Hasan, Civil Engineering Department, South Dakota State University, Brookings, S. Dak. 57007-0495. B. Lunde, Office of Research, South Dakota Department of Transportation, 700 Broadway Avenue East, Pierre, S. Dak. 57501-2586.

5. The long-term effectiveness of undersealing depends on preventing free moisture from accumulating in the pavement structure. All joints and cracks should be properly sealed, and subdrains should be placed to get rid of moisture (*2*).

Finally, the success of a pavement undersealing project also depends on other rehabilitation work that should be performed in conjunction with undersealing.

The main objectives of this paper are to summarize the pertinent results obtained from the survey of current practices.

SUMMARY OF CURRENT PRACTICES

Summarized in this section is part of the survey of current practices dealing with PCC pavement undersealing. The survey was sent out to all 50 states and Puerto Rico (referred to here as a state for data analysis purposes). The relevant questions on undersealing were

1. The criteria used to establish when to implement undersealing work,
2. The types of grouts used in undersealing,
3. The construction methods used in undersealing, and
4. The criteria used to determine the long-term effectiveness of undersealing.

To collect the needed information two survey techniques were used: the initial information request and follow-up requests. Thirty-three states responded to the survey. As shown in Figure 1, of the 33 states that responded only 16 are implementing undersealing as a rehabilitation strategy. The other 17 states do not implement undersealing for the following reasons:

1. The difficulty of locating voids beneath the slab,
2. The difficulty of filling all voids,
3. The damage to the pavement that overgrouting could cause,
4. The dependence of undersealing on the experiences and skills of the contractors, and
5. The lack of cost-effectiveness of undersealing.

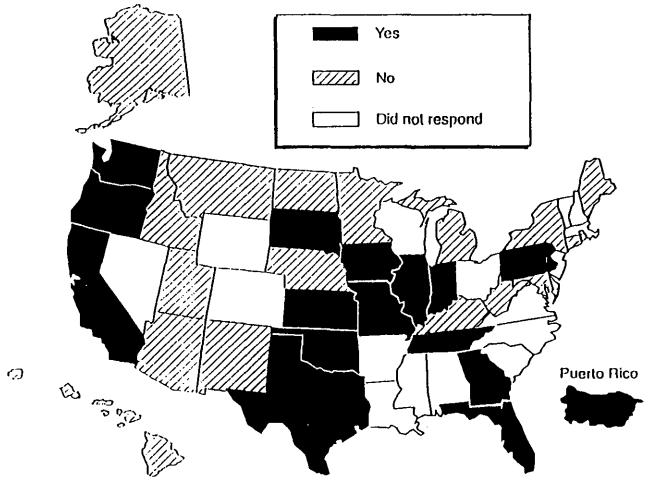

FIGURE 1 States that responded to survey.

However, even some of those states that underseal their PCC pavements do so only on a limited basis for the above-mentioned reasons. Only Indiana is clearly satisfied with its undersealing operation. However, the Indiana Department of Transportation is seeking more information on the means of locating voids beneath the pavement slab.

Criteria Used in Implementation of Undersealing Work

Of the 16 states that use undersealing in their pavement restoration work, 9 use visual surveys, as indicated by pumping or faulting in combination with nondestructive testing, to locate voids beneath a slab. The other seven states rely on nondestructive testing for void detection. Table 1 presents the means used by the various states to determine the locations of slabs that need undersealing work. The falling-weight deflectometer (FWD) and the Benkelman beam are the most commonly used equipment.

Table 2 presents the criteria used for determining the slabs that need undersealing. These values are also used for determining the effectiveness of an undersealing operation. Generally, corner deflections greater than 0.025 cm (0.01 in.) to greater than 0.09 cm (0.035 in.) are adopted. Some states such as Pennsylvania and Missouri use a load transfer efficiency (LTE) value of less than 65 percent as a criterion for determining those slabs that need undersealing. Load transfer at joints and cracks can be determined by using one of the following equations:

$$\text{LTE} = (d_{UL}/d_L) \times 100 \quad (1)$$

or

$$\text{LTE} = [(2d_{UL})/(d_L + d_{UL})] \times 100$$

where

LTE = load transfer efficiency (percent),
d_{UL} = deflection of the unloaded slab, and
d_L = deflection of the loaded slab.

Types of Grouts Used in Undersealing

Figure 2 shows the types of grouts used in the various states. As shown in Figure 2, pozzolan (fly ash)-cement grout is the most popular material used in the states. Indiana is the only state that uses asphalt cement, with very satisfactory results. For pozzolan-cement grouts, a 7-day compressive strength of 4138 kPa (600 lb/in.^{2}) to 5517 kPa (800 lb/in.^{2}) and an average flowability of 10 to 16 sec are generally recommended and used.

Construction Methods Used in Undersealing

All 16 states except Puerto Rico limit their undersealing operations to those conditions when the temperature is above 0°C

TABLE 1 Techniques Used To Determine Locations of Slabs That Need Undersealing

State	Visual	Benkelman	FWD[a]	GPR[b]	Dynaflect	Road Rater
California	x					
Florida	x	x				
Georgia	x	x				
Kansas	x		x			
Illinois	x		x			
Indiana					x	
Iowa	x			x		x
Missouri	x		x			
Oklahoma[c]						
Oregon			x			
Pennsylvania		x	x			
Puerto Rico		x				
South Dakota	x	x	x			
Texas[d]	x		x	x		
Tennessee[e]						
Washington		x	x			

a: Falling Weight Deflectometer.
b: Ground Penetrating Radar.
c: Not specified.
d: The Spectral Analysis of Surface Waves (SASW) technique is also used.
e: A pre-rolling method is used.

(32°F). In cold weather states undersealing also is not allowed if the subgrade is frozen.

The maximum allowable pumping pressure (excluding the initial pumping pressure) used by highway agencies varies from 138 kPa (20 lb/in.^{2}) to 1035 kPa (150 lb/in.^{2}). Pumping pressures ranging from 345 kPa (50 lb/in.^{2}) to 414 kPa (60 lb/in.^{2}) seemed to be the most preferred values. Table 3 presents the maximum allowable pumping pressures specified by state highway agencies.

Maximum vertical slab movement allowed during pumping varies from 0.04 cm (0.0175 in.) to 0.64 cm (0.25 in.). Table 4 shows the maximum allowable vertical slab movements specified by the states.

The survey also revealed that pumping should be stopped when one of the following conditions prevails:

1. The maximum allowable pumping pressure has been attained.
2. The maximum allowable vertical slab movement has been measured.
3. The time limit for pumping grout into the holes has been attained (recommended by some states).
4. The grout starts to flow from adjacent holes or comes out of the joints (recommended by some states).

Finally, all states adopt some type of pavement restoration work in conjunction with undersealing. This may include joint or crack sealing, patching, the use of edge drains, grinding, dowel retrofitting, the use of overlays, spall repair, and full-depth repair.

Long-Term Effectiveness of Undersealing Operations

All 16 state highway agencies use the corner deflection measurements and joint transfer efficiency values presented in Table 2 to establish the acceptance of undersealing work. If a joint fails the contractor may be required to rework the slab. No guidelines were provided to establish the long-term effectiveness of undersealing. All states rely on long-term monitoring of the concrete panels to observe that pumping and faulting are not resumed.

CONCLUSIONS

The survey revealed the following:

1. Undersealing is performed on a limited basis by 16 state highway agencies.
2. Visual surveys and FWD testing are the most common means used for void detection.
3. Corner deflections greater than 0.025 cm (0.01 in.) to greater than 0.09 cm (0.035 in.) or a load transfer efficiency of less than 65 percent are adopted as criteria in the determination of those slabs that need undersealing.
4. Fly ash–cement grout is the preferred material used in undersealing.
5. Pumping pressures are generally limited to a maximum of 414 kPa (60 lb/in.^{2}).

TABLE 2 Corner Deflection and Joint Efficiency Values (cm) Used To Determine Location of Slabs That Need Undersealing

State	> 0.025	> 0.038	> 0.051	> 0.064	> 0.076	> 0.089	JE[a] < 65
California[b]							
Florida		x					
Georgia					x		
Kansas[c]							
Illinois[b]							
Indiana[d]							
Iowa[b]							
Missouri[e]							x
Oklahoma[b]							
Oregon[f]				x			
Pennsylvania			x				x
Puerto Rico					x		
South Dakota	x						
Texas			x				
Tennessee					x		
Washington						x	

1 in. = 2.54 cm

a: JE = Joint Efficiency.
b: Not specified.
c: If corner deflections are greater than a base value established from the interior slab deflection.
d: Judgement + Modified Majidzadeh Criteria.
e: Corner deflection greater than 0.045 cm is also used.
f: Darter/Crovetti slope intercept method is also used (based on a deflection of 10 mils).

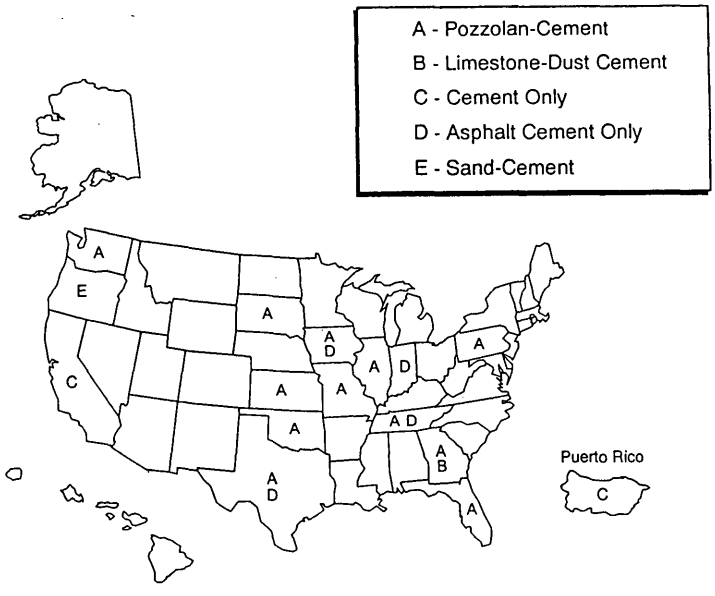

FIGURE 2 Typical undersealing materials used by different states.

TABLE 3 Maximum Allowable Pumping Pressures (kPa) Specified by Various Highway Agencies

State	138	276	345	414	690
California	x				
Florida[a]					
Georgia					x
Kansas				x	
Illinois		x			
Indiana[b]					
Iowa	x				
Missouri			x		
Oklahoma				x	
Oregon[b]					
Pennsylvania[b]					
Puerto Rico[b]					
South Dakota				x	
Texas			x		
Tennessee			x		
Washington[b]					

1 psi = 6.9 kPa

a: As low as possible.
b: Not specified.

TABLE 4 Maximum Allowable Vertical Slab Movements (cm) Specified by Various Highway Agencies During Pumping

State	0.089	0.127	0.254	0.318	0.508	0.635
California[a]						
Florida				x		
Georgia		x				
Kansas				x		
Illinois		x				
Indiana						x
Iowa			x			
Missouri					x	
Oklahoma	x					
Oregon[b]						
Pennsylvania		x				
Puerto Rico		x				
South Dakota				x		
Texas				x		
Tennessee			x			
Washington[c]						

1 in. = 2.54 cm

a: Zero to profile grade of surface.
b: A deflection of 0.064 cm is specified.
c: A deflection of 0.051 cm is specified.

6. The maximum vertical slab movement allowed during pumping varies from 0.04 cm (0.0175 in.) to 0.64 cm (0.25 in.).

7. All states adopt some type of pavement restoration work in conjunction with undersealing.

8. The long-term effectiveness of undersealing is generally established by observing that pumping and faulting distresses are not resumed in the concrete panels.

ACKNOWLEDGMENTS

The survey results presented in this paper were part of a research study sponsored by the South Dakota Department of Transportation. The authors express their appreciation for the information provided by the various state highway agencies.

REFERENCES

1. Allen, H. Final Report of Committee on Maintenance of Concrete Pavements as Related to the Pumping Action of Slabs. *HRB Proc.*, Vol. 28, 1948.
2. Darter, M. I., E. J. Barenberg, and W. A. Yrjanson. *NCHRP Report 281: Joint Repair Method for Portland Cement Concrete Pavements.* TRB, National Research Council, Washington, D.C., 1985.
3. Ransom, R. C., and J. T. Kunz. Nondestructive Detection of Voids Beneath Pavements. *Public Works*, Vol. 117, 1986.
4. Steinway, W. J., J. D. Echard, and C. M. Luke. *NCHRP Report 237: Locating Voids Beneath Pavement Using Pulse Electromagnetic Waves.* TRB, National Research Council, Washington, D.C., 1981.
5. Sudol, J. J., and J. W. Muncaster. Undersealing Concrete Pavements: The Indiana Method. *Public Works*, Vol. 117, 1986.
6. Sliffer, J. C., M. McPeter, and W. E. Burns. Experimental Project on Grout Subsealing in Illinois: A 20-Month Evaluation. In *Transportation Research Record 1041*, TRB, National Research Council, Washington, D.C., 1985.
7. *Pavement Rehabilitation Manual.* Report FHWA-ED-88-025. FHWA, U.S. Department of Transportation, 1985.
8. Neal, B. F. *California PCC Pavement Faulting Studies: A Survey.* Report FHWA-CA-TL-85-06. California Department of Transportation, 1985.

Publication of this paper sponsored by Committee on Pavement Rehabilitation.

New Predictive Modeling Techniques for Pavements

YING-HAUR LEE AND MICHAEL I. DARTER

Statistical regression algorithms have been utilized extensively in pavement engineering for more than three decades. Multiple linear regression, stepwise regression, and nonlinear regression techniques are the most popular ones for pavement predictive modeling. The advantages, the deficiencies, and the limitations of these regression techniques are reviewed. To minimize these problems, the projection pursuit regression (PPR) introduced by Friedman and Stuetzle (1981) was selected to assist in the proper selection of functional forms. Through the use of local smoothing techniques, the PPR attempts to model the response surface as a sum of nonparametric functions of projections of the explanatory variables. The projected terms are essentially two-dimensional curves that can be graphically represented, easily visualized, and properly formulated. As a result a two-step predictive modeling approach is proposed and demonstrated in a case study for the prediction of the edge stress of a pavement slab. It is also demonstrated that statistical regression techniques should not be used alone to obtain a more reliable and comprehensive predictive model. The importance of subject-related engineering knowledge, the principles of dimensional analysis, the proper selecton of functional forms, and applicable engineering boundary conditions are considered essential and are also demonstrated. A comparison of the predictive models previously developed and the proposed approach to "prediction" and "extrapolation" clearly shows the preference of the proposed approach and the promising features of the PPR algorithm.

Statistical regression techniques have been utilized extensively in predicting complicated pavement performance indicators for more than three decades. Multiple linear regression, stepwise regression, and nonlinear regression techniques are the most popular ones among transportation engineers. Undoubtedly, regression analysis is a very important statistical tool for many sciences. This paper starts with a review of the advantages and the limitations of these currently used regression techniques. Some specific problems in the selection of proper functional forms and the violation of some embedded statistical assumptions by use of these techniques are discussed.

Traditional parametric regression techniques such as linear and nonlinear regressions require the imposition of a parametric form on the functions and then obtaining the parameter estimates afterward. In situations in which little knowledge about the shape and the form of a function exists, several new nonparametric regression techniques developed over the past 10 years have gradually gained popularity. Without imposing an unjustified parametric assumption, nonparametric regression techniques strive to estimate the actual functional form that best fits the data through the use of scatter plot smoothers (*1*).

The alternating conditional expectation (ACE) algorithm developed by Breiman and Friedman (*2*) for optimal transformation of multiple regression and correlation does an excellent job in maximizing the squared multiple correlation, R^2 (*1–3*). By using the same alternative backfitting procedures for variable transformations as used in the ACE algorithm, Tibshirani (*4*) introduced the additivity and variance stabilization (AVAS) algorithm, which tries to achieve the constant error variance assumption of regression (*1,4*). Both techniques provide an invaluable tool in suggesting proper transformations of variables. However, neither the ACE nor the AVAS algorithm is capable of modeling interactions between the explanatory variables. The variable interactions must be explicitly specified in the assumed model form.

Consequently, the projection pursuit regression (PPR) introduced by Friedman and Stuetzle (*5*) and Friedman (*6*) is selected because of its ability to handle variable interactions. As a result a two-step predictive modeling approach is proposed and demonstrated in a case study for the prediction of concrete pavement edge stress owing to the finite slab length effect.

The demonstration is based on a comparison between the previous modeling approaches from the zero-maintenance study (*7*), a stress analysis procedure (*8*), and the proposed methodology. The importance of incorporating subject-related engineering knowledge such as the use of the principles of dimensional analysis and the proper selection of functional forms is demonstrated. The proposed modeling procedure illustrates how to select a proper functional form through the use of the PPR as well as the aid of graphical representation and visual inspection. Nonlinear regression is used to obtain the parameter estimates for the specified functional forms. The proper selection of initial parameter estimates is also discussed to guarantee convergence of the iterative nonlinear regression routines. The applications of the resulting predictive models to "prediction" and "extrapolation" are also discussed.

MULTIPLE REGRESSION

Multiple regression is one of the most time-honored and widely used regression techniques for the study of linear relationships among a group of measurable variables. Suppose there exists a true model to describe the relationship between response variables (y's) and explanatory variables (or predictors, x's) (*9–11*):

$$y_i = x_i^T\beta + \epsilon_i \qquad (i = 1, \ldots, n) \tag{1}$$

where x_i^T is the ith row of the $(n \times p)$ matrix X of the column of 1's if an intercept and the explanatory variables are included. The superscript T denotes the transpose of the column vector x_i. β is a $p \times 1$ vector of unknown regression coefficients, and p and n are the number of parameter estimates in the model and the total number of observations, respectively.

Y.-H. Lee, Department of Civil Engineering, Tamkang University, E725, #151, Ying-Chuan Road, Tamsui, Taipei, Taiwan 25137, Republic of China. M. I. Darter, Department of Civil Engineering, University of Illinois, NCEL #1212, 205 North Mathews Avenue, Urbana, Ill. 61801.

The basic assumptions are usually that the random errors (ϵ's) are mutually uncorrelated and normally distributed with zero mean and constant variance and are additive and independent of the expectation function. For any arbitrary β value of $\hat{\beta}$, the residuals $r_i(\hat{\beta})$ can be determined by the following expression:

$$r_i(\hat{\beta}) = y_i - x_i^T\hat{\beta} \qquad (i = 1, \ldots, n) \tag{2}$$

On the basis of the above assumptions multiple regression tries to find a set of parameters $\hat{\beta}$ such that the sum of the squared residuals given in Equation 3 is minimized, which is also best known as the least-squares (LS) method.

$$RSS(\hat{\beta}) = \sum_{i=1}^{n} [r_i^2(\hat{\beta})] = r_1^2(\hat{\beta}) + r_2^2(\hat{\beta}) + \cdots + r_n^2(\hat{\beta}) \tag{3}$$

The LS method is best known and most frequently adopted because of its simple structure, elegant LS theory, fast computation time, as well as its estimators, which can be obtained explicitly from the data and are interpretable to its user.

As far as variable selection is concerned, all-subset regression and stepwise regression techniques are often utilized for automatic variable selection for preliminary and exploratory analyses of linear relationships among a group of important variables.

ALL-SUBSET REGRESSION AND STEPWISE REGRESSION

All-subset regression procedure finds all possible combinations of variables in the model when the set of candidate variables is not too large. To select the "best" subset of variables, different measurements including the coefficient of determination (R^2), adjusted R^2 (adj-R^2), and the C_p statistics due to Mallows have been proposed (*11,12*). The Mallows C_p statistic can be defined as follows:

$$C_p = \frac{RSS}{s^2} + 2p - n \tag{4}$$

where RSS represents the residual sum of squares of the regression, p is the number of parameters, and s^2 is the estimate of the residual variance from the full regression model. According to Draper and Smith (*12*), a regression model with "a low C_p value about equal to p" is preferred such that the model fits the actual data better with the least number of parameters (*11,12*).

Stepwise regression uses a forward selection or a backward elimination procedure that iteratively adds or deletes one explanatory variable at a time to find the "best" subset of significant independent variables in the model (*13*). However, this procedure does not necessarily produce the "best" subset among a group of candidate variables. The first variable added or deleted may not necessarily be the best or the worst overall. It is quite possible that the first variable selected by forward selection becomes unnecessary in the presence of the other variables entered afterward or vice versa. In other words, forward selection and backward elimination techniques may result in totally different subsets of variables with similar summary statistics. "It is unlikely that there is a single best subset, but rather several equally good ones," as observed by Gorman and Toman (*14*).

In comparison with the high computational cost of all-subset regression, stepwise regression is one of the most popular techniques used in transportation research because of its fast computation, simplicity of use, and capability in progressively adding or dropping variables in a regression model. It is expected that some latent or lurking variables may be included in a regression model.

Because of the ease of use and the efficiency of computation, stepwise regression may be easily abused in some respects if one fails to recognize possible physical interpretations on the parameter estimates and the embedded basic assumptions. A very long regression model with dozens of parameter estimates may be the typical result of a stepwise regression that fits the data very well but with no comprehensive engineering insight into the data analyzed. Often, some applicable engineering boundary conditions are violated as well.

NONLINEAR REGRESSION

Practical real-world problems are often found to be nonlinear in nature. Because of its favorable feature of handling a complicated nonlinear model, nonlinear regression has been widely used as a modeling technique for pavement research. In addition, some applicable boundary conditions may be incorporated into the specified nonlinear model form and the parameter estimates may have their own physical meanings as well. However, nonlinear models are more difficult to specify and develop than linear models.

Suppose there exists a true model that best describes the relationship between response variables (y's) and explanatory variables (x's) (*10,15*):

$$y_i = F(\beta, x_i) + \epsilon_i \qquad (i = 1, \ldots, n) \tag{5}$$

where $F(\beta, x_i)$ is a nonlinear function based on the predictors x_i. β is a $p \times 1$ vector of unknown regression coefficients to be estimated, and n is the total number of observations. Similar to linear regressions, the disturbance (or error) term is usually assumed to be additive, mutually uncorrelated, and normally distributed with zero mean and constant variance. For any arbitrary β value of $\hat{\beta}$, the residuals $r_i(\hat{\beta})$ are

$$r_i(\hat{\beta}) = y_i - F(\hat{\beta}, x_i) \quad (i = 1, \ldots, n) \tag{6}$$

Unlike linear regressions whose parameters can be explicitly estimated by a closed-form expression, nonlinear regressions must use an iterative routine to find the best parameter estimates ($\hat{\beta}$) such that the sum of the squared residuals as given in Equation 3 is minimized.

Before carrying out a nonlinear regression, engineers must first assume a feasible descriptive (or conceptual) model form with the most important parameters prespecified on the basis of previous experience and engineering knowledge. In a two-dimensional factor space the model form can be determined as easily as it can be visualized in a scatter plot. Subsequently, reliable parameter estimates may be obtained.

The situation is quite different for the case of multidimensional (three or higher) factor space, where the data trend and the possible interactions among candidate variables cannot be easily identified. Unfortunately, real engineering problems most likely belong to the latter case, in which higher dimensions are concerned and

the true functional forms are rarely known to engineers. Thus, the proper selection of a plausible functional form from a multidimensional factor space provides a real challenge for pavement engineers.

Guessing initial parameter estimates for a multidimensional model is also a very time-consuming process. It is not uncommon that the resulting model does not converge or contains insignificant parameter estimates, with poor initial parameter estimates and an improper model form. In addition, parameter estimates are sometimes toward the wrong direction of their physical interpretations, and they may depend heavily on the initial starting values as well. Specifying bounds for some parameters is not uncommon, although the final resulting model may eventually reach the assumed bounds but without achieving the specified convergence criterion. Thus, "some models are difficult to fit, and there is no guarantee that the procedure will be able to fit the model successfully" (*10*,p.576).

Furthermore, even when parameter estimates are successfully obtained, the assumption of constant error variance is frequently violated, as indicated by residual analyses. This problem, which is probably due to improper selection of the model form, is often unrecognized, and there is no quick remedy for this situation.

Thus, it is very dangerous to develop such a nonlinear model without acquiring more knowledge of the complicated relationships between the predictors and the dependent variable. The prediction based on an inadequate model specification is also very questionable.

PROJECTION PURSUIT REGRESSION

Unlike the ACE and the AVAS algorithms previously discussed, the projection pursuit regression introduced by Friedman and Stuetzle (*5*) and Friedman (*6*) is capable of modeling interactions between predictor variables when suggesting nonparametric transformations to improve the fit. This algorithm is an exploratory nonlinear regression technique that tries to model the response surface (y's) as a sum of nonparametric functions of projections of the predictor variables (x's) through the use of super smoothers (*5,6*). Assume there exists a true model given as follows (*16*, Vol. 2):

$$y = \bar{y} + \sum_{m=1}^{M_0} \beta_m \Phi_m(a_m^T x) + \epsilon \tag{7}$$

where x is equal to $(x_1, x_2, \ldots, x_p)^T$ and denotes the vector of predictor variables and $\bar{y}$ is the expected value (or mean) of the response variable. The "projection" part of the "projection pursuit regression" indicates that the vector of predictors, x, is projected onto the direction vectors, a_m, to get the lengths of the projection $a_m^T x$, where $m = 1, \ldots, M_0$. The "pursuit" part indicates that an optimization technique is used to find the best direction vectors, a_m. $\Phi_m(a_m^T x)$ stands for the unknown nonparametric transformation functions of the projected lengths $a_m^T x$ to be estimated. ϵ is the random error. Notice that Φ_m has been standardized to have zero mean and the unity variance given in the following expression:

$$E[\Phi_m(a_m^T x)] = 0 \qquad E[\Phi_m^2(a_m^T x)] = 1$$

$$(m = 1, \ldots, M_0) \tag{8}$$

The PPR algorithm strives to minimize the mean squared residuals, $E[r^2]$, over all possible combinations of β_m, Φ_m, and a_m values. This algorithm first performs a forward stepwise fitting procedure starting with a single term and ending up with M_{max} terms. Supersmoother is used to estimate the conditional expectation functions. After having fitted the M_{max} term model in a forward stepwise manner, a backward stepwise procedure is followed and stopped with an M_{min} term model. Notice that M_{max} and M_{min} are the user-specified maximum and minimum number of terms in the model, respectively. The relative importance of each term can be measured by the absolute value of β_m as well. The expectation function of the squared residuals is given as follows:

$$E[r^2] = E\left[y - \bar{y} - \sum_{m=1}^{M_0} \beta_m \Phi_m(a_m^T x) \right]^2 \tag{9}$$

Conceptually, the explanatory variables x's are projected onto the direction vectors $a_1, a_2, \ldots, a_m$, to find good nonlinear transformations $\Phi_1, \Phi_2, \ldots, \Phi_m$ for the multidimensional response surface. In other words, the response surface is broken down into a series of smooth projected terms adding all together. Thus, the largest trend in the factor space is captured as the first projected term Φ_1, and the residuals become the sources for additional projections afterward. More technical details about the development process, the application, and the demonstration on modeling interactions of the PPR algorithm can be found elsewhere (*5,6,16*).

PROPOSED TWO-STEP MODELING APPROACH

The proper selection of regression techniques is one of the most important factors in the success of prediction modeling. Since most of the regression algorithms currently available do not directly consider interaction effects during the modeling process, the interaction terms must be subjectively determined prior to performing a regression analysis. With the multidimensional pavement engineering problems in mind, several unresolved deficiencies are frequently identified in the use of stepwise regression and nonlinear regression. These include problems in the selection of correct functional form, violations of the embedded statistical assumptions, and failure to satisfy some engineering boundary conditions as previously discussed.

The projection pursuit regression, however, appears to have the most favorable features in handling these problems. As a result a two-step regression analysis procedure is proposed herein to better find the correct functional form and to better fit the response surface as well.

1. With the help of the PPR a multidimensional response surface is broken down into the sum of several smooth projected curves that are graphically representable in two dimensions. Plausible functional forms and applicable boundary conditions may then be easily identified and specified through visual inspection or engineering knowledge of the physical relationships to model these individual projected curves separately.
2. Traditional parametric regression techniques such as linear and nonlinear regressions are then utilized for these purposes with higher confidence in the parameter estimates.

The overall regression statistics and the goodness of fit often clearly show the advantages of the proposed two-step modeling

approach over the traditional counterparts. The S-PLUS statistical package (*16–19*), which has been widely used by statisticians, was selected for the analysis due because of the availability of this new regression technique.

EDGE STRESS DUE TO LOADING AND FINITE SLAB LENGTH EFFECTS: CASE STUDY

Since transverse cracking is one of the major structural distresses in jointed concrete pavements, the determination of the maximum bending stress at the longitudinal edge (midway between the transverse joints) is very crucial in any mechanistic or mechanistic-empirical design procedures.

However, the theoretical Westergaard edge stress solution (*20*) based on an infinite slab assumption may not be well suited for the actual finite slab size conditions. To assess the effect of a finite slab length, a series of finite-element (FE) runs are often performed. Unfortunately, the FE model cannot be easily implemented as a part of a design procedure because of the required running time.

Several attempts in edge stress prediction that proved to be very successful in the past are reviewed and discussed below. The basic concepts behind those analysis procedures were to design and perform a full factorial of FE runs under various combinations of different conditions. Statistical regression techniques were utilized to develop predictive models for different situations. The predictive equations were then used as alternatives for design purposes with sufficient accuracy in estimating stresses.

To demonstrate the proposed two-step predictive modeling procedures, the following case study was performed. The purpose of this case study was to demonstrate the advantages of incorporating dimensional analysis and selecting proper functional forms for the predictive models analyzed. Three different approaches are discussed in the following sections:

1. Use arbitrary but "best" linear combinations of individual variables with interaction terms for regression;
2. Introduce as many mechanistic variables as possible on the basis of engineering knowledge, and also find the "best" linear combinations of these variables with interaction terms for regression; and
3. Introduce as many mechanistic variables (or clusters of variables) as before, and also try to find the best functional forms on the basis of the proposed two-step predictive modeling procedures.

Principles of Dimensional Analysis

According to Westergaard (*20,21*), the closed-form stress solution due to a circular edge loading on a semi-infinite slab over a dense liquid foundation on the basis of medium-thick plate theory is given as follows:

$$\sigma = \frac{3(1+\mu)P}{\pi(3+\mu)h^2}\left[\log_e \frac{Eh^3}{100ka^4} + 1.84 - \frac{4\mu}{3} + \frac{1-\mu}{2} + 1.18(1+2\mu)\frac{a}{l}\right] \quad (10)$$

where

σ = theoretical Westergaard edge stress (FL^{-2}),
P = total applied wheel load (F),
a = radius of the applied circular load (L),
E = elastic modulus of the concrete slab (FL^{-2}),
h = slab thickness (L),
μ = slab Poisson's ratio,
k = modulus of subgrade reaction (FL^{-3}), and
l = radius of relative stiffness of the slab subgrade system (L) given by

$$l = \sqrt[4]{\frac{Eh^3}{12(1-\mu^2)k}} \quad (11)$$

[Note that the basic dimensions are abbreviated as length (L) and force (F).]

Through the use of the principles of dimensional analysis, the above stress equation may be reduced to the following equation form in which both sides of the equation are dimensionless (*22,23*).

$$\frac{\sigma h^2}{P} = f\left(\frac{a}{l}\right) \quad (12)$$

Therefore, the above normalized stress equation ($\sigma h^2/P$) is simply a function of the dominating variable, a/l, representing the combination effect of the input parameters, namely E, h, k, and a, for constant μ (usually $\mu \approx 0.15$).

To account for the finite slab length effect, Ioannides et al. (*21*) introduced a normalized length term, L/l, when comparing FE results with the theoretical Westergaard solution. Similarly, a normalized width term, W/l, was introduced to account for the effect of finite slab width. Note that L and W represent slab length and slab width, respectively. However, it is also recognized that the finite slab width effect (W/l) is not as significant as the other two dimensionless parameters (i.e., a/l and L/l), as suggested by earlier investigators (*8,23*).

An adjustment (or multiplication) factor may be introduced to account for the theoretical difference between the Westergaard solution (σ) and the results from the FE model by using only these two dimensionless factors (a/l and L/l). The adjustment factor (R) is defined by the following expression:

$$R = \frac{\sigma_i}{\sigma} = f\left(\frac{a}{l}, \frac{L}{l}\right) \quad (13)$$

where σ_i is the edge stress determined by the FE model.

The advantages of using the principles of dimensional analysis to derive the above formulation are evident. They can be very helpful in identifying the governing dependent and independent variables (or clustered variables) of a given relationship. In addition, they may also help to reduce the number of factorial FE runs needed for the analysis. The above formulation is not only easy to comprehend but is also dimensionally correct. Thus, the resulting edge stress from FE studies (σ_i) can be determined by multiplying the theoretical Westergaard solution and the adjustment factor (R) together, if it is properly formulated.

Use of Arbitrary Linear Combination of Variables

The analysis of edge stress due to different axle loads, slab lengths, slab thicknesses, foundation supports, thermal gradients, and edge supports was initially studied by Darter (*7*). A large full factorial of FE runs was performed to determine the edge stresses for different conditions, and subsequently separate predictive models were developed. For the case of loading only, an 18-kip single axle loading was applied on the following factorial pavement sections:

1. Slab length L = 15, 20, 25, and 30 ft;
2. Slab thickness h = 8, 10, and 14 in.;
3. Foundation support k = 50, 200, and 500 pci; and
4. Edge support ES = 0, 12, 36, and 60 in.

where other pertinent input parameters are

$E = 5 \times 10^6$ psi lb/in^2,
W = 12 ft,
μ = 0.15, and
loaded area per wheel = 12 × 15 in.^{2}.

The results of these FE runs were directly used to derive a regression model for edge stress (σ_L) prediction.

Stepwise regression procedure was utilized to pick the "best" linear combinations of individual variables including interaction terms during the modeling process. The slab length (L) was not proved to affect the edge stress prediction significantly and thus was excluded from the model. The proposed predictive model for single axle load without the loss of edge support (ES = 0) is given as follows:

$$\sigma_L = \frac{\text{load}}{18 \cdot h^2} \cdot \left(17.35783 - 0.05388 \cdot \frac{h^3}{k} + 7.41722 \cdot \log_{10}\frac{h^3}{k}\right) \quad (14)$$

Using Equation 14 to predict the actual calculated edge stresses from the above FE runs, a fairly good agreement is observed.

However, this model does not contain the elastic modulus of the concrete slab (E) and the finite slab length (L) because of the limitations of the factorial runs conducted. The variables included in this model are numerically significant, but they are not the actual dominating factors with correct dimensions. Thus, the applicability of using this equation beyond the ranges of the data for which the model was originally developed such as different E values and other shorter slabs is very questionable.

Introducing Mechanistic Variables (Clustered Variables)

The analysis of edge stress was further studied by Salsilli-Murua (*8*). The concept of equivalent single axle radius (ESAR) was utilized for analyzing different load configurations including dual wheels, tandem gears, and tridem gears. The effects of slab sizes, widened outer lanes or tied shoulders, subbase and subgrade layers, and thermal curling were also analyzed separately. Through the use of the principles of dimensional analysis, a series of small factorial FE runs covering most practical engineering conditions were performed and separate predictive models were developed.

As previously discussed, the effects of wheel loading and finite slab length can be best represented by two dimensionless factors: a/l and L/l. Thus, only a minimum number of factorial FE runs on the basis of these two factors were performed. The adjustment (or multiplication) factor (R) as defined in Equation 13 was also introduced for edge stress prediction. Note that the Westergaard solution (σ) for infinite slab condition is approximated by the resulting ILLI-SLAB edge stress (σ_∞) for L/l = 7.0 herein when calculating the adjustment factor ($R = \sigma_i/\sigma_\infty$).

A multiple stepwise regression procedure was utilized again because of its favorable feature of progressively adding and dropping variables in a regression model. The proposed predictive model is given as follows:

$$R = 0.582282 - 0.533078\left(\frac{a}{l}\right) + 0.181706\left(\frac{L}{l}\right) - 0.019824\left(\frac{L}{l}\right)^2 + 0.109051\left(\frac{a}{l}\right)\left(\frac{L}{l}\right) \quad (15)$$

Statistics: N = 12, R^2 = 0.996, SEE = 0.0028, CV = 0.29 percent
Limits: $3 \le L/l \le 5$, $0.05 \le a/l \le 0.3$

N is number of datum points, R^2 is the coefficient of determination, SEE is the standard error of estimates, and CV is the coefficient of variation).

His work has repeatedly demonstrated the advantages of using dimensional analysis to discover the underlying dominating factors for the analysis. In addition, the proposed predictive model not only has fairly good agreement with the data analyzed, but it may also be applied to a wide range of input parameters (i.e., E, h, k, and a). This model is also dimensionally correct. The prediction of edge stress is simply a matter of multiplying the theoretical Westergaard solution by the predicted R value on the basis of this model.

Nevertheless, the conclusions should be restricted to the ranges of the data for which the model was originally developed. This is also true for any regression technique chosen to develop such a predictive model. Besides, a reasonable doubt is raised as to the adequacy of the functional form, especially when an asymptotic trend of the relationship between R and L/l is observed. This asymptotic trend could not be captured simply because of the multiple stepwise regression technique chosen. Thus, the usefulness of the model beyond the specified limits is highly questionable.

Selecting Proper Functional Forms

The importance of incorporating subject-related engineering knowledge into the modeling process, as has been done in the previous example in identifying dominating clustered variables, cannot be overemphasized. In addition, the selection of proper functional forms to satisfy some applicable engineering boundary conditions is a crucial component of a successful predictive model. The proposed two-step modeling approach was adopted herein to illustrate this point. The following factorial ILLI-SLAB runs were performed:

a/l: 0.05, 0.1, 0.2, and 0.3 and
L/l: 2.0, 2.5, 3.0, 3.5, 4.0, 4.5, 5.0, 6.0, and 7.0.

Note that W/l was set to 7.0 for all runs. The FE grids were generated according to the recommendations of Ioannides (*24*, pp. 187–188) to provide sufficient accuracy. The pertinent input parameters and the results of these factorial runs are presented in Table 1. A three-dimensional perspective plot providing a very clear picture of the relationship among R, a/l, and L/l is shown in Figure 1.

Because the relationship is a nonlinear three-dimensional surface, a nonlinear regression model may be better suited for this prediction purpose than an arbitrarily selected linear or polynomial model form. But, what kinds of functional forms to be used in the model and how to choose a proper one remain unanswered.

The proposed two-step modeling approach is aimed at search-

TABLE 1 ILLI-SLAB Runs on Slab Size Effects

a/l	L/*l*	c	*a*	P	*l*	L	W	E	k	h	σ
0.05	2.0	2.5	1.995	1250	39.89	79.79	279.26	5	200	10.59	40.868
0.05	2.5	2.5	1.995	1250	39.89	99.74	279.26	5	200	10.59	43.559
0.05	3.0	2.5	1.995	1250	39.89	119.68	279.26	5	200	10.59	45.458
0.05	3.5	2.5	1.995	1250	39.89	139.63	279.26	5	200	10.59	46.744
0.05	4.0	2.5	1.995	1250	39.89	159.58	279.26	5	200	10.59	47.536
0.05	4.5	2.5	1.995	1250	39.89	179.52	279.26	5	200	10.59	47.973
0.05	5.0	2.5	1.995	1250	39.89	199.47	279.26	5	200	10.59	48.180
0.05	6.0	2.5	1.995	1250	39.89	239.37	279.26	5	200	10.59	48.287
0.05	7.0	2.5	1.995	1250	39.89	279.26	279.26	5	200	10.59	48.293
0.10	2.0	5.0	2.821	2500	28.21	56.42	197.47	4	300	8.23	100.494
0.10	2.5	5.0	2.821	2500	28.21	70.52	197.47	4	300	8.23	109.154
0.10	3.0	5.0	2.821	2500	28.21	84.63	197.47	4	300	8.23	115.240
0.10	3.5	5.0	2.821	2500	28.21	98.73	197.47	4	300	8.23	119.399
0.10	4.0	5.0	2.821	2500	28.21	112.84	197.47	4	300	8.23	121.952
0.10	4.5	5.0	2.821	2500	28.21	126.94	197.47	4	300	8.23	123.347
0.10	5.0	5.0	2.821	2500	28.21	141.05	197.47	4	300	8.23	123.999
0.10	6.0	5.0	2.821	2500	28.21	169.26	197.47	4	300	8.23	124.304
0.10	7.0	5.0	2.821	2500	28.21	197.47	197.47	4	300	8.23	124.311
0.20	2.0	10.0	5.642	10000	28.21	56.42	197.47	3	400	9.97	178.536
0.20	2.5	10.0	5.642	10000	28.21	70.52	197.47	3	400	9.97	201.014
0.20	3.0	10.0	5.642	10000	28.21	84.63	197.47	3	400	9.97	216.928
0.20	3.5	10.0	5.642	10000	28.21	98.73	197.47	3	400	9.97	227.837
0.20	4.0	10.0	5.642	10000	28.21	112.84	197.47	3	400	9.97	234.529
0.20	4.5	10.0	5.642	10000	28.21	126.94	197.47	3	400	9.97	238.158
0.20	5.0	10.0	5.642	10000	28.21	141.05	197.47	3	400	9.97	239.822
0.20	6.0	10.0	5.642	10000	28.21	169.26	197.47	3	400	9.97	240.510
0.20	7.0	10.0	5.642	10000	28.21	197.47	197.47	3	400	9.97	240.443
0.30	2.0	10.0	5.642	10000	18.81	37.61	131.64	2	500	7.16	251.011
0.30	2.5	10.0	5.642	10000	18.81	47.02	131.64	2	500	7.16	292.598
0.30	3.0	10.0	5.642	10000	18.81	56.42	131.64	2	500	7.16	322.461
0.30	3.5	10.0	5.642	10000	18.81	65.82	131.64	2	500	7.16	342.758
0.30	4.0	10.0	5.642	10000	18.81	75.23	131.64	2	500	7.16	355.316
0.30	4.5	10.0	5.642	10000	18.81	84.63	131.64	2	500	7.16	362.178
0.30	5.0	10.0	5.642	10000	18.81	94.03	131.64	2	500	7.16	365.327
0.30	6.0	10.0	5.642	10000	18.81	112.84	131.64	2	500	7.16	366.408
0.30	7.0	10.0	5.642	10000	18.81	131.64	131.64	2	500	7.16	365.845

a = radius of loaded area, in.
c = load dimensions are c x c, except those cases with c = 2.5 use 2c x c instead, in.
l = radius of relative stiffness, in.
h = slab thickness, in.
E = elastic modulus of concrete, $*10^6$ psi
k = modulus of subgrade reaction, pci
L = slab length, in.
W = slab width, in.
P = total applied load, lb
σ = edge bending stress, psi

The tire pressure was held constant at 100 psi for all the runs.
Note: 1 inch = 2.54 cm, 1 psi = 6.89 kPa, 1 pci = 0.27 MN/m^3, 1 lb = 0.454 kg.

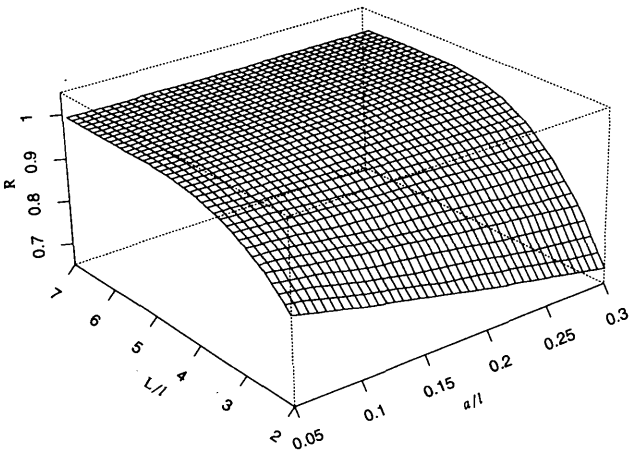

FIGURE 1 Slab size effect: three-dimensional plot.

ing for a series of two-dimensional projected curves first to ease these important modeling decisions. First, the PPR technique was utilized to determine the direction vectors for a/l and L/l and the suggested single-term nonlinear transformation $\Phi_1(a_1^T x)$ by using only those datum points within the specified limits of Equation 15. The results of this PPR trial are given in the following equations:

$$R = 0.9667 + 0.0330\Phi_1(\text{ATX1}) \tag{16}$$

$$\text{ATX1} = -0.8945\frac{a}{l} + 0.4471\frac{L}{l} \tag{17}$$

A graphical representation of this PPR trial is shown in Figure 2. The first two plots are the scatter plots of the one-to-one relationships of R versus a/l and L/l. The next plot shows the resulting first PPR projected term versus the length of the projection, that is, $\Phi_1(a_1^T x)$ versus $a_1^T x$. Notice that $a_1^T x$ is represented by the axis label ATX1, whereas $\Phi_1(\text{ATX1})$ is represented by the axis label "1st Projected Term" in this plot. The goodness-of-fit of this PPR model including a plot of the predicted versus actual values and a plot of the residual versus predicted values is displayed in the last two plots. If this curve is properly modeled and the above two equations are used, fairly good predictions with a relatively high R^2 of 0.995 may be obtained.

Thus, the task was reduced to simply finding a feasible model for this projected curve. An asymptotic trend was clearly identified through visual inspection. Therefore, an asymptotic nonlinear model with two to three (or at most four) parameters may describe this curve adequately. The following four-parameter equation form was selected to offer the maximum flexibility in the modeling process:

$$\Phi_1(\text{ATX1}) = a_1 + \frac{1}{a_2 + a_3\text{ATX1}^{a_4}} \tag{18}$$

The nonlinear regression technique was then used to obtain the parameter estimates. The first derivative of this equation form with respect to each parameter was also provided to help the iterative regression routine converge faster. The starting value of each parameter was carefully chosen so that a_1 and a_4 were large negative values, for example, -4.0, and a_1 was the minimum possible value of Φ_1. Since a_2 and a_3 were still undecided, two small positive values, for example, 0.01, were chosen as their starting points. The following equation satisfies the convergence criteria even with many other different starting values:

$$\Phi_1(\text{ATX1}) = -5.5869 + \frac{1}{0.1473 + 0.2627\text{ATX1}^{-5.1659}} \tag{19}$$

The overall statistics for the prediction of R (or σ_i/σ_∞) because of the slab length effect by using Equations 16, 17, and 19 are summarized as follows:

Statistics: $N = 20$, $R^2 = 0.994$, SEE = 0.0027, CV = 0.28 percent
Limits: $3 \leq L/l \leq 5$, $0.05 \leq a/l \leq 0.3$

To illustrate how the three-dimensional response surface (Figure 1) might be broken down into the sum of a series of two-dimensional curves, the PPR algorithm was utilized again to obtain a two-term model and a three-term model as shown in Figures 3 and 4, respectively. By analogy, the axis labels "ATX2" and "ATX3" represent $a_2^T x$ and $a_3^T x$, respectively, whereas the axis labels "2nd Projected Term" and "3rd Projected Term" represent $\Phi_2(\text{ATX2})$ and $\Phi_3(\text{ATX3})$ in Equation 7, respectively. The other plots are similar to the plots defined in Figure 2.

As an example, the results of the two-term PPR model are given in the following equations:

$$R = 0.9667 + 0.0330\Phi_1(\text{ATX1}) + 0.00210\Phi_2(\text{ATX2}) \tag{20}$$

$$\text{ATX1} = -0.8945\frac{a}{l} + 0.4471\frac{L}{l} \tag{21}$$

$$\text{ATX2} = 0.9970\frac{a}{l} + 0.07787\frac{L}{l} \tag{22}$$

The second projected term contributes little to the prediction of R, since its coefficient is very small when compared with the coefficient of the first projected term (i.e., $\beta_2 = 0.0021$, whereas $\beta_1 = 0.0330$). The third projected term also contributes very little to the accuracy of the prediction when compared with the first one and the second one, and thus the associated equations for the three-term model are not presented herein. In fact, the use of only one or two projected curves can adequately describe this three-dimensional response surface, as suggested by these figures.

The plausible model forms suggested by these PPR trials are an asymptotic nonlinear model for the first projected curve, a second-degree polynomial for the second projected curve, and a third-degree polynomial for the third projected curve if necessary. Of course, some piecewise linear and nonlinear curves may also be formulated for these purposes without much loss of generality.

Prediction and Extrapolation

From the above demonstration, it is evident that using different regression procedures may result in totally different predictive models, but with excellent agreement with the same set of data.

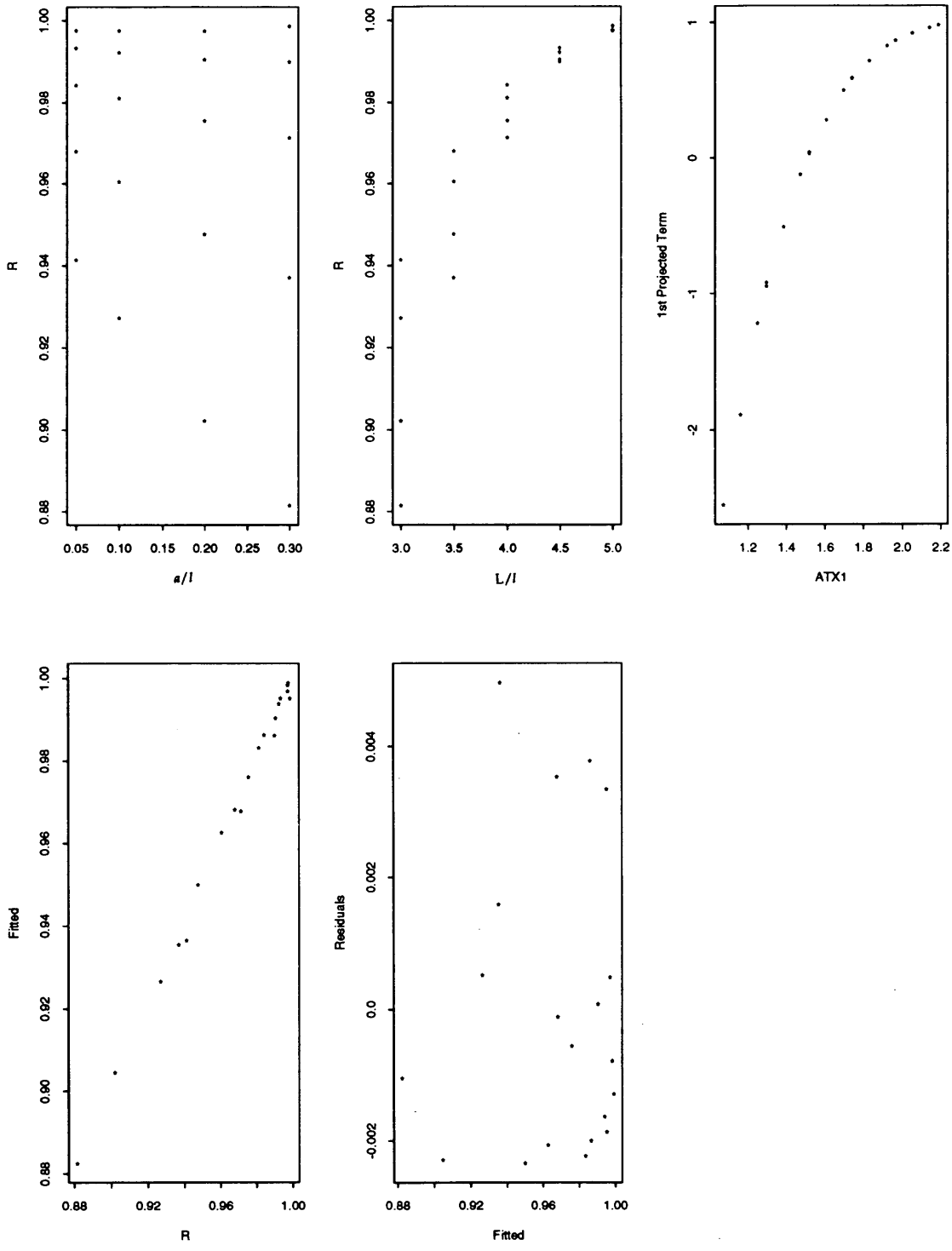

FIGURE 2 Slab size effect: one-term PPR model.

Under the umbrella of statistical regression analysis, they are all feasible solutions of the targeted problem as long as the conclusions are restricted to the range of the data. In other words "extrapolation beyond the range of the data" is never considered feasible with statistical regression analysis procedures.

However, it is also recognized that "extrapolation" is often necessary in actual engineering practice because of the limited resources available and technical limitations. To judge which equation is preferable, both Equations 15 and 16 were checked by plotting the predicted versus the actual R values within the specified data ranges as displayed by the symbol "○" in Figures 5(a) and 5(b), respectively. It is clearly shown that both equations result in very good predictions within the range of the data from which they were originally developed. In addition, Figures 5(a)

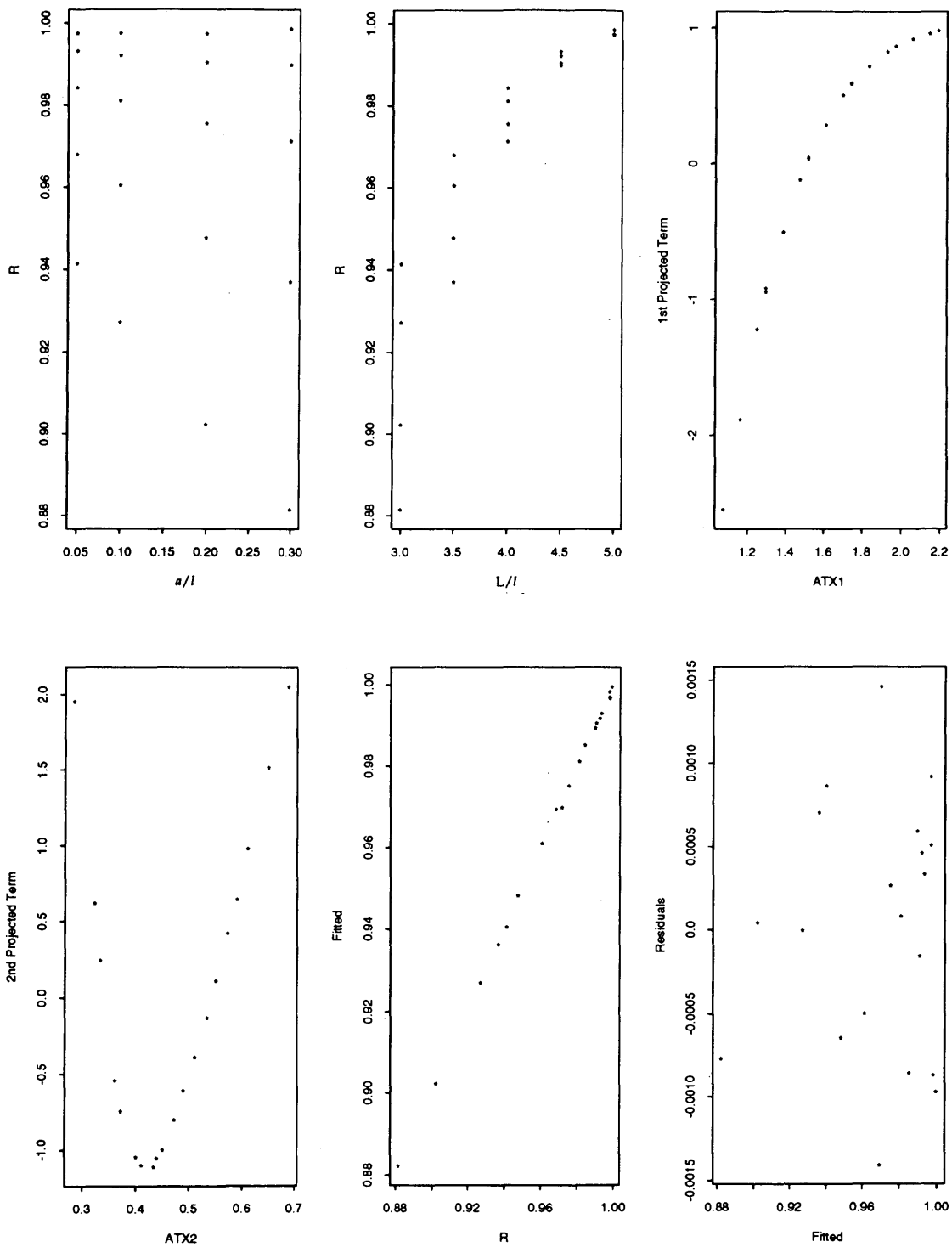

FIGURE 3 Slab size effect: two-term PPR model.

and 5(*b*) present the results when extrapolating beyond the specified limits by using these two models and the data from all of the 36 FE runs, respectively. These datum points, as displayed by the symbol "*" in the graphs, clearly show the difference.

Extrapolation by using Equation 15 results in totally unacceptable predictions outside the specified limits as shown in Figure 5(*a*). However, this problem is less pronounced as shown in Figure 5(*b*) when using Equation 16. In fact, the extrapolation of L/l greater than 5.0 provides excellent agreements with the actual data, since the functional form was properly selected to be asymptotic such that the predicted R values are very close to unity, as they should be. Nevertheless, some discrepancies still exist when extrapolating Equation 16 to smaller L/l values, that is, $L/l < 3.0$, which generally result in smaller R values.

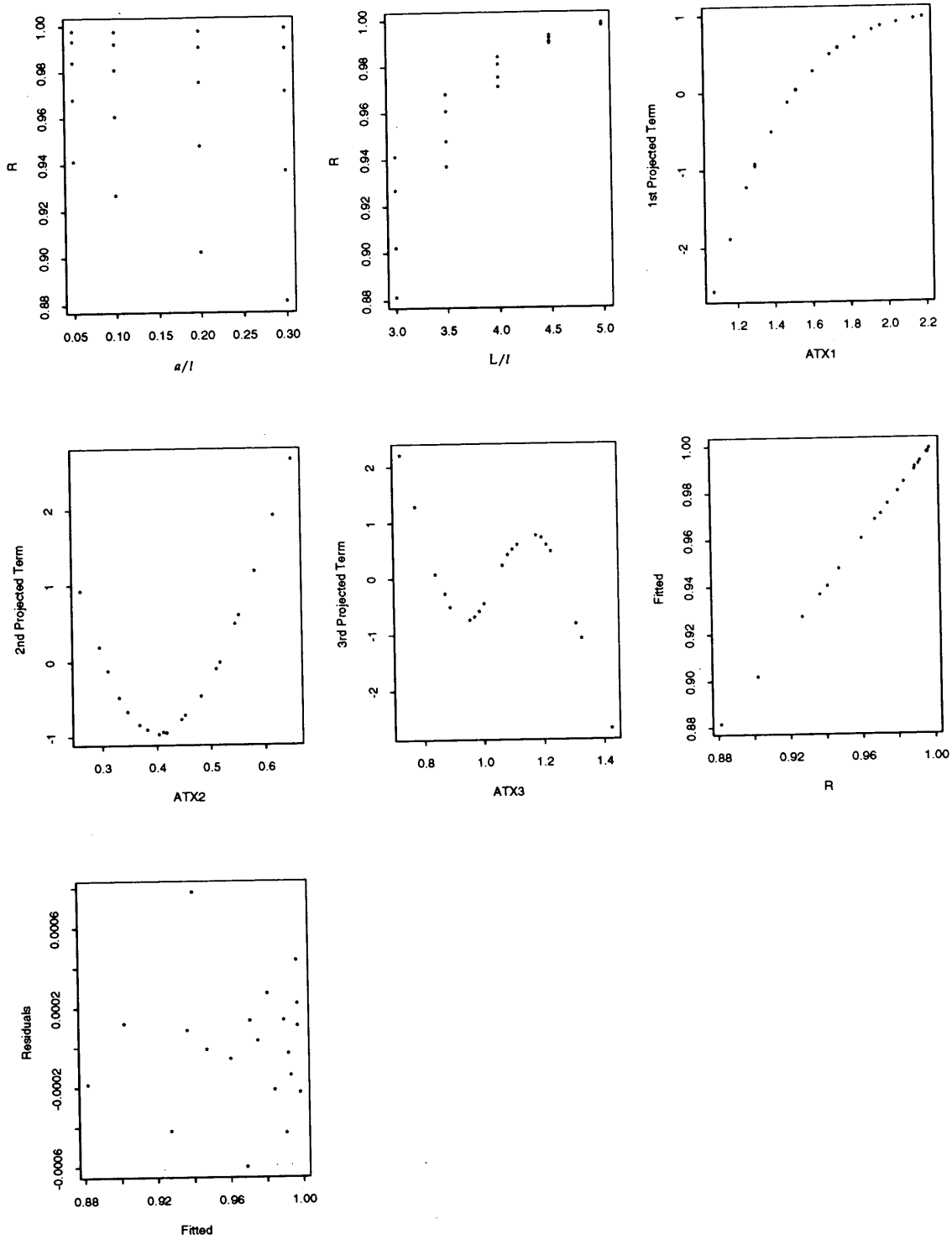

FIGURE 4 Slab size effect: three-term PPR model.

This result may be explained by the fact that the first parameter [a_1, or the minimum possible value of Φ_1(ATX1)] of Equation 19 was estimated to be -5.5869, such that Equation 16 will never result in a value below 0.7823. This approximation is acceptable for the ranges of data that were used to develop Equations 16, 17, and 19. However, it may not be as accurate when extrapolating too far away from this specified range. If the minimum possible value of R is known, this boundary condition may also be imposed on the predictive model. Thus, better agreement with the data can be obtained even in the case of extrapolation.

In summary, this case study not only demonstrates the benefits of using mechanistic variables through the use of the principles of dimensional analysis but it also emphasizes the importance of selecting proper functional forms. Correct functional forms pro-

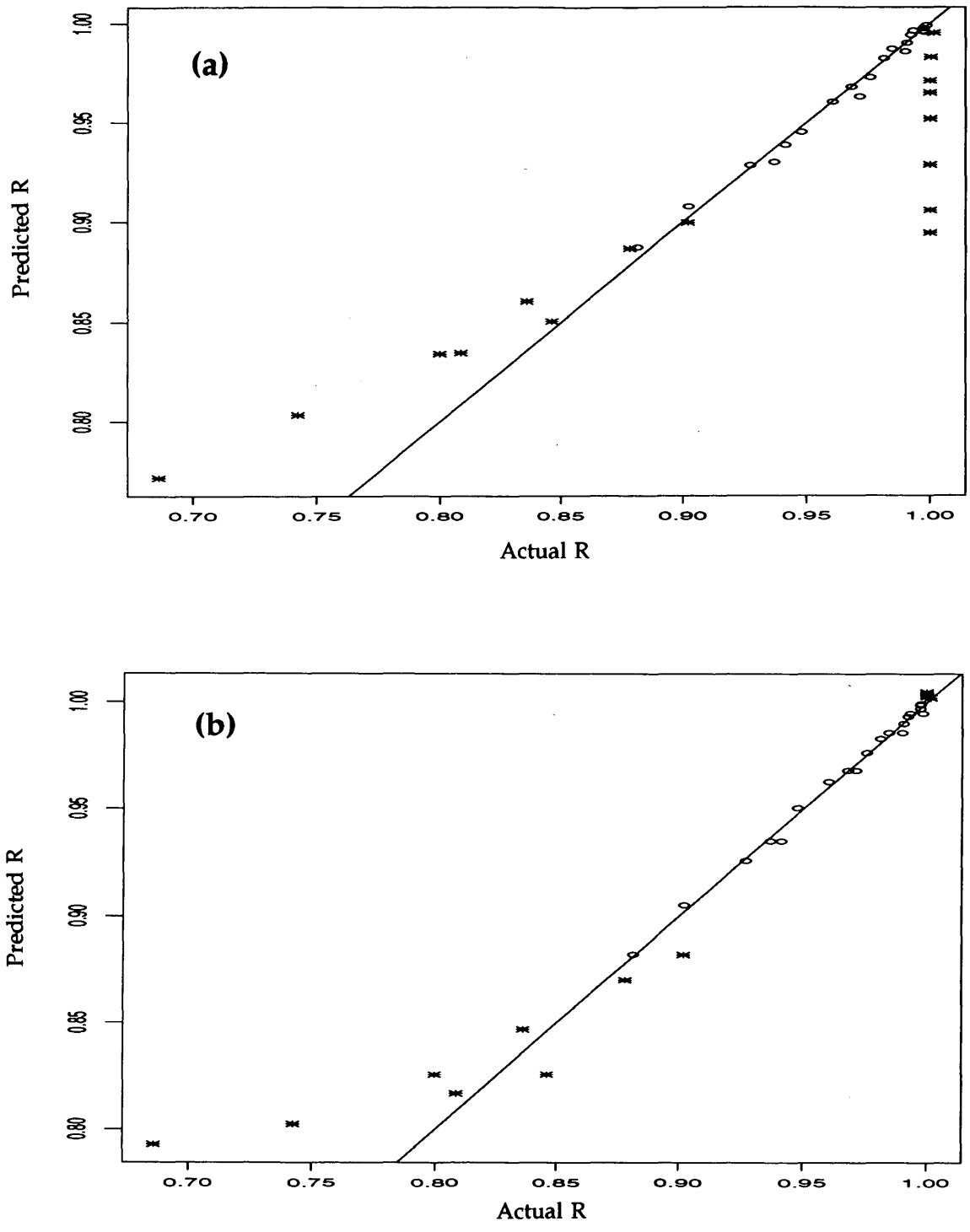

FIGURE 5 Extrapolated prediction plots using (*a*) existing model; (*b*) new model.

vide more comprehensive insights into the performance of the predictive model and may also lead to reasonable results even when extrapolation beyond the range of the data is required. It can be concluded that proper functional form is also a very crucial component in the success of a modeling process. The proper selection of functional forms to satisfy some applicable physical boundary conditions and subject-related engineering knowledge are the best supplements to statistical regression algorithms.

CONCLUSIONS

Several traditional linear and nonlinear regression techniques that have been widely adopted in pavement research were reviewed. Their advantages and limitations were discussed. Application of these regression techniques to practical engineering problems often shows the deficiencies in the selection of proper functional forms, the violation of some embedded statistical assumptions,

and failures to satisfy some applicable engineering boundary conditions.

Through the use of projection pursuit regression technique, a two-step predictive modeling approach was proposed in an attempt to minimize these problems. The proposed modeling approach was demonstrated in a case study for edge stress prediction owing to the finite slab length effect. Without imposing an unjustified parametric assumption, the PPR provides a unique routine for breaking down higher-dimensional engineering problems into a series of sensible projected curves. By doing so the individual projected curves may be formulated separately with better choices of feasible functional forms as well as possible boundary conditions. Not only did the demonstration reemphasize the advantages of using the principles of dimensional analysis but it also illustrated the importance of the proper selection of functional forms. Correct functional form provides more comprehensive insights into the performance of the predictive equation and may also lead to reasonable results even when extrapolation beyond the range of the data is required.

The demonstration was based on the data from the theoretical FE solutions in which no erroneous data are expected. As for applying the PPR to field or laboratory data with some possible errors, the promising features of the PPR algorithm are also helpful for identifying any extremely strange behavior because of data errors. Engineering knowledge of the physical mechanism of the problem may be applied in identifying the possible bad datum points as well.

It is also believed that only through the application of both engineering and statistical knowledge and techniques will a more theoretically correct predictive equation be developed. If properly developed it may also be applied beyond the range of the data. Nevertheless, the conclusions should be restricted to the range of the data.

ACKNOWLEDGMENTS

This research work was partially sponsored by the Illinois Department of Transportation under the project titled Implementation of Illinois Pavement Feedback System, for which different modern regression techniques were utilized for predictive model development. The authors would like to express much appreciation to James Hall, Illinois Department of Transportation, for valuable assistance in this project.

REFERENCES

1. Hastie, T. J., and R. J. Tibshirani. *Generalized Additive Models.* Monographs on Statistics and Applied Probability 43. Chapman & Hall, 1990.
2. Breiman, L., and J. H. Friedman. Estimating Optimal Transformations for Multiple Regression and Correlation (with Discussion). *Journal of the American Statistical Association*, Vol. 80, 1985, pp. 580–619.
3. Buja, A. Remarks on Functional Canonical Variates, Alternating Least Squares Methods and ACE. *Annals of Statistics*, Vol. 18, No. 3, 1990, pp. 1032–1069.
4. Tibshirani, R. Estimating Transformations for Regression via Additivity and Variance Stabilization. *Journal of the American Statistical Association*, Vol. 83, 1987, pp. 394–405.
5. Friedman, J. H., and W. Stuetzle. Projection Pursuit Regression. *Journal of the American Statistical Association.* Vol. 76, 1981, pp. 817–823.
6. Friedman, J. H. *SMART User's Guide.* Technical Report No. 1. LCS, Department of Statistics, Stanford University, Stanford, Calif., 1984.
7. Darter, M. I. *Design of Zero-Maintenance Plain Jointed Concrete Pavement, Vol. I. Development of Design Procedures.* FHWA Report FHWA-RD-77-111. FHWA, U.S. Department of Transportation, June 1977.
8. Salsilli-Murua, R. A. *Calibrated Mechanistic Design Procedure for Jointed Plain Concrete Pavements.* Ph.D. thesis. University of Illinois, Urbana, 1991.
9. *SAS User's Guide: Basics*, Version 5 edition. SAS Institute, Inc., 1985.
10. *SAS User's Guide: Statistics*, Version 5 edition. SAS Institute, Inc., 1985.
11. Weisberg, S. *Applied Linear Regression*, 2nd ed. Wiley Series in Probability and Mathematical Statistics. John Wiley & Sons, Inc., New York, 1985.
12. Draper, N. R., and H. Smith. *Applied Regression Analysis*, 2nd ed. Wiley Series in Probability and Mathematical Statistics. John Wiley & Sons, Inc., New York, 1981.
13. Rousseeuw, P. J., and A. M. Leroy. *Robust Regression and Outlier Detection.* Wiley Series in Probability and Mathematical Statistics. John Wiley & Sons, Inc., New York, 1987.
14. Gorman, J. W., and R. J. Toman. Selection of Variables for Fitting Equations to Data. *Technometrics*, Vol. 8, 1966, pp. 27–51.
15. Bates, D. M., and D. G. Watts. *Nonlinear Regression Analysis and Its Applications.* Wiley Series in Probability and Mathematical Statistics. John Wiley & Sons, Inc., New York, 1988.
16. *S-PLUS User's Manual*, Vol. 1 and Vol. 2. Statistical Sciences, Inc., Seattle, Wash., Nov. 1991.
17. *S-PLUS Reference Manual.* Statistical Sciences, Inc., Seattle, Wash., Nov. 1991.
18. Chambers, J. M., and T. J. Hastie. *Statistical Models in S.* Wadsworth & Brooks/Cole Computer Science Series. AT&T Bell Laboratories, 1992.
19. Becker, R. A., J. M. Chambers, and A. R. Wilks. *The New S Language—A Programming Environment for Data Analysis and Graphics.* The Wadsworth & Brooks/Cold Computer Science Series. AT&T Bell Laboratories, 1988.
20. Westergaard, H. M. New Formulas for Stresses in Concrete Pavements of Airfields. *Transactions, ASCE*, Vol. 113, pp. 425–444, 1948. Also in *Proceedings, ASCE*, Vol. 73, No. 5, May 1947.
21. Ioannides, A. M., M. R. Thompson, and E. J. Barenberg. The Westergaard Solutions Reconsidered. In *Transportation Research Record* 1043, TRB, National Research Council, Washington, D.C., 1985.
22. Tayabji, S. D., and D. J. Halpenny. Thickness Design of Roller-Compacted Concrete Pavements. In *Transportation Research Record 1136*, TRB, National Research Council, Washington, D.C., 1987.
23. Ioannides, A. M., and R. A. Salsilli-Murua. Temperature Curling in Rigid Pavements: An Application of Dimensional Analysis. In *Transportation Research Record 1227*, TRB, National Research Council, Washington, D.C., 1989.
24. Ioannides, A. M. *Analysis of Slabs-on-Grade for a Variety of Loading and Support Conditions.* Ph.D. thesis. University of Illinois, Urbana, 1984.

Publication of this paper sponsored by Task Force on Statistical Methods in Transportation.